BIOPHYSICAL CHEMISTRY 2 (1974) 1–22. © NORTH-HOLLAND PUBLISHING COMPANY

COMPARATIVE BINDING STUDY OF THE INTERACTION OF QUINACRINE AND ETHIDIUM BROMIDE WITH DNA AND NUCLEOHISTONE

José BONTEMPS and Eugène FREDERICQ
Laboratoire de Chimie Physique, Université de Liège au Sart-Tilman, B4000 Liège, Belgium

Received 28 December 1973
Revised manuscript received 11 March 1974

The degree of binding of quinacrine dihydrochloride and ethidium bromide to DNA and nucleohistone has been determined by direct and indirect methods.

The results obtained by the equilibrium dialysis experiments have been analyzed in terms of various theoretical models and have led us to propose for the interaction of the dyes with DNA at low ionic strength a structural scheme where the external binding sites are next to the intercalative ones.

The equilibrium dialysis results were used to check those obtained by the indirect methods, i.e. absorption and fluorescence titrations, and to identify the origin of the discrepancies.

The comparative study of the binding of these dyes to DNA and nucleohistone has shown that the accessible part of DNA in the nucleoprotein is to some extent different from free DNA itself.

1. Introduction*

When starting a study on the interaction of a ligand with a macromolecule, one is always faced with the difficult problem of making a choice between various methods (direct and indirect) for the binding curve determination, and between the different procedures for analyzing the binding data in terms of number of binding sites and binding constants. One of the aims of this paper is to compare the adequacy of the various methods available in different situations to help the users in making the appropriate choice for their particular system. To our knowledge, a throughout comparison of this kind never appeared in the literature.

In most of the published works, the binding parameters of the interaction between quinacrine [1,2] and ethidium bromide [3–12] with nucleic acids have been determined by indirect methods, mainly by absorption spectrophotometry and fluorescence titrations, without taking care to verify the validity of such methods. The indirect binding curve calculations are based on theoretical hypotheses which can only be checked by a comparison with a direct method, such as equilibrium dialysis.

As for many other drugs, the interaction of quinacrine with nucleic acids seems to involve two consecutive stages: intercalation [13–16] and external binding [15, 16]. A particular feature of quinacrine, compared to other acridines such as proflavine and acridine orange, is the presence on the acridine ring of an aliphatic side-chain with a positively charged terminal diethylamino group. It creates additional interactions with the phosphate groups of DNA [17] and, although this 9-amino substituent is two to three times more extended than the acridine ring, more binding sites of DNA are occupied by quinacrine than by the 9-aminoacridine itself [1]. Due to the presence of such bulky side chains, the first intercalation model of Lerman [18] has been modified [1, 16, 19]. The second stage of the binding process is not well defined [15, 16]. Detected at moderate ionic strength, it would occur on the outside of the DNA helix, as in the case of proflavine [16]. In several works, the

* Abbreviations used in this article: DNH, deoxyribonucleohistone; EB, ethidium bromide; Q, quinacrine dihydrochloride (atebrin); PF, proflavine.

complexes of quinacrine with biological macromolecules have been compared to those formed with proflavine [2,16,20], ethidium bromide [4,16,21–23], and methylene blue [15].

Reported quantitative data are very scarce and binding experiments by means of equilibrium dialysis are still lacking. The stoichiometry of the strong binding process with DNA has been estimated as four nucleotides per dye molecule [15]. Binding curves derived from spectrophotometry data and presented in figs. 6 and 7 by Drummond et al. [1] seem contradictory and the evaluation of the binding parameters from fluorescence titrations is not very precise [2].

In view of the lack of unambiguous binding studies and of the recent application of quinacrine and its alkylated derivative to chromosome characterization [24], it appeared worthwhile determining the binding curves of this antimalarial acridine on both calf thymus DNA and nucleohistone by direct (equilibrium dialysis) and indirect (absorption spectrophotometry, fluorescence intensity and polarization) procedures. We will draw the attention to the uncertainties which arise when using such indirect methods. Further information will be obtained from the analysis of the binding process in terms of theoretical models. The binding parameters of quinacrine will be compared to those obtained for the trypanocidal phenanthridine, ethidium bromide, on the same macromolecules. The comparison between dye-DNA and dye-nucleohistone complexes will bring some indication about the screening effect of the histones on these dyes and about the state of DNA in the nucleoprotein.

2. Materials and methods

2.1. Samples

The preparation and characterization of DNA [25] and nucleohistone [26] samples from calf thymus have been already described. The nucleohistone was prepared in a gel-form but used in a soluble form by stirring the diluted gel (concentration: 0.5 mg DNA per ml). The concentrations of the DNA and nucleohistone solutions were calculated from their absorbance at 260 nm, using the molar extinction coefficient per mononucleotide residue: $\epsilon = 6450$ and 6700 $M^{-1}cm^{-1}$ respectively. All solutions were made in pure water or in NaCl, unbuffered but adjusted at pH 6.5 by NaOH. Micrococcus Lysodeikticus DNA was a gift of J. Ramstein (Orleans) [27].

Quinacrine dihydrochloride (from the Nutritional Biochemical Corporation) was crystallized three times in ethanol; absorption, excitation and emission fluorescence spectra were found identical before and after this operation. Molar extinction coefficients were determined in water at neutral pH after drying at 90°C to constant weight and were found to be independent of the ionic strength (1 mM to 0.1 M NaCl in unbuffered solutions). We measured $\epsilon = 8400$, 8900, 4600, 50000 and 20000 $M^{-1}cm^{-1}$ at $\lambda = 445$, 425, 345, 280 and 225 nm respectively; these values are in good agreement with those of various authors [15,28], except those of Drummond et al. [1]. Ethidium bromide (from the British Drug House) was used without further purification; we did not detect any trace of impurity by thin-layer chromatography on silicagel according to LePecq [29]. The concentrations of free ethidium bromide solutions were determined from their absorbance at 480 nm, using $\epsilon = 5600$ $M^{-1}cm^{-1}$ [3].

2.2. Equilibrium dialysis

The equilibrium dialysis apparatus was identical to that described by Fredericq and Houssier [25]. The total dye concentration of the "inner" and "outer" compartments were determined spectrophotometrically, after desorption of the bound dye from the macromolecule for the "inner" one (table 1) to eliminate the possible effect due to the adsorption of the dye on the vessels and on the cellulose membrane. In each case, complete liberation of the dye was checked by differential spectrophotometry. Moreover, it was widely checked that the same equilibrium level was reached whether the total amount of dye was added in one of the compartments or equally distributed in each of them. In the range of electrolyte, macromolecular and dye concentrations used in our experiments, the influence of the Donnan effect was calculated and was found to be inferior to 5% of the bound-dye concentration, i.e. inferior to the accuracy of the equilibrium dialysis experiments.

The amount of binding is expressed in terms of r, defined as the number of bound-dye molecules per nucleotide phosphorus, and (D_f) will denote the

Table 1
Desorption of the bound-dye from the macromolecule in the "inner" compartment

Dye macromolecule complex	Composition of the medium	Wavelength λ(nm)	Molar extinction coefficient $\epsilon(M^{-1}cm^{-1})$
Quinacrine-DNA in 0.1 M NaCl	Ethanol 60% (V/V)	445	9200
		425	9900
	Dimethylformamide	445	5800
	50% (V/V)	425	7700
Quinacrine-DNA in 1 mM NaCl	Dimethylformamide 50% (V/V) 0.1 M NaCl	425	7900
Quinacrine-nucleohistone in 1 mM NaCl	Methanol 60% (V/V) and 0.08 M NaOH	416	7860
Ethidium bromide-nucleohistone in 1 mM NaCl	Methanol 37.5% (V/V) and 0.125 M NaOH	494	5600

free-dye concentration. Owing to the relatively low molar extinction coefficients of quinacrine and ethidium bromide compared to proflavine and acridine orange, low values of r were not available since we used absorption spectrophotometry to determine (D_f).

2.3. Absorption spectrophotometry

The absorption spectra were registered on a Zeiss RPQ 20A spectrophotometer and precise absorbances were measured on a Shimadzu QV-50 spectrophotometer, using in the reference cell a macromolecular solution at the same concentration as in the complex.

The different methods used for the determination of the binding curves from absorption experiments are listed in table 2.

It is very critical to have a precise value of the parameters ϵ_b and $\Delta\epsilon_{lim} = \epsilon_f - \epsilon_b$ (where subscripts f and b denote free and bound dye respectively) for the calculation of the bound fraction, $1-\alpha$, according to the well-known method of Peacocke and Skerrett [30]. This is the reason why we will compare several methods for estimating these parameters which are less easily accessible at high ionic strength. In the case of dye-nucleic acids complexes, the linear range of the reported extrapolation methods 1a and 1b [31, 32] appears very short, so that both may be empirically improved if the same parameters, $(\Delta\epsilon)^{-1}$ and ϵ_{app} (the apparent molar extinction coefficient, defined

Table 2
Binding curves derived from absorption spectrophotometry

Method	Graphical determinations	Ref.
1. Titration at one total dye concentration [30]: calculation of $1-\alpha$	Determination of $\Delta\epsilon_{lim} = \epsilon_f - \epsilon_b$	
	1a: $(\Delta\epsilon)^{-1} = (\epsilon_f - \epsilon_{app})^{-1}$ versus P^{-1}	[31]
	1b: ϵ_{app} versus D/P	[32]
	1c: $(\Delta\epsilon)^{-1}$ versus P^{-2}	this work
	1c: ϵ_{app} versus $(D/P)^2$	this work
	1d: $\Delta A/P$ versus D/P	this work
2. Titration at one total dye concentration: calculation of k and n	k and n determinations	
	2a: ϵ_{app} versus D/P and P/D	[32]
	2b: n from $\epsilon_{app}/\epsilon_f$ versus P/D	this work
	2b: k from $1-\alpha$ versus P/D	[33]
3. Titration at two different total dye concentrations [34]	property used for the calculation of r and (D_f) $\Delta A/P$ versus P	this work

as the measured absorbance, A, divided by the total dye concentration, D) are plotted versus P^{-2} and $(D/P)^2$ respectively (method 1c). We suggest an other graphical procedure (method 1d) in which $\Delta A/P$ (where ΔA and P denote the variation of absorbance at a given wavelength and the DNA molar nucleotide concentration respectively) is plotted as a function of D/P according to the following equation:

$$\Delta A/P = \sum_i \Delta\epsilon_{\mathrm{lim},i} r_i \qquad (1)$$

valid for several binding processes if $\epsilon_{b,i}$ does not vary with r_i. As D/P goes to zero, it tends to become identical to r_1 and the slope of this plot gives $\Delta\epsilon_{\mathrm{lim},1}$. In this representation, the range of linearity is much larger for the titrations at low ionic strength than for those at high ionic strength. This suggests that the determination of $\Delta\epsilon_{\mathrm{lim}}$ would be made by some measurements at low salt concentration, even when studying a binding process at high ionic strength.

Owing to the limited range of linearity of the plot ϵ_{app} versus D/P used in the recent method of Terada and Miyake [32] (method 2a), we developed another procedure for the direct determination of the parameters k and n in the case of a single binding process (method 2b). If $\Delta\epsilon_{\mathrm{lim}}$ has been determined by one of the methods mentioned above (methods 1c and 1d), n is easily calculated from the slope at the origin of the plot $\epsilon_{\mathrm{app}}/\epsilon_{\mathrm{f}}$ versus P/D since r becomes identical to n as P/D goes to zero:

$$\epsilon_{\mathrm{app}}/\epsilon_{\mathrm{f}} = 1 - r(\Delta\epsilon_{\mathrm{lim}}/\epsilon_{\mathrm{f}})(P/D). \qquad (2)$$

The binding constant, k, is then estimated by the method of Schwarz [33]. When $1-\alpha$ is plotted against P/D, the straight line passing by the points $(0,0)$ and $(1,2/n)$ intercepts the experimental curve at a point M whose ordinate value is related to k.

It is possible to avoid the determination of $\Delta\epsilon_{\mathrm{lim}}$ when the titration experiments are made at two different dye concentrations. This procedure, suggested by Halfman and Nishida [34] for different polymer concentrations was adapted for the case of two dye concentrations, D_1 and D_2 $(D_1 > D_2)$ (method 3). $\Delta A/P$ is plotted versus P. For a given value of $\Delta A/P$, P_1 and P_2 are determined by the intercepts of the horizontal with curves 1 and 2. The parameters r and (D_{f}) are then calculated as follows:

$$r = (D_1 - D_2)/(P_1 - P_2) \qquad (3)$$

$$(D_{\mathrm{f}}) = (D_2P_1 - D_1P_2)/(P_1 - P_2). \qquad (4)$$

2.4. Fluorescence

The fluorescence apparatus and the calculations of $(\phi_{\mathrm{app}}/\phi_{\mathrm{f}})$, the ratio of quantum yields, and of μ_{app}, the emission anisotropy, have been previously described [25]. The different corrections which are to be made for the calculation of the ratio of quantum yields from the measured quantities, $(I_{\mathrm{app}}/I_{\mathrm{f}})_{\mathrm{mes}}$, were found of the same order of magnitude as the precision of the measurements, i.e. 2–5%, when excitation occurs in the isosbestic point or range. For quinacrine and ethidium bromide, the excitation wavelengths were 458 and 510 nm and the emission wavelengths were 500 and 590 nm respectively. The latter values are not the maxima of the true fluorescence spectra [2, 7, 23]. In order to follow the variation of the fluorescence parameters with increasing binding, the fluorescence parameters of the complex (subscript c) were calculated as described by Fredericq and Houssier [25].

The relations allowing binding curves calculations from fluorescence intensities and polarizations have been taken from LePecq and Paoletti [4] and Ellerton and Isenberg [35] respectively.

2.5. Analysis of the binding curves

In table 3, we summarize the methods of analysis of the binding curves with references to previous works. When the Scatchard equation (procedure 1) or the exclusion model (procedure 2) are used, the parameters r, n and k will be noticed with roman and arabic subscripts respectively.

Among the various representations used for determining the binding parameters k and n, the direct representation (r versus (D_{f})) and the Scatchard plot ($r(D_{\mathrm{f}})^{-1}$ versus r), will be used throughout this work. The former permits an easy visual and qualitative comparison between different systems and offers the advantage of being additive with respect to r at a given value of (D_{f}); the latter provides a very sensitive analysis of the data at low r and (D_{f}) values and its shape is very much affected by the existence of several sets of binding sites and by the heterogeneity of the binding process. The double logarithmic plot, introduced by Thompson and Klotz [36], was found improper

Table 3
Procedures of analysis of the binding curves. Procedures 1 and 2 can be used to characterize the first binding process at low ionic strength, and consequently to analyse the second binding process; while procedure 3 may simultaneously fit both processes as a whole

Procedure	Model used	Parameters and symbols	Ref.
1	One set of homogeneous binding sites (classical Scatchard eq.)	k_1, $n_1(r_1)$	[41]
2	Exclusion of adjacent binding sites (eq. (6) of Fredericq and Houssier [25])	k_1, $n_1 = 0.25(r_1)$	[25,40,42–45]
3	Heterogeneous model of Chambron	$\bar{k}$, n, $\bar{w}$	[46–48]

in our case because of the scattering of the experimental points and the lack of results at low r values.

The problem of the decomposition of complex binding curves has been recently reviewed by Feldman [37]. In the case of dye-nucleic acids complexes at low ionic strength, a quite simple procedure can be adopted since the experimental data are satisfactorily fitted using two groups of binding sites, the existence of which has been widely suggested for quinacrine [15,16] and ethidium bromide [3,4,38–40].

The calculations were made according to the following scheme. As the binding constants for both processes appear very different, the parameters of the stronger one are determined from the Scatchard plot by procedures 1 or 2 of table 3. The direct plot relative to this process, r_{th} versus $(D_f)^{-1}$, is then subtracted from the experimental one, r_{exp} versus $(D_f)^{-1}$, and the second binding process is quantitatively analyzed by plotting $(r_{exp} - r_{th})(D_f)^{-1}$ as a function of $(r_{exp} - r_{th})$.

In the simplest approach, i.e. two sets of homogeneous sites (procedure 1) the values of k_1 and n_1 are determined from the slope and intercept on r axis of the asymptote to the experimental Scatchard plot. A more refined procedure is to take into account the intercalation model with exclusion of adjacent binding sites (procedure 2), which seems rather convenient for the intercalation of various dyes at high ionic strength [25,40,42–44]. These results suggest a common binding capacity of the DNA helix, the binding constant (denoted k_1, as in eq. (6) of Fredericq and Houssier [25]) depending upon the dye and the salt concentration. In the Scatchard representation, the curvature introduced by the exclusion model is only important in the region of large binding ($r > 0.2$), so that it may be difficult to distinguish it from a straight line (Scatchard eq.) on the limited range of r values available here. The third model adopted for the fitting has been presented by Chambron et al. [46] for proflavine-DNA complexes and applied by different authors to proflavine-nucleohistone complexes [47,48]. Contrary to procedures 1 and 2, the single or complex binding curve is analyzed as a whole and mean values of the binding parameters, $\bar{k}$ and $\bar{n}$ are obtained, in addition to a factor of interaction, $\bar{w}$.

3. Results and discussion

3.1. Equilibrium dialysis

Quinacrine-DNA complexes in 0.1 M NaCl. The results of our binding experiments with Q are compared in two ways in fig. 1 to those obtained by Houssier et al. [40] with EB. The Scatchard plot with Q presents a more pronounced curvature than that expected from the exclusion model, which is illustrated by curve 2. This makes the analysis according to this model impossible, although the Scatchard representation suggests a saturation value close to 0.25.

In order to correct the equation of the exclusion model (eq. (6) of Fredericq and Houssier [25]) for the fitting of the experimental results, we used the method of Chambron (procedure 3 of table 3) which includes an exponential term. As indicated in table 4 (fitting no. 1), this treatment yields a value of n equal to 0.24, i.e. close to the limiting value expected from the exclusion model. This suggests a fitting which takes into account both models (procedures 2 and 3

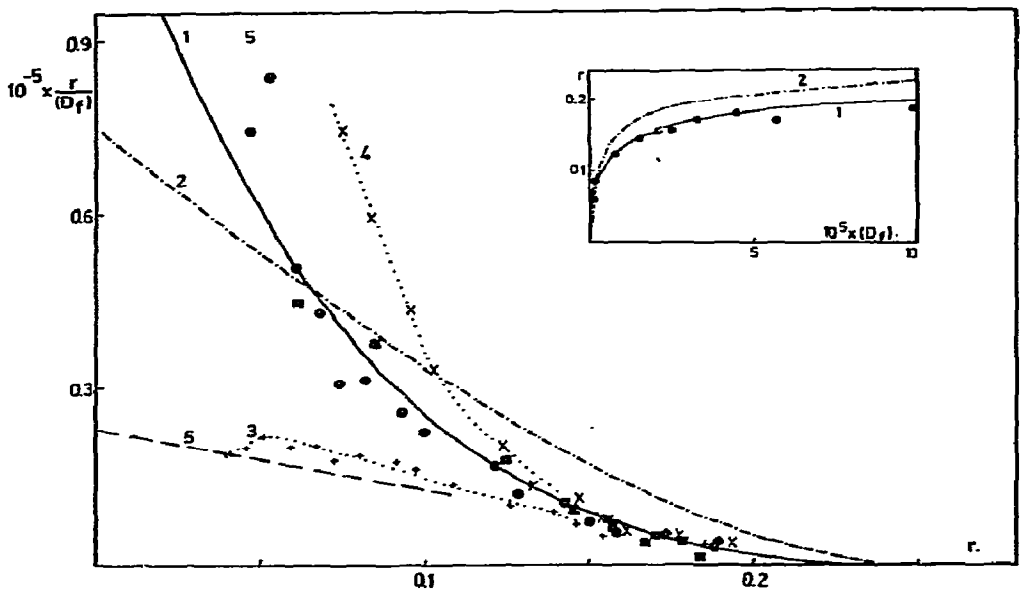


Fig. 1. Binding curves of quinacrine-DNA complexes in 0.1 M NaCl. Main figure: Scatchard plot. ▪: Mean values of equilibrium dialysis experiments. ×, • and +: absorption spectrophotometry at λ = 421 nm for $\Delta\epsilon_{lim}$ = 4910, 5000 and 5150 M^{-1} cm^{-1} respectively, total dye concentration equal to 7 × 10^{-5} M
Curve 1: theoretical curve calculated from eq. (5) with k_1 = 2.55 × 10^5 M^{-1} and w_1 = 0.66 kcal mol^{-1} (fitting no. 2 of table 4).
Curve 2: illustrates the model with exclusion of the adjacent binding sites (eq. (6) of Fredericq and Houssier [25]), with the k_1 value obtained by Houssier et al. [40] for the ethidium bromide DNA-complexes in 0.1 M NaCl.
Line 5: Results obtained by the method of Terada and Miyake [32] (method 2a of table 2).
Insert figure: direct representation. •: Mean values of equilibrium-dialysis experiments.

Table 4
Fittings of the equilibrium dialysis experiments according to the procedures listed in table 3

Fitting no.	System	Site numbers			Binding constants ($10^{-5}M^{-1}$)		$\bar{w}$	Fig. and curve no.
		1st process	2nd process	Σn_i	1st process	2nd process	(kcal mol^{-1})	
1	Q-DNA 0.1 M NaCl	n = 0.24	–	0.24	$\bar{k}$ = 4.0	–	0.73	–
2	Q-DNA 0.1 M NaCl	n_1 = 0.25	–	0.25	k_1 = 2.55	–	0.66	1–1
3	PF-DNA 0.1 M NaCl [46]	n = 0.225	–	0.225	$\bar{k}$ = 3.2	–	0.065	–
4	EB-DNA 0.1 M NaCl [40]	n_1 = 0.25	–	0.25	k_1 = 1.5	–	–	1–2
5	Q-DNA 1 mM NaCl	n_I = 0.21	n_{II} = 0.16	0.37	k_I = 110	k_{II} = 1.7	–	2–1
6	Q-DNA 1 mM NaCl	n_1 = 0.25	n_{II} = 0.125	0.375	k_1 = 60	k_{II} = 1.5	–	2–2
7	Q-DNA 1 mM NaCl	n = 0.47	–	0.47	$\bar{k}$ = 200	–	2.21	2–3
8	Q-DNH 1 mM NaCl	n_I = 0.16	n_{II} = 0.13	0.29	k_I = 55	k_{II} = 0.64	–	2–1'
9	Q-DNH 1 mM NaCl	n = 0.42	–	0.42	$\bar{k}$ = 100	–	2.83	2–3'
10	EB-DNA 1 mM NaCl	n_I = 0.25	n_{II} = ?	?	k_I = 20	k'_{II} = 0.020*	–	4–1
11	EB-DNA 1 mM NaCl	n_1 = 0.25	n_{II} = 0.27	0.52	k_1 = 30	k_{II} = 0.13	–	4–2
12	EB-DNH 1 mM NaCl	n_I = 0.20	n_{II} = ?	?	k_I = 15	k'_{II} = 0.025*	–	4–1'

* k' denotes the constant value observed in horizontal Scatchard plots.

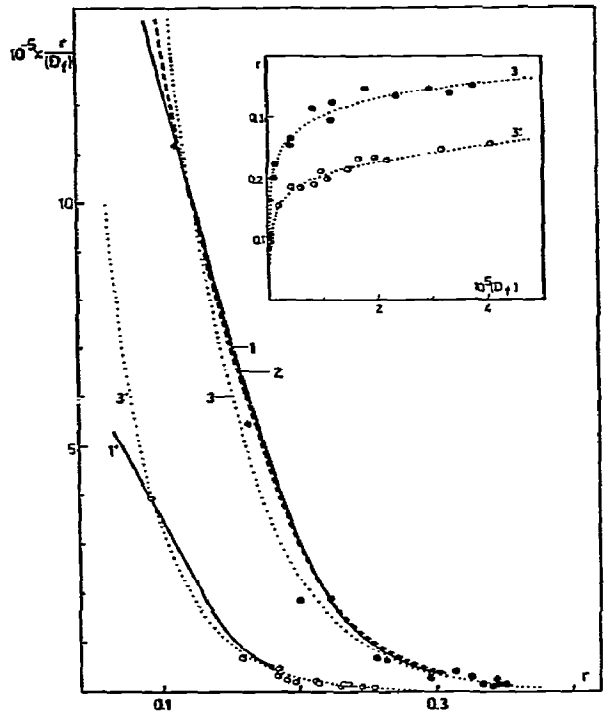


Fig. 2. Binding curves of quinacrine to DNA (•) and nucleohistone (○) in 1 mM NaCl determined by the equilibrium dialysis method. Main figure: Scatchard plot. Insert figure: direct representation. The different curves correspond to the fittings listed in table 4.

of table 3, fitting no. 2 of table 4, curve 1 in fig. 1), i.e.:

$$\frac{r}{(D_f)} = \frac{k_1(1-4r)^2}{2(1-2r)} \exp\left(-\frac{2w_1 r}{0.25\,RT}\right). \qquad (5)$$

The value of $k_1 = 2.55 \times 10^5\ M^{-1}$ determined in this way is of the same order of magnitude as those reported for EB [40] and acridine orange [25] under similar conditions. The positive value of the interaction energy, w_1, indicates the repulsive nature of the exponential term of eq. (5).

It is interesting to note that in a study of EB-closed circular SV40 DNA complexes, Bauer and Vinograd [43] have introduced an exponential term in the same equation.

Quinacrine-DNA/nucleohistone complexes in 1 mM NaCl. As shown in fig. 2, the Scatchard plot for the binding of Q to DNH is shifted towards lower r values, compared to DNA. In the range of the strong binding process, this shifting may be considered as due (1) to a simultaneous reduction of the parameters k and n in DNH compared to DNA or (2) to a lower value of n only, without modification of the binding constant, k.

(1) In the first hypothesis, binding sites are different in nature and in number in DNH compared to DNA because the histones modify the conformation of DNA in the nucleoprotein and sterically block the accessibility of the dye to the DNA helix. These lower binding parameters in DNH may be considered as constant on the whole binding range. The difference between the first binding site of the dye on DNA and DNH may be characterized by extrapolation to zero binding ratio from the plot $R = r_{DNH}/r_{DNA}$ versus r_{DNA} or r_{DNH} (fig. 3), where r_{DNH} and r_{DNA} denote the binding ratio for DNH and DNA respectively, for a given value of (D_f). The extrapolated value of R, denoted R_0, is equal to the ratio kn_{DNH}/kn_{DNA}. Experimental and calculated values of R_0 are listed in table 5, a and b respectively.

(2) In the second hypothesis, DNA in DNH would react with the dye exactly in the same way as free DNA (k identical) except that only some regions of DNA in the nucleoprotein could be complexed by the dye. In order to explain the variation of R with r_{DNH} (fig. 3), it must be assumed that the accessibility of these regions increases with the binding, which could be due to the release of some histone fractions more loosely bound. The binding strengths being identical, R becomes equal to n_{DNH}/n_{DNA} and $R_0 = (n_{DNH}/n_{DNA})_0$ estimates the amount of "free DNA" in DNH. So, the variations of R with r_{DNH} reflect those of n_{DNH}. This quantity can only be estimated graphically (fig. 3 and table 5a).

In numerous works [7,9,10,49], n values in the latter expression of R_0 are taken identical to the numbers of primary binding sites determined from linear extrapolation at low $r(D_f)^{-1}$ values in the Scatchard representation, without considering k values. This approximation may explain the very different values obtained for the amount of "free DNA" in DNH (0.16 to 0.68). For our complexes, such values are given in

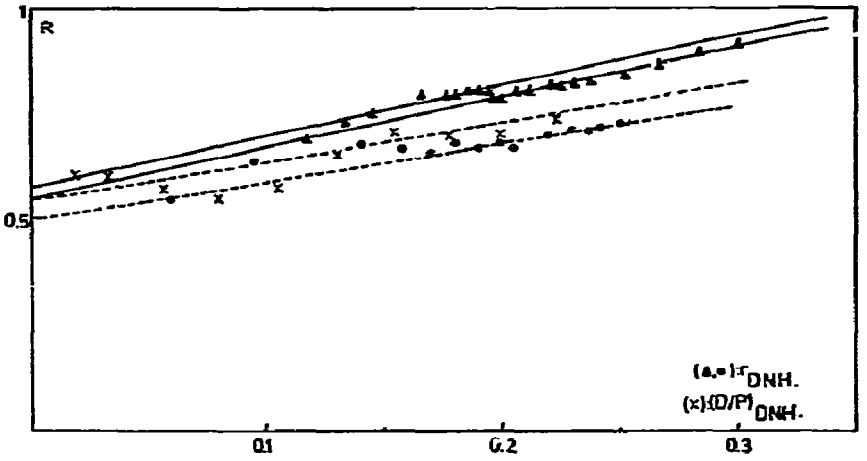


Fig. 3. Reduction of the binding parameters of quinacrine (●) and ethidium bromide (▲) in nucleohistone compared to DNA in 1 mM NaCl, from binding data and from fluorescence intensities in the case of ethidium bromide (x). In the former case (● and ▲), the binding ratios were compared at a given (D_f) value, while in the latter, fluorescence intensities were compared with respect to D/P, at $D = 5 \times 10^{-5}$ M (fig. 10B).

table 5c, such estimations may be wrong if the reactive part of DNH is a variable quantity.

In the second hypothesis, contrarily to the first one, all physico-chemical properties of the dye depending upon the binding would extrapolate to the same value at r or D/P equal to zero, whether the dye is bound to DNA or to DNH. Moreover, the extrapolated value of R, would be independent of the nature of the dye. If our extrapolations of fig. 3 are meaningful, they argue for the first hypothesis, but not unambiguously because of the scattering of the points and the lack of experimental data at low r_{DNH} values. Other more convincing indications will be obtained from the fitting calculations, in the fluorescence polarization study (section 3.3) and from circular dichroism measurements (not reported here).

The two hypotheses presented above will be now considered in the various treatments of the binding curves (table 3 in section 2.5).

Procedure 3 yields different mean binding constants, $\bar{k}$, and different total numbers of sites, n, for DNA and DNH (fittings no. 7 and 9 of table 4). The quantity R_0 may be calculated as mentioned above since the exponential term goes to unity as r decreases.

Table 5
Experimental and calculated values of R_0: extrapolated value to zero binding of r_{DNH}/r_{DNA}, r_{DNH} and r_{DNA} being determined at a given value of (D_f) in the direct representation.

	Mode of calculation	Quinacrine	Ethidium bromide
a. Experimental value of fig. 3	–	0.50–0.54	0.54–0.57
b. k and n different	$(k_I n_I)_{DNH}/(k_I n_I)_{DNA}$	0.38 (no.5 and 8 [a])	0.60 (no. 10 and 12)
	$(\bar{k}n)_{DNH}/(\bar{k}n)_{DNA}$	0.45 (no. 7 and 9)	–
c. k values not considered, $n = n_I$ from the Scatchard plot	$(n_I)_{DNH}/(n_I)_{DNA}$	0.76 (no. 5 and 8)	0.80 (no. 10 and 12)
			0.68 [b]

a) The numbers between brackets refer to the fitting numbers of table 4.
b) Spectrophotometric results of Angerer and Moudrianakis [7].

Table 6
Comparison between our results with quinacrine and those reported by Chambron with proflavine [46], analyzed according to procedure 3 of table 3

Log I		−3	−2	−1	0
$\log \bar{k}$	quinacrine	7.3	–	5.6	–
	proflavine	–	6.4	5.5	4.7
n	quinacrine	0.47	–	0.24	–
	proflavine	–	0.370	0.225	0.200
$\bar{w}$(kcal/mol)	quinacrine	2.21	–	0.73	–
	proflavine	–	0.230	0.065	0

A value of 0.45, i.e. close to the experimental one, was found (table 5, a and b).

Our values of $\bar{k}$ for Q-DNA complexes in 0.1 M and 1 mM NaCl are in perfect agreement with those reported by Chambron [46] for proflavine-DNA complexes, as shown by the linear relation between $\log \bar{k}$ and the logarithm of the ionic strength, I (table 6). The same is true for the n values. The term of electrostatic interaction, $\bar{w}$, higher in the case of Q, may be easily explained by the double positive charge of Q compared to the proflavine cation.

Procedure 1 permits a quantitative characterization of the binding parameters of the second binding process, k_{II} and n_{II} (fittings no. 5 and 8 of table 4). The latter quantities are found smaller in DNH compared to DNA, to the same extent as for the strong binding parameters, k_I and n_I. The value of $R_0 = 0.38$ calculated in this way is very similar to that obtained by procedure 3 (table 5b). On the contrary, if the binding strengths are not taken into account, the calculated value of $R_0 = 0.76$ is the most discrepant among the calculated ones (table 5c).

Using procedure 2, results similar to procedure 1 were obtained for the estimation of k_{II} and n_{II} for Q-DNA complexes in 1 mM NaCl. In both treatments, for a (D_f) value of about 5×10^{-5} M, the ratio of the number of externally bound molecules to the number of intercalated ones, r_{II}/r_I (meaning of subscripts given in section 2.5) for procedures 1 and 2 respectively, is around 0.50.

Ethidium bromide-DNA/nucleohistone complexes in 1 mM NaCl: Our equilibrium dialysis experiments with EB-DNH complexes at low ionic strength are compared in fig. 4 with those obtained by Houssier et al. [40] in the case of DNA. At free-dye concentrations below 5×10^{-5} M, DNA binds more Q than EB molecules, while the contrary is observed for DNH. Consequently, a higher value of R is attained for EB compared to Q (fig. 3). The most striking feature of the Scatchard plots is the linearity observed at low r values for both macromolecules. As already noticed for Q, the initial slope of this representation is smaller in the case of DNH.

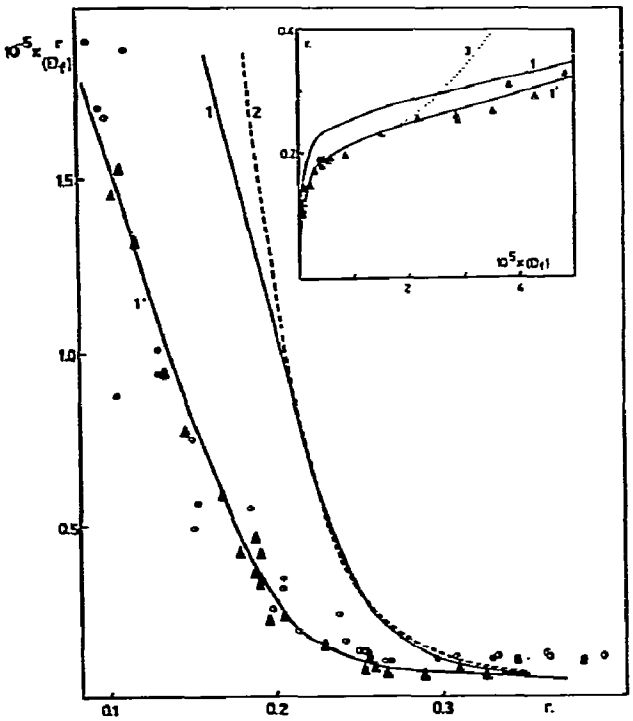


Fig. 4. Binding curves of ethidium bromide to DNA and nucleohistone in 1 mM NaCl. Main figure: Scatchard plot. Insert figure: direct representation. Curves 1 and 2 refer to the fittings of table 4 calculated from the equilibrium dialysis results of Houssier et al. [40] with DNA. The results with nucleohistone were obtained by the equilibrium dialysis method (▲) and by absorption spectrophotometry (○, ●) at $\lambda = 480$ and 465 nm and a total dye concentration of 5×10^{-5} M. Curve 3 in the insert figure gives the shape of the spectrophotometric results at r values higher than 0.25.

Still higher differences in the strength of EB binding by these macromolecules have been reported by Angerer and Moudrianakis [7] under the same conditions but using spectrophotometry. On the contrary,

in the case of avian erythrocyte nucleohistone and using the same spectroscopic method, binding constants were found to be similar [9,10]. A reduction was also observed with proflavine [48], while the strong binding process of actinomycin D was enhanced in DNH compared to DNA [49].

As for Q, procedures 1 and 2 (table 3) were successively used for characterizing process II of EB-DNA complexes (fittings no. 10 and 11 of table 4) and of EB-DNH complexes (fitting no. 12) in 1 mM NaCl. The affinity for this process appears very low compared to Q, so that n_{II} was not determinable by procedure 1. The Scatchard plot relative to this process is horizontal and seems to be of the same magnitude for both macromolecules. This constant value is noticed k'_{II} in table 4. Such a behaviour was also observed by Peacocke and Skerrett [30] for proflavine-DNA complexes. However, using procedure 2, we were able to determine both parameters of process II (fitting no. 11 of table 4). n_{II} has a value of 0.27, i.e. very close to that of the intercalation model with exclusion of adjacent binding sites. It is low compared to the one reported by LePecq and Paoletti [4]. As in the case of Q, for the highest (D_f) values examined, i.e. 5×10^{-5} M, the ratio r_{II}/r_I is around 0.50. From a simple calculation, one could estimate that it should attain unity for $(D_f) = 10^{-4}$ M.

The calculated value of R_0 by the fitting procedure which assumes different k values in DNH and in DNA (fittings no. 10 and 12, table 5b) is closer to the experimental one, i.e. 0.50–0.57, than the other calculated value (table 5c), as already noticed in the case of Q.

3.2. Absorption spectrophotometry

In this section, we will examine the different methods allowing binding calculations (table 2) from the spectrophotometric data.

Method 1:

Quinacrine-DNA complexes in 0.1 M and 1 mM NaCl: Typical titrations at $\lambda = 421$ nm, the wavelength of maximum hypochromism, are given in fig. 5B. Spectral shifts were found similar to those reported in the literature [1,2,15,28]. In 0.1 M NaCl, a well-defined isosbestic point was observed at 458 nm, which was not present in 1 mM NaCl. The modification of shape of the bound-dye spectrum upon binding was checked

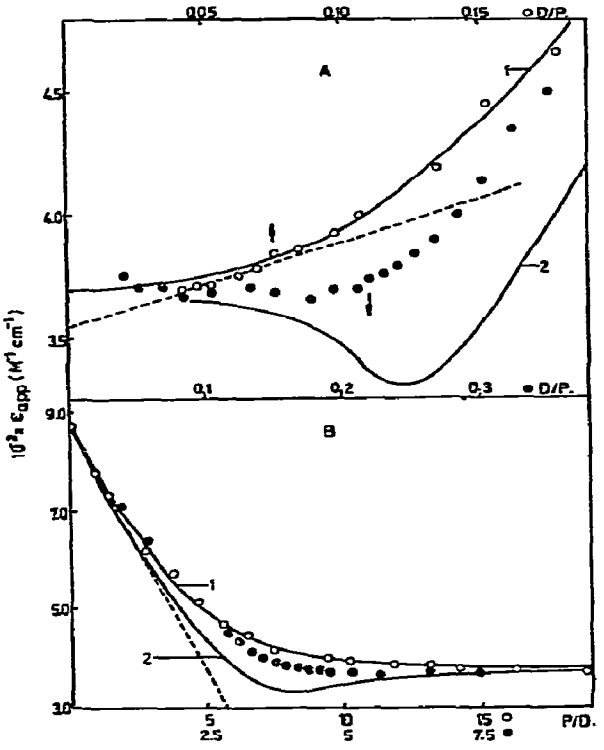


Fig. 5. Illustration of the spectrophotometric method of Terada and Miyake [32] (methods 1b and 2a of table 2) for the complexes of quinacrine with DNA in 0.1 M (○) and 1 mM NaCl (●), at $\lambda = 421$ nm and a total dye concentration of 7×10^{-5} M. Curves 1 and 2 were calculated from eq. (6) (see text).

by the method suggested by Li and Crothers [50]. Variations of the ratio of the trough to the peak (variation of absorbances at $\lambda = 421$ and 465 nm respectively) at low P/D values were more important as the salt concentration was decreased (not shown in the figures).

The decrease of ϵ_{app} with P/D (fig. 5B) suggests a common value of $\epsilon_b = 3700$ at both ionic strengths. This limiting value is rapidly reached in 1 mM NaCl, at $P/D = 5$. On the contrary, in 0.1 M NaCl, this value is only reached for P/D values higher than 20. Thus, precise values of ϵ_b are more difficult to determine at high ionic strength.

Therefore, different methods for estimating this critical parameter of the method of Peacocke and Skerrett were compared (figs. 5 and 6, table 7). In a

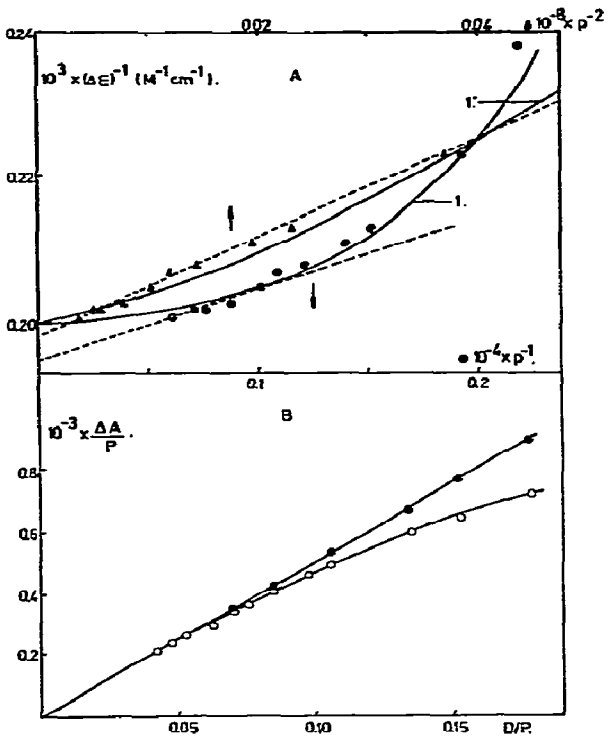


Fig. 6. Methods of determination of $\Delta\epsilon_{lim}$ for the complexes of quinacrine with DNA, at $\lambda = 421$ nm and a total dye concentration of 7×10^{-5} M.
Part A: ● and ▲: methods 1a and 1c of table 2 for the complexes in 0.1 M NaCl. Curves 1 and 1′ were calculated from eq. (6) (see text).
Part B: method 1d of table 2, based on eq. (1), for the complexes in 0.1 M (○) and 1 mM NaCl (●).

first step, we have applied the two reported linear extrapolation methods (methods 1a and 1b of table 2) which yield similar values of $\Delta\epsilon_{lim}$ (table 7a) but 3% higher than the one calculated from fig. 5B; assuming an identical value at both ionic strengths ($\Delta\epsilon_{lim}$ = 8700 − 3700 = 5000 $M^{-1}cm^{-1}$ at $\lambda = 421$ nm). A lower value, i.e. 4910 $M^{-1}cm^{-1}$, was obtained by averaging the absorbance at high polymer concentrations: $P/D > 12$ in fig. 5B. In the plots illustrating methods 1a and 1b (figs. 6A and 5A respectively), the apparent experimental range of linearity is very short. Moreover, the calculated curves 1 (figs. 5A and 6A) and 1′ (fig. 6A) show a regular curvature without linear part, the value of ϵ_b or $\Delta\epsilon_{lim}$ being given by the intercept of the ordinate axis with the tangent to the curve at the origin. This tangent can not be estimated from our experimental results. Such measurements were tried (P/D ratios higher than 20) but showed a contribution of turbidity to the absorbance, even when a DNA solution was used in the reference compartment. Curves 1 and 1′ were calculated from the following equation:

$$\epsilon_{app} = \alpha\epsilon_f + (1-\alpha)\epsilon_b \qquad (6)$$

where ϵ_f and ϵ_b were respectively taken as 8700 and 3700 $M^{-1}cm^{-1}$; α and $1-\alpha$ were calculated from the binding results obtained from equilibrium dialysis (fitting no. 2 of table 4).

The influence of the value of $\Delta\epsilon_{lim}$ upon the binding curves is shown in fig. 1. If this parameter is taken equal to 5000 $M^{-1}cm^{-1}$ (filled circles), the agreement with the equilibrium dialysis results is satisfactory (curve 1 of fig. 1 from fitting no. 2 of table 4), while strong deviations are observed for other values (curves 3 and 4 for $\Delta\epsilon_{lim}$ = 5150 and 4910 $M^{-1}cm^{-1}$ respectively). It is important to notice that the binding curve is significantly shifted towards higher r values for a small underestimation (2%) of $\Delta\epsilon_{lim}$ (n_1 = 0.125 from the linear part of curve 4). A 3% overestimation of the same parameter strongly reduces the binding strength and makes the lowest $r(D_f)^{-1}$ values to increase with r (curve 3) for r between 0.040 and 0.055, which would suggest the existence of a cooperative process.

We suggest (1) an empirical improvement of methods 1a and 1b which yields a satisfactory value of $\Delta\epsilon_{lim}$, and (2) a second method, based on eq. (1), which emphasizes the advantage of some measurements at low ionic strength even when studying a system at high ionic strength (methods 1c and 1d of tables 2 and 7 illustrated in figs. 6A and 6B respectively). As shown in fig. 6A, the linear extrapolation of method 1c is better justified than in the case of methods 1a and 1b (figs. 6A and 5A respectively). The slight curvature of the calculated curve 1′ can be neglected and a linear extrapolation of the data furnished a good value of $\Delta\epsilon_{lim}$.

Let's now examine the results of the Q-DNA titrations in 1 mM NaCl which are compared in fig. 7 to the equilibrium dialysis results in the same range of $r(D_f)^{-1}$ values. Despite the disagreement between both methods at low binding, it is striking to notice

Table 7
Determination of ϵ_b and $\Delta\epsilon_{lim}$ by the different methods listed in table 2

Complex	Method	$\Delta\epsilon_{lim}$ ($M^{-1}cm^{-1}$)	% deviation	Fig. no.
a. Q-DNA complexes in 0.1 M NaCl	1a	+ 5130	+ 3	6A
	1b	+ 5150	+ 3	5A
λ = 421 nm	Averaging of absorbances	+ 4910	− 2	−
ϵ_f = 8700	at high *P/D* values			
	1c	+ 5040	+ 1	6A
	1d	+ 5000	0	6B
b. EB-DNH complexes in 1 mM NaCl				
λ = 480, ϵ_f = 5600	1d	+ 3260	−	−
λ = 465, ϵ_f = 5220	1d	+ 3660	−	−
c. EB-DNA complexes in 0.1 M NaCl				
λ = 538 nm	1d	− 2200	−	−
ϵ_f = 1440				

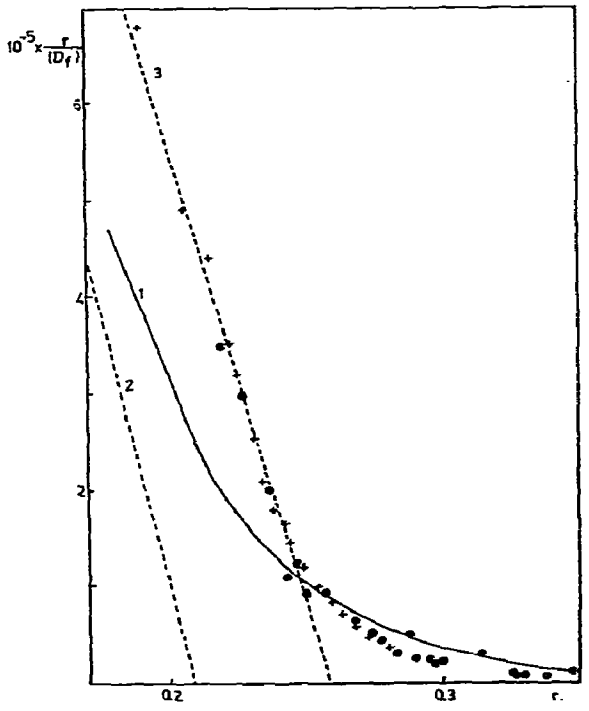


Fig. 7. Comparison between the results obtained by the equilibrium dialysis method (curve 1 from the fitting no. 5 of table 4, line 2 is the first component of the complex binding curve) and by absorption spectrophtometry (•) at λ = 421 nm and a total dye concentration of 7 × 10^{-5} M, for the complexes of quinacrine with DNA in 1 mM NaCl. (+): points calculated after smoothing the experimental curve ΔA versus *P/D*.

the similarity between the first slope of the spectrophotometric results (line 3, with n_1 = 0.26 and k_1 = 93 × 10^5 M^{-1}) and that obtained with the equilibrium dialysis data by two sets of homogeneous sites. The curve 1 illustrates the complete fitting no. 5 of table 4, line 2 giving the first component, with n_1 = 0.21 and k_1 = 110 × 10^5 M^{-1}. The differences between equilibrium dialysis and spectrophotometric data are undoubtedly due to the different spectrum of the second bound species compared to the first one. Its effect upon the measured absorbances is to contribute more positively to ϵ_{app}, which is clearly shown in fig. 5 by the difference between the experimental values (filled circles) and the calculated curve for the first binding process (curve 2). This difference has been quantitatively related to the bound fraction of the second bound species to estimate $\epsilon_{b,2}$ at λ = 421 nm. A value of 2800 ± 300 $M^{-1}cm^{-1}$ was found. Curve 2 was calculated from eq. (6) as mentioned above, except that the first bound species was only estimated, taking the mean value between fittings no. 5 and 6 of table 4.

Analogous titrations with DNH were made and showed an increasing turbidity contribution as one goes to low *P/D* values, i.e. as the electroneutrality of the complexes was approached.

Ethidium bromide-nucleohistone complexes in 1 mM NaCl: In contrast to the results of Angerer and Moudrianakis [7], no constant isosbestic point was observed in the whole range of *P/D* values, at *D* = 5 × 10^{-5} M. As *P/D* decreases, the isosbestic wavelength progressively shifts from 506 to 510 nm.

Similar observations have been reported for proflavine-DNA complexes [50].

Compared to the equilibrium dialysis results in fig. 4, the binding curve derived from spectrophotometric measurements (table 7b) is similar for r values up to 0.25. The discrepancy between both methods appears as an overestimation of r, which increases with the binding ratio, as observed for EB-DNA complexes in 1 mM NaCl [40]. The differences are better displayed in the direct representation (curve 3 in insert fig. 4).

A treatment similar to the case of Q-DNA complexes in 1 mM NaCl was realized in order to estimate $\epsilon_{b,2}$. We found 1200 ± 300 and 2900 ± 1000 $M^{-1}cm^{-1}$ at λ = 480 and 465 nm respectively.

Method 2:

The method developed by Terada and Miyake [32] (method 2a of table 2) was found inconvenient for studying dye-nucleic acids complexes, even at high ionic strength. The two graphical representations used for the direct calculation of the parameters k and n in the case of a single Langmuir process are given in figs. 5A and 5B, for Q-DNA complexes at two ionic strengths. The extrapolations were only possible for the experiments in 0.1 M NaCl (dashed lines of figs. 5A and 5B). Values of 0.225 and 1×10^5 M^{-1} were obtained for n and k respectively: the corresponding straight line (marked 5 in fig. 1) in the Scatchard plot satisfactorily fits other data at large r values only. Similar discrepancies were observed with the EB-DNA complexes in 0.1 M NaCl, although this system is simpler than the Q-DNA complexes described above (see fig. 1 and section 3.1). These two low k values mainly arise from the overestimation of the initial slope of the plot ϵ_{app} versus D/P (fig. 5A).

Results obtained by our original method (method 2b of table 2, illustrated in fig. 8 for EB-DNA complexes in 0.1 M NaCl) were found to be more satisfactory. At both dye concentrations, values of 0.19 and 1.76×10^5 M^{-1} were obtained for the parameters n and k respectively. The corresponding straight line (line 4 in fig. 9B) fits the data as well as the calculated curve from the exclusion model (curve 3) in the range of r values between 0.04 and 0.15.

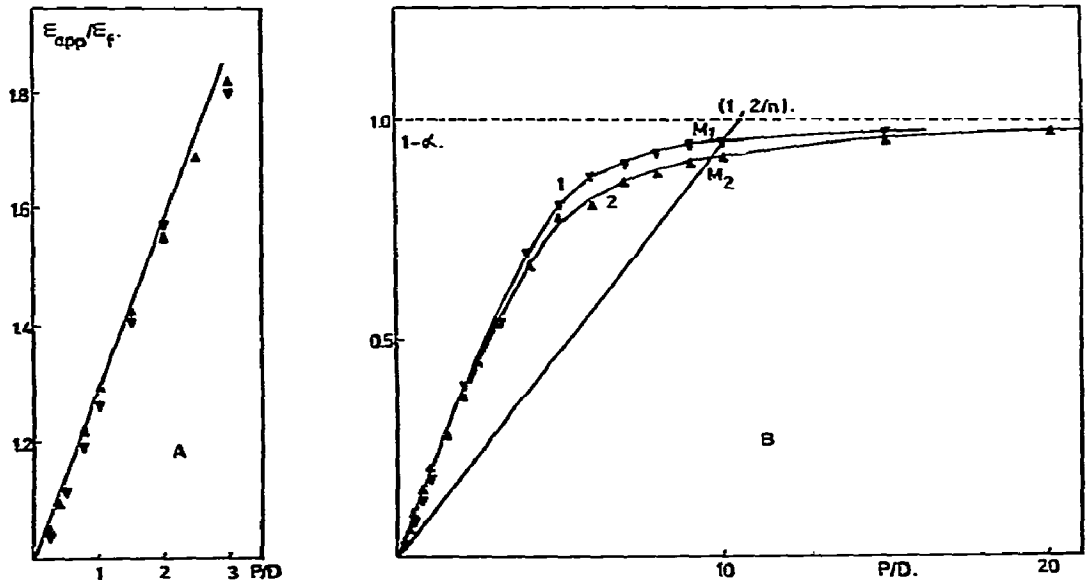


Fig. 8. Direct determination of the binding parameters k and n from the spectrophotometric data (method 2b of table 2) for the complexes of ethidium bromide with DNA in 0.1 M NaCl, at λ = 538 nm and at two different total dye concentrations, ▼: D_1 = 12.05×10^{-5} M (curve 1); ▲: D_2 = 6.52×10^{-5} M (curve 2).
Part A: determination of n according to eq. (2).
Part B: determination of k by the method of Schwarz [33].

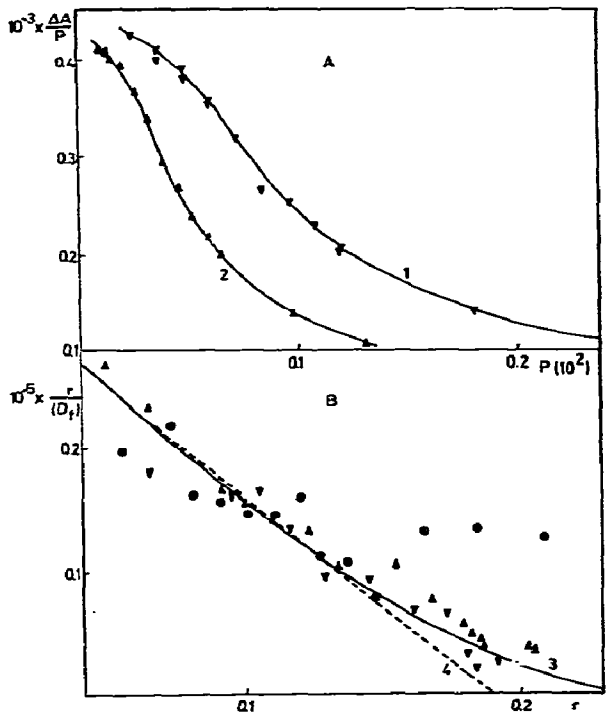


Fig. 9. Binding curve of ethidium bromide to DNA in 0.1 M NaCl by two spectrophotometric methods.

Part A: property depending upon the binding ratio as a function of the molar nucleotide concentration of the complexes. The ΔA were measured at $\lambda = 538$ nm at two different total dye concentrations, ▼: $D_1 = 12.05 \times 10^{-5}$ M (curve 1); ▲: $D_2 = 6.52 \times 10^{-5}$ M (curve 2).

Part B: comparison of the results obtained by the classical method (▼and ▲) (method 1d of table 2) and by the method inspired from Halfman and Nishida [34] (●), based on eqs. (3) and (4) (method 3 of table 2). Curve 3 was calculated from the equation of the exclusion model with $k_1 = 0.7 \times 10^5$ M^{-1} (eq. (6) of Fredericq and Houssier [25]).

Line 4 illustrates the results obtained by the method 2b of table 2.

Method 3:

The complexes of EB with DNA in 0.1 M NaCl were chosen because of their relative simplicity to compare the results obtained by method 3 (table 2) and by the classical method (method 1 of table 2, table 7c). Results compared in the Scatchard representation (fig. 9B) are satisfactory for r values below 0.15. The imprecision on low ΔA measurements is sufficient to explain the discrepancy between both methods at large r values. The full curve is the theoretical curve corresponding to the model of exclusion (curve 3) with $k_1 = 0.7 \times 10^5$ M^{-1}, which is somewhat lower than that reported by Houssier et al. [40]. The precision of method 3 would be improved by using more different dye concentrations ($D_1/D_2 > 2$).

3.3. Fluorescence intensity and polarisation

The experimental dependence of the fluorescence intensity (ϕ_{app}/ϕ_f) and anisotropy (μ_{app}) upon D/P, at constant dye concentration, is given in figs. 10 and 11 for Q and EB bound to DNA and DNH. At low D/P, the measured quantities are equal to those of the bound dye, i.e. (ϕ_b/ϕ_f) and μ_b. Their respective extrapolated values at $D/P = 0$, $(\phi_{app}/\phi_f)_{lim}$ and μ_{app}^{lim}, represent the effect of the first binding site upon the fluorescence property of the first intercalated molecule. The variation of the fluorescence parameters from these limiting values may be due to three factors: (1) the increase of the binding ratio for the various processes, (2) the increasing free-dye concentration, and (3) the interactions between bound and free dye molecules.

Extrapolated values of (ϕ_{app}/ϕ_f): Upon binding to DNA and DNH, the quantum yield of fluorescence of EB is increased by a factor 20, which is in good agreement with reported data for DNA [4] and poly(dG-dC) [23]. With respect to this property, EB behaves similarly to acridine orange [25]. In contrast to EB, a quenching is observed in the case of Q. The limiting value of 0.8 for Q-calf thymus DNA complexes was found strongly depressed to 0.06 with Micrococcus Lysodeikticus DNA. A similar behaviour has already been observed for Q and other dyes such as acriflavine, proflavine and quinacrine mustard (older works are mentioned in refs. [2, 20, 34, 48, 51, 52]): A–T and G–C binding sites respectively increase and decrease the fluorescence of the bound dye and this reflects the presence of base-specific binding sites. Compared to DNA, the limiting value for Q-DNH complexes is significantly lower (around 0.50).

In order to explain the difference in the values of $(\phi_{app}/\phi_f)_{lim}$ in terms of base composition, two conditions must be satisfied: (1) the binding must occur at random, i.e. without base-specificity, and (2) the

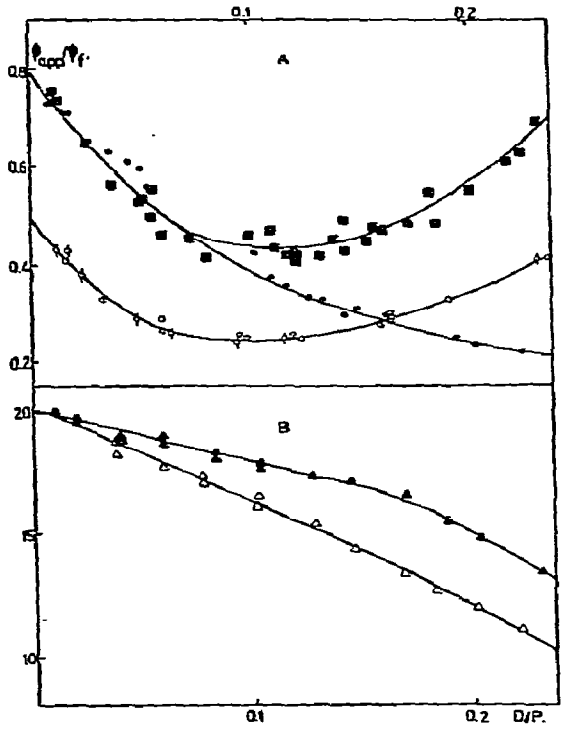


Fig. 10. Dependence of the fluorescence intensity upon D/P at D constant.
Part A: Complexes of quinacrine with DNA in 0.1 M NaCl (■) and 1 mM NaCl (●) at a total dye concentration of 5.53×10^{-5} M. Complexes of quinacrine with nucleohistone in 1 mM NaCl at a total dye concentration of 2.5×10^{-5} (○) and 1.88×10^{-5} M (◊). $\lambda_{ex} = 458$ nm and $\lambda_{em} = 500$ nm.
Part B: Complexes of ethidium bromide with DNA (▲) and nucleohistone (△) in 1 mM NaCl at a total dye concentration of 5×10^{-5} M. $\lambda_{ex} = 510$ nm and $\lambda_{em} = 590$ nm.

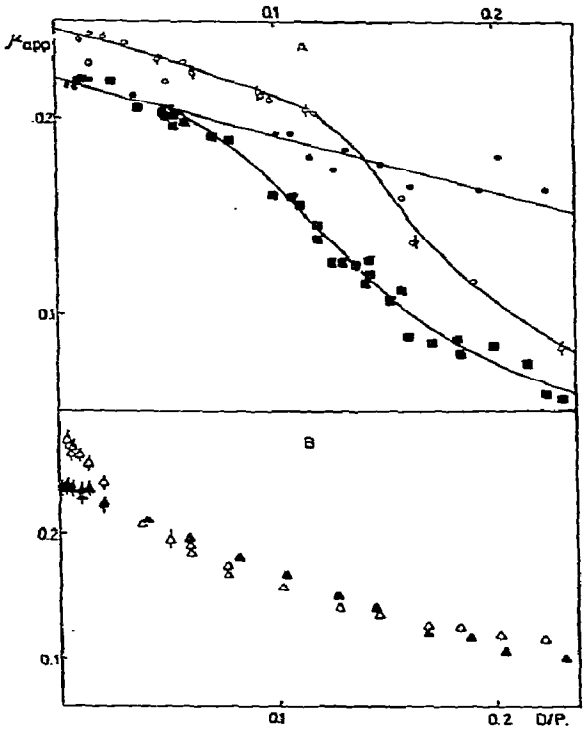


Fig. 11. Dependence of the fluorescence anisotropy upon D/P at D constant.
Part A: same symbols as in fig. 10A.
Part B: same symbols as in fig. 10B, except (▲) and (◊) for the complexes of ethidium bromide with DNA and nucleohistone, at a total dye concentration of 5×10^{-6} M.
Same excitation and emission wavelengths as in fig. 10.

fluorescence of the bound dye must be dependent upon the base composition of the binding site. The fact that equilibrium dialysis results at high ionic strength can be fitted by a theoretical relation with homogeneous sites (eq. (6) of Fredericq and Houssier [25]) for Q and other dyes [25,40,42–44] favours this interpretation. In the particular case of EB, the fluorescence [4] and the binding parameters [3,43] were found independent of the base composition of DNA. On the contrary, identical values of $(\phi_{app}/\phi_f)_{lim}$ will be observed: (1) if the base composition does not affect neither the binding process, nor the fluorescence property or (2) if the binding process is specific. In the latter case, the fluorescence property may or may not depend upon the nature of the bases.

Moreover, quenching and enhancement factors may be simultaneously present and the various dyes may be differently affected. For dyes of class I (ethidium bromide and acridine orange), whose fluorescence is increased upon binding to DNA, the effect is due to a property common to "all" binding sites of DNA, i.e. its hydrophobicity [4,25]. This behaviour is that expected when a molecule passes from an aqueous medium to an apolar and rigid one. On the contrary, "some" of the binding sites of DNA are able to quench

Table 8
Extrapolated values of emission anisotropies from binding data and Perrin plots in glycerol (τ, fluorescence lifetime, V, molecular volume)

Dye	λ_{ex} (nm)	λ_{cm} (nm)	μ_0	τ (nsec)	V (A^3)	μ_{app}^{lim} DNA	μ_{app}^{lim} DNH	$\Delta\mu_1$	$\Delta\mu_2$
Proflavine [35]	466	525	0.38	4.7	154	0.29	–	0.11	–
Acridine orange [25]	490	530	0.35	–	–	0.25	–	0.10	–
Ethidium bromide	510	590	0.36	24*	195	0.24	0.29	0.12	0.050
Quinacrine	445	500	0.32	4 [56]	250	–	–	–	–
	458	500	0.33†	–	–	0.22	0.245	0.11	0.025

* The fluorescence lifetime of free EB in glycerol was taken equal to that obtained by Wahl et al. [57] for EB bound to DNA.
† Recalculated from the fluorescence polarization spectrum (not reported here).

the fluorescence of dyes of class II (acriflavine, proflavine, quinacrine and quinacrine mustard). They have been identified as the G-C rich regions of DNA and the mechanism of quenching has been related to the formation of a charge-transfer complex in the excited state [2,20,35,48,51,52]. The different π-acceptor character of the various dyes may easily explain why quenching depends upon the nature of the dye.

In the case of dye-DNH complexes compared to DNA, we believe that the identical and different limiting values obtained for EB and Q respectively may be explained by the considerations developed above. The additional quenching of Q fluorescence in DNH compared to DNA indicates that the first Q molecule binds to a G-C rich region, i.e. that the initially reactive part of DNA in DNH has a higher apparent G-C content than DNA itself. In view of the reported works on the location of histone on DNA [53,54], it seems that the lysine-rich fractions, which are associated with A-T rich DNA regions, would be responsible for the effect observed here, as in the case of the accessibility of DNA to DNase [55]. Another explanation is that the effect may be related to the different nature of the binding site in DNH compared to DNA.

Extrapolated values of μ_{app}: The emission anisotropies of free dye in glycerol extrapolated to $T/\eta = 0$ in a Perrin plot, μ_0, are compared in table 8 to those obtained from binding extrapolations to $D/P = 0$, μ_{app}^{lim}. The difference between those values, $\Delta\mu_1 = \mu_0 - \mu_{app}^{lim}$, defines a first depolarization process which is of the same magnitude for the different dyes bound to DNA. Like Wahl et al. [57], we believe that this depolarization is the result of internal motions in DNA which are transmitted to the intercalated dye molecules.

For a given dye (EB or Q), however, the value of μ_{app}^{lim} is different whether the dye is bound to DNA or to DNH, which is easily explained by assuming that the presence of histone reduces such internal motions. This would also demonstrate that the reactive part of DNH is somewhat different from DNA itself, in opposition to the presumed presence of "free" DNA in nucleohistone. Moreover, the difference $\Delta\mu_2 = (\mu_{app}^{lim})_{DNH} - (\mu_{app}^{lim})_{DNA}$ is two times higher for EB compared to Q. This difference may be related to other published observations: (1) in a new intercalation model, the torsion angle for Q is lower than for EB [16], (2) the extent of ribosome destabilization is higher for EB compared to Q [21,22] and (3) a salt-induced cooperative conformational transition of a synthetic DNA is reversed by the addition of EB, but not by Q [23], although both dyes bind on the same site on DNA [4]. Compared to DNA, the intercalation of a dye molecule into the base-pairs of DNH may require more structural modifications of the double helix, for which EB seems more efficient than Q.

Variations of $(\phi_b/\phi_f)_c$ *upon binding*: For Q bound to DNA or DNH (fig. 12B), the experimental values of the fluorescence of the complexes fall close to the theoretical curve for about one third of the intercalation range. These curves were calculated according to Ellerton and Isenberg [35] who assumed that nearest-neighbour interaction between bound dyes quenches

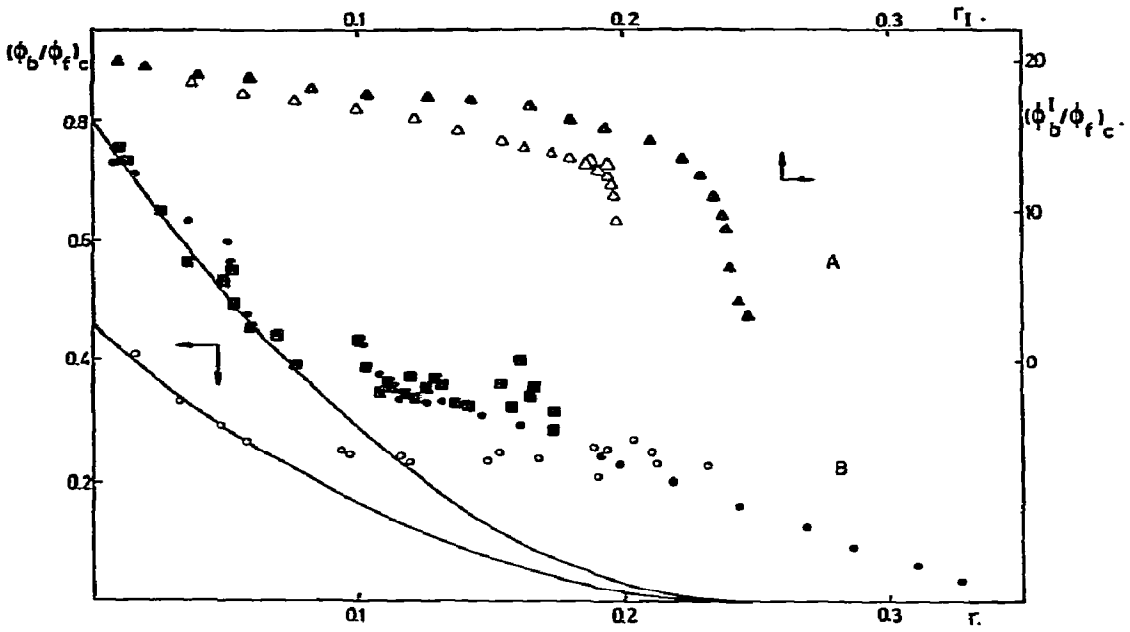


Fig. 12. Fluorescence of the complexes as a function of the binding ratio.
Part A: Complexes of ethidium bromide with DNA (▲) and nucleohistone (△) in 1 mM NaCl, in the intercalation range.
Part B: Complexes of quinacrine with DNA in 0.1 M (■) and in 1 mM NaCl (●), and with nucleohistone in 1 mM NaCl (○), on the whole binding range. The curves were calculated from eq. (7) taking $(\phi_{app}/\phi_f)_{lim}$ equal to 0.80 and 0.46 for DNA and nucleohistone respectively.
Same excitation and emission wavelengths as in fig. 10.

the fluorescence and derived the following equation:

$$(\phi_b/\phi_f)_c/(\phi_{app}/\phi_f)_{lim} = (1 - r/n)^2. \quad (7)$$

At higher r values, the quenching process is not as efficient as predicted by this simple hypothesis. We believe that this is mainly due to a structural modification of the binding site of DNA or DNH.

The same considerations are not valid in the case of EB (fig. 12A) where the quenching rate is smaller compared to Q. The ratio (ϕ_{app}/ϕ_f) of fig. 10B was only found constant at very low binding ($D/P < 0.01$) as already reported in the earlier works of Lepecq and Paoletti [4] who attributed the variations at higher r values to interactions (quenching process) between the two different bound species. Such variations clearly demonstrate that binding calculations derived from fluorescence titration are not valid at this ionic strength, which makes questionable the results presented by Angerer and Moudrianakis [7]. This quenching process may be precisely related to the second binding stage in the following way.

Assuming that the fluorescence of the externally bound species is totally quenched, ϕ_b, in eq. (7), represents the quantum yield of the intercalated molecules, ϕ_b^I. The quantity $\phi_b^I/\phi_f = (\phi_{app}/\phi_f) - \alpha$ was then divided by the bound fraction, $(1-\alpha)_I$, to obtain $(\phi_b^I/\phi_f)_c$ which has been plotted against r_I in fig. 12A. Mean values of fittings no. 10 and 11 of table 4, and fitting no. 12 for DNA and DNH were used respectively for this purpose. It is observed that $(\phi_b^I/\phi_f)_c$ linearly decreases with r_I up to $r_I = 0.20$, and then rapidly drops. In view of the similarity of shape between this plot and the plot r_{II} versus r_I (not shown here, but easily calculable from fitting results of table 4), we can conclude that the externally bound molecules are responsible for the quenching of the fluorescence of the complex as the binding increases.

More precise information is obtained by treating

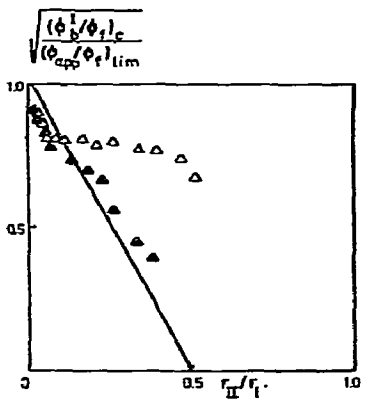


Fig. 13. Quenching of the fluorescence of the intercalated ethidium bromide molecules by interactions with the externally bound ones, for the complexes with DNA (▲) and nucleohistone (△) in 1 mM NaCl.

these data in a way derived from that suggested by Ellerton and Isenberg [35]. In fig. 13, the abscissa r/n of eq. (7) has been replaced by r_{II}/r_I. Assuming a spatial proximity between the intercalation and the external binding sites so that in interactions between the two kinds of bound molecules could take place, the ratio r_{II}/r_I represents, for a given value of r ($r = r_I + r_{II}$), the probability that an externally bound molecule be next to an intercalated one. From the satisfactory linearity observed for EB-DNA complexes (fig. 13), it appears that the fluorescence of the intercalative complex is totally quenched for a value of r_{II}/r_I around 0.50, as if an externally bound molecule was able to quench quantitatively the high fluorescence emitted by two intercalated ones.

The discrepancy from the theoretical line drawn in fig. 13, low for DNA and higher for DNH, may be explained by the fitting calculations listed in table 4. Indeed, in fittings no. 10 and 12, the direct representation for process II is a straight line which, compared to fitting no. 11, underestimates the lower r_{II} values (and consequently the ratio r_{II}/r_I) and overestimates the higher ones. For DNA, the use of the mean value between fittings no. 10 and 11 partially corrects the discrepancy, but not for DNH, for which only the "wrong" fitting no. 12 may be used.

With regard to the variations of $(\phi_b/\phi_f)_c$ upon binding, Q behaves similarly to proflavine [35] and EB similarly to acridine orange [25].

Variations of μ_c upon binding: For free dyes (Q and EB) in water, an anisotropy $\mu_f = 0.020$–0.025

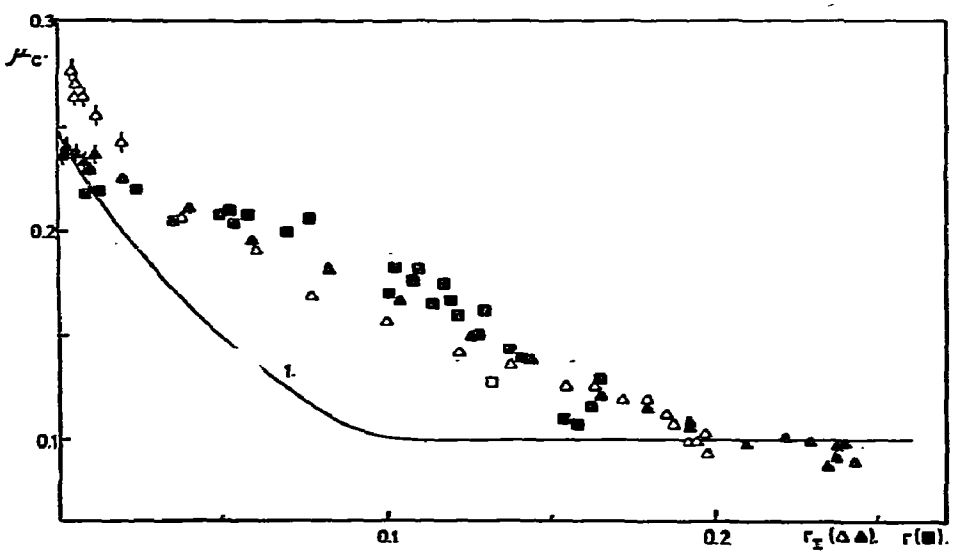


Fig. 14. Emission anisotropy of the complexes as a function of the binding ratio. Same symbols and wavelengths as in fig. 11. Curve 1 was taken from the results of Fredericq and Houssier [25] for the complexes of acridine orange with DNA.

was measured. These values were used for calculating the anisotropy of the complex, μ_c. In fig. 14, our results are compared to previous data obtained for acridine orange-DNA complexes (curve 1 after ref. [25]). The minimum anisotropy of 0.10 corresponding to maximum energy transfer is reached at higher r values for EB and Q, which is in perfect agreement with the lower overlapping of the absorption and emission bands of these dyes compared to acridine orange.

Binding calculations: As mentioned above, the method of LePecq and Paoletti [4] based on the fluorescence intensities cannot be applied to EB-DNA and DNH complexes in 1 mM NaCl. In the case of Q, the same procedure yields negative values of the bound fraction, which is easily predicted by the shape of fig. 10A.

The relation of Ellerton and Isenberg [35] based upon the anisotropies also gives negative values of $1-\alpha$ for EB complexes. Erratic points in the Scatchard plot were obtained for Q-DNA complexes in 1 mM NaCl. In 0.1 M NaCl, for the same complexes, a very poor linearity was observed (not shown here), giving $n = 0.15$ and $k = 2.2 \times 10^5\ M^{-1}$. Compared to the equilibrium results (fitting no. 1 of table 4) on the same range of $r(D_f)^{-1}$ values, this corresponds to an underestimation of r by 20–30%.

4. General conclusions

4.1. Structural scheme for the dye-DNA complexes at low ionic strength

If the total dye concentration of the "inner" compartment is measured after desorption of the dye from the macromolecule and if the influence of the Donnan effect is negligible, the equilibrium dialysis method is the most accurate for the quantitative study of the complexes between dyes and nucleic acids. Contrary to the indirect methods (see section 4.2 below) in which the deviations may be systematic and lead to a shifting of the Scatchard curve, the scattering of the experimental points obtained by the equilibrium dialysis method is apparently statistic.

From the fitting calculation based on our equilibrium dialysis experiments with the complexes of quinacrine and ethidium bromide with DNA and nucleohistone, the complex binding curves at low ionic strength may be satisfactorily decomposed into two components (figs. 1, 3 and 4, table 4).

A quantitative picture of the second binding process was obtained using two different models to characterize the first intercalative process, i.e. the classical set of homogeneous sites and the more refined model with exclusion of the adjacent binding sites, without base-specificity (procedures 1 and 2 of table 3). The small difference between both models, mainly at high r values, was found of importance for the determination of the low binding constant in the external binding process of ethidium bromide to DNA (fitting no. 11 of table 4).

The more distinctive features between both dyes appear in the strengths and the maximum site numbers of the second binding process. The higher k_{II} and lower n_{II} values observed with quinacrine may be due to the double charge of the dye compared to the ethidium cation. This charge enhances the electrostatic attractive forces between the phosphate groups and the dye molecules, and consequently the binding constant. As two negative charges of DNA may interact with one quinacrine molecule, the number of external binding sites is reduced by a factor two compared to ethidium bromide (see fittings no. 6 and 11 of table 4). This particularity of quinacrine has already been emphasized [28] and the side-chain of the dye has been structurally related to polyamines [17] which are thought to bridge the narrow groove of DNA [58].

Moreover, the stoichiometry of both processes seems to be interdependent. This relation suggests a spatial proximity between the intercalation site and

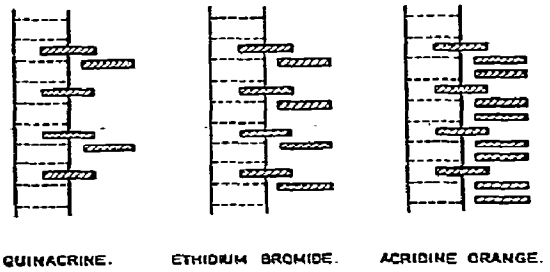


Fig. 15. Proposed structural scheme for the binding of quinacrine and ethidium bromide to DNA at low ionic strength compared to that suggested for acridine orange [25], for a free-dye concentration of about 10^{-4} M.

the external one, due in part to attractive interactions between the dye molecules. From our calculations, the ratio of intercalated to external molecules differs according to the dye. For a free-dye concentration of quinacrine or ethidium bromide about 5×10^{-5} M, the intercalative sites of DNA are nearly completely occupied ($n_1 = 0.25$ according to the exclusion model) and an additional external molecule is bound near half of them ($r_{II} = 0.125$). This value of 0.125 corresponds to the saturation level of the second binding process for quinacrine ($n_{II} = 0.125$ from fitting no. 6 of table 4), but only to half that of ethidium bromide ($n_{II} \approx n_1 \approx 0.25$ from fitting no. 11 of table 4). So that, in the case of ethidium bromide, all the second sites are only occupied for a free-dye concentration about 10^{-4} M. These considerations are illustrated in fig. 15, where the different dyes have been classified with respect to the increasing complexity of their interaction with DNA. The spatial proximity between the two kinds of binding sites doesn't necessarily imply the formation of a dimer, for which we actually have no evidence.

4.2. Binding curves derived from spectrophotometric and fluorescence titrations

The comparison between the direct (equilibrium dialysis) and the indirect methods (spectrophotometry and fluorescence) for the binding curves determination allows us to identify the origin of some of the discrepancies between the two kinds of methods.

(i) If the critical quantity, $\Delta\epsilon_{lim}$, has been determined by proper methods (methods 1c and 1d of table 2), the classical spectrophotometric method of Peacocke and Skerrett [30] is perfectly valid in the absence of externally bound species, i.e. at high ionic strength. In the presence of them, their influence on the determination of the binding parameters of the strong binding, according to the Scatchard plot for instance, is negligible if the strength of the external process is relatively low, as in the case of ethidium bromide (fig. 4, $k_{II}/k_1 = 0.004$ from fitting no. 11 of table 4). On the contrary, if k_{II} is higher as in the case of quinacrine (fig. 7, $k_{II}/k_1 = 0.025$ from fitting no. 6 of table 4), the spectrophotometric data yield an overestimation of the primary site number. The number of secondary binding sites does not appear to be a limiting parameter.

These drawbacks may be avoided if the titrations are made at two different dye concentrations (fig. 9, method 3 of table 2), which should differ by a factor higher than two.

In the case of a single binding process which follows a Langmuir isotherm, the binding parameters k and n can be directly calculated from the measured absorbances. By the recent method of Terada and Miyake [32] (fig. 5, method 2a of table 2), we only found satisfactory values for the parameter n. We developed a new method (fig. 8, method 2b of table 2) which, moreover, yields satisfactory values of the binding constant, k, but has the same limitations.

(ii) For the various complexes at low ionic strength examined throughout this work, the binding curves derived by the fluorescence methods (based on the intensity [4] or the anisotropy [35]) were found either completely erratic or underestimate the results obtained by equilibrium dialysis to an appreciable extent (20–30%). The main explanation for these discrepancies is that the fluorescence parameters (quantum yield and emission anisotropy) of the bound molecules vary as the binding ratio increases (figs. 12–14).

By correcting the measured quantities for the free-dye contribution, we were able to explain some of these variations. (1) In the case of quinacrine, the variations of the quantum yield of fluorescence in the range of intercalation may be described in terms of interaction between intercalated molecules, which results in a quenching whose efficiency decreases with the extent of binding. (2) For the ethidium bromide complexes, similar interactions also occur, but between intercalated and externally bound molecules. (3) While the binding process of these dyes occurs without base-specificity, the quantum yield of the fluorescence of quinacrine strongly depends upon the nature of the binding site, contrarily to the case of ethidium bromide which is not affected by the base composition. (4) The emission anisotropy of the bound molecules is also modified during the binding process, in a manner which depends on the relative position of the dye molecules and on the overlapping between the absorption and the fluorescence spectra.

For an accurate study of the fluorescence parameters, it is obvious that the intensities must be measured using polarized light because (1) the light emitted by the intercalated molecules is highly polarized, (2) this

polarization depends upon the binding ratio and (3) the monochromators of the apparatus partially polarize the light.

4.3. State of DNA in nucleohistone

The amount of DNA covered by the histones in nucleohistone is still controversial and depends upon the method used for its study: dye binding [6,7,9, 10,47–49,59] (older works reviewed by Fredericq [53]) or enzyme accessibility [55,60]. From our approach, it is very likely that there is not a complete identity between the first binding site of a dye molecule on DNA and on the accessible regions of DNA in nucleohistone. Such an identity should yield identical binding constants of the dye on both macromolecules and identical values of the physico-chemical properties depending upon the binding when they are extrapolated to r or D/P equal to zero. Thus, we reject the concept of "free DNA" in nucleohistone, for the following reasons:

(i) The best agreement between the experimental value of R_0 (a parameter which estimates the reduction of the binding in nucleohistone compared to DNA) and the calculated ones was found when both parameters of the intercalative process were considered as lower in nucleohistone compared to DNA (fig. 3 and table 5). Moreover, in the case of quinacrine, the fitting calculations showed that the external binding process is reduced to a similar extent as the intercalative one (fittings no. 5 and 8 of table 4). This behaviour did not appear with ethidium bromide, mainly because of the low value of the binding strength of the external process.

(ii) The fluorescence polarization measurements also allowed us to distinguish clearly the first binding site of the dye to DNA from the one to nucleohistone (fig. 11 and table 8). This optical parameter reflects the mobility of the first bound dye molecule. So, the torsional motions detected by Wahl in DNA [57] appear to be reduced by the presence of the chromosomal proteins. This difference is better shown with ethidium bromide than with quinacrine, which is in good agreement with other observations [16,21–23].

(iii) Results obtained by the circular dichroism technique on the complexes of ethidium bromide with DNA and nucleohistone in 1 mM NaCl (not reported here) were found completely similar to the recent observations of Dalgleish et al. with proflavine [61]. These authors concluded that "the conformation of all of the DNA is altered by its incorporation into the nucleoprotein complex".

In summary, these results indicate that in nucleohistone there are no completely free regions structurally identical to DNA itself.

Acknowledgements

The authors gratefully acknowledge the financial support of this work provided by the Institut pour l'encouragement de la Recherche Scientifique dans l'Industrie et l'Agriculture and by the Fonds de la Recherche Fondamentale Collective.

Thanks are also due to Dr. C. Houssier for valuable discussions of the results and to Miss J. Linet for her assistance in carrying out some of the experiments.

References

[1] D.S. Drummond, V.F.W. Simpson-Gildemeister and A.R. Peacocke, Biopolymers 3 (1965) 135.
[2] U. Pachmann and R. Rigler, Exp. Cell Res. 72 (1972) 602.
[3] M.J. Waring, J. Mol. Biol. 13 (1965) 269.
[4] J.B. LePecq and C. Paoletti, J. Mol. Biol. 27 (1967) 87.
[5] R. Bittman, J. Mol. Biol. 46 (1969) 251.
[6] D.E. Olins, J. Mol. Biol. 43 (1969) 439.
[7] L.M. Angerer and E.N. Moudrianakis, J. Mol. Biol. 63 (1972) 505.
[8] J.R. Hutton and J.G. Wetmur, Biopolymers 11 (1972) 2337.
[9] P.F. Lurquin and V.L. Seligy, Biochem. Biophys. Res. Commun. 46 (1972) 1399.
[10] R.E. Williams, P.F. Lurquin and V.L. Seligy, Eur. J. Biochem. 29 (1972) 426.
[11] S. Aktipis and A. Kindelis, Biochemistry 12 (1973) 1213.
[12] C.H. Lee, C.T. Chang and J.G. Wetmur, Biopolymers 12 (1973) 1099.
[13] L.S. Lerman, Proc. Nat. Acad. Sci. U.S. 49 (1963) 94.
[14] L.S. Lerman, J. Cell. Comp. Physiol. 64, suppl. 1 (1964) 1.
[15] N.B. Kurnick and I.E. Radcliffe, J. Lab. Clin. Med. 60 (1962) 669.
[16] J.M. Saucier, B. Festy and J.B. LePecq, Biochimie 53 (1971) 973.
[17] R.L. O'Brien, J.G. Olenick and F.E. Hahn, Proc. Nat. Acad. Sci. U.S. 55 (1966) 1511.

[18] L.S. Lerman, J. Mol. Biol. 3 (1961) 18.
[19] N.J. Pritchard, A. Blake and A.R. Peacocke, Nature (London) 212 (1966) 1360.
[20] N. Weisblum and P.L. De Haseth, Proc. Nat. Acad. Sci. U.S. 69 (1972) 629.
[21] A.D. Wolfe, in: Progress in Molecular and Subcellular Biology, ed. F.E. Hahn (Springer-Verlag, Berlin and Heidelberg, 1971) vol. 2, p. 247.
[22] A.D. Wolfe, R.G. Allison and F.E. Hahn, Biochemistry 11 (1972) 1569.
[23] F.M. Pohl, R.M. Jovin, W. Baehr and J.J. Holbrook, Proc. Nat. Acad. Sci. U.S. 69 (1972) 3805.
[24] T. Caspersson, L. Zech, E.J. Modest, G.E. Foley, U. Wagh and E. Simonsson, Exp. Cell Res. 58 (1968) 128.
[25] E. Fredericq and C. Houssier, Biopolymers 11 (1972) 2281.
[26] E. Fredericq, Biochim. Biophys. Acta 55 (1962) 300.
[27] J. Ramstein, M. Dourlent and M. Leng, Biochim. Biophys. Acta 47 (1972) 874.
[28] J.L. Irvin and E.M. Irvin, J. Biol. Chem. 210 (1954) 39.
[29] J.B. LePecq, in: Methods of Biochemical Analysis, ed. D. Glick (John Wiley, New York, 1971) vol. 20, p. 41.
[30] A.R. Peacocke and J.N.H. Skerrett, Trans. Faraday Soc. 67 (1956) 261.
[31] S.N. Cohen and K.L. Yielding, J. Biol. Chem. 240 (1965) 3123.
[32] H. Terada and K. Miyake, Kolloid-Z.Z. Polym. 251 (1973) 139.
[33] G. Schwarz, Eur. J. Biochem. 12 (1970) 442.
[34] C.J. Halfman and T. Nishida, Biochemistry 11 (1973) 3493.
[35] N.F. Ellerton and I. Isenberg, Biopolymers 8 (1969) 769.
[36] C.J. Thompson and I.M. Klotz, Arch. Biochem. Biophys. 147 (1971) 178.
[37] H.A. Feldman, Anal. Biochem. 48 (1972) 317.
[38] I. Sela, Biochim. Biophys. Acta 190 (1969) 216.
[39] C. Houssier, in: Abstracts of the first European Biophysics Congress, eds. E. Broda, A. Locker and H. Springer-Lederer (Verlag der Wiener Medizinischen Akademie, Baden (Vienna) 1971) vol. 1, p. 239.
[40] C. Houssier, B. Hardy and E. Fredericq, Biopolymers, in press.
[41] G. Scatchard, Ann. N.Y. Acad. Sci. 51 (1949) 660.
[42] W. Müller and D.M. Crothers, J. Mol. Biol. 35 (1968) 251.
[43] W. Bauer and J. Vinograd, J. Mol. Biol. 47 (1970) 419.
[44] R.W. Armstrong, T. Kurucsev and U.P. Strauss, J. Am. Chem. Soc. 92 (1970) 3174.
[45] D.M. Crothers, Biopolymers 6 (1968) 575.
[46] J. Chambron, M. Daune and C. Sadron, Biochim. Biophys. Acta 123 (1966) 306.
[47] B.L. Gittelson and I.O. Walker, Biochim. Biophys. Acta 138 (1967) 619.
[48] J.J. Lawrence and M. Louis, Biochim. Biophys. Acta 272 (1972) 231.
[49] L. Kleinman and R.C.C. Huang, J. Mol. Biol. 55 (1971) 503.
[50] H.J. Li and D.M. Crothers, Biopolymers 8 (1969) 217.
[51] A.M. Michelson, C. Monny and A. Kovoor, Biochimie 54 (1972) 1129.
[52] R.K. Selander, Biochem. J. 131 (1973) 749.
[53] E. Fredericq, in: Histones and Nucleohistones, ed. D.M.P. Phillips (Plenum Press, London and New York, 1971) p. 136.
[54] R.J. Clark and G. Feldsenfeld, Nature (London) New Biol. 240 (1971) 226.
[55] A.E. Mirsky and B. Silverman, Proc. Nat. Acad. Sci. U.S. 69 (1972) 2115.
[56] R.V. Chen, G.G. Vurek and N. Alexander, Science 156 (1967) 949.
[57] P. Wahl, C. Paoletti and J.B. LePecq, Proc. Nat. Acad. Sci. U.S. 65 (1970) 417.
[58] A.M. Liquori, L. Constantino, V. Crescenzi, V. Elia, E. Giglio, R. Pulitri, M. De Santis Savino and V. Vitagliano, J. Mol. Biol. 24 (1967) 113.
[59] J.L. Irvin and E.M. Irvin, J. Biol. Chem. 206 (1954) 39.
[60] A.E. Mirsky, B. Silverman and N.C. Panda, Proc. Nat. Acad. Sci. U.S. 69 (1972) 3243.
[61] D.G. Dalgleish, E. Dingsøyr and A.R. Peacocke, Biopolymers 12 (1973) 445.

BIOPHYSICAL CHEMISTRY 2 (1974) 23–31. © NORTH-HOLLAND PUBLISHING COMPANY

THEORETICAL ANALYSIS OF THE OXIDATION OF AMYLOSE BY PERIODATE ION AS AN EXAMPLE OF COOPERATIVE EFFECTS IN POLYMER KINETICS

José J. GONZÁLEZ
Institute of Theoretical Physics, NTH, University of Trondheim, Norway

Received 11 October 1973

It is shown that oxidation of amylose by periodate ions can be described by a stochastic model of random sequential polymer reactions with nearest-neighbour cooperative effects. The reaction is completely described by a second-order rate constant k, and two reactivity coefficients a and c which measure the degree of inhibition.

Simple and rapid methods for the determination of k, a and c for a wide class of polymer reactions with nearest-neighbour cooperative effects are given.

1. Introduction

Polymer reactions often display cooperative effects, because reaction of one residue in a given chain can enhance the reactivity of other units in the same chain (auto-activatory, auto-cooperative or auto-catalytic reactions) or diminish the reactivity of other units (auto-inhibitory or, less appropriately, hetero-cooperative reactions). Usually, the effects are short-ranged and of special interest are those affecting the $r = 1, 2, 3\ldots$ consecutive neighbouring reactive sites only.

The theoretical analysis of a wide class of cooperative reactions has been described elsewhere (ref. [1], hereafter referred to as GHH). Here, we apply the results to the oxidation of amylose by periodate ion. The chemical principles and the experimental data are given by Painter and Larsen [2]. For the present purpose it is sufficient to recognize that amylose consists of a linear chain of (cyclic) glucose units, each containing a vicinal-diol function. The degree of polymerization of the amylose employed was 2700, so that we shall neglect finite size effects for the time being (cf. discussion in section 3.2). Amylose behaves in solution as a random coil [3–5]. It is natural to assume that the monomer units are attacked at random. Upon oxidation by the metaperiodate ion, each vicinal-diol is converted into two aldehyde groups. Once formed, an aldehyde group can react either with water, to give a hydrate (a geminal diol), or, if there are nearest-neighbouring unoxidized units, with the closest hydroxyl group in an adjacent monomer, to give a six-membered, cyclic hemiacetal. In careful analyses [2, 6–8] Painter and Larsen have shown that the auto-inhibitory effects in periodate oxidation of amylose and other 1,4-linked polysaccharides is due to the spontaneous formation of such hemiacetals. They block the vicinal-diol functions of nearest-neighbouring unoxidized units, thus protecting them from attack by periodate. An equilibrium is very rapidly established between the two states of combination of the aldehyde groups. The simplest assumption is that oxidation of an unit instantaneously reduces the reactivity of its nearest-neighbouring units to a constant fraction. When an oxidized unit is flanked by two unoxidized monomers, the asymmetric form of the glucose implies that the stereochemistry of the two hemiacetals is different and hence that the position of the two equilibria will be different. When an unoxidized unit is between two oxidized ones, the inhibitory effects of the two equilibria will be compounded. Moreover, the extreme stability of six-membered hemiacetals rings, compared to larger ones, assures that the inhibitory effect of oxidized units is exerted upon nearest-neighbours only [7].

The preceding discussion suggests the following idealized model for the oxidation of amylose: a one-dimensional chain consists of an infinite number of identical units, each capable of undergoing a reaction. A unit that

has undergone the reaction is assumed to remain in the reacted state. The probability that a given unit reacts during the time interval dt is assumed to be equal to zero, if the unit has already reacted, equal to $k\,dt$, if the unit and its nearest-neighbours have not reacted, and equal to $a_R k\,dt$, $a_L k\,dt$ or $ck\,dt$ depending on whether the left, the right or both nearest-neighbours of the (unreacted) unit have reacted[†]. At the initial time, $t = 0$, the chain is assumed to be in the unreacted state.

This model takes no account of the depletion of the attacking reagent that takes place in a bimolecular reaction. This is equivalent to using an idealized time-scale, t, which assumes that the concentration of the attacking reagent (x_2) remains constant throughout the reaction (cf. section 2 for transformation to real units of time). The rate constant k is, when expressed in proper units, the initial second-order rate constant of the reaction. The reactivity coefficients a_R, a_L and c are measures of the inhibition (or activation).

This stochastic model was treated in section 3.1 of GHH as special case $r = 1$ of a general model describing cooperative effects relating to r consecutive neighbouring units. The degree of oxidation $y(t)$, called extent of reaction in GHH, is given by

$$y(t) = 1 + (a-c)^{-1}\left\{-e^{-kct} + (2c-a) \times \exp[-kat-(2-a)(1-e^{-kt})] + (3c-c^2-a)e^{-kct} \times \int_0^{kt} ds \exp[(c-a-1)s-(2-a)(1-e^{-s})]\right\}, \quad (1)$$

where the abbreviation $a = a_R + a_L$ has been used. The results for the average densities $q_l(t)$, $l = 1,2,\ldots$ of sequences of l contiguous, unoxidized units are

$$q_1(t) = 1-y(t)-(2-e^{-kt}) \times \exp[-kat-(2-a)(1-e^{-kt})], \quad (2)$$

and for $l \geqslant 2$

$$q_l(t) = (1-e^{-kt})^2 \times \exp[-kat-(2-a)(1-e^{-kt})]\exp[-(l-2)kt]. \quad (3)$$

[†] Note that the chemical considerations presented above also suggest $c = a_R a_L$. We return to this point in section 3.2.

Since only the symmetric combination $a = a_R + a_L$ enters our formulae, this model is essentially equivalent to one with *symmetric* cooperative effects of nearest-neighbours. Models of the last type have been studied by several authors [9–14].

Finally, we remark that Smidsrød et al. (ref. [15], here after referred to as SLP), with minor differences to be commented later, applied the stochastic model presented above by means of computer simulation to account for the experimental data of Painter and Larsen [2].

We shall begin in section 2 by developing simple and rapid techniques for determining a and c from experimental data, and will then show in section 3 that the values obtained are able to account completely for the reaction curve reported by Painter and Larsen. In section 4 we briefly discuss the basis for a theoretical description of oxidation of sodium alginate [6, 7] and xylan [8].

2. Treatment of experimental data

2.1. Calibration of the time-scale

In order to convert the idealized time-scale, t, into real units of time, t^*, we note that the idealized time, dt, that is required to bring about an increment in the degree of oxidation will be multiplied by a factor $x_2/x_1(t)$ in the experimental situation [15], x_2 being the (constant) concentration of monomeric units and $x_1(t)$ the concentration of periodate ions at time t.

Now, $x_1(t) = x_1(0) - x_2 y(t)$, and hence

$$dt^* = dt[x_1/x_2 - y(t)]^{-1}, \quad (4)$$

or

$$t^* = \int_0^t dt[x_1/x_2 - y(t)]^{-1}, \quad (5)$$

where $x_1 \equiv x_1(0)$.

2.2. Determination of k and a from the initial stages of the oxidation

Expanding eq. (1) for $kt \ll 1$, we get

$$y(t) = kt - \tfrac{1}{2}(3-a)k^2t^2 + O(k^3t^3). \quad (6)$$

Similarly, eq. (5) yields

$$t^* = \frac{t}{x_1/x_2} + \frac{k}{2}\left(\frac{t}{x_1/x_2}\right)^2 + O(k^3 t^3). \quad (7)$$

Therefore, the initial stages of the reaction will be described by

$$y(t^*) \simeq (x_1/x_2)k\left\{t^* - \tfrac{1}{2}k[1+(x_1/x_2)(3-a)]t^{*2}\right\}. \quad (8)$$

From this it is seen that a plot of $y(t^*)/t^*$ against t^* gives a straight line whose intercept and slope permit calculation of k and a.

It may be noted that, at the very beginning, the reaction obeys second-order kinetics, because

$$y(t^*) = (x_1/x_2)kt^* + O(t^{*2}) \quad (9)$$

and hence the familiar equation

$$\frac{1}{x_1-x_2}\ln\frac{x_2[x_1-x_2y(t^*)]}{x_1[x_2-x_2y(t^*)]} \simeq \frac{k}{x_2}t^* \quad (10)$$

holds true.

2.3. Determination of a and c from the asymptotic tail of the reaction curve

Eq. (1) can be written:

$$y(t) = 1 - Be^{-kct} + (a-c)^{-1}\{(2c-a) \times \exp[-kat-(2-a)(1-e^{-kt})] - (3c-c^2-a)e^{-kct} \times \int_0^{e^{-kt}} dx\, x^{a-c}\exp[-(2-a)(1-x)]\}, \quad (11)$$

where

$$B = (a-c)^{-1}\{c - (3c-c^2-a) \times \int_0^1 dx\, x^{a-c}\exp[-(2-a)(1-x)]\}. \quad (12)$$

For the case $a > c > 0$, which applies in the oxidation of polysaccharides, the asymptotic behaviour will be

$$y(t) \simeq 1 - B\,e^{-kct}, \quad (13)$$

because

$$e^{-kct}\int_0^{e^{-kt}} dx\, x^{a-c}\exp[-(2-a)(1-x)] = e^{a-2}\sum_{n=0}^{\infty}\frac{(2-a)^n}{n!}\frac{\exp[-(n+a+1)t]}{n+a-c+1}. \quad (14)$$

To find the asymptotic behaviour of the degree of oxidation as a function of the real, experimental time t^*, we assume that eq. (13) holds for $t > t_0$ and write eq. (5) as

$$t^* \simeq K + \int_{t_0}^{t} d\tau\,[(x_1-x_2)/x_2 + B\exp(-kc\tau)]^{-1}, \quad (15)$$

where

$$K = \int_0^{t_0} d\tau\,[x_1/x_2 - y(\tau)]^{-1}. \quad (16)$$

The particular value of K (and of L, C and D, which we introduce below) is irrelevant for determination of a and c.

Integrating eq. (15) and solving for t one finds that

$$t \simeq [(x_1-x_2)/x_2]t^* - (1/kc)\ln[x_1/x_2 - y(t^*)] + L. \quad (17)$$

Inserting this into eq. (13) and solving for $y(t^*)$ one gets

$$y(t^*) \simeq 1 - \frac{(x_1-x_2)/x_2}{D\exp\{kc[(x_1-x_2)/x_2]t^*\}-1}. \quad (18a)$$

Eq. (15), and hence also eq. (18a), contains an uncontrolled approximation. However, the error committed by using the asymptotic approximation (13) in the integrand of the integral

$$\int_{t_0}^{t} d\tau\,[x_1/x_2 - y(t)]^{-1}$$

can be made as small as desired by choosing t_0 large enough. A necessary condition for the validity of eq. (18a) is, of course, that

$$\exp(-kct) \gg \exp(-kat), \qquad \text{for } t \geq t_0.$$

Eventually, when

$$D\exp\{kc[(x_1-x_2)/x_2]t^*\} \gg 1,$$

eq. (18a) simplifies to

$$y(t^*) = 1 - C \exp\{-[(x_1 - x_2)/x_2]\, kct^*\}. \quad (18b)$$

As a consequence of eq. (18a),

$$\ln\{1 + [(x_1 - x_2)/x_2]\,[1 - y(t^*)]^{-1}\} = \ln D + [(x_1 - x_2)/x_2]\, kct^*. \quad (19a)$$

And because of eq. (18b)

$$\ln[1 - y(t^*)] = \ln C - [(x_1 - x_2)/x_2]\, kct^*. \quad (19b)$$

Note that eq. (19b) is a special case of eq. (19a) for very large time values.

Thus, according to which of the asymptotic formulae (18a, b) is applicable, a logarithmic plot of the appropriate function will yield a straight line whose slope determines the reactivity constant c.

Once c is known, the fact that the intercept of the straight line (19a) [or (19b)] depends upon a only (i.e., different values of a give a family of parallel straight lines), suggests the following procedure for determination of a: If the experimental values for large times are plotted according to eq. (19a), for instance, the theory predicts a straight line. Once the best fit to the data has been found, the slope of the straight line determines c. The reactivity constant a is determined by finding by means of eqs. (1), (5) and (19a) the particular value of a that reproduces the straight line determined by the experimental data. In practice, a is found by interpolation. We exemplify this method in section 3.

When one of the reactivity constants vanishes, the degree of oxidation goes asymptotically to a limit value less than unity. Knowledge of the limit value permits determination of the other reactivity constant (cf. section 3 of GHH).

It is again noted that in the asymptotic region the oxidation proceeds according to second-order kinetics. Using eq. (18a) one verifies:

$$\frac{1}{x_1 - x_2} \ln \frac{x_2[x_1 - x_2 y(t^*)]}{x_1[x_1 - x_2 y(t^*)]} \simeq \frac{k}{x_2} ct^* + \text{constant}. \quad (20)$$

2.4. A different method for determination of a and c

When the approximate values of a and c are known beforehand (for instance, when studying the temperature dependence of the reactivity coefficients of a given substance), the following procedure will be advantageous: One computes t_1^*, the value of t^* for which a given value, say 0.4, of the degree of oxidation is obtained, as a function of a for different values of the parameter c. Similarly, t_2^*, the value of t^* for which $y(t_2^*) = 0.5$, say, is computed as a function of a for different values of the parameter c. A plot of t_2^* against t_1^* yields a family of curves, c being the family parameter. Similarly, a family of curves with a as family parameter is plotted. In this way, a chart is obtained that permits determination of a and c from the experimental values for t_1^* and t_2^*.

3. Theoretical analysis of the oxidation of amylose by periodate ion

3.1. Results

In the experiment to be analysed [2], x_1 was 5 mM, x_2 was 3 mM, and the data given in table 1 were obtained.

Applying the procedure of section 2.2, we try to determine the rate constant k and the reactivity coefficient a from the initial stages of the reaction (fig. 1). However, it is seen from fig. 1 that the linear approximation to $y(t^*)/t^*$ applies during the initial 2 minutes of the reaction only, where merely two measurements were done.

When, in cases like this, the domain of applicability of the linear approximation to $y(t^*)/t^*$, eq. (8), is rather short, it is advisable to make a special study of the initial stages of the reaction by using a low concentration of the attacking reagent in order to slow down the reaction. This is important, because the large initial rate of a typical oxidation reaction makes measurements of the degree of oxidation during the first few minutes difficult and comparatively inaccurate.

The slope of the straight line that has been drawn in fig. 1 corresponds to $a = 0.460$. This value, which is the one found more accurately from the asymptotic part, is consistent with the initial data, but these data are clearly insufficiently accurate to allow determination of a. The intercept of the straight line gives the rate constant $k = 0.01875\ \text{min}^{-1}$. Given as a second-order rate constant $k = 225\ \ell\ \text{mole}^{-1}\text{h}^{-1}$. This value, which is the

Table 1

Oxidation of amylose (3mM with respect to vicinal-diol groups and of a viscosity-average degree of polymerization of 2700) in 5mM sodium metaperiodate at 20°. Experimental degrees of oxidation ($y_{expt.}$) are compared with those ($y_{anal.}$) calculated in this work by means of the analytical formula (1) derived in GHH and with those ($y_{M.C.}$) computed in SLP by means of Monte Carlo simulation. Reactivity coefficients are: (1) This work: $a = 0.460 \pm 0.030$; $c = 0.0337 \pm 0.0030$. (2) SLP: $a = 0.437 \pm 0.030$; $c = 0.0330 \pm 0.0030$ (errors estimated only)

Time (min)	$y_{expt.}$	$y_{anal.}$	Diff.	$y_{M.C.}$	Diff.
1.00	0.018	0.018	0.000	0.018	0.000
2.00	0.036	0.035	0.001	0.035	0.001
3.25	0.057	0.056	0.001	0.056	0.001
4.00	0.068	0.067	0.001	0.068	0.000
5.00	0.082	0.082	0.000	0.082	0.000
6.00	0.097	0.096	0.001	0.096	0.001
8.00	0.124	0.121	0.003	0.122	0.002
9.00	0.135	0.133	0.002	0.134	0.001
15.0	0.217	0.195	0.022	0.196	0.021
30.0	0.316	0.299	0.017	0.300	0.016
45.0	0.373	0.363	0.010	0.364	0.009
60.0	0.409	0.407	0.002	0.408	0.001
90.0	0.465	0.465	0.000	0.467	−0.002
120	0.496	0.502	−0.006	0.502	−0.006
150	0.528	0.528	0.000	0.529	−0.001
180	0.550	0.549	0.001	0.550	0.000
210	0.566	0.565	0.001	0.566	0.000
240	0.580	0.579	0.001	0.580	0.000
270	0.591	0.591	0.000	0.592	−0.001
300	0.594	0.602	−0.008	0.602	−0.008
330	0.602	0.611	−0.009	0.611	−0.009
360	0.612	0.620	−0.008	0.620	−0.008
390	0.618	0.627	−0.009	0.628	−0.010
420	0.625	0.634	−0.009	0.635	−0.010
450	0.630	0.641	−0.011	0.641	−0.011
555	0.653	0.660	−0.007	0.661	−0.008
630	0.670	0.672	−0.002	0.673	−0.003
690	0.679	0.681	−0.002	0.683	−0.004
750	0.689	0.689	0.000	0.690	−0.001
810	0.698	0.697	0.001	0.698	0.000
870	0.707	0.704	0.003	0.705	0.002
930	0.712	0.711	0.001	0.712	0.000
990	0.723	0.717	0.006	0.719	0.004
1200	0.743	0.738	0.005	0.739	0.004
1320	0.751	0.749	0.002	0.750	0.001
1440	0.753	0.759	−0.006	0.760	−0.007
1560	0.766	0.769	−0.003	0.770	−0.004
1680	0.778	0.778	0.000	0.778	0.000

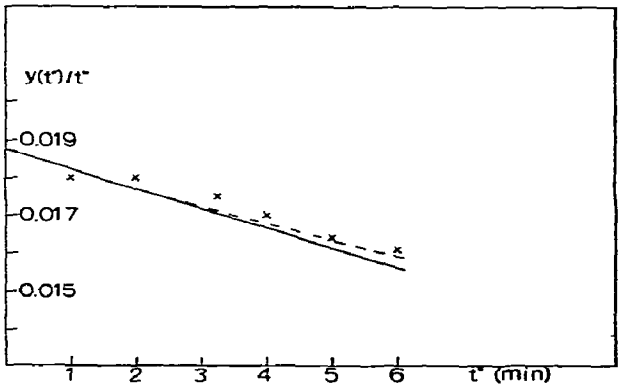


Fig. 1. Determination of k and a from the initial stages of the reaction (for explanation, see text). The experimental values of $y(t^*)/t^*$ are denoted by crosses. Solid line: linear fit to the data for $t^* < 3$ min. Broken line: exact theoretical curve for $y(t^*)/t^*$ with $k = 0.01875$ min^{-1}; $a = 0.460$ and $c = 0.0337$.

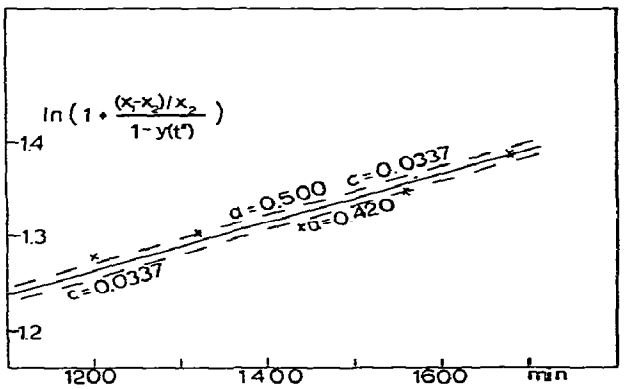


Fig. 2. Determination of a and c from the asymptotic tail of the reaction curve (for explanation, see text). The crosses denote experimental values for

$$\ln\{1 + [(x_1-x_2)/x_2][1-y(t^*)]^{-1}\}.$$

The slope of the straight line determined by the data (solid line) determines c to $c = 0.0337$. The broken lines are two theoretical curves with identical values of $c = 0.0337$ and different values of a.

one found in ref. [2] by a different method, is consistent with the data but, due to the apparent uncertainty of the first few experimental values, a slightly different value cannot be excluded.

The reactivity constants a and c were determined by applying the method described in section 2.3 to the last five experimental values, taken at times 1200, 1320, 1440, 1560 and 1680 min. These values are safely within the domain of applicability of eq. (18a). The slope of the straight line (fig. 2) gave $c = 0.0337 \pm 0.0030$.

To find the experimental value of a the eqs. (1) and (5) were used to compute

$$\ln\{1 + [(x_1-x_2)/x_2][1-y(t^*)]^{-1}\}$$

for $t^* = 1200$ min and $t^* = 1600$ min for different values of a. Each pair of values determines a straight line. Fig. 2 shows two such straight lines (broken lines) which readily allow us to conclude that $a = 0.460$ yields a good fit to the data.

Using the values for k, a and c found, we computed, by means of a programmable Wang 700B calculator, $y(t^*)$ for different values of t^*. In practice, one first computes the degree of oxidation for a given value of the ideal time, t, by numerical integration of eq. (1). The corresponding value of the experimental time, t^*, is found by numerical integration of eq. (5). Since $y(t)$ appears in the integrand of eq. (5), computation of t^* involves as intermediate calculation the evaluation of $y(t)$ for a sufficiently high number of values of t in the integration range. Care was taken to compute $y(t)$ with high accuracy in order to hold the error in computing t^* below one part per thousand. The results are found in table 1 and fig. 3 displays the theoretical curve as well as the experimental values.

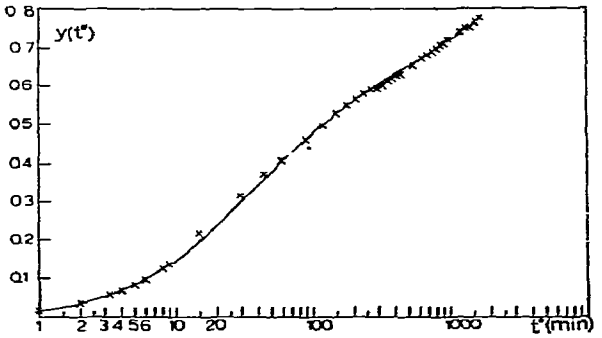


Fig. 3. Theoretical oxidation curve according to eqs. (1) and (5) for $k = 0.01875$ min^{-1}; $a = 0.460$ and $c = 0.0337$. The crosses denote experimental values for the degree of oxidation of amylose.

3.2. Comparison with Smidsrød et al. (SLP)

From table 1 we conclude that the Monte Carlo simulation empoyed in SLP essentially gives results very close to ours. The slightly different values for a and c are probably due to the fact that in SLP an array simulating a degree of polymerization $N = 80$ was used, whereas our model presupposes $N = \infty$.

In the experiment [2], amylose of a viscosity-average degree of polymerization of $N = 2700$ was employed. The analytical estimation of the error introduced by operating with $N = \infty$ is difficult, because the reactivity of the end residues of the amylose chains is unknown. However, we may state with confidence that the error is negligible as compared to the experimental errors. Already in SLP it was found that higher values than $N = 80$ for the simulated degree of polymerization only resulted in changes that were negligible. Still, this argument does not take account of the modified reactivity of the terminal residues but, clearly, whether the two terminal residues are oxidated or not only contributes to the oxidation degree by maximally $\pm 4/N$ (including maximal nearest-neighbour effects).

The following dissimilarity should be noted: the Monte Carlo simulation technique employed by Smidsrød et al. presupposed discrete time units: the attack of periodate was simulated by random sequential introduction of integers into an array and the passage of time was recorded as the number of random integers supplied [15].

The discretization of time, which clearly is an unrealistic feature, leads to additional terms of the order of $1/N$ in the degree of oxidation† as may be seen from the simple case of $a_R = a_L = c = 1$. It is easily seen that the degree of oxidation for a chain of N molecules after n attacks is given by

$$y_N(n) = 1 - (1-1/N)^n. \qquad (21)$$

Introducing in the limit $N \to \infty$ the time-scale $kt = n/N$, eq. (21) yields

$$y(t) = 1 - e^{-kt} - kt/N + O(N^{-2}), \qquad (22)$$

which differs from the exact result given by eq. (1) by terms of the order $1/N$.

† I am grateful to Professor Hemmer for bringing this fact to my attention.

Finally, the chemical considerations presented in the introduction make the assumption $c = a_R a_L$ a natural one [15]. Once this is done, a_R and a_L can be determined separately. Our results are

$$a_R = 0.369 \quad \text{and} \quad a_L = 0.091,$$

to be compared with $a_R = 0.340$ and $a_L = 0.097$ reported in SPL.

3.3. Discussion

Although it would be interesting to try to find the best matching of k, a and c with the data, no attempt in this direction was done because this time-consuming task would be very simplified if one could dispose of sufficient data to apply the procedures of sections 2.2 and 2.3 with desirable accuracy.

The applicability of the stochastic model is beyond doubt. New experiments studying the oxidation of amylose by periodate ions at different temperatures are needed in order to scan the region of validity of the stochastical model employed.

Since the model predicts the average density of sequences of $l \geqslant 1$ contiguous, unoxidized glucose residues in the chains it would be worthwhile to try a measurement of sequence distributions. For illustration, the density functions for $l = 1, 2, 3, 4, 5$ for this experiment are displayed in table 2 and fig. 4. They were computed by means of eqs. (2, 3).

4. Other oxidation experiments

Oxidation experiments with sodium alginate [6, 7] and xylan [8] also manifested strong auto-inhibitory effects and, here too, the auto-inhibitory effects were due to the formation of six-membered hemiacetal rings.

However, sodium alginate is not a homopolymer but a block copolymer [16, 17] so that the stochastic model used here cannot without modification be used to describe chain molecules of this type.

Xylan ought, in principle, be suitable for description by the model. Still, attempts to fit the model to the data of ref. [5] failed. This is apparently due to the fact that xylan, in contrast to amylose, is not soluble in water and that oxidized xylan becomes increasingly soluble with

Table 2
Average density of sequences $q_l(t^*)$ of l = 1, 2, 3, 4, 5 contiguous, unoxidized glucose residues in amylose during oxidation by periodate [2]

Time (min)	q_1	q_2	q_3	q_4	q_5
1	0.0003	0.0003	0.0003	0.0003	0.0003
2	0.0013	0.0012	0.0011	0.0011	0.0011
3.25	0.0031	0.0030	0.0028	0.0026	0.0025
4	0.0046	0.0043	0.0040	0.0037	0.0034
5	0.0079	0.0063	0.0058	0.0053	0.0048
6	0.0095	0.0086	0.0077	0.0069	0.0062
8	0.0154	0.0137	0.0118	0.0102	0.0088
9	0.0186	0.0164	0.0139	0.0118	0.0101
15	0.0407	0.0331	0.0254	0.0196	0.0150
30	0.0983	0.0637	0.0407	0.0246	0.0149
45	0.1469	0.0861	0.0416	0.0201	0.0097
60	0.1851	0.0943	0.0367	0.0143	0.0055
90	0.2377	0.0941	0.0242	0.0062	0.0016
120	0.2704	0 0853	0.0147	0.0025	0.0004
150	0.2914	0.0746	0.0087	0.0010	0.0001
180	0.3055	0.0642	0.0051	0.0004	–
210	0.3150	0.0548	0.0030	0.0001	–
240	0.3215	0.0467	0.0017	–	–
270	0.3258	0.0397	0.0010	–	–
300	0.3285	0.0338	0.0006	–	–
330	0.3300	0.0287	0.0003	–	–
360	0.3306	0.0244	0.0002	–	–
390	0.3305	0.0208	0.0001	–	–
420	0.3298	0.0177	–	–	–
450	0.3286	0.0151	–	–	–
555	0.3220	0.0087	–	–	–
630	0.3157	0.0059	–	–	–
690	0.3102	0.0043	–	–	–
750	0.3045	0.0032	–	–	–
810	0.2986	0.0023	–	–	–
870	0.2928	0.0017	–	–	–
930	0.2868	0.0012	–	–	–
990	0.2811	0.0009	–	–	–
1200	0.2614	0.0003	–	–	–
1320	0.2508	0.0001	–	–	–
1440	0.2408	–	–	–	–
1560	0.2311	–	–	–	–
1680	0.2220	–	–	–	–

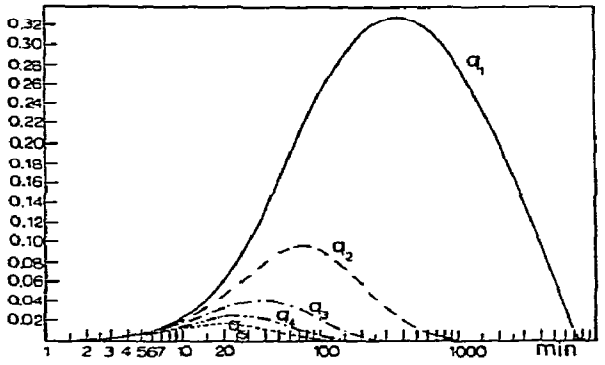


Fig. 4. Theoretical average densities of $l = 1, 2, 3, 4, 5$ contiguous, unoxidized glucose residues according to eqs. (2, 3). The values of k, a and c used, apply to the oxidation of amylose by periodate ion [2].

growing degree of oxidation†. A poorly soluble chain molecule clearly is not randomly attacked by the oxidizing reagent. The solubility being dependent upon the degree of oxidation, it is extremely difficult to account for its influence during the oxidation process.

Acknowledgement

It is a great pleasure to thank Professor P.C. Hemmer, Dr. T.J. Painter and Dr. O. Smidsrød for valuable comments and fruitful discussion. Dr. Painter is also thanked for help with the manuscript.

† This explanation was suggested by Painter [18].

References

[1] J.J. González, P.C. Hemmer and J.S. Høye, Chem. Phys. 3 (1974) 228.
[2] T. Painter and B. Larsen, Acta Chem. Scand. 24 (1970) 2724.
[3] W. Banks and C.T. Greenwood, Carbohyd. Res. 7 (1968) 349.
[4] W. Banks and C.T. Greenwood, Carbohyd. Res. 7 (1968) 414.
[5] V.S.R. Rao, N. Yathindra and P.R. Sundararajan, Biopolymers 8 (1969) 325.
[6] B. Larsen and T.J. Painter, Carbohyd. Res. 10 (1969) 186.
[7] T. Painter and B. Larsen, Acta Chem. Scand. 24 (1970) 813.
[8] T. Painter and B. Larsen. Acta Chem. Scand. 24 (1970) 2366.
[9] J.B. Keller, J. Chem. Phys. 37 (1962) 2584.
[10] T. Alfrey, Jr. and W.G. Lloyd, J. Chem. Phys. 38 (1963) 318.
[11] C.B. Arends, J. Chem. Phys. 38 (1963) 322.
[12] J.B. Keller, J. Chem. Phys. 38 (1963) 325.
[13] L. Lazare, J. Chem. Phys. 39 (1963) 727.
[14] E.A. Boucher, J.C.S. Faraday I 68 (1972) 2295.
[15] O Smidsrød, B. Larsen and T. Painter, Acta Chem. Scand. 24 (1970) 3201.
[16] A. Haug, B. Larsen and O. Smidsrød, Acta Chem. Scand. 21 (1967) 691.
[17] B. Larsen, O. Smidsrød, A. Haug and T.J. Painter, Acta Chem. Sand. 23 (1969) 2375.
[18] T.J. Painter, private communication.

BIOPHYSICAL CHEMISTRY 2 (1974) 32–41. © NORTH-HOLLAND PUBLISHING COMPANY

ANALYSIS OF RELAXATION KINETICS DATA BY A NONLINEAR LEAST SQUARES METHOD

M.L. JOHNSON* and T.M. SCHUSTER‡

Biochemistry and Biophysics Section, Biological Sciences Group, University of Connecticut, Storrs, Connecticut 06268, USA

Received 15 October 1973
Revised manuscript received 25 February 1974

Recent improvements in measuring and data acquisition techniques have increased greatly the precision of chemical relaxation data. This has necessitated more accurate methods for data analysis in cases of complex relaxation spectra, as is often observed in biochemical systems. We have developed and applied a method capable of decomposing a wave form containing up to three overlapping exponentials. The method is based upon a nonlinear least squares algorithm. Analysis of the method shows that when it is applied to a two exponential function where the signal-to-noise ratio, $\Delta S/N$, is fifty, using 100 data points, the resulting four coefficients (two amplitudes and two relaxation times) are each accurate to within 5–10 % over a wide range of conditions, i.e., relative amplitudes from 10–90 % and ratios of relaxation times of 2.5 or greater. The influence of the number of data points and of random noise is as expected from statistical theory. Applications of the curve fitting methods to experimental temperature-jump data from oxygen binding to hemoglobin and hemocyanin yields internally consistent results. The values of the root-mean-square of the residuals of the fit approach those expected on the basis of the experimental signal-to-noise ratios.

1. Introduction

Curve fitting to nonlinear equations is a common problem in data analysis. Several methods are available in principle; the success of a particular method in practice depends upon the magnitude and kinds of noise in the data. We have applied a well-known nonlinear least squares method ([9], p. 451; [13], p. 149; [2]; [6]) specifically to simulated and real temperature-jump relaxation kinetics data. The method has been tested and used for more than one year in the form of a user oriented Fortran IV program and has proved to be practical and reliable in a variety of applications to the analysis of temperature-jump kinetics data from the binding of oxygen to hemocyanin and hemoglobin.

It has been shown theoretically that chemical relaxation (the time course of the change in concentration of some dependent variable) is described exactly as the sum of exponential curves [5]. The following analytical expressions apply to any problem involving fitting to multiple exponential curves, such as fluorescent decay kinetics [4, 16], isotope exchange kinetics [12], equilibrium sedimentation [7, 21] and the correlation spectrum of concentration fluctuations from equilibrium [3].

In a relaxation kinetics experiment the time course of the approach to an equilibrium state is given by

$$y(t) = \sum_i A_i \exp(-t/\tau_i). \qquad (1)$$

A_i is some dependent variable which is related to the extent of the reaction, such as optical absorbance or conductivity; t, the time is the independent variable; and τ_i the relaxation times. The quantities A_i and τ_i are the direct observables which can be related to the "normal reaction variables" of the reaction matrix for a given kinetic mechanism [5]. The accuracy with which A_i and τ_i can be evaluated from the experimen-

* Present address: Department of Biochemistry, University of Virginia, Medical School, Charlottesville, Virginia 22903.

‡ A preliminary account of these results was presented at the IUPAB Symposium on "Relaxation Methods in Molecular Biology", Copenhagen, August, 1972.

tal kinetics curve determines the accuracy with which the rate constants, enthalpies, and activation parameters of the corresponding reaction meachanism can be determined. In a more general sense it determines the number of elementary chemical reactions which can be characterized and thus defines the resolution of the entire kinetic analysis [5, 8, 20].

Recent developments in photometric detection [15] and on-line computer assisted data acquisition systems [17] have made it possible to obtain sufficiently accurate data to warrant the evaluation and use of improved curve fitting methods for obtaining A_i and τ_i.

2. Methods

The Gauss–Newton method (and any other method of successive approximation) is an algorithm for refining guesses of the values of the coefficients of a function. The algorithm can thus be applied repeatedly until the guesses have been refined to any specified precision. For example, for a 2 exponential fit, given a set of data points t_i (independent variable, in this case time) and y_i (dependent variable, in this case concentration) and initial guesses $\alpha_1^{(0)}$, $\alpha_2^{(0)}$, $\alpha_3^{(0)}$, and $\alpha_4^{(0)}$ (coefficients, i.e., amplitudes and reciprocal time constants) the algorithm generates a new set of improved guesses $\alpha_1^{(1)}$, $\alpha_2^{(1)}$, $\alpha_3^{(1)}$, and $\alpha_4^{(1)}$ (using Magar's notation [13]). The Gauss–Newton iteration generates a series of approximations for each variable (such as $\alpha_j^{(0)}$, $\alpha_j^{(1)}$, $\alpha_j^{(2)}$, ..., α_j) which approach the convergence values of the coefficients (α_1, α_2, α_3 and α_4). These convergence values yield a minimum root-mean-square (RMS) of the residuals for fitting to the function, F, for m data points.

$$F(\alpha_1, \alpha_2, \alpha_3, \alpha_4, t) = \alpha_1 e^{-t\alpha_2} + \alpha_3 e^{-t\alpha_4}, \tag{2}$$

$$(\mathrm{RMS})^2 = (1/m)\sum_{i=1}^{m} [F(\alpha_1, \alpha_2, \alpha_3, \alpha_4, t_i) - y_i]^2. \tag{3}$$

The Gauss–Newton method calls for approximation of the function $F(\alpha, t_i)$ by the Taylor expansion

$$y_i \approx F(\boldsymbol{\alpha}^{(q)}, t_i) \approx F(\boldsymbol{\alpha}^{(q-1)}, t_i) + \sum_{j=1}^{n} [\delta F(\boldsymbol{\alpha}^{(q-1)}, t_i)/\delta\alpha_j]\epsilon_j \tag{4}$$

at each of the i data points ([13], p. 150). In this equation α is a vector whose elements are the parameters $\alpha_1, \alpha_2, \alpha_3, \alpha_4$ and ϵ_j is the difference between the values of the jth parameter for successive iterations (q and $q-1$). This set of equations can then be rewritten in matrix notation as

$$\boldsymbol{y}^* = \mathbf{P}\epsilon, \tag{5}$$

where $\boldsymbol{y}^*$ is the vector whose elements are $y_i - F(\alpha^{(q-1)}, t_i)$ and ϵ is the vector whose elements are $\epsilon_1, \epsilon_2, \epsilon_3, \epsilon_4$, and $\mathbf{P}$ is the matrix of the partial derivatives in eq. (4). The vector ϵ can be evaluated from its matrix equivalent

$$\epsilon = (\mathbf{P}'\mathbf{P})^{-1}\mathbf{P}\boldsymbol{y}^*, \tag{6}$$

where $\mathbf{P}'$ is the transpose of $\mathbf{P}$.

The correction vector, ϵ, can then be added to α to get a better approximation of α,

$$\alpha^{(q)} = \alpha^{(q-1)} + \Pi\epsilon \tag{7}$$

where $\Pi \leqslant 1$, which is used to speed convergence ([13], p. 146). It should be noted that this constant is unity at convergence and is varied during the iterative process if required to prevent divergence.

The computer program we have developed [11] chooses the initial values of α by first approximating the reciprocal time constants and then using a linear least squares fit to obtain the best amplitudes corresponding to these time constants. For a two exponential fit the initial values of the reciprocal time constants are found by fitting a straight line to a log plot of the first and last half of the data points. For a three exponential fit the starting values for the reciprocal time constants are obtained using the values of the reciprocal time constants (α_2, α_4) determined in a prior two exponential fit. The starting values of the reciprocal time constants for a three exponential case are taken to be (1) the average of α_2 and α_4, (2) a number 20 % greater than either α_2 or α_4, and (3) a number 20 % less than the other.

For a linear least squares fit the standard errors (SE) of the coefficients, α_j, would be given by ([9], p. 258)

$$\mathrm{SE}_j = [(\mathbf{P}'\mathbf{P})^{-1}_{jj}(\mathrm{RMS})^2]^{1/2}, \tag{8}$$

where $(\mathbf{P}'\mathbf{P})^{-1}_{jj}$ is the jth diagonal element of the ma-

trix $(P'P)^{-1}$.

3. Results and discussion

The use of eq. (8) for nonlinear fitting is only an approximation which in this case involves three assumptions, (1) that the nonlinear problem is linear at the solution [see eq. (4)], (2) that the error in each parameter is independent and normally distributed, and (3) that the variance of the noise is given by the RMS of the fit. For convenience of notation the parameters obtained in a two exponential fit [see eq. (2)] are denoted by a, b, c, d for $\alpha_1, \alpha_2, \alpha_3, \alpha_4$, respectively, and a_0, b_0, c_0, d_0 are the values used in generating the test data.

We have used this approximation as a measure of the standard error of the parameters of a fit and refer to it as the "confidence limit" (CL). A more complete statistical analysis of standard errors can be obtained by an analysis of the confidence contours of the parameters as shown by Magar ([13], p. 252). However, the interpretation of such analysis is complex for more than three parameters.

One method of defining the meaning of the CL of a parameter is to compare it with the SE of the mean (correct) value obtained by analysis of a single set of test data perturbed by several different sets of random noise. This procedure can be used to calibrate the CL.

Table 1

Test of the algorithm for finding the "confidence limit" (CL) of a variable using a linear approximation [eq. (8)]. For the function,

$$y = a_0 e^{-b_0 t} + c_0 e^{-d_0 t}$$

one hundred data points equally spaced in time were calculated and perturbed by six different sets of pseudo-random noise (RMS = 0.02; $\Delta S/N = 50$). CL, the "confidence limit", is seen to be about three times the standard error (SE)

True value	Mean value	SE of mean	Mean CL
$a_0 = 0.50$	$a = 0.4956$	0.008	0.033
$b_0 = 1.00$	$b = 0.998$	0.013	0.051
$c_0 = 0.50$	$c = 0.5009$	0.010	0.034
$d_0 = 5.00$	$d = 5.054$	0.15	0.511

Table 1 shows the results of a typical test of this definition of the "confidence limit". In this case the CL was about three times the standard error of the mean.

Extensive testing of the method was performed by analyzing generated data and comparing the calculated and the true time constants and amplitudes under a variety of conditions. These conditions, although realistic, do not always represent the optimum ones available with present instrumentation. For example, the Δ signal-to-noise ratio ($\Delta S/N$) used for most of these evaluations is 50 but in practice values of 200 can be obtained, depending on the system under study. Also, although the use of one hundred data points represents a reasonable number for analog recording, more recent digital recording methods provide for as many as one thousand data points with time spacing varying according to the particular transient [17]. The present method does not require equally spaced data points.

The examples shown in figs. 1–5 are all for a two exponential fit to generated data. In each case all four parameters, two time constants and two amplitudes, were varied simultaneously. In all cases the time range of the data extended to three times the slowest time constant and, except for fig. 4, the baseline was assumed.

Fig. 1 shows that as $\Delta S/N$ decreases the uncertainty of each of the four parameters varies in about the same way. At $\Delta S/N = 100$ the CLs of the time constants are within 5 %, and of the amplitudes within 2 %, of the correct values. It should be recalled that the corresponding standard error is about one-third of these CLs (see table 1).

The detection and measurement of a second relaxation having a small amplitude can be accomplished over a rather wide range of relative amplitudes, as shown in fig. 2. Between the relative amplitudes of 0.10 and 0.90 the time constants were determined to within 8 % in both cases.

Fig. 3 shows the influence of the number of data points on the CL of each coefficient. An accuracy of about 5 % is obtained with 100 data points in all but one case, the faster time constant, for which it is about 10 %. If, however, the data points had been taken unequally spaced in time so as to increase the fraction of points within the fast phase, the CL of the faster time constant can be brought to within 5 %. Such a procedure is possible in practice by optimizing the data sampling profile.

In practice, determining the baseline can cause er-

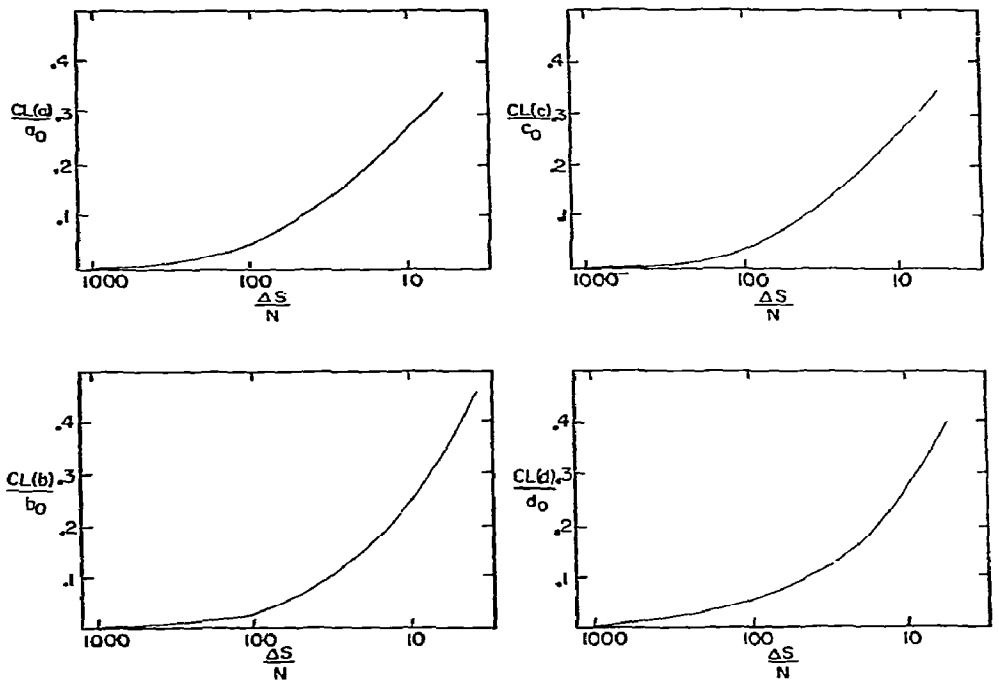


Fig. 1. Error in amplitudes and time constants as a function of $\Delta S/N$. Ordinate: Confidence limit (CL, approximately 3 × SE) of the calculated variable (a, b, c, d) divided by the true value of that variable; $CL(a)/a_0$, $CL(b)/b_0$, $CL(c)/c_0$, or $CL(d)/d_0$. Abscissa: Absolute difference in signal level before and after reaction divided by RMS noise, $\Delta S/N$. Calculated using the function $y = a_0e^{-b_0t} + c_0e^{-d_0t}$, where $a_0 = 0.5$, $b_0 = 1.0$, $c_0 = 0.5$, $d_0 = 5.0$. All four parameters were varied simultaneously using 100 data points equally spaced in time.

rors and the influence of such errors is shown in fig. 4. A 1 % error in the baseline causes about 5 % uncertainty in each of the four coefficients, emphasizing the importance of the accuracy of this measurement.

Baseline error is basically an instrumental problem which results from cooling after the temperature perturbation and/or very slow decay processes which are not complete by the time cooling occurs. These sources of baseline error can be minimized significantly by precise calibration procedures and automated data acquisition methods with varying sampling profiles. This has been found to essentially solve this problem for baseline corrections of a few percent [11].

The present method yields reliable values when the ratio of the time constants is as small as about 2.5, as shown in fig. 5. For more closely overlapping time constants, which display essentially a spectrum of coefficients, it is possible to use average techniques [18].

We have avoided data smoothing procedures since, without a priori knowledge of the form of the noise, such methods are expected to bias the data. If all data points have the same absolute accuracy and are equally spaced in time, no weighting factors should be used. This is because the present method does not introduce any weighting factors. However, weighting factors should be used if the data are recorded using a variable band width or if there are any unusual or time dependent noise distributions [9].

The above analysis has demonstrated the sensitivity and limitations of the method emphasizing a two exponential function. Selected analyses for a three exponential function have revealed similar trends. A presentation of the corresponding complete analysis for a three exponential function would be too extensive for this report. In principle, the method can be applied to a function having a larger number of exponential terms, provided the data justify such an analysis. Furthermore, the method can be extended to transcendental, nonhomogeneous and periodic functions making it useful for the analysis of a variety of data.

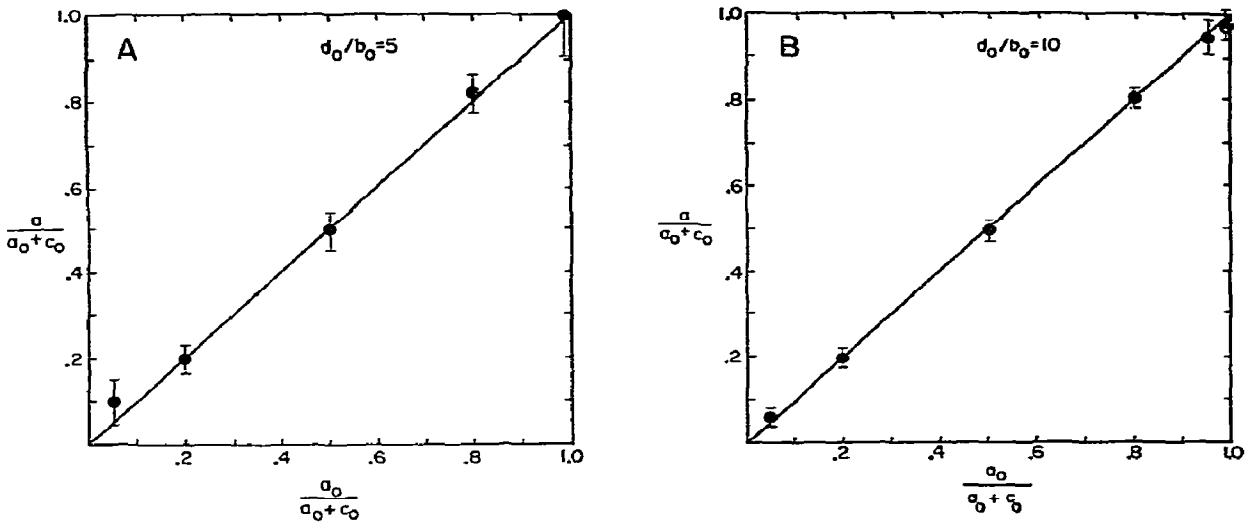


Fig. 2. Influence of relative amplitudes on determination of true amplitudes. Ordinate: Calculated relative amplitude. Abscissa: True relative amplitude. Definitions as in fig. 1, $\Delta S/N = 50$, 100 data points equally spaced in time, all four parameters were varied simultaneously for two different ratios of relaxation times, $d_0/b_0 = 5$ (A), 10 (B). Straight lines indicate unity slope.

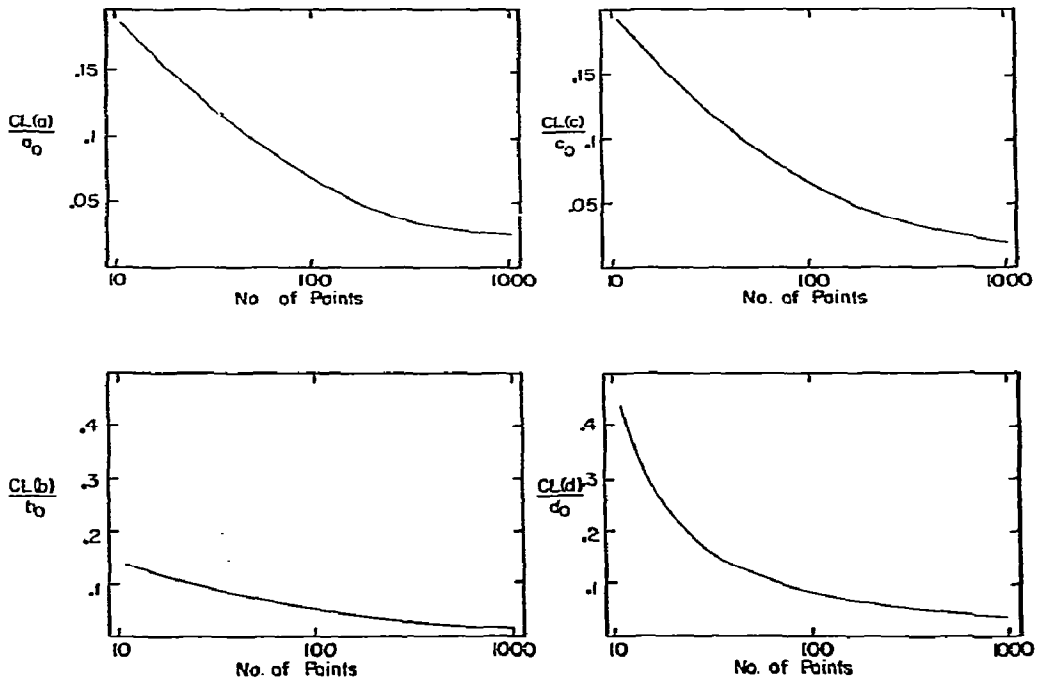


Fig. 3. Influence of the number of data points on the determination of amplitudes and time constants. Ordinate: As in fig. 1. Abscissa: Total number of data points spaced equally in time over identical time ranges. $\Delta S/N = 50$ and a_0, b_0, c_0, d_0 as in fig. 1.

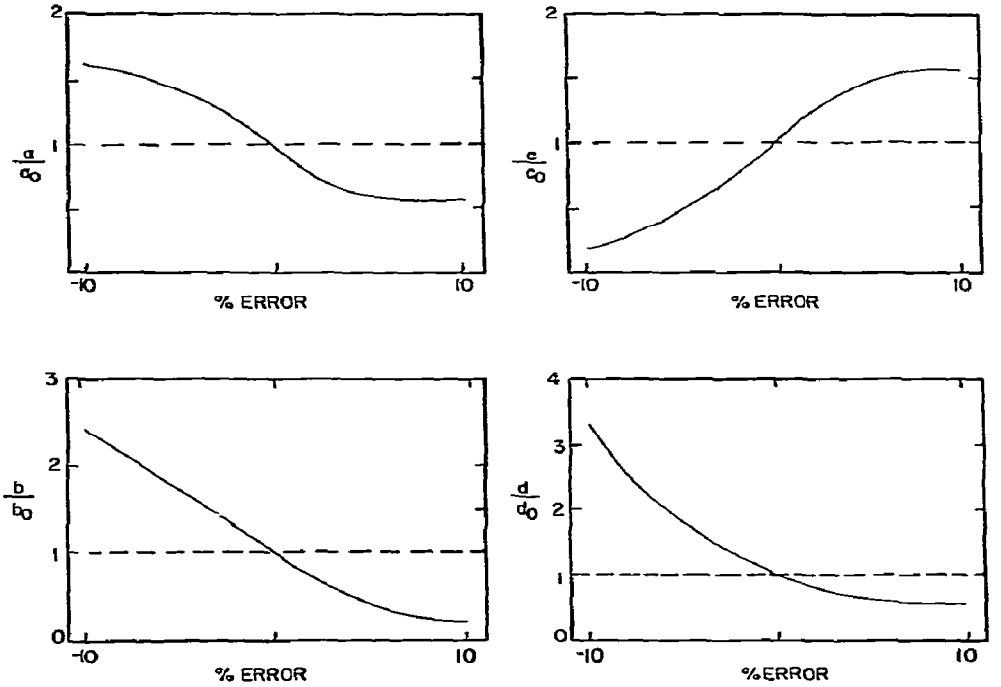


Fig. 4. Influence of baseline error on the determination of amplitudes and time constants. Ordinate: Parameters have same meaning as in fig. 1. Abscissa: Baseline error, as percent of total amplitude. All four parameters were varied simultaneously, using 100 equally spaced points. Other parameters as in fig. 1.

The computer program in which the present method has been used for analyzing relaxation data containing up to three exponentials includes options which allow for (1) determining baselines by fitting to polynomials, (2) making cooling corrections, (3) signal averaging from repetitive experiments, (4) amplitude normalization, (5) conversion of data from transmittance to absorbance, (6) data sorting and editing according to the RMS noise, (7) a routine for simulating and refitting relaxation spectra based upon measured relaxation times, amplitudes and RMS noise, and (8) evaluation of average relaxation times and amplitudes [18].

4. Experimental applications

We have applied this method of analysis to data from equilibrium centrifugation [11] and temperature-jump relaxation kinetics [14, 17] and cite briefly examples of the latter. Two proteins whose mechanism of oxygen binding are presently under investigation are hemocyanin and hemoglobin, examples of which are summarized in tables 3, 4, and fig. 6.

Numerically, there is "no satisfactory way" ([13], p. 255) of determing the number of exponential terms required to describe a set of experimental data. However, knowledge of the chemical properties, composition or structure of the system under study often provides information about the minimum number of parameters required to describe the time course of the reaction. We have used two numerical methods to attempt to determine the minimum number of exponential terms: (1) comparison of the RMS of each fit with the expected RMS based on a determination of the magnitude of noise in the data, and (2) an analysis of the randomness of the residuals of the fit. The determination of the number of exponentials is made using data from replicate experiments since both methods are sensitive to nonrandom noise.

We estimate the randomness of the residuals by fit-

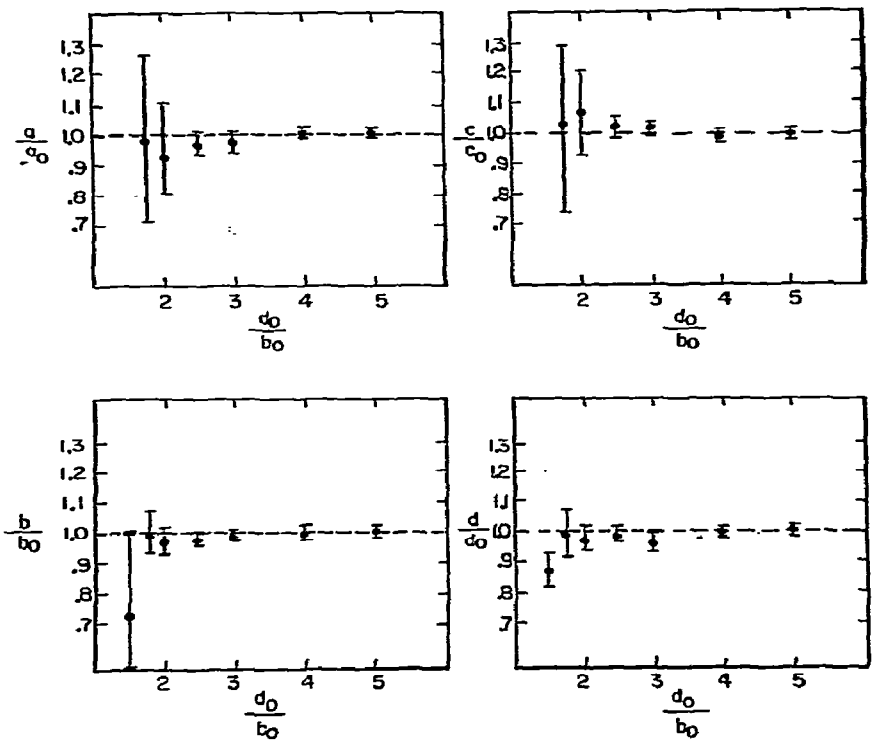


Fig. 5. Influence of the ratio of time constants on the determination of time constants and amplitudes. Ordinate: As in fig. 1, ± CL. Abscissa: Ratio of true time constants. All four parameters were varied simultaneously using 1000 data points equally spaced in time, equal amplitudes, and $\Delta S/N = 100$.

ting the residuals as a function of the independent variable (time) to four polynominals, of degree zero through three (yielding ten coefficents), and comparing the value of each coefficient with twice its standard error ([9], p. 258). If the residuals were truly random all of the coefficients would be approximately zero and statistically only one in ten would be larger than twice its standard error. This simple approach is utilized by counting the number of coefficients which are greater than twice the respective standard error thus giving an estimate of the nonrandomness which will vary between zero and ten, where the larger numbers indicate less randomness.

Table 2 demonstrates this measure of randomness for a test case where the data were calculated for two exponential terms. The RMS and nonrandomness are seen to decrease when the correct minimum number of exponential terms is used. (Observe that the confidence limits increase when analyzing this two exponential data as three exponentials.) Fitting to three exponentials does not improve the fit as judged from the RMS or the nonrandomness. In addition, the uncertainty of each coefficient is increased in the three exponential fit as seen in the values of CL, as expected from eq. (8).

Table 3 and fig. 6 show that under some conditions at least three exponentials are required to describe the kinetics of O_2 binding to hemoglobin. This can be seen from the decrease in the RMS of the fits and nonrandomness of the residuals. However, since even the three exponential fit yields a high value for the estimate of the nonrandomness and the value of ΔS/RMS is only about 75 % of the value expected on the basis of the RMS noise monitored prior to the temperature-jump,

Table 2

Analysis of the behavior of the nonrandomness of the residuals as a function of the number of exponential terms included in the fit. One thousand data points were calculated according to the function

$$y_i = 0.5 \exp^{10.0 t_i} + 0.5 \exp^{3.0 t_i},$$

where the time values were equally spaced from zero to one. These data were then perturbed with pseudo-random noise, normally distributed, such that the Δ signal-to-noise ratio, $\Delta S/\mathrm{RMS}$, was 50.0

Fit	RMS (volt)	$\Delta S/\mathrm{RMS}$	NR[1)]	$A_i/\Delta S \pm \mathrm{CL}$[1)]	$1/\tau(\mathrm{sec}^{-1}) \pm \mathrm{CL}$[1)]
One exp.	0.02994	33.2	9	100.0 ± 0.45	4.48 ± 0.028
Two exp.	0.01995	50.0	0	46.2 ± 2.5	10.77 ± 0.49
				53.8 ± 2.8	3.11 ± 0.07
Three exp.	0.01993	50.0	0	27.7 ± 52.4	13.6 ± 7.8
				32.6 ± 28.6	6.1 ± 9.0
				39.7 ± 58.6	2.8 ± 1.0

1) See text for meaning of NR, "nonrandomness", and CL, "confidence limit".

Table 3

Analysis of temperature-jump relaxation data from oxygen binding to human hemoglobin-A. Protein concentration 10^{-4} M (heme); 22 percent saturated with O_2; pH 7.0, 0.1 M phosphate plus 1.25×10^{-3} M inositol hexaphosphate; initial temperature = 16°C, $\Delta T = 4$°C; wavelength of observation 365 nm; heating time about 3 microseconds. Total change in optical absorbance $\Delta S = 4.42$ volt (0.0230 A). Data were recorded using an on-line computer for data acquisition [17]. One thousand ten-bit data points were recorded digitally at 100 kilohertz band width with a sampling frequency that decreased with the slope of the transient

Fit	RMS (volt)	$\Delta S/\mathrm{RMS}$	NR[1)]	$A_i/\Delta S \pm \mathrm{CL}$[1)]	$1/\tau(\mathrm{sec}^{-1}) \pm \mathrm{CL}$[1)]
One exp.	0.281	15.6	10	100.0 ± 0.89	201.0 ± 4.2
Two exp.	0.0617	71.2	8	67.4 ± 0.49	977.0 ± 10.7
				32.6 ± 0.32	62.0 ± 0.8
Three exp.	0.0259	169.0	7	57.0 ± 0.33	1386.0 ± 12.2
				33.7 ± 0.28	150.0 ± 2.2
				9.3 ± 0.25	19.5 ± 0.6

1) See text for the meaning of NR, "nonrandomness", and CL, "confidence limit".

$\Delta S/\mathrm{RMS} = 290$, it is possible that a fourth term is required to adequately characterize these data.

In contrast, the oxygen binding reaction with *Limulus* (horseshoe crab) hemocyanin monomer with a single binding site (table 4) is characterized by a minimum of two exponentials under some conditions. This conclusion is arrived at by noting that the RMS of the two exponential fit is approximately what would be expected from the magnitude of the noise before the temperature jump, $\Delta S/\mathrm{RMS} \approx 120$, and the marked decrease in the nonrandomness which results from including the second exponential.

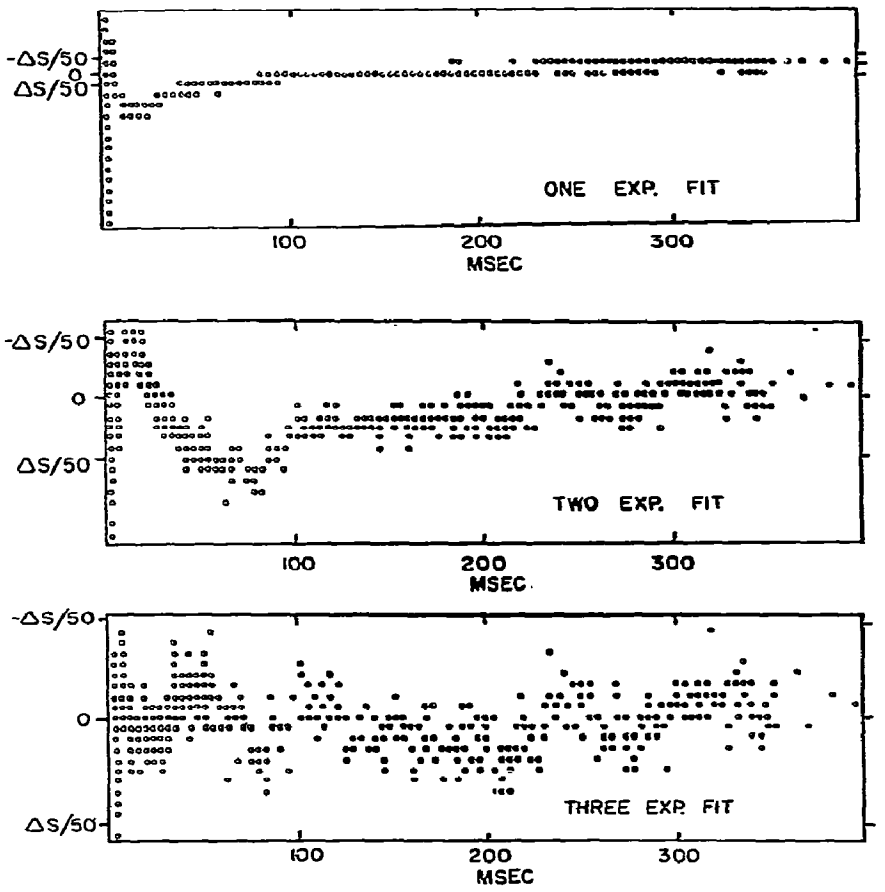


Fig. 6. Plots of residuals for the three fits of hemoglobin data as described in table 3. Ordinate: Deviation of residuals defined as the difference between the data point and the corresponding fitted function at that time. *Note scale differences.* Abscissa: Time in milliseconds. In each case all parameters were varied simultaneously. Baseline was determined independently and is the same for all fits. Experimental conditions and data recording are as described in table 3. Note the increasing randomness in the residuals with increasing number of time constants, this is an additional criterion for the significance of the minimum number of coefficients.

Acknowledgement

The advice of Dr. D.A. Yphantis and the stimulation of Dr. R. Dyson are gratefully acknowledged. This research was supported by the following grants: National Science Foundation, GJ-9 to the University of Connecticut Computer Center, GB-30825X (to D.A.Y.), GB-31097X (to T.M.S. and D.A.Y.). USPHS-NIH: GM-18472 (to T.M.S.) and Training Grant GM-00317 (M.L.J.).

References

[1] P.R. Bevington, Data reduction and error analysis for the physical sciences (McGraw-Hill, New York, 1969).
[2] G. Box, N.Y. Acad. Sci. 86 (1960) 792.
[3] B. Chu, Ann. Rev. Phys. Chem. 21 (1970) 2507.
[4] R.D. Dyson and I. Isenberg, Biochemistry 10 (1971) 3233.
[5] M. Eigen and L. DeMaeyer, Techniques of organic chemistry, eds. S.L. Friess, E.S. Lewis and A. Weissberger, 2nd Ed., Vol. VIII, Part II (Interscience, New York, 1963) p. 895.
[6] B. Fletcher, Computer J. 10 (1967) 392.

Table 4

Analysis of temperature jump relaxation data from oxygen binding to hemocyanin (*Limulus*). Protein concentration was 3 mg/ml and about 70 % saturated with oxygen: pH 8.5; 0.45 M KCl; 0.05 M Tris-HCl; initial temperature = 16°C with $\Delta T \approx 4$°C; heating time about 3 microseconds; wavelength of observation 363 nm. Total change in optical absorbance ΔS = 14.4 volt (−0.0072 A). Under these conditions the molecular weight is about 70 000, corresponding to one oxygen binding site per molecule [11]. Data were recorded as described in table 3

Fit	RMS (volt)	ΔS/RMS	NR[1)]	$A_i/\Delta S \pm$ CL[1)]	$1/\tau(\text{sec}^{-1}) \pm$ CL[1)]
One exp.	0.566	25.5	8	100.0 ± 0.37	93.3 ± 0.8
Two exp.	0.114	127.0	2	72.5 ± 0.55	172.0 ± 1.1
				27.5 ± 0.43	30.7 ± 0.4
Three exp.	0.112	129.0	2	63.9 ± 6.2	186.0 ± 5.8
				19.3 ± 2.9	63.9 ± 18.7
				16.8 ± 5.2	24.3 ± 2.8

1) See text for the meaning of NR, "nonrandomness", and CL, "confidence limit".

[7] H. Fujita, Mathematical theory of sedimentation analysis (Academic Press, New York, 1962).
[8] G. Hammes, Adv. Protein Chem. 23 (1968) 1.
[9] F.B. Hildebrand, Introduction to numerical analysis (McGraw-Hill, New York, 1956).
[10] G. Ilgenfritz and T.M. Schuster, Kinetics of Oxygen Binding to Human Hemoglobin, J. Biol. Chem., in press.
[11] M.L. Johnson, Ph.D. Thesis, Univ. of Connecticut, Storrs, Conn. (1973).
[12] S.L. Laiken and M.P. Printz, Biochemistry 9 (1970) 1547.
[13] M.E. Magar, Data analysis in biochemistry and biophysics (Academic Press, New York, 1972).
[14] R. Pennathur and T.M. Schuster, unpublished results.
[15] C.R. Rabl, in: Dechema Monographien: Technische Biochemie, ed. H.S. Rehm, Vol. 71 (Verlag Chemie, Weinheim, 1973) p. 187.
[16] R. Rigler and M. Ehrenberg, Quart. Rev. Biophys. 6 (1973) 139.
[17] T.M. Schuster and D. Hess, A Computer Assisted Data Acquisition System for Rapid Reaction Kinetics, in preparation.
[18] G. Schwarz, Rev. Mod. Phys. 40 (1968) 206.
[19] H. Strehlow and J. Jen, Chem. Instr. 3 (1971) 47.
[20] A.F. Yapel, Jr. and R. Lumry, in: Methods of biochemical analysis, ed. D. Glick, Vol. 20 (Wiley–Interscience, New York, 1971) p. 169.
[21] D.A. Yphantis, Biochemistry 3 (1964) 297.

BIOPHYSICAL CHEMISTRY 2 (1974) 42–48. © NORTH-HOLLAND PUBLISHING COMPANY

APPLICATION OF POLYELECTROLYTE LIMITING LAWS TO VIRIAL AND ASYMPTOTIC EXPANSIONS FOR THE DONNAN EQUILIBRIUM

David I. DEVORE* and Gerald S. MANNING
School of Chemistry, Rutgers University, New Brunswick, New Jersey 08903, USA

Received 2 January 1974

We have applied a general polyelectrolyte theory to an analysis of the Donnan equilibrium. The polyelectrolyte concentration is measured by a dimensionless parameter x, equal to the ratio of the equivalent polyelectrolyte concentration to the concentration of salt in the external compartment. For small x, virial series – expansions in powers of x – are developed for the Donnan salt-exclusion, osmotic pressure, and electromotive force. For large x, asymptotic expansions for these effects are presented. Polyion–polyion interactions are explicitly neglected, so that the physical significance of the virial series differs from its meaning in neutral polymer chemistry. Numerical results illustrate large deviations from ideal Donnan behavior as well as satisfactory agreement with published data on the salt-exclusion and emf effects. However, results for the Donnan osmotic pressure disagree with the data, except in the case of zero salt concentration in the external compartment, for which agreement is almost exact.

1. Introduction

Limiting laws for equilibrium and transport properties of dilute polyelectrolyte solutions, analogous to the Debye–Hückel–Onsager theory for ordinary ionic solutions, have recently been developed [1–7]. Agreement with experimental measurements appears to be quite good without recourse to adjustable parameters. In this article we extend the theory to the calculation of virial series for the three Donnan effects; that is, for the emf, pressure difference, and difference in simple salt concentration generated at equilibrium between two compartments when one contains a mixed solution of polyelectrolyte and simple salt and is separated from the other by a barrier which is permeable to the ions of the simple salt but not to the polyion.

The line charge model on which the general theory is based has been amply discussed elsewhere [1, 5, 7]. Here we wish only to recall the assumption [1] that interactions among different polyions contribute negligibly to the free energy. In view of the commonly held interpretation of the nth virial term as representing interactions among n polymers, it is important to realize that the virial expansions to be presented below do *not* have such significance. Rather, the nth term calculated here represents a contribution due to interactions of small counterions and co-ions with only *one* polyion. We will argue in a later section that polyion–polyion interactions are indeed negligible, at least for dilute solutions. Of course, for neutral polymers or polyelectrolytes in the presence of simple salt concentrations sufficiently high to screen out electrostatic interactions, polymer–polymer interactions are entirely responsible for the existence of the higher terms in the virial series.

2. Calculations

2.1. Donnan salt-exclusion

Unprimed quantities will refer to the compartment which contains the polyelectrolyte; primed, to the external (polyelectrolyte-free) compartment. Let n_s and n'_s, then, be the respective concentrations of simple salt (molecule cm^{-3}). We restrict attention to uni-uni-

* Present address: Department of Physiology, College of Physicians and Surgeons, Columbia University, New York, New York.

valent salt, so that n_s is also the concentration of the co-ion in the polyelectrolyte compartment. Now n_s may be expanded as a power series in the equivalent polyelectrolyte concentration n_e. Since n_s equals n_s' when n_e is zero, we may write

$$n_s - n_s' = n_e \sum_{i=1}^{\infty} A_i x^{i-1}, \tag{1}$$

where

$$x = n_e/n_s', \tag{2}$$

and the coefficients A_i are independent of concentration. This form for the series is dictated by an obvious dimensional analysis.

Alternate forms for the salt exclusion are obtained by considering the ratio n_2/n_2', where species 2 is the co-ion. Since $n_2 = n_s$ and $n_2' = n_s'$ eqs. (1) and (2) imply that,

$$n_2/n_2' = 1 + \sum_{i=1}^{\infty} A_i x^i. \tag{3}$$

The counterion ratio n_1/n_1' is obtained from eq. (3) by noting that $n_1 = n_e + n_2, n_1' = n_2'$:

$$n_1/n_1' = 1 + \sum_{i=1}^{\infty} \bar{A}_i x^i, \tag{4}$$

where

$$\bar{A}_1 = 1 + A_1, \qquad \bar{A}_i = A_i \ (i > 1). \tag{5}$$

The coefficients A_i may be determined starting from the general equilibrium criterion that the activities of the electroneutral simple salt component in each compartment must be equal:

$$\gamma_\pm^2 \, n_s(n_e + n_s) = (\gamma_\pm')^2 \, (n_s')^2, \tag{6}$$

where $\gamma_\pm, \gamma_\pm'$ are the respective mean activity coefficients of the simple salt. The required theoretical expression for $\gamma_\pm$ is given by the limiting law derived previously [1],

$$\ln \gamma_\pm = -\tfrac{1}{2} \, \xi \, n_e/(n_e + 2n_s), \qquad \xi \leqslant 1, \tag{7}$$

where it will be recalled that ξ is a dimensionless parameter defined by

$$\xi = e^2/\epsilon kTb, \tag{8}$$

with e the protonic charge, k Boltzmann's constant, T the absolute temperature, ϵ the dielectric constant of the bulk solvent, and b the average distance along the axis of the polyion chain between neighboring charged groups (contour length divided by total number of charged groups on the chain). Thus, ξ is a measure of the linear charge density of the polyion. There is also a limiting law for $\gamma_\pm$ valid for $\xi > 1$, but, as we shall see, it will not be needed. To conform with the requirement for the validity of the limiting law that the solution be very dilute (strictly speaking, infinitely dilute), we take $\gamma_\pm'$ equal to unity.

If eq. (7) is used in eq. (6) together with the expansion for n_s, eq. (1), a power series in n_e is obtained which is identically equal to zero. The coefficient of the nth term in the series contains A_n as well as all A_i for $i < n$. Thus, if each coefficient is set equal to zero, a recursion relation for the A_i is found. In this tedious but straightforward manner we have calculated A_i up to $i = 5$. For $\xi \leqslant 1$, then,

$$A_1 = -\tfrac{1}{2}(1 - \tfrac{1}{2}\xi)$$

$$A_2 = \tfrac{1}{8}(1 - \tfrac{1}{4}\xi^2)$$

$$A_3 = -\tfrac{1}{16}(\xi - \tfrac{1}{6}\xi^3)$$

$$A_4 = -\tfrac{1}{128}(1 - \tfrac{9}{2}\xi^2 + \tfrac{9}{16}\xi^4)$$

$$A_5 = \tfrac{1}{16}(\tfrac{1}{4}\xi - \tfrac{1}{3}\xi^3 + \tfrac{1}{30}\xi^5).$$

The above coefficients, together with eq. (1), provide a virial series for the salt exclusion provided that $\xi \leqslant 1$. If the polyion chain is characterized by a value of ξ which exceeds unity, we recall [1] that the general theory predicts a consequent instability which is resolved when sufficiently many counterions condense on the polyion to lower its *net* value of ξ to unity. Therefore the expansion for n_s when $\xi > 1$ may be obtained from that for $\xi \leqslant 1$ by the following transformation of the latter: $n_e \to \xi^{-1} n_e, A_i(\xi) \to A_i(1)$. The resulting coefficients for $\xi > 1$ are,

$$A_1 = -\tfrac{1}{4}\xi^{-1}, \quad A_2 = \tfrac{3}{32}\xi^{-2}, \quad A_3 = -\tfrac{5}{96}\xi^{-3},$$

$$A_4 = \tfrac{47}{2048}\xi^{-4}, \quad A_5 = -\tfrac{1}{320}\xi^{-5}.$$

2.2. Donnan osmotic pressure

The pressure difference Π_D between polyelectrolyte and external compartments is easily calculated from the difference of osmotic pressures in each compartment,

$$\Pi_D/kT = \phi(n_p + n_e + 2n_s) - 2\phi' n_s', \tag{9}$$

where ϕ and ϕ' are osmotic coefficients. The concentration n_p is that of the polyion; it is much smaller than the equivalent polyelectrolyte concentration n_e. In the derivation [1] of the limiting law for ϕ, it was permissible to neglect n_p in comparison with n_e. In the present context the result of this highly accurate approximation would be the omission of the ideal leading term in the virial series for Π_D. It is a trivial matter to retain n_p in the derivation of the limiting law, and the modified result is

$$\phi(n_p + n_e + 2n_s) = \phi_p n_e + n_p + 2n_s, \tag{10}$$

where

$$\begin{aligned} \phi_p &= 1 - \tfrac{1}{2}\xi, && \xi \leqslant 1, \\ &= \tfrac{1}{2}\xi^{-1}, && \xi > 1. \end{aligned} \tag{11}$$

The osmotic coefficient ϕ' is taken as unity to correspond with the requirement of infinite dilution. Eq. (9) reduces to the relation,

$$\Pi_D/kT = n_p + \phi_p n_e + 2(n_s - n_s'). \tag{12}$$

The virial series for Π_D is now immediately obtained by direct substitution of eq. (1) into eq. (12):

$$\Pi_D/kT = n_p + 2n_e \sum_{i=2}^{\infty} A_i x^{i-1}, \tag{13}$$

where the coefficients A_i are given through $i = 5$ in the previous subsection for both $\xi \leqslant 1$ and $\xi > 1$. Note the cancellation of the linear term in n_e.

The coefficient A_2 in eq. (13) has already been derived by Varoqui and Schmitt [9] for use in their discussion of diffusion in polyelectrolyte solutions.

2.3. Donnan emf

The electromotive force at equilibrium is obtained from the condition that the electrochemical potentials of the co-ions in each compartment must be equal (as must those of the counterions, a condition which can also be used to calculate the emf):

$$kT \ln \gamma_2 n_2 + z_2 e\psi = kT \ln \gamma_2' n_2' + z_2 e\psi', \tag{14}$$

or

$$\Delta\psi \equiv \psi - \psi' = -(kT/z_2 e) \ln (\gamma_2 n_2/\gamma_2' n_2'). \tag{15}$$

Here z_2 is the valence of the co-ion, ψ is the electrostatic potential of the polyelectrolyte compartment, and ψ' is the electrostatic potential of the external compartment. The limiting law for γ_2 is [1],

$$\ln \gamma_2 = -\tfrac{1}{2}\xi n_e/(n_e + 2n_s), \qquad \xi \leqslant 1. \tag{16}$$

The value of γ_2' is taken as unity to conform with the requirement for eq. (16) of infinite dilution.

Eq. (1) may be used to substitute for n_s in eq. (16) and an expansion of $\ln \gamma_2$ in powers of x is then obtained. An expansion of $\ln(n_2/n_2')$ is found from eq. (3). When substituted into eq. (15), these expansions lead to the result,

$$\Delta\psi \doteq -(RT/z_2 F) \sum_{i=1}^{\infty} B_i x^i, \tag{17}$$

where F is Faraday's constant and the B_i are given in terms of the A_i. We calculated the first three coefficients for $\xi \leqslant 1$:

$$B_1 = -\tfrac{1}{2}, \quad B_2 = \tfrac{1}{8}\xi, \quad B_3 = \tfrac{1}{16}(\tfrac{1}{3} - \tfrac{3}{4}\xi^2). \tag{18}$$

For $\xi > 1$, the coefficients may be obtained from eqs. (17) and (18) by the transformation $x \to \xi^{-1}x$, $B_i(\xi) \to B_i(1)$:

$$B_1 = -\tfrac{1}{2}\xi^{-1}, \quad B_2 = \tfrac{1}{8}\xi^{-2}, \quad B_3 = -\tfrac{5}{192}\xi^{-3}. \tag{19}$$

2.4. Donnan effects for large x

In the previous subsections we have developed vir-

ial series for the Donnan effects. These series are valid for small values of the concentration of the impermeable species, as measured by the dimensionless parameter $x = n_e/n'_s$. We may also inquire about the behavior of the Donnan equilibrium for large x, although the corresponding problem does not exist for neutral polymer solutions.

For large x, we may write the asymptotic expansion,

$$n_s/n'_s = \sum_{i=1}^{\infty} a_i x^{-i}. \tag{20}$$

By using this expansion in eqs. (6) and (7), we calculated the first three coefficients for $\xi \leqslant 1$:

$$a_1 = e^{\xi}, \quad a_2 = 0, \quad a_3 = -e^{2\xi}(1 + 2\xi). \tag{21}$$

The same "condensation transformation" applied previously yields the first three coefficients for $\xi > 1$,

$$a_1 = e\xi, \quad a_2 = 0, \quad a_3 = -3e^2\xi^3, \tag{22}$$

where e is the base of natural logarithms.

The Donnan osmotic pressure Π_D is obtained by applying eq. (20) to eq. (12) and omitting the negligible term n_p:

$$\Pi_D/kTn_e = \phi_p - \sum_{i=1}^{\infty} \bar{a}_i x^{-i}, \tag{23}$$

where ϕ_p is given by eq. (11) and

$$\bar{a}_1 = 2, \quad \bar{a}_i = -2a_{i-1} \quad (i \geqslant 2). \tag{24}$$

Finally, the Donnan emf may be calculated in a manner analogous to the case of small x. The result is

$$\Delta\psi = (RT/z_2F)[\ln x - \tfrac{1}{2}\xi + (1 + \xi)e^{\xi}x^{-2} + \ldots], \quad \xi \leqslant 1, \tag{25}$$

and

$$\Delta\psi = (RT/z_2F)(\ln x - \ln \xi - \tfrac{1}{2} + 2e\xi^2x^{-2} + \ldots), \quad \xi > 1, \tag{26}$$

where e is the base of natural logarithms.

2.5. Implicit method for any value of x

For $\xi \leqslant 1$ we may combine the general equilibrium condition, eq. (6), with the limiting law, eq. (7), to obtain the salt-exclusion ratio n_s/n'_s as an implicit function of x:

$$y(x + y)\exp[-\xi x(x + 2y)^{-1}] = 1, \quad \xi \leqslant 1, \tag{27}$$

where

$$y = n_s/n'_s. \tag{28}$$

For $\xi > 1$, the "condensation transformation" yields

$$y(\xi^{-1}x + y)\exp[-\xi^{-1}x(\xi^{-1}x + 2y)^{-1}] = 1, \quad \xi > 1. \tag{29}$$

For given values of x and ξ, y may be found numerically from eq. (27) or eq. (29) and used in eq. (12) for the Donnan pressure or in eq. (15) for the emf.

2.6. Reduction to ideal Donnan case

If electrostatic interactions among the various ionic species are neglected, and only the restriction of electroneutrality in each compartment retained, then the general criterion of equal activities of simple salt components reduces from eq. (6) to the relation,

$$n_s(n_e + n_s) = (n'_s)^2, \tag{30}$$

since the mean activity coefficient in each compartment becomes unity. Eq. (29) may be solved exactly as a quadratic equation for n_s:

$$n_s/n'_s = -\tfrac{1}{2}x + (1 + \tfrac{1}{4}x^2)^{1/2}. \tag{31}$$

If the r.h.s. of eq. (31) is expanded in powers of x, the first few terms are identical to eq. (3) with the A_i evaluated at $\xi = 0$. In other words, the ideal Donnan case is obtained from the polyelectrolyte theory by setting the charge density along the polyion chain equal to zero at fixed n_e. It may be verified that the same result holds for the other Donnan effects, for large as well as small x. That such must be the case can

Table 1
Example of Donnan salt-exclusion

x[a]	n_S/n'_S (ideal)	n_S/n'_S (calc)	n_S/n'_S (obs)
0.52	0.77	0.94	0.94
1.03	0.61	0.88	0.90
1.54	0.49	0.84	0.85
1.95	0.42	0.80	0.81
2.85	0.32	0.75	0.77
13.7	0.07	0.31	0.28
19.5	0.05	0.24	0.10

[a] For $x \leq 2.85$, $n'_S = 1.00 \times 10^{-2}$ mole liter^{-1}; for $x \geq 13.7$, $n'_S = 1.03 \times 10^{-3}$ mole liter^{-1}.

Table 2
Example of Donnan electromotive force

x[a]	$\Delta\psi$(ideal)[b]	$\Delta\psi$(calc)[b]	$\Delta\psi$(obs)[b]
0.52	- 6.7	- 3.4	- 1.8
1.03	-12.7	- 6.2	- 3.2
1.54	-18.3	- 8.8	- 5.0
1.95	-22.3	-10.7	- 5.6
2.85	-29.3	-14.6	- 8.1
13.7	-68.3	-41.1	-31.8
19.5	-77.0	-49.1	-40.0

[a] For $x \leq 2.85$, $n'_S = 1.00 \times 10^{-2}$ mole liter^{-1}; for $x \geq 13.7$, $n'_S = 1.03 \times 10^{-3}$ mole liter^{-1}.
[b] Units in mV.

be seen immediately from eq. (7), for example, which indicates that the value predicted by the polyelectrolyte limiting law for $\gamma_\pm$ is unity when $\xi = 0$.

3. Numerical results

In tables 1–3 we have presented numerical results and a comparison with published data. In all three tables the value of ξ has been chosen as 1.85 to obtain the calculated values. For $x < 3$ the virial series for small x were used; for $x > 10$ the asymptotic expansions for large x were used. The exact implicit method of calculation, was used only to check that for the

Table 3
Example of Donnan osmotic pressure

x[a]	Π/c (ideal)[b]	Π/c (calc)[b]	Π/c (obs)[b]
0.52	19.8	3.86	0.42
1.03	41.7	7.36	0.68
1.54	58.1	10.0	0.91
1.95	69.7	11.9	1.14
2.85	89.9	16.1	1.57
13.7	149	29.2	9.54
19.5	155	33.0	12.7

[a] For $x \leq 2.85$, $n'_S = 1.00 \times 10^{-2}$ mole liter^{-1}; for $x \geq 13.7$, $n'_S = 1.03 \times 10^{-3}$ mole liter^{-1}.
[b] Units in cm H_2O cm^{-2}/gram liter^{-1}.

worst cases – $x = 2.85$ for the virial series and $x = 13.7$ for the asymptotic expansion – the l.h.s. of eq. (29) deviated from unity by less than 5%. The ideal Donnan values were calculated from the thermodynamically exact (for the ideal case) eq. (31). The observed values are taken from the paper of Nagasawa et al. [10], which, as far as we are aware, is the only published account of a *complete* set of Donnan data (salt-exclusion, osmotic pressure, and emf). These authors used a sample of sodium polyvinyl alcohol sulfate with NaCl as the permeable salt. The polyion was characterized by a degree of esterification of 0.65. Since a vinylic polymer with one charge per monomer corresponds to the value $\xi = 2.85$ at 25°C, the proper value of ξ is 0.65 × 2.85 = 1.85, and this value was used in the theoretical calculations as mentioned above.

One may note from tables 1–3 the dramatic difference between both calculated and observed values and the ideal values. There has been a tendency in the literature to ascribe such differences to the "binding" of counterions by the polyion. However, as has been repeated stressed in previous publications [1–7], deviations from ideality due to the limiting laws are caused not only by a direct condensation of counterions on the polyion, a mode of interaction which may properly be called binding (although it is not governed by the mass-action law), but also by a diffuse Debye–Hückel type of interaction between the polyion and a surrounding ionic atmosphere which includes co-ions as well as counterions. The word "binding" may not be used to

describe such long-range interactions, just as it cannot, and is not, used to describe Debye–Hückel deviations from ideality in ordinary ionic solutions. For example, the important coefficient A_1 equals $-\frac{1}{2}$ for the ideal case $\xi = 0$ but rises to $-\frac{1}{4}$ when $\xi = 1$, even though no condensation occurs for intermediate values of ξ and the entire effect is due to the ion atmosphere.

If attention is now given to a comparison of calculated with observed values, it will be seen that the results are mixed. For the salt-exclusion ratio (table 1) there is almost exact agreement except at $x = 19.5$; for the emf (table 2) the agreement is reasonably good, but the calculated values are systematically less than those observed; the calculated values of the osmotic pressure (table 3) are an order of magnitude greater than the observed values for small x, while for the two large values of x, they are greater by a factor of 3.

We believe that the anomaly at $x = 19.5$ in table 1 may be due to experimental difficulties in the determination of n_s at such low values of the salt concentration. We have noted that in table 1 of the paper by Nagasawa et al. [10] the independently measured value of the chloride ion *activity* in the polyelectrolyte compartment is larger by a factor of two than the measured chloride *concentration*. Only for this entry ($x = 19.5$) is the activity found to be larger than the concentration; moreover, an activity coefficient equal to two cannot be explained on any convincing basis. That it is the concentration and not the activity which is probably in error is indicated by the fact that the product of the listed chloride activity with the listed sodium activity is in good agreement with the square of the known sodium chloride mean activity in the external compartment.

We are unable to offer any explanation for the serious disagreement between calculated and observed values of the Donnan osmotic pressure. In view of previous interpretations of the virial series, there may be some temptation to ascribe the discrepancy to the neglect in the theory of polyion–polyion interactions. This possibility, however, is remote. It is not consistent with the good results obtained in tables 1 and 2, for example. Nor is it consistent with the observation that disagreement between theory and experiment is *least* in table 3 for the *higher* values of x, for which polyion–polyion interactions would be greatest. With this point in mind we also compared our calculations with the more recent osmotic pressure data of Takahashi et al. [11] for the Na polystyrenesulfonate–NaCl system. Again, calculated values for small x were almost an order of magnitude greater than those observed, but for $x = \infty$ (i.e., no extraneous salt, a case not reported in ref. [10]) agreement was almost exact. Moreover, the general theory has been found to be reliable for a large variety of equilibrium and transport properties [5], a fact which also suggests that polyion–polyion interactions do not contribute in an important way.

Finally, we wish to point out that some experimental work has focused on the second virial coefficient, a quantity which, according to the present theory, does not have the special significance for dilute polyelectrolyte solutions which it possesses in neutral polymer chemistry. For $x = 1.54$, for example, the third virial term is fully half as large as the second for the system analyzed in tables 1–3. Moreover, the terms are of alternating signs (in particular, the third virial coefficient is negative) and a plot of the first five virial terms shows that Π/c does not appear to deviate much from linearity, so that a purely experimental plot may easily be misinterpreted as reflecting only the second virial term, whereas it may in fact be determined by the first few virial terms. Therefore, we have not regarded as reliable any reported values of the second virial coefficient, but have chosen to use values of Π/c.

Note added in proof

It is interesting that if the osmotic pressure data are converted to osmotic coefficients by use of eq. (9) together with measured pressure and concentrations, then the disagreement with theory does not appear to be so bad. A typical example is ϕ(obs) = 0.3, while a calculation from the appropriate limiting law in ref. [1] gives ϕ(calc) = 0.4.

References

[1] G.S. Manning, J. Chem. Phys. 51 (1969) 924.
[2] G.S. Manning, J. Chem. Phys. 51 (1969) 934.
[3] G.S. Manning, J. Chem. Phys. 51 (1969) 3249.
[4] G.S. Manning, Biopolymers 9 (1970) 1543.
[5] G.S. Manning, Ann. Rev. Phys. Chem. 23 (1972) 117.
[6] G.S. Manning and A. Holtzer, J. Phys. Chem. 77 (1973) 2206.

[7] G.S. Manning, in: Charged and Reactive Polymers, I, Polyelectrolytes, E. Selegny, ed. (Reidel, Dordrecht, 1974) to be published.
[8] R.W. Armstrong and U.P. Strauss, in: Encyclopedia of polymer science and technology, H.F. Mark, N.G. Gaylord and N.M. Bikales, Eds., Vol. 10 (Wiley, New York, 1969).
[9] R. Varoqui and A. Schmitt, Biopolymers 11 (1972) 1119.
[10] M. Nagasawa, A. Takahashi, M. Izumi and I. Kagawa, J. Polymer Sci. 38 (1959) 213.
[11] A. Takahashi, T. Kato and M. Nagasawa, J. Phys. Chem. 74 (1970) 944.

BIOPHYSICAL CHEMISTRY 2 (1974) 49–52. © NORTH-HOLLAND PUBLISHING COMPANY

PROTON MAGNETIC RESONANCE STUDIES OF HUMAN ADULT HEMOGLOBIN IN WATER †

Joseph J. BREEN, Dolores A. BERTOLI, Josef DADOK and Chien HO *

Received 25 January 1974

The preferential binding of oxygen to the α hemes of normal human adult hemoglobin in the presence of organic phosphates in D_2O at neutral pD has been confirmed in H_2O. Additionally, it has been found that the preferential binding of oxygen is pH dependent with random ligation being observed at pH ~ 9.

1. Introduction

Proton magnetic resonance (PMR) studies of human normal and abnormal hemoglobins have successfully provided detailed and unique information about the heme environment, functional properties of the α and β heme groups, and the subunit interactions during the ligand binding process [1–3]. Such studies normally utilize deuterium oxide as the solvent medium in order to reduce the intense proton signal from water, to simplify the spectra by eliminating signals from exchangeable protons, and to facilitate the observation of the aromatic proton resonances close to the water proton resonance. It is known however, that deuteration of proteins may not only alter their conformations but also their functional properties. The effects of partial deuteration on the properties of human adult hemoglobin (Hb A) have been reported and suggest that the cooperativity of oxygen binding as measured by the Hill coefficient, n, is greatly reduced by partial deuteration with a subsequent return to the normal value upon extensive deuteration [4]. These observations have important implications to all studies of proteins involving D_2O as the solvent.

In order to confirm the validity of our PMR studies of hemoglobins in D_2O, we have repeated our PMR experiments in H_2O in the presence and absence of organic phosphates. Additionally, we have extended our PMR studies to monitor oxygen binding to hemoglobin as a function of pH.

2. Experimental

2.1. Materials

HbCO A was prepared from fresh whole blood obtained from a local blood bank by standard procedure [5]; distilled water was used to lyse the cells. The hemoglobin was made phosphate-free by gel filtration with a Sephadex G-25 column (2.5 x 40 cm); 0.01 M Tris·HCl–0.1 M NaCl, pH 7.45, was used as a buffer [6]. Stock solutions of either 0.15 M 2,3-diphosphoglycerate (P_2-glycerate) obtained from Calbiochem or 0.09 M inositol hexaphosphate (Ins-P_6) obtained from Sigma and 1.0 M Bis-Tris (Aldrich) were added, so the solutions used for measurement were ~ 9% Hb A, 32mM P_2-glycerate, 0.1 M Bis-Tris·HCl at pH 6.8, or 11% Hb A, 10 mM Ins-P_6, 0.1M Bis-Tris·HCl at pH 6.6. The pH of the solutions was determined with a Radiometer Model 4 pH meter equipped with a Backman 39030 frit junction combination electrode. The carbon monoxide was re-

† From the Department of Biophysics and Microbiology and the Department of Biochemistry, Faculty of Arts and Sciences, University of Pittsburgh, Pittsburgh, Pennsylvania 15260 USA (J.J.B., D.A.B., and C.H.) and the Mellon Institute of Science, Carnegie-Mellon University, Pittsburgh, Pennsylvania 15213 USA (J.D.). Part of this paper was presented at the 17th Annual Meeting of the Biophysical Society, Columbus, Ohio, USA February 27 – March 2, 1973.

* Address all correspondence to Dr. C. Ho, Department of Biophysics and Microbiology, University of Pittsburgh, 378 Crawford Hall, Pittsburgh, Pennsylvania 15260, USA.

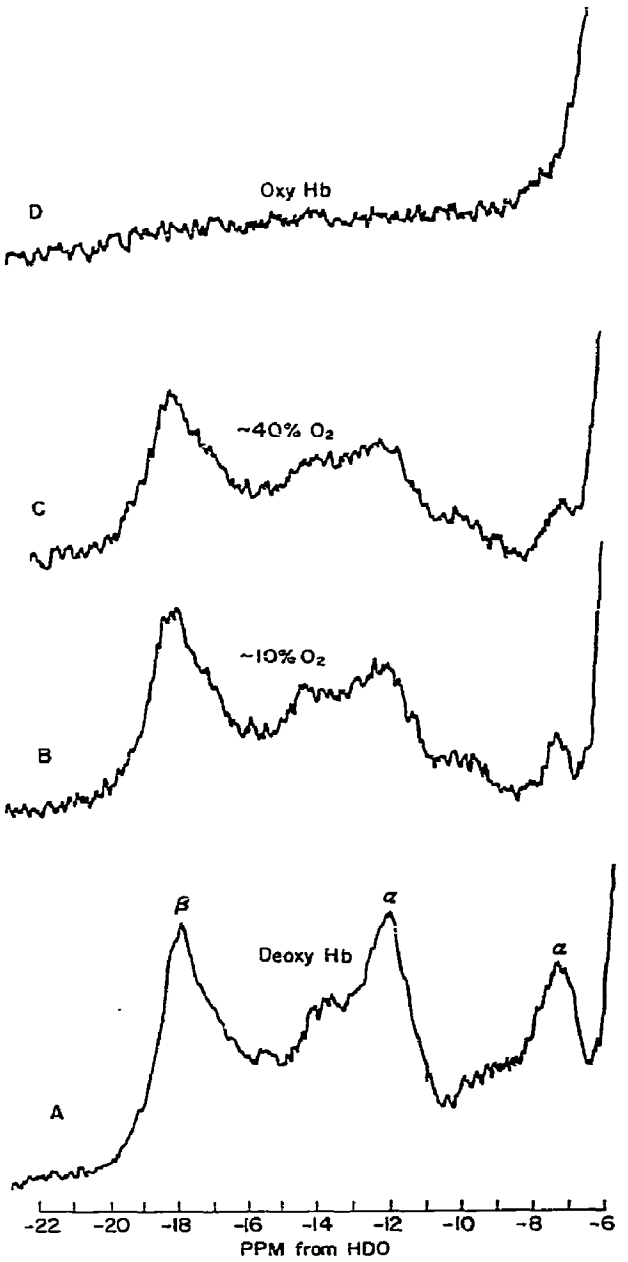


Fig. 1. 250 MHz PMR spectra of HbA as a function of O_2 saturation in 0.1M Bis-Tris buffer plus 32 mM 2,3-diphosphoglycerate at pD 6.75 and 31°C. Deuterium oxide is the solvent medium. This figure taken from ref. [11] is included to allow comparison of PMR spectra obtained in deuterium oxide and water.

placed by oxygen by flushing the solution in a rotory evaporator in an ice-water bath under a Sylvania 150-W flood lamp. Oxygen was removed by flushing the solution with purified nitrogen. Partially oxygenated samples were obtained by mixing deoxy and oxyhemoglobin in the appropriate proportions.

2.2. Method

PMR spectra were obtained on the MPC-HF 250MHz superconducting nuclear magnetic resonance spectrometer [7]. 5mm NMR tubes were used and the probe temperature was 31°. The lines were of low intensity and relatively broad, thereby requiring signal to noise improvement by standard time averaging techniques and the utilization of high transmitter power and short sweep times (0.8 sec). The number of scans per sample was de-

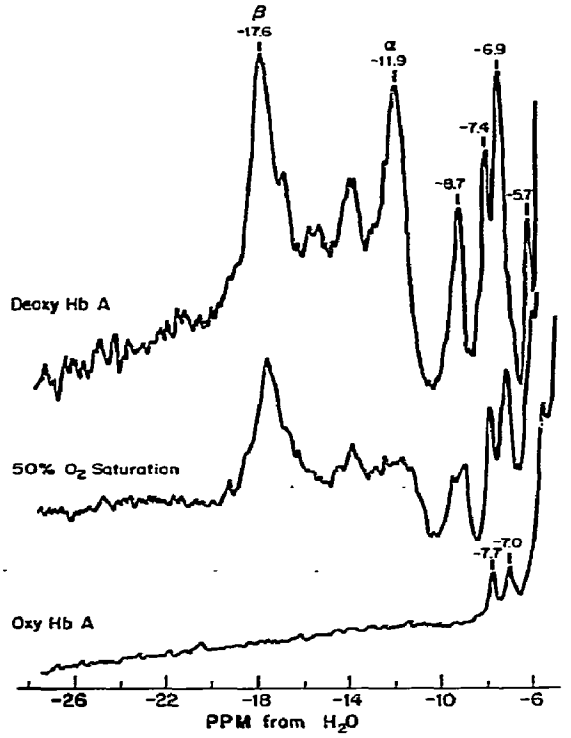


Fig. 2. 250 MHz PMR spectra of HbA in 0.1M Bis-Tris buffer plus 10 mM inositol hexaphosphate at pH 6.6 in 100% H_2O at 31°C. The HDO signal is 4.72 ppm downfield from the proton resonance of a standard, 2,2-dimethyl-2-silapentane-5-sulfonate (DSS) at 31°C.

pendent upon the degree of ligand saturation with the general requirement between 100 and 500 transients. PMR spectra of hemoglobin in water may be obtained routinely with the spectrometer in this configuration. Chemical shifts are referenced to the H_2O signal and are accurate to ±0.1 ppm.

3. Results

Figs. 1 and 2 show the hyperfine shifted PMR signals of deoxyhemoglobin A in 32 mM P_2-glycerate and 10 mM Ins-P_6 at various stages of oxygenation in D_2O and H_2O respectively. The three prominent hyperfine shifted proton resonances for the D_2O sample have been previously reported and assigned to the α (−7.4 and −12.1 ppm) and β (−17.9 ppm) chains [8]. The downfield resonances of the α and β chains appear to experience a small diamagnetic shift in H_2O while the upfiled portion of the hyperfine region presents additional signals from exchangeable N–H protons [9, 10].

In both H_2O and, as previously described, D_2O [11] the addition of oxygen to the deoxygenated samples at pH 6.6 results in the preferential decrease in the intensity of the low field α resonances as compared with that resonance attributed to the β chains. This selective diminuation in the α signal's intensity is indicative of preferential ligand binding to the iron atom of the α heme groups with the loss of the iron's paramagnetic moment and occurs in the presence of organic phosphate. In contrast to the preferential binding of oxygen observed at pH 6.6, one finds random ligation of oxygen at pH 9.3 for Hb A in the presence of either P_2-glycerate or Ins-P_6 (fig. 3). While it is known that the binding of organic phosphates to hemoglobin is pH dependent and that this binding decreases above pH 6.5, Bunn and Guidotti [12] have examined the effect of Ins-P_6 on the P_{50} of hemoglobin, i.e., the partial pressure of O_2 (in Torr) necessary to saturate 50% of the hemoglobin, and found it to be substantial at pH 9.0 indicating significant binding of Ins-P_6 to deoxyhemoglobin even at pH 9.0. This is attested to in the PMR spectra by a reduced downfield shift of the β chain resonance in the presence of organic phosphate. The addition of organic phosphates shifts the β-chain signal downfield ca. 1.0 ppm at neutral pH [13, 14] and this perturbation is reduced at high pH to 0.3 ppm with the α-chain signals undergoing no chemical shift changes. The shift of the β-chain signal may be considered to be a direct result of the interaction between the organic phosphate with the binding site located on the β chains of the hemoglobin tetramer.

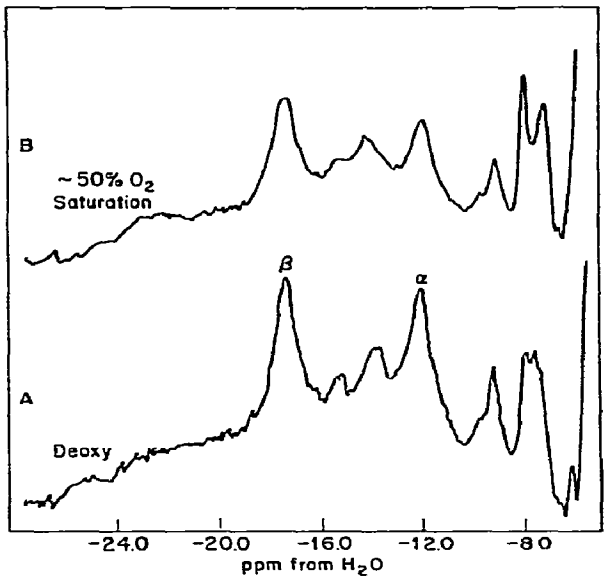


Fig. 3. 250 MHz PMR spectra of HbA in 0.05M glycine buffer plus 9.4 mM inositol hexaphosphate at pH 9.3 in 100% H_2O at 31°C. The HDO signal is 4.72 ppm downfield from the proton resonance of a standard, 2,2-dimethyl-2-silapentane-5-sulfonate (DSS) at 31°C.

Diamagnetic HbO_2 and HbCO samples in H_2O have two signals of approximately equal intensity at −7.7 and −7.0 ppm which are not observed in deuterated media. This spectral region of the chemically modified hemoglobin des(His-146β) presented data which were indistinguishable from normal hemoglobin thereby precluding assignment of these exchangeable PMR signals to an alkaline Bohr proton at β146. More significantly, however, was the observation of random binding of oxygen for Hb des(His-146β) at neutral pH in the presence of organic phosphates [15].

4. Discussion

These results confirm the preferential binding of oxygen molecules to the α-chain hemes of normal Hb A in the presence of high concentrations of organic phoshates at neutral pH. This preference exists under

these conditions in both D_2O and H_2O thereby substantiating the premise that experimental information obtained from PMR studies of hemoglobins in D_2O is relevant to those carried out in H_2O.

Additionally, it has been shown here that hemoglobin's ligand binding is pH dependent with random ligation of oxygen being observed at alkaline pH. This pH dependence in normal Hb A when coupled with the observation of random ligation in the chemically modified Hb des(His-146β) at neutral pH serves to suggest the importance of the conformation of the carboxyl terminal residue of the β chains in the ligand binding process of human hemoglobin. This residue is believed to stabilize the deoxy conformation through the formation of salt bridges with lysine 40α by its carboxyl group and with the aspartate 94β by its imidazole side chain [16]. The disruption of these salt bridges facilitates the transition to the liganded or oxy conformation [16]. The recent direct measurement of the histidine 146β pK value of 8.0 for deoxyhemoglobin and of 7.1 for carbonmonoxyhemoglobin provides support for the reasonableness of the pH dependence observed in normal adult hemoglobin [17]. The importance of the histidine 146β residue in eliciting α and β heme functional non-equivalence in the ligand binding process of hemoglobins is presently under continued investigation.

Acknowledgement

This work was supported by research grants from the National Institutes of Health (HL-10383, HL-15165, and RR-00292) and National Science Foundation (GB 37096X). J.J.B. is a recipent of the Public Health Service Postdoctoral Fellowship (1 FO 2 GM55395-01).

References

[1] D.G. Davis, S. Charache and C. Ho, Proc. Natl. Acad. Sci. US 63 (1969) 1403.
[2] D.G. Davis, T.R. Lindstrom, N.H. Mock, J.J. Baldassare, S Charache, R.T. Jones and C. Ho, J. Mol. Biol. 60 (1971) 101
[3] T.R. Lindstrom, J.S. Olson, N.H. Mock, Q.H. Gibson and C. Ho, Biochem. Biophys. Res. 45 (1971) 22.
[4] S. Tomita and A. Riggs, J. Biol. Chem. 245 (1970) 3104.
[5] D.L. Drabkin, J. Biol. Chem. 164 (1946) 703.
[6] M. Berman, R. Benesch and R.E. Benesch, Arch. Biochem. Biophys. 145 (1971) 236.
[7] J. Dadok, R.F. Sprecher, A.A. Bothner-by and T. Link, Abstracts, Section C-2 of the 11th Experimental NMR Conference, Pittsburgh, Pa. (1970).
[8] T.R. Lindstrom, C. Ho and A.V. Pisciotta, Nature New Biol. 237 (1972) 263.
[9] D.J. Patel, L. Kampa, R.G. Shulman, T. Yamone and M. Fujiwara, Biochem. Biophys. Res. Commun. 40 (1970) 1224.
[10] J.D. Glickson, C.C. McDonald and W.D. Phillips, Biochem. Biophys. Res. Commun. 35 (1969) 492.
[11] T.R. Lindstrom and C. Ho, Proc. Natl. Acad. Sci. US 69 (1972) 1707.
[12] H.F. Bunn and G. Guidotti, J. Biol. Chem. 247 (1972) 2345.
[13] S. Ogawa and R.G. Shulman, J. Mol. Biol. 70 (1972) 315.
[14] C. Ho, T.R. Lindstrom, J.J. Baldassare and J.J. Breen, Ann. N.Y. Acad. Sci. 222 (1973) 21.
[15] J.J. Breen, J.V. Kilmartin and C. Ho, unpublished results.
[16] M.F. Perutz and L.F. Ten Eyck, Symp. Quant. Biol. 36 (1971) 295.
[17] J.V. Kilmartin, J.J. Breen, G.C.K. Roberts and C. Ho, Proc. Natl. Acad. Sci. US 70 (1973) 1246.

BIOPHYSICAL CHEMISTRY 2 (1974) 53–63. © NORTH-HOLLAND PUBLISHING COMPANY

PHYSICAL CHEMICAL STUDIES OF SHORT-CHAIN LECITHIN HOMOLOGUES. PHASE SEPARATION AND LIGHT SCATTERING STUDIES ON AQUEOUS DIOCTANOYLLECITHIN SOLUTIONS

R.J.M. TAUSK, C. OUDSHOORN and J.Th.G. OVERBEEK
Van 't Hoff Laboratory, State University, Transitorium III, Padualaan 8, Utrecht – De Uithof, The Netherlands

Received 31 January 1974

Some phase separation phenomena in aqueous dioctanoyllecithin solutions including the effects of NaCl and on the phase diagram are reported. At low electrolyte concentrations (below 0.2 M) both salts cause the upper c solute temperatures (u.c.t.) to decrease, probably due to a decrease of electrostatic attraction between the lipid r cules. At higher salt concentrations the effect of LiI continues in the same direction (salting-in) but NaCl leads t increase of the u.c.t. (salting-out).

Micellar weight determinations could be performed at room temperature in homogeneous lecithin solutions c taining 0.2 M LiI. An attempt was made to interpret the light scattering data with the help of the open associatic model (equal association constants for aggregation steps beyond a certain step) and the Flory–Huggins type of thermodynamic nonideality. The angular dependence of the light scattering points to very large and extended mi celles. The radii of gyration are approximately proportional to the square root of the micellar weights.

1. Introduction

Characterisation of the association properties of dioctanoyllecithin (diC_{8-}) is important for the understanding of certain biochemical and physical chemical phenomena. In the course of the study [1] of the kinetics of the hydrolysis of different lecithin homologues by pancreatic phospholipase A it was found that the enzyme activity is strongly dependent on the chain length of the lecithin, probably through a dependence on the lipid aggregation structure. The highest activities were encountered with dioctanoyllecithin as the substrate. Dissolved in water this lecithin associates, at concentrations just above the the critical micelle concentration (CMC) into thermodynamically stable aggregates (micelles), whereas the next higher homologue (diC_{9-}) forms liquid crystalline dispersions (liposomes). At slightly higher concentrations of diC_{8-} a phase separation sets in. The enzyme kinetics were actually studied in these inhomogeneous solutions.

Pugh [2] has performed light scattering measurements to obtain the micellar weight of diC_{8-}. In his thesis he reported a micellar weight of but gave no further details. Furthermore he mention a phase separation.

Even in homogeneous solutions the inter of the aggregation phenomena will be hamp the strong thermodynamic nonideality conn with the proximity of the phase separation. ficulties have also arisen during studies on o factants [3–5].

We first studied the demixing of dioctan in aqueous solutions. We were interested in fluence of inorganic electrolytes on the dem two reasons. In the first place the enzymati ysis by phospholipase A reveals large salt ef Moreover salt effects on the demixing migh formation on the electrostatic contribution free energy of mixing. The influence of the out agent NaCl and the salting-in electrolyte the CMC [6] have been discussed in part I c series [7] (hereafter referred to as I). The ir of NaCl on the micellar weights of diC_{6-} an

lecithin has been described in II [8]. Correlations between effects on the CMC's and the phase diagrams are to be expected.

To study the association phenomena we performed light scattering experiments in homogeneous solutions aiming in particular at the influence of temperature changes when approaching the phase separation. The study of the influence of the lecithin concentration was facilitated by the finding that the phase separation at room temperature could be suppressed by addition of LiI.

2. Methods and materials

The synthesis and purification of dioctanoyllecithin as well as the preparation of the aqueous solutions, containing variable concentrations of electrolytes have been described in I [7]. The lecithin was not completely free of surface active impurities since the γ versus log c curve (γ = surface tension) showed a minimum around the CMC [7].

2.1. Phase diagram

Phase separation was determined in 1 ml graduated pipets in a regulated constant temperature bath. A glass joint with a stopper was fused to the lower end of each pipet. This spoiled the calibration of the lower part, which was therefore filled with mercury. The open upper end of the pipet was sealed with parafilm (Marathon). To homogenise the solution at elevated temperatures a small piece of iron sealed in a plastic tube was moved up and down in the pipet by a magnet. The temperature was slowly lowered and the cloud points were noted visually. A few times the solutions were left for 12 to 24 hours at temperatures below the cloud points in order to determine the phase volumes and concentrations in both phases. However, with increasing duration of the experiments reproducibility of the diagrams decreased and the cloud point curves tended towards lower temperatures, probably due to decomposition of the diC_{8}-. Since rather limited amounts of material were available dilution series were carried out in the pipets. Lecithin monohydrate concentrations were determined from phosphor analysis [9].

2.2. Light scattering

The light scattering technique and the calibration of the Fica 50 instrument of the Société Française d'Instruments de Contrôle et d'Analyse have been described in II [8]. The angular dependence of the scattering was checked with aqueous solutions of fluorescein, bovine serum albumin and polystyrene latex (diameter: 109 nm) and with a solution of poly-α-methylstyrene [10] (molecular weight: 1×10^6) in toluene. The temperature of the toluene outer vessel was regulated and the temperature in the light scattering cells was recorded with a thermistor. We never waited for full temperature equilibrium since the experiments had to be performed rather quickly due to the decomposition of the lecithin. The solutions were filtered under pressure through millipore filters (0.45 or 0.1 μ). Before measuring the light scattering of homogeneous solutions at high dilutions and room temperature (25.0°C, 0.2 M LiI) the cuvettes were centrifuged for 1 hour at 20000 rpm. Before studying the temperature dependence of the scattering in systems showing phase separation at 45°C the solutions were filtered at elevated temperatures (ca 80°C).

2.3. Refractive index increments

The increment at room temperature was measured in a Rayleigh interferometer (Aus Jena). The temperature dependence of the increment was obtained with a Brice-Phoenix differential refractometer. The instrument was calibrated with sucrose solutions.

3. Light scattering equations

The light scattering, in excess over the solvent scattering, from a solution containing various macromolecules with different molecular weights M_i, weight fractions f_i and equal refractive index increments dn/dc is given [11] by the equation

$$Kc(1+\cos^2\theta)/R_\theta = \{M_w\langle P_1(\theta,c)\rangle\}^{-1} + c\langle Q(\theta,c)A_{ij}(c)\rangle + \ldots . \quad (1)$$

R_θ stands for the excess Rayleigh ratio at an angle θ to the incident beam, if no polariser or analyser are used. $K = 2\pi^2 n_0^2 (dn/dc)^2 \lambda_v^{-4} N_0^{-1}$, where n_0 is the

refractive index of the solvent, λ_v is the wavelength in vacuum and N_0 is Avogadro's constant. c is the total solute concentration in mass per unit volume. $A_{ij}(c)$ is a concentration dependent interaction parameter, discussed in more detail in II. $\langle P_1(\theta, c)\rangle$ is an average of angle and concentration dependent factors, resulting from intramolecular (internal-) interferences. $Q(\theta, c)$ also corrects for interferences but contains contributions from both intra- and intermolecular (external-) interferences. M_w equals the weight average molecular weight given by

$$M_w = \sum_i f_i M_i = \int_0^\infty M f(M)\,dM \qquad (2)$$

where $f(M)$ stands for the weight distribution function of the macromolecules.

By using the "single contact approximation" Zimm [12] showed that for large molecules at low concentrations in a two component system $Q(\theta, c)$ equals unity. Vrij and van den Esker [13] obtained the same result by quite a different method. $Q(\theta, c)$ is very difficult to estimate in our case. As an approximation we will also assume $Q = 1$, although our micelles might in fact have structures very different from flexible polymers. For particles with rather small radii of gyration, r_g, or small angles, θ, the light scattering equation reads:

$$Kc(1 + \cos^2\theta)/R_\theta = A + B\sin^2(\theta/2) \qquad (3)$$

with

$$A = (RT)^{-1}\,d\Pi/dc = 1/M_{w,app.} = 1/M_w + A_2 c \qquad (4)$$

and

$$B = 16\pi^2(3\lambda^2)^{-1}\langle r_g^2\rangle_z/M_w = 16\pi^2(3\lambda^2)^{-1}q^2. \qquad (5)$$

Π is the osmotic pressure and λ equals the wavelength in solution ($\lambda = \lambda_v/n$). For simplicity's sake we abbreviated $\langle A_{ij}(c)\rangle$ by A_2 as is common practice. $\langle r_g^2\rangle_z$ stands for the z-average of the radius of gyration squared and is defined by

$$\langle r_g^2\rangle_z = M_w^{-1}\int_0^\infty M f(M) r_g^2\,dM. \qquad (6)$$

Considering the fact that our system consists of only two components the use of $d\Pi/dc$ in eq. (4) is justified. The interpretation in terms of several lecithin species (second equality in eq. (4)) implies that relations between concentrations and activity coefficients (incorporated in A_2) exist [8]. Eqs. (3) and (4) form the basis of the well known "Zimm plots" [12].

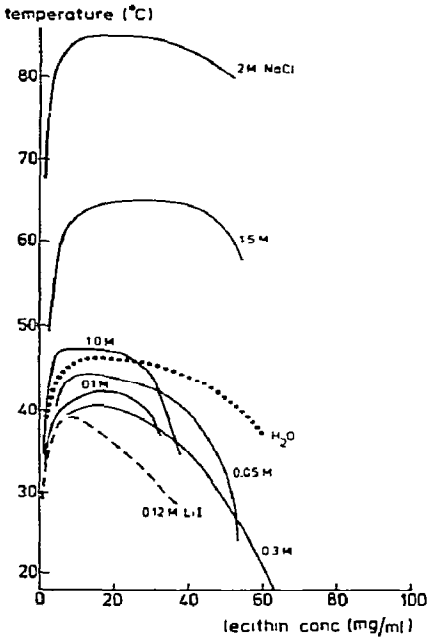


Fig. 1. Phase separation diagrams of dioctanoyllecithin in aqueous selutions. The dotted line (...) was obtained in electrolyte free solutions. The fully drawn lines (——) and the broken line (– – –) refer to solutions containing NaCl and LiI respectively.

Contrary to the lecithins with shorter chains, studied in our previous paper [8], dioctanoyllecithin forms very large micelles. The critical micelle concentration is rather low (0.12–0.16 mg/ml). These two properties enable us to use the "Debye approximation" [14], in which micellar concentrations (c_m = total concentration – CMC) are substituted in eqs. (3) and (4).

In systems close to a phase separation ($d\Pi/dc \to 0$) [15] or composed of very large particles [16] the scattering becomes so large that one should take the attenuation and the multiple scattering into account. The former correction is easily performed. For systems whose scattering can be described by eq. (3) one can use the relations given by Debye [15]. The correction for multiple scattering is more difficult to evaluate

exactly. It can, however, be shown that this correction is small compared to other experimental accuracies and was therefore disregarded.

4. Results

4.1. Phase separation diagrams

In fig. 1 the influence of various concentrations of NaCl on the phase separation diagram are shown. In electrolyte free solutions and at room temperature the demixing sets in at about 0.8 mg/ml. The CMC (0.12–0.16 mg/ml [7]) was virtually temperature independent up to 50°C (the highest temperature used). Addition of the salt in relatively low concentrations leads to a lowering of the cloud point curve. At higher concentrations the demixing region rises again. The temperatures in the maxima of the diagrams (critical temperatures) as a function of the NaCl concentration are plotted in fig. 2. The cloud point curves were not very reproducible from one lecithin sample to the other. We found for another separately synthesized sample a maximal temperature of 50.6°C in NaCl free solutions. The general behaviour on increasing NaCl concentrations remained the same.

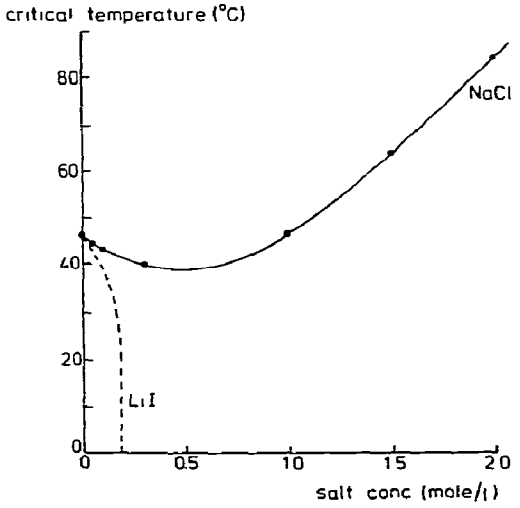


Fig. 2. Critical temperatures of the phase separations as a function of the salt concentrations. ——: NaCl, – – –: LiI.

The influence of 0.12 M LiI on the phase diagram is also shown in fig. 1. Addition of higher concentrations of LiI brings about a further lowering of the curve (as can be seen from fig. 2). It appeared to be impossible to obtain phase separation at high LiI contents.

The combined effects of NaCl and LiI were qualitatively investigated. Continuous addition of NaCl to a solution containing 0.12 M LiI first led to a decrease and then to an increase of the cloud point temperatures. The cloud point curve lowered again upon a further addition of LiI. The same phenomena can be obtained with KCNS instead of LiI.

The critical concentration was difficult to estimate due to the flatness of the upper part of the curves. At the critical concentration and temperature the volumes of both phases should be finite. By investigation of the phase volumes in salt free solutions we obtained a critical concentration of about 21 mg/ml.

4.2. Refractive index increments

The refractive index increments measured at room temperature in 0.2 M LiI and with an accuracy of ± 0.0005 ml/g were 0.118^0, 0.118^3 and 0.119^5 ml/g at wavelengths of 578, 546 and 436 nm respectively. The results of studies of the temperature dependence of the increments in 10^{-2} M phosphate buffer (pH = 6.9 ± 0.1) and at temperatures above the phase separation are shown in fig. 3. Linear extrapolations of these

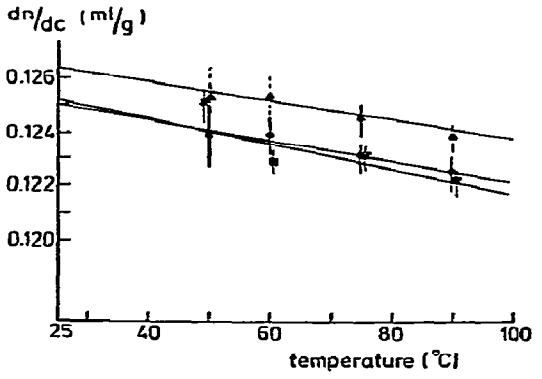


Fig. 3. Temperature and wavelength dependence of the refractive index increments in 10^{-2} M phosphate buffer (pH = 6.9 ± 0.1). ■: λ_v = 578 nm, ●: λ_v = 546 nm, ▲: λ_v = 436 nm.

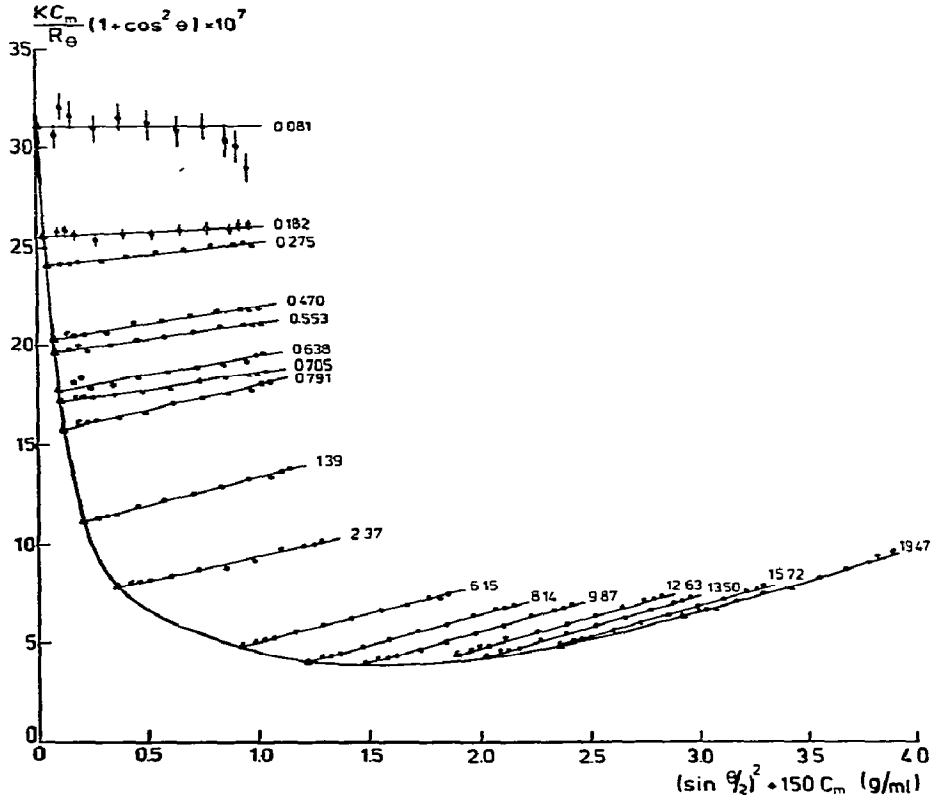


Fig. 4. "Zimm plot" of dioctanoyllecithin at 25.0°C, 0.2 M LiI and λ_v = 546 nm. The numbers on the right hand side of the lines refer to micellar concentrations in mg/ml.

increments to 25°C yield 0.125 ml/g for 578 nm and 546 nm and 0.126 ml/g for 436 nm. The accuracy of these extrapolated values is about 0.001 ml/g. The differences between these values and the increments directly measured at room temperature can be explained by the increase in the solvent refractive index due to the presence of LiI [8]. Our values are significantly smaller than the value reported by Pugh (0.138 ml/g) [2].

4.3. Concentration dependence of the light scattering in 0.2 M LiI

The results of the scattering experiments in 0.2 M LiI at 25°C and λ_v = 546 nm are given in fig. 4. The concentrations c_m used in this graph are the micellar concentrations. A CMC value of 0.128 mg/ml was used. This value was obtained by extrapolation of the results at low micellar concentrations in a manner explained in part II of this series [8]. The lines of constant concentration were extrapolated to $\theta = 0°$. The values of $R_0/(2Kc_m) = M_{w,app.}$ as a function of the micellar concentration are replotted in fig. 5. Within the measuring accuracy of about 2% the same data were obtained with the two other wavelengths.

The values of $q = [\langle r_g^2\rangle_z/M_w]^{1/2}$ as calculated from the slopes with the help of eqs. (3) and (5) at various concentrations are plotted in fig. 6. At low concentrations ($c_m < 2$ mg/ml) these slopes are of course rather inaccurate. The values of q at λ_v = 578 nm and λ_v = 546 nm were equal within the experimental error. The values at λ_v = 436 nm, however, were always about 4% smaller. Part of this effect can be explained by taking the depolarisation into account. This

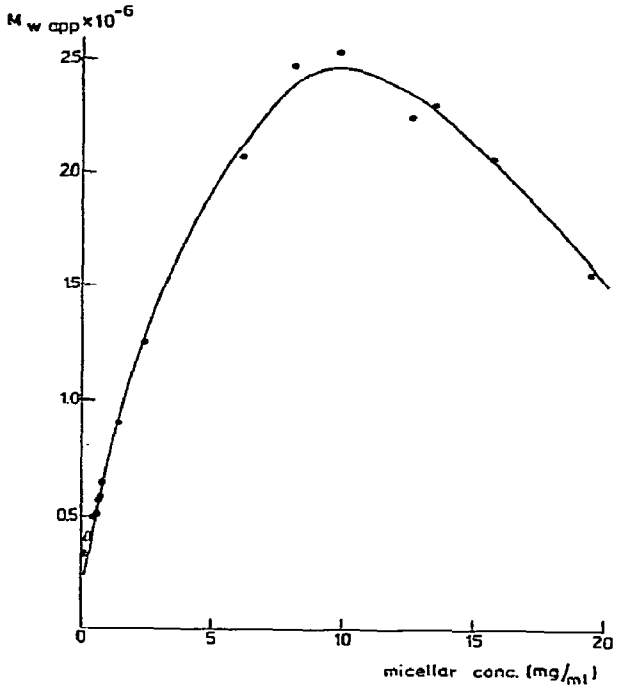


Fig. 5. Apparent weight average micellar weights as a function of micellar concentrations. The curve was obtained by least square curve fitting with eqs. (9) and (10).

depolarisation ($\rho_u = U_h/U_v$) was wavelength dependent and increased notably at lecithin concentrations above 13 mg/ml. The values of ρ_u at $\theta = 90°$ in the whole concentration range increased at $\lambda_v = 578$ nm from 0.005 to 0.009, at $\lambda_v = 546$ nm from 0.006 to 0.009 and at $\lambda_v = 436$ nm from 0.01 to 0.018.

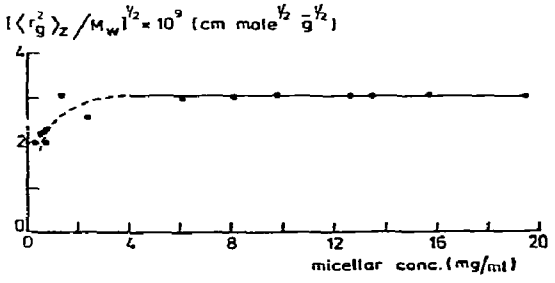


Fig. 6. $[\langle r_g^2 \rangle_z / M_w]^{1/2}$ from eqs. (3) and (5) as a function of the micellar concentrations.

4.4. Temperature dependence of the light scattering in salt free solution

A few preliminary experiments at $\lambda_v = 546$ nm on the temperature dependence of the light scattering near phase separation have been performed at total lecithin concentrations of 13.6, 16.7, 19.1 and 22.5 mg/g. From the angular dependence we determined the scattering at $\theta = 0°$ and the slope of the regression line representing the reciprocal value of the scattering versus $\sin^2(\theta/2)$. The results are given in figs. 7, 8 and 9. The scattering envelopes at high temperatures were not so well behaved as those obtained at room temperature and 0.2 M LiI. This is very likely due to the

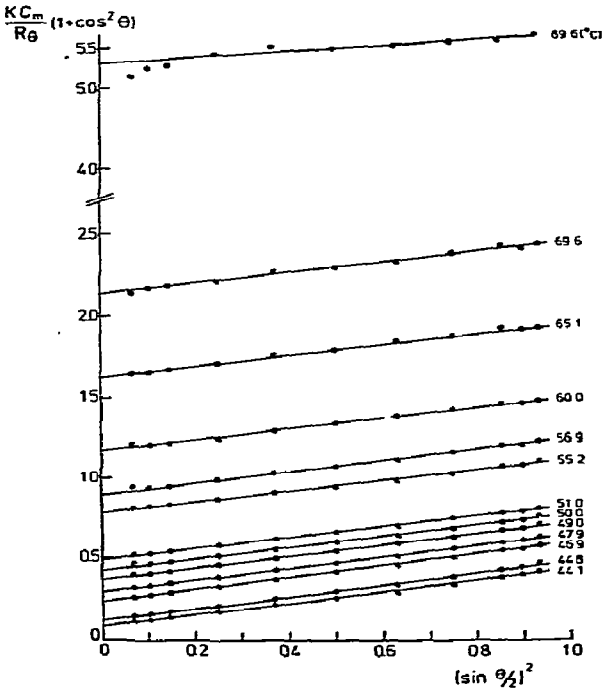


Fig. 7. Temperature dependence of the reciprocal scattering at $\lambda_V = 546$ nm and a lecithin concentration of 22.5 mg/g in salt free solutions. The numbers on the right-hand side of the lines refer to the temperatures. Phase separation occurred at 44.0°C.

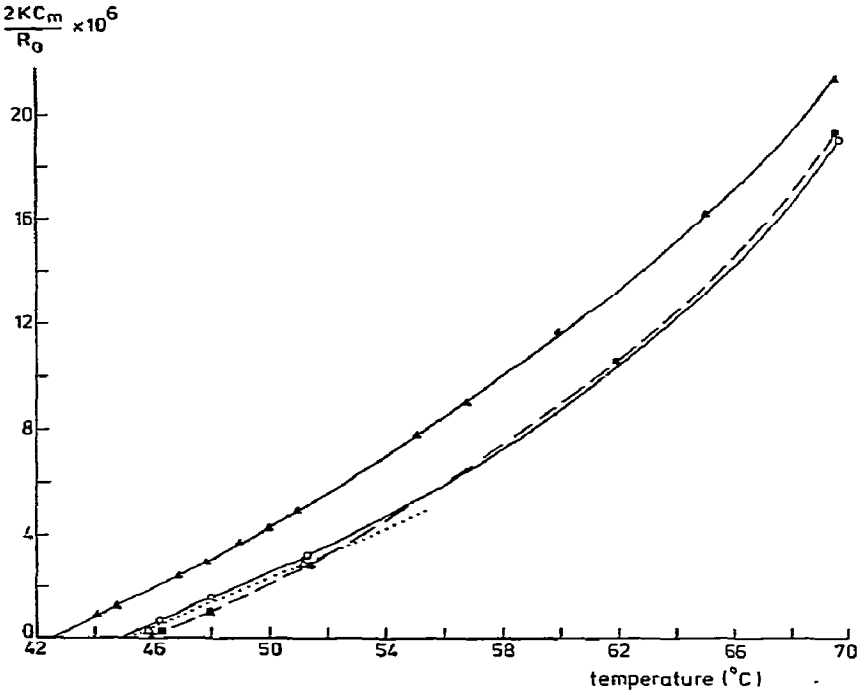


Fig. 8. Temperature dependence of $2Kc_m/R_0$. The four lecithin concentrations in mg/g are o: 13.6, ■: 16.7, △: 19.1 and ▲: 22.5.

presence of dust, which is difficult to remove quantitatively at high temperatures. The depolarisation strongly increased when approaching the phase separation region (at 10°C from the spinodal ρ_u was 0.01, at 3°C ρ_u was 0.03 whereas at 0.5° from the spinodal ρ_u rose to about 0.08). This effect could be due to multiple scattering.

If the lines of fig. 8 are extrapolated to $2Kc_m/R_0 = 0$ we obtain points from the spinodal [17]. Except for the critical point this curve lies below the binodal, that is the cloud point curve. In fig. 10 we have plotted parts of the binodal (visually determined) and the spinodal obtained from the light scattering experiments. The whole cloud point curve from these experiments

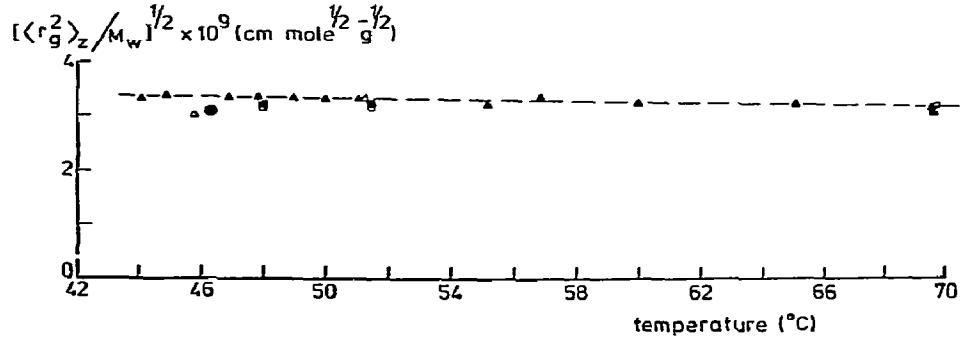


Fig. 9. Temperature dependence of $[\langle r_g^2\rangle_z/M_w]^{1/2}$ in salt free solutions. The lecithin concentrations in mg/g were o: 13.6, ■: 16.7, △: 19.1 and ▲: 22.5

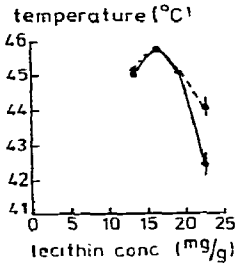


Fig. 10. The broken line (– – –) represents a part of the binodal (phase separation curve). The fully drawn line (——) is a part of the spinodal.

lies somewhat below and has a smaller width than the curve obtained in the experiments shown in fig. 1 (dotted line).

5. Discussion

5.1. Light scattering at room temperature in 0.2 M LiI

The aggregation properties of dioctanoyllecithin at room temperature in homogeneous solutions could only be obtained by increasing the solubility by addition of salt. We thus dissolved the lecithin in 0.2 M LiI. This leads to a lowering of the upper consolute temperature below 0°C.

5.1.1. Micellar weight

In fig. 5 we see a very strong increase of the apparent micellar weight already at low micellar concentrations. Normal thermodynamic nonideality effects can be expected to play a minor role in that region. In particular it would be difficult to visualise such a large negative virial coefficient. We therefore have to assume that the real micellar weight strongly increases with the concentration. This also implies a polydisperse micellar system [8]. In association phenomena a large polydispersity is obtained when all equilibrium constants (K_i) for successive aggregation steps (beyond a certain point) are equal [8, 18].

$$K_i = K = C_i/(C_{i-1} \times C_1) \qquad (7)$$

where C_i equals the molar concentration of the i-mer. In nonideal solutions eq. (7) also holds if the chemical potentials of the different species are related [19] according to

$$\mu_i = \mu_i^0(P, T, c') + RT[\ln c_i + M_i(B_1 c + B_2 c^2 + \ldots)]. \qquad (8)$$

Eq. (7) leads to an approximately linear increase of the weight average micellar weight with the square root of the micellar concentration c_m (in mass per unit volume) according to

$$M_w = k(c_m)^{1/2}. \qquad (9)$$

In order to interpret the apparent micellar weights more in detail we need a theory for estimating the thermodynamic nonideality in eqs. (4) and (8), that is to say we need values for the second and higher virial coefficients. The micellar weights are, however, so high that the calculation of the second virial coefficient on the basis of noninteracting rigid molecules, as performed in II [8], becomes very questionable. One can easily show that the use of that theory, in conjunction with the experimental data is unjustified above concentrations of 6 to 8 mg/ml since the excluded volume of cylinders of reasonable diameters would be larger than the volume of the whole solution. Higher virial terms should then be taken into account, but they are difficult to estimate. We therefore considered another model. We assumed the real micellar weight to increase according to eq. (9) and expanded the apparent micellar weight concentration dependence into virial terms according to

$$1/M_{w,app.} = 1/M_w + A_2 c_m + A_3 c_m^2. \qquad (10)$$

Such an expansion into constants is in agreement with eq. (8), which yields virial coefficients that are independent of the molecular weight. We next performed least square curve fitting procedures [20] to obtain the value for k from eq. (9) and A_2 and A_3. Taking $A_3 = 0$ we obtained a very bad fit. Including A_3 as an adjustable parameter a good fit could be obtained. We found $k = 2.38 \times 10^7$ ml$^{1/2}$g$^{1/2}$mole^{-1}, $A_2 = -2.36 \times 10^{-5}$ mole ml g^{-2} and $A_3 = 2.1 \times 10^{-3}$ mole ml^2 g^{-3}. The accuracy of these values depends almost entirely on the accuracy of the CMC. We estimated the maximal error in the CMC to be ± 0.014 mg/ml. The systematic errors in the parameters k, A_2 and A_3 then are $\pm 0.1 \times 10^7$, $\mp 0.5 \times 10^{-5}$ and $\mp 0.2 \times 10^{-3}$ respectively.

We interpreted these parameters in terms of the

classical Flory–Huggins theory [21] developed for the interaction of large polymer molecules. In this case we use

$$2Kc_m/R_0 = 1/M_w + v_1^2(M_0v_0)^{-1}(1-2\chi)c_m + v_1^3(M_0v_0)^{-1}c_m^2 \quad (11)$$

where M_0 and v_0 are the solvent molecular weight and specific volume respectively. v_1 is the specific volume of the solute (assumed to be 0.90 ml/g) and χ is an interaction parameter which is concentration dependent. In order to calculate χ from the parameters A_2 and A_3 we have to expand χ according to

$$\chi = \chi_0 + gc_m. \quad (12)$$

This procedure leads to $\chi_0 = 0.50025 \pm 6 \times 10^{-5}$ and $g = 0.428 \pm 0.002$ ml/g. Fitting eq. (11) to the experimental data with χ independent of the concentration gave $\chi = 0.506$. This would, however, imply a phase separation ($2Kc_m/R_0 \leq 0$) at concentrations between 5 and 13 mg/ml. In the theories on the thermodynamics of macromolecules a value for χ above 0.5 indicates that the system is near a phase separation, which in our system is indeed the case.

5.1.2. Micellar shape

A remarkable feature of our Zimm plot (fig. 4) is the parallelism of the lines at constant concentration. This implies that $q = [\langle r_g^2\rangle_z/M_w]^{1/2}$ as calculated with the help of eqs. (3) and (5) is also constant (fig. 6). The value for q is 3.1×10^{-9} cm mole$^{1/2}$g$^{-1/2}$. At low micellar concentrations q tends to lower values, but the accuracy is of course less in that region. Using the association model (M_w is dependent on the concentration) this implies that q is also independent of M_w.

We will now discuss the constant value for q with the help of three alternative models for the geometry of the micelles: a) the disk, b) the rigid rod, c) the random coil.

a) *Disk.* The z-average radius of gyration is connected with the z-average radius (R) of a circular disk according to [22]

$$\langle r_g^2\rangle_z = \tfrac{1}{2}\langle R^2\rangle_z. \quad (13)$$

Since $\langle R^2\rangle_z$ is proportional to the z-average particle weight (and also to the weight average weight), q is independent of the average micellar weight if the system consists of disks of equal thickness and different radii. The open association model with $M_w/M_n = 2$ leads to $M_z = \frac{3}{2}M_w$ [8]. Using a thickness of the disks of 2 × 20 Å we find $q = 0.95 \times 10^{-9}$ cm mole$^{1/2}$ g$^{-1/2}$, whereas the experimentally observed value ($q = 3.1 \times 10^{-9}$) would be consistent with disks of thickness 2 × 1.8 Å. The area per molecule would be 440 Å^2. The disk model would thus lead to absurd dimensions of the lecithin molecules and can therefore be discarded.

b) *Rigid rod.* The z-average radius of gyration squared is proportional to the ρ-average rod length L_ρ squared according to [23]

$$\langle r_g^2\rangle_z = \tfrac{1}{12}\langle L^2\rangle_\rho \quad (14)$$

where $\langle L^2\rangle_\rho$ is connected with the ρ-average molecular weight $\langle M^2\rangle_\rho$ according to [24]

$$M_\rho = [(1/M_w)\int_0^\infty M^2 f(M)\,dM]^{1/2}. \quad (15)$$

The "most probable distribution" ($M_w/M_n = 2$) [8, 25] leads to

$$M_\rho = \sqrt{3}M_w.$$

q^2 is therefore proportional to M_w. The open association model of rigid rods is therefore incompatible with our constant value of q. If the micellar system were monodisperse a value for q of 3.1×10^{-9}, together with a rod radius of 20 Å, would be consistent with a micellar weight of 800 000 and a rod length of 960 Å. For several reasons this monodisperse model is also not satisfactory. It would in the first place be very unlikely for a rod of 960 Å length and 40 Å diameter to be rigid. Moreover in the low concentration range we have measured micellar weights well below 800 000 (our lowest value was 320 000). In that concentration range q tends to lower values which can be interpreted as arising from a concentration dependent micellar weight. There seems, however, no justification for the hypothesis that the micellar size first increases and then remains constant at 800 000. A further increase would then be expected. In the previous section (5.1.1) we also gave another reason for postulating a polydisperse system.

c) *Random coil.* The z-average radius of gyration squared of a random coil is proportional to the z-average end to end distance squared ($\langle h^2\rangle_z$) and thereby

proportional to the z-average micellar weight [23], implying q independent of the micellar size

$$\langle r_g^2 \rangle_z = \tfrac{1}{6} \langle h^2 \rangle_z. \qquad (16)$$

If we assume the real micellar weight to increase according to eq. (8), with $k = 2.38 \times 10^7$ ml$^{1/2}$g$^{1/2}$ mole^{-1}, we can calculate the end to end distance and compare it with the contour length (length L of a rigid rod with a radius of 20 Å). We now for instance obtain at a concentration of 10 mg/ml, $M_w = 2.38 \times 10^6$, $\langle h^2 \rangle_z^{1/2} = 1170$ Å and $L_z = 4260$ Å. The end to end distance is too large compared to the contour length to apply the random coil statistics.

The most likely picture of the micellar shapes, that emerges from the considerations given above, is that of a very extended structure, probably wormlike with an increasing flexibility with increasing size (the more classical wormlike structure yields q values that still depend on the micellar size). Perhaps we should not think of unbranched rods but visualize the micelles more as an extended network.

5.2. Temperature dependence of the scattering in salt free solutions

As can be seen from figs. 7 and 8 the scattering increases very much on approaching the phase separation. The complete interpretation of this decrease in $d\Pi/dc$ can not yet be given. Probably two effects operate at the same time: the average micellar weight and thermodynamic nonideality (concentration fluctuations) both increase with decreasing temperature.

It is remarkable that in this case too $\langle r_g^2 \rangle_z / M_w$ remains approximately constant (see fig. 9). Since the value for q equals $(3.2 \pm 0.15) \times 10^{-9}$ cm mole$^{1/2}$ g$^{-1/2}$ we may conclude that the micellar structures in this case closely resemble the structures obtained at room temperature and 0.2 M LiI ($q = 3.1 \times 10^{-9}$, fig. 6).

5.3. Phase separation diagrams

We propose the rise of the upper consolute temperature at high NaCl concentrations as shown in figs. 1 and 2 to be due to a general salting-out effect [6,7], which is also reflected by the decrease of the CMC. This salting-out is most likely based upon two effects that both lead to an increase of the demixing temperatures. Addition of NaCl will probably lead to an increase of the average micellar weight (as was the case with the shorter homologues [8]) and to an increase of the interaction parameter χ (reduction of the solvent quality).

The initial decrease of the critical temperature can be explained by a decrease in electrostatic attractions between the lecithin molecules. This is quite reasonable if we assume Coulomb attraction forces between the phosphate group of one molecule and the choline group of a neighbouring molecule. The exact orientations and the resulting interactions between the polar groups are still very much debated (see, e.g., refs. [26,27]).

The opposite effect of LiI and NaCl in mixtures of these salts at high concentrations, as described in section 4.1 has its analogue in the change of the CMC in mixtures of the same electrolytes [7]. Again we assume a general salting-in effect due to LiI. Although the CMC of the lecithin in water is only slightly influenced by addition of LiI the micellar properties are probably greatly effected.

It is worthwhile mentioning that other theories exist for the appearance of demixing in solutions of macromolecules. Flory [28] and Onsager [29] proved that a phase separation in solutions of asymmetrical molecules can also appear even without taking χ into account. A strict application of their theories, however, is rather difficult in our associating system. Moreover these theories require an anisotropic concentrated phase, which in our case is not formed.

5.4. General conclusions on the aggregation properties of the short-chain lecithin homologues and the phospholipase A enzyme kinetics

In summarising the results from the micellar weight determinations on dihexanoyl-, diheptanoyl- and dioctanoyllecithin we arrive at our main conclusion concerning the general aggregation properties: The average micellar weight at a certain micellar concentration increases strongly with elongation of the chain length. This effect is most likely due to an increase of the micellar polydispersity, which accompanies the micellar weight-concentration dependence. Simple inorganic electrolytes, added in high concentrations, affect the micellar properties by general salting-out and salting-in (change of the hydrophobic bond). In this case too

we postulate an influence through a change of the polydisperisyt. In part IV of this series [31] we will present a simple association model which is in agreement with these observations.

This research project was initiated mainly to find correlations between the micellar aggregation properties and the phospholipase A enzyme kinetics [1,30]. Our thermodynamic data of the general behaviour of these lecithins do not provide detailed information of the local orientations and interactions of the lecithin molecules in the micelles. It is therefore impossible to test different hypotheses concerning the influence of the local environment of the lipid molecules on the enzyme kinetics. If hydrophobic bonds play an important role, we would expect the enzyme activity to increase with increasing chain length of the lecithins and with increasing concentrations of salting-out agents. A salting-in agent (for instance LiI) should in principle lead to a lowering of the activities. These effects have indeed been observed [1,30]. The "enzyme-substrate complex dissociation constants" change in the directions in agreement with this hydrophobic bond hypothesis. The details of the influences of the chainlength of the lipids and the salt concentrations are, however, still obscure, since the main effects on the enzyme activities stem from changes in the "maximal velocity" and not from changes in the dissociation constant. We therefore have to assume the maximal velocity to depend also on the hydrophobic bond, through changes in the environment of the lipid molecules bound at the active site of the enzyme.

Acknowledgements

The authors are indebted to Mr. P.J.M.J. Kok for introductory experiments on the phase separation and to Professor A. Vrij for the many helpful and stimulating discussions. We would also like to thank Dr. D.J. Goedhart of the physico-chemical department of AKZO-Research Laboratories in Arnhem for the use of the Brice-Phoenix differential refractometer and Dr. W. Mandema of Koninklijke/Shell-Laboratorium, Amsterdam, for his generous gift of poly-α-methylstyrene.

References

[1] G.H. de Haas, P.P.M. Bonsen, W.A. Pieterson and L.L.M. van Deenen, Biochim. Biophys. Acta 239 (1971) 252.
[2] W.J. Pugh, Thesis, London (1970).
[3] K.W. Herrman, J.G. Brushmiller and W.L. Courchene, J. Phys. Chem. 70 (1966) 2909.
[4] J.M. Corkill, J.F. Goodman and T. Walker, Trans. Faraday Soc. 63 (1967) 759.
[5] P. Mukerjee, J. Phys. Chem. 76 (1972) 565.
[6] P. Mukerjee, J. Phys. Chem. 69 (1965) 4038.
[7] R.J. M. Tausk, J. Karmiggelt, C. Oudshoorn and J.Th.G. Overbeek, Biophys. Chem. 1 (1974) 175.
[8] R.J.M. Tausk, J. van Esch, J. Karmiggelt, G. Voordouw and J.Th.G. Overbeek, Biophys. Chem. 1 (1974) 184.
[9] C.H. Fiske and Y. Subbarow, J. Biol. Chem. 66 (1925) 375.
[10] P.F. Mijnlieff and D.J. Coumou, J. Coll. Interf. Sci. 27 (1968) 553.
[11] H. Yamakawa, Modern theory of polymer solutions (Harper & Row, New York, 1971) ch. 5.
[12] B.H. Zimm, J. Chem. Phys. 16 (1948) 1093.
[13] A. Vrij and M.W.J. van den Esker, J. Chem. Soc. Faraday Trans. II 68 (1972) 513.
[14] P. Debye, Ann. N.Y. Acad. Sci. 51 (1949) 575.
[15] B. Chu, Molecular forces (Wiley, New York, 1967) p. 161.
[16] S.H. Maron and R.L.H. Lou, J. Polym. Sci. XIV (1954) 29.
[17] H. Tompa, Polymer solutions (Butterworth, London, 1956) ch. 2.
[18] P. Mukerjee, J. Phys. Chem. 76 (1972) 565.
[19] E.T. Adams and J.W. Williams, J. Am. Chem. Soc. 86 (1964) 3454.
[20] W.E. Wentworth, J. Chem. Ed. 42 (1965) 96.
[21] P.J. Flory, Principles of polymer chemistry (Cornell University Press, Ithaca, 1953) ch. 12.
[22] C. Picot, G. Weill and H. Benoit, J. Coll. Interf. Sci. 27 (1968) 360.
[23] K.A. Stacey, Light-scattering in physical chemistry (Butterworth, London, 1956) p. 28.
[24] G. Ehrlich and P. Doty, J. Am. Chem. Soc. 76 (1954) 3764.
[25] H. Fujita, Mathematical theory of sedimentation analysis, eds. E. Hutchinson and P. van Rysselberghe (Academic Press, New York, 1962) p. 296.
[26] M.C. Phillips, E.G. Finer and H. Hauser, Biochim. Biophys. Acta 290 (1972) 397.
[27] P.H.J.Th. Ververgaert, A.J. Verkley, P.F. Elbers and L.L.M. van Deenen, Biochim. Biophys. Acta 311 (1973) 320.
[28] P.J. Flory, Proc. Roy. Soc. London A 234 (1956) 60.
[29] L. Onsager, Ann. N.Y. Acad. Sci. 51 (1949) 627.
[30] W.A. Pieterson, Thesis, Utrecht (1973).
[31] R.J.M. Tausk and J.Th.G. Overbeek, Biophys. Chem. 2 (1974) to be published.

BIOPHYSICAL CHEMISTRY 2 (1974) 64–69. © NORTH-HOLLAND PUBLISHING COMPANY

ON THE BINDING OF ACTINOMYCIN AND OF DAUNOMYCIN TO DNA: A CALORIMETRIC AND SPECTROSCOPIC INVESTIGATION

F. QUADRIFOGLIO and V. CRESCENZI*
Laboratory of Macromolecular Chemistry, Institute of Chemistry, University of Trieste, Trieste, Italy

Received 19 December 1973

The "strong" binding of two antibiotics, actinomycin D and daunomycin, to native DNA (calf-thymus) in dilute aqueous solution has been studied by means of calorimetric and spectroscopic measurements. In essence our results show:

(1) Daunomycin interaction with DNA is an exothermic process, all features of which depend in a discontinuous way on the fraction of DNA binding sites engaged by the drug. Fluorescence data indicate that such a discontinuous trend should be independent of the GC content of DNA.

(2) Actinomycin binding to DNA is, on the contrary, characterized by a positive enthalpy. For such binding, no discontinuity appears discernible with increasing the molar ratio of drug to DNA (phosphorous) on the basis of calorimetric and fluorescence data.

(3) Both antibiotics can be bound simultaneously to DNA: our results would suggest that their binding sites on the biopolymer are independent.

Discussion is focussed on the possible information derivable from our data on whether or not intercalation may indeed be the main process through which each antibiotic considered "strongly" interacts with DNA.

1. Introduction

The interaction of the antibiotic actinomycin D and DNA has been widely studied by different techniques [1, 2]. The results have been interpreted by a number of workers in terms of intercalation of the aromatic moieties of the actinomycin D molecules into dG–dC sequences of DNA, with the cyclic pentapeptide rings located in the minor groove [2, 3]. This interaction mechanism would be, however, limited to molar ratios r of antibiotic to DNA nucleotides less than 0.1, because of severe steric interference between intercalation sites spaced more closely than six (or more) base pairs apart along the biopolymer chains [4, 5].

Qualitatively similar conclusions have been reached in the case of the "strong" interaction of the other antibiotic daunomycin and DNA [6–12].

* Mailing address: V. Crescenzi, Laboratorio di Chimica delle Macromolecole, Istituto di Chimica, Università di Trieste, 34127 Trieste (Italy).

The thermodynamic characterization of the specific binding of either actinomycin or daunomycin by DNA in dilute aqueous solution is, however, still somewhat lacking. As a matter of fact, for such binding only apparent equilibrium constants, K_I, have been reported and no systematic efforts seem to have been made to resolve the free energy of binding in terms of enthalpic and entropic contributions. In this connection the only results which can be found in the literature are those due to Gellert et al. [4] who conclude, on the basis of the dependence on temperature of K_I from spectroscopic data, that the enthalpy of binding, ΔH_I, of actinomycin by calf-thymus DNA is close to zero at near room temperature and for low ionic strengths. Similarly, Cavalieri and Nemchin [13] report that $\Delta H \approx 1$ kcal/mole at 25°, always for native calf-thymus DNA with actinomycin. On the other hand it appears established that interaction of actinomycin with mononucleotides is characterized by association constants much lower than those with DNA but by large and negative enthalpy changes [4, 14]. For the mononucleotides, complex

formation with actinomycin is understood to involve a stacking of the aromatic ring systems [15, 17]. The deduction of Gellert et al. [4] is that since "a common mechanism of interaction should imply similar thermodynamic parameters ... the interaction of actinomycin with DNA on one hand and with deoxyguanosine-5'-monophosphate or deoxyguanosine on the other must be fundamentally different", thus disfavouring intercalation of the antibiotic into DNA. Such a reasoning, although a weak one being essentially based on thermodynamic information, cannot however be easily dismissed.

In this connection, it is relevant to point out that in the case of the "strong" binding of proflavine and of ethidium bromide to DNA, which takes place via dye molecules intercalation, our calorimetric and spectroscopic data show that the enthalpy of dye–DNA interaction is quite similar to that of dye self-association [18]. The antibiotic–DNA case may, though, be more complicated so that deductions based on a comparison of the energetics of supposedly similar processes must be taken with care. In any event, obvious prerequisite to any further discussion in this direction is that more, accurate thermodynamic data be eventually available for the systems of our concern.

We thought worthwhile to start an investigation on the interaction of actinomycin and daunomycin with calf-thymus DNA in dilute aqueous solution with the aid of calorimetric measurements as well as spectroscopic (UV absorption, circular dichroism and fluorescence) measurements.

We wish to report here the results obtained so far, as these seem to add useful information to our knowledge on the difference between the mode of binding of the two antibiotics to DNA.

2. Experimental

2.1. Samples

Actinomycin D was a Schwarz-Mann product, used without further purification. The concentration of the solutions was determined spectroscopically using a molar extinction coefficient of 24800 M^{-1} [4] at 440 nm.

Daunomycin ·HCl sample was a kind gift of Farmitalia. The concentration of the solution was determined weighing the sample after drying in vacuo for 24 h.

Calf-thymus DNA was a Sigma product (type I, sodium salt, highly polymerized). A molar (phosphorous base) extinction coefficient of 6400 M^{-1} at 259 nm was used.

Micrococcus lysodeikticus-DNA was a Miles product. A molar extinction coefficient (phosphorous base) of 6800 M^{-1} at 260 nm was given by the producer.

A 0.01 M phosphate buffer (pH = 7) solution was employed as solvent throughout the work, unless otherwise specified.

Glass bidistilled water was used in all cases.

2.2. Apparatus

Microcalorimetric measurements were performed at 25°C with a LKB Model 10700 batch-type microcalorimeter equipped with glass cells.

Circular dichroism measurements were made with a Jouan Mod. 185 Dichrograph.

Spectrophotometric measurements were carried out with a Hitachi Perkin Elmer Mol. EPS-3t spectrophotometer.

Fluorescence measurements were carried out with a Perkin Elmer Mod. MPF-3L in the ratio mode.

2.3. Procedure

The microcalorimetric measurements were performed as previously described [18–20]. We can safely exclude possible errors due to adsorption of the antibiotics on the calorimeter cell walls, because the reproducibility of the results, using different initial concentrations and different volumes of drug solutions, was pretty good.

As regards the kinetics of interactions of the two antibiotics with DNA, our calorimetric measurements show that the reaction is complete within 5 min after mixing. Successsive mixing did not involve, in fact, further heat exchanges besides, obviously, those due to friction.

In calculating ΔH_I for actinomycin and daunomycin we have assumed complete binding of the antibiotics. This is certainly correct for low values of r where the binding constants for the two substances is of the order of magnitude of 10^6 M^{-1} (see text).

The concentration of the antibiotics in the solutions

used in the microcalorimetric measurements was around 10^{-4} M. The concentration of DNA solutions for the same measurements was in the range $3 \times 10^{-4} - 10^{-3}$ M (phosphorous base).

3. Results and discussion

3.1. Remarks on some physico-chemical properties of actinomycin and of daunomycin in dilute aqueous solution

Prior to a presentation of the data on the interaction of the two drugs with DNA it appears useful to briefly comment a few data concerning their behaviour in solution.

Our calorimetric experiments indicate that at the ionic strengths employed in our study the enthalpy of dilution of actinomycin is quite small. In the literature, dimerization constants K_D of the order of 10^3 M^{-1} have been reported for actinomycin at higher ionic strengths, together with estimated enthalpies ΔH_D ranging from −7 [21] to −15 [14] kcal/mole. Elaboration of our heat of dilution data as already explained in another instance [20], leads to the conclusion that, under our experimental conditions, either K_D or ΔH_D (or both) must be much lower, and thus evaluable only with difficulty.

In the case of daunomycin, on the contrary, the heat of dilution is well measurable and its dependence on concentration may be interpreted in terms of a dimerization of the antibiotics. We shall present these results in a separate communication, in full details [24].

In any case, the above mentioned data, together with data on the heat of dilution of DNA, were used in this work to correct the calorimetric results obtained upon mixing DNA and antibiotics solutions.

Furthermore, the final concentrations of both actinomycin and daunomycin in the presence of DNA were already such that their extent of dimerization could be completely neglected, and the (corrected) heats of mixing could be unambiguously attributed to *monomeric* antibiotic molecules–DNA interactions. Accordingly, the stoichiometric ratios of antibiotic to DNA nucleotides had in practice to be limited to values lower than about 0.2 in the calorimetric experiments.

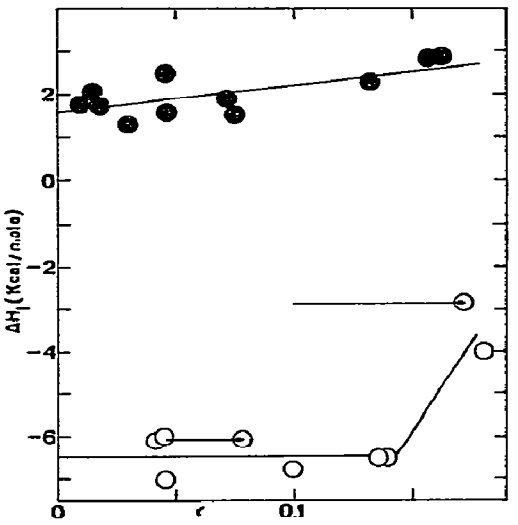


Fig. 1. Enthalpy of interaction (see text) of native calf-thymus DNA with: (a) actinomycin D (full symbols), (b) daunomycin hydrochloride (open symbols). Solvent: 0.01 M phosphate buffer, pH 7.0. r is the final stoichiometric ratio between the molar concentration of antibiotic and the molar (phosphorous base) concentration of DNA. $T = 25°C$. In two experiments with daunomycin, solutions of DNA already containing a given amount of the drug were added of more daunomycin to span the Δr indicated by the arrows.

3.2. Interactions with DNA

The results of the calorimetric experiments on the heat of binding of actinomycin and of daunomycin, respectively, to DNA are reported in fig. 1. In ordinate ΔH_I is the enthalpy of interaction in kcal per mole of antibiotic bound to DNA; in abscissa r is the molar ratio of antibiotic to DNA (nucleotides) in the solutions. All measurements were taken at 25° using 0.01 M phosphate buffer (pH = 7.0). Under these conditions the binding constants K_I of both antibiotics to DNA are greater than 10^6 M^{-1} [4, 5, 12, 22].

Data of fig. 1 clearly show that: (1) binding of actinomycin to DNA is an endothermic process taking place without apparent discontinuities (from a "calorimetric" standpoint, and within the accuracy of our data) in the range of r values considered; (2) binding of daunomycin to DNA is an exothermic process with a nearly constant enthalpy up to r about 0.13, above which $-\Delta H_I$ drops to distinctly lower values.

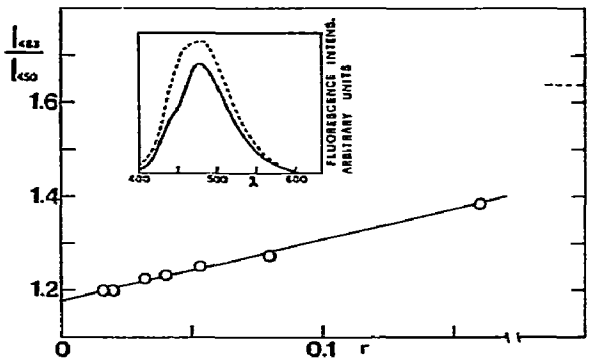


Fig. 2. Ratio of the fluorescence intensity at 483 and 450 nm of actinomycin D as a function of the stoichiometric molar ratio actinomycin/DNA. Excitation wavelength 360 nm. The broken line of the right ordinate gives the fluorescence intensity ratio for actinomycin at the same concentration (1.88×10^{-5} M) but in the absence of DNA. Solvent: 0.01 M phosphate buffer, pH 7.0. The insert shows the fluorescence spectra of the antibiotic in the absence and in the presence of DNA ($r = 0.016$; dotted curve).

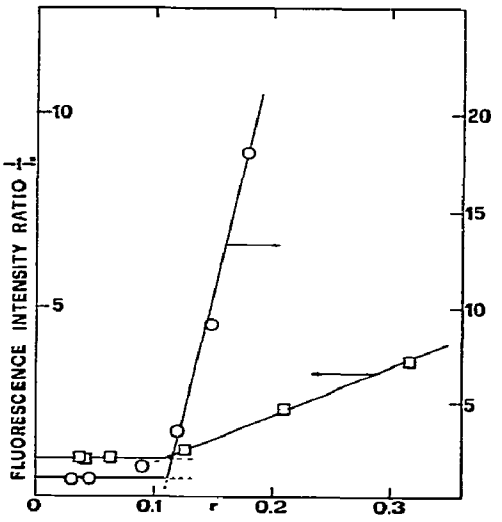


Fig. 3. Dependence of the fluorescence intensity (at 565 nm) of daunomycin-HCl on the stoichiometric molar ratio antibiotic/DNA, r. In ordinate is given the ratio of the fluorescence intensity measured at a given r (I) to that measured at the lowest r value considered (I_0). Solvent: 0.01 M phosphate buffer, pH 7.0. (□) DNA from calf-thymus (daunomycin conc., 1.48×10^{-4} M); (○) DNA from *micrococcus-lysodeikticus* (daunomycin conc., 3.0×10^{-5} M). The fluorescence of daunomycin in the absence of DNA is markedly reduced with increasing drug concentration (e.g., from 3.0×10^{-5} to 1.48×10^{-4} M). Such quenching has to be ascribed essentially to partial dimerization of the drug [24].

The diverse trends of ΔH_I with increasing r for actinomycin and daunomycin find their counterpart in the results of the fluorescence measurements which are reported in figs. 2 and 3.

In the case of actinomycin (fig. 2) the fluorescence spectrum undergoes only relatively minor changes upon interaction with DNA. One change consists in the increase of the intensity of emission at 450 nm (a shoulder in the fluorescence spectrum of the free antibiotic) with respect to that of the maximum (480 nm) in bound actinomycin spectrum (excitation wavelength: 380 nm). The ratio of the intensity of fluorescence at 450 and 483 nm of actinomycin is also plotted in fig. 2 as a function of r. It is seen that this ratio changes little upon increasing r, without any detectable discontinuity up to $r \approx 0.25$. The physical meaning of this behaviour is still obscure, however.

On the contrary, when daunomycin is bound to DNA for $r \leqslant 0.12$ its fluorescence (excitn. at 468 and maximum of emission at 565 nm) is strongly reduced [6]. Furthermore, as it is shown in fig. 3, the trend of daunomycin fluorescence with increasing r exhibits a clear discontinuity at around $r \approx 0.12$. Spectral perturbations brought about by binding to DNA in the case of daunomycin are clearly evidenced also by circular dichroism (CD) measurements typical results of which are given in fig. 4. It is seen in fact that the CD spectrum of bound daunomycin exhibits bands which are distinctly red-shifted and of increased amplitude with respect to those of the unbound species.

Comparing the calorimetric and spectroscopic results of figs. 1, 2 and 3, one would deduce that in the case of daunomycin, *as distinct* from the case of actinomycin, binding to DNA takes place with at least two different mechanisms depending on r. At very low r values, for which a number of evidences indicates that daunomycin is "intercalated" into DNA, we thus find an "enthalpy of intercalation" of -6.5 ± 0.5 kcal/mole (see fig. 1). Taking for the equilibrium binding constant a value of 3×10^6 M^{-1}, the entropy of daunomycin intercalation then amounts to +7.7 e.u., approximately. For r greater than 0.12, daunomycin interacts more weakly with DNA [12] according to a less exothermic process (fig. 1) which leads to only minor perturbations in the characteristic fluorescence of this an-

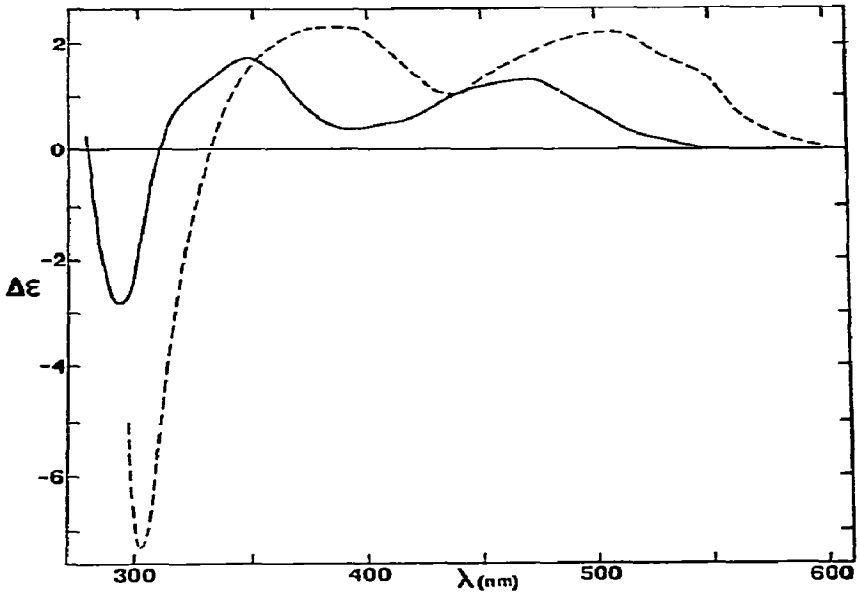


Fig. 4. Circular dichroism spectra of daunomycin·HCl (2.62×10^{-5} M) in 0.01 M phosphate buffer, pH 7.0. (–) without DNA; (– – –) with DNA ($r = 0.12$).

tibiotic (fig. 3). In this connection it is interesting to recall that we have found for the enthalpy of intercalation of proflavine and of ethidium bromide into DNA nearly identical values, averageable to -6.5 ± 0.5 kcal per mole of dye bound. This figure is also close to the enthalpy of self-association in water of both dyes said above, always at 25° [18].

We conclude that our calorimetric data provide additional, original evidence in favour of the intercalation mechanism through which daunomycin is sought to be bound to DNA at very low r values. On the contrary, in the case of actinomycin we cannot say that our present data lead to a similar conclusion. The following deductions may, however, be safely made. Since the total enthalpy of actinomycin–DNA interaction is about +2 kcal/mole (at the lowest r values; see fig. 1), this interaction would imply intercalation of the actinocyl chromophore between adjacent base pairs of native DNA and were this intercalation characterized by an enthalpy of, say, –6 kcal/mole per sec, then other events occurring upon actinomycin binding would require 8 kcal/mole. One such event might be a conformational change of the cyclic pentapeptide rings being located in the minor groove of DNA [5]. More important, the binding of actinomycin is entirely an entropy driven process (about +39 e.u., taking $\Delta H_I = 2$ kcal/mole and $K_I = 1.2 \times 10^7$ M^{-1} [5]) which means that a relatively large number of water molecules of hydration is released in such a process. This, in turn, can imply an unfavourable enthalpy. Our reasoning cannot, however, be pushed too far as it would necessitate, among other things a knowledge of the thermodynamics of the actinocyl chromophore (and of related model compounds) intercalation into DNA as well as more accurate data on the interaction of actinomycin with deoxynucleotides by direct calorimetric measurements.

We wish to add here however that the binding of actinomycin and daunomycin to DNA are not only characterized by different thermodynamic features but must also occur on at least "independent" sites along the biopolymer chains. We have found in fact that when a DNA solution containing daunomycin at $r_{\text{Dau.}} = 0.11$ is added of actinomycin so that $r_{\text{Act.}} \approx 0.6$, the fluorescence of the former antibiotic is unchanged. This type of measurement was feasible since the excitation wavelength used is far from absorption regions of either DNA or actinomycin (see fig. 3).

Being the binding constants to DNA for the two an-

tibiotics of the same order of magnitude, and were their binding sites the same, we should expect a displacement of a fraction of intercalated daunomycin molecules and thus an increase in fluorescence of the solution. Moreover, the fluorescence spectrum of actinomycin recorded in such conditions (after correction for the very small fluorescence contributed by daunomycin) exhibited an intensity ratio I_{483}/I_{450} (see fig. 2) typical for $r = 0.07$ with DNA alone.

Finally, in a separate set of calorimetric experiments we have also found that the heat exchange accompanying the interaction of actinomycin with DNA ($r_{Act.} = 0.08$) is very nearly the same whether or not the DNA solutions already contained bound daunomycin molecules ($r_{Dau.} = 0.11$).

In our opinion these results show, in agreement with different types of observations reported by others [23], that the two antibiotics can be bound to DNA at independent sites.

One possibility might be that daunomycin as opposed to actinomycin strongly prefers dA–dT pairs. We have checked this possibility using DNA from *micrococcus lysodeikticus* with a GC content of 72 %, much higher than that of calf-thymus DNA (41 %) and studying the dependence of daunomycin fluorescence with increasing r. The results, reported in fig. 3, show that saturation of daunomycin strong binding sites (intercalation) with the two DNA samples occurs at the same r value thus disproving any preference of this antibiotic for dA–dT pairs. Therefore, if it is correct to postulate that intercalation is a process limited in extent by the distortion it induces in the helical structure of DNA, when daunomycin and actinomycin are added to DNA exceeding such limits competition between the two antibiotics should take place. This, as mentioned above, is not the case: a possible limiting conclusion would then be that actinomycin does not intercalate at all into DNA. Other less drastic interpretations of the set of results reported here might of course be advanced.

Not to increase the speculative character of our discussion, we think it advisable however to postpone further arguments until more thermodynamic data on the systems of our concern will be accumulated.

Acknowledgement

This work has been sponsored by the Italian Consiglio Nazionale delle Ricerche, Rome. Thanks are due to Miss Gabriella Zumin and to Miss Loredana Spadaro for their skilful contribution.

References

[1] E. Reich and I.H. Goldberg, Progr. Nucl. Acad. Res. Mol. Biol. 3 (1964) 183.
[2] H.M. Sobell, Progr. Nucl. Acad. Res. Mol. Biol. 13A (1972).
[3] H.M. Sobell and S.C. Jain, J. Mol. Biol. 68 (1972) 21.
[4] M. Gellert, C.E. Smith, D. Neville and G. Felsenfeld, J. Mol. Biol. 11 (1965) 445.
[5] W. Müller and D.M. Crothers, J. Mol. Biol. 35 (1968) 251.
[6] E. Calendi, A. di Marco, R. Reggiani, B. Scarpinato and L. Valentini, Biochim. Biophys. Acta 103 (1965) 25.
[7] W. Kersten, H. Kersten and W. Szybalski, Biochemistry 5 (1966) 236.
[8] A. di Marco, in: Antibiotics, eds. D. Gottlieb and P.D. Shaw (Springer Verlag, Berlin, 1967) p. 190.
[9] M. Waring, J. Mol. Biol. 54 (1970) 247.
[10] F. Zunino, FEBS Letters 18 (1971) 249.
[11] W.J. Pigram, W. Fuller and L.D. Hamilton, Nature New Biol. 235 (1972) 17.
[12] F. Zunino, R. Gambetta, A. di Marco and A. Zaccara, Biochim. Biophys. Acta 277 (1972) 489.
[13] L.F. Cavalieri and R.G. Nemchin, Biochim. Biophys. Acta 87 (1964) 641.
[14] D.M. Crothers, S.L. Sabol, D.I. Ratner and W. Muller, Biochemistry 7 (1968) 1817.
[15] S.S. Danyluk and T.A. Victor, Jerusalem Symp. Quant. Chem. Biochem. II (1970) 395.
[16] B.H. Arison and K. Hoogsteen, Biochemistry 9 (1970) 3976.
[17] T.R. Krugh and J.W. Neely, Biochemistry 12 (1973) 1775.
[18] F. Quadrifoglio, V. Crescenzi and V. Giancotti, Biophys. Chem. 1 (1974) 319.
[19] V. Crescenzi, F. Delben, F. Quadrifoglio and D. Dolar, J. Phys. Chem. 77 (1973) 539.
[20] V. Crescenzi and F. Quadrifoglio, Eur. Polymer J. 10 (1974) 329.
[21] N.S. Angerman, T.A. Victor, C.L. Ball and S.S. Danyluk, Biochemistry 11 (1972) 2402.
[22] D. Carroll and R. Botchan, Biochem. Biophys. Res. Commun. 46 (1972) 1681.
[23] A. Rusconi, Biochim. Biophys. Acta 123 (1966) 627.
[24] F. Quadrifoglio and V. Crescenzi, manuscript in preparation.

BIOPHYSICAL CHEMISTRY 2 (1974) 70–75. © NORTH-HOLLAND PUBLISHING COMPANY

ON SOME STOCHASTIC MODELS FOR PROTEIN BIOSYNTHESIS

J. HIERNAUX
Université Libre de Bruxelles, Faculté des Sciences, Brussels, Belgium

Received 24 May 1973
Revised manuscript received 19 November 1973

The stability of the solutions of a model proposed by Gibbs et al. to describe the protein biosynthesis is studied in terms of the relative values of the kinetic parameters characterizing the three main steps of the polymerization process, i.e., initiation, elongation and termination. When the rate of initiation is equal to the rate of termination, the stationary state is unstable and depends thus on the perturbations imposed to the system. A comparison with results established by Vassart et al. suggests that initiation could be the rate determining step in protein biosynthesis.

1. Introduction

Theoretical studies of open chemical reaction networks with non-linear kinetics have shown that such systems may become unstable far from equilibrium and evolve to a new regime depending on time and/or space. Non-linear evolution equations may also allow far from equilibrium for multiple stationary states. Such situations have been called by Prigogine *dissipative structures* [1–3].

The object of this paper is to analyze in similar terms a model proposed by Gibbs et al. [4, 5] for the translation process of the protein biosynthesis. This model describes the diffusion of the ribosomes along the messenger RNA and gives the steady state distribution of nascent polypeptide chains.

Further models [6–8] have also been elaborated to simulate the protein biosynthesis. These models deal essentially with the polymerization process which is the basis of the protein biosynthesis. Here, we shall focus on Gibbs' results, which are the only ones to give rise to many possible types of stationary states. Our purpose will be to study the properties of these states in terms of the values of certain characteristic parameters of the system, by simulation on a C.D.C. 6400 computer. As we shall see, this numerical study will permit us to find again results established by Gibbs, to interpret them in terms of a transition between different polymerization states of the system as the parameters vary and to study properties such as the stability of these states.

2. The model

In their model, Gibbs et al. assimilate the diffusion of the ribosomes along the mRNA to the diffusion of segments along a one-dimensional lattice of K sites. Every site of the lattice represents one codon. The segment of length $L (L < K)$, representing the ribosome, may cover one ($L = 1$) or several ($L > 1$) sites of the lattice. This description of the protein biosynthesis is represented schematically on fig. 1.

This complex phenomenon has an irreversible character due to the polarity of the message contained in the mRNA. Moreover, this irreversible process requires continuous flow of tRNA and ribosomes. Thus, the biosynthetic apparatus can be looked upon as an open system operating in the nonlinear domain of thermodynamics of irreversible processes. The protein synthesis includes three main steps: initiation, elongation and termination [9] which are respectively characterized by the kinetic constants $k_f^{(0)}$, k_f and $k_f^{(K)}$.

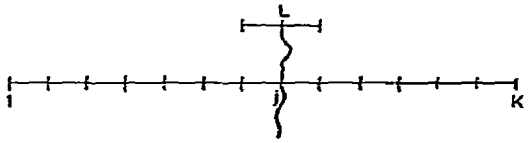


Fig. 1. The ribosome is represented by the segment of length L which diffuses along the lattice of length K representing the mRNA.

The probability $n_j(t)$ that the site j of the lattice be occupied by the polymerization site of the segment at time t is given by the following equation:

$$\frac{dn_j(t)}{dt} = q_{j-1}(t) - q_j(t) \qquad (1)$$

where $q_j(t)$ is the forward flow of the polymerization centre from site j to site $j+1$.

The value of this forward flow is given by the relation:

$$q_j(t) = k_f \frac{n_j(t)\left(1 - \sum_{s=1}^{L} n_{j+s}(t)\right)}{1 - \sum_{s=1}^{L} n_{j+s}(t) - n_{j+L}(t)} \qquad (2)$$

which has been derived by Gibbs et al. by adopting a markovian approximation for the motion of the ribosome. This assumption is perhaps far from biological reality because the motion of the ribosome results from a complex reaction including several chemical factors, most of which are not taken into account in this description*.

The kinetic equation (1) assumes a particular form at the boundaries of the system, where q_j becomes, for the first site:

$$q_0(t) = k_f^{(0)}\left(1 - \sum_{s=1}^{L} n_s(t)\right), \qquad (3)$$

for $1 \leqslant j \leqslant L-1$:

$$q_j(t) = k_f \frac{n_j(t)\left(1 - \sum_{s=1}^{L} n_{j+s}(t)\right)}{1 - \sum_{s=1}^{L} n_{j+s}(t) + n_{j+L}(t)}, \qquad (4)$$

for $K - L + 1 \leqslant j \leqslant K - 1$:

$$q_j(t) = k_f\, n_j(t), \qquad (5)$$

for the last site:

$$q_K(t) = k_f^{(K)}\, n_K(t). \qquad (6)$$

* A well known result in stochastic theory is that a process which is markovian in a certain space may become non-markovian when "projections" to smaller subspaces are made.

Eqs. (1) to (6) define for the K sites of the lattice, a set of coupled non-linear differential equations. Gibbs has shown that the behaviour of their solutions will depend on the relative values of the three parameters $k_f^{(0)}$, k_f and $k_i^{(K)}$. The different types of solutions are presented in the following section. A certain analogy between the occurrence of multiple solutions for those equations and some results obtained in biochemical models giving rise to dissipative structures [10–13] suggest that it is essential to study the stability of these solutions in order to determine the particular regime which will be physically realizable for different ranges of values of the parameters. This will be carried out in the following section.

3. Numerical analysis

We have investigated the evolution of the system towards the stationary state for various initial conditions and various values of the parameters by integrating the system of differential equations [1] which represents the progression of the segments along the lattice by the Runge Kutta method.

3.1. The segment covers only one site of the lattice (L = 1)

As shown by Gibbs et al., at the stationary state, we have three possibles types of solutions according to the boundary conditions and the rate constants.

n_{LD}: uniform low-density solution, which prevails when the initiation is the rate-determining step. This implies that $k_f^{(0)} < k_f^{(K)}$ and $k_f^{(0)} < k_f/(1+\sqrt{L})$.

n_{HD}: uniform high-density solution, which prevails when the termination is the rate-determining step. This implies that $k_f^{(K)} < k_f^{(0)}$ and $k_f^{(K)} < k_f/(1+\sqrt{L})$.

$n_{L/H}$: in this case, the rates of initiation and termination are of comparable magnitude and rate-determining, i.e. $k_f^{(0)} \simeq k_f^{(K)} < k_f/(1+\sqrt{L})$. This solution corresponds to a transition between n_{LD} and n_{HD}. The situation is analogous to a traffic jam in automobile traffic. Fig. 2 shows the three types of solutions.

We have tested the stability of these solutions with respect to small and large fluctuations for various values of the parameters.

(a) $k_f^{(0)} < k_f^{(K)} < k_f/(1+\sqrt{L})$.

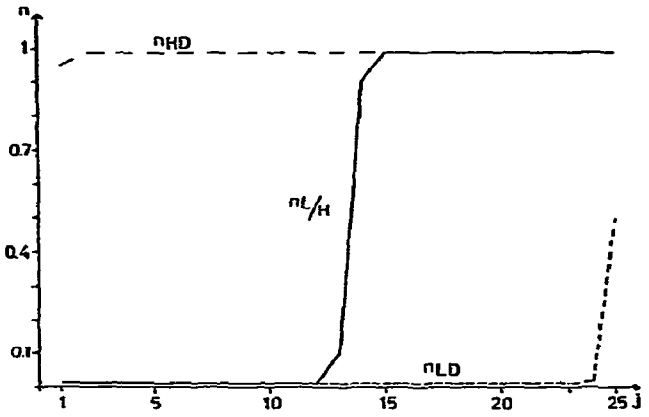


Fig. 2. The probability as a function of j.

If one discards the boundary conditions, two solutions are obtained at the stationary state: n_{LD} and n_{HD}. But the fact that the initiation is the rate-determining step eliminates n_{HD} and leaves us with only one stationary state solution, the low-density one. This solution is stable with respect to all disturbances.

(b) $k_f^{(K)} < k_f^{(0)} < k_f/(1+\sqrt{L})$.

As in the preceding case, the fact that the termination is the rate-determining step restricts us to one solution, the high-density one which is always stable.

(c) $k_f^{(0)} = k_f^{(K)} < k_f/(1+\sqrt{L})$.

The only solution satisfying the boundary conditions is $n_{L/H}$ which corresponds to an accumulation of nascent proteins near the site K of the lattice. This implies that the high-density part of the solution should be unstable at the level of the first sites of the lattice and that the

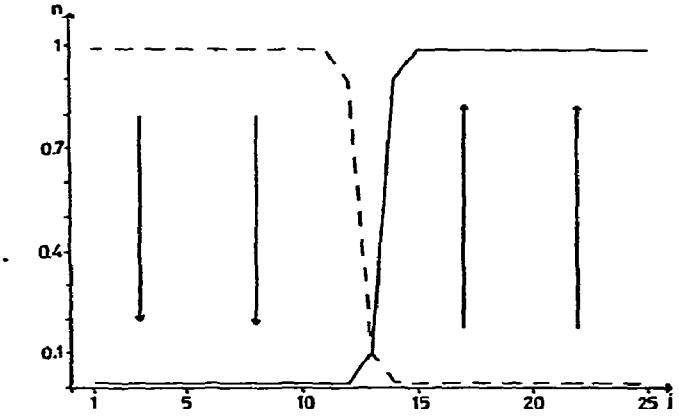


Fig. 3. As initial conditions, one has a "population inversion" (—). The arrows show the evolution of the system to a stationary state which is characterized by an accumulation of segments at the level of the last sites. The numerical values chosen for the parameters are: $K = 25$, $k_f^{(0)} = k_f^{(K)} = 0.1$, $k_f = 10.0$.

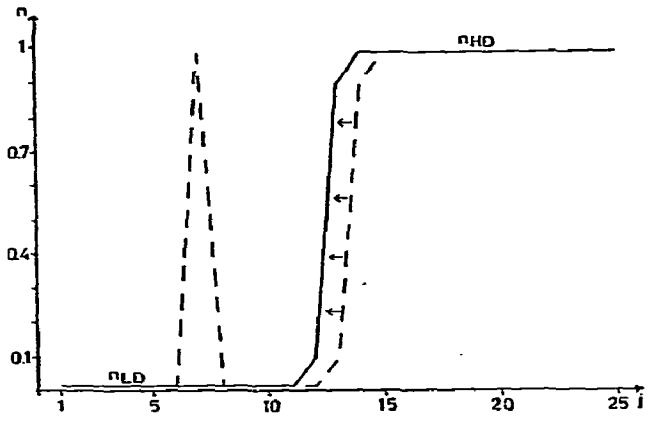


Fig. 4. A perturbation result in a displacement of the transition point. The initial transition point is situated at the level of the sites 13, 14. If one imposed the value of n_{HD} for the site 8, one observes a displacement of the transition point to the sites 11, 12. The numerical values chosen for the parameters are: $k_f^{(0)} = k_f^{(K)} = 0.1$, $k_f = 10.0$, $K = 25$.

low-density one should be unstable at the level of the last sites of the lattice. This is confirmed by the numerical calculations described in fig. 3. An interesting point is that the position of the transition between the two branches depends on the perturbations imposed on the system: any perturbation results in a displacement of the transition as shown in fig. 4.

3.2. The segment covers more than one site of the lattice ($L > 1$)

This case is more realistic, because it is known that a ribosome covers several codons of the mRNA

(a) $k_f^{(0)} < k_f^{(K)} < k_f/(1+\sqrt{L})$.

As in the previous case ($L = 1$), at the stationary state, the only possible solution is the low-density one.

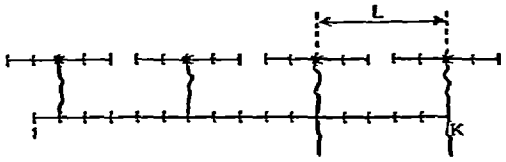


Fig. 5. Spatial periodicity observed when $L > 1$. Here $L = 5$ and $K = 17$.

(b) $k_f^{(K)} < k_f^{(0)} < k_f/(1+\sqrt{L})$.

These values of the parameters correspond to the uniform high-density solution, when $L = 1$. In this case, the uniform high-density solution does not exist at the stationary state. One observes instead spatial oscillations with "period" L around this solution. These oscillations result from the fact that the boundary conditions only concern the polymerization sites. The latter are distant from each other by a length L. Thus, the other "inactive" sites of the segments block the remaining sites of the lattice as shown on fig. 5. Obviously, this spatial periodicity is not a spatial dissipative structure, as it is the only solution available to the system for the given values of the parameters.

Clearly, this situation is a direct consequence of the assumption that the segments cannot overlap.

In this case, the oscillatory solution is unique and stable. Fig. 6 represents this type of solution

(c) $k_f^{(0)} = k_f^{(K)} < k_f/(1+\sqrt{L})$.

One observes a transition from the low-density solution which prevails at the level of the first sites, to the oscillatory one, which prevails at the level of the last sites. As in the previous subsection, the position of the transition appears to depend on the initial conditions and on the type of perturbations imposed on the system. Fig. 7 present such a solution.

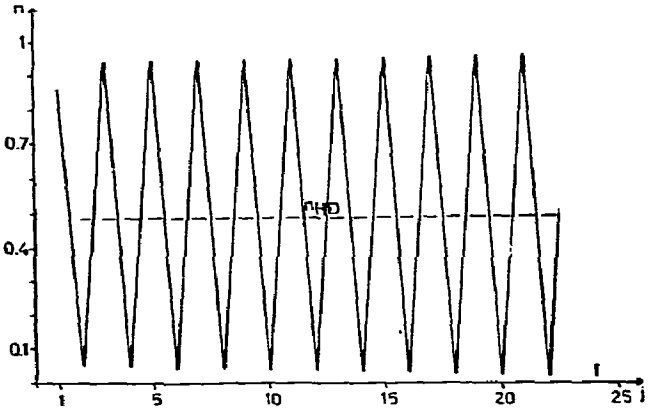


Fig. 6. Oscillations around n_{HD}. The numerical values chosen for the parameters are: $L = 2$, $K = 25$, $k_f^{(0)} = 1.0$, $k_f^{(K)} = 0.1$, $k_f = 10.0$.

4. Discussion

We have studied in some detail the transitions between polymerization states occuring in a model proposed by Gibbs et al. for the protein biosynthesis. Our results show that the nature of the steady states depends on the boundary conditions imposed on the system and, in certain cases, on the initial conditions.

Three domains can be determined, depending on the relative values of the kinetic constants.

The first domain corresponds to $k_f^{(0)} < k_f^{(K)} < k_f/(1+\sqrt{L})$. The uniform low-density solution is the only possible one. Biologically, this situation would correspond to a fast reading of the mRNA when the initiation is the rate-determining step.

The second domain correspond to $k_f^{(0)} = k_f^{(K)} < k_f/(1+\sqrt{L})$ a transition between the low- and the high-density solutions is observed. It is the only case in which we observe multistationarity: this results from the fact the position of the transition is undetermined since it depends on the initial conditions and on the perturbations imposed on the system. Thus, in this case, various solutions coexist for given values of the parameters. Experimentally, this domain would correspond to the accumulation of nascent proteins at variable positions near the 3 end of the mRNA.

The third domain corresponds to $k_f^{(K)} < k_f^{(0)} < k_f/(1+\sqrt{L})$. When $L = 1$, the high-density solution is stable. When $L > 1$, as shown by Gibbs et al., oscillations occur around the high-density solution. This situation would correspond to an accumulation of nascent proteins along a mRNA which is slowly read.

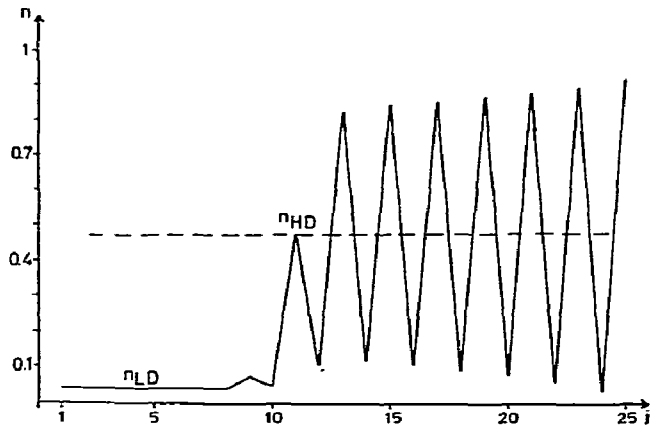


Fig. 7. Solution with transition. The numerical values chosen for the parameters are: $L = 2$, $K = 25$, $k_f^{(0)} = k_f^{(K)} = 0.1$, $k_f = 10.0$.

Summarizing, the only region of existence of multiple stationary states for given values of the parameters is $k_f^{(0)} = k_f^{(K)} < k_f$. In this case, each point at the interior of the lattice may occur at the high density as well as the low density state, depending on the initial conditions. This behavior corresponds therefore entirely to the one analyzed by Prigogine et al. for systems exhibiting dissipative structures.

In the other regions of values of the parameters the solution are unique and therefore cannot be regarded as dissipative structures. Still, a certain analogy exists with multiple solutions and dissipative structures owing to the fact that the variation of the different parameters induces transitions between different types of steady state solutions. In a sense, one can say that we have "parametrical" transitions inducing qualitative changes in the character of the solution.

The purpose of our stability analysis was to establish a relation between the value of the parameters and the physicaliy realizable situations. Next, we must compare these stable solutions provided by the model with the situations observed in living cells.

The model discussed in this paper describes protein biosynthesis in a rather simplified way. It is therefore difficult to establish a tangible link between such a model and the biological reality. However, one can compare the number of ribosomes which constitute a polysome and the number of segments which are moving along the lattice. Vassart et al. [8] have evaluated that the mRNA of hemoglobin is composed of 150 codons, that a ribosome covers 10 codons and that a polysome is formed of 5 ribosomes. In our treatment, for $L = 2$, and $K = 25$ which have the same ratio as $L = 10$ and $K = 150$, we have indeed obtained five ribosomes when the initiation and the termination are of comparable magnitude and rate-determining, we have obtained between seven and nine ribosomes. When the termination is the rate-determining step, we have obtained eleven ribosomes. Similar results were also obtained by Vassart et al. [8], who have concluded that the initiation is the rate-determining step of the protein biosynthesis.

In order to better approach the biological reality, which is probably far from the rather restrictive approximation for the polymerization flow (eq. 2), it

would be interesting to develop a nonmarkovian stochastic model to represent the protein biosynthesis.

Acknowledgement

We are indebted to Professor I. Prigogine for his interest in this work. We are also indebted to Professor G. Nicolis and to Dr. A. Goldbeter for many stimulating discussions. We acknowledge financial support from the Institut pour l'Encouragement de la Recherche Scientifique dans l'Industrie et l'Agriculture.

References

[1] P. Glansdorff and I. Prigogine, Thermodynamic theory of structure, stability and fluctuations (Wiley–Interscience, New York, 1971).
[2] G. Nicolis, Stability and dissipative structures in open systems far from equilibrium, Advan. Chem. Phys. 19 (1971).
[3] I. Prigogine and G. Nicolis, Biological order, structure and instabilities, Quarterly Reviews of Biophysics 4 (1971) 107.
[4] C.T. Mac Donald, J.H. Gibbs and A.C. Pipkin, Biopolymers 6 (1968) 1.
[5] C.T. Mac Donald and J.H. Gibbs, Biopolymers 7 (1969) 707.
[6] R. Gordon, J. Theor. Biol. 22 (1969) 515.
[7] U.N. Singh, J. Theor. Biol. 25 (1969) 444.
[8] G. Vassart, J.I. Dumont and F.R.L. Cantraine, B.B.A. 247 (1971) 471.
[9] J. Lucas-Lenard and F. Lipmann, Ann. Rev. of Biochem. 40 (1971) 409.
[10] R. Blumenthal, J.-P. Changeux and R. Lefever, J. Membrane 2 (1970) 371.
[11] A. Babloyantz and G. Nicolis, J. Theor. Biol. 34 (1972) 185.
[12] A. Goldbeter and G. Nicolis, Biophysik 8 (1972) 212.
[13] M. Sanglier and A. Babloyantz, FEBS Letters 23 (1972) 364.

BIOPHYSICAL CHEMISTRY 2 (1974) 76–81. © NORTH-HOLLAND PUBLISHING COMPANY

MONTE CARLO GENERATION OF POLYPEPTIDE RANDOM COIL CONFORMATIONS; THE PERSISTENCE VECTOR AND THE CHAIN VECTOR DISTRIBUTION

F.Th. HESSELINK*

Van 't Hoff Laboratorium der Rijksuniversiteit, Trans. III, Utrecht, The Netherlands

Received 2 January 1974

Polypeptide random coil conformations of various chain lenghts (N = 5, 10, 20, 40, 80 peptide units) are generated by a Monte Carlo procedure. The characteristic ratio obtained for the sets of generated conformations is identical with the exact value calculated with the average transformation matrix procedure, indicating the equivalence of the two treatments. On the basis of the generated sets of conformations the length and direction of the persistence vector (the averaged chain vector expressed in the reference frame of the first two skeletal bonds) are investigated for various chain lengths. The radial distribution function for the chain vector shows the length of the chain vector for small polypeptides (N = 5, 10) not to deviate far from its most probable value. Also for larger chains up to chains of 80 peptide units very significant deviations from a gaussian distribution are observed.

The distribution of the length of the vector connecting the remote end of the chain with the end of the persistence vector exhibited behavior much closer to the gaussian approximation, an improvement especially significant for the short chains.

1. Introduction

Recently, Flory [1] has called attention to the mean displacement vector $\boldsymbol{a}$, the conformational average of the chain vector $\boldsymbol{r}$ expressed in a reference frame fixed with respect to the first two skeletal bonds of the polymer chain. The interest in this vector $\boldsymbol{a}$ resides in Flory's assumption that, especially for short chains, the density distribution of the vector $\boldsymbol{\rho}$, with $\boldsymbol{\rho} = \boldsymbol{r} - \boldsymbol{a}$, should behave in better approximation according to gaussian statistics than the distribution of the chain vector itself. In this paper we shall investigate this assumption for polypeptide random coil conformations, using a previously described [2] Monte Carlo procedure.

Monte Carlo generation of polymer chains has become an increasingly popular method to obtain information of the conformational behavior of polymer molecules. This technique has been applied to various conformational problems, such as the influence of volume exclusion on chain dimensions [3–7], the conformational behavior of macromolecules near interfaces [8, 9], the behavior of short chains [10] and ring closure problems [11], etc. Recently, a set of Monte Carlo generated poly L-lysine random coil conformations served as a basis for the calculation of the electrical free energy of a polylysine random coil [2]. However, this set contained only a rather small number (200) of conformations, and so a second purpose of this paper is to investigate further the validity of the proposed generation procedure by a calculation of the chain vector length and distribution for larger sets of conformations and for various chain lengths. Our calculations are based on a set of preferred conformations for the L-lysine residue, but presumably they apply to any (co)poly α-L-amino acid containing C^{β} atoms.

2. Method of calculation

The Monte Carlo generation procedure has been described elsewhere [2]; it is based on the assumption that the conformation of a residue in a randomly coiled polypeptide chain is independent of neighboring residues [12],

* Present address: Shell Research, P.O. Box 60, Rijswijk, The Netherlands.

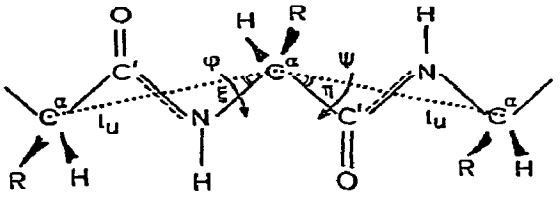


Fig. 1. Polypeptide chain indicating the meaning of the fixed angles η and ξ and of the variable angles φ and ψ.

whereas the conformation of each residue (i.e. the rotational angles φ and ψ, see fig. 1) is determined by the short range interatomic interaction within the peptide residue. The probabilities for various (φ, ψ) combinations are tabulated [2], and the Monte Carlo procedure consists essentially in the random picking of (φ, ψ) combinations for the consecutive residues in the polypeptide chain. The coordinates of the atoms of the macromolecule are then calculated using the peptide geometry and transformation matrix procedure described by Ooi et al. [13]. This procedure should generate the unperturbed dimensions of the polypeptide random coil.

The characteristic ratio, C_N, given by

$$C_N = \langle r^2 \rangle / N l_u^2, \qquad (1)$$

$\langle r^2 \rangle$ being the mean square end-to-end distance of a chain of N peptide units each of length l_u, has been calculated from the generated sets of conformations for various chain lengths, with $l_u = 3.80$ Å. Exact values for C_N for various N are also calculated on the basis of the preferred set of (φ, ψ) combinations (table 4 in ref. [2]), using the average transformation matrix procedure described by Brant and Flory [14, 12]. In these calculations the value used for the angle between the virtual bond and the C–N bond ξ was 13.5° and the value of the angle between the virtual bond and the C–C′ bond η was 21.9° (see fig. 1). The peptide bond between C′–N has been taken as flat and rigid.

3. Results and discussions

3.1. Characteristic ratio

Sets of random coil conformations have been generated for polypeptides with chain lengths, ranging from $N = 5$ up to $N = 80$ peptide units. In table 1 the number of generated conformations and the obtained values for the characteristic ratio are given, together with the exact values for C_N, obtained using Brant and Flory's average transformation matrix procedures ([12] p. 25; [14]) and our set of preferred (φ, ψ) combinations. The agreement between the values of the characteristic ratio obtained with these two different methods is such that we can state confidently that the generated sets of conformations are indeed representative for the polypeptide random coil. The present Monte Carlo procedure to generate polypeptide conformations proves to be a significant improvement over previous procedures [4, 5], which produced too low values for the characteristic ratio.

Due to differences in the chosen peptide geometry and in the set of prefered (φ, ψ) angles, our values for the characteristic ratio are somewhat higher than those obtained by Brant and Flory [14], possibly indicating that the dimensions of our sets of random coil conformations are somewhat larger than would correspond with "unperturbed dimensions". However, since polypeptide molecules have the tendency to form regular structures (α-helix, β-structure) in poor solvents, we usually only find random coil conformations in good solvents, i.e., under conditions when polypeptides have much larger dimensions than would correspond with unperturbed dimensions. Therefore, the differences between the generated conformations and the unperturbed dimensions, if any, are thought to be of little importance.

3.2. Persistence vector

When the chain vector $\boldsymbol{r}$, which connects to two ends of the chain, is expressed in terms of an external reference frame, the averages of the components of $\boldsymbol{r}$ become zero. However, expressed in a reference frame defined by the first two skeletal bonds of the chain the averages of the components of vector $\boldsymbol{r}$ represent a finite displacement $\boldsymbol{a}$ from the origin. Flory [1] calls this vector $\boldsymbol{a}$ the persistence vector of the chain, since it is obviously related with the persistence length a of the Kratky–Porod [15] chain model. For a discussion of this relationship we refer to Flory's paper [1]. From our sets of random coil conformations values for this persistence vector are obtained for polypeptide chains of various chain lengths, and these values are given in table 1. As Flory expected, the length of $\boldsymbol{a}$ increases with chain length for short chains,

Table 1
Results of the Monte Carlo generation of sets of polypeptide random coil conformations

Number of peptide units	Number of generated conformations	$\langle C_N \rangle_{M.C.}$	$\langle C_N \rangle_{exact}$	Persistence vector a (Å)	$\|a\|$ (Å)	$\langle r^2 \rangle^{1/2}$ (Å)	$\langle \rho^2 \rangle^{1/2}$ (Å)
5	20000	2.981	2.982	(10.9 −3.5 − 5.6)	12.7	14.7	7.31
10	10000	4.900	4.899	(16.3 −4.5 − 9.6)	19.4	26.6	18.2
20	5000	7.166	7.174	(20.8 −6.3 −12.6)	25.1	45.5	37.9
40	5000	9.113	9.053	(23.2 −5.4 −13.4)	27.4	72.6	67.2
80	2000	10.112	10.151	(20.9 −7.8 −15.0)	26.9	108.1	104.7

and it levels off for longer chains to a finite length we find to be of about 27 Å.

Figure 2 shows the orientation of these persistence vectors for various chain lengths in the (x, y) plane, the plane defined by the also shown orientation of the first peptide unit. The origin is chosen at the first C^{α} atom.

As can be seen, the length of the persistence vector increases up to a certain length, but its orientation is predominantly determined by the orientation of the first residue. Because of the asymmetric character of chains composed of L-amino acids, the z-coordinate of the persistence vector (see table 1) deviates from the orientation of the first residue.

Because of the non-zero values of the average coordinates of the chain vector when expressed in the frame of reference of the first peptide unit ($\langle x \rangle$, $\langle y \rangle$, $\langle z \rangle$), the distribution of the cartesian components of the chain vector is also far from symmetric around the origin. As an example, fig. 3 shows the distribution of the x, y, and z component of the chain vector for a chain of 20 peptide units. Note that these distributions are not symmetric either around $\langle x \rangle$, $\langle y \rangle$ or $\langle z \rangle$ respectively.

3.3. The chain vector r and its radial distribution function

The radial distribution function of the chain vector for chains of 5, 10, 20, 40 and 80 peptide units is shown in figs. 4–8, whereas the rms end-to-end distance $\langle r^2 \rangle^{1/2}$ corresponding with these distributions is given in table 1. Using these values for $\langle r^2 \rangle^{1/2}$, radial distribution functions $R(r)$ are calculated according to the gaussian approximation with

$$R(r) = 4\pi(3/2\pi\langle r^2 \rangle)^{3/2} r^2 \exp(-3r^2/2\langle r^2 \rangle) \qquad (2)$$

and these distributions are also shown in figs. 4–8.

Comparison of the actual and the gaussian distributions indicates the extreme deviation from gaussian behavior for short chains. For chains up to 10 peptide units the actual distribution is extremely peaked around a most probable value for the end-to-end distance, a value shown to be not very much shorter than the length of a completely extended polypeptide chain (with $\varphi = \psi = 180°$). For longer chains the actual and gaussian distri-

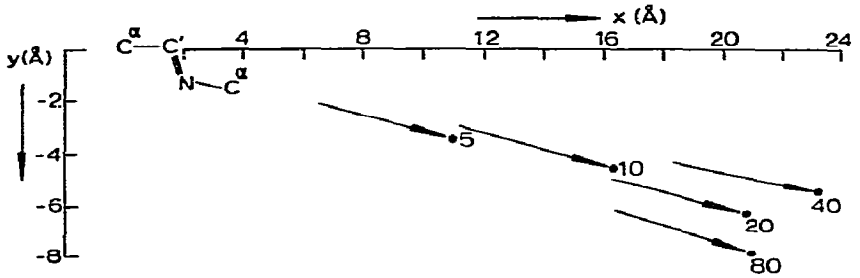


Fig. 2. Orientation of the first peptide unit in the $x-y$ plane and the persistence vectors for polypeptide chains of 5, 10, 20, 40, and 80 peptide units.

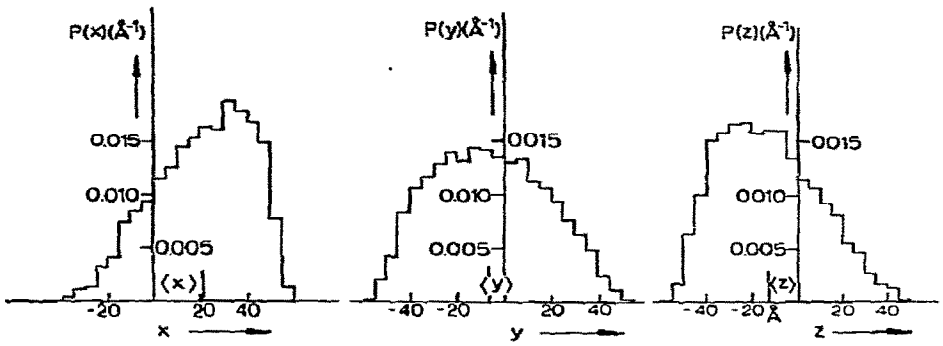


Fig. 3. Distribution $P(x)$, $P(y)$ and $P(z)$ of respectively the x, y and z component of the chain vector for a chain of 20 peptide units, expressed in the frame of reference of the first two skeletal bonds of the chain.

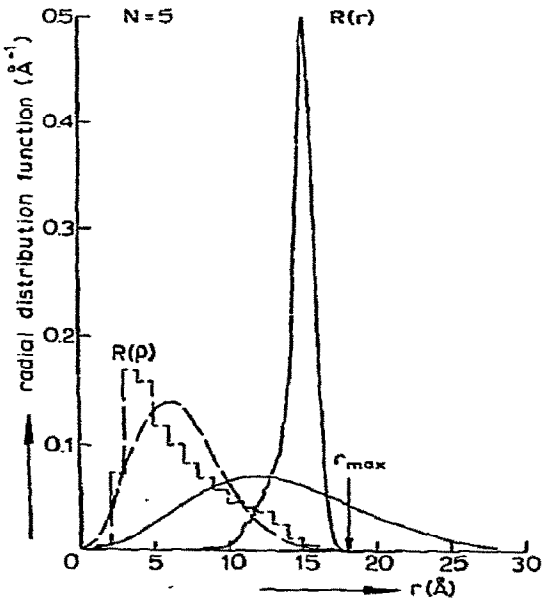


Fig. 4. The radial distribution function $R(r)$ for the chain vector and its gaussian approximation (full curves); further, the distribution $R(\rho)$ of Flory's ρ vector and its gaussian approximation (broken curves) both for a chain of 5 peptide units. r_{max} indicates the length of the fully extended chain.

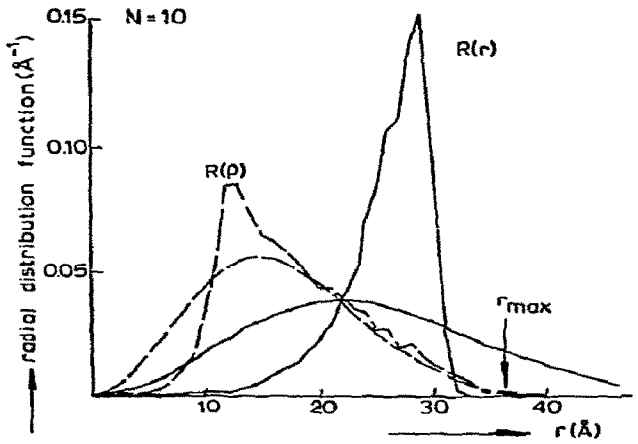


Fig. 5. Same as fig. 4, for a chain of 10 peptide units.

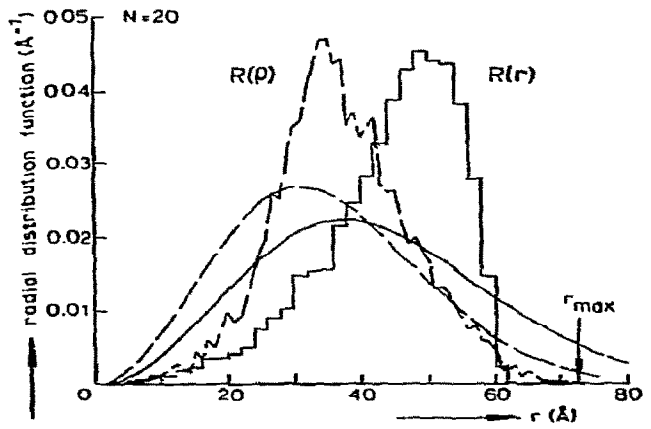


Fig. 6. Same as fig. 4, for a chain of 20 peptide units.

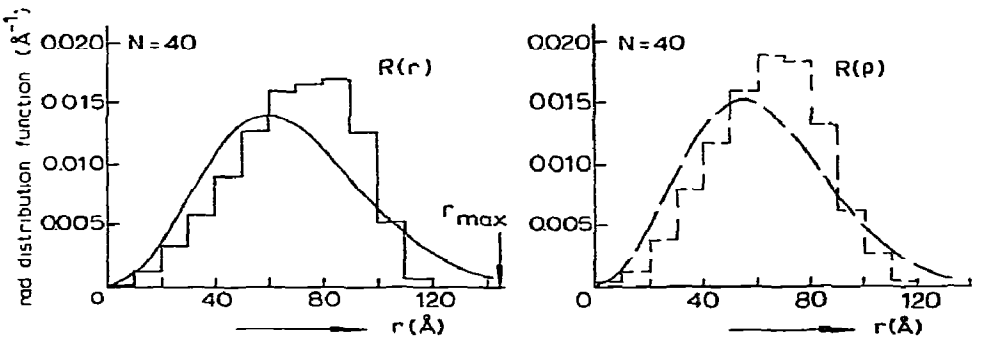


Fig. 7. Same as fig. 4, for a chain of 40 peptide units.

butions are closer together, but we still see systematic deviations in three regions of the distribution curves.

Deviation I: The actual probability of chains having a chain vector longer than about $2\langle r^2\rangle^{1/2}$ is overestimated by the gaussian distribution, a well known deficiency of this distribution which is only valid for chains not extended too much.

Deviation II: The actual distribution exceeds the gaussian distribution in the region where r is somewhat larger than $\langle r^2\rangle^{1/2}$. This hump found in the actual distribution over the gaussian distribution (see figs. 4–8) becomes smaller for longer chains, and it has almost vanished for $N = 80$.

Deviation III: The probability of a short chain vector ($r < \langle r^2\rangle^{1/2}$) is overestimated by the gaussian distribution. This effect is very important for short chains and it has again almost vanished for chains of 80 peptide units. It has also been found for other types of polymers, such as polynucleotides [11], polymethylene and polysiloxanes [16] and it plays an important role in the formation of polymer rings. Actually, Delisi and Crothers [11] obtained a radial distribution function for a polynucleotide of 7 units, which looks very similar to our results for a chain of 20 peptide units.

Comparison of the actual distributions with more sophisticated treatments of the freely jointed chain ([11] ch. 8; [17]) is not expected to remove the observed deviations II and III, since Jernigan and Flory [18] showed the gaussian approximation to function very well as long as $r \ll Nl_u$.

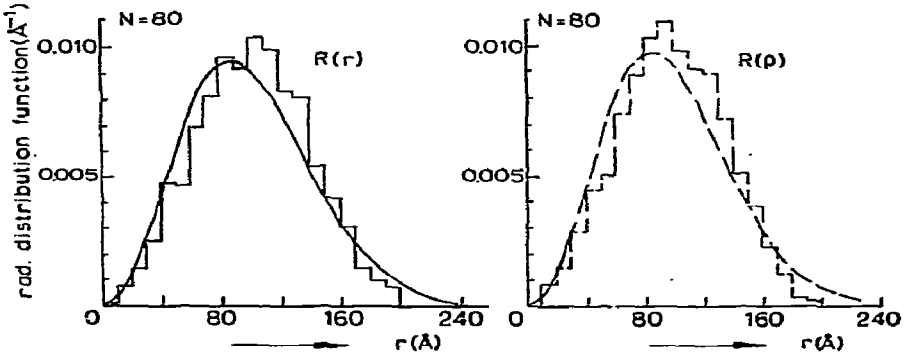


Fig. 8. Same as fig. 4, for a chain of 80 peptide units.

3.4. The vector ρ and its distribution

Now, we consider the distribution of the remote end of the chain relative to the terminus of the persistence vector, defining [1] a vector ρ according to

$$\rho = r - a \tag{3}$$

or

$$\rho = \begin{bmatrix} x - \langle x \rangle \\ - \langle y \rangle \\ z - \langle z \rangle \end{bmatrix}, \tag{4}$$

where x, y and z are the coordinates of the remote end of the chain in the reference frame of the first residue and $\langle x \rangle$, $\langle y \rangle$ and $\langle z \rangle$ the elements of the persistence vector.

The mean square value of ρ is then given by [1]

$$\langle \rho^2 \rangle = \langle r^2 \rangle - a^2. \tag{5}$$

After generation of the sets of conformations for each chain length the elements of the persistence vector are calculated. Then the elements of the vector ρ are calculated for each conformation according to eq. (4), and the resulting value for $\langle \rho^2 \rangle^{1/2}$ is given in table 1. These values for $\langle \rho^2 \rangle$ obey eq. (5).

The radial distribution function for the vector ρ, $R(\rho)$, is shown for various chain lengths in the figs. 4–8, together with the gaussian distribution for the value of $\langle \rho^2 \rangle$ (broken lines). For short chains ($N = 5$ and $N = 10$, chains with respectively 16 and 31 backbone atoms) the distribution $R(\rho)$ exhibits behavior very much closer to the gaussian approximation than the distribution for the chain vector $R(r)$. For longer chains, however, the distribution $R(\rho)$ behaves only slightly more like the gaussian approximation than the distribution of the chain vector $R(r)$. Therefore, the vector ρ could be useful for ring closures of small rings, whereas for larger rings the use of ρ instead of r would not result in great improvements.

After completion of this manuscript a paper appeared by Premilat and Hermans, Jr. [19], in which similar results are reported for the radial distribution function $W(r)$ for polypeptide chains of 5, 10 and 20 peptide units. These results, however, are not discussed in terms of Flory's persistence vector but in terms of the Kratky–Porod wormlike chain model.

Acknowledgement

The author wishes to thank Professor H.A. Scheraga for the inspiration which led to the present work.

References

[1] P.J. Flory, Proc. Natl. Acad. Sci. 70 (1973) 1819.
[2] F.Th. Hesselink, T. Ooi and H.A. Scheraga, Macromolecules 6 (1973) 541.
[3] J. Mazur and F.L. McCrackin, J. Chem. Phys. 49 (1968) 648.
[4] H.E. Warvari, K.K. Knaell and R.A. Scott, J. Chem. Phys. 57 (1972) 1161.
[5] S. Tanaka and A. Nakajima, Macromolecules 5 (1972) 708.
[6] S.D. Stellman and P.J. Gans, Macromolecules 5 (1972) 720.
[7] Z. Alexandrowicz and Y. Accad, Macromolecules 6 (1973) 251.
[8] E.A. DiMarzio and F.L. McCrackin, J. Chem. Phys. 43 (1965) 539.
[9] E.J. Clayfield and E.C. Lumb, Macromolecules 1 (1968) 133.
[10] M. Fixman and R. Alben, J. Chem. Phys. 58 (1973) 1553.
[11] C. Delisi and D.M. Crothers, Biopolymers 10 (1971) 1809.
[12] P.J. Flory, Statistical mechanics of chain molecules (Interscience, New York, 1969) Ch. VII.
[13] T. Ooi, R.A. Scott, G. Vanderkooi and H.A. Scheraga, J. Chem. Phys. 46 (1967) 4410.
[14] D.A. Brant and P.J. Flory, J. Am. Chem. Soc. 87 (1965) 2791.
[15] O. Kratky and G. Porod, Rec. Trav. Chim. 68 (1949) 1106.
[16] M.S. Beevers and J.A. Semlyen, Polymer 13 (1972) 385.
[17] H. Yamakawa, Modern theory of polymer solutions (Harper and Row, New York, 1971) p. 12.
[18] R.L. Jernigan and P.J. Flory, J. Chem. Phys. 50 (1969) 4185.
[19] S. Premilat and J. Hermans, Jr., J. Chem. Phys. 59 (1973) 2602.

BIOPHYSICAL CHEMISTRY 2 (1974) 83–96. © NORTH-HOLLAND PUBLISHING COMPANY

MODEL CALCULATIONS ON THE KINETICS OF OLIGONUCLEOTIDE DOUBLE HELIX COIL TRANSITIONS. EVIDENCE FOR A FAST CHAIN SLIDING REACTION

Dietmar PÖRSCHKE

Max-Planck-Institut für biophysikalische Chemie, 34 Göttingen, GFR

Received 25 March 1974
Revised manuscript received 6 May 1974

Relaxation data obtained previously for the double helix coil transition of oligoriboadenylates and oligoribouridylates are compared to the results of numerical calculations according to various models. In these models the helix coil transition is described by individual rate constants for the first steps of helix formation, whereas the rate constants of the following steps of helix chain growth are assumed to be uniform. The existence of various helix intermediates containing the same number of base pairs is accounted for by statistical factors. First a quasistationary treatment of a zipper model is used for an analysis of the influence of various model parameters. Then relaxation spectra are calculated including helix coil intermediates explicitly without any assumption of quasistationarity. The relaxation spectrum calculated for any chain length N comprises $N-1$ fast processes with time constants in the range of 0.1 to 0.5 μs and one slow process with a time constant τ depending upon the nucleotide concentration (τ is usually in the ms time range). The fast processes are associated mainly with the unzippering at helix ends and are usually characterized by relatively small amplitudes, whereas the slow process represents the overall helix coil transition usually characterized by a very large amplitude.

Consideration of staggered helix series (where the different helix series are coupled to each other by the single stranded state) leads to a spectrum of slow relaxation processes with one separate relaxation process for each helix series. It is shown that this "non-sliding" staggering zipper model is not consistent with the experimental results. The measured relaxation curves can be represented by single exponentials for nucleotide chain lengths 8 to 11 (within experimental accuracy). This is also true for conditions where several, clearly separated time constants should be expected according to the theoretical model. The experimental data suggest the existence of a direct coupling between different series of staggered helices by a chain sliding mechanism with a time constant < 1ms. Chain sliding may be explained by diffusion of helix defects along the double helix such as diffusion of small loops. A simple model calculation for the diffusion of a bulge loop assuming quasistationarity suggests a sliding time constant around 100 μs for a helix comprising 10 base pairs.

Finally some thermodynamic and kinetic parameters are evaluated according to the "sliding" staggering zipper model: The negative activation enthalpy observed for helix recombination can be described using a series of nucleation parameters indicating reduced stability constants for the first three base pairs. Nucleation may usually be achieved with the formation of the third or fourth base pair depending upon the magnitude of the chain growth parameter. The rate constant of helix chain growth is around 10^6 s^{-1} at 0.05 M [Na^+] and increases to about 4×10^6 s^{-1} at 0.17 M [Na^+].

1. Introduction

Convenient models for the investigation of the dynamics of base recognition in nuclei acids are helix complexes formed from oligonucleotides [1–6]. The oligomer systems allow direct determinations of elementary reaction parameters. Of the systems analyzed until now, the base pairing between oligoriboadenylates and oligoribouridylates was studied in most detail.

Helices from oligo(A) and oligo(U) are formed according to a second order mechanism [3]. It was found that the rate constants of recombination are almost independent of the chain length, suggesting that the rate determining step is a nucleation process identical for various chain lengths. When a nucleus is present, formation of further base pairs is a comparatively fast process. The negative enthalpy of activation observed for the recombination rate demonstrates that the nucleation is not a simple elementary step. From the value of the activation enthalpy (around −9kcal/mole),

it has been concluded that about three base pairs are required for (A) · (U) helix nucleation [3, 5]. In contrast to the rate of recombination, the rate of dissociation is strongly chain length dependent; increasing chain lengths lead to decreasing rates of dissociation. The magnitude of the activation enthalpies observed for the dissociation is close to that of the reaction enthalpies associated with helix dissociation.

Hitherto, the analysis of these data was based upon simple all or none models and upon quasistationary treatments. The purpose of the present investigation is a more detailed quantitative treatment of the data obtained from oligo(A) · oligo(U) model helices. Starting from some model calculations assuming quasistationarity, the kinetics of the oligomer helix coil transition is described quantitatively by explicit consideration of partly melted helix species without the assumption of quasistationarity. Comparison of calculated relaxation spectra to those measured by the temperature jump method leads to the suggestion of a new mechanism involved in the helix coil transition. Finally some kinetic model parameters are evaluated.

2. Elementary rate constants and statistical factors

The formation of a double helix from complementary nucleotide chains is not a simple one-step process, but involves a series of elementary steps (fig. 1). The determination of each of the corresponding rate constants is impossible. However, many of the steps, like the steps of helix growth, are expected to be very similar and may be described by a uniform rate constant. On the other hand, individual rate constants will be required for the description of the nucleation process. For the present system it is useful to introduce two different kinds of correction factors (cf. fig. 1; cf. ref. [7]).

a) A series of constants σ_n describing the reduction of the stability constant of the nth base pair compared to that found for a base pair in an infinitely long helix sequence where

$$\lim_{n\to\infty} \sigma_n = 1 . \tag{1}$$

It cannot be decided a priori whether a variation in the stability constant is associated mainly with the rate constant of dissociation or the rate constant of recombination. For the purpose of the present model calculations, it is most convenient to associate the σ factors with the rate constants of dissociation.

b) A second series of correction factors γ_n is used for scaling of forward and backward rate constants, k_f and k_b, respectively (see fig. 1). In analogy to eq. (1)

$$\lim_{n\to\infty} \gamma_n = 1 . \tag{2}$$

The various possibilities of forming helix species are considered by statistical factors. These factors are discussed below within the framework of a simple zipper model (cf. ref. [5]), i.e., staggered helical species are not yet included. When oligonucleotides with N complementary bases recombine, a first base pair may be formed at N different positions. Thus the rate constant for the formation of a first base pair will be

$$k_{01} = N \gamma_1 k_f . \tag{3}$$

If the first base pair is formed at one end of the strands, there is only one way of forming an adjacent base pair (cf. fig. 2). If the helix formation does not start at one of the nucleotide ends, however, there are two ways of helix growth with equal probability. When all

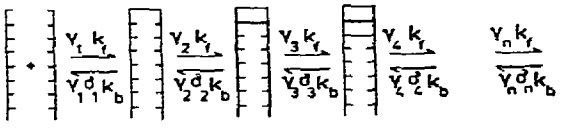


Fig. 1. Schematic representation of helix formation.

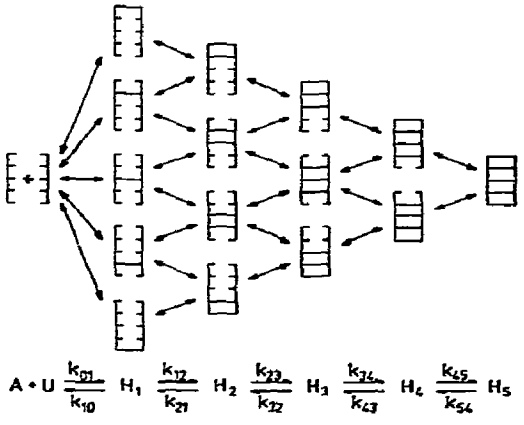


Fig. 2. Schematic representation of helix formation with intermediates according to a zipper model.

the different helices with one base pair are considered as one class of species, the probability of conversion to the class of helix species with two base pairs – i.e., the number of helix growth pathways divided by the number of initial helix states – can be calculated according to the general formula

$$\nu_n = \frac{2(N-n)+2}{N-n+2} \quad \text{for } n \geq 2, \tag{4}$$

where n is the number of base pairs in the class of helix species formed. Thus the individual rate constants are given by

$$k_{n-1,n} = \nu_n \gamma_n k_f \quad \text{for } n \geq 2. \tag{5}$$

Base pairs may dissociate at both ends of a helix sequence with the same probability. For this reason the rate constants of dissociation are given by

$$k_{n,n-1} = \nu'_n \gamma_n \sigma_n k_b, \tag{6}$$

With $\nu'_n = 2$ for $n \geq 2$. A single base pair may dissociate in one way only, thus $\nu'_1 = 1$.

It is impossible to determine all the individual kinetic parameters defined above. However, the number of independent variables is reduced by consideration of the thermodynamic parameters evaluated previously [8]. By definition the chain growth parameter s is

$$s = k_f/k_b \tag{7}$$

and the nucleation parameter β is

$$\beta = 1/\prod_{n=1}^{\infty} \sigma_n . \tag{8}$$

Furthermore the various σ_n factors will be assigned according to the expectation that a first base pair will be less stable than a second base pair less stable than a third one. Thus

$$\sigma_2 > \sigma_3 \ldots \geq 1 . \tag{9}$$

The exact thermodynamic functions for the calculation of s and β for oligo(A) · oligo(U) helix coil transitions are described in ref. [8]. The chain growth parameter s is in the range of 10 at 0°C to 2 at 40°C. Analysis of the oligo(A) · oligo(U) melting curves demonstrated that the nucleation parameter β depends upon the temperature too. At 0°C β is 4×10^{-4} M^{-1}, whereas at 40°C β is 8×10^{-4} M^{-1}.

3. Quasistationary model calculations

In previous discussions of the helix coil kinetics according to quasistationary calculations [1, 2, 5, 9–11], the general expressions derived for a sequential mechanism of double helix formation (cf. ref. [2]) were simplified by consideration of special model cases. In the present investigation the rates of recombination and dissociation are calculated directly by means of a computer, allowing free variation of any of the individual rate constants involved.

3.1. Influence of σ parameters

The influence of the model parameters upon the overall rate constants k_R and k_D may be analyzed in two different steps. In the first step an equilibrium parameter σ is varied without changing any of the γ parameters ($\gamma_i = 1$ for all i). The dependence of the rate of recombination k_R and the associated enthalpy of activation AE_R upon σ_2 (at $\sigma_i = 1$ for $i > 2$) is represented in fig. 3. At low values of σ_2 the formation of the second base pair is the rate determining step, since $k_{21} < k_{23}$ (and $k_{10} > k_{12}$). Under these conditions the activation enthalpy is the sum of the enthalpy for the formation of the first base pair ΔH_{01} and the activation enthalpy associated with the formation of the second base pair AE_f. An increase of σ_2 leads to a change of the mechanism. At high values of σ_2 (i.e., $\sigma_2 > 10$) the formation of the third base pair becomes the rate determining step, since $k_{21} > k_{23}$ (and $k_{32} < k_{34}$). For these conditions, the activation enthalpy is the sum of the enthalpy for the formation of the first two base pairs $\Delta H_{01} + \Delta H_{12}$ and the activation enthalpy associated with the formation of the third base pair. The model calculation presented in fig. 3 illustrates the possibility of fitting experimental enthalpies of activation by an appropriate choice of σ_i parameters. It also shows the order of magnitude of σ_i parameters required for a shift of the rate determining step in (A) · (U) helix formation.

3.2. Influence of γ parameters

An example for the influence of a γ parameter is given in fig. 4. At low values of γ_1 the formation of the first base pair is the rate determining step and the recombination rate is proportional to γ_1. At $\gamma_1 \geq 1$

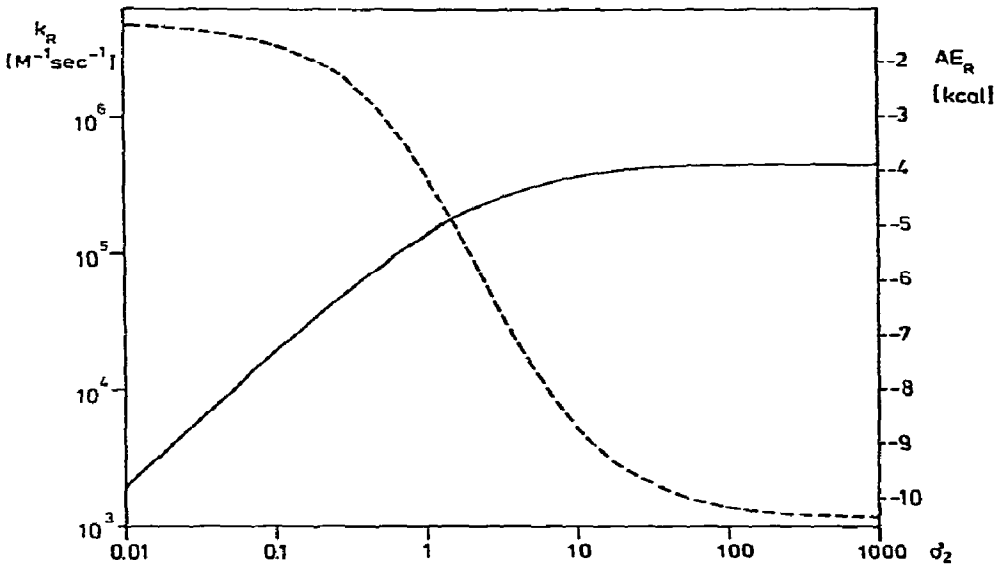


Fig. 3. Rate constant of recombination k_R and its enthalpy of activation AE_R as a function of σ_2 calculated according to the quasistationary model. ($N = 10$, 25°C, $k_f = 5 \times 10^6$ s^{-1}, $AE_f = 2$ kcal/mole, $\gamma_i = 1$ for all i, $s = 3.74$, $\beta = 5.88 \times 10^{-4}$ M^{-1})

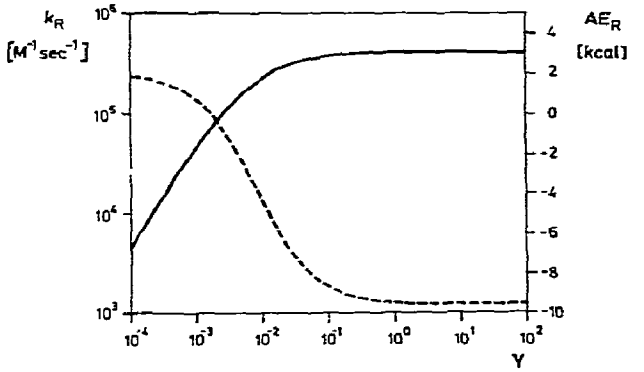


Fig. 4. Rate constant of recombination k_R and its enthalpy of activation AE_R as a function of γ_1 calculated according to the quasistationary model. ($N = 10$, 25°C, $k_f = 5 \times 10^6$ s^{-1}, $AE_f = 2$ kcal/mole, $\sigma_2 = 20$, $\gamma_i = 1$ for $i > 1$, $s = 3.74$, $\beta = 5.88 \times 10^{-4} M^{-1}$)

the formation of the third base pair becomes the rate determining step (due to $\sigma_2 = 20$ used in this example) and the rate constants of the first step no longer influence the overall rate of recombination. The change in the rate determining step is reflected in the enthalpy of activation going from +2 kcal/mole (corresponding to the activation enthalpy of the first step) to about −10 kcal/mole (corresponding to $\Delta H_{01} + \Delta H_{12} + AE_f$). The model calculation presented in fig. 4 demonstrates that the value of γ_1 does not influence the overall rate parameters significantly as long as γ_1 is greater than 0.1.

3.3. Model parameters of oligo(A) · oligo(U) helix formation

A recent determination of the rate constant of binding a monomer base to a complementary polynucleotide template [12] yielded a value of 7.5×10^7 M^{-1} s^{-1}. Due to sterical factors and due to electrostatic repulsion, the rate of forming a first base pair in oligomer helices, i.e., $\gamma_1 k_f$, will be lower than that, probably between 10^6 and 10^7 M^{-1} s^{-1}. According to previous estimates [3, 5] the value of k_f is expected to be of the same order of magnitude, thus $\gamma_1 \approx 1$. As long as definite evidence for possible deviations is not available, it will be assumed that all the γ_i parameters are unity. Then the set of rate constants measured for the helix coil transition of oligo(A) · oligo(U)

(at 0.05 M salt) can be represented by the following model parameters: $k_f = 3.2 \times 10^6\ s^{-1}$ (25°C) $AE_f = 2$ kcal, $\sigma_2 = 20$, $\sigma_3 = 4$.

4. Relaxation spectrum according to a zipper model

4.1. Results of the model calculations

For a more accurate description of the kinetics of the helix-coil transition the helix coil intermediates have to be included directly without assuming quasi-stationarity. However, the following simplifications are made in order to reduce the number of rate equations:

1) Helix species containing the same number of base pairs in different configurations are considered to be one kind of intermediate (cf. fig. 2).

2) Staggered helix species are excluded.

Furthermore, the set of rate equations resulting from the kinetic scheme is linearised. Thus the results of the calculations are valid for small perturbations (as is the case for the experimental data obtained from relaxation measurements).

The helix coil transition of complementary oligonucleotides of chain length N is described by the following set of linearised rate equations:

$$\dot{x}_A = \dot{x}_U = -k_{01}(C_A + C_U)\,x_A + k_{10}\,x_{H_1},$$

$$\dot{x}_{H_1} = -(k_{10}+k_{12})\,x_{H_1} + k_{01}(C_A+C_U)\,x_A + k_{21}\,x_{H_2},$$

$$\dot{x}_{H_2} = -(k_{21}+k_{23})\,x_{H_2} + k_{12}\,x_{H_1} + k_{32}\,x_{H_3},$$

$$\vdots$$

$$\dot{x}_{H_N} = -k_{N,N-1}\,x_{H_N} + k_{N-1,N}\,x_{H_{N-1}}. \qquad (10)$$

The rate constants are equivalent to those used in the quasistationary treatment. C_A and C_U are the concentrations of the complementary single stranded oligonucleotides. The parameters x_i are the differences between the concentrations of species i at any time t and these concentrations at $t = \infty$ (i.e., at equilibrium). $\dot{x}_i$ are the corresponding differentials dx_i/dt. Due to the conservation of mass:

$$x_A + \sum_{n=1}^{N} x_{H_n} = 0. \qquad (11)$$

Using this condition one rate equation may be eliminated and the remaining system of rate equations may be represented in the form of a matrix with N columns and N rows. The mathematical procedure for the evaluation of relaxation times (as well as relaxation amplitudes) from this matrix has been discussed by Eigen and De Maeyer [13]. In the present investigation numerical solutions were obtained using a Fortran program developed by G. Ilgenfritz (unpublished). A general subroutine was written, which in connection with the main program allows the calculation of relaxation spectra (time constants as well as amplitudes) for any oligomer helix coil transition.

The helix coil transition of a helix containing N base pairs involves N independent reaction steps, which should be reflected in a relaxation spectrum including N time constants. Two examples of time constants and amplitudes of such relaxation spectra are shown in table 1. The helix coil transition of octanucleotides is represented by 8 time constants and that of octadecanucleotides by 18 time constants. In both cases, however, the main amplitude of the reaction is associated with the lowest $1/\tau$ value, i.e., with the slowest reaction. The amplitudes are calculated with the assumption, that each base pair formed contributes the same unit change to the total optical effect. Although this model may not be accurate in detail, it is expected to represent the general character of the amplitudes correctly.

Further model calculations show, that the relaxation process with the lowest $1/\tau$ value is strongly concentration dependent, whereas the majority of the other relaxation processes do not exhibit any concentration dependence. It can also be shown, that the relative amplitude of the "slow process" decreases at low degrees of the helix coil transition, whereas the relative amplitudes of the fast processes increase in that range.

Due to the coupling of the individual reaction steps, it is not possible to associate each of the calculated relaxation processes with an individual base pairing reaction (cf. ref. [13]). The calculated relaxation times are associated with normal modes of the coupled reaction system. In the present system, the slowest relaxation process (with the lowest $1/\tau$ value) represents the all or none helix coil reaction between separated single strands and complete double helices. Its time constant is close to that calculated from an all or

Table 1
Relaxation spectra according to a zipper model

Example 1 [a]		Example 2 [b]	
$1/\tau_i$	A_i	$1/\tau_i$	A_i
2.77 E+2	9.90 E−1	7.90 E+1	7.53 E−1
2.66 E+6	8.40 E−3	2.05 E+6	1.30 E−1
4.40 E+6	1.79 E−3	2.97 E+6	7.02 E−2
6.45 E+6	2.15 E−4	4.31 E+6	3.07 E−2
8.35 E+6	4.68 E−5	5.98 E+6	1.12 E−2
1.03 E+7	4.64 E−7	7.86 E+6	3.58 E−3
1.38 E+7	7.16 E−7	9.83 E+6	1.09 E−3
3.43 E+7	9.14 E−9	1.17 E+7	2.57 E−4
		1.36 E+7	6.73 E−5
		1.51 E+7	5.78 E−6
		1.65 E+7	2.48 E−6
		1.77 E+7	1.48 E−7
		2.34 E+7	1.32 E−6
		6.25 E+7	3.54 E−8

a) N=8, $C_t = 5 \times 10^{-5}$, 0 → 3.4°C, $k_f = 3.84 \times 10^6 s^{-1}$, s = 8.45, θ = 0.211.
b) N=14, $C_t = 10^{-3}$, 9.2 → 16.9°C, $k_f = 4.55 \times 10^6 s^{-1}$, s = 4.43, θ = 0.917. θ is the fraction of nucleotide residues involved in base pairing.

none model. The amplitude of the process is close to the total amplitude of the helix coil reaction at low chain lengths. For high chain lengths, in particular at low degrees of the helix coil transition, another helix coil reaction becomes important. This reaction is the unzippering of helices at helix ends, i.e., the dissociation of a few base pairs, which does not necessarily lead to the dissociation of the complete helix (cf. ref. [14]). Due to the high elementary time constant of intramolecular base pairing, this reaction is very fast. Since it is an intramolecular reaction, it does not show any concentration dependence. There is a series of different unzippering reactions coupled to each other without high activation barriers. This kind of coupling leads to the broad relaxation spectrum shown in table 1. The results of the present model calculations are consistent with the results obtained for a simple sequential model by Elson [15].

4.2. Comparison with experimental relaxation data

The relaxation spectra calculated according to the zipper model agree quite well with the experimental relaxation curves obtained for the helix coil transition of oligo(A) · oligo(U). Both relaxation phases predicted by the theoretical calculations were observed, clearly separated from each other. As expected the time constant of the fast process is independent of nucleotide concentration [14], whereas the reciprocal time constant of the slow "all or none" process is a linear function of the free nucleotide concentration [3].

The agreement of the theoretical calculations according to the zipper model with the experimental data does not mean, however, that the zipper model describes the helix coil kinetics in oligo(A) · oligo(U) accurately. As discussed in the following section, staggered helices, which are neglected in the zipper model, influence the relaxation spectrum associated with the helix coil transition of oligo(A) · oligo(U) significantly. The "simple" zipper model allows a correct description of helix coil kinetics only, when staggered helices are present at negligible concentrations, as may be expected for block-oligomers (e.g., AAAAUUUU [5]) and for hetero-oligomers containing GC base pairs (e.g., AAGCUU [6]).

5. Relaxation spectrum according to a "non-sliding" staggering zipper model

5.1. Results of the model calculations

In addition to the helix species with exactly aligned nucleotide chains, included in the zipper model, oligo(A) and oligo(U) form staggered helix species with a few nucleotide units extending at each helix end. These staggered helix species, which are considered in the staggering zipper model [8, 16], contribute significantly to the helix population. Thus the contributions of staggered helix species must also be included in kinetic model calculations.

Two series of staggered helix species, shown schematically in fig. 5 for pentanucleotides, are considered in the following model calculations. Statistical factors for helix formation and dissociation are assigned according to the same schema as shown for the aligned zipper helices in fig. 2. The intrinsic rate constants for formation or dissociation of individual base pairs are also the same as defined for the aligned zipper helices. However, one has to take into account that there are two different kinds of staggered helix species for each series: a) one of the strands may be shifted in the

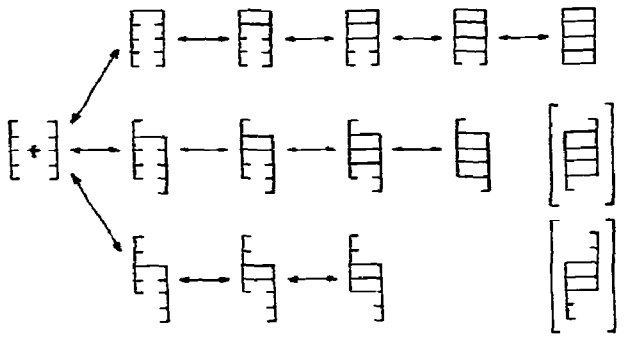


Fig. 5. Scheme of helix formation according to a staggering zipper model with two series of staggered helices. The helix species shown in brackets indicate the two different kinds of helices within each series of staggered species.

"3′–5′ direction" with respect to its complementary partner or b) in the opposite direction (cf. fig. 5). The thermodynamic and kinetic parameters of both will be identical. The existence of the two kinds is considered in the kinetic model simply by a factor of 2 in the rate constant for the formation of a first base pair for each series of staggered helices.

The influence of staggered helix series upon the type of calculated relaxation spectra is illustrated in table 2. All the relaxation spectra are calculated for the same chain length and for the same intrinsic equilibrium and rate parameter, yet according to different models. The total number of relaxation times μ increases with the number of helix species considered in the calculation. Most of these relaxation times are associated with the unzippering reactions of the helix series and are characterized by high $1/\tau$ values and by rather low amplitudes. However, the calculated relaxation spectra also show relaxation effects with quite different properties, characterized by low $1/\tau$ values and high relative amplitudes. In contrast to the time constants of most of the fast processes, the time constants of the slow processes are concentration dependent. For each helix series considered in the model calculation one slow relaxation process is obtained. Obviously the three slow relaxation processes calculated according to the staggering zipper model with 2 staggered helix series are associated with the overall helix coil transitions of the following three helix series: (1) the series with aligned oligomer strands, (2) the series with one nucleotide unit staggering at each end, and (3) the helix series with two nucleotide units staggering at each end. These three helix series constitute three separated reaction pathways – each with a number of relaxation times corresponding to the number of helix

Table 2
Relaxation spectra according to 1) a zipper model, 2) a "non sliding" staggering zipper model with one series of staggered helices (one residue staggering), 3) a "non sliding" staggering zipper model with two series of staggered helices (one and two residues staggering)

	1		2		3	
	$1/\tau_i$	A_i	$1/\tau_i$	A_i	$1/\tau_i$	A_i
"slow"	2.32 E+1	9.60 E−1	7.05 E+0	2.34 E−1	6.84 E+0	2.44 E−1
			6.32 E+1	7.23 E−1	4.86 E+1	4.45 E−1
					1.56 E+2	2.66 E−1
"fast"	2.41 E+6	2.65 E−2	2.41 E+6	2.31 E−2	2.41 E+6	2.36 E−2
	3.48 E+6	9.66 E−3	2.45 E+6	5.89 E−3	2.45 E+6	6.03 E−3
	4.96 E+6	2.93 E−3	3.48 E+6	8.40 E−3	2.54 E+6	7.72 E−4
	6.71 E+6	6.54 E−4	3.77 E+6	1.83 E−3	3.48 E+6	8.61 E−3
	8.53 E+6	1.03 E−4	4.96 E+6	2.55 E−3	3.77 E+6	1.87 E−3
	.	.	.	.	.	.
	.	.	.	.	.	.
	.	.	.	.	.	.
	6.71 E+7	1.57 E−7	6.71 E+7	1.34 E−6	6.71 E+7	1.66 E−6
i_{max}	10		19		27	

$N = 10$, $C_t = 10^{-4}$M, $T = 0 \rightarrow 3.4$°C, $k_f = 3.84 \times 10^6$ s^{-1}, $s = 7.63$, $\sigma_2 = 20$, $\theta = 0.774$.

species. The pathways are coupled to each other by the single stranded state, resulting in three slow relaxation processes. The time constants of these processes are determined by the overall rate constants of recombination k_R and of dissociation k_D. Since the k_R values are almost equivalent for the different helix series, the difference of the three time constants is due to the difference of the k_D values, which differ by factors of s for the different helix series.

The amplitudes of the three slow relaxation processes depend upon the degree of the helix coil transition. At temperatures where most of the helices are converted to the coil form, the main amplitude is associated with the slow relaxation process, i.e., associated with the helix series with aligned oligomer strands. At high helix content the amplitudes associated with the staggered helix species increase and may even become predominant (cf. fig. 6).

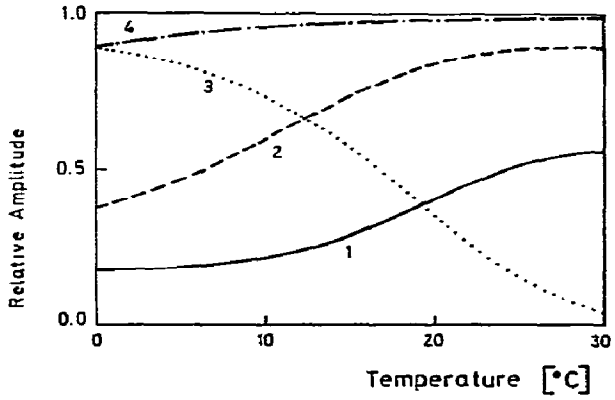


Fig. 6. Relaxation amplitudes according to a staggering zipper model with consideration of two staggered helix series as a function of the temperature. At each temperature the section between the abscissa and the first line (—) represents the relative amplitude A_1 of the slowest process no. 1, the section between the first (—) and the second (– – –) line, the relative amplitude of the process no. 2 and the section between the second (– – –) and the third (—·—) line, the relative amplitude of process no. 3. The rest amplitude (range no. 4) is due to the fast unzippering at helix ends. The dotted line represents the $N = 10$, $C_t = 5 \times 10^{-4}$ M fraction of nucleotides being in the helical state.

5.2. *Comparison to experimental relaxation data*

Provided that the staggering zipper model is correct, a relatively broad spectrum of relaxation times should be expected. The separation of the different time constants should be most pronounced at high chain growth parameter s. Optimal amplitude ratios for a convenient resolution of the spectrum should be found at high helix content.

Previously the experimental relaxation curves were fitted by single exponentials and in general the fitting was surprisingly accurate. Deviations from a single exponential response were observed mainly for rather long oligonucleotides of chain length 14 or 18 [3]. In view of the results of the model calculations the experimental relaxation curves were reexamined carefully. Virtually all of the relaxation curves measured for chain lengths 8, 9, 10 and 11 could be described by single exponentials within experimental error. In particular those measurements, that could be performed with high experimental accuracy (i.e., low lamp fluctuations, high signal change, etc.), were in excellent agreement with single exponentials.

It is well known, that the analysis of relaxation curves with more than one time constant is rather difficult, unless the time constants are clearly separated from each other. When the time constants differ by a factor of two, for instance, the resulting function may be approximated by a single exponential with great accuracy [17]. For the present oligomer systems, however, the model calculations predict time constants separated by factors of 5 under certain conditions. If these relaxation processes were present in reality, it should be possible to detect them rather easily. A sample of a measured and a corresponding calculated relaxation function is given in fig. 7. It is readily seen that the experimental and theoretical results are not consistent.

6. Relaxation spectrum according to a "sliding" staggering zipper model

6.1. *Chain sliding by defect diffusion*

Since the experimental relaxation function and the relaxation function predicted by a direct application of a staggering zipper model are not consistent, the basis of the kinetic model has to be analyzed in more detail. The broad relaxation spectrum predicted by the model is due to the existence of the series of staggered helices, which are coupled to each other only by

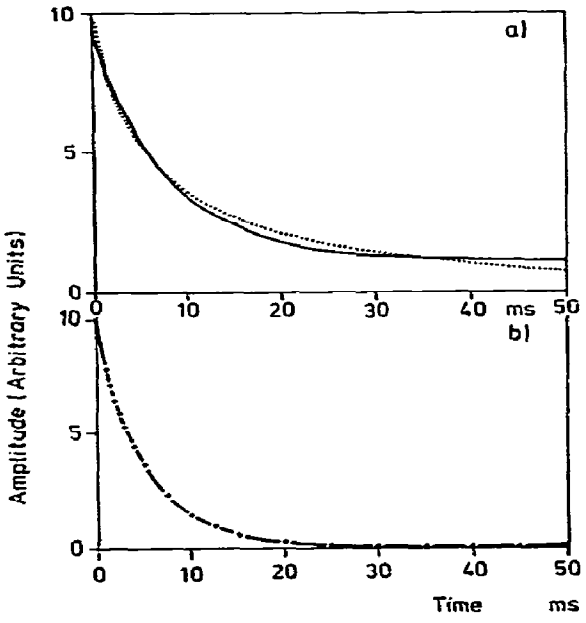


Fig. 7. Theoretical (a) and experimental (b) relaxation curves. The theoretical points (a) are calculated according to a staggering zipper model including two series of staggered helices $\tau_1 = 1.47$ ms, $A_1 = 0.105$; $\tau_2 = 5.54$ ms, $A_2 = 0.477$; $\tau_3 = 28.3$ ms, $A_3 = 0.391$. Both curves are fitted to a single exponential [$A = A_0 \exp(-t/\tau) + B$] by a least squares procedure (line) ($N = 10$, $C_t = 3.33 \times 10^{-5}$M oligomers, 10.5 → 15.5°C, 0.15 M salt).

the single stranded state. Because of this kind of coupling the different helix series are separated from each other by relatively high activation barriers.

However, the predicted relaxation spectrum may be changed completely when a new mechanism in the helix coil transition is considered. The theoretical relaxation spectrum with its various slow time constants may be converted into a relaxation function with a single slow time constant by introduction of a relatively fast coupling reaction between the different helix series. The most direct way of coupling the different staggered helix series seems to be a chain sliding reaction of one nucleotide strand along its complementary partner. In order to explain the observation of a single exponential in the helix coil transition of oligo(A) · oligo(U), the sliding reaction must be relatively fast.

Any mechanism requiring a simultaneous dissociation of many base pairs is characterized by very high activation energies resulting in relatively low rates of reaction. Thus a mechanism has to be found with intermediates that can be formed without high energies of activation. This condition could be fulfilled by the following type of mechanism:

With a certain probability the intramolecular base pairing reaction of the nucleotide residues, being in the single stranded state adjacent to a helix sequence, will not lead to a proper continuation of the helix sequence. In the most simple case, a single nucleotide residue may loop out of the helix sequence. The formation of such a "bulge" loop certainly distorts the helix geometry. Thus, the equilibrium concentration of bulge loops may be relatively low. However, bulge loop formation is not negligible. According to a recent estimate [18], the equilibrium concentration of a helix containing one bulge loop compared to that of a helix with the same number of base pairs in an undistorted helix sequence is lower by a factor η of about 0.01.

When a bulge loop is present in a helix sequence, the loop base will be subjected to the rapid base pair formation and dissociation process. As a consequence of this rapid equilibration, a bulge loop may move quite rapidly along the helix sequence. The probability for bulge movement in a double helix formation from homopolynucleotides is equal for both directions. If a bulge loop is formed at one end of a helix sequence and disappears at the opposing end, the bulge loop diffusion will result in a shift of the nucleotide strands by one nucleotide residue against each other (fig. 8).

6.2. Quasistationary model of chain sliding by bulge loop diffusion

Such a defect-diffusion mechanism may be described quantitatively by assuming quasistationarity of the bulge loop intermediates. The repeating steps of bulge

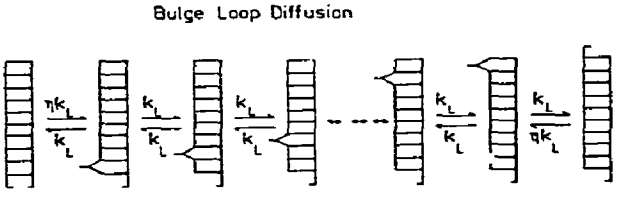


Fig. 8. Scheme of bulge loop diffusion resulting in chain sliding.

loop movement may be characterized by uniform rate constants k_L. Individual rate constants are required for loop initiation. For simplicity, it is assumed, that the nucleation barrier for the introduction of a bulge loop is associated with the first step exclusively. Starting from a helix with unpaired nucleotide residues at the helix ends, a bulge loop may be introduced without changing the total number of base pairs. In that case the nucleation factor η is simply related to the free energy of bulge loop formation ΔG_L by

$$\eta = \exp(-\Delta G_L/RT) \tag{12}$$

and the rate of the first step of bulge loop nucleation may be described by $\eta\, k_L$. The evaluation of the overall rate constant of chain sliding k_s assuming quasi-stationarity of the intermediates yields

$$k_s = \eta\, k_L/N, \tag{13}$$

where N is the number of base pairs of the helix sequence. The rate constant of loop movement k_L is expected to be of the same irder of magnitude as the rate constants found for the elementary steps of base pairing. Using a value of $k_L = 5 \times 10^6\ s^{-1}$ and $\eta = 0.01$, the rate constant of chain sliding will be $5 \times 10^3\ s^{-1}$ for helix chain length $N = 10$. The relaxation time associated with the chain sliding reactions $\tau_s = 1/(2k_L)$ will then be about 100 μs. Although this estimate of the chain sliding relaxation time may be a rough approximation only, it shows that the chain sliding reaction in helices formed from homopolynucleotides should be expected to proceed in a relatively short time range.

6.3. Relaxation spectrum

When the fast coupling due to chain sliding is included in the model calculations, the main amplitude of the relaxation spectrum is associated with a single slow time constant τ_1 (cf. table 3). This time constant reflects the overall helix association–dissociation process and $1/\tau_1$ is a linear function of the free single strand concentration. Since three different helix series are considered in the present treatment of the staggering zipper model, the chain sliding reaction is reflected by two relaxation processes. These processes are associated with rather small amplitudes, at least for short chain lengths. Thus, the chance to measure the chain sliding reaction directly is very small. For higher chain lengths, i.e., $N = 14$ and 18, some relaxation amplitude was measured in the time range between the slow ("all or none") process and the fast unzippering spectrum [3]. This amplitude could be due to chain sliding. However, some part of this amplitude could also be due to the existence of hairpin loops, which may become important in this range of chain lengths.

Table 3
Relaxation spectrum according to a "sliding" staggering zipper model (two series of staggered helices). The data are for the 7 slowest of 27 relaxation processes. Chain length and experimental conditions are the same as in table 2. Rate constant of chain sliding $10^5\ s^{-1}$

$1/\tau_i$	A_i
8.62 E+1	9.16 E−1
6.23 E+4	2.85 E−2
1.17 E+5	4.68 E−3
2.41 E+6	2.89 E−2
2.46 E+6	4.65 E−3
2.55 E+6	3.00 E−3
3.48 E+6	8.81 E−3

$N=10$, $C_t = 10^{-4}$M, 0→3.4°C, $k_f = 3.84 \times 10^6 s^{-1}$, $s = 7.63$, $\theta = 0.774$.

6.4. Experimental and model parameters

Some model calculations using the simplified quasi-stationary approach already showed the influence of the various kinetic model parameters upon the overall rate constants. In general the same relations will be valid for the more complex staggering zipper model. However, the extension of the kinetic staggering zipper model by consideration of chain sliding gives rise to some change in the relation between the elementary and the overall rate constants. As a consequence of the fast chain sliding effect, a helix with aligned nucleotide strands containing the maximal number of base pairs may be formed according to an increased number of reaction pathways including those starting from an initial formation of staggered helices with subsequent chain sliding reactions. Obviously the reaction pathways via chain sliding will increase the overall rate of recombination for a given set of elementary rate constants. Since all the reactions are reversible, the same is true for the rate of dissociation.

An exact evaluation of the overall rate constants would require an accurate knowledge of the rate of

chain sliding as a function of chain length, temperature, etc. Without this exact information about the chain sliding it is not possible to judge, e.g., whether helix species containing few base pairs and many residues staggering at each end will have a chance for chain sliding within their lifetime.

In the present model calculations only two series of staggered helices are considered: those with one and with two nucleotide residues staggered at each end. If the neglected helix series would contribute significantly to the overall rate of the helix coil transition, the elementary rate constants evaluated from fitting of the overall k_R and k_D values would decrease by factors of about 2 to 3.

A reasonable fit of the measured overall rate constants k_R and k_D using the present model with two staggered helix series is obtained with the following elementary parameters:

$k_f = 10^6\ s^{-1}$ (25°C), $AE_f = 2$ kcal, $\sigma_2 = 20$, $\sigma_3 = 4$

($\gamma_i = 1$ for all i).

The theoretical rate constants given in fig. 9a and b were derived from calculated relaxation spectra using the time constant of the slow relaxation process. Although there are some obvious differences of the theoretical and the experimental rate constants, it is apparent that these differences are mainly due to some scatter in the experimental parameters. The experimental rate constants of recombination obtained for chain lengths 9 and 11, for example, are relatively low, whereas those obtained for chain lengths 10 and 14 are relatively high. It is certainly not expected that there are any such maxima and minima of these rate constants depending upon chain length. Thus these deviations are attributed mainly to experimental errors. In general terms the experimental data can be represented correctly.

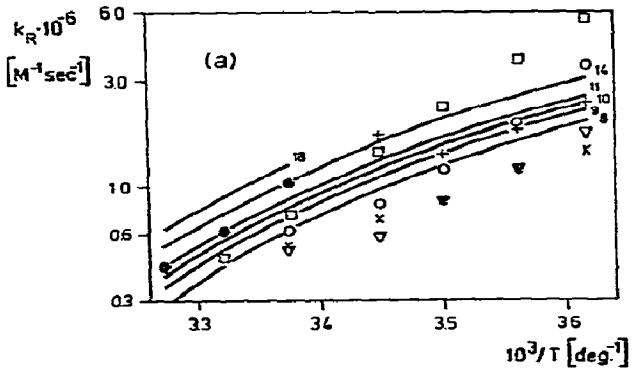


Fig. 9a.

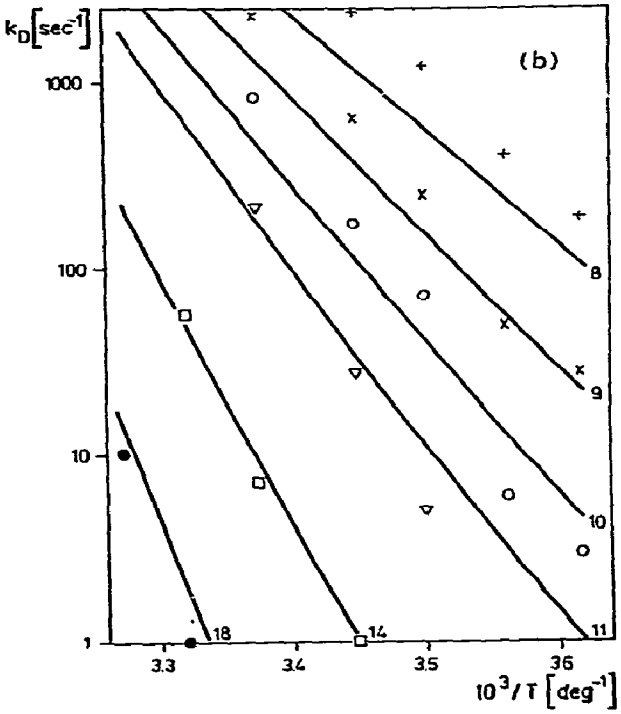


Fig. 9. Experimental and theoretical rate constants of recombination (a) and of dissociation (b) as a function of the reciprocal absolute temperature for different chain lengths (0.05 M salt). Experimental values are from ref. [3] and theoretical curves are calculated according to a staggering zipper model (two series of staggered helices) with chain sliding (model parameters as given in the text). Experimental data symbols: N = 8 (+), 9 (×), 10 (○), 11 (△), 14 (□) and 18 (●).

6.5. *Ionic strength dependence*

The above set of model parameters was derived for the rate constants measured at 0.05 M ionic strength. Some experimental data obtained recently for the helix coil transition of tetradecanucleotides allow a comparison of model parameters at different ionic strengths. The experimental results obtained at 0.1 and

Table 4
Elementary rate factors evaluated from recombination rate constants k_R measured for $A(pA)_{13} + U(pU)_{13}$ at different ionic strengths (25°C)

Ionic strength	k_R(exp.)	k_f(theor.)	$\bar{\gamma}$
0.05	6.4×10^5	1.0×10^6	0.125
0.1	2.6×10^6	2.2×10^6	0.28
0.166	8.7×10^6	3.7×10^6	0.46

0.166 M [Na^+] are summarized in table 4. The activation enthalpies are close to those obtained previously in 0.05 M [Na^+]. Compared to the rate measured in 0.05 M [Na^+], the rates obtained in 0.1 and 0.166 M [Na^+] are higher by factors of about 4 and 13 respectively. Part of this increase is simply due to an increase of the chain growth parameter with increasing ionic strength (calculated according to ref. [11]; fitting of melting curves obtained for $A(pA)_{13} + U(pU)_{13}$ at 0.1 and 0.166 M [Na^+] did not yield evidence for an ionic strength dependence of the nucleation parameter β within experimental error). The rest of the increase is attributed to a dependence of the rate constants upon the ionic strength. An evaluation according to the model including two staggered helix series leads to the elementary rate constants given in the third column of table 4. If the rate obtained from the direct measurement of helix unzippering is used as a limiting value of the elementary rate constant, γ_i factors may be derived. Obviously this type of evaluation allows a rough comparison only. The γ parameters given in table 4 represent average values over the first series of base pairs.

7. Discussion

Numerical model calculations can be very useful for the investigation of complex reaction mechanisms, when analytical solutions of the set of rate equations are not accessible. By facilitating simple comparisons between theoretical and experimental data, numerical model calculations may help to select possible reaction mechanisms. In the present investigation several models of increasing complexity were used to simulate the experimental data. A summary of the various models is presented in table 5.

One major outcome of the comparison between theory and experiment is the suggestion of a fast chain sliding mechanism in oligo(A) · oligo(U) helices. The existence of a chain sliding reaction in nucleotide double helices may have been expected. However, the suggested high rate of chain sliding is surprising. The experimental evidence for the high rate of chain sliding is supported by the results of a model calculation: chain sliding by diffusion of a loop is expected to occur with a time constant around 100 μs for a helix with 10 base pairs. This time constant is estimated on the basis of a relatively simple mechanism using model parameters that were determined independently.

With a fast chain sliding reaction in (A) · (U) helices, it can be understood more easily that the recombination of poly(A) and poly(U) can be described by a second order rate law up to very high extents of reaction (up to more than 90% of the total reaction amplitude, for conditions with exclusive formation of double helices [19]). Since helix nuclei will be formed statistically along the polymer strands, intermediate formation of helix structures with incomplete base pairing is expected. If the annealing of these structures were characterized by relatively low rates, deviations of the measured rate of helix formation towards a first order mechanism should be observed. However, since intermediate mismatched helix structures are annealed by a fast chain sliding reaction, helix formation poly(A) and poly(U) can be described by a simple second order rate law.

Although direct evidence for a fast chain sliding reaction only is presented for the (A) · (U) system, corresponding reactions may occur in any helix formed from homopolymer strands. In general, the rate of chain sliding will decrease with increasing length of the helix. The rate of sliding in helices formed from heteropolymers will be smaller than that in helices formed from homopolymers, since the formation of intermediate loop structures of low free energy will be less likely in heteropolymer than in homopolymer sequences. Nevertheless, chain sliding reactions are also expected for helices formed from heteropolymers.

Sliding of nucleotide chains may be involved in the processing of the genetic information. Some in vitro experiments suggest the existence of chain sliding effects in the transcription by DNA polymerase. The synthesis of long polynucleotides using short template

Table 5
Models used for the description of oligomer helix coil kinetics

	Model			
	Zipper quasistationary	Zipper	Non-sliding staggering zipper	Sliding staggering zipper
Described in section	3	4	5	6
Without stationary assumption	–	+	+	+
Staggered helices included	–	–	+	+
Model describes				
1: overall transitions of entire helices	+	+	+	+
2: unzippering at helix ends	–	+	+	+
3: chain sliding	–	–	–	+
Validity	simple approximation valid for small N and large s	for all N [a] and s at negligible concentrations of staggered helices	for all N [a] and s chain sliding faster than overall helix dissociation	for all N [a] and s chain sliding slower than overall helix dissociation
Appropriate model system	oligo(A) at acidic pH (refs. [1, 3b]	block- and hetero-oligomers (cf. refs. [5, 6] good approximation for unzippering in oligo(A) · oligo(U) (cf. ref. [14]		oligo(A) · oligo(U)

[a] Except for chain lengths $N >$ "cooperative length".

sequences by DNA polymerase has been explained on the basis of chain sliding [20].

The model calculations performed on the helix coil transition of oligo(A) · oligo(U) are also useful for the evaluation of elementary rate parameters. The theoretical model provides a link between two relaxation processes, that can be analyzed directly by experiments: (1) the overall helix coil reaction [3], and (2) the unzippering reaction at helix ends [14]. Both reactions were measured independently. The fact that the elementary rate constants evaluated from the different measurements are not completely identical, should not be suprising. It is expected that base pairing at helix ends is a faster process than base pairing in the helix nucleus or close to the helix nucleus. The contributions of electrostatic interactions in the helix nucleus will be different from those at helix ends. In addition, the rate of base pairing will also depend upon the length of adjacent nucleotide chains. From this point of view the present kinetic model still presents a simplified picture of the helix coil transition. Nevertheless, the present state of the model is sufficiently detailed for a satisfactory analysis of the elementary processes involved in genetic information transfer.

Acknowledgement

The author is indebted to Dr. G. Ilgenfritz for his advice in the computations and for free use of his Fortran programs, to Drs. E. Neumann and G.W. Hoffman for critical comments on the manuscript and to Dr. M. Eigen for his interest and support. Computer calculations were performed on the Univac 1108 of the Ges. f. wiss. Datenverarbeitung m.b.H., Göttingen.

References

[1] D. Pörschke, Diplomarbeit, Universität Göttingen (1966).
[2] M. Eigen, in: Nobel Symposium 5: Fast reactions and primary processes in chemical kinetics, ed. S. Claeson (Almquist and Wiksell, Stockholm, 1967) pp. 355–361.
[3] D. Pörschke, Thesis, Universität Braunschweig (1968); D. Pörschke and M. Eigen, J. Mol. Biol. 62 (1971) 361–381.
[4] J.G. Hoggett and G. Maass, Ber. Bunsenges. Phys. Chem. 75 (1971) 45–54.
[5] M.E. Craig, D.M. Crothers and P. Doty, J. Mol. Biol. 62 (1971) 383–401.
[6] D. Pörschke, O.C. Uhlenbeck and F.H. Martin, Biopolymers 12 (1973) 1313–1335.
[7] G. Schwarz, J. Mol. Biol. 11 (1965) 64–77.
[8] D. Pörschke, Biopolymers 10 (1971) 1989–2013.
[9] M. Saunders and P.D. Ross, Biochem. Biophys. Res. Commun. 3 (1960) 314–317.
[10] N.R. Kallenbach, D.M. Crothers and R.G. Mortimer, Biochem. Biophys. Res. Commun. 11 (1963) 213–216.
[11] R.D. Blake, L.C. Klotz and J.R. Fresco, J. Amer. Chem. Soc. 90 (1968) 3556–3562.
[12] G.W. Hoffman and D. Pörschke, Biopolymers 12 (1973) 1625–1638.
[13] M. Eigen and L.C. De Maeyer, in: Technique of organic chemistry, eds. S.L. Friess, E.S. Lewis and A. Weissberger, Vol. III-2 (Interscience, New York, 1963).
[14] D. Pörschke, Biophys. Chem. 2 (1974) 97–101.
[15] E.L. Elson, Biopolymers 11 (1972) 1499–1520.
[16] J. Applequist and V. Damle, J. Amer. Chem. Soc. 87 (1965) 1450–1458.
[17] H. Strehlow and J. Jen, Chem. Instr. 3 (1971) 47–69.
[18] I. Tinoco, P.N. Borer, B. Dengler, M.D. Levine, O.C. Uhlenbeck, D.M. Grothers and J. Gralla, Nature New Biol. 246 (1973) 40–41.
[19] R.D. Blake and J.R. Fresco, J. Mol. Biol. 19 (1966) 145–160.
[20] M. Chamberlin and P. Berg, J. Mol. Biol. 8 (1964) 708–726.

BIOPHYSICAL CHEMISTRY 2 (1974) 97–101. © NORTH-HOLLAND PUBLISHING COMPANY

A DIRECT MEASUREMENT OF THE UNZIPPERING RATE OF A NUCLEIC ACID DOUBLE HELIX

Dietmar PÖRSCHKE
Max-Planck-Institut für biophysikalische Chemie, 34 Göttingen, GFR

Received 25 March 1974
Revised manuscript received 6 May 1974

The rate of double helix unzippering was determined directly by application of a fast temperature jump method to a nucleotide system of partly unzippered helices formed from oligoriboadenylates and oligoribouridylates of equal chain lengths (14 and 18 nucleotide residues). These helices showed a relaxation process in the time range of 0.1 to 0.3 μsec, that is assigned to the unzippering reaction. Measurements at 0.05 M and 0.1 M [Na^+] demonstrated a rather small dependence upon the ionic strength. Increase of temperature increases the rate of unzippering. Simulation of the unzippering relaxation by a zipper model yielded a rate constant of base pair formation adjacent to a helix sequence of 8×10^6 sec^{-1} at 25°C associated with an activation enthalpy of 4 kcal/mole. This elementary rate constant is higher than that obtained from a simulation of the overall recombination and dissociation rates of entire helices. The difference is attributed to reduced electrostatic and steric hindrance effects for base pair equilibration at helix ends.

1. Introduction

It is well known that the recognition of complementary base pairs in nucleic acids is a cooperative process [1]. Both thermodynamic and kinetic parameters of base pair recognition depend upon the state of the neighboring residues. When complementary nucleotide strands associate to double helical structures, the formation of the first few base pairs, the nucleation, is a relatively slow process, whereas the addition of base pairs to a helix nucleus, the chain growth, is a relatively fast reaction [2–5]. Thus the nucleation reaction could be studied directly in great detail, whereas the parameters of the chain growth reaction were not accessible to a direct experimental characterization. The experimental techniques available either did not have the required high time resolution or were not sensitive enough. Thus indirect methods were used to determine the rate of this reaction. The most reliable value was evaluated from relaxation data obtained for the "all or none" helix coil transition of oligonucleotides. Evaluation according to simple kinetic models yielded rate constants in the range of 10^7 sec^{-1} for the addition of AU base pairs to preexisting AU helix sequences [4, 5].

A direct measurement of the elementary step of base pairing requires a nucleotide system with a high population of partly melted helices. This condition is met by equimolar mixtures of oligoriboadenylates and oligoribouridylates of medium chain lengths at temperatures below the midpoint of the helix coil transition. A temperature jump performed in this range will change the helix population mainly by transitions of a few base pairs at the helix ends, called the unzippering reaction. Under these conditions the "all or none" helix coil transition involving the entire oligomer helix will contribute a relatively small reaction amplitude only. Relaxation measurements performed previously with oligoriboadenylates and oligoribouridylates of chain length 14 and 18 at low degrees of the helix coil transition demonstrated the existence of a very fast relaxation process, that was attributed to an unzippering reaction [4]. In the present investigation this reaction was quantitatively analysed by application of a fast temperature jump technique.

2. Materials and methods

The oligoriboadenylates and the oligoribouridylates of chain length 14 and 18 used in the experiments were isolated and characterised as described in ref. [6]. Buffers and salt reagents were of analytical grade. Melting curves were taken as described in ref. [7]. Relaxation data were obtained by the fast temperature jump apparatus developed by Hoffman [8].

3. Experimental results

A necessary condition for a convenient measurement of the rate of double helix unzippering is a nucleotide system with a low triple helix content. As was shown previously the amount of triple helices in the oligo AU system may be appreciably reduced by using low ionic strengths [4, 6]. A second condition for the resolution of the unzippering relaxation is the existence of a sufficiently high relaxation amplitude. In order to resolve the unzippering relaxation the parameters of the experimental systems had to be optimised carefully leaving very little chance for a variation, e.g., of the nucleotide concentration. The unzippering was observed by changes of the hypochromicity in the wavelength range of 240 to 260 nm (cf. ref. [9]). (The nucleotide quantities available did not allow measurements in the hyperchromic wavelength range around 285 nm.)

An example of a relaxation experiment is given in fig. 1. The relaxation signal can be fitted by a single exponential with a time constant of 0.23 μsec. However, the low signal to noise ratio does not allow the exclusion of a possible spectrum of relaxation times that is suggested by model calculations (cf. below and ref. [10]). Within the range of nucleotide concentrations for which satisfactory signal to noise ratios can be obtained (C = 1.5 to 5 × 10^{-4} M nucleotide residues), the time constant of the unzippering reaction is independent of the nucleotide concentration as should be expected for an intramolecular reaction.

A plot of the logarithm of the reciprocal relaxation time constant measured for a 1:1 mixture of riboadenylates and ribouridylates of chain length 18 as a function of the reciprocal absolute temperature is given in fig. 2. The apparent activation enthalpy associated with the reciprocal relaxation time constant is 3 to 4

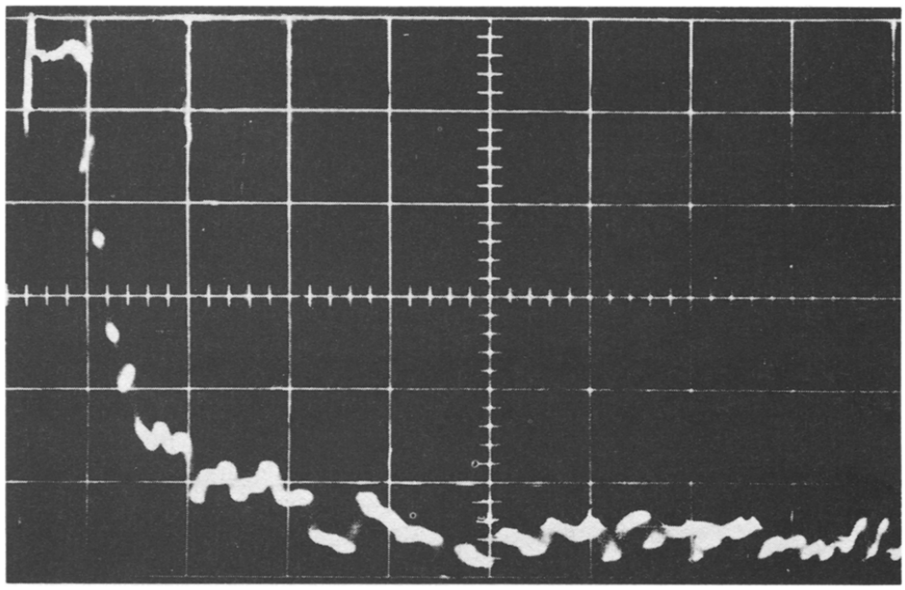


Fig. 1. Relaxation measured for $A(pA)_{13} + U(pU)_{13}$ in 0.05 M NaCl, 0.05 M sodium cacodylate pH 7 at 24°C (C_t = 3 × 10^{-4} M monomers, λ = 248 nm). Abscissa: time (time base 0.1 μs/small scale unit), ordinate: amplitude (arbitrary units).

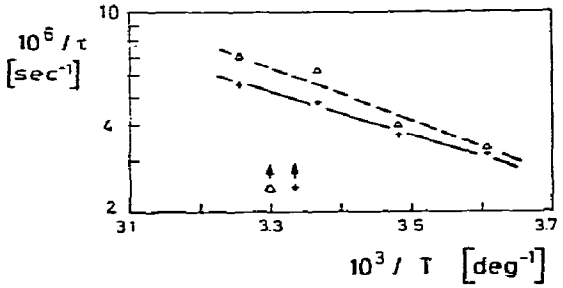


Fig. 2. Arrhenius plot of the reciprocal relaxation time of helix unzippering; $A(pA)_{17} + U(pU)_{17}$ in 0.05 M (—, +) and 0.1 M (– – –, Δ) sodium cacodylate pH 7; the melting points of the helix coil transition are in the range of 25°C (0.05 M) to 30°C (0.1 M) (indicated by arrows) for the nucleotide concentrations used in the relaxation experiments.

kcal/mole. (The activation enthalphy associated with the rate constant of base formation is derived in the following section.) Data were obtained for ionic strengths of 0.05 and 0.1 M. The relaxation time constants are almost independent of the salt concentration in this range (cf. fig. 2). Relaxation measurements at 0.2 M [Na^+] revealed two relaxation time constants in the fast range at about 0.2 μsec and about 0.8 μsec: the smaller one seems to be equivalent to the time constant observed at the lower ionic strength whereas the larger one may be associated with triple stranded helices [6].

The kinetic measurements were performed with nucleotides of chain lengths 14 and 18. As might be expected it was found that the relaxation data obtained for unzippering of the oligomer helices used did not depend on the chain length.

4. Model calculations

The relaxation spectrum of double helix unzippering cannot be described by simple model equations. Although the kinetic scheme of the unzippering reaction seems to be very simple [10], the evaluation of rate equations and relaxation times is rather complicated, because many individual consecutive reaction steps participate in the unzippering reaction. Even if the rate constants of the individual steps are equivalent, mutual coupling of these steps gives rise to a relatively complicated relaxation pattern. The problem is similar to that encountered in the kinetics of α-helix coil transitions. In that case Schwarz [11] derived relatively simple expressions, valid for certain limiting conditions. For the present system simple analytical solutions of the set of coupled rate equations are not available. (For some recent approach to the problem cf. refs. [12, 13].)

Due to these difficulties in a rigorous theoretical treatment of the unzippering reaction a different approach was used in order to evaluate the elementary rate constants of base pairing. The system of rate equations was solved numerically by use of a digital computer. The kinetic model and its solution is described in an accompanying paper [10]. Within the framework of the present investigation a zipper model will suffice to derive kinetic parameters. The zipper model considers all the helix species that are involved in the helix coil transition of helices with aligned nucleotide strands [10, 14]. Helix species containing staggered nucleotide residues are neglected. Although the consideration of staggered helix series would increase the number of parallel reactions, the mean unzippering relaxation time would not be changed essentially, since the time constants of the fast parallel reactions in the individual helix series are very similar and the relaxation spectra associated with the unzippering of the individual helix series are not coupled to each other (cf. ref. [10]). Furthermore, application of the zipper model reduce the computer time required for evaluation.

The relaxation spectrum calculated according to a zipper model for oligonucleotides of chain length N comprises N relaxation processes. The slowest process, associated with the overall helix coil transition of the entire oligomer helix, is clearly separated from the rest of the relaxation spectrum with many fast processes, associated mainly with the unzippering reaction [10]. Figure 3 gives a graphical presentation of a relaxation curve calculated according to the zipper model. In order to compare the experimental with the theoretical relaxation data the relaxation spectrum calculated for the short time range was approximated by a single exponential using a least squares procedure. Such exponentials were evaluated for various elementary rate constants associated with variable activation parameters and then compared to the experimental data. A fit is obtained with a rate constant $k_f = 8 \times 10^6$ sec^{-1} (25 °C) for the formation of a base pair adjacent to a helix sequence. The temperature dependence observed for

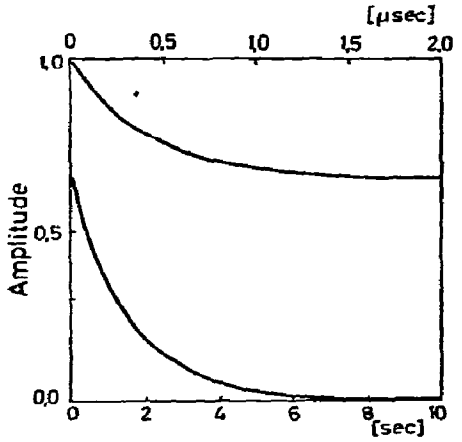


Fig. 3. Relaxation curve calculated according to a zipper model for $A(pA)_{17} + U(pU)_{17}$ (14°C, $C_t = 3.6 \times 10^{-4}$ M monomers, $k_f = 4.4 \times 10^6$ sec^{-1}). Upper curve reflects the unzippering reaction (upper time scale), whereas the lower curve reflects the "overall" helix coil transition (lower time scale); signal is in relative normalised units.

the unzippering relaxation could be fitted using an activation enthalpy of 4 kcal/mole associated with k_f (cf. fig. 4). For evaluation of these elementary parameters only the data measured at 4 and 14°C were used,

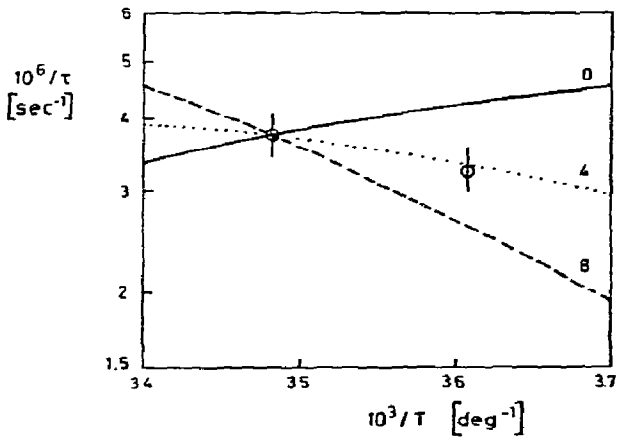


Fig. 4. Average reciprocal relaxation time calculated according to a zipper model as a function of the temperature for different activation enthalpies AE_f associated with the elementary rate of base pair formation $AE_f = 0$ (—), 4 kcal/mole (····), 8 kcal/mole (– – –), measured relaxation times (○).

in order to avoid interference with the single strand stacking relaxation (cf. section 5 and ref. [9]).

The model calculations predict a decrease of the unzippering relaxation time with increasing temperature in a certain range of experimental conditions, even if the elementary rate constant k_f is associated with a zero activation enthalpy (cf. fig. 4). Similar results were obtained for the relaxation time constants evaluated for α-helix coil transitions in polypeptides [15].

5. Discussion

The unzippering reaction of oligoriboadenylate–oligoribouridylate helices can be observed only in a restricted temperature range below the melting transition. In the range of the melting transition the relaxation amplitude due to unzippering decreases whereas the relaxation amplitude due to the stacking reaction of single stranded riboadenylate chains increases [9]. These two reactions are characterised by almost the same time constants and thus cannot be distinguished on the basis of their reaction rates. The only reason to assign the relaxation process observed below the melting transition to the helix unzippering reaction is its relatively large amplitude. The measured amplitude is much higher than expected from single strand stacking of riboadenylate chains, since below the melting transition most of the adenylic acid residues are bound in double helical structures.

The data obtained previously for the stacking reaction in riboadenylate chains [9] demonstrate, that the base pairing in AU helices is not a simple conversion between two states only. Relaxation measurements showed, that there are at least three independent conformations of riboadenylate chains [9]. A complete reaction scheme has to account for these three conformations, leading to a rather complicated reaction scheme characterised by several relaxation time constants. At present, however, the individual rate constants of the complete reaction scheme are not known and the accuracy of the fast relaxation measurements does not allow the resolution of possibly existent separate relaxation processes. It is conceivable that base pairs are formed from all the different conformations of the riboadenylate chain with similar rates. However, it is also possible that base pairs are formed from one specific conformation with a particularly high rate. As

long as detailed information about the individual steps is not available, the AU base pairing reaction may be approximately described by a simple two state reaction mechanism.

Such a mechanism was used for the evaluation of rate constants according to a zipper model. The resulting rate constant $k_f = 8 \times 10^6$ sec^{-1} (25°C, 0.05 M salt) is very close to that obtained from previous indirect evaluations [4, 5]. The measurements at different salt concentrations showed a relatively small dependence of the unzippering relaxation upon the ionic strength. Since the unzippering reaction involves formation and dissociation of a few base pairs at helix ends, this process will be accompanied by relatively small changes in the electrostatic interactions between the oligomer strands. A more distinct dependence upon the ionic strength is expected for the elementary rate constants of the first steps in the double helix formation, since the encounter of the oligonucleotide strands faces strong repulsive electrostatic potentials. Evidence for this is obtained from model calculations on the experimental overall rate constants of helix association [10]. It may also be expected, that the rate of base pair formation depends upon the number of nuleotide residues adjacent to the base pair due to steric hindrance effects and due to reduced rates of diffusion with increasing chain length. Therefore an exact representation of the double helix coil kinetics will require the introduction of quite a number of individual rate parameters (cf. ref. [10]).

Acknowledgement

The author is indebted to Drs. E. Neumann and G.W. Hoffmann for critical comments on the manuscript and to Dr. M. Eigen for his interest and support. Computer calculations were performed on the Univac 1108 of the Ges. f. wiss. Datenverarbeitung m.b.H., Göttingen.

References

[1] D. Poland and H.A. Scheraga, Theory of helix–coil transitions in biopolymers (Academic Press, New York and London, 1970).
[2] P.D. Ross and J. M. Sturtevant, J. Amer. Chem. Soc. 84 (1962) 4503–4507.
[3] R.D. Blake, L.C. Klotz and J.R. Fresco, J. Amer. Chem. Soc. 90 (1968) 3556–3562.
[4] D. Pörschke, Thesis, Universitat Braunschweig (1968); D. Pörschke and M. Eigen, J. Mol. Biol. 62 (1971) 361–381.
[5] M.E. Craig, D.M. Crothers and P. Doty, J. Mol. Biol. 62 (1971) 383–401.
[6] D. Pörschke, Biopolymers 10 (1971) 1989–2013.
[7] G.W. Hoffman and D. Pörschke, Biopolymers 12 (1973) 1611–1623.
[8] G.W. Hoffman, Rev. Sci. Instr. 42 (1971) 1643–1647.
[9] D. Pörschke, Eur. J. Biochem. 39 (1973) 117–126.
[10] D. Pörschke, Biophys. Chem. 2 (1974) 83–96.
[11] G. Schwarz, Biopolymers 6 (1968) 873–897.
[12] E.L. Elson, Biopolymers 11 (1972) 1499–1520.
[13] T.R. Chay and C.L. Stevens, Biopolymers 12 (1973) 2563–2588.
[14] J. Applequist and V. Damle, J. Amer. Chem. Soc. 87 (1965) 1450–1458.
[15] G. Schwarz, Habilitationsschrift, Universität Braunschweig (1966).

BIOPHYSICAL CHEMISTRY 2 (1974) 102–115. © NORTH-HOLLAND PUBLISHING COMPANY

ANALYSIS OF CONFORMATIONALLY-LINKED DISSOCIATION OF PROTEINS

Kenneth E. NEET

Department of Biochemistry, Case Western Reserve University, Cleveland, Ohio 44106, USA

Received 3 January 1974

Conformationally-linked dissociation equilibria of dimeric proteins have been examined to determine how experimentally obtainable parameters, such as the apparent dissociation constant, K_D, and the apparent conformational transition constant, K_{conf}, are related to intrinsic subunit interaction constants, K_A or K_B, and intrinsic isomerization constants, K_1 or K_2. Limiting models are considered in which either the conformational change occurs before dissociation or in which the dissociation occurs before the conformational change, as well as a general model including both possibilities. Models are also considered in which three conformations are allowed or in which four subunits (tetramers) are involved. Simulated data for the dimer equilibria are presented to show how variation of protein concentration and variation of certain constants affect the proportion of various molecular species, the weight-average molecular weight, and the overall extent of conformational change. Methods are suggested to distinguish between the different limiting cases based upon the dependence of K_D and/or K_{conf} on protein concentration, perturbant concentration, and temperature. It is concluded that methods used to calculate self-dissociation constants of oligomeric proteins include linked isomerization reactions such that the equilibrium constant obtained should not be considered as a true subunit interaction term. Indeed, dissociation can occur under the influence of a perturbant with no change in the intrinsic affinity of the subunits but with the sole effect of the perturbant being on a linked conformational change. Additional experiments on the thermodynamics of the conformational change are required to determine the actual relationship. Depending on the complexity of the equilibria involved and the relative value of the equilibrium constants, the extent of the conformational change can vary directly with, vary inversely with, or be independent of the total protein concentration. Even when intrinsic subunit affinities are not affected by the perturbant, the extent of conformational change can vary with protein concentration. Interpretation of data from proteins which may be involved in conformationally-linked dissociation reactions, therefore, must be made with caution.

1. Introduction

The importance of subunit interactions and conformational changes of proteins for diverse processes, such as allosteric transitions of enzymes, has become evident in recent years [1]. The concept that a conformational change occurs in a subunit, alters the interactions with neighboring subunits, and thereby transmits an effect, e.g., site–site interactions, is implicit in many of the allosteric enzyme models [2–5]. However, the possible quantitative effects that conformational changes may have upon subunit interactions, and vice versa, have not been completely examined. The total interaction between two or more subunits is in principle measurable by the affinity, i.e., the equilibrium constant for formation of the oligomer from protomers. Elegant methods for calculation of apparent association constants, based on such techniques as ultracentrifugation, have been developed [6–8].

Since many proteins are known to undergo conformational changes upon dissociation [9,10], the apparent dissociation constant calculated from molecular weight data will be a complex constant involving several equilibria. This fact has been pointed out by Henn and Ackers [10] and by Gratzer and Beaven [9] in discussion of specific experimental systems. Such considerations are necessarily a special case of the linkage relations discussed by Wyman [11] and the thermodynamic constraints. For multimeric proteins in which no true dissociation occurs, Weber [12] has analyzed the energetic relationship between ligand binding, conformational changes, and interactions between polypeptide chains (macro-associations). However, a discussion of the special case of conformationally-linked dissociation of proteins with emphasis on analysis of experimental data would appear to be useful at this time. A clear understanding of such systems is important because of their increasing frequency and because

of the relationship of such linked systems to interpretation of allosteric enzymes. The present paper systematically analyzes the equilibria in systems in which dissociation (or association) of an oligomer is linked to conformational changes within the subunit. The proportion of each protein species is calculated under various simulated conditions and related to measurable parameters of the system. Equilibria involving dimers and monomers are examined in detail and consequences of conformational changes are discussed. Criteria are suggested to distinguish between possible sequential pathways for a multi-step process of dissociation and conformational change using observable experimental parameters. Several interesting conclusions concerning the interpretation of measured equilibrium constants for self-association result from this analysis.

2. Theory

2.1. The general case of a dimer with two possible conformations available

Consider a dimer that may dissociate into monomers and either the monomer or the dimer may exist in two conformations, A and B, as diagrammed in fig. 1. The equilibrium constants for the various steps are given in eqs. (1) through (4),

$$K_A = [A]^2/[A_2] \quad (1)$$

$$K_B = [B]^2/[B_2] \quad (2)$$

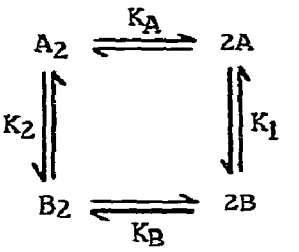
$$K_1 = [B]/[A] \quad (3)$$

$$K_2 = [B_2]/[A_2] , \quad (4)$$

where [A], [B], $[A_2]$, and $[B_2]$ represent the concentrations, in weight per volume, of the species A, B, A_2, and B_2, respectively. The constants K_A and K_B are written as dissociation constants on a weight basis and K_1 and K_2 are conformational transitional constants for the individual processes. Since this is a closed system only three constants are independent with the restriction given by eq. (5).

$$K_A K_1^2 = K_B K_2 . \quad (5)$$

The constants as written represent intrinsic properties



$$K_A = \frac{A^2}{A_2} \qquad K_1 = \frac{B}{A}$$

$$K_B = \frac{B^2}{B_2} \qquad K_2 = \frac{B_2}{A_2}$$

$$K_A K_1^2 = K_2 K_B$$

Fig. 1. Equilibria of conformationally-linked dissociation of a dimer. A_2 and B_2 represent two conformations of the dimer and A and B represent the same two conformations of the monomer. K_A and K_B are intrinsic or microscopic dissociation constants for the steps shown and K_1 and K_2 are intrinsic conformational transition constants of the dimer and monomer, respectively.

of the system under study and do not necessarily denote measurable experimental quantities. The latter will be discussed later. With the above equations and the conservation equation

$$P_0 = [A]+[B]+[A_2]+[B_2] , \quad (6)$$

the system can be solved for the fraction of each individual species present. P_0 represents the total protein concentration. The parameters used to describe the system will be the weight fraction of each individual species, f, as defined in the following equation:

$$f_X = [X]/P_0 , \quad X = A, B, A_2, B_2 . \quad (7)$$

From eqs. (1) – (6) the fraction of each species can be calculated as a function of P_0, K_1, K_2, K_A, and K_B. The coefficients of the quadratic equations obtained are given in tables 1 and 2 for the B_2 and B species for several special cases to be discussed. The real, positive roots that are obtained upon solving these quadratic equations for the scheme in fig. 1 are given for all four protein species in table 3.

Table 1
The quadratic equation for f_{B2} for cases V, II', III, 15, 12, and 13

Dimer with two available conformations	Coefficients [1]		
	α	β	γ
Case V–general	$P_0(1+1/K_2)^2$	$-[K_B(1+1/K_1)^2 + 2P_0(1+1/K_2)]$	P_0
Case II'–sequential: monomeric intermediate	P_0	$-[K_B + 2P_0(1+1/K_2)]$	P_0
Case III–sequential: oligomeric intermediate	$P_0(1+1/K_2)^2$	$-[K_B + 2P_0(1+1/K_2)]$	P_0
Dimer with three available conformations			
Case 15	$P_0(1+1/K_{21})^2$	$-[2P_0(1+1/K_{21}) + K_B(1+K_{12})^2]$	P_0
Case 12	P_0	$-[2P_0 + K_B(1+K_{12}+1/K_{11})^2]$	P_0
Case 13	$P_0(1+K_{22}+1/K_{21})^2$	$-[2P_0(1+K_{22}+1/K_{21}) + K_B]$	P_0

[1] α, β, and γ are coefficients of the quadratic equation: $\alpha f_{B2}^2 + \beta f_{B2} + \gamma = 0$.

Table 2
The quadratic equation for f_B for cases V, II', III, 15, 12, 13

Dimer with two available conformations	Coefficients [1]		
	α'	β'	γ'
Case V–general	$P(1+1/K_2)$	$K_B(1+1/K_1)$	$-K_B$
Case II'–sequential: monomeric intermediate	P	$K_B(1+1/K_1)$	$-K_B$
Case III–sequential: oligomeric intermediate	$P(1+1/K_2)$	K_B	$-K_B$
Dimer with three available conformations			
Case 15	$P(1+1/K_{21})$	$K_B(1+K_{12})$	$-K_B$
Case 12	P	$K_B(1+K_{12}+1/K_{11})$	$-K_B$
Case 13	$P(1+K_{22}+1/K_{21})$	K_B	$-K_B$

[1] α', β', and γ' are coefficients of the quadratic equation: $\alpha' f_B^2 + \beta' f_B + \gamma' = 0$.

Table 3
Solutions of the quadratic equation for the general case V

Term	Dimer with two conformations–case V
f_A	$[-(1+1/K_1)K_2K_B + Z](2K_1P_0)^{-1}(1+K_2)^{-1}$
f_B	$[-(1+1/K_1)K_2K_B + Z](2P_0)^{-1}(1+K_2)^{-1}$
f_{A2}	$[K_2K_B(1+1/K_1)^2 + 2P_0(1+K_2) - (1+1/K_1)Z](2P_0)^{-1} \times (1+K_2)^{-2}$
f_{B2}	$K_2[K_2K_B(1+1/K_1)^2 + 2P_0(1+K_2) - (1+1/K_1)Z] \times (2P_0)^{-1}(1+K_2)^{-2}$
Z	$[K_2^2K_B^2(1+1/K_1)^2 + 4P_0K_2K_B(1+K_2)]^{1/2}$

Several special cases may be considered. If dissociation is occurring with no conformational change at all, then either $K_2 = K_1 = 0$ or $K_2 = K_1 =$ infinity (case I), in which case pure dissociation from the A_2 to the A species or B_2 to the B species will be observed. This is the situation normally assumed for associating systems when calculation of dissociation constants is made. At the other extreme, if conformational changes are occurring with no dissociation then $K_A = K_B = 0$ or $K_A = K_B =$ infinity (case VI) in which case only the conformational transition of either the dimeric or the monomeric species is observed.

Some interesting intermediate cases II, III, IV, and V will be described and discussed below. Case II: The sequential case with a monomeric intermediate:

Case II: when $K_2 = 0$ and $K_B = \infty$; $A_2 \rightleftharpoons 2A \rightleftharpoons 2B$ (8)

Case II′: when $K_2 = \infty$ and $K_A = \infty$; $B_2 \rightleftharpoons 2B \rightleftharpoons 2A$. (8′)

Since A and B are arbitrary designations, case II and case II′ are equivalent to each other. Generally, only II will be treated but occasionally for clarity the other will also be considered. Case III: Similarly, a sequential case with an oligomeric intermediate may be defined by

Case III: when $K_1 = \infty$ and $K_A = 0$; $A_2 \rightleftharpoons B_2 \rightleftharpoons 2B$ (9)

Case III′: when $K_1 = 0$ and $K_B = 0$; $B_2 \rightleftharpoons A_2 \rightleftharpoons 2A$ (9′)

The two sequential situations differ in that in case II (sequential with monomeric intermediate) dissociation occurs before the conformational change is involved, whereas in case III (sequential with oligomeric intermediate) the conformational change precedes the dissociation. These two cases not only differ in pathway but would appear to differ in the driving force for the linked equilibria. Hence, it will be useful to determine if these can be distinguished experimentally from the molecular weight data and the proportion of conformations present at equilibrium. Case IV: The special case in which A_2 would appear to dissociate directly into two B subunits, as given by

Case IV: when $K_1 \gg K_A$ and $K_B \gg K_2$; $A_2 \rightleftharpoons 2B$, (10)

will not be treated explicitly but will be considered as a subcase of the other situations in which the constants are such that no detectable intermediates are found. It should be noted however, that in principle, two equilibria still occur in this situation, and would be described as in eq. (9). Case V: The general case V occurs when all four equilibrium constants have a finite value and, consequently, all four protein species are present (fig. 1).

The expression for the coefficients of the quadratic equations describing the f_B and f_{B2} in the sequential cases are given in tables 1 and 2. The expressions for the fractions of the individual protein species in the sequential cases can be easily derived from the expressions in table 3 for the general case with the appropriate restrictions on the equilibrium constants. The transformation equation (5) will be used when necessary to express the equations for the fractions of species in terms of K_B instead of K_A.

In general, the fractions of individual components are not experimentally obtainable parameters. To be able to interpret models of this sort then, one must determine how the experimental parameters vary under different conditions. From the definition of the weight-average molecular weight, $\bar{M}_w$, and the weight fractions, f, the following equation can be derived for a heterogeneous mixture of macromolecules:

$$f_{A2} + f_{B2} = \bar{M}_w/m - 1. \quad (11)$$

The molecular weight of the monomeric species is given by m. Thus, the sum of the dimer fractions is directly related to the observed weight average molecular weight. Alternatively, an apparent dissociation constant, K_D, for the dimer to monomer equilibrium can be cal-

culated in the usual manner from experimental data disregarding any conformational changes involved. K_D is related to the intrinsic values of constants in the model as follows:

$$K_D = (A+B)^2/(A_2+B_2) = K_A(1+K_1)^2/(1+K_2)$$
$$= K_B[K_2/(1+K_2)](1+K_1)^2/K_1^2. \quad (12)$$

Eq. (12) is derived from eqs. (1) – (4) and (7). A similar expression has been derived by Gratzer and Beaven [9] for an example analogous to case II and by Henn and Ackers [10] without full analysis.

An apparent conformational equilibrium constant, K_{conf}, may be defined as the summation of all forms in the second conformation, B, divided by the summation of all forms in the first conformation, A. This then represents the experimentally obtained conformational constant if a transition is assumed between the starting conformation A and the second or final conformation B. The conformations are assumed to be measured regardless of whether they are in a monomeric or dimeric environment. Such a conformational constant is given in terms of the intrinsic constants of the models by

$$K_{conf} = \sum(f_B + f_{B2})/\sum(f_A + f_{A2})$$
$$= [2K_1K_A(1+K_2)+K_2\mathcal{T}]/[2K_A(1+K_2)+\mathcal{T}], \quad (13)$$

where

$$\mathcal{T} = -(1+K_1)K_A + [K_A(1+K_1)^2 + 4P_0K_A(1+K_2)]^{1/2};$$

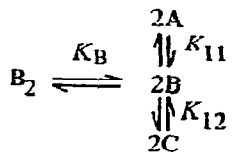
and is identical to eq. (19) of Henn and Ackers [10]. The consequences and interpretations of these apparent equilibrium constants will be discussed in the next section. For the special cases II and III', K_{conf} is obtained by letting $K_2 = 0$ or $K_1 = 0$, respectively.

2.2. Dimer with three available conformations

If we now consider the case of a dimer–monomer equilibrium in which three conformations are available, the model and the equations become much more complex. We will only consider here three interesting limiting cases† of such a model.

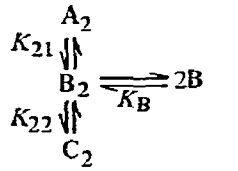
† The numbers used to designate these cases are arbitrary and have no special significance.

(a) Case 12 in which the monomer can exist in two other conformations not available to the dimer:



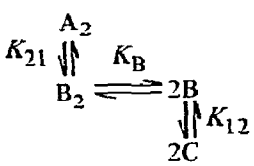
Case 12 (14)

(b) Case 13 in which the dimer can exist in two other conformations not available to the monomer:



Case 13 (15)

(c) Case 15 in which the dimer can exist in two conformations and the monomer can exist in two conformations but only one conformation is common to monomer and dimer:

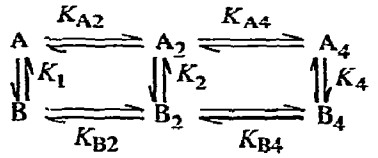


Case 15 (16)

The terms of the quadratic equations are again given in table 1 and 2 for the three cases cited above with three available conformations. It can be seen that the form of the equations is similar to the two conformational cases but now the constants can take on additional values because of the relationship to the conformational transition constants. The apparent dissociation constants, K_D, are given in table 4 for these three cases.

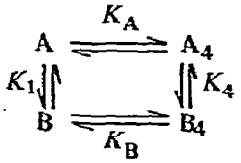
2.3. Tetramer with two available conformations

For tetramer association the existence of intermediate molecular weight species must be considered. The most probable of these is the monomer–dimer–tetramer association with two available conformations for each species:



Case VII (17)

Case VII has two independent equilibrium constants more than the dimer case V. A limiting case of the tetramer association would occur when no significant amounts of dimer are formed (case VIII):



Case VIII (18)

The relationship of the observed dissociation constants, K_D, to the intrinsic constants of case VII and VIII are given in table 4. Because of the degree of complexity and the additional constants, the tetramer association cases have not been explicity solved and simulated.

Table 4
Apparent dissociation constants in terms of intrinsic equilibrium constants

Case	K_D
Dimer V	$K_B[K_2/(1+K_2)]/(1+K_1)^2/K_1^2 = K_A(1+K_1)^2/(1+K_2)$
Dimer 12	$K_B(1+K_{12}+1/K_{11})^2$
Dimer 13	$K_B(1+K_{22}+1/K_{21})^{-1}$
Dimer 15	$K_B(1+K_{12})^2(1+1/K_{21})^{-1}$
Tetramer VII	$K_{D2} = K_{A2}(1+K_1)^2/(1+K_2)$ and $K_{D4} = K_{A4}(1+K_2)^2/(1+K_4)$
Tetramer VIII	$K_B[(1+K_1)/K_1]^4K_4/(1+K_4) = K_A(1+K_1)^4/(1+K_4)$

3. Results

Values of the various constants have been assumed and data have been simulated based upon the equations derived in the theoretical section. Weight fractions of various components under various conditions and experimental parameters that can be obtained from real systems have been calculated. Computations were carried out on a Hewlett Packard 9100A calculator.

Fig. 2 shows the dependence of the weight fraction of the four components of this dimer system on the protein concentration and on various values of the constants. Fig. 2e, or case II, can be considered one extreme in which there is no B_2 present because of the values of K_2 and K_B. Fig. 2a, or case III, would occur at the other extreme when there is no A present because of the values of K_A and K_1. One set of values for the constants of case V is simulated in fig. 2b, c, and d in which $K_A = K_B = 1$ and represents a similar contribution of the four equilibria. In fig. 2, the weight fraction, f, is plotted against the parameter P, which is the ratio of the total protein concentration to K_B (or K_A in fig. 2e). The consequences of this normalization will be discussed later. Other values of the constants have been assumed for case V (not shown) and approach case II or III in the extreme. Case V (fig. 2b, c, d) is thus an intermediate, complex description of what could occur and case II (fig. 2e) and case III (fig. 2a) are limiting, simple cases.

In all cases presented, the proportion of the dimeric species increases with increasing protein concentration as dictated by the mass action principle. At low values of K_2, f_A and f_{A2} predominate at low and high protein concentration, respectively. At high values of K_2, the equilibria shift to the B conformation so that f_B and f_{B2} predominate. For case V, when K_A is not equal to K_B (data not shown) similar curves are obtained to fig. 2b, c, d except that the point of equivalence of f_{B2} and f_{A2} does not occur when $K_2 = 1$, as it does when $K_A = K_B = 1$ (fig. 2c).

Although examination of fig. 2 shows that protein species vary differently with assumed constants, this is not a satisfactory procedure to distinguish one case from another. The weight fraction of individual components is not directly measurable. The measured parameter is usually the total amount of conformation B and/or the total amount of the dimer. We will now examine the experimentably obtainable parameters and how they vary both with protein concentration and with the conformational transition constants. Fig. 3 shows the variation of the dimeric species with pro-

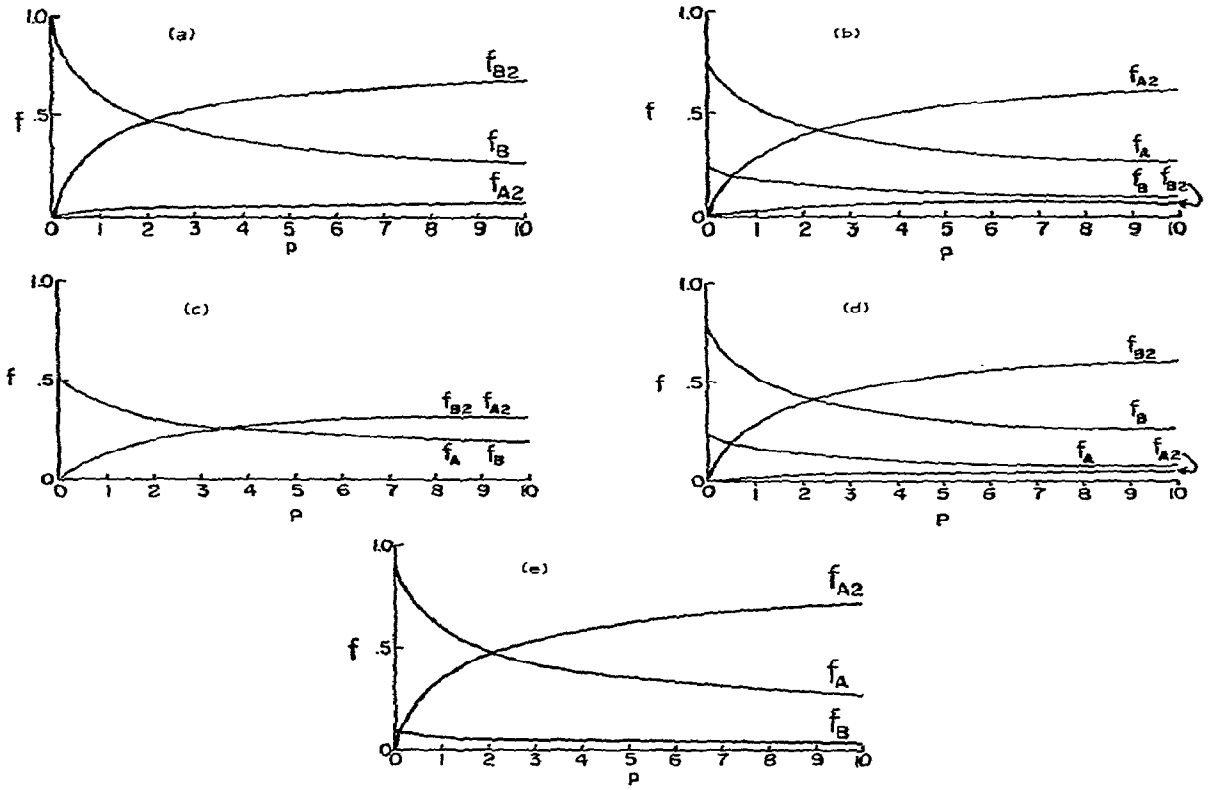


Fig. 2. Weight fractions, f, of individual protein forms as a function of protein concentration at K_1 and K_2 values. $P = P_0/K_B$ (or $P = P_0/K_A$). (a) Case III: $K_2 = 10$, $K_1 = \infty$, $K_A = 0$. (b) Case V: $K_2 = 10^{-3}$, $K_1 = 0.316$, $K_A = 1$. (c) Case V: $K_2 = 1$, $K_1 = 1$, $K_A = 1$. (d) Case V: $K_2 = 10$, $K_1 = 3.16$, $K_A = 1$. (e) Case II: $K_2 = 0$, $K_1 = 10^{-1}$, $K_A = 1$.

tein concentrations for case II, III, and V which is directly related to the weight average molecular weight by eq. (11). Fig. 3a shows that in the case where the monomer may go on to a second conformation, the midpoint of the distribution curve (the point where $f_X = 0.5$) of the dimeric species will be shifted to higher protein concentrations than if the second conformation of the monomer does not exist (i.e., $K_1 < 10^{-3}$). Conversely, fig. 3b shows that if the conformational change occurs before the dissociation, then the midpoint of the molecular weight distribution curve shifts to lower protein concentrations than if the conformational change did not occur (i.e., $K_2 > 10^2$). Thus, the position of these molecular weight distribution curves can be shifted quite markedly as a perturbant is varied depending upon whether a conformational transition of either the monomer or dimer can occur. Fig. 3c shows that if conformational changes can occur in both the monomer and the dimer, case V, then the observed values of molecular weight distribution can be either higher or lower than that which would exist in the absence of conformational changes. In fact, as K_2 increases the midpoint of the molecular weight distribution curve (fig. 3c) shifts to higher values of P_0 and then shifts back to lower concentrations. Eq. (12) can be differentiated with respect to K_1 to prove that the apparent dissociation constant, K_D, passes through a maximum value when K_1 is equal to K_A/K_B. Thus, complex behavior of the weight average molecular weight can be expected if two or more conformations

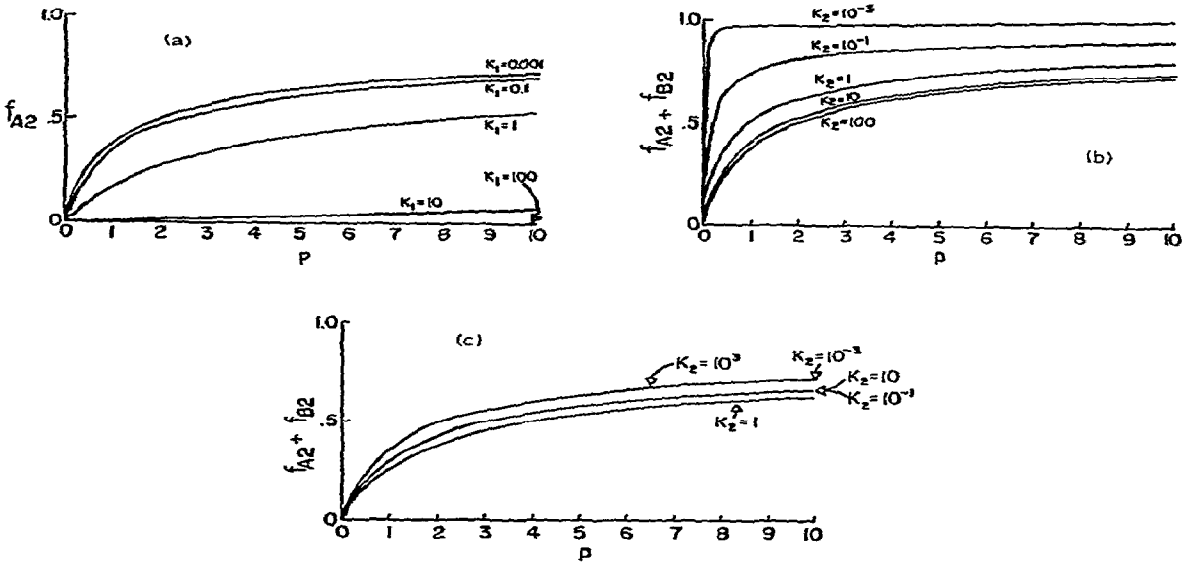


Fig. 3. The variation of the total demeric fraction ($f_{A2} + f_{B2}$) as a function of protein concentration at different values of K. (a) Case II. (b) Case III. (c) Case V ($K_A = K_B = 1$). $f_{A2} + f_{B2}$ is equivalent to ($\bar{M}_w/m - 1$).

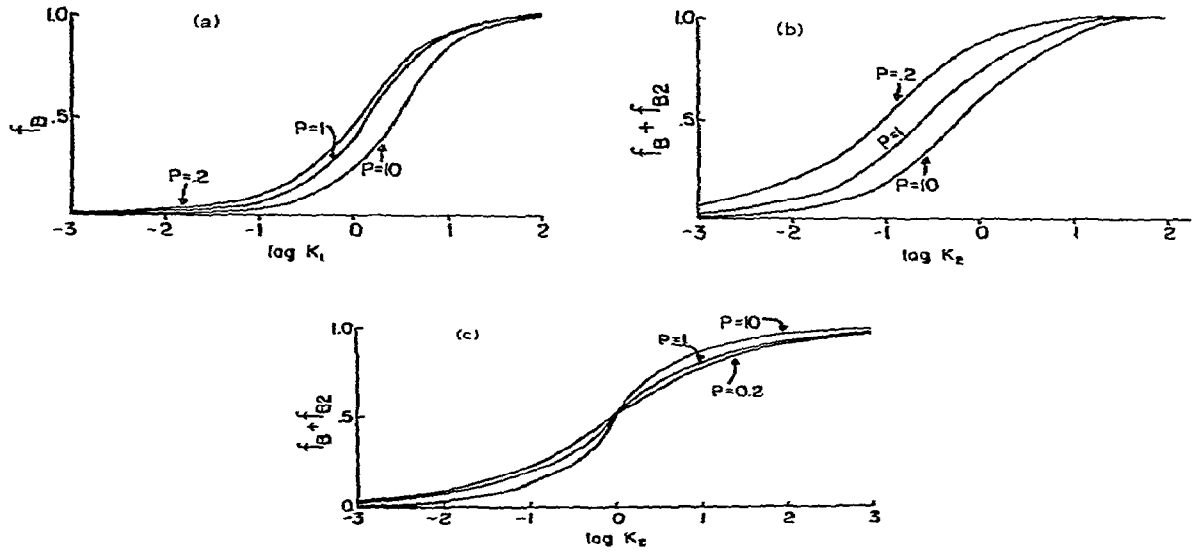


Fig. 4. The variation of the total fraction in conformation B ($f_B + f_{B2}$) as a function of K_1 or K_2 at different protein concentrations. (a) Case II. (b) Case III. (c) Case V ($K_A = K_B = 1$).

are available to the monomer and dimer in the equilibria.

The distribution curves of fig. 3 are not as easily interpretable as it might appear since these curves have been normalized to a K_B or K_A of unity (or $P = P_0/K_B$) for ease of presentation as was done in fig. 2. The position, and therefore the appearance, of the curves is not enough to distinguish among the various possibilities since experimentally P_0 would be varied where the largest change in molecular weight occurred and all curves would appear similar. Additional data are needed to choose among the possibilities as will be discussed later.

The other experimental quantity that can be measured is the conformational change, which will be represented here as $f_B + f_{B2}$. This parameter is normally measured by some spectroscopic method, such as optical rotation, and is then calculated as the fractional change from one state to another. The dependence of this conformational parameter on protein concentration, temperature, salt concentration, etc. can be determined. Fig. 4 demonstrates the dependence of $f_B + f_{B2}$ on K_1 or K_2 at different protein concentrations for case II, III and V ($K_A = K_B = 1$). It can be assumed for these purposes that the variation of some external parameter such as salt concentration or temperature causes variation of K_1 or K_2. Case II and case III differ quantitatively in the manner in which the conformation changes with a change in K_1 or K_2. Case V again can exhibit complex behavior and can either shift up or down depending on the value of the various constants. Strikingly, under some conditions the fraction of $B + B_2$ may not change with protein concentration even though this might be expected from a system undergoing association. Hence, the independence of a conformational change on protein concentration is not sufficient evidence to conclude that no association–dissociation is occurring. Shifting of the value of K_2 away from the intersection point (fig. 4) by adjusting pH or salt concentration may allow observation of protein concentration dependency of the conformational parameter.

For the case where three conformations are possible and either the monomer or the dimer can exist in three conformations (case 12, case 13) the curves for the fractions versus protein concentration are essentially the same in form as those shown in fig. 2 for two conformations. For example, $\bar{M}_w$ versus protein concentration would be unable to demonstrate the presence of the additional conformations. Different combinations of intrinsic constants contribute to the value of the apparent equilibrium constants (K_{conf} or K_D, table 4). However, the dependence of the weight fractions on the intrinsic conformational constant does change (tables 1 and 2) and limits are set by the relationship of the constants involved. Fig. 5 shows how various weight fractions of components vary with K_{11}, K_{21}, K_{12}, or K_{22} and thus expected behavior if a varied perturbant were affecting one intrinsic constant. Unless conformation B can be distinguished from conformation C and A it is unlikely that these cases could be resolved from the case where only two conformations exist, by this type of experiment.

The association of a tetramer linked to a conformational change raises additional difficulties. The mode of association may be either monomer–tetramer (no intermediates) or monomer–dimer–tetramer. (The conclusion of trimer is also possible but would seem less likely.) The methods to distinguish between the different modes of association have been outlined [7, 8] and would be the initial information necessary for a system under investigation. The monomer–tetramer case (case VIII) introduces no new parameters over the monomer–dimer cases discussed above with the exception that the dependency on protein concentration would be steeper due to the fourth power term in the association expression. The relationship of the observed dissociation constant, K_D, to the intrinsic constants for the case of a monomer–tetramer equilibrium with two allowed conformations of each species is given in table 4. Analysis of K_D and conformational changes would be similar to that already discussed for the dimer.

The monomer–dimer–tetramer association with two conformations (case VII) is complicated by the fact that conformational transition constants of each species may be different, giving rise to different proportions of different conformational-oligomeric species. Analysis of K_D can be performed by analyzing both the monomer–dimer and the dimer–tetramer observed association constants [8] as a function of temperature or perturbant concentration as suggested for the simple dimer case discussed previously. This procedure amounts to treating each step of the association separately in order to determine its characteristics. Conformational analysis of case VII depends upon whether the conformational probe is sensitive to

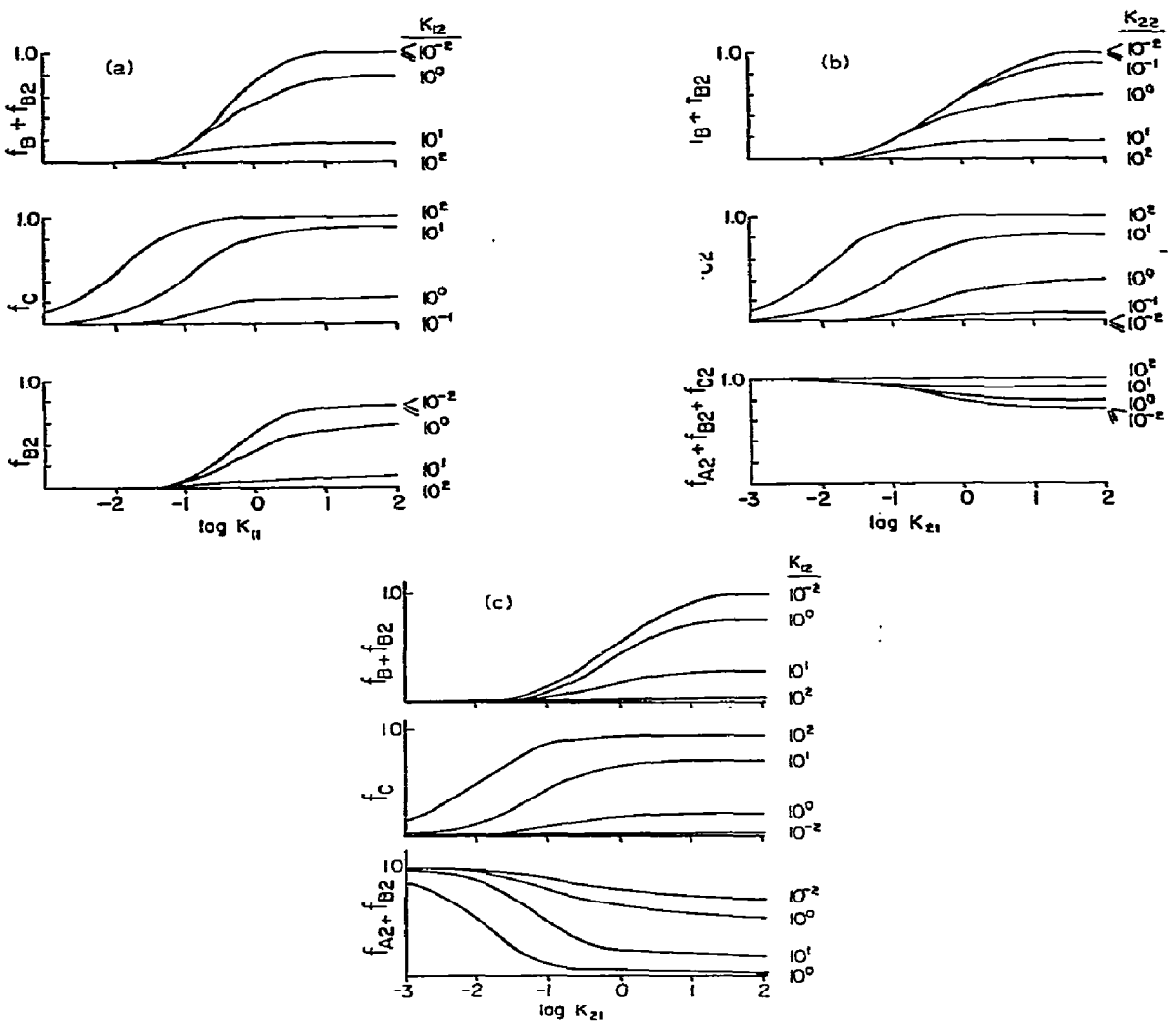


Fig. 5. Dimer with three conformations. Variations of the total dimeric fraction, the total fraction in conformation B, and the total fraction in conformationC as a function of K_{11} or K_{22} at different values of K_{12} or K_{21} and at $P = 10$. (a) Case 12. (b) Case 13. (c) Case 15.

changes that occur at the dimer level, the tetramer level, or both. Simulations of such situations are beyond the scope of this report, but the expectations of the results follows from those given here for the dimer case. For example, if all three intrinsic conformational transition constants are the same, no dependency of the second conformation on protein concentration should be expected. However, if two of the transition constants are the same and the third different, the conformational change could occur over a higher or lower range of protein concentration than would be expected, and become essentially constant over a range of protein concentration in which it is known from molecular weight determinations that association or dissociation is ocurring. Alternatively, if the association constants are the same regardless of the conformation concerned, i.e., $K_{A2} = K_{B2}$ and $K_{A4} = K_{B4}$, a protein concentration dependent change in conformation might occur with appropriate values of the other intrinsic constants. For general values of the intrinsic constants

complex behavior could occur and extensive experiments would be necessary for a thorough analysis. The effect of an external perturbant could be primarily on a conformational step even though the primary observation was dissociation (or association), as was noted for the dimer cases.

4. Discussion

The analysis presented here of the dissociation equilibria of dimers and monomers in which two or three conformations have been considered is a simplified model and is similar to models previously mentioned briefly [9,10]. The present paper attempts to establish the experiments necessary to discriminate between different situations based on the type of curves and a consideration of the limits involved. Additional complexities not discussed here include the extension to hybrid conformational forms, such as an AB dimeric configuration, as well as the presence of initially dissimilar subunits. These additional complexities do not appear to be amenable to a general analysis but should be considered as possible in any specific protein.

Several interesting features are found in the simple dimer case analyzed here. If a perturbant, such as temperature or ionic strength, is introduced into a system and a dissociation occurs, the dissociation is not necessarily due to a direct effect on the forces between subunits but can be due to an effect on a secondary change, K_1. In other words, the apparent K_D, calculated from the molecualr weight distribution, is not necessarily a direct measurement of the subunit affinities. This is true regardless of the method [7,8,13,14] used to calculate the K_D, the extent of association (e.g., tetramer), and the mode of association (e.g., monomer–dimer–tetramer). Additional conformational experiments need to be performed to elucidate the true series of events. Indeed, the apparent K_D can be either larger than the intrinsic affinity constant, as in case II, or smaller than the intrinsic affinity constant, as in case III. With more complex systems, such as the tetramer, such considerations hold true regardless of the mode of the association.

Henn and Ackers [10] have noted that the apparent conformational constant is a function of the protein concentration. It is clear from eq. (13) that this apparent conformational constant approaches K_1 at low protein concentrations and approaches K_2 at protein concentrations high relative to K_D. In practice, K_{conf} would have to be measured over an accessible range of protein concentration and extrapolated to zero and infinite concentration to determine K_1 and K_2. Variation of the perturbant (i.e., K_1 or K_2) at high enough or low enough protein concentration so that dissociation or association could not appreciably occur would allow a distinction to be made between an allowed conformational change in the dimer (case III) or in the monomer (case II), respectively. Furthermore, the trend of K_{conf} with the change in the protein concentration (i.e., shape of the curve) can give an indication of whether case II or case III best represents what is occurring with the protein. Table 5 shows that a plot of ln K_{conf} versus P_0 will have a negative slope for case V when $K_1 > K_2$ and a positive slope when $K_2 > K_1$. Thus with a careful definition of the native and the induced conformations and with a single experiment of this nature discrimination between the limiting cases could be made.

If K_1 is being altered by some external perturbant, then the molecular weight distribution and the apparent K_D actually can go through a maximum value (case V, fig. 2c). This important fact must be considered in interpreting experimental data, e.g., the observation of both increased association and dissociation under different conditions could be solely due to effects in one direction on K_1 (or K_2) and not increased or decreased subunit affinities. Somewhat surprisingly, when K_A equals K_B, i.e., the subunit affinity is dependent of the conformation of the dimer, the amount of the second conformation can still be a function of the protein concentration, if the constants are appropriate (fig. 2). The measurable value, $f_B + f_{B2}$, can either increase or decrease with protein concentration depending upon the relative value of K_2 and K_1 (fig. 5, table 5). In contrast

Table 5
Limits of K_{conf} and the differential of K_{conf} at high and low protein concentration [1)]

	K_{conf}	d ln K_{conf}/d P
$P \to 0$	K_1	$(K_2-K_1)/K_1K_A(1+K_1)$
$P \to \infty$	K_2	$(K_2-K_1)[K_A(1+K_2)]^{1/2}/2K_2P^{3/2}$

[1)] Obtained from analysis of eq. (13).

to the general conclusion of Henn and Ackers [10] and others, there are conditions for a conformationally-linked dissociation system in which the conformational change is not dependent upon protein concentration. Namely, when $K_1 = K_2$ then the intrinsic affinities of the two conformations are not identical but now K_{conf} [eq. (13)] becomes independent of P_0 and $f_B + f_{B2}$ is constant. This situation would imply that the conformational transition is independent of the state of association of the molecule and appears to hold for the dissociation of muscle aldolase in $MgCl_2$ [15].

Some methods used to measure conformational changes, such as ultraviolet difference spectra, may also be sensitive to the simple act of dissociation, e.g., of tyrosine residues occur at the subunit binding domains. Indeed, this has been the method developed by Fisher and Cross [16] to calculate dissociation constants from spectroscopic data [17,18]. This is satisfactory if only the $A_2 \rightleftharpoons 2A$ equilibrium is present. However, if the B conformation also contributes to the conformational probe then this method is not applicable. In this complex situation, summation curves, using fig. 2 to add the contributions of the dissociation to A and the conformation of B, could be calculated. Alternatively, the data could be combined with molecular weight data to determine the contribution of each form.

The question arises as to whether an analysis for a two state transition, as discussed by Tanford,[19], will distinguish the four species of fig. 1 as individual states. The most definitive analysis, comparison of several different techniques to monitor the conformational transition, will not demonstrate more than two states if all techniques are sensitive only to changes in tertiary structure. However, if one conformational technique is sensitive to the dissociation per se, i.e., $A_2 \rightleftharpoons 2A$, then the data from this technique would not change concommitantly with the others Thus, it is important to use techniques that are more sensitive to tertiary structural changes such as circular dichroism and techniques that are also sensitive to simple exposure of groups, such as ultraviolet difference spectroscopy. The second analysis for two states is the plot of $\log K_{conf}$ versus $\log C$ (where C is the concentration of added reagent) which is usually linear for a two state transition. Tanford [20] has shown that eq. (19) adequately represents the experimental situation in which it is assumed that the reagent, C, binds to n sites on the protein molecule in the second state with an association constant, k.

$$\frac{\partial \ln K_{conf}}{\partial \ln C} = \frac{nkC}{1+kC} . \qquad (19)$$

The right hand side of eq. (19) is often essentially constant over the region in which K_{conf} is experimentally measurable. For a conformationally-linked dissociation, an equation analogous to eq. (19) will be much more complex. Qualitatively, the plot of $\log K_{conf}$ versus $\log C$ will be linear at low protein concentration ($A \rightleftharpoons B$) and will be linear at high protein concentration ($A_2 \rightleftharpoons B_2$) but with a slope, n, twice as large as at low concentration. Thus, for intermediate protein concentrations, in which C is actually causing dissociation, the $\log K_{conf}$ versus $\log C$ plot will be concave down as the slope changes from high to lower. For a reaction in which added reagent is causing association, the relationships will be reversed and the plot will be concave up. On the other hand, for a monomeric protein which undergoes a transition with intermediates, the $\log K_{conf}$ versus $\log C$ plot can curve either up or down depending upon the relative values of reagent bound, n, in each step. Therefore, if it is known that the reagent causes either dissociation or association, analysis by this procedure may rule out certain possibilities for the number of conformational states.

In the figures illustrated in this paper, K_1 or K_2 has been treated as the variable that is altered by the perturbant while K_A or K_B is constant. This approach has been used to demonstrate that the dissociation can be 'pulled' or 'pushed' by the conformational change. The effect of the perturbant instead could be on K_A or K_B or, in general, the perturbant could alter both the intrinsic affinities and the intrinsic conformational constants. An increase in K_A, for example, would qualitatively affect the molecular weight curves for case II in the same manner as an increase in K_1. However, by following the procedures outlined in this paper, the constants which are most affected by a perturbant can be ascertained.

Qualitatively, the type of intrinsic constant (conformational or dissociation) that has been mainly affected can be determined with an appropriate plot of the experimental data. In general, a change in K_1 or K_2 will cause a sharp transition in an observed molecular weight parameter in a linked system. For example,

Henn and Ackers [10] observed an abrupt change in a van 't Hoff plot of K_D data for D-amino acid oxidase, which they attributed to a conformational change in a linked reaction. This expected behavior can be described mathematically if the normal dependence of each intrinsic constant on temperature:

$$\frac{\partial \ln K}{\partial (1/T)} = \frac{-\Delta H^0}{R} \quad , \tag{20}$$

is assumed and inserted into the differential form of eq. (12). The result shows the dependency of the observed K_D on temperature:

$$\frac{\partial \ln K_D}{\partial (1/T)} = \frac{-\Delta H_B}{R} - \frac{\Delta H_2}{(1+K_2)R} + \frac{2\Delta H_1}{(1+K_1)R} \quad . \tag{21}$$

ΔH_B, ΔH_2, and ΔH_1 in this equation are the changes in enthalpy corresponding to K_B, K_2 and K_1, respectively. Sharp breaks of ln K_D as $1/T$ varies are due to the magnitude of K_2 or K_1 compared to unity [K_2 and K_1 are still functions of temperature in eq. (21)]. The expected behavior of a van 't Hoff plot of K_D data for different relationships of K_1 and K_2 is outlined in table 6 (lines A and B). For positive values of ΔH_2 and ΔH_1, the van 't Hoff plot would bend down if K_2 were varying with temperature and would bend up if K_1 were varying with temperature. Since the *sign* of ΔH_2 or ΔH_1 should be determinable by temperature studies of K_{conf} at high or low protein concentrations, distinctions between the predominance of case II or case III could be made from the shape of log K_D versus $1/T$ data. In contrast, a linear or only slowly changing van 't Hoff plot (K_D) would indicate the lack of an important, linked isomerization. A very sharp transition between linear portions, such as observed for D-amino acid oxidase [10], could only occur if both K_1 and K_2 varied in an appropriate way with temperature. In fact, the temperature dependence data of Henn and Ackers [10] can be adequately fit by the general case V with the following values of the various parameters: $\Delta H_B = 0$; $\Delta H_2 = 2$; $\Delta H_1 = 140$ kcal/m; $\Delta S_B = 25.2$ eu; $\Delta S_1 = 250$ eu; $\Delta S_2 = 532$ eu. Since no other very different values of these parameters (e.g., $\Delta H_1 = 0$) have been found to fit the data, it is most likely that significant proportions of both conformations of both monomer and dimer of D-amino acid oxidase exist in equilibrium.

A similar analysis can be applied if perturbants other than temperature are used to study dissociation. The only requirement is to establish the manner in which the data should be plotted in order to examine the possibility of an unusually sharp transition. The

Table 6
Behavior of K_D with change in temperature of perturbant concentration

	$K_1(T)$	$K_2(T)$	Van 't Hoff plot (K_D)	
			R(slope)	Description
(A)	constant	$\ll 1$	$[-\Delta H_B+2\Delta H_1/(1+K_1)]-\Delta H_2$	concave down for $\Delta H_2 > 0$
	constant	$\gg 1$	$[-\Delta H_B+2\Delta H_1/(1+K_1)]-\Delta H_2/K_2$	and concave up for $\Delta H_2 < 0$
(B)	$\ll 1$	constant	$-[\Delta H_B+\Delta H_2/(1+K_2)]+2\Delta H_1$	concave up for $\Delta H_1 > 0$
	$\gg 1$	constant	$-[\Delta H_B+\Delta H_2/(1+K_2)]+2\Delta H_1/K_1$	and concave down for $\Delta H_1 < 0$
	$K_1(C)$	$K_2(C)$	ln K_D versus ln C plot	
			Slope	Description
(C)	constant	$\ll 1$	$[(n_B k_B C/(1+k_B C)](K_1-1)/(K_1+1)$	concave down
	constant	$\gg 1$	$[n_B k_B C/(1+k_B C)](K_1-1)/(K_1+1)-n_{B2}k_{B2}C/(1+k_{B2}C)$	
(D)	$\ll 1$	constant	$[-n_{B2}k_{B2}C/(1+k_{B2}C)]K_2/(1+K_2)+n_B k_B C/(1+k_B C)$	concave up
	$\gg 1$	constant	$[-n_{B2}k_{B2}C/(1+k_{B2}C)]K_2/(1+K_2)+n_B k_B C/(1+k_B C)$	

addition of chemical reagents is a commonly used method to study dissociations. If we again follow the treatment of Tanford [20] in which the effect of reagent is to bind to B or B_2 (as designated by subscript), differentiation of eq. (12) with respect to the reagent concentration, C, yields

$$\frac{\partial \ln K_D}{\partial \ln C} = \frac{n_B k_B C}{1+k_B C}\ \frac{K_1-1}{K_1+1} - \frac{n_{B2} k_{B2} C}{1+k_{B2} C}\ \frac{K_2}{1+K_2}. \quad (22)$$

Therefore, a plot of $\ln K_D$ versus $\ln C$ will be linear or only slowly curving if no important isomerization reactions are present. When K_1 or K_2 (still functions of C) vary sharply near unity, abrupt changes in slope of the indicated plot will occur. The shape of the $\ln K_D$ versus $\ln C$ plot can distinguish, in an unequivocal manner, between case II and case III (table 6, lines C and D). Variation of K_2 with C should lead to a plot that is concave down whereas variation of K_1 should yield a plot that is concave up. The data for α-chymotrypsin dimerization (Aune and co-workers [21,22]) show a nearly linear dependence of $\ln K_D$ on pH below or above pH 4 [21] and a linear dependence of $\ln K_D$ on ln concentration of NaCl or $CaCl_2$ [22]. These data and other evidence [23] are therefore consistent with the conclusion that no conformational change is occurring upon association.

Of the two limiting dimer cases, II and III, one represents the case (II) where dissociation occurs first and is followed by a conformational change, whereas the other (III) represents a change in conformation which is followed by a dissociation. These models, then, essentially exhibit 'cause and effect'. In case II the dissociation 'allows' an isomerization, or the conformational change 'pulls' the dissociation depending upon which step (K_I or K_A) the perturbant affects. In case III the conformational change 'allows' the dissociation, or the dissociation 'pulls' the isomerization. Similar statements could be made in considering subunit interactions without dissociation. If a system in the presence of an external perturbant or upon binding of a ligand satisfies one of these limiting models, interpretations of statements about allosteric enzymes such as 'a change in conformation caused a change in the subunit interaction so that the second subunit was altered' may be better understood and distinguished from the converse relationship. The outline of simulated data given here indicates ways in which these two extreme cases can be delineated. Intermediate cases will be much more difficult to clarify but with appropriate experiments it should be possible to determine most of the constants.

Acknowledgement

This work was supported by grants from the NSF (GB-8175) and from the USPHS (AM-12881). K.E.N. was a Faculty Research Awardee (PRA-55) of the American Cancer Society during the period of this work.

References

[1] D.E. Koshland, Jr., in: The enzymes, ed. P.D. Boyer, 3rd Ed., Vol. I(Academic Press, New York, 1970) p. 342.
[2] J. Monod, J. Wyman and J.P. Changeux, J. Mol. Biol. 12 (1965) 88.
[3] D.E. Koshland, Jr., G. Nemethy and D. Filmer, Biochemistry 5 (1966) 365.
[4] C. Frieden, J. Biol. Chem. 242 (1967) 4045.
[5] L.W. Nichol, W.J.H. Jackson and D.J. Winzor, Biochemistry 8 (1967) 2449.
[6] R.F. Steiner, Arch. Biochem. Biophys. 49 (1954) 400.
[7] E.T. Adams, Jr., Biochemistry 6 (1967) 1864.
[8] E.T. Adams, Jr., Fractions 3 (1967) 1. Technical Bulletin of Spinco Division of Beckman Instruments.
[9] W.B. Gratzer and G.H. Beaven, J. Biol. Chem. 244 (1969) 6675.
[10] S.W. Henn and G.K. Ackers, Biochemistry 8 (1969) 3829.
[11] J. Wyman, Advan. Prot. Chem. 19 (1964) 224.
[12] G. Weber, Biochemistry 11 (1972) 864.
[13] D.E. Roark and D.A. Yphantis, Ann. New York Acad. Sci. 164 (1969) 245.
[14] R.H. Haschemeyer and W.F. Bowers, Biochemistry 9 (1970) 435.
[15] L.S. Hsu and K.E. Neet, submitted for publication (1973).
[16] H.F. Fisher and D.G. Cross, Arch. Biochim. Biophys. 110 (1965) 217.
[17] H.F. Fisher, L.L. McGregor and D.G. Cross, Biochim. Biophys. Acta 65 (1962) 175.
[18] J.A. Rupley, R.D. Renthal and M. Praissman, Biochim. Biophys. Acta 140 (1967) 185.
[19] C. Tanford, Advan. Prot. Chem. 24 (1970) 1.
[20] C. Tanford, Advan. Prot. Chem. 23 (1968) 121.
[21] K.C. Aune and S.N. Timasheff, Biochemistry 10 (1971) 1609.
[22] K.C. Aune, L.C. Goldsmith and S.N. Timasheff, Biochemistry 10 (1971) 1617.
[23] K.E. Neet, K.M. Sackrison, G.R. Ainslie and L.C. Barritt, Arch. Biochem. Biophys. 160 (1974) 569.

BIOPHYSICAL CHEMISTRY 2 (1974) 116–126. © NORTH-HOLLAND PUBLISHING COMPANY

A STUDY OF THE EFFECTS OF EXTERNALLY APPLIED SODIUM-IONS AND DETECTION OF SPATIAL NON-UNIFORMITY OF THE SQUID AXON MEMBRANE UNDER INTERNAL PERFUSION

I. INOUE, I. TASAKI and Y. KOBATAKE

Department of Pharmaceutical Sciences, Hokkaido University, Sapporo, Japan and Laboratory of Neurobiology, National Institute of Mental Health, Bethesda, Maryland 20014, USA

Received 11 January 1974

Electrical properties of the axon membrane were examined under internal perfusion of squid giant axons with a dilute solution of NaF or CsF. The rate of propagation of the action potential was markedly enhanced when NaCl was added to the external $CaCl_2$ solution. The membrane conductance both at rest and during the action potential was increased with increasing Na-concentration in the external medium. In the perfusion zone of these axons, the action potentials in different parts of the membrane were found to terminate in a more-or-less spatially random and temporally irregular fashion. When the electric field outside the axon membrane was examined with hyperfine glass-pipette electrodes, small rectangular potential changes of uniform amplitude were observed. The small potential changes, which resemble those obtained by Bean in EIM-treated lipid bilayer, were interpreted as indicating spatial non-uniformity of the axon membrane during excitation. The importance of long-range electric interaction between different parts of the axon membrane is emphasized.

1. Introduction

Under internal perfusion with a dilute sodium salt solution, squid giant axons are known to remain electrically excitable in a medium containing only $CaCl_2$ and a non-electrolyte solution [1–3]. Addition of a sodium salt to the external $CaCl_2$ solution considerably increases the amplitude and the duration of the prolonged action potential of these axons. When a potassium salt is introduced into the interior of axons under these conditions, the duration of the action potential developed is shortened and its time-course approaches that of intact axons immersed in normal sea water.

During experimental studies of the properties of the axons under internal perfusion with a dilute salt solution, we found that the action potential duration was highly variable within the perfusion zone of the axon. This finding, which suggests the coexistence of domains of the membrane in the excited state side-by-side with areas in the resting state, prompted us to the present study. We found in the first place that addition of a sodium salt to the external $CaCl_2$ solution greatly enhanced the rate of propagation of the action potential and the electric conductance of the membrane at the peak of excitation. Following this finding, we explored spatial non-uniformity of the squid axon membrane with hyperfine glass-pipette electrodes. We could record small electrical signals from the perfusion zone of the axon which resembled those discovered by Bean et al. [4] in their studies of a bi-layer membrane into which a small amount of EIM [5] had been incorporated. These experimental findings and their possible significance are described in this paper.

2. Methods

The giant axons used in the present studies were taken from the squid, Doryteuthis bleekeri, caught in the northern part of the Sea of Japan. The technique of internal perfusion was the same as that used in the preceding study [3]. The flow rate of the internal perfusion fluid was maintained at a level between 10 and 30 μl/min. There was a continuous flow of the external

fluid medium at a rate of approximately 20 ml/min except during the period when microelectrode recordings were made from the surface of the axon. The length of the perfusion zone was usually between 15 and 20 mm. A long glass-pipette electrode (approximately 100 μ in diameter and filled with 1 M KCl making contact with a Ag—AgCl wire) was used to record action potentials intracellularly from the perfusion zone. Agar-gel was filled near the tip to reduce outflow of KCl from the tip of the electrode. When measurements of the rate of propagation of action potentials were required, a pair of glass-pipette electrodes held by a common electrode-holder (see fig. 1) was introduced into the perfusion zone through the outlet cannula used for internal perfusion. The recording tips of these paired electrodes were separated by a distance of approximately 6.5 mm. These electrodes had a dc resistance of about 2 megohms. Electric stimuli to the perfusion zone of the axon were applied through a short metal electrode inserted into the axon through the outlet cannula.

The electric impedance of the axon membrane was determined by introducing a platinized platinum electrode (approximately 2 mm in length) into the perfusion zone. The impedance bridge used was substantially the same as that described previously [6]. A large platinum wire in the external medium and the intracellular platinum electrode were connected to the unknown arm of the bridge. The ratio arms of the bridge consisted of fixed resistors at a ratio of 1:10 or 1:5. The frequency of the ac used for measurements was either 10 or 3kHz. The membrane potential was monitored simultaneously with a glass-pipette electrode.

Hyperfine glass-pipette electrodes were prepared by a Narishige microelectrode-puller and were filled with a 3 M KCl solution by the alcohol method. A Narishige micropositioner and a Nihon Kohden microelectrode-amplifier (type MZ-4) were used for potential recording with microelectrodes.

In most of the present series of experiments, the internal perfusion fluid was prepared by mixing a 600 mM NaF solution with a 12 % (by volume) glycerol solution and then by strongly buffering with a Na-phosphate solution. The ratio of the concentration of the fluoride ions to that of phosphate-ions in the mixture (expressed in mequiv/ℓ) was usually 2:1. The total Na-ion concentration was either 30 or 15 mequiv/ℓ, and its pH was 7.3 ± 0.1. In one series of experiments, a dilute CsF solution was employed instead of a NaF solution; this solution was prepared in a similar manner by using CsF and Cs-phosphate. The external fluid medium was prepared by mixing a 400 mM $CaCl_2$, a 600 mM NaCl and a 12 % glycerol solution; the pH was adjusted to 8.0 ± 0.1 with a small amount of Tris buffer. All the experiments described in this paper were carried out at room temperature (17—21°C).

3. Results

3.1. Effects of NaCl added to external $CaCl_2$ solution

In axons internally perfused with a 30 mM Na-salt solution (see section 2), the rate of propagation of the action potential was very low when the external medium contained only $CaCl_2$ and glycerol (see fig. 1). The observed rate was found to vary widely from preparation to preparation; the highest rate encountered was around 1 m/sec. In some preparations, only decremental conduction of an impulse was observed.

The propagation rate was profoundly enhanced when NaCl was added to the external medium (see middle and right records in fig. 1). In a medium containing 100 mM $CaCl_2$ and 100 NaCl, the observed rate was around 3 m/sec. In the medium containing 40—100 mM $CaCl_2$ and 400 mM NaCl, the rate was higher than 6 m/sec. It is important to note that the concentrations of both the divalent cations and Na-ions in the last external medium are very similar to those in normal sea water and the internal Na-ion concentration used is not very different from that in normal axons.

Addition of NaCl affected not only the propagation rate but also both the resting and action potentials of the axon. The action potential amplitude was between 40 and 60 mV in the absence of Na-ions in the external medium; the resting membrane potential was between −30 and −40 mV under these conditions. These values are very close to those reported previously [1]. Addition of 100 mM NaCl to the medium increased the amplitude to about 70 mV and decreased the resting potential to a level between −20 and −30 mV. In the medium containing 100 mM $CaCl_2$ and 400 mM NaCl, the amplitude was usually between 70 and 90 mV and the resting potential was roughly −10 mV. Under these conditions, repetitive firing of action potentials or fixation of the membrane potential at the depolarized

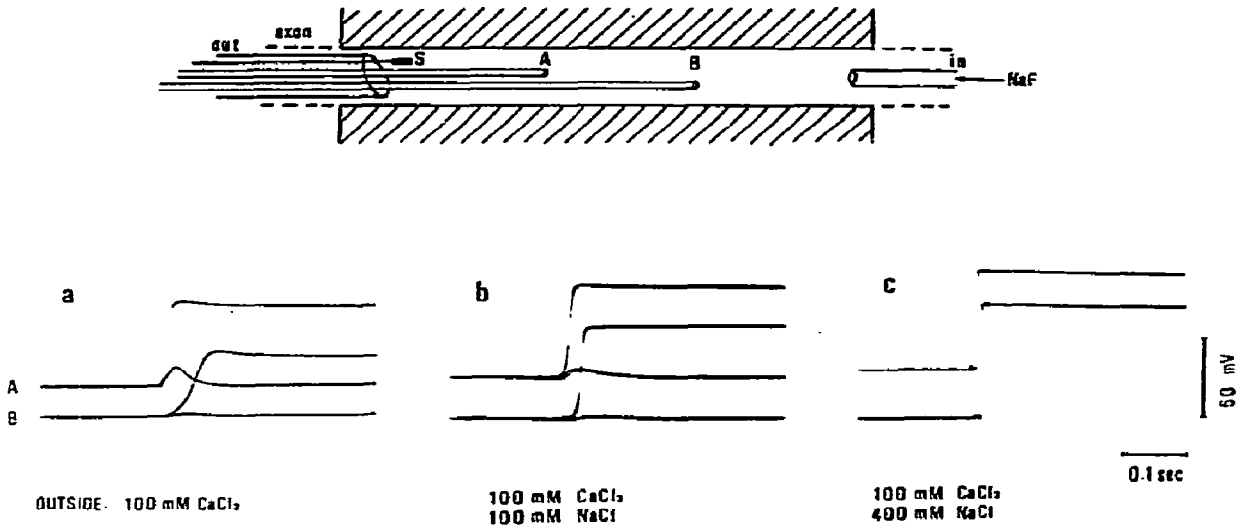


Fig. 1. Top: A schematic diagram (not to scale) showing the arrangement of the electrodes used for recording action potentials at two points in a squid giant axon. S represents the stimulating platinum electrode; A and B indicate the recording glass-tubing electrodes. "Out" and "In" refer to the outlet and inlet cannula, respectively. The axon used was approximately 450 μ in diameter and was internally perfused with a dilute NaF solution. The perfusion zone was roughly 20 mm long. The portion of the axon immersed in the external medium (shaded area) was 32 mm.

Bottom: Oscillograph records showing the effect of NaCl added to the external $CaCl_2$ solution on the action potentials recorded simultaneously from two points (6.5 mm apart) in the axon. The electrolyte compositions of the external media are given. In record a and b, the effects of subthreshold stimuli are shown. Temperature 20°C.

level was often observed.

Attempts were made to measure the extent of the conductance change in the axon membrane at the peak of an action potential observed under these conditions. Both the voltage-clamp and ac impedance techniques were used for this purpose. The results of these measurements are illustrated in figs. 2 and 3.

In the presence of only $CaCl_2$ (and glycerol) in the external medium, the membrane resistance at rest was between 7 and 10 kilohm cm^2; at the peak of the action potential, the membrane resistance fell to about 1/10 of the value at rest. (These values were estimated from the slopes of the linear parts of the voltage-current relationship.) After addition of 100 mM NaCl to the external medium, the membrane resistance at rest decreased to roughly 3 kilohm cm^2 and the resistance at the peak of excitation was around 0.2 kilohm cm^2. In the medium containing 400 mM NaCl and 100 mM $CaCl_2$, the membrane resistance at rest was between 1 and 2 kilohm cm^2 and the value at the peak of excitation was about 0.1 kilohm cm^2.

A few examples of oscillograph records of the membrane currents under voltage-clamp are shown on the left in fig. 2. These records indicate that the time-courses of the observed membrane currents are strongly influenced by the voltage level used for clamping. In the presence of a mixture of $CaCl_2$ and NaCl in the external medium, initiation of a strong inward current was followed by a rapid decline in the current intensity. A possible interpretation of this finding is presented in section 4. When the applied voltage was only slightly lower than the peak level of the action potential, a weak inward current was maintained during the entire length of the clamping voltage pulse.

The ac impedance method was applied to the perfused zone of the axon membrane in order to obtain qualitative information as to the time course of the membrane conductance during the action potential. As can be seen in fig. 3, there was a sudden change in the balance of the impedance bridge at the onset of an action potential. (The disturbance produced by the action potential in the ac amplifier tuned to the frequency of the bridge ac was adjusted to last not more than about 1 msec at 10 kHz frequency by reducing the

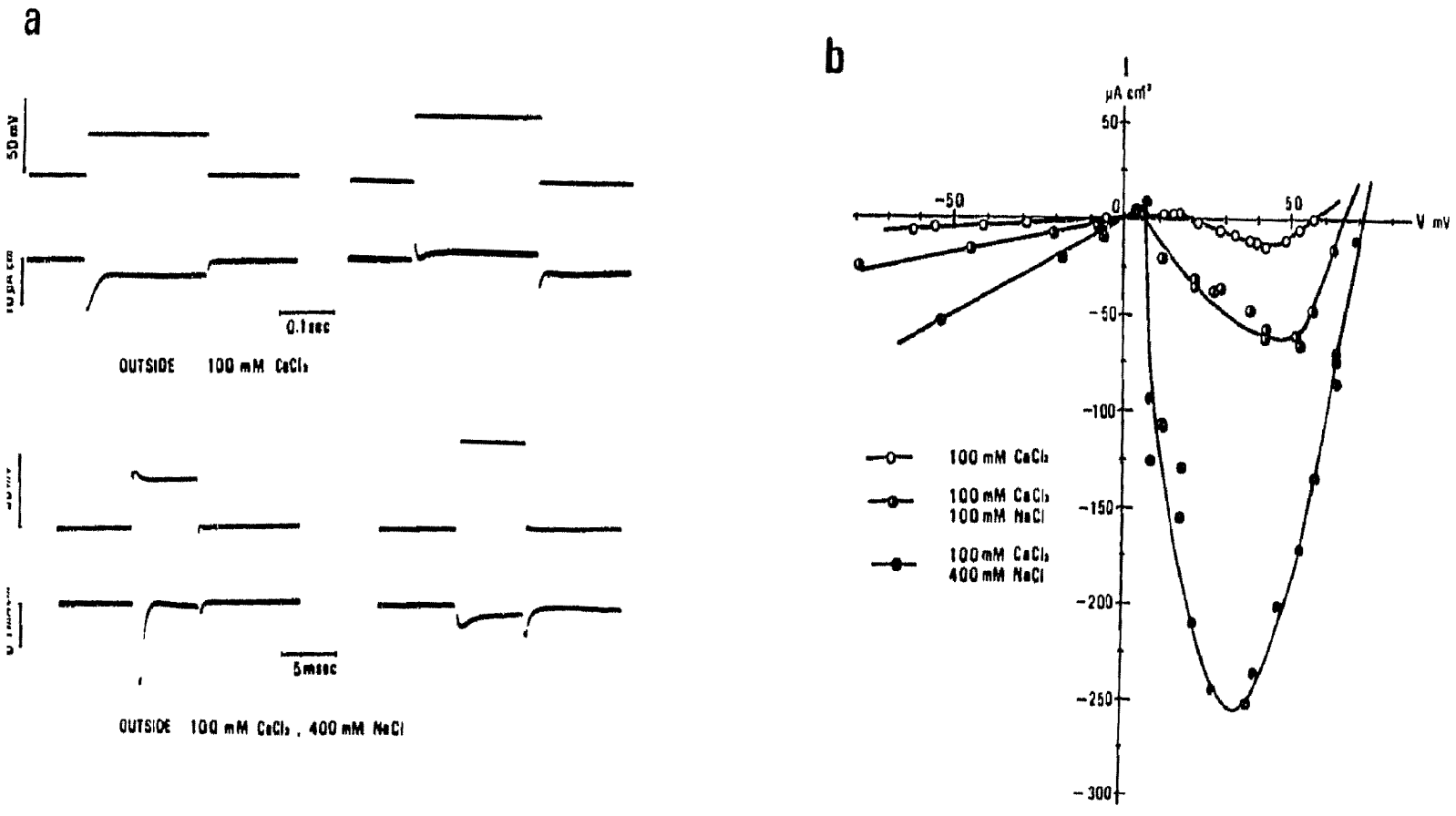


Fig. 2. Oscillograph records used for determination of the membrane resistance at rest and at the peak of excitation (a) and a plot of the results of these measurements (b). Records "a" and the data shown in "b" were taken from two different axons. The axon diameter was approximately 400 μ in both cases. The internal perfusion fluid was 30 mM NaF solution. The electrolyte compositions of the external solutions are given. Temperatures 21°C.

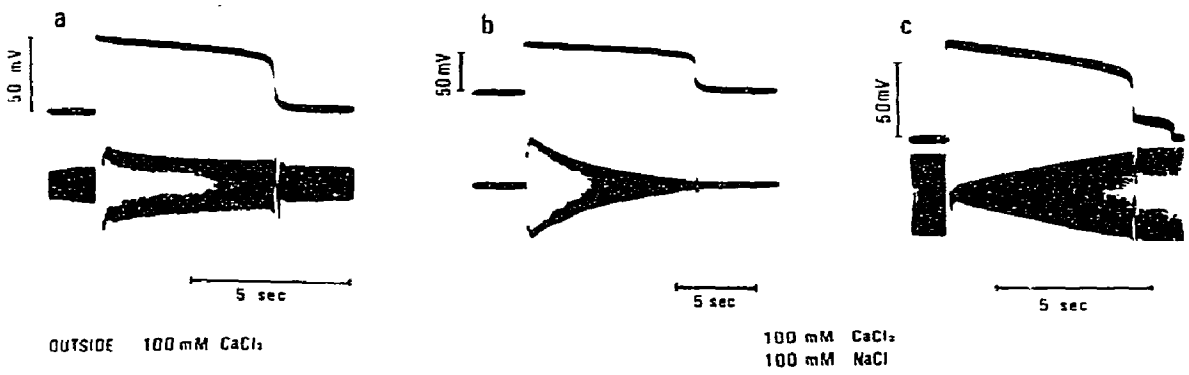


Fig. 3. Simultaneous recording of the action potential (top trace) and the output of an impedance bridge for measuring changes in the membrane resistance during excitation (bottom trace). The electrolyte compositions of the external solutions are given. In record c, the known arms of the impedance bridge were so adjusted that the best balance was observed at the onset of the action potential.

sharpness of tuning.) In the presence of both Ca- and Na-ions in the external medium, the change in the bridge balance was largest at the onset of the action potential; the balance was gradually restored during the plateau of the action potential, indicating a slow rise in the membrane resistance during this period. Immediately before termination of a prolonged action potential, the membrane impedance was very close to that of the membrane at rest. A similar finding has been reported previously based on observations of giant axons treated with tetraethylammonium ions [6].

3.2. Asynchronous termination of the action potential in the perfusion zone

Using the experimental setup employed for measurements of the rate of propagation of the action potential (see fig. 1, top), the process of termination of a prolonged action potential was examined. As is well known, the end of a prolonged action potential is characterized by a distinct potential jump toward the resting state of the membrane. Under internal perfusion with a dilute Na-salt solution, however, the terminal

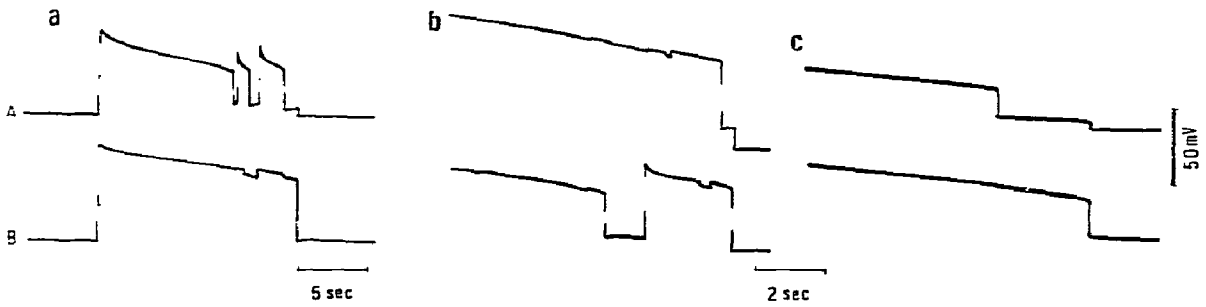


Fig. 4. Action potentials recorded simultaneously at two different points (approximately 6.5 mm apart) in an axon internally perfused with a dilute NaF solution. The experimental arrangement shown at the top of fig. 1 was used. Oscillograph traces marked A and B represent the deflections observed with electrodes A and B in fig. 1, respectively. The internal perfusion fluid was a 15 mM NaF solution. The external medium contained 100 mM $CaCl_2$ and 400 mM NaCl. Each record was taken from a different axon. In record b and c, only the terminal portions of the action potentials are shown.

portion of the action potential was frequently complex and irregular. Occasionally a rapid succession of abrupt potential changes of considerable amplitude was seen repetitively toward the end of a prolonged action potential.

Oscillograph records taken simultaneously at two points in the perfusion zone separated by a short distance revealed that the action potentials terminate asynchronously within the perfusion zone. Fig. 4 shows the experimental findings obtained by this technique from axons immersed in a medium containing 100 mM $CaCl_2$ and 400 mM NaCl. In some instances, the response recorded with the proximal electrode (the one closer to the stimulating electrode) came to an abrupt end before termination of the response recorded with the distal electrode; in other instances, the sequence of termination of the responses was reversed. Even in one and the same axon, the sequence of termination was found to vary from trial to trial. Occasionally the action potential was seen to terminate in two distinct steps, indicating that the recording tip of the electrode was located at the boundary between two zones where the action potential duration was quite different.

The observations described above strongly suggest that, at least in axons internally perfused with a dilute Na-salt solution, the action potential terminates more-or-less randomly within the perfusion zone. This is in sharp contrast to what happens at the onset of a prolonged action potential. In this case the boundary between the excited and the resting parts of the membrane moves distally at a more-or-less uniform rate.

Between the resting and excited parts of the axon membrane, there is unquestionably an electric current produced by a difference in the membrane potential between the two parts. This current is inwardly directed in the excited part of the membrane and consequently tends to bring about a transition of the membrane to the resting state. The resting part of the membrane is, on the other hand, traversed by an outwardly directed current which tends to excite this area. Because of this electric interaction between the excited part of the membrane and the area at rest, there is a strong tendency for the membrane to assume either a uniformly excited or a uniformly resting state. Toward the end of a prolonged action potential, this electric interaction is weak because the membrane resistance is relatively high both in the resting and excited parts of the membrane. Obviously, this weakness of the interaction is the major factor which makes the action potential in the perfusion zone terminate in a more-or-less random manner. The experimental results shown in fig. 4 indicated that, at least toward the end of a prolonged action potential, domains of the axon membrane in the excited state coexist with the areas at rest. In other words, the process of repolarization of the membrane proceeds in a spatially non-uniform fashion in the perfusion zone.

3.3. Demonstration of domains of the axon membrane in the excitedand resting states

To demonstrate spatial non-uniformity of the axon membrane at rest and during the action potential, microelectrode studies were conducted on axons under continuous intracellular perfusion. A serious difficulty arises in such a study from the fact that potential changes produced by excitation of a small domain can not be restricted to a small area due to the so-called cable or core-conductor property of the axon. The extent of spread of electricity within the axon can be diminished considerably by lowering the salt concentration inside the axon. When the internal NaF or CsF concentration is decreased to a level of 15 mM, a formal calculation of the space constant yields a value of about 1 mm. Thus, raising the resistivity of the perfusion fluid is a powerful means of restricting the spread of the electric potential produced by a small domain in the excited state.

An axon internally perfused with either a 15 mM NaF or CsF solution was immersed in an external medium containing 40 mM $CaCl_2$ and 400 mM NaCl. At the time when the axon was firing action potentials repetitively, the surface of the axon was gently pressed with the recording tip of a microelectrode. Care was taken to indent the surface without actually penetrating the membrane. (Penetration could readily be recognized by the appearance of strong negativity at the tip of the recording microelectrode.) Action potentials of the axon were continuously monitored with a large internal glass-pipette electrode (approximately 100 μ in diameter) introduced into the perfusion zone through the outlet cannula used for internal perfusion. It was found by this technique that small potential changes with rectangular time courses could be recorded from the surface of an internally perfused squid axon (see fig. 5).

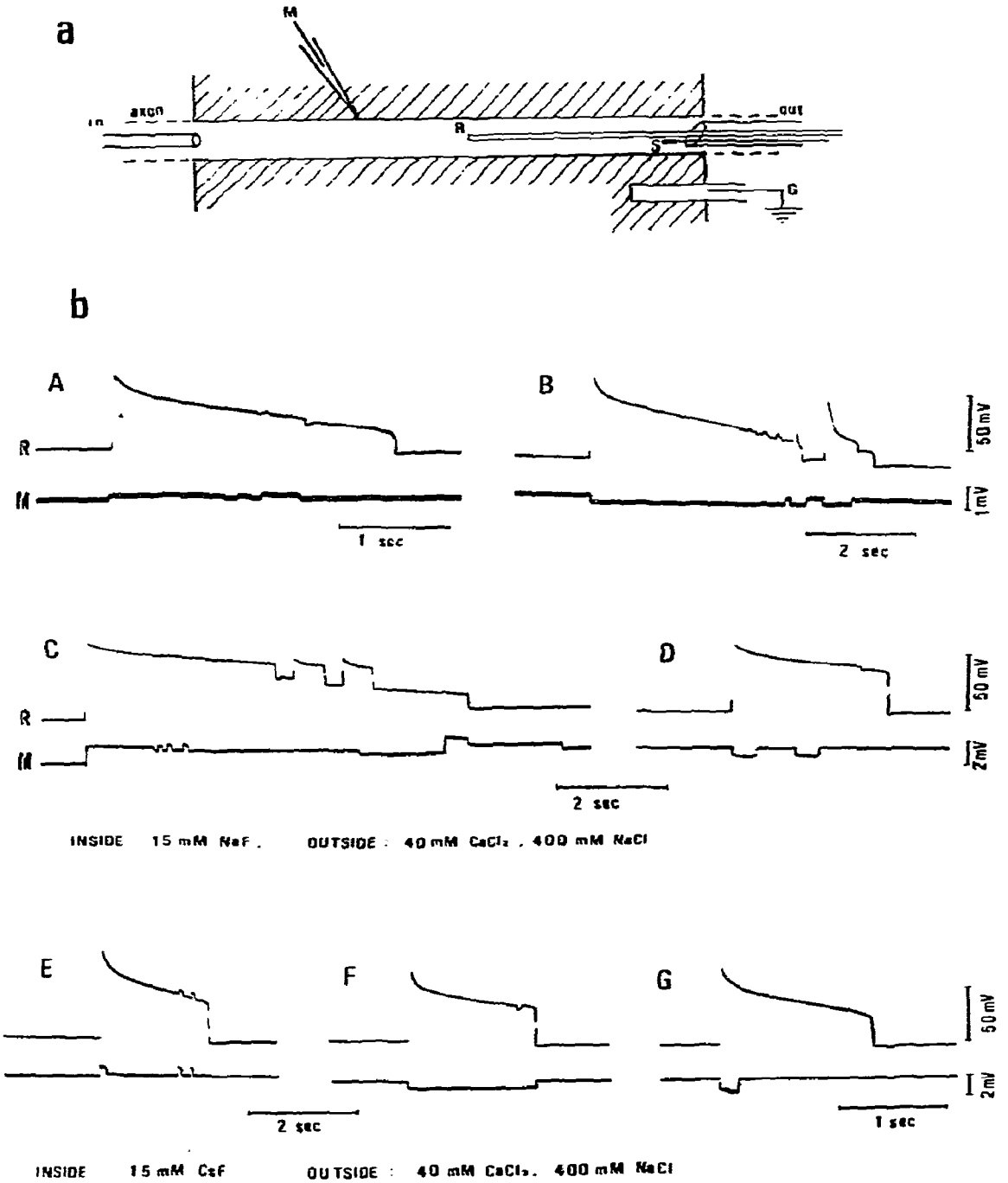


Fig. 5. Demonstration of small rectangular potential changes by the use of a microelectrode pressing on the surface of the membrane during excitation. The oscillograph trace marked M shows the potential changes observed with the microelectrode (M). The trace marked R shows the changes in the membrane potential recorded with an intracellular electrode (R). The electrolyte compositions of the external fluid media are given. Each record was taken from a different axon. Note that the small responses are positive in records A, C and E and negative in other records.

The time-courses of the small potential changes observed with a microelectrode were generally very different from the response recorded simultaneously with a large intracellular electrode. Frequently these rectangular potential changes appeared repetitively during the plateau of a single action potential. These changes represented either a rise or a fall in potential recorded with a microelectrode referred to a large extracellular ground electrode. A small fall in the recorded potential (a small downward deflection of the trace marked "M" in fig. 5) was encountered less frequently than a small rise in potential. The amplitude of the observed potential changes was usually smaller than 1 mV. It was only when the tip of the microelectrode was pushed toward the tip of the large intracellular electrode that the time-course of the potential changes recorded with the microelectrode resembled that observed with the large intracellular electrode.

In most instances the small rectangular potential changes observed had a uniform amplitude at a given position of the microelectrode. In some instances, there were two distinct "unitary" responses superimposed on each other. On few occasions, the observed "unitary" responses showed initial transients which resembled those present in internally recorded action potentials. All these findings gave us an impression that these potential changes have something in common with those observed by Bean et al. [4] and by Ehrenstein et al. [7] in EIM-treated bi-layer membranes. It is important to note that these "unitary" responses in squid axon membranes have never been observed when the tip of the recording microelectrode was larger than about 2μ.

There were many spots on the membrane surface where no potential changes could be detected with a microelectrode. Once "unitary" responses were detected at one particular site, responses with the same amplitude, sign and similar discharge patterns could be recorded from the same sites for many minutes. When "unitary" responses recorded from a particular site had a negative sign, it was always possible to detect responses of the reversed (i.e., positive) sign simply by slightly displacing the recording microelectrode either longitudinally or transversely. It was more difficult to record "unitary" responses of the negative sign than those with a positive sign. A reasonable interpretation of this finding is described in section 4.

It was not surprising to find that an electric stimulus applied at one end of the perfusion zone invariably evoked "unitary" responses. Examples of oscillograph records of "unitary" responses evoked by electric stimuli are shown in fig. 5. Both the sign and the amplitude of the responses evoked by electric stimuli were the same as those associated with spontaneous discharges of action potentials.

4. Discussion

4.1. Properties of squid axon membrane under internal perfusion

Physiological implications of the experimental data illustrated in fig. 1 are almost self-explanatory. Here, we point out only that the sign of the action potential is independent of the sign and the magnitude of the concentration gradient of sodium-ions across the membrane. It is obvious that, in the absence of sodium salt in the medium, Na-ions are transported across the membrane from the axon interior to the external medium. Yet, the polarity of the observed action potential is the same as that of an unperfused axon immersed in normal sea water. The large increase in the membrane conductance observed after addition of Na-ions to the external medium is attributable to a high mobility of Na-ions in the membrane. (The intramembrane mobility of Ca-ion is considered to be two orders of magnitude smaller than that of Na-ion [8].) We believe that the increase in the action potential amplitude is brought about by a larger change in the phase-boundary potential in the presence of Na-ions in the external medium [3].

The maximum of the inward current observed in the experiment of fig. 2 is definitely smaller than that in normal axons. This is at least partly ascribable to the effect of pronase on the axon [9]. After addition of Na-ions to the external medium, the major portion of the inward current under voltage-clamp must be carried by Na-ions. We have noted that this inward current loses its intensity, or is "inactivated" (Hodgkin and Huxley [10]), more rapidly when the clamping voltage is lower. This behavior of the membrane may be interpreted in the following manner: In the external fluid medium, the mobility of Ca-ions is comparable to that of Na-ions (see e.g., Robinson and Stokes [11]). Within the membrane, however, Ca-ions are far

less mobile than Na-ions. Consequently, a strong inward current tends to increase the Ca-ion concentration in the external surface layer of the membrane. A high Ca-ion concentration in this layer is expected to increase the membrane resistance, resulting in a rapid decline in the intensity of the inward current.

4.2. Significance of "unitary responses"

We are now ready to discuss the significance of the experimental results illustrated in fig. 5. Microelectrodes pressed against the external surface of the axon membrane in the perfused zone revealed the existence of small rectangular potential changes of uniform amplitude. We call these potential changes "unitary" responses without any implication as to their origin. It is not difficult to speculate how these "unitary" responses are generated. Let us consider a situation in which a patch of the membrane in the excited state is surrounded by a large area of the membrane in the resting state. For the sake of simplicity, we assume that the membrane is planar and also that the patch under consideration, which may be referred to as the "active domain", is very small. Due to the difference in the membrane potential in these two distinct parts of the membrane, the active domain is traversed by a strong inward current and the resting area by a weak outward current. The space on the inner side of the membrane is occupied by a conducting fluid medium with conductivity σ_i. The structure on the outer side of the membrane (connective tissues and Schwann cells) are also treated as a uniform conductor with conductivity σ_o. The electric potentials produced by these currents in the inner and outer conducting media are denoted by ϕ_i and ϕ_o, respectively. These potentials satisfy the Laplace equation

$$\nabla^2\phi_i = 0 \quad \text{and} \quad \nabla^2\phi_o = 0. \tag{1}$$

In the media in the immediate vicinity of the active domain

$$i = \sigma_i\partial\phi_i/\partial n = -\sigma_o\partial\phi_o/\partial n \tag{2}$$

where i is the surface density of the inwardly-directed membrane-current and $\partial/\partial n$ denotes the gradient in the direction normal to the membrane. In the media in direct contact with the resting area of the membrane, there is an electric current directed outwardly through the membrane. The density of this current is given by $(\phi_i - \phi_o)/r$, where r is the resistance of the membrane in the resting state. Therefore,

$$-\sigma_i\partial\phi_i/\partial n = \sigma_o\partial\phi_o/\partial n = (\phi_i - \phi_o)/r. \tag{3}$$

Equations (2) and (3) show that both $(\sigma_i\phi_i)$ and $(-\sigma_o\phi_o)$ satisfy the Laplace equation and the same boundary conditions. Therefore, near the surface of the membrane, we have

$$\sigma_i = -(\sigma_o/\sigma_i)\phi_o + \text{constant}, \tag{4}$$

which indicates the existence of a mirror-image relationship between ϕ_i and $(\sigma_o/\sigma_i)\varphi_o$.

Within the limit of the present formal treatment, eq. (4) is applicable to the case where there is more than one domain in the membrane. However, the potential ϕ_i in the internal medium has to be referred to the average potential inside the axon in this case. Under the condition of the experiments shown in fig. 5, σ_o is far greater than σ_i, indicating that potential changes produced by an active domain in the external fluid medium is far smaller than those recorded intracellularly. This is actually the case; the potential changes observed after penetration of the membrane was far larger than those recorded extracellularly.

Under the conditions of the experiments shown in fig. 5, the maximum of the inward current through the membrane in the perfusion zone is of the order of 0.3 mA/cm^2. In order to evaluate the IR-drop outside the membrane produced by this current, the resistance s/σ_o has to be determined, s being the total thickness of the layer consisting of Schwann cells and connective tissue. The resistance was determined with a long platinized platinum electrode introduced into an axon of which the membrane was destroyed by internal perfusion with sea water. Using the result of this determination, 3.5 ohm cm^2, the amplitude of a negative "unitary" response is expected not to exceed about 1 mV (i.e., 0.3 mA/cm^2 times 3.5 ohm cm^2). Experimentally, we found that this is actually the case. This finding gives additional support to the notion that the negative responses in fig. 5 were recorded when the recording microelectrode was located directly outside an active domain.

The axon membrane at rest located in the immediate

vicinity of an active domain is traversed by a relatively strong outwardly directed current. It is possible that some of the positive "unitary" responses were recorded in this manner. However, a more probable arrangement for obtaining these positive "unitary" responses is by the formation of a deep pocket in the membrane by strong pressure applied at the tip of the microelectrode. The legitimacy of this argument is supported by the following experiences:

(1) Partial recording of the intracellular potential changes without being accompanied by the resting potential is well known in frog nerve fibers [12].

(2) When the tip of a microelectrode was pushed toward the orifice of the internal recording electrode, the pattern of discharge recorded through the microelectrode is usually the same as that recorded with the internal electrode.

(3) On one occasion, we recorded a gradual change of negative "unitary" responses into positive ones while pressing the tip of a microelectrode against the axon membrane; such a reversal of the sign is known to occur in the cell body membrane of a neuron in tissue culture [13]. Thus, we may conclude that many of the positive "unitary" responses were recorded with the tip of the microelectrode pressing against the external surface of the membrane at rest in the vicinity of an active domain.

Two distinct series of "unitary" responses superimposed on each other (record C in fig. 5) may be interpreted as being recorded with a microelectrode located at a point in the resting area of the membrane between two neighboring active domains. This interpretation is supported by the experience that superposition of two negative "unitary" responses has never been encountered. Based on this and other experiences, we are inclined at present to believe that the size of a single active domain is larger than the dimension of the microelectrode, namely, 1 μ, and is far smaller than the radius of the axon.

Repetitive firing of "unitary" responses may be interpreted in the following manner. A transition of a small domain of the membrane from its resting state to the active state is induced by an increase in the external Na^+–Ca^{++} concentration ratio [3]. Since this active domain is traversed by a strong inward current, the excitation process in this domain is prematurely terminated. When the domain returns to its resting state, the properties of this domain gradually return to normal. [The mechanism of this return is similar to that of the recovery process following an abolished action potential (p. 125 in ref. [14]).] Thus, the same domain is again thrown back into its excited state.

It is reasonable to assume that there is some variation in the critical Na^+–Ca^{++} concentration ratio at different parts of the axon membrane. Hence, a number of active domains could be produced simultaneously in the membrane under a variety of conditions. When there is more than one active domain in the membrane, a strong interaction must exist between these domains by virtue of electric currents spreading among these domains. These currents are different from the well-known "local currents", i.e., Hermann's Stromchen [15], in the sense that the streamlines of these currents are not in general alignment in the direction of the long axis of the axon. From our demonstration of active domains and of spatial non-uniformity in the axon membrane, it follows immediately that long-range interactions between different parts of the membrane through the mediation of electric currents play an essential role in the process of excitation of the axon membrane.

4.3. Relation between the properties of intact and internally perfused axons

Under internal perfusion of a squid giant axon with a dilute sodium salt solution, the action potential duration is very long (see fig. 1). Previous studies [1, 2] have shown that partial or total replacement of the internal sodium salt with a potassium salt markedly shortens the action potential duration. In fact, when the composition of both internal and external fluid media is brought close to that of the normal environment of an intact squid axon, these prolonged responses are converted immediately into brief conventional action potentials. Therefore, it is evident that internal perfusion of an axon with a sodium salt solution *does not* bring about any undesirable irreversible alteration of the macromolecular architecture of the axon membrane. For this reason, we believe that analysis of the experimental results described in this paper leads us to a better understanding of the membrane of an intact axon in normal ionic environment.

According to the present state of our knowledge, the process of action potential production may be visualized in the following manner: An excitable axon

membrane under continuous perfusion can be treated as a labile cation-exchanger membrane which may undergo a "phase transition" under the influence of perturbations of various forms [1–3]. Application of an electric current pulse, changes in the chemical composition of the external medium, and changes in the temperature are examples of such perturbations. A change in the ratio of univalent–divalent cations within the membrane is considered to trigger such a transition.

A transition of the axon membrane from one state to the other is associated with a large change in the intramembrane ion-mobilities, selectivities and effective charge-density of the membrane. Therefore, there is a sudden shift in the membrane potential at the moment when the membrane undergoes such a transition; this sudden potential shift represents initiation of an action potential. In excitation of an axon immersed in a Na-free medium (fig. 1a), a large increase in the Ca-ion mobility appears to be the major factor contributing to the potential shift. Following such a transition, the distribution of various ions in- and outside the membrane changes as a function of time as a result of a marked enhancement of the interdiffusion fluxes, bringing about a gradual change in the membrane potential. Particularly, in axons with both Na- and Ca-ion externally and K-ion internally, the interdiffusion fluxes are intensified because of high mobilities of univalent cations; this is considered as the major factor which makes the action potential duration in the normal environment very short.

We have demonstrated the appearance of active domains under particular experimental conditions. Although it seems technically difficult to make a similar demonstration in intact (i.e., internally unperfused) axons, we may assume that the behavior of the membrane macromolecules in these axons is not fundamentally different from that in axons internally perfused with dilute salt solutions. Thus, we may generalize our conclusions to include axon membranes under other experimental conditions. In the well-known equivalent-circuit model of the axon membrane [10], the membrane is treated as a spatially uniform structure and a transition from the resting state to the active state is assumed to be continuous. Based on the experimental findings described in this paper, we may conclude that it is the fraction of the membrane in the active active state that is a continuous function of the chemical composition of the external medium or of the potential difference applied across the membrane [14]. The state of the membrane in every small domain of the membrane changes discontinuously; but, the probability of being in one particular state changes continuously with the averaged state variables of the system. A similar conclusion was reached by Ehrenstein et al. [7] who studied the properties of lipid bi-layer membranes containing a limited number of EIM molecules.

Further experimental studies are required to reach a better understanding of the process of nerve excitation from a molecular point of view.

Acknowledgement

We are deeply indebted to Mr. Kawai and to Mr. Tada at the Otaru Aquarium, and to Mr. Shinta of the Oshoro Marine Laboratory, Hokkaido University, for a continuous supply of squid during the present investigation. This work was partly supported by a grant from the Ministry of Education in Japan. One of the authors (I.T.) is indebted to the Naito Science Foundation for a travel fund for carrying out the present work.

References

[1] A. Watanabe, I. Tasaki, and L. Lerman, Proc. Natl. Acad. Sci. US 58 (1967) 2246.
[2] I. Tasaki, L. Lerman and A. Watanabe, Amer. J. Physiol. 216 (1969) 130.
[3] I. Inoue, Y. Kobatake and I. Tasaki, Biochim. Biophys. Acta 307 (1973) 471.
[4] R.C. Bean, W.C. Shepherd, H. Chan and J.T. Eichner, J. Gen. Physiol. 53 (1969) 741.
[5] P. Mueller and D.O. Rudin, Nature 217 (1968) 713.
[6] I. Tasaki and S. Hagiwara, J. Gen. Physiol. 140 (1957) 859.
[7] G. Ehrenstein, in: Biophysics and Physiology of Excitable Membranes, ed. W.J. Adelman, Jr. (Van Nostrand–Reinhold, New York, 1971).
[8] I. Tasaki, A. Watanabe and L. Lerman, Amer. J. Physiol. 213 (1967) 1465.
[9] H. Sato, I. Tasaki, E. Carbone and M. Hallett, J. Mechanochem. Cell Motility, 2 (1973) 209.
[10] A.L. Hodgkin and A.F. Huxley, J. Physiol. 117 (1952) 500.
[11] R.A. Robinson and R.H. Stokes, Electrolyte Solutions (Butterworths, London, 1959).
[12] I. Tasaki, Japan. J. Physiol. 3 (1953) 73.
[13] W. Hild and I. Tasaki, J. Neurophysiol. 25 (1962) 277.
[14] I. Tasaki, Nerve Excitation (Thomas, Springfield, Ill., 1968).
[15] L. Hermann, Handbuch der Physiologie, Band II, Theil I (Verlag F.C.W. Vogel, Leipzig, 1879).

BIOPHYSICAL CHEMISTRY 2 (1974) 127–136. © NORTH-HOLLAND PUBLISHING COMPANY

A DYE-BINDING INDUCED CONFORMATIONAL TRANSITION OF POLY-(METHACRYLIC ACID) BY AURAMINE O IN AQUEOUS SOLUTIONS

I. EXPERIMENTAL RESULTS

W.H.J. STORK, J.A.M. VAN BOXSEL, A.F.P.M. DE GOEIJ, P.L. DE HASETH and M. MANDEL
Gorlaeus Laboratoria der Rijksuniversiteit Leiden, afdeling Fysische Chemie III, Leiden, The Netherlands

Received 7 February 1974

Binding of auramine O to poly-(methacrylic acid) (PMA) has been established over a large range of C_p^0/C_d^0 values using spectroscopic methods (UV absorption and visible fluorescence emission spectra), equilibrium and sedimentation dialysis, potentiometric and viscosimetric titrations. All the results show qualitative agreement with those obtained previously with the system crystal violet–PMA although the binding seems to be less strong for auramine O than for crystal violet. From dialysis experiments binding isotherms were obtained at three different degrees of neutralization α'; at $\alpha' = 0.10$ the results could be fitted to a Langmuir isotherm but at α' equal to 0.40 and 0.65 deviations with respect to such an isotherm occur. The results of potentiometric and viscosimetric titrations confirm that the conformational transition which the dye-free PMA exhibits upon ionization is affected by the dye binding. The region in which the conformational transion occurs is broadened and is less sharply defined in the presence of auramine O.

1. Introduction

In two previous papers [1, 2] the binding of crystal violet (CV) to poly-(methacrylic acid) (PMA) has been investigated as a model for dye binding to weak polyelectrolytes exhibiting a conformational transition upon ionization. Such an investigation using an extensively studied synthetic polyelectrolyte may be helpful for a better understanding of the very important interactions between charged dyes and biopolymers.

The results obtained by several experimental techniques all pointed to strong binding of CV to PMA. Furthermore it was found that the positively charged CV does not bind specifically to the charged carboxylate groups of PMA, particularly in view of the fact that completely undissociated PMA still strongly interacts with CV. The results also suggested that the binding of CV is stronger to the compact conformational state of PMA, predominantly present at low degrees of neutralization α' in dye-free systems, than to the more extended conformational states which appear at higher values of α'. Under most experimental conditions it was found that either the fraction f of bound dye was equal to unity or the amount of bound dye per monomeric unit r had it maximum value r_m. Therefore no quantitative evaluation of the binding equilibrium was possible and the conclusions remained purely qualitative.

In the present paper an analogous investigation of the interaction between PMA and the cationic dye auramine O in aqueous solutions will be presented. Qualitatively the phenomena observed are the same as those for the CV–PMA system. The interaction between dye and polyelectrolyte is weaker however and makes a more quantitative description possible. In particular it has been possible to obtain information about the influence of the dye binding on the conformational transition of PMA.

In part I of this series the experimental results will presented; in part II [13] these results will be interpreted and critically discussed.

2. Experimental

2.1. Materials

Atactic PMA was prepared and fractionated as des-

cribed previously [3]. The sample used in the present investigation had a molecular weight of 1.3×10^6 according to viscosimetric determinations [4]. It was the same sample as used previously [1, 2]. Solutions of PMA were prepared with conductance water of specific conductivity lower than $10^{-6}\Omega^{-1}m^{-1}$. Concentrations were determined potentiometrically. Different degrees of neutralizations were obtained by adding known amounts of NaOH 0.1 M prepared from Fixanal or Merck ampullae (with the usual precautions to avoid contamination by carbonate).

Auramine O or bis [4-(dimethylaminophenyl)] methylidene ammonium chloride was of commercial origin. In view of the possible presence of inorganic salts and organic impurities its purification was attempted in several ways. The method of Noll [5] and Graebe [6] yielded the best results. 10 g auramine O ("Eastman") was recrystallized from 75 cm^3 ethanol. The crystals were filtered at 0°C, washed twice with ice-cold ethanol and dried in vacuum at 40°C over P_2O_5. The final product seemed to contain half a mole of water per mole dye judging from elementary analysis (performed by H. Pieterse, Laboratory of Organic Chemistry, University of Amsterdam); C: 64,2%, N: 13,6%, H: 7,0%, Cl: 10,1%, O: 2,5% (theoretically C: 65,2%, N: 13,4%, H: 7,4%, Cl: 11,3%, O: 2,5%). Repeated recrystallization did not yield further improvement. The purified sample exhibited a maximum extinction coefficient of $4.8 \times 10^4 \ell.mol^{-1}cm^{-1}$ in water of 20°C at 23 300 cm^{-1}. Its melting point was 263°C compared to the literature values of 267°C [6] and 265°C [7].

Auramine O slowly decomposes with time and was therefore stored at low temperature in the dark. Checks on the purity were performed regularly. In aqueous solutions at pH ≈ 7 AuO is completely dissociated into the dye cation and the chloride anion; these solutions when stored in the dark are quite stable. Hence stock solutions were prepared about once a week.

At low pH decomposion into Michler's ketone has been established. This reaction has been studied in detail by Holmes and Darling [8] who found that the reaction, which proceeds according to first order kinetics at constant pH, is accelerated by an increase in H^+ concentration. In the present investigation the velocity constant k was measured at 20°C at various pH values; $k = 5 \times 10^{-4}min^{-1}$ at pH = 2.2 and $k = 10^{-4}min^{-1}$ at pH = 2.8, the latter corresponding to a half life of about 6 days. At pH = 4 no decomposition at all was observed even after a few days. These results are in accordance with the observations by Holmes and Darling.

In alkaline solutions the dye reacts with OH^-. This reaction was investigated by Goldacre and Phillips [9] who established that it proceeds in two steps. In the first step addition of water yields a carbinol. Equilibrium is reached only after a few days and is characterized by a pK = 9.8.

In accordance with these results we have found that for $3.5 < pH < 8.0$ the absorption spectrum and the fluorescence quantum yield of AuO solutions are independent of the H^+ concentration.

Auramine O has been found [10] to obey Beer's law up to concentrations of 10^{-3}M. Hence it is generally assumed that auramine O does not aggregate in aqueous solutions up to this concentration [11] in contrast to crystal violet. In the present investigation it was found that AuO obeys Beer's law up to the highest concentration measured, i.e., 2.5×10^{-3}M.

Salts and *buffer* materials were all of p.a. quality.

2.2. *Techniques*

All experimental techniques have already been described extensively [1, 2]. They will only be outlined here. All measurements were carried out at 20°C. Equilibrium dialysis was performed in the dark for 24 hours with Sigma 250-11 dialysis sacks prewashed to remove inhibitors. The dye concentration in the polyelectrolyte-free (outer) solution was determined spectroscopically and assumed to be equal to the dye activity (dye concentration $C_d < 10^{-3}$M). In the polyelectrolyte solutions the total dye concentration was calculated from the total amount of dye present in the complete system and the amount in the outer solution at equilibrium. The fraction of dye bound to PMA was obtained assuming the deviations of the activity coefficients with respect to unity to be negligible for the free dye cations even in the presence of polyions (this assumption will be discussed in part II of this series). Corrections for the adsorption of the dye to the dialysis sacks and glassware were applied.

For sedimentation dialysis either a Beckman Spinco E analytical ultracentrifuge or a Beckman L II preparative ultracentrifuge was used. In both cases correc-

tions for the adsorption of the dye to the centrifuge tubes were necessary.

Absorption spectra were determined with a Zeiss PMQ II spectrophotometer. Fluorescence measurements were performed either with the Zeiss PMQ II spectrophotometer with fluorescence attachment ZFM 4 and a Hanau St.75 mercury lamp or a Farrand spectrofluorimeter with xenon lamp. The AuO solutions were excited at 23 300 cm^{-1}. Background emission was found to be negligible all solutions investigated. Corrections for primary absorption effects (in case the Farrand spectrofluorimeter was used) and the spectral sensitivity of the instruments were applied. From corrected spectra the quantum yield would be obtained as described previously [1].

Potentiometric titrations were performed discontinously with Radiometer equipment using G 202C glass electrodes and K 401 calomel electrodes. Viscosimetric titrations were carried out automatically with the aid of a Viscometer Reader and Printing Counter VR-P2 of Rehovot Instruments using two Ubbelohde viscosimeters with flow time for water of 49.3 and 94.9 s respectively at 20.00 ± 0.02°C.

3. Results

3.1. Absorption spectroscopy

The absorption spectrum of AuO in aqueous solutions is characterized by an important maximum near 23 300 cm^{-1} in the visible region. In the near ultraviolet there are further absorption maxima the first of which is situated at 27 000 cm^{-1}. According to Adam [12] these maxima correspond to different absorption bands.

The absorption spectrum of AuO undergoes modifications when increasing amounts of PMA are added at constant dye concentration C_d^0. Some representative spectra of PMA–AuO systems at constant $C_d^0 = 2 \times 10^{-4}$M and NaCl concentration $C_s^0 = 2 \times 10^{-3}$ M and different polyelectrolyte concentrations C_p^0 (expressed as number of moles monomer per unit volume) at constant degree of neutralization α' are given in fig. 1. Although both the absorption band at 23 300 and 27 000 cm^{-1} are affected by the presence of PMA the spectral changes are less spectacular than for corresponding PMA–CV systems [1]. The apparent extinction coefficient at 23 300 cm^{-1} decreases with increasing C_p^0

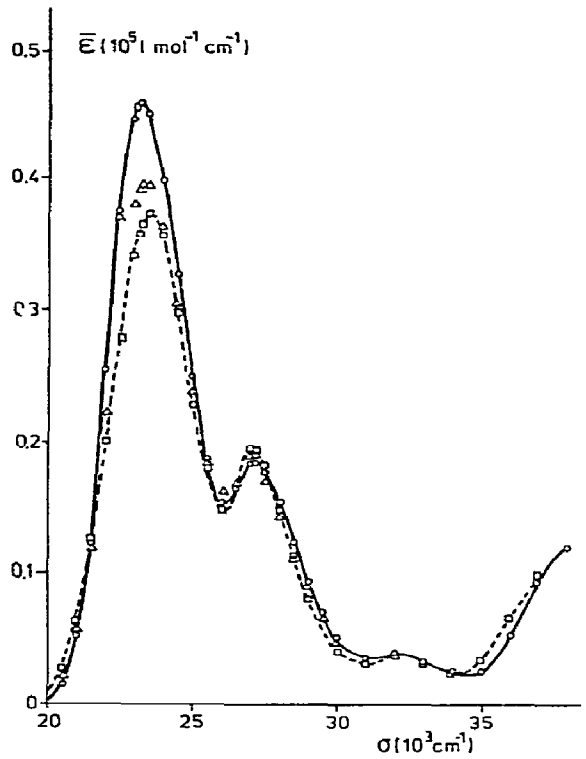


Fig. 1. Absorption spectra of AuO–PMA solutions; $C_d^0 = 2 \times 10^{-4}$M, $C_{NaCl} = 2 \times 10^{-3}$M; PMA at $\alpha' = 0.65$; C_p^0: 0 M (○), 1.7×10^{-4}M(△) and 8.7×10^{-9}M(□).

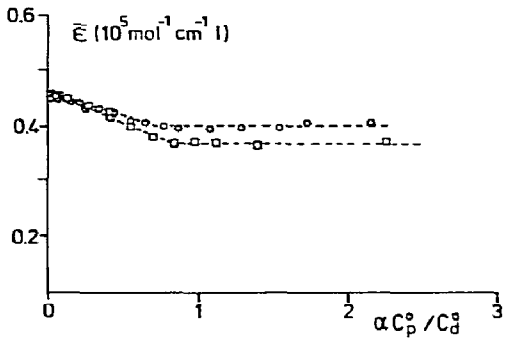


Fig. 2. Apparent absorption coefficient of AuO at 23 300 cm^{-1} versus $\alpha' C_p^0 / C_d^0$; $C_d^0 = 2 \times 10^{-4}$M, $C_{NaCl} = 2 \times 10^{-3}$M; $\alpha' = 0.10$ (○) and 0.65 (□).

until it reaches a constant value over a broad region of C_p^0 values (fig. 2), in qualitative agreement with the observations at the absorption maximum of CV in PMA–CV systems. The relative decrease for the former is much smaller however. Furthermore, for all the systems

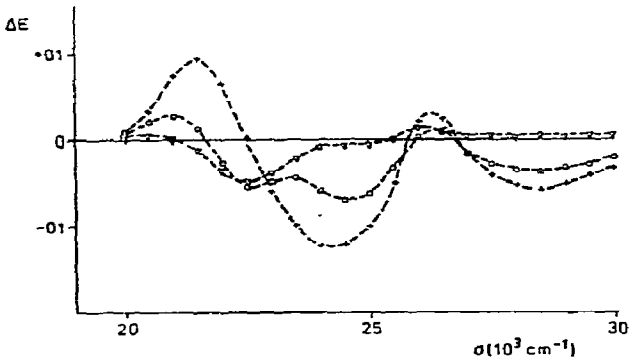


Fig. 3. Difference spectra of AuO–PMA systems with respect to PMA free AuO solution; ΔE is difference in extinction for a pathlength of 0.1 cm. $C_d^0 = 1.5 \times 10^{-5}$M, $C_{NaCl} = 2 \times 10^{-3}$M, PMA, $C_p^0 = 9.3 \times 10^{-4}$M at $\alpha' = 0.10$ (+), 0.50 (○) and 1.00 (▽).

investigated no new absorption bands due to bound dye were observed between 20 000 and 40 000 cm^{-1} which suggests that in this spectral region the spectrum of free and bound dye overlap considerably. This is confirmed by difference spectra between AuO and AuO–PMA (fig. 3). These also demonstrate that at constant C_p^0/C_d^0 the spectrum of the bound dye may depend on α', as was also observed for CV.

Therefore, although the spectral modification point to dye binding, no quantitative evaluation has been attempted of the concentration of free and bound dye from the spectra of the different solutions. As will be shown below the fraction f of total dye concentration bound to the polyelectrolyte is still well below unity even at the highest concentration C_p^0 investigated in contrast to what was observed in the PMA–CV systems (e.g., $f = 0.70$ at $C_p^0 = 2.6 \times 10^{-3}$M for PMA–AuO against $f = 1.0$ for $C_p^0 > 4 \times 10^{-4}$M for PMA–CV; $\alpha' = 0.65$ and $C_d^0 = 2 \times 10^{-4}$M). This points to a much weaker interaction between AuO and PMA than for CV and PMA and could partially be responsible for the small spectral changes observed with the former.

3.2. Equilibrium dialysis

The binding was studied extensively at three different pH values using phosphate buffers of low ionic strength ($I \approx 10^{-3}$M). For pH = 5.5 (corresponding to $\alpha' \approx 0.10$) the buffer composition is given by $C_{KH_2PO_4} = 2.3 \times 10^{-3}$M; $C_{Na_2HPO_4} = 7.3 \times 10^{-3}$M. For pH = 6.8 ($\alpha' \approx 0.40$), $C_{KH_2PO_4} = 7.1 \times 10^{-4}$M, $C_{Na_2HPO_4} = 5.4 \times 10^{-4}$M and for pH = 7.65 ($\alpha' \approx 0.65$), $C_{KH_2PO_4} = 1.07 \times 10^{-4}$M and $C_{Na_2HPO} = 8.9 \times 10^{-4}$. For each set of experimental conditions an adsorption isotherm of the dye to the dialysis sacks was constructed. The reproducibility of these isotherms was poor. However, since the decrease in the free dye concentration due to adsorption of AuO

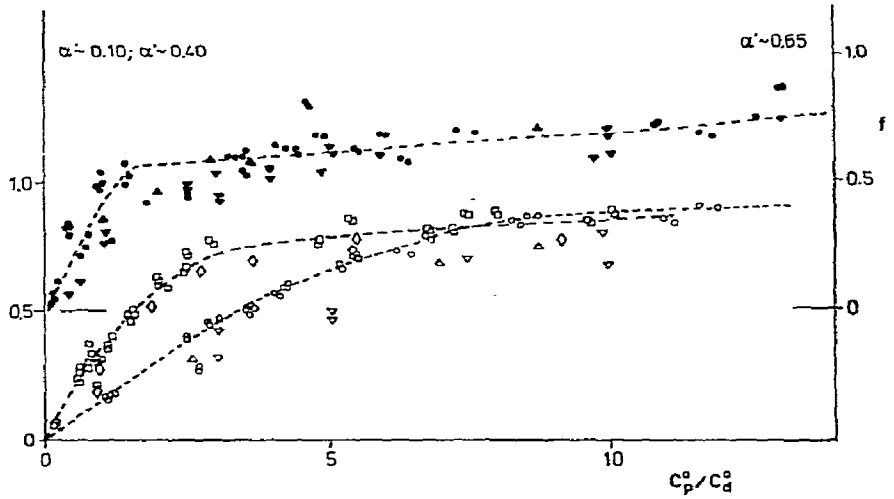


Fig. 4. Fraction f of bound auramine O versus C_p^0/C_d^0 determined by equilibrium dialysis (D) and sedimentation dialysis by preparative (P) and analytical (A) ultracentrifuge (see text); $10^{-4} < C_d^0 < 3 \times 10^{-4}$M. PMA at $\alpha' = 0.10$: D (○), P(▽), A(△); $\alpha' = 0.40$: D(□), P(◇); $\alpha' = 0.65$: A(●), P(▼), A(▲). (Ionic strength of small ions ~2×10^{-3}M).

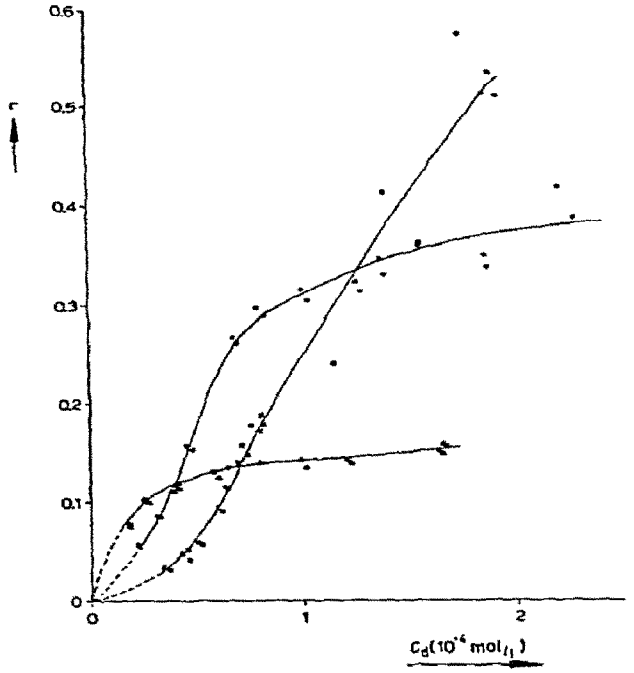


Fig. 5. Binding isotherms for the AuO–PMA systems using only the equilibrium dialysis data of fig. 4; $\alpha' = 0.10$ (▲), 0.40 (●) and 0.65 (■).

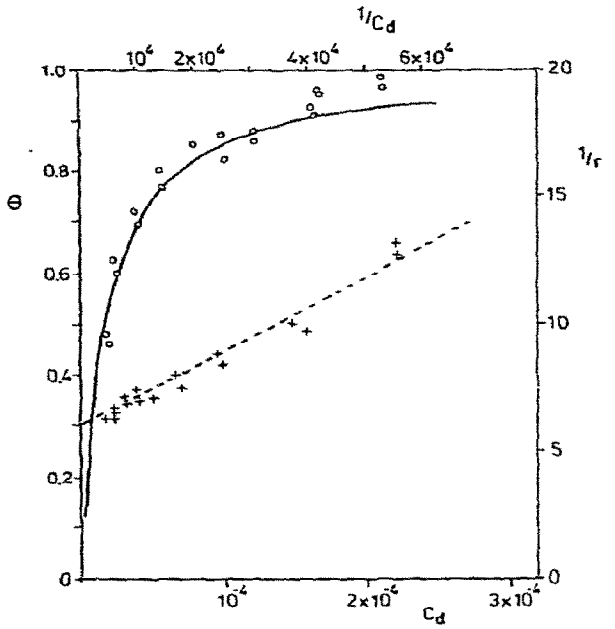


Fig. 6. Plot of $1/r$ against $1/C_d$ (+) for the equilibrium dialysis data of fig. 4 and 5 for AuO–PMA at $\alpha' = 0.10$ and corresponding Langmuir isotherm $\theta = r/r_{max}$ versus C_d (○) with the parameters $K_a = 5 \times 10^{-4}$ l mol^{-1} and $r_{max} = 0.16$ as determined from the linear plot $1/r$ versus $1/C_d$.

to the bags never exceeded 12%, significant binding curves for auramine O to PMA could be obtained. The fraction f of dye bound to PMA as function of C_p^0/C_d^0 (corresponding to several sets of experiments where both C_p^0 and C_d^0 were varied) measured at the three different pH values are represented in fig. 4. As can be seen, under the experimental conditions f remains always smaller than unity and increases only slowly with C_p^0/C_d^0 at the highest ratios investigated. These results are also represented as binding isotherms in fig. 5. The number of dye ions bound per monomeric unit, $r = fC_d^0/C_p^0$, tends with increasing concentration of free dye C_d to a value of the same magnitude as α', at least for $\alpha' \approx 0.10$ and $\alpha' \approx 0.40$. In the case of $\alpha' \approx 0.65$ an estimate of r_m is not possible. As can be seen from fig. 6 where $1/r$ is plotted against $1/C_d$ the isotherm for the system with $\alpha' \approx 0.10$ fits to a Langmuir isotherm. At higher values of α' the binding process does not conform to such an isotherm, however, as follows already from the increasing slope of the curve r versus C_p at low values of C_p (see fig. 5).

Binding was also studied in unbuffered PMA solutions at $\alpha' \approx 0.65$ with 2×10^{-3}M NaCl. The same general characteristic features as in the buffered solutions at pH = 7.65 were observed, although the results themselves were not identical, as was to be expected.

Dye interaction to acidified PMA was also investigated as it was found previously [1] that CV strongly binds to the completely undissociated PMA. Owing to the decomposition of AuO under prevailing experimental conditions it was impossible to draw conclusions about possible binding. As AuO is generally less strongly bound to PMA than CV under comparable conditions the decomposition of the dye may mask completely its rather weak interaction with the macromolecule at low pH. Finally it should be mentioned that the extent of binding of the dye found from equilibrium dialysis was not influenced by the way in which the solutions were prepared.

3.3. Sedimentation experiments

Experiments were carried out at $\alpha' = 0.10$, 0.40 and 0.65 in the presence of 2×10^{-3}M NaCl. In all cases widely scattered results were obtained probably due to the rather large irreproducibility of the dye adsorption to the centrifuge tubes and cells. Qualitatively the values of f found both with the analytical and the preparative ultracentrifuge, assuming that the sedimentation does not perturb the binding equilibrium, are of the same magnitude as those obtained with the help of equilibrium dialysis under comparable conditions although the former always seems to be somewhat smaller (fig. 4).

3.4. Potentiometric titrations

The pH of PMA titrated with NaOH in the presence of AuO depends on the way in which the titration is performed, as was already observed with the PMA–CV systems. If PMA is neutralized to a certain value of α' and the dye is added hereafter (neutralization before dye procedure NBD) the pH is not time dependent and identical to the pH found by completely neutralizing the PMA–AuO solutions and subsequently acidifying with HCl to the required α'. If however, PMA–AuO solutions were directly neutralized up to a certain α' value (dye before neutralization procedure, DBN) the pH was found to decrease for a period of several hours after preparation of the solution (especially near $\alpha' = 0.50$) reaching finally a value which was always larger than the pH found by the NBD procedure. This difference in pH was dependent on C_p^0/C_d^0 and largest in the α' region where the polyacid in the absence of the dye exhibits a conformational transition [3]. (In general $0.1 < \Delta\,\mathrm{pH} < 0.3$.) Although it may be safely assumed that the NBD procedure yields the true equilibrium values of pH some titration curves of PMA in the presence of AuO, at constant C_d^0 and in the presence of a small excess of NaCl, obtained by both procedures are represented in fig. 7 to demonstrate that the qualitative features of the titration curves are the same for both cases and analogous to those observed with PMA–CV systems [2]. At rather low α' values the pH of the PMA–AuO solutions fall below the reference titration curve fo the dye-free PMA solution. At larger α' values the pH is always larger than the reference pH of the dye free system, the difference increasing with increasing C_d^0. It should be noted that the initial lowering of the titration curve of PMA by AuO is much larger than the corresponding lowering due to a corresponding increase in the NaCl concentration. In fact the pH of the PMA–NaCl system is not significantly affected if C_s is increased from 2×10^{-3} to 2.3×10^{-3}M. This observation together with the anomalous change of the titration curve at higher α' with increasing C_d^0 proves that the influence of AuO cannot be explained in terms of variations in the ionic strength only but that specific interaction effects leading to dye binding should be held responsible for the phenomena observed.

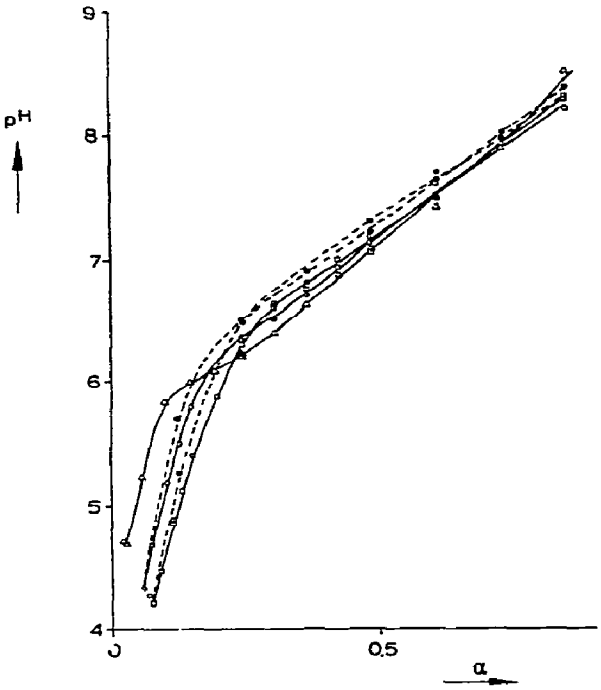


Fig. 7. Potentiometric titration curves (pH versus α') of AuO–PMA solutions. $C_p^0 = 7.8 \times 10^{-4}$M, $C_{NaCl} = 2 \times 10^{-3}$M. $C_d^0 = 0$ M (△); 10^{-4}M, NBD (○); 10^{-4}M, DBN (●); 2×10^{-4}M, NBD (□); 2×10^{-4}, DBN (■).

In the investigation of PMA–CV system [2] it has been concluded that, up to a first approximation, the dye binding may be assumed to affect the dissociation of the carboxylic groups on the polyelectrolyte only through the change of the net charge density of the polyion and its influence on the mean electrostatic potential on the surface of the macromolecule. In view of the similarity of the effect on the titration curves of PMA observed with both dyes this conclusion may

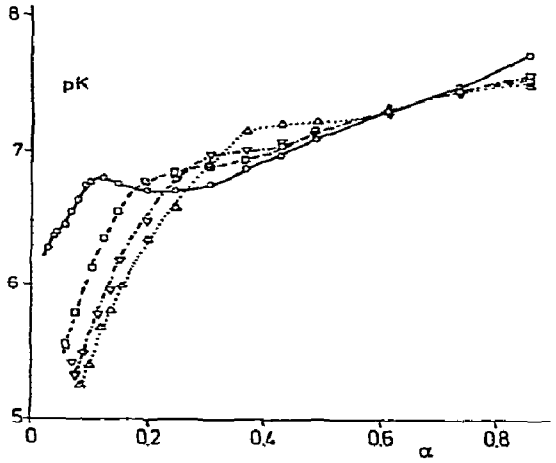


Fig. 8. pK versus α' for AuO–PMA solutions (NBD only); $C_p^0 = 7.8 \times 10^{-4}$ M, $C_{NaCl} = 2 \times 10^{-3}$ M, $C_d^0 = 0$ (○), 10^{-4} (□), 2×10^{-4} (▽), 3×10^{-4} M (△).

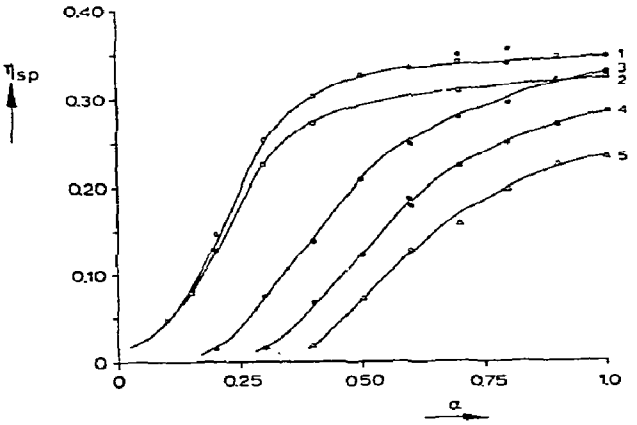


Fig. 9. η_{sp} versus α' for AuO–PMA solutions, $C_p^0 = 7.8 \times 10^{-4}$ M, $C_{NaCl} = 2 \times 10^{-3}$ M, $C_d^0 = 10^{-4}$ (●), 2×10^{-4} (■) and 3×10^{-4} M (△); reference curves $C_p^0 = 7.8 \times 10^{-4}$ M, $C_d^0 = 0$, $C_{NaCl} = 2 \times 10^{-3}$ (○) and 2.2×10^{-3} M (□).

be extended to PMA–AuO systems. Therefore the titration curves may be transformed into plots of $pK \equiv pH + \log|[(1-\alpha)/\alpha]|$ against α (where K is the apparent dissociation constant and α the degree of dissociation which can be calculated under the above assumption from α' and the correction for the autodissociation of the polyacid). These plots for the titrations according to the NBD procedure are represented in fig. 8. (A physically more significant representation would have been a plot of pK versus the net degree of charge of the polyion, $(\alpha - r)$; in principle r can be calculated from binding isotherms for any value of α'. As only binding isotherms at three different values of α' were determined it has not been possible to estimate r over the whole titration range however.) For the dye-free PMA systems three different regions may be distinguished in such plots [3]. At low charge densities up to $\alpha \approx 0.10$, corresponding to the compact conformational state (state a) of PMA, pK is a rapidly increasing function of α. For α larger than 0.35 PMA is in a much more extended mean conformation (state b) and $dpK/d\alpha$ is much smaller. Between $\alpha = 0.15$ and $\alpha = 0.35$ the conformational transition takes place and the pK slightly decreases with α or remains nearly constant. Although it should be borne in mind that for the PMA–AuO systems α is not a true measure of the real change density (which is decreased by the positively charge dyes bound to the polyelectrolyte) the curves pK versus α clearly suggest that for these systems the a state is increasingly stabilized by increasing C_d^0 as the first region (characterized by nearly the same value of $dpK/d\alpha$ as for dye-free PMA) is extended over a broader interval of α values. For the region $\alpha > 0.50$ all the curves nearly coincide indicating that in all cases probably an analogous b state is present. These conclusions are confirmed by the viscosimetric results shown below.

3.5. Viscosimetric results

The specific viscosity $\eta_{sp} = (\eta - \eta_0)/\eta_0$ (with η and η_0 standing for the viscosity of the solution and the reference solvent respectively) of PMA in aqueous salt solutions (NaCl) in the absence and presence of AuO as function of the degree of neutralization (at constant C_p^0 and C_d^0) are represented in fig. 9. No effect of the way in which the PMA–AuO solutions were prepared was detected for these viscosity measurements and time effects were also absent. The curves of fig. 9 demonstrate that the overall change of η_{sp} with α' characteristic for the PMA system exhibiting a conformational transition is conserved in the presence of the dye. At low α, η_{sp} is very small and changes only slowly with α, due to the compact structure of the conformational a state. In the region of the conformational transition η_{sp} rises to much higher values and remains practically constant in the region of the conformational b state (at least in the presence

of 2×10^{-3}M NaCl). The influence of AuO on η_{sp} differs significantly from the effect of NaCl of equal ionic strength in agreement with what was observed by potentiometry. The region of low η_{sp} is extended to higher α values and the interval of α values in which the viscosity rises up to a practically constant value is also broadened in comparison to the AuO-free PMA solutions. Also the limiting η_{sp} at high α is somewhat lowered with respect to the corresponding viscosity of a solution with equal ionic strength but without AuO. These results, completely analogous to those observed with the PMA–CV system [2], supports the assumption that AuO has a marked stabilizing effect on the compact conformational a state of PMA and probably also slightly affects the conformations in the b state. It is also clear from these results that the interaction between AuO and PMA cannot be explained in terms of electrostatic interactions only.

3.6. *Fluorescence spectroscopy*

The interaction between AuO and PMA was also investigated by fluorescence spectroscopy. Fluorescence spectra were measured of PMA–AuO solutions over a wide range of PMA concentrations at different α' and C_d^0. The results were quite similar to those obtained with PMA–CV systems [1]. Auramine O is almost nonfluorescent in aqueous solutions; the quantum yield was found to be $\phi = 5 \times 10^{-4}$ at $C_d^0 = 2 \times 10^{-4}$ M. At constant C_d^0 the fluorescence intensity is increased by the presence of PMA without important alterations of the fluorescent spectrum. Hence relative values for the apparent fluorescence intensity could be obtained from readings at the maximum of the spectrum.

The influence of increasing C_p^0/C_d^0 ratio at constant α' is demonstrated in fig. 10 for $C_d^0 = 3 \times 10^{-4}$ M. Analogous results were obtained also at $C_d^0 = 10^{-5}$ M, not shown here. At very low values of C_p^0/C_d^0 the fluorescence increases more or less linearly with increasing PMA concentration independently of α'. At higher values of this ratio the results diverge for different degrees of neutralization, however, as at each α' a maximum in the fluorescence intensity is reached at a value of C_p^0/C_d^0 which is the lower the higher α'. Note that in all cases the fluorescence intensity of the PMA–AuO systems were higher than for the PMA-free system with equal C_d^0 (which in fig. 10 would be represented by $I \approx 6$). As we know that the fraction of bound dye f increases monotonously with increasing C_p^0 at low α' values up to the highest ratio C_p^0/C_d^0 investigated by fluorescence measurements (see fig. 4) it may be assumed that the increase in quantum yield is correlated to the binding under these circumstances.

If at constant C_d^0 and C_p^0 the fluorescence intensity is plotted against the degree of neutralization curves analogous to fig. 11 are obtained. This particular curve represents the change of the quantum yield with α' at

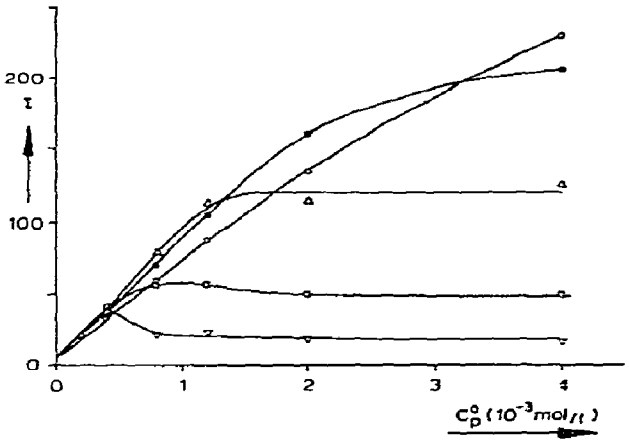


Fig. 10. Fluorescence intensity I (arbitrary units) of AuO–PMA solutions versus C_p^0; $C_d^0 = 3.2 \times 10^{-4}$M; PMA at $\alpha' = 0.1$ (○), 0.2 (●), 0.3 (△), 0.5 (□) and 0.75 (▽).

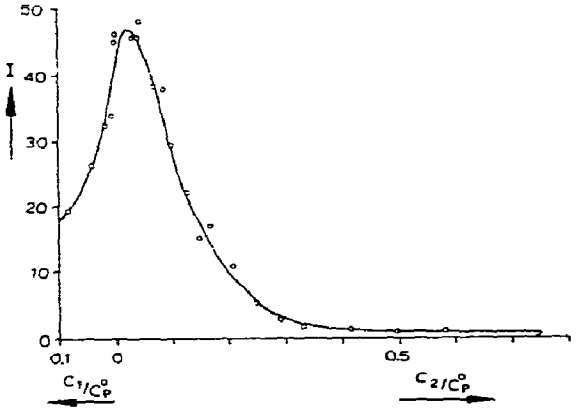


Fig. 11. Dependence of the fluorescence intensity I (in arbitrary units) on the charge of th polyelectrolyte for AuO–PMA solutions; $C_d^0 = 10^{-5}$M, $C_p^0 = 2.3 \times 10^{-3}$M; C_1/C_p^0 represents the ratio of the concentration of added HCl to the concentration of PMA and $C_2/C_p^0 = \alpha'$ the analogous ratio for NaOH.

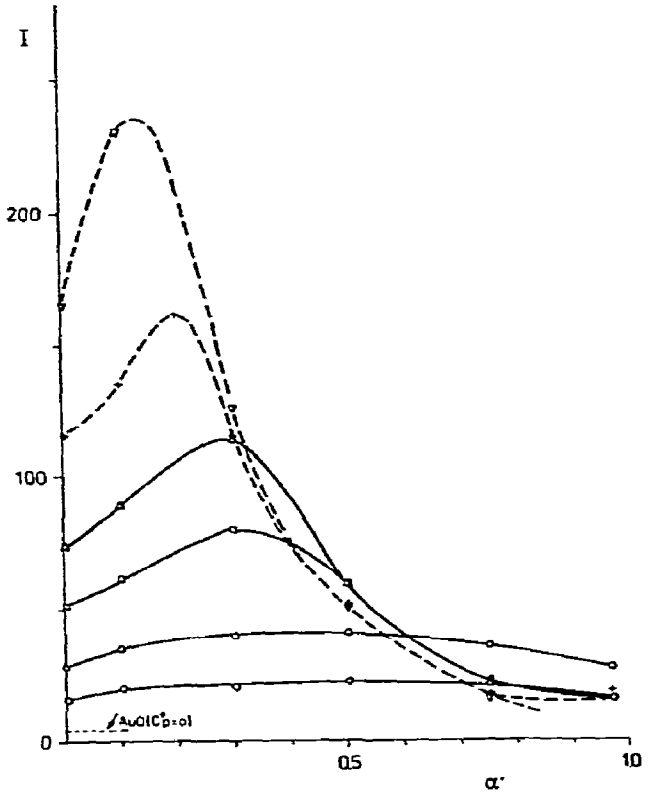


Fig. 12. Dependence of the fluorescence intensity I (in arbitrary units) on α' for AuO–PMA solutions; $C_d^0 = 3 \times 10^{-4}$ M, $C_p^0 = 2 \times 10^{-4}$ (○), 4×10^{-4} (○), 8×10^{-4} (□), 12×10^{-4} (△), 20×10^{-4} (+) and 40×10^{-4} M (▽).

a high C_p^0/C_d^0 ratio and is characterized by a maximum near $\alpha' = 0.05$. At lower ratios of polyelectrolyte over dye this maximum shifts to larger values of α' as can easily be seen from fig. 12. Apparently in the presence of a large excess of PMA with respect to the dye, i.e., for large values of f but small r, the fluorescence has a maximum in the α' region where dye-free PMA is in its compact conformational a state. On the other hand when the concentrations of PMA and AuO are of comparable magnitude, i.e., when f is small but r much larger than in the previous case, the lower intensity is practically independent of α'.

In slightly acidified PMA solutions the fluorescence intensity was found to decrease with decreasing pH although it remains well above the intensity level observed with PMA–free AuO solutions. This differs from the behaviour of the PMA–CV system [1] where the fluorescence intensity was found to increase with decreasing pH (fig. 11) but may be due to the weaker interaction of AuO with PMA as compared to CV and perhaps also to the decomposition of the dye, as discussed above. (Note that for practically all acidified solutions represented in fig. 10 the pH is lower than 3.5!)

4. Conclusions

The results both from equilibrium and sedimentation dialysis show that auramine O can be bound to PMA at low and high values of the degree of neutralization. The fraction f of dye bound to PMA increases with increasing ratio C_p^0/C_d^0 but up to the highest value investigated ($C_p^0/C_d^0 < 12$) no total binding of the dye was observed ($f < 1$). If the results are transformed into binding isotherms they can be fitted to a Langmuir isotherm at $\alpha' = 0.10$ but not so at $\alpha' = 0.40$ and $\alpha' = 0.65$.

The binding of AuO to PMA is accompanied by some modifications in the rather complex spectrum of the dye. Due to a considerable overlap of the spectrum of the free and the bound dye ions these results do not lend themselves for an estimation of f.

Potentiometric and viscosimetric results indicate that the behaviour of PMA is strongly affected by the presence of the dye and that AuO has a stabilizing effect on the compact conformational state of PMA which in the absence of dye is predominantly present only for the uncharged or slightly charged polyelectrolyte.

Fluorescence measurements show that the emission intensity for AuO–PMA systems is always larger than for the corresponding PMA free dye solutions but depends on C_p^0/C_d^0 and α' and thus also on f and the amount of dye r bound per monomeric unit. The maximum in the fluorescence intensity of AuO–PMA solutions with increasing α' is shifted to larger α' values and becomes flatter the larger r.

Qualitatively all these results are analogous to those observed for the CV–PMA systems [1, 2]. From a quantitative point of view the binding of AuO to PMA is weaker than the binding of CV.

In part II of this series these results will be discussed and interpreted by assuming a direct influence of dye-binding on the conformational equilibrium of PMA.

Acknowledgement

The authors are indebted to Mr. G.J.M. Lippits, who carried out the viscosimetric measurements.

References

[1] W.H.J. Stork, P.L. de Haseth, W.B. Schippers, C.M. Körmeling and M. Mandel, J. Phys. Chem. 77 (1973) 1772.
[2] W.H.J. Stork, P.L. de Haseth, G.J.M. Lippits and M. Mandel, J. Phys. Chem. 77 (1973) 1778.
[3] J.C. Leyte and M. Mandel, J. Polymer Sci. A2 (1964) 1879.
[4] N.M. Wiederhorn and A.R. Brown, J. Polymer Sci. 8 (1952) 651.
[5] A. Noll, Papierfabrikant 24 (1926) 593.
[6] C. Graebe, Ber. dtsch. Chem. Ges. 20 (1887) 3260.
[7] G. Breuer and J. Schnitzer, J. Chem. Soc. (1940) 461.
[8] W.C. Holmes and J.F. Darling, J. Am. Chem. Soc. 46 (1924) 2343.
[9] R.J. Goldacre and J.N. Phillips, J. Chem. Soc. (1949) 1724.
[10] G. Oster and Y. Nishijama, J. Am. Chem. Soc. 78 (1956) 1581.
[11] M.K. Pal and M. Schubert, J. Phys. Chem. 67 (1963) 1821.
[12] F.C. Adam, J. Mol. Spectry. 4 (1960) 359.
[13] M. Mandel and W.H.J. Stork, Biophys. Chem. 2 (1974)137.

BIOPHYSICAL CHEMISTRY 2 (1974) 137–143. © NORTH-HOLLAND PUBLISHING COMPANY

A DYE-BINDING INDUCED CONFORMATIONAL TRANSITION OF POLY-(METHACRYLIC ACID) BY AURAMINE O IN AQUEOUS SOLUTIONS

II. THEORETICAL INTERPRETATION AND DISCUSSION OF THE EXPERIMENTAL RESULTS

M. MANDEL and W.H.J. STORK

Gorlaeus Laboratoria der Rijksuniversiteit Leiden, afdeling Fysische Chemie III, Leiden, The Netherlands

Received 7 February 1974

The binding of Auramine O to poly-(methacrylic acid) (PMA) is explained using a two-state model for the polyelectrolyte and preferential binding of the dye to the hypercoiled conformational state of PMA predominantly present for the dye-free polyelectrolyte at low degrees of neutralization. Bound-dye interactions were neglected leading to a binding isotherm as given by Monod et al. to which the experimental dialysis results could be fitted. It is shown that this model predicts a conformational transition from the more extended conformational state of PMA to the hypercoiled one upon progressive binding of the dye. The experimental results obtained by potentiometric and viscosimetric titrations as well as the fluoresence intensity measurements of the AuO–PMA system are consistent with the conclusions based on this model.

1. Introduction

In part I of this series [1] it has been shown with the help of several experimental techniques that the cationic dye auramine O (AuO) binds to poly-(methacrylic acid) (PMA) at all different degrees of neutralization α' but to an extend which depends both on α' and the ratio C_p^0/C_d^0 (where C_d^0 and C_p^0 stand for the total concentration of dye and polyelectrolyte respectively, the latter expressed as number of moles monomer per unit volume). This binding affects the macromolecular properties of the weak polyacid which exhibits in the absence of the dye a conformational transition upon ionization in a rather limited range of α' values roughly situated between $\alpha' = 0.15$ and $\alpha' = 0.35$. The experimental evidence, particularly from potentiometric and viscosimetric determinations points to a stabilization of the compact conformational state of PMA (in the absence of the dye predominantly present at low values of α') through the binding of AuO. This was also the qualitative conclusion drawn in a previous investigation of the interaction between PMA and another cationic dye, crystal violet (CV), where no significant binding isotherms could be obtained, however, due to the saturation of the PMA under all accessible experimental conditions [2, 3]. In the latter study it could also be demonstrated that the interaction between dye and polyelectrolyte differs considerably from the interaction between PMA and small monovalent cations and that other than purely electrostatic interactions play an important role in this binding. That justified the assumption that the dissociation equilibrium of the carboxylic groups of PMA was not directly affected by the binding of the dye. Owing to experimental difficulties this was much more difficult to demonstrate for the PMA–AuO interactions but the qualitative simularity between the results for both systems permits extension of these conclusions to the binding of AuO to PMA.

For the PMA–AuO system binding isotherms were obtained at three different values of the degree of neutralization of PMA: At $\alpha' = 0.10$ a Langmuir type of isotherm was found; both at $\alpha' = 0.40$ and $\alpha' = 0.65$ the isotherm was not of this simple shape. In this part it will be shown how the latter binding isotherm can be interpreted in terms of a preferential binding of the dye to the compact conformational state (state a) of PMA which induces a conformational transition of PMA from the more open conformational state

(state b), predominantly present at $\alpha' = 0.40$ and $\alpha' = 0.65$ in the absence of the dye, to state a. The other experimental results of the PMA–AuO will then be shown to be consistent with these conclusions.

2. Theoretical approach

The peculiar properties of PMA have been extensively investigated in recent years, also in this laboratory. All experimental evidence shows that PMA undergoes a cooperative conformational transition from an anomalous compact conformational state a, characteristic for the uncharged or slightly charged poly-acid and the exact nature of which has not yet been established, to a more open conformational state within a narrow range of α' values given above. From an analysis of the potentiometric titration and ultra-violet spectral data it has been possible to derive the average fraction $x_a^{(0)}$ of polyelectrolyte molecule present in state a as a function of the degree of dissociation [4, 5]. Furthermore Leyte [6] has been able to show that this conformational transition can be described in terms of cooperative transformations of sequences of the macromolecule consisting of a number of monomeric units S which is of the order of 20 to 30 monomers. Therefore up to a first approximation a solution of PMA can be represented as a solution containing per unit volume M *independent and identical* units, consisting of S monomers, which can be either in the "a state" or the "b state" (not to be further specified) according to the experimental conditions, particularly the value of α' if the temperature is kept constant. Clearly $M = N_{av} C_p^0 / S$ where N_{av} stands for Avogadro's constant.

A molecular partition function (including eventually the influence of the solvent) may be defined for any of the M units either in the a or b state, say $q_a^{(0)}$ and $q_b^{(0)}$ respectively, which in turn determine the equilibrium constant $L^{(0)}$ between both conformational states of PMA.

$$L^{(0)} = q_b^{(0)} / q_a^{(0)} . \tag{1}$$

All three quantities, $q_a^{(0)}$, $q_b^{(0)}$ and $L^{(0)}$ depend on the state of charge of the units which under the assumption of a randomly charged polyelectrolyte can be characterized by α'. The superscripts (0) indicate that these quantities refer to a system where no dye is present. With the help of $q_a^{(0)}$ and $q_b^{(0)}$ it is also possible to determine the fraction $x_a^{(0)}$ of all units which are in the state according to

$$x_a^{(0)} = q_a^{(0)} / (q_a^{(0)} + q_b^{(0)}) = (1 + L^{(0)})^{-1} . \tag{2}$$

It will now be assumed that each unit may bind up to $s < S$ dye ions. No detailed model for this binding is necessary: the only assumptions that have to be made is that the bound dye ions are in a thermodynamically distinguishable state with respect to the dye ions which are free in solution and that they can be treated as localized particles. In general s will be a functions of α' in as far as the binding equilibrium does not perturb the dissociation equilibrium of the carboxylic groups. The partition function of a unit bearing i bound dye ions will be different in the a and b state and be represented by $q_a(i)$ and $q_b(i)$ respectively. Each partition function will depend on the number of dye ions bound, the charge borne by the unit, the interactions between bound dye particles, etc. In general they may be represented by the following expressions.

$$q_a(i) = q_a^{(0)} q_{d,a}^i \sum_{(c)} \exp[-E_{c,a}(i)/kT]$$

$$= q_a^{(0)} q_{d,a}^i \phi_a(i), \tag{3}$$

$$q_b(i) = q_b^{(0)} q_{d,b}^i \sum_{(c)} \exp[-E_{c,b}(i)/kT]$$

$$= q_b^{(0)} q_{d,b}^i \phi_b(i) . \tag{4}$$

Here $q_{d,a}$ and $q_{d,b}$ stand for the molecular partition function of a dye bound to the a and b state respectively (including the electrostatic interaction between the charge of the dye ion and the charge of the macromolecular unit); $E_{c,a}(i)$ corresponds to the configurational interaction energy of i dye ions bound to the a state in a given configuration and $E_{c,b}(i)$ to the corresponding quantity for the b state. The summation $\Sigma_{(c)}$ goes over all distributions of the i dye ions over the s binding sites of the unit. The quantities $\phi_a(i)$ and $\phi_b(i)$ can in principle be explicited using an assumption about the interactions between the bound dye ions, e.g., by using a linear Ising model.

According to the procedure outlined by Hill [7] a grand ensemble partition function Ξ for the system consiting of M independent adsorbing units bearing each s binding sites may be written as

$$\Xi = \xi^M , \tag{5}$$

where ξ is the grand partition function of a unit defined by

$$\xi = q_a^{(0)} + q_b^{(0)} + \sum_{i=1}^{s} [q_a(i) + q_b(i)] \lambda_d^i . \tag{6}$$

Here λ_d stands for the absolute activity of the bound dye in equilibrium with the free dye ions in solutions which is characterized by the activity a_d. Thus

$$\lambda_d = \exp(\mu^0/kT) a_d , \tag{7}$$

with μ_d^0 representing the standard chemical potential of the free dye ions in solution. It follows from the general expressions of statistical thermodynamics that the average number of bound dye particles per unit volume $\bar{N} = fC_d^0 N_{av}$, where f is the fraction of the total amount of dye bound to the macromolecule is given by

$$\bar{N} = \lambda_d \frac{\partial \ln \Xi}{\partial \ln \lambda_d} = \frac{M \Sigma_{i=1}^{s} i [q_a(i) + q_b(i)] \lambda_d^i}{q_a^{(0)} + q_b^{(0)} + \Sigma_{i=1}^{s} [q_a(i) + q_b(i)] \lambda_d^i} . \tag{8}$$

If use is made of eqs. (3), (4) and (7) and the definition of $L^{(0)}$ according to (1) is introduced as well as the definitions of the bonding constants K_a and K_b of dye ions to the units in the a and b state respectively

$$K_a = q_{d,a} \exp(\mu_d^0/kT) , \tag{9}$$

$$K_b = q_{d,b} \exp(\mu_d^0/kT) , \tag{10}$$

$$h = K_b/K_a , \tag{11}$$

the following expression for the fraction θ of dye bound with respect to the maximum amount of dye which can be bound may be derived from (8) ($\theta = f/f_{max} = r/r_{max} = \bar{N}/sM$, with $r = fC_d^0/C_p^0$ representing the amount of dye bound per monomeric unit).

$$\theta(a_d) = \frac{\Sigma_{i=1}^{s} (i/s) z^i [\phi_a(i) + L^{(0)} h^i \phi_b(i)]}{1 + L^{(0)} + \Sigma_{i=1}^{s} z^i [\phi_a(i) + L^{(0)} h^i \phi_b(i)]} . \tag{12}$$

Here $z = K_a a_d$. In the same way the fraction x_a of all units which are in the a state under the given conditions of the binding equilibrium is given by

$$x_a(a_d) = \frac{1 + \Sigma_{i=1}^{s} z^i \phi_a(i)}{1 + L^{(0)} + \Sigma_{i=1}^{s} z^i [\phi_a(i) + L^{(0)} h^i \phi_b(i)]} . \tag{13}$$

The binding isotherm represented by (12) is characterized by a large number of parameters: there are the five fundamental quantities S, s, K_a, $L^{(0)}$, h and a certain additional number necessary to explicate the interaction functions $\phi_a(i)$ and $\phi_b(i)$. The equation of the isotherm considerably simplifies into the following expression for θ' if either $L^{(0)} = 0$ (all units in the a state) or $h = 1$ and $\phi_a(i) = \phi_b(i)$ (no difference in binding and interaction between bound dye ions in the a and b state).

$$\theta'(a_d) = \frac{\Sigma_{i=1}^{s} (i/s) z^i \phi_a(i)}{1 + \Sigma_{i=1}^{s} z^i \phi_a(i)} . \tag{14}$$

The latter isotherm θ' may still differ considerably from a Langmuir-type (LM) isotherm through the interaction function $\phi_a(i)$. If it is assumed however that the reduced interactions energies $E_{c,a}/kT$ are negligible small, then $\phi_a(i) = s!/i!(s-i)!$ and the LM isotherm $\theta' = z/(1+z)$ is obtained. It has been found that for the binding of AuO to PMA at $\alpha' = 0.10$, for which it is known [4, 5] that $x_a^{(0)}$ is practically equal to unity and therefore $L^{(0)}$ negligible small, the results could be fitted to a LM isotherm. Within the framework of the model this would indicate that under these conditions the interactions between bound dye-ions could be neglected. Although it does not follow necessarily that for PMA at $\alpha' = 0.40$ and $\alpha' = 0.65$ where r may attain considerably larger values, these interactions are negligible too, this may be assumed in a first approximation. The expressions (12) and (13) then simplify to

$$\theta(a_d) = \frac{(1+z)^{s-1} z + L^{(0)} h (1+hz)^{s-1} z}{(1+z)^s + L^{(0)} (1+hz)^s} = \frac{z}{1+z} \frac{1 + L^{(0)} h y^{s-1}}{1 + L^{(0)} y^s} , \tag{15}$$

$$x_a(a_d) = (1 + L^{(0)} y^s)^{-1} , \tag{16}$$

$$y(a_d) = (1 + hz)(1 + z)^{-1} . \tag{17}$$

The isotherm (15) is identical with the Monod–Wyman–Changeux (MWC) isotherm [8] which was derived thermodynamically using essentially the same approximations as introduced in the present statistical approach.

The latter has however the advantage that it can easily be extended to the case where the interactions between bound dye ions is not negligible. That this has not been attempted presently is due to the consideration that, owing to the rather large scattering of the points in the experimentally determined isotherms, it would be impossible to ascertain whether these interactions play an important role in the binding of AuO to PMA or not. Furthermore the attractive interactions between AuO ions are possibly not too important in view of the reduced tendency of AuO to aggregate in solution as compared to other dyes.

From (15) it may be seen that the MWC isotherm deviates from the LM isotherm, (characterized by K_a) by a factor which depends on a_d only through the function $y(a_d)$. In the case where preferential binding of the dye to the a state is assumed, i.e., $K_a > K_b$, $h < 1$, this function is smaller than unity ($y < 1$) and decreases monotonically with increasing z. It then follows from (15) that with increasing z the MWC isotherm tends to an LM isotherm. For experimental conditions (α') where $L^{(0)}$ differs significantly from zero increasing dye binding will have the effect of increasing $x_a(a_d)$ with respect to $x_a^{(0)}$ as can be seen from (16). Whenever $L^{(0)}y^s$ becomes negligible small as compared to unity all units will be in a state and for higher activities a_d the MWC isotherm will coincide with the LM isotherm as defined above. Thus the dye binding may induce a conformational transition of the macromolecule from the b state to the a state. As will be shown below this seems to be the case for the PMA–AuO systems at the higher values of the degrees of neutralization.

Finally it is interesting to note that the isotherm (15) can also be written in a slightly different form which emphasizes its deviation with respect to a LM isotherm characterized by K_b.

$$\theta(a_d) = \frac{hz}{1+hz}\,\frac{y(1+hL^{(0)}y^{s-1})}{h(1+L^{(0)}y^s)}. \qquad (18)$$

From this expression it may be seen that at very low values of a_d, where $z \ll 1$ and $y \approx 1$, θ becomes a linear function of z with a slope equal to $(1+hL^{(0)})(1+L^{(0)})^{-1}$.

3. Discussion

The binding isotherms of AuO to PMA at $\alpha' = 0.40$ and $\alpha' = 0.65$ can be fitted to an MWC isotherm according to (15). Owing to the large scattering of the experimental points, due to experimental difficulties as exposed in part I of this series, no computerized least-squares fitting procedure was attempted. Rather a simple trial-and-error graphical procedure was used. Five parametres are needed for such a fit: S, s, K_a, h and $L^{(0)}$. Values for $L^{(0)}$ could be derived from the titration curve of PMA in the absence of dye [4, 5]. For S a value of approximately 20 monomers was chosen and the other parameters were adjusted. The activity of the free dye ions was put equal to the experimentally determined concentration $C_d = (1-f)C_d^0$. This can be justified by the fact that all interactions of the dye with the charged polyelectrolyte are in a first approximation taken into account through the so-called binding equilibrium and the interactions between the free dye ions themselves can be neglected because of the low concentration.

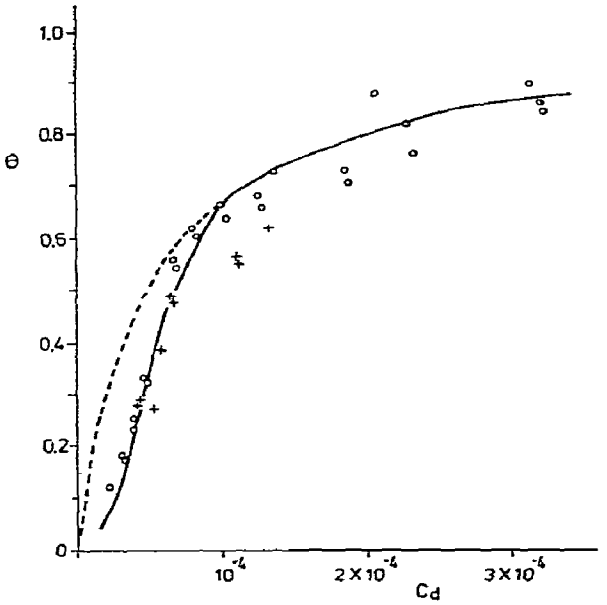


Fig. 1. Binding isotherm of AuO to PMA at $\alpha' = 0.40$. Experimental points from equilibrium dialysis (○) and sedimentation dialysis with preparative ultra-centrifuge (+). Full curve: MWC isotherm according to eq. (15) with parameters as given in table 1; dotted curve: LM isotherm with same K_a.

In spite of the crudeness of the fitting procedure the results are surprisingly satisfactory as can be seen from figs. 1 and 2, particularly at the lower end of the con-

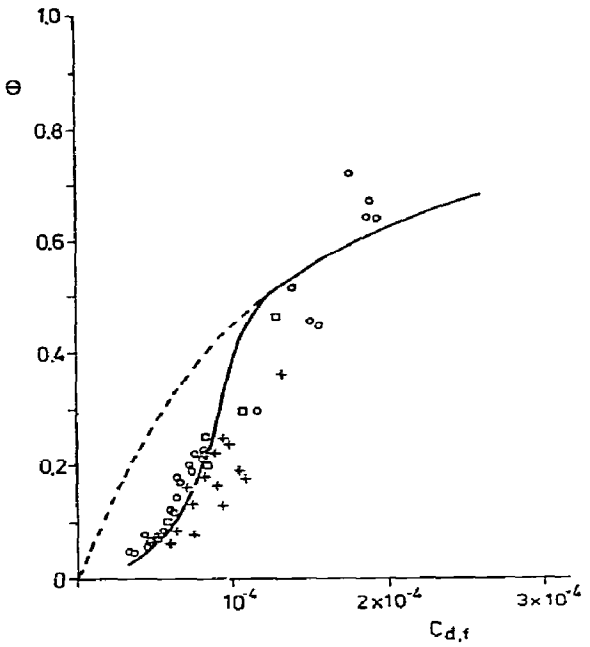


Fig. 2. Binding isotherm of AuO to PMA at $\alpha' = 0.65$. Experimental points from equilibrium dialysis (○), sedimentation dialysis with preparative (+) and analytical (□) ultra-centrifuge. Full curve: MWC isotherm according to eq. (15) with parameters as given in table 1; dotted curve: LM isotherm with same K_a.

Table 1
Parameters of the binding isotherms of AuO and CV to PMA

	AuO–PMA					CV–PMA	
α'	$L^{(0)}$	h	S	r_m	K_a	r_m	K_a
0	—	—	—	—	—	0.12	10^5
0.10	—	—	—	0.16	5×10^4	—	—
0.25	—	—	—	—	—	0.27	$>10^6$
0.40	300	0.1	21	0.48	2×10^4	0.35	$>10^6$
0.65	2000	0.1	20	0.80	9×10^3	—	—
0.75	—	—	—	—	—	0.80	$>10^6$

centration scale where more experimental points are available. The values of the different parameters of the corresponding MWC isotherms are collected in table 1. It should be pointed out that the same value of h could be used for both isotherms. In the same table are also given the parameters derived from the LM isotherm for the AuO binding to PMA at $\alpha' = 0.10$ and some results obtained for the system PMA–CV

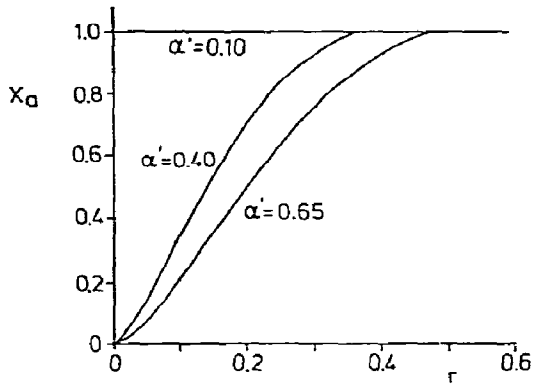


Fig. 3. The variation of x_a with increasing r at three different values of α' according to eqs. (15) and (16) using the parameters as given in table 1.

[2, 3]. Quantitative confirmation is obtained that under all circumstances K_a for AuO is at least one order of magnitude smaller than K_a for CV. There seems to be a decrease of K_a with α' for the AuO–PMA system but in view of the crude fitting procedure it may be questioned whether this decrease is significant. As was pointed out in section 2, $q_{d,a}$ and therefore also K_a will depend on α'. A slight increase of K_a with increasing α' would have been expected however.

With the help of (15) and (16) the change of x_a as function of the amount of dye bound per monomeric unit r may be calculated using the values of the parameters given in table 1. This is represented in fig. 3 and demonstrates the induced conformational transition of PMA at $\alpha' = 0.40$ and $\alpha' = 0.65$ by the binding of AuO. As can be seen PMA, which at these α' values is in the b state in the absence of dye, is completely reverted to a state at $r = 0.40$ and $r = 50$ respectively. At $\alpha' = 0.10$ where PMA is already completely in the a state, no influence of dye binding on x_a is noticeable. Although no experimental results are available which would permit the calculation of such curves at other values of α' the latter may be assumed to be of analogous shape as those of fig. 3. For values of α' situated in the transition region of dye-free PMA the curves will start at $r=0$ with an x_a value equal to $x_a^{(0)}$, (e.g., $x_a^{(0)} = 0.50$ for $\alpha' = 0.17$).

This influence of dye binding on the conformational transition is, qualitatively at least, consistent with the experimental results of the potentiometric titrations as given in part I of this series. From fig. 3 it

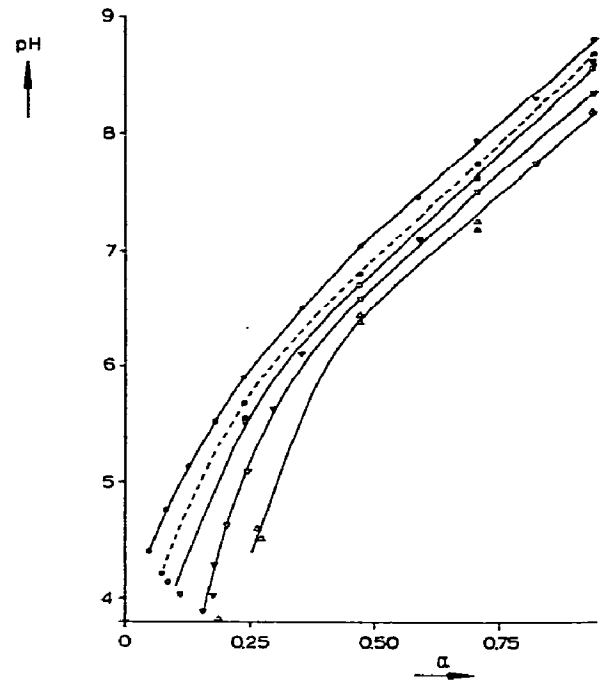


Fig. 4. Potentiometric titration curves (pH versus α) for AuO–PAA solutions. $C_p = 8.4 \times 10^{-4}$M. (○): $C_d^0 = 0$. (●): $C_{NaCl}^0 = 4 \times 10^{-4}$M, $C_d^0 = 0$. (□,▽, △): $C_{NaCl}^0 = 0$; $C_d^0 = 8.7 \times 10^{-5}$, 17.4×10^{-5} and 26.1×10^{-5}M respectively.

may be concluded that at a constant value of r (corresponding more or less to a constant ratio C_p^0/C_d^0) the conformational transition of PMA upon ionization will reveal a broader domain of α' values both for the region where the a state is predominantly present and the region in which the a–b transformation occurs, as was observed experimentally. A quantitative interpretation of these titration curves is not yet possible. The model used presently to discuss the binding isotherms is far too simple for understanding the detailed influence of dye binding on the potentiometric and viscosimetric behaviour of PMA. There can be no doubt however that the pecularities of the titration curves of PMA in the presence of AuO are due to the interference between dye binding and the conformational transition. Preliminary results for the potentiometric titration of poly-(acrylic acid) (PAA), which in dye free solutions is not characterized by a cooperative conformational transition upon binding, in the presence of AuO show that the addition of dye results in a complete lowering of the pH versus α' curve with respect to the dye-free system (fig. 4). Although it may be seen that the effect of the dye cannot be attributed to the increase in ionic strength solely indicating specific binding effects, the curves of fig. 4 differ considerably from the analogous ones obtained with AuO–PMA which must be connected with the occurence of special conformations in the latter polyelectrolyte.

Also consistent with these conclusions based on the combined binding and conformational equilibrium are the results of the fluorescence measurements. As shown in part I of this series the fluorescence intensity of the AuO–PMA system exhibits quite remarkable features depending on the C_p^0/C_d^0 ratio and α'. As the free dye ions practically do not fluoresce this intensity will be determined essentially by two factors:

1) the concentration of the bound dye ions fC_d^0;

2) the quantum yield of bound molecules.

In the discussion of fluorescence measurements on the CV–PMA [2, 3], in which qualitatively identical results as for the AuO–PMA system were obtained, it was already pointed out that the quantum yield of bound dye ions may differ according to the conformational state of PMA. It was inferred that the unfolding of the PMA molecule in the course of its conformational transition from the a to the b state makes new degrees of freedom available to the bound dye and increases the possibility of quenching the excited dye through interaction with the solvent thus reducing its quantum yield. If it is assumed that the quantum yield of AuO bound to the a state is much larger indeed than for the same dye ion bound to the b state, the dependence of the fluorescence intensity as function of C_p^0/C_d^0 and α' can be explained taking into account the influence of the bound dye ions on the conformational transition of PMA.

Consider the results represented in fig. 10 of part I of this series. At very low values of the ratio C_p^0/C_d^0 the concentration of bound dye ions will be low but the value of r may be rather large, particularly for higher values of α' (see fig. 4 of part I). Therefore PMA will be predominantly in the a state also at the higher values of α'. Hence the fluorescence intensity may be expected to be low but only slightly dependent on α', as has been found experimentally. When at constant C_d^0 the concentration of PMA is increased, fC_d^0 also increases but r will generally tend to decrease in view of the non-linear increase of f with C_p^0/C_d^0. This will result in a conformational transition from the a

to the b state which will set in at lower ratios C_p^0/C_d^0 the higher α'. Whereas at the lower α' values the fluorescence intensity is expected to increase, at higher values of α' the reduced quantum yield of dye ions bound to the b state may level off this increase and even lower the fluorescence intensity, as is also observed. For $\alpha' = 0.10$ where the dye binding has been assumed to have no effect on the conformational transition of PMA, which is always present in the a state, no such leveling off has been observed as expected. On the same basis the dependence of the fluorescence intensity with α' at constant C_p^0/C_d^0 is also understandable. As was already pointed out for the CV–PMA system [2, 3], the decrease of the fluorescence intensity with increasing α' for the larger values of α' cannot be explained by a gradually unbinding of the dye, as assumed by some authors [9] in view of all the other results which show that AuO binds to PMA also at these values of α' where the fluorescence intensity is greatly reduced.

From the investigation of the CV–PMA system it was concluded that non-electrostatic interactions must also be held responsible for the binding of the dye to PMA. In view of the similarities of the results obtained for CV–PMA and AuO–PMA systems this conclusion may be extended to the latter. This may explain to some extent why the binding constant K_a is smaller for AuO with only two phenyl rings than for CV which has three phenyl rings and should give rise to larger van der Waals forces and enhanced hydrophobic binding. A detailed picture of the binding is still lacking and no statements can be made on the exact sites to which the dyes bind. The role of the methyl groups in PMA is probably only secondary as it has been shown that binding between PAA and AuO as well as CV [10] may occur. The much weaker interactions between both dyes and PAA as compared to PMA should be compared to the binding of both dyes to the b state of PMA. The enhancement of the binding of the dyes to the a state must obviously be connected to the particular hypercoiled conformations of this state but here again no detailed picture can be advanced as long as the structure and the stabilization of the a state is not fully understood.

Summarizing it may be concluded that the properties of AuO–PMA systems may be understood by assuming a stronger binding to the compact conformational state of PMA than to the more extended one. Through this preferential binding a conformational transition may be induced if PMA is predominantly present in the b state. The AuO–PMA system may thus be considered to be a very simple model system for the allosteric effects attributed to enzymes.

References

[1] W.H.J. Stork, J.A.M. Van Boxsel, A.F.P.M. de Goeij, P.L. de Haseth and M. Mandel, Biophys. Chem. 2 (1974) 127.

[2] W.H.J. Stork, P.L. de Haseth, W.B. Schippers, C.M. Körmeling and M. Mandel, J. Phys. Chem. 77 (1973) 1772.

[3] W.H.J. Stork, P.L. de Haseth, G.J.M. Lippits and M. Mandel, J. Phys. Chem. 77 (1973) 1778.

[4] J.C. Leyte and M. Mandel, J. Polymer Sci. A2 (1964) 1879.

[5] M. Mandel, J.C. Leyte and M.G. Stadhouder. J. Phys. Chem. 71 (1967) 60.

[6] J.C. Leyte, Polymer Letters 4 (1966) 245.

[7] T.L. Hill, An introduction to statistical thermodynamics (Addison-Wesley, Reading, Mass., 1960).

[8] J. Monod, J. Wyman and J.P. Changeux, J. Mol. Biol. 12 (1965) 88.

[9] E.V. Anufrieva and T.M. Sheveleva, J. Polymer Sci. C16 (1968) 3514.

[10] T. Soda and K. Yoshioka, J. Chem. Soc. Japan 87 (1966) 324.

BIOPHYSICAL CHEMISTRY 2 (1974) 144–150. © NORTH-HOLLAND PUBLISHING COMPANY

CONFORMATION CHANGES IN rRNA INDUCED BY ELECTRIC IMPULSES

Arnold REVZIN* and Eberhard NEUMANN
Max-Planck-Institut für biophysikalische Chemie, D-34 Göttingen, GFR

Received 26 March 1974
Revised manuscript received 6 June 1974

We have investigated the effects of electric field pulses (of about 44 kV/cm magnitude and 30 μsec duration) on E. coli ribosomal RNA in solution (5×10^{-4} M sodium cacodylate buffer, pH 7, 20°C). The time course of changes in ultraviolet absorbance and electric dichroism can be resolved into contributions from orientational and conformational changes. The fast part of the relaxation spectrum (completed in less than 1 μs) is attributed to alignment of double-helical segments of rRNA with the external electric field; the slower part (relaxation times in the ms and μs range) is shown to be due to changes in orientation of the entire rRNA molecule, concomitant with electric field-induced helix–coil transitions of oligomeric base-paired regions.

1. Introduction

The analysis of electric field-induced changes in electrical and optical properties of anisotropic polyelectrolytes [1] has yielded basic information about macromolecular size and shape, and about the relationship between the polyion and its surrounding cloud of counterions. In particular, some unusual electric birefringence data and dielectric measurements led to speculation that the polyelectrolyte ionic atmosphere might be responsible for the observed effects [2,3]. It remained for Eigen and Schwarz, using ac conductivity measurements [4], to demonstrate convincingly that rod-like polyions may be oriented by interaction of the applied electric field with dipoles induced through displacement of the counterion atmosphere parallel to the long axis of the molecule. Indeed, numerous electrical and electrooptical studies on polyelectrolytes can be consistently interpreted in terms of such ion-atmosphere polarization (cf., e.g., refs. [4–11]), and theories have been developed to account quantitatively for the phenomena [12–15].

Recently it has been demonstrated that electric impulses cause conformational changes in macromolecules. Schwarz and Seeling [16] have presented evidence that electric fields may bring about helix–coil transitions in polypeptides (in nonaqueous solutions). Long-lived conformational changes induced in the multi-stranded polynucleotide complex poly(rA)·2 poly(rU) by electric impulses have been analysed in terms of shifts in the counterion cloud causing strand repulsion and unwinding of helical structures [17]. As part of investigations on metastable secondary structures in macromolecules [18] we have studied the behavior of ribosomal RNA in the presence of electric fields. Previous work on electric birefringence and dichroism of rRNA has been aimed at characterizing the molecular configuration of rRNA in solution [19,20]. In this study we present direct evidence that electric fields may cause not only changes in orientation of rRNA but also helix–coil transition in double-helical sections of the polyelectrolyte.

2. Materials and methods

The rRNA was a mixture of 16S and 23S species from Escherichia coli (strain MRE 600). Preparation and handling of RNA and of buffer solutions has been previously described [21].

* Present address: Institute of Molecular Biology, University of Oregon, Eugene, Oregon 97403, USA.

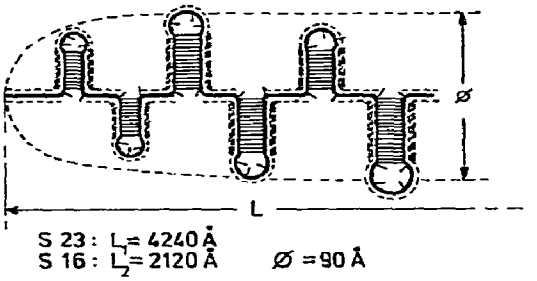


Fig. 1. Model for rRNA at pH 7 (after Spirin [24]). Lengths of major axis, L, for 16S and 23S particles and of minor axis, ϕ, were calculated under the following assumptions: (i) the 23S (16S) particle contains about 3550 (1775) bases, of which 2500 (1250) are in double-helical regions and 1050 (525) are in single-stranded stretches. (ii) At the low ionic strength used (5×10^{-4} M) the rRNA is rather extended, and the average distance between partially stacked bases in single-stranded regions is taken to be about 4 Å. (iii) The double-helical "arms" contain on average 15 base pairs. The distance between base pairs is taken to be 3 Å [A'-RNA; S. Arnott, Progr. Biophys. Mol. Biol. 21 (1970) 265]. Thus, the average length of an arm is about 45 Å, and its diameter is about 20 Å.

The electric impulse experiments were performed with a high power pulse generator equipped with a fast spectrophotometric detection system [22,23] and polarization optics [23]. This apparatus permits easy measurement of the time course of field-induced changes in several optical properties of the sample solution.

The design of the measuring cell permits application of high field intensities while minimizing temperature increase [17]. Two flat, gold covered electrodes form the base planes of the cylindrical volume (≈ 0.4 ml) of a thermostated Teflon cell. The light beam of the detection system crosses the cell through quartz windows, perpendicular to the direction of the applied electric field. When the device is used in its polarizing mode, the light may be polarized at any angle to the applied electric field [23].

3. Theoretical aspects

According to the generally accepted model, rRNA at neutral pH is a single polymeric chain in which coil regions alternate with double-helical stretches ("arms") containing about 4–20 base pairs (of the Watson–Crick type). About 70% of the bases are in base-paired regions even at rather low ionic strengths [20]. (For review see ref. [24].) We may assume that the helical portions align approximately perpendicular to the long axis of the stretched molecule (fig. 1), especially for the case of the high electrostatic repulsion which is present at low ionic strength (e.g. 5×10^{-4} M).

3.1. Relaxation times

When polyelectrolytes are subjected to an external electric field a rapid polarization is induced by displacement of the counterion cloud. The time constant for this process in rRNA under our experimental conditions may be estimated to be $\ll 1$ μs. (See, e.g., eqs. 11–14 of ref. [17]; calculations using these equations are based on Mandel's model [13] for polarization of rod-like polyelectrolytes, and account for saturation effects and dependencies on counterion type and neutral salt concentration.) Thus, when a field is applied to an rRNA solution a set of dipoles rapidly develops. Since there is some rotational freedom about sugar-phosphate bonds, the double-helical "arms" will tend to align along the direction of the applied field (fig. 2b). Concomitantly there will be rotation of the entire macromolecule into the field direction because of the overall induced dipole moment (fig. 2c) [20].

When the field is removed, the system relaxes to its resting state (fig. 2a). Time constants, τ, for rotational relaxation of arms and of the entire molecule may be estimated from the equation $\tau = (6D_r)^{-1}$ (see ref. [2]) using Gans' formula for the rotational diffusion coefficient, D_r, for non-charged ellipsoids of revolution in the absence of intermolecular interactions [25].

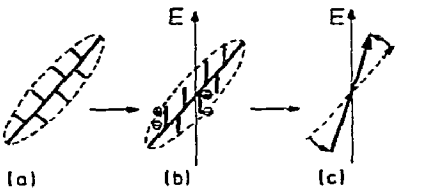


Fig. 2. Some effects of applied electric fields on rRNA.
(a) Schematic diagram of configuration in absence of field.
(b) Applying field results in dipole formation (indicated by ± signs on two of the "arms") and in fast alignment of "arms" with the field.
(c) Overall dipole moment causes slower rotation of entire molecule into field direction.

$$\tau = \frac{\pi\eta}{18kT}\,\frac{L^3}{[\ln(2L/\phi)-0.5]}. \qquad (1)$$

In eq. (1), η is the solution viscosity, k the Boltzmann constant, T the absolute temperature, L is the major axis and ϕ the minor axis of the ellipsoid. Using for average dimensions $L = 45$ Å, $\phi = 20$ Å, we calculate for the arms τ (arm) ≈ 0.01 μs. With the dimensions given in fig. 1 we estimate $\tau(16S) \approx 120$ μs, $\tau(23S) \approx 820$ μs for rotational relaxation of the entire molecules 16S and 23S rRNA. Thus the arms relax much faster than the molecules can rotate.

Study of multistranded polynucleotide complexes [17] suggests that the applied field may cause helix–coil transitions of base pairs in the double-helical arms of rRNA. It is also conceivable that there may occur field-induced single-strand destacking of bases although so far there is no evidence in the literature for such effects. In any case, the time constant for stacking–destacking processes in single-stranded polynucleotides may be estimated from studies on oligo- and polyriboadenylates [26] to be about 0.5 μs.

As mentioned above, ion-atmosphere polarization may induce dipole moments in the arms of rRNA. At the negative end of such a dipole double-helical section, counterion screening of the negatively charged phosphate residues is reduced and base pairs can open. When the field is switched off and the ion cloud rapidly relaxes there will be a large driving force favouring base pair closure.

Assuming that n base pairs are involved in an intramolecular "all-or-none" coil–helix transition [27], the time constant for this process is given by

$$\tau_n^{-1} = k_n^a + k_n^d = k_n^a(1 + 1/\alpha s^n), \qquad (2)$$

where k_n^a and k_n^d are the (overall) rate constants for the association and dissociation of n base pairs, respectively, s is the mean stability constant for a base pair adjacent to a base pair sequence, and α is a mean nucleation parameter. When the driving force strongly favors helix formation, i.e., $s \gg 1$, eq. (2) reduces to

$$\tau_n^{-1} = k_n^a. \qquad (3)$$

If a nucleus is already present (i.e. formally $\alpha = 1$), k_n^a is the rate constant for the association of n base pairs adjacent to a pre-existing nucleus. Denoting by k^a the association rate constant of a single base pair (adjacent to a nucleus), we may write for small n ($\leqslant 10$),

$$k_n^a \leqslant k^a/n. \qquad (4)$$

Using eqs. (3) and (4) we thus may estimate the maximum number of base pairs which may be associated with a measured τ_n.

In rRNA, k^a is an average over A·U and G·C base pairs. However, no direct data are available for k_n^a or k^a at the low ionic strength of 5×10^{-4} M [Na^+] we have used. Kinetic studies of helix–coil transitions in hetero-oligonucleotides with $n = 6$ to 10 [28] show that the recombination rate constants (k_n^a) decrease with decreasing ionic strength. It seems reasonable that k^a values will be lower at low ionic strength because of higher repulsion between charged polynucleotide backbones. On the other hand, the oligonucleotide studies [28] show that the helix *dissociation* rates are independent of ionic strength; this implies that k^a is also independent of ionic strength and that the observed ionic strength dependence of k_n^a lies solely in the increased difficulty of nucleation at low salt concentrations. Thus it is not yet established whether the k^a value of 10^7 s^{-1} reported by Pörschke and Eigen [29] for oligo (rA) · oligo (rU) helixes at 0.05 M ionic strength will apply to our system, or whether a k^a of, say, 10^5 s^{-1} is more appropriate for our ionic conditions.

3.2. Rotational and conformational contributions to dichroism

If we assume that the overall polarizability of rRNA is symmetric with respect to the long axis (L, fig. 1), it follows from eq. 13 of ref. [30] that

$$A_\parallel^{rot} - A_0 = -2(A_\perp^{rot} - A_0) = \Delta A_\parallel^{rot} = -2\Delta A_\perp^{rot}, \qquad (6)$$

where A_0 is the isotropic absorbance (in the absence of an applied field) and $A_\parallel^{rot}$, $A_\perp^{rot}$ are the absorbances of light polarized parallel and perpendicular to the field direction, respectively, when the molecules are rotated by the external field. When conformational changes, ΔA^{conf}, as well as rotational effects, ΔA^{rot}, occur, we may write for the measured *total* absorbance changes

$$\Delta A_\parallel = \Delta A_\parallel^{conf} + \Delta A_\parallel^{rot}, \quad \Delta A_\perp = \Delta A_\perp^{conf} + \Delta A_\perp^{rot}. \qquad (7)$$

Since the conformational contribution is isotropic,

$$\Delta A_{\parallel}^{\mathrm{conf}} = \Delta A_{\perp}^{\mathrm{conf}} = \Delta A^{\mathrm{conf}}. \qquad (8)$$

Using eqs. (6) and (8) we may solve eqs. (7) for the conformational and rotational contributions to the electric dichroism:

$$\Delta A^{\mathrm{conf}} = \tfrac{1}{3}(2\Delta A_{\perp} + \Delta A_{\parallel}), \quad \Delta A_{\parallel}^{\mathrm{rot}} = \tfrac{2}{3}(\Delta A_{\parallel} - \Delta A_{\perp}),$$
$$\Delta A_{\perp}^{\mathrm{rot}} = -\tfrac{1}{3}(\Delta A_{\parallel} - \Delta A_{\perp}). \qquad (9)$$

4. Results and discussion

4.1. Electric birefringence

We have used the usual optical arrangement for measurement of electric birefringence, with polarizers, on either side of the cell, rotated to 45° with respect to the field direction. We find that the light intensity emerging through crossed polarizers is increased in the presence of the field while the intensity emerging through parallel polarizers is decreased. Due to the small signal amplitudes, the experimental arrangement does not produce birefringence curves which can be analyzed in detail, but the results establish that we are indeed observing a field-induced effect and not an artefact from, for example, cell distortion.

4.2. Electric dichroism

Fig. 3 shows the result of a typical electric dichroism experiment. The time course of each intensity change, ΔI, is seen to be rather complex. There are rapid changes when the rectangular pulse starts at t_0 and when it ends at t_e; the changes during and after the pulse reflect slower processes. The long time values ($t \geqslant 10$ ms) for $\Delta I_{\parallel}$ and $\Delta I_{\perp}$ are small, indicating that contributions to destacking and base-pair opening due to temperature increase (≈ 1°C under the given conditions) are negligible when compared with field-induced intensity changes.

The time constants for the fast processes at t_0 and t_e are $\leqslant 1$ μs. We note also that the contribution of these fast processes to $I_{\parallel}$ is about twice as large and is of opposite sign to the contribution to $I_{\perp}$. According to the theoretical considerations discussed in section 3.2, we may attribute the fast changes to (partial) rotation of double-helical arms into the field direction. This interpretation is consistent with the observation that $I_{\parallel}$ increases when the arms are being aligned. As in DNA, the transition moments of the π-electron systems of the bases are roughly perpendicular to the helix axis of the arm, which means that $I_{\parallel}$ will grow (and $I_{\perp}$ diminish) as the arms line up along the field. It is also seen that when the field is switched off at t_e, the fast change is largely reversed, as the arms relax quickly to their original configuration. This analysis of the fast changes is in agreement with the interpretation of electric birefringence data on rRNA by Golub and Nazarenko [20].

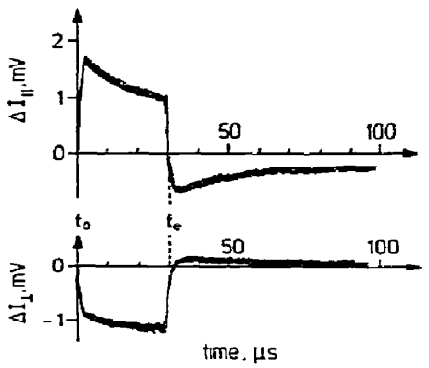


Fig. 3. Electric dichroism data for rRNA at 20°C, 5×10^{-4} M Na^+-cacodylate, pH 7; rRNA concentration of 2×10^{-4} M phosphate residues. A 44 kV/cm pulse was applied for 30 μs. The impulse begins at t_0 and ends at t_e. The data shown were transcribed from the actual photograph. $\Delta I_{\parallel}$ and $\Delta I_{\perp}$ are intensity changes at 280 nm for light polarized parallel and perpendicular to the field direction, respectively.

To facilitate further analysis of our dichroism results, we formally delete the amplitudes of the rapid changes (due to arm rotation) at t_0 and t_e. For instance, for the data in the upper part of fig. 3, the fast intensity change of about 1.6 mV (completed in a negligible time after the field is applied) is subtracted from each value of $\Delta I_{\parallel}$. The slow intensity decrease from t_0 to t_e is thus referred to a value of $\Delta I_{\parallel} = 0$ at $t = t_0$. Likewise, the rapid decrease in $\Delta I_{\parallel}$ at $t = t_e$ is removed. Since the fast changes at t_0 and t_e have about equal magnitudes, the initial value of $\Delta I_{\parallel}$ for the slow, field-free, intensity increase coincides with the corrected final ($t = t_e$) value of $\Delta I_{\parallel}$ for the slow intensity decrease in the presence of the field. The slow changes thus separated out were converted to absorbance changes and are shown (schematically) in fig. 4. (Since $\Delta I \ll I_0$, I_0 being the light intensity in the absence of the external field, we may approximate $\Delta A = -\Delta I / I_0'$, where $I_0' = 2.3\, I_0$, and

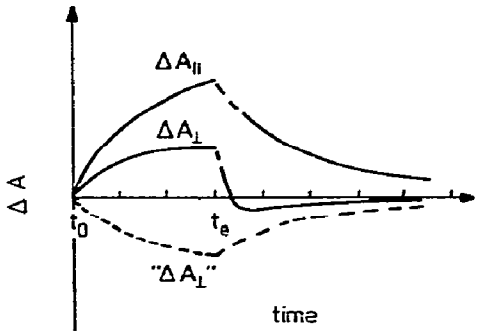


Fig. 4. Time course of electric dichroism in rRNA; the fast changes at t_0 and t_e have been deleted. (See fig. 3 and text.) Upper curves, $\Delta A_\parallel$ and $\Delta A_\perp$, (schematically) represent the observed absorbance data. The lower dotted line is the curve which $\Delta A_\perp$ would follow if field-induced optical changes were purely rotational.

I_0 = 24.5 mV). The fact that both $\Delta A_\parallel$ and $\Delta A_\perp$ have the same sign shows immediately that the slower changes are not merely orientational. Were the changes purely rotational, the relationship $\Delta A_\parallel = -2\Delta A_\perp$ would hold. *Therefore, there must be conformational changes in addition to orientation.* For the experiment shown in fig. 3 we find the absorbance changes (neglecting arm rotation) at $t = t_e$ to be $\Delta A_\parallel = 0.7$ mV/I_0' and $\Delta A_\perp = 0.3$ mV/I_0'. Referring the different contributions to the sum $\Delta A_\parallel + \Delta A_\perp = 1.0/I_0'$ and using eqs. (9) we derive the magnitudes of the relative rotational and conformational contributions: rel. $\Delta A^{conf} = \Delta A^{conf}/(\Delta A_\parallel + \Delta A_\perp) = 0.43$, rel. $\Delta A_\parallel^{rot} = 0.27$ and rel. $\Delta A_\perp^{rot} = -0.135$. It is seen that the field-induced conformational changes provide a large fraction of the overall absorbance changes. From the negative value for $\Delta A_\perp^{rot}$ we infer that as the RNA molecules rotate into alignment with the field the helix axes of the double-helical arms rotate out of the field. This implies that the limit of arm alignment is predominantly steric and electrostatic, rather than being due to randomizing tendencies of thermal motion.

4.3. Absorbance

Figure 5 presents typical absorbance versus time data for an electric field pulse experiment. The changes, ΔA, in such a measurement are larger than are the changes in $A_\parallel$ or $A_\perp$, so we use the absorbance data for kinetic analysis. Since the time constants of processes involving electric polarization are dependent on the field intensity in a complex manner [4], we limit the analysis of our absorbance data, $\Delta A(t)$, to the ("field-free") time range $t \geqslant t_e$. In fig. 6 the logarithm of the absorbance changes of a series of impulse experiments is plotted as a function time. The curvature of this plot shows that, as expected, rRNA displays a spectrum of relaxation times. Thus, we may write for $t \geqslant t_e$,

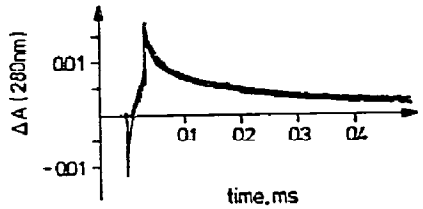


Fig. 5. Field-induced absorbance change, ΔA, for rRNA as a function of time. Experimental conditions as in fig. 3.

$$\Delta A(t)/\Delta A(t_e) = \sum_i \beta_i \exp(-t/\tau_i), \qquad (10)$$

where β_i is the relative amplitude of process i having

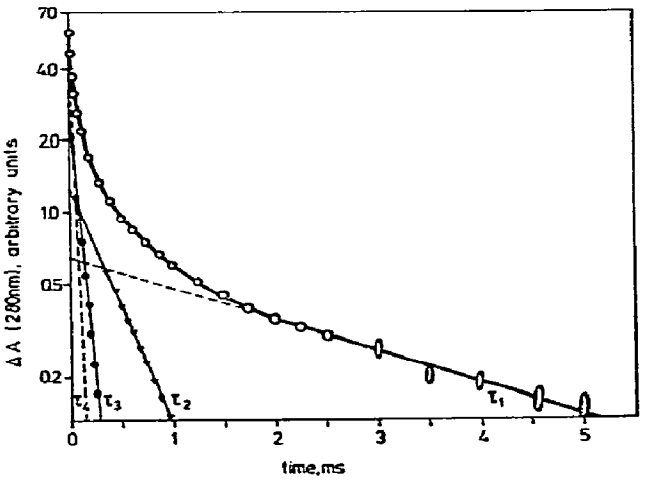


Fig. 6. Kinetic analysis of absorbance data, $\Delta A(t)$ (open circles), for $t \geqslant t_e$; $\Delta A(t)$ is the difference between the absorbance value at time $t(\geqslant t_e)$ and the value at $t \to \infty$. The initial slope of the log $\Delta A(t)$ versus t curve gives the limit, τ_4, for the relaxation of the fastest process of the relaxation spectrum.

the relaxation time τ_i [31]. Such a spectrum may be decomposed by starting with the slowest process (characterized by τ_1), subtracting contributions from this process to permit evaluation of τ_2, etc. This approach shows that we may associate at least four time constants with the relaxation spectrum. The values obtained are: $\tau_1 = 3200\ \mu s$, $\tau_2 = 460\ \mu s$, $\tau_3 = 80\ \mu s$ and $\tau_4 = 30\ (\pm 10)\ \mu s$; τ_4 is determined from the initial slope of the relaxation spectrum.

An analysis of this type, in which the relaxation times differ by factors of only 6 or 7 can give "meaningful" τ values only if the relative amplitudes, β_i, are approximately equal [32]. Extrapolation of the straight lines used to evaluate the τ_i to the time at which the field is switched off shows that $\beta_1 \approx 0.10$, $\beta_2 \approx 0.10$ and $\beta_3 \approx 0.18$. Thus our analysis of the relaxation spectrum fulfils the requirement of proper amplitude ratios. Finally, the relative contribution from processes having $\tau < \tau_3$ is given by $\beta_4 \approx 0.62$.

The β_i values also give insight into the actual processes to which the τ_i may correspond. The total amplitude for the faster processes is about *four* times larger than that for the two slower processes. Since our experimental arrangement is such that $\Delta A \approx \Delta A_{\parallel} + \Delta A_{\perp}$, it follows from eq. (7) that

$$\Delta A \approx 2\Delta A^{\mathrm{conf}} + \tfrac{1}{2}\Delta A_{\parallel}^{\mathrm{rot}}. \qquad (11)$$

Using the values for ΔA^{conf} and $\Delta A_{\parallel}^{\mathrm{rot}}$ calculated in section 4.2, we find that the conformational contribution to the absorbance change at $t = t_e$ (neglecting the fast arm orientation) should be roughly *six* times larger than the rotational contribution. Comparing this with the β_i values implies that the conformational changes are associated with the time range between the two smaller τ_i values, τ_3 and τ_4, while rotational effects are characterized by the two larger τ_i values τ_1 and τ_2.

This interpretation is consistent with the actual values of the τ_i. If τ_1 corresponds to overall rotation of 23S RNA and τ_2 to 16S RNA, we see that the measured values of these quantities are somewhat larger than those estimated by eq. (1). However, the theoretical values of τ are very sensitive to the choice of the molecular dimension L; errors in the calculations may partially cancel if we consider the *ratio* of relaxation times. This ratio is 3200/460 = 7.0 for measured τ values and is found to be 6.8 from the theoretical calculation. Thus τ_1 and τ_2 may indeed reflect rotation of the entire RNA molecules. This analysis is also in agreement with the results of electric birefringence studies on rRNA where time constants in the msec range have been associated with macromolecular orientation [20].

Finally, the fast part of the relaxation spectrum characterized by $\tau_4 = 30\ \mu s$ and $\tau_3 = 80\ \mu s$ is clearly associated with conformational changes and probably reflects coil–helix transitions. Since most of the fast changes due to arm bending [$\tau(\mathrm{arm}) \ll \tau_4$ or τ_3] are reverted immediately upon switching off the field, we infer that the arms are not grossly changed by the field, i.e., the extent of helix–coil transition caused by the field is not very large.

If in fact $k^a = 10^5\ s^{-1}$, then using the values of τ_4 and τ_3 in eqs. (3) and (4) we find that the field pulse causes opening of 3–8 base pairs. This would imply that few arms are totally unwound by the field. On the other hand, if k^a is much larger than $10^5\ s^{-1}$, our data may reflect a rate-limiting nucleation step in arm refolding. The τ_3 and τ_4 values reported here are similar to those measured for double-helical tRNA fragments [33] (after rough corrections have been made for different ionic conditions and for different values of s). In any case, our results indicate that the conformational changes induced by the electric field involve base pair separation of short stretches in the arms of rRNA.

5. Concluding remarks

The orientation of macromolecules by electric fields is often used to deduce information about molecular size and shape. The present study of rRNA indicates that such electro-optical studies may be complicated by conformational changes which occur in addition to orientation, especially for long impulses of high field intensity in solutions of low ionic strength. Conversely, possible orientation of molecules should be considered when analyzing optical changes in temperature-jump experiments, since a large electric field is present as the capacitor is discharged during the jump [31]. The various contributions to field-induced changes in optical parameters may be separable by analysis similar to that used here for rRNA electric dichroism results.

Acknowledgement

We thank H.H. Grünhagen for generous help in using the electric impulse apparatus, D. Pörschke for critical comments, and the Stiftung Volkswagenwerk for a grant to E.N.

References

[1] E. Fredericq and C. Houssier, Electric dichroism and electric birefringence (Clarendon Press, Oxford, 1973).
[2] C.T. O'Konski and B.H. Zimm, Science 111 (1950) 113.
[3] H.M. Dintzis, J.L. Oncley and R.M. Fuoss, Proc. Natl. Acad. Sci. USA 40 (1954) 62.
[4] M. Eigen and G. Schwarz, Z. Physik. Chem. N.F. 4 (1955) 380; J. Coll. Sci. 12 (1957) 181; in: Electrolytes, ed. B. Pesce (Pergamon Press, Oxford, 1962) p. 309.
[5] C.T. O'Konski and A.J. Haltner, J. Am. Chem. Soc. 79 (1957) 5634;
C.T. O'Konski and S. Krause, J. Phys. Chem. 74 (1970) 3243.
[6] N. Ise, M. Eigen and G. Schwarz, Biopolymers 1 (1963) 343.
[7] S.Z. Jakabhazy and S.W. Fleming, Biopolymers 4 (1966) 793.
[8] C. Horninck and G. Weill, Biopolymers 10 (1971) 2345.
[9] D.-W. Ding, R. Rill and K.E. van Holde, Biopolymers 11 (1972) 2109.
[10] F. van der Touw, J.W.H. Briedé and M. Mandel, Biopolymers 12 (1973) 111.
[11] E. Charney and J.B. Milstien, Biopolymers, in press.
[12] G. Schwarz, Z. Physik 145 (1956) 563.
[13] M. Mandel, Mol. Physics 4 (1961) 489.
[14] J.P. McTague and J.H. Gibbs, J. Chem. Phys. 44 (1966) 4295.
[15] F. Oosawa, Biopolymers 9 (1970) 677; Polyelectrolytes (Marcel Dekker, New York, 1971).
[16] G. Schwarz and J. Seelig, Biopolymers 6 (1968) 1263.
[17] E. Neumann and A. Katchalsky, Proc. Natl. Acad. Sci. USA 69 (1972) 993.
[18] E. Neumann, Angew. Chem. 85 (1973) 430; Angew. Chem. Intern. Edit. 12 (1973) 356.
[19] G.A. Dvorkin and A.S. Spirin, Dokl. Akad. Nauk SSSR 135 (1960) 987.
[20] E.I. Golub and V.G. Nazarenko, Biophys. J. 7 (1967) 13.
[21] A. Revzin, E. Neumann and A. Katchalsky, J. Mol. Biol. 79 (1973) 95.
[22] G. Ilgenfritz, Ph.D. Thesis, Göttingen (1966).
[23] H.H. Grünhagen, Biophysik 10 (1973) 347; Ph.D. Thesis, Braunschweig (1974); Messtechnik, in press.
[24] A.S. Spirin and L.P. Gavrilova, The ribosome (Springer Verlag, Berlin, 1969).
[25] R. Gans, Ann. Physik 86 (1928) 652.
[26] D. Pörschke, Eur. J. Biochem. 39 (1973) 117.
[27] M. Eigen, in: Nobel Symp. Vol. 5, ed. S. Claesson (Almquist and Wiksell, Stockholm, 1967) p. 333.
[28] D. Pörschke, O.C. Uhlenbeck and F.H. Martin, Biopolymers 12 (1973) 1313.
[29] D. Pörschke and M. Eigen, J. Mol. Biol. 62 (1971) 361.
[30] W. Kuhn, H. Dürkop and H. Martin, Z. Physik. Chem. B45 (1940) 121.
[31] M. Eigen and L. De Maeyer, in: Techniques of organic chemistry, Vol. 8 part 2, eds. S.L. Friess, E.S. Lewis and A. Weissberger (John Wiley, New York, 1963) p. 895.
[32] H. Strehlow and J. Jen, Chem. Instrum. 3 (1971) 47.
[33] D. Riesner, R. Römer and G. Maass, Eur. J. Biochem. 15 (1970) 85.

BIOPHYSICAL CHEMISTRY 2 (1974) 151–157. © NORTH-HOLLAND PUBLISHING COMPANY

EFFECT OF METAL BINDING ON THE INTRINSIC FLUORESCENCE OF BOVINE CARBONIC ANHYDRASE

Alessandro FINAZZI AGRÒ, Laura MORPURGO * and Bruno MONDOVI
Institutes of Biological Chemistry and Applied Biochemistry, University of Rome and Center of Molecular Biology, National Research Council, Rome, Italy

Received 2 January 1974
Revised manuscript received 30 April 1974

Bovine carbonic anhydrase shows an intrinsic fluorescence which results from tryptophans located in different microenvironments. It is possible to attribute the whole fluorescence to at least two types of tryptophan.

This fluorescence is differently affected by the binding of different metals. In fact while Zn^{2+} causes an increase of the fluorescence yield, the binding of Co^{2+}, Cu^{2+} and Hg^{2+} is followed by a quenching of the fluorescence. The quenching is about 40% for the cobalt, 80% for the copper and 60% for the mercury derivative. The binding of Cu^{2+} and Hg^{2+} induces also a change in the shape of the fluorescence emission spectrum. This fact suggests a different influence of the metals on the various types of tryptophan.

The fluorescence quenching induced by iodide which can bind to the metal and act as a fluorescence perturbing agent is also indicative of the presence of different tryptophans.

1. Introduction

Fluorescence spectroscopy has recently been found very useful in the study of metal binding to proteins [1–5]. Metal binding often causes a significant quenching of the intrinsic fluorescence. Among metalloproteins, carbonic anhydrase is very peculiar since it can bind a number of different metals at the same site producing derivatives with different spectroscopic parameters, i.e., absorption, circular dichroism, electron paramagnetic resonance, etc. [6].

Previous work has suggested that the addition of zinc slightly increases the fluorescence of the protein [7] and that a tryptophan is located very near to the metal site since a triplet–triplet energy transfer can take place between the aromatic aminoacid and an aromatic sulfonamide bound to the metal [8].

In the present paper we report a study on the effect of several metals and inhibitors on the fluorescence of bovine carbonic anhydrase. It gives evidence that the various types of tryptophan contained in the protein can be, at least in part, discriminated on the basis of fluorimetric measurements. The relevance of tryptophan environment to the mechanism of quenching is discussed.

2. Materials and methods

Bovine carbonic anhydrase was obtained as a by-product in the preparation of superoxide dismutase [9]. The first peak eluted from the DEAE cellulose column has carbonic anhydrase activity. This fraction was rechromatographed on a DEAE-Sephadex column equilibrated with 0.025 M Tris-HCl buffer pH 8.7. For the elution 0.1 M Tris-HCl pH 8.5 was used.

The removal of zinc was achieved by incubating the protein in the presence of o-phenanthroline according to Lindskog and Malmström [10].

The esterolytic activity of the protein was tested by the method of Pocker and Stone [11].

* On leave from the Laboratory of Cromatography, National Research Council, Rome, Italy.

Absorption spectra were obtained with a Beckman DK 2A spectrophotometer. Fluorescence spectra were measured with a Fica L55 Spectrofluorimeter which gives spectra corrected for the energy of excitation and for the response of the photodetector. The band widths were either 10 Å or 25 Å for the excitation and 25 Å for the emission. The experiments were conducted at 25°C.

The recombination experiments were performed in rather concentrated apoprotein solution (~ 10^{-4} M) where the binding to a stoichiometric amount of metal ion occurs at reasonably fast rate. Once completely recombined, the solutions can be diluted down to the fluorescence experiments range (~ 10^{-6} M) without significant dissociation.

The apparent stability constant for Cu-carbonic anhydrase iodide complex was calculated from the absorbance at 445 nm as a function of iodide concentration.

3. Results

The fluorescence spectra of holo and apo carbonic anhydrase have been already reported [7]. They present an excitation maximum at 280 nm and an emission maximum at 340 nm, which is typical of tryptophan containing proteins. At the resolution used in the present experiments (excitation bandwidth 1 nm; emission bandwidth 2.5 nm) it is possible to observe a shoulder on the short wavelength side of the emission peak (328 nm), while the excitation peak shows a secondary peak at 290 nm (fig. 1). The overall shape is not affected by the presence of zinc, but the metal containing sample has a 10% greater quantum yield. Excitation with 300 nm light still gives an emission maximum around 340 nm (see figs. 1 and 4) but the shoulder at 328 nm is clearly decreased. The quantum yield of fluorescence increases on going from 280 to 290 nm but it sharply decreases between 290 and 300 nm. The excitation spectra at isoemissive wavelengths respectively on the short wavelength side (309–318 nm) and on the long wavelength side (368–380 nm) of the emission peak are significantly different (fig. 2). It seems that the emission of carbonic anhydrase may result from the contribution of spectroscopically different tryptophans. A contribution of tyrosine to this effect cannot be ruled out.

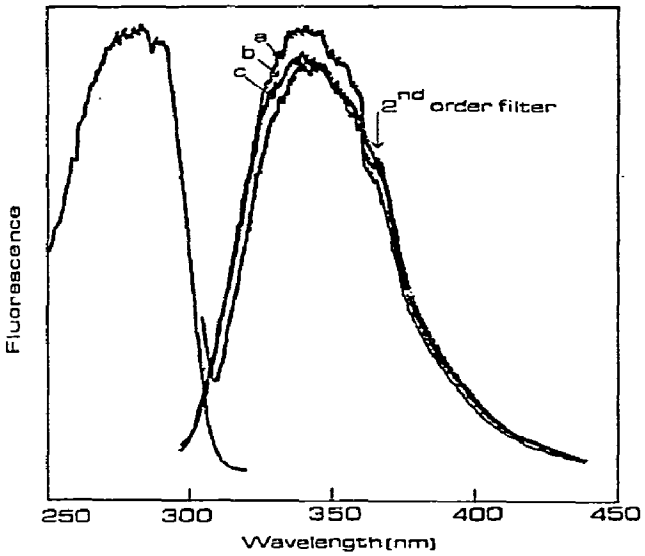


Fig. 1. Fluorescence spectra of apocarbonic anhydrase. The sample contained 3 × 10^{-6} M apocarbonic anhydrase in 0.05 M Tris HCl pH 7.6.

Excitation bandwidth 10 A. Emission bandwidth 25 A.

Excitation wavelength: curve *a* = 280 nm; curve b = 290 nm; curve c = 300 nm. Emission wavelength = 340 nm. The amplifier settings of curve c were higher than those og curve a and b. The spectra obtained with protein dissolved in 0.05 M acetate buffer pH 5 are qualitatively identical, but with a 15–20% lower quantum yield.

The addition of cobalt to apocarbonic anhydrase causes a 40% quenching of the fluorescence yield without a significant change of shape (fig. 3a and b).

The addition of copper to the apoprotein has a different effect. The quantum yield is reduced to about 1/5 of the original value and the shape is drastically changed (fig. 3, d). In fact the maximum is shifted to 328 nm and a shoulder at 313 nm becomes apparent. It appears that the shift is due to a preferential quenching of the tryptophans which have their emission at higher wavelength (see fig. 4).

The addition of azide which is known to bind with high affinity to the metal at the active site of carbonic anhydrase, causes a further decrease of fluorescence of both cobalt- and copper-derivatives (fig. 3, c and e). In both cases azide binding results in a somewhat better resolution of the fine structure.

The presence of absorption bands in the region 500–300 nm due to metal binding and to azide binding

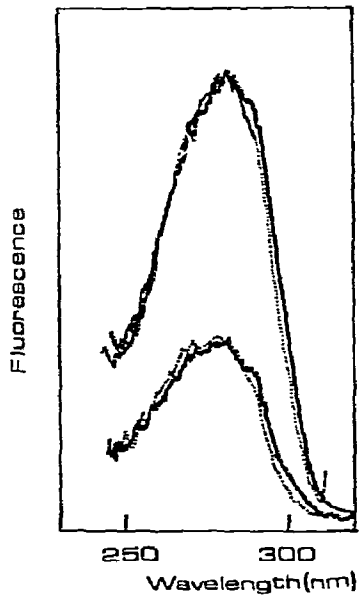


Fig. 2. Excitation spectra of apocarbonic anhydrase and of its copper derivative at two isoemissive wavelengths. The samples contained 3×10^{-6} M apocarbonic anhydrase (upper curves) and copper-treated apocarbonic anhydrase (lower curves) in 0.05 M acetate buffer pH 5. The isoemissive wavelengths are 315 (dotted line) and 372 nm (continuous line) for the apocarbonic anhydrase.

For the copper derivative they are 315 (dotted line) and 340 nm (continuous line).

Excitation bandwidth 10 Å; emission bandwidth 25 Å.

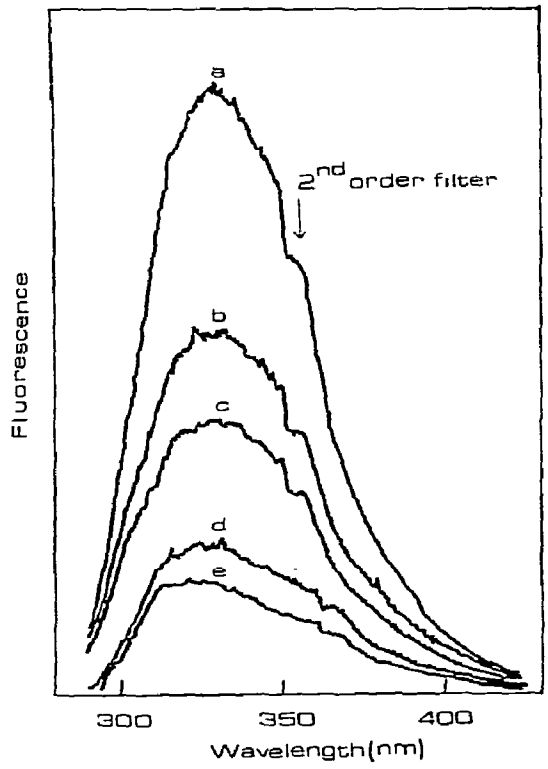


Fig. 3. Effect of metals and azide binding on fluorescence. The sample contained 2×10^{-6} M carbonic anhydrase in 0.05 M Tris HCl pH 7.6 as such (curve a) or in the presence of cobalt (b); cobalt-azide (c); copper (d) and copper-azide (e).

Excitation and emission band widths 25 Å. Excitation wavelength 280 nm.

(fig. 5) could explain the observed quenching since there is overlap with the emission of tryptophan, a prerequisite for energy transfer phaenomena.

However, the addition of stoichiometric mercuric acetate to apocarbonic anhydrase causes a 60% fluorescence quenching (see fig. 6), a value which is intermediate between those of cobalt and copper, without a corresponding increase of absorption in the spectral region 500–300 nm.

The addition of iodide to carbonic anhydrase derivatives is also followed by a quenching of fluorescence. In the case of apocarbonic anhydrase the quenching is linearly related to the amount of added iodide, with a change of slope above ~ 0.1 M iodide (fig. 7, a, and b) whereas it goes to saturation in the case of the copper derivative (fig. 7, b). The cobalt carbonic anhydrase behaves in an intermediate fashion, that is with a fast decrease of fluorescence at low iodide concentrations, whilst at higher iodide concentrations the decrease tends to become parallel to that of apocarbonic anhydrase (fig. 7, a). The quenching effect at low iodide concentrations observed for cobalt and copper carbonic anhydrase seems to be related to the coordination of this anion to the metal, and is concomitant to the appearance of new absorption bands in the visible range (fig. 8). The apparent stability constants evaluated from fluorescence spectra are in reasonable agreement with the value found in the literature [12] or obtained from optical spectra. The found value of the apparent stability constant for the Cu carbonic anhydrase is about 4×10^3 in 0.04 M phosphate buffer pH 6. It is strongly dependent on pH and buffer concentration

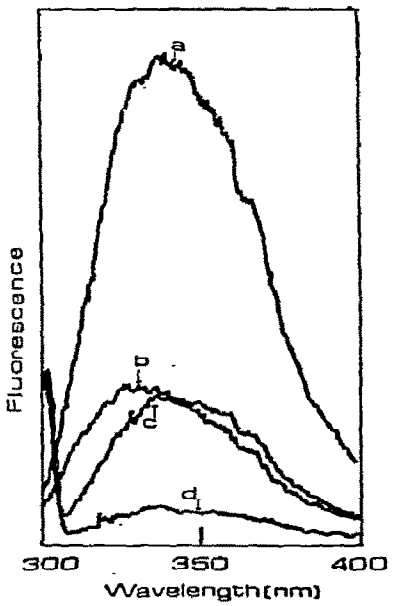


Fig. 4. Fluorescence of apocarbonic anhydrase and its copper derivative at different excitation wavelengths. The samples contained 2×10^{-6} M apocarbonic anhydrase (curves a and c) or its copper derivative (curves b and d) in 0.05 M Tris HCl pH 7.6.

Excitation wavelengths: 280 nm for the curves a and b; 300 nm for the curves c and d.

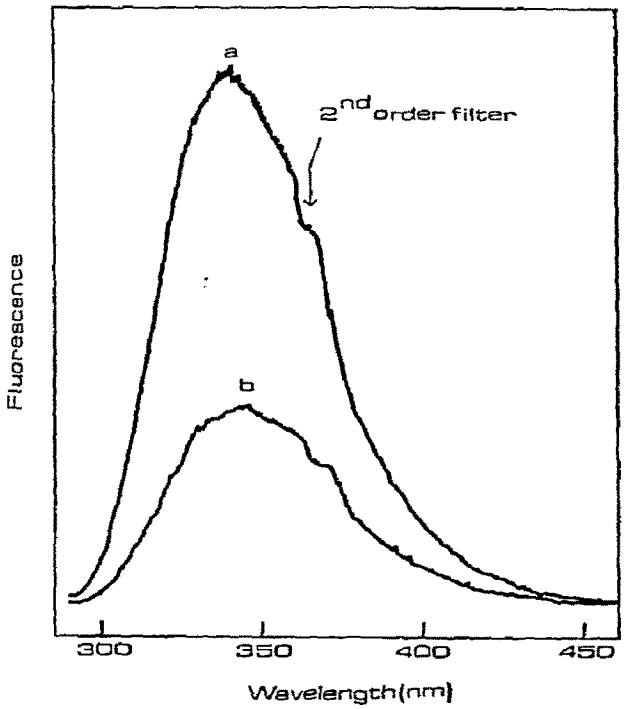


Fig. 6. Fluorescence of mercury derivative of apocarbonic anhydrase. To 6×10^{-6} M apocarbonic anhydrase in 0.05 M Tris HCl buffer (a) equimolar amounts of mercuric acetate were added (b). Excitation wavelength: 280 nm.

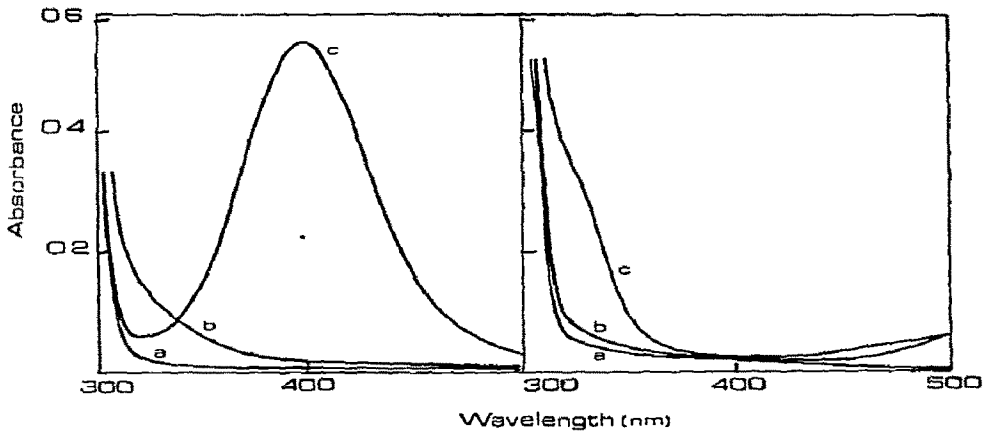


Fig. 5. Absorption spectra of copper and cobalt derivatives of apocarbonic anhydrase.

Left: to 2×10^{-4} M apocarbonic anhydrase (a) in 0.05 M Tris HCl pH 7.6 equimolar amounts of cupric sulfate (b) and then 4×10^{-4} M sodium azide (c) were added.

Right: to 4×10^{-4} M apocarbonic anhydrase (a) in 0.05 M Tris HCl pH 7.6 equimolar amounts of cobalt chloride (b) and then 8×10^{-4} M sodium azide (c) were added.

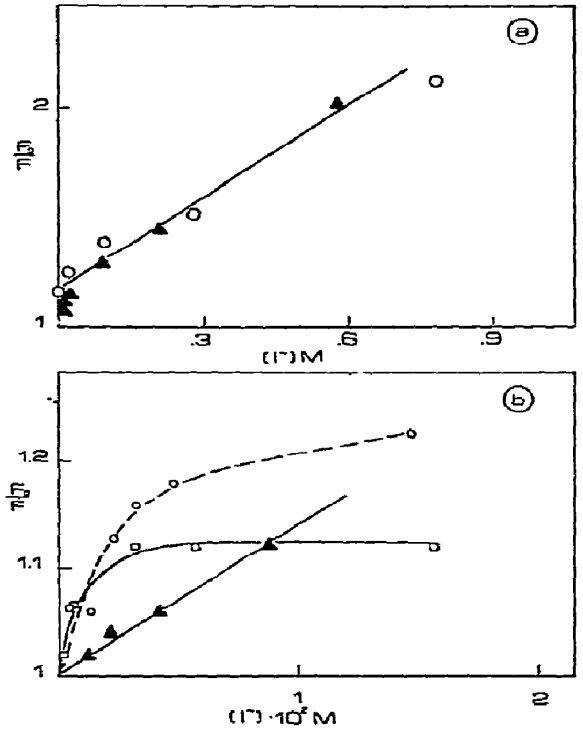


Fig. 7. Effect of iodide on carbonic anhydrase fluorescence. To the carbonic anhydrase derivatives (1 to 3 × 10^{-6} M in 0.04 M phosphate buffer pH 6) increasing amounts of freshly prepared concentrated solutions (low concentration experiments) or weighed amounts (high concentration experiments) of potassium iodide were added. The fluorescence spectra were recorded immediately after the addition of iodide. F_0/F was taken at the maximum emission of any sample. Excitation wavelength: 280 nm. (o): Cobalt carbonic anhydrase; (□): copper carbonic anhydrase; (▲): apocarbonic anhydrase.

(L. Morpurgo, to be published).

In the case of the zinc enzyme neither quenching nor new absorption bands are observed at low iodide concentrations although iodide is an inhibitor of the zinc as it is of the cobalt enzyme [12]. At high iodide concentrations there is a quenching analogous to that of apocarbonic anhydrase.

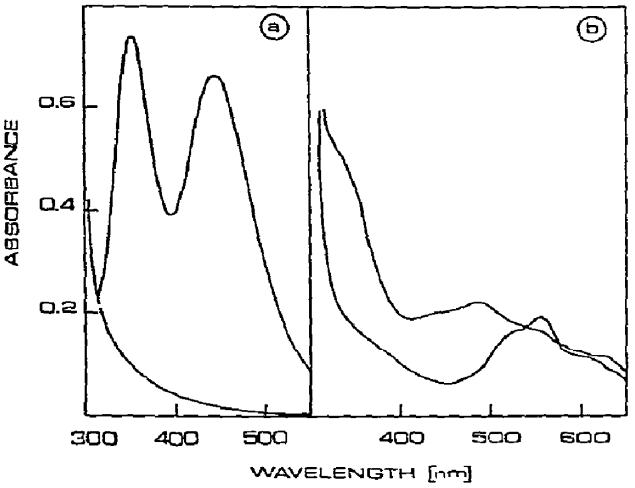


Fig. 8. Binding of iodide by cobalt and copper carbonic anhydrases.

a) 2.5 × 10^{-4} M Cu carbonic anhydrase in 0.01 M phosphate buffer pH 6 (lower curve); plus 3 × 10^{-2} M KI (upper curve).

b) 7.8 × 10^{-4} M Co carbonic anhydrase in 0.01 M phosphate buffer pH 6 (lower curve); plus 0.14 M KI (upper curve).

4. Discussion

It is known that the microenvironment is responsible for the energy and quantum yield of tryptophan fluorescence [13]. Thus the fluorescence of proteins containing more than one tryptophan could be thought in principle as the sum of the fluorescences from each tryptophan. In fact it seems most reasonable to expect that each tryptophan is located in a different environment both in terms of dielectric constant and rotational freedom. However very few cases have been described where it was possible to resolve spectroscopically the contribution of different tryptophans to the overall fluorescence [14]. More frequently the fluorescence of a protein seems to originate from only a type of tryptophan the others being nonfluorescent. In some cases it was demonstrated that the nonfluorescent tryptophans were transferring their excitation energy to the fluorescent ones [13]. From the data reported above it appears that the fluorescence of differently located tryptophans of carbonic anhydrase can be spectroscopically resolved. In fact the emission spectrum of the protein shows a shoulder at 328 nm,

a wavelength typical of buried tryptophans [12]. The excitation spectra performed at isoemissive wavelengths are (fig. 2) different and the emission spectra obtained with wavelengths higher than 290 nm show a progressive disappearance of the shoulder at 328 nm and a shift of the emission peak to lower energy (see fig. 1). A contribution from tyrosines cannot be ruled out. However, had they a major role, a monotonous decrease in quantum yield between 280 nm and 300 nm would be expected. The presence of differently solvated tryptophans in carbonic anhydrase was already proposed by Lindskog and Nilsson [15] on the basis of solvent perturbation experiments, which showed that only 40% out of the seven tryptophans contained in the protein are freely accessible to the solvent. These authors studied human and bovine carbonic anhydrases. By comparison with the molecular model of carbonic anhydrase C they proposed that only one tryptophan is really buried and only one is completely exposed to the solvent. Of the other five tryptophans, which are partly sticking into the molecule, two seem to have a greater rotational freedom which would allow interaction with the solvent.

The addition of various metal ions to apocarbonic anhydrase produces fluorescence changes which are specific for the added metal. Zinc, as previously reported by Brewer et al. [7], increases the fluorescence of the protein, and this is not surprising as it is known that zinc complexes can often be strongly fluorescent [16]. The quenching effects exerted by cobalt, copper and mercury are different both qualitatively and quantitatively. Copper and mercury affect both the height and the shape of the emission. The former seems to affect more the tryptophans with emission at higher wavelength since it shifts the emission maximum from 340 to 328 nm, whilst the latter causes a small shift toward longer wavelengths. All of these metals cause very small and scarcely significant changes of the ORD spectrum [17] in the region of the aromatic amino-acids. However their coordination geometries are different: distorted tetrahedral in the case of cobalt, [18] axial in the case of copper [19] so that the fluorescence variations can partly be attributed to conformational changes. Little can be firmly established about the mechanism of the fluorescence quenching. The most straightforward explanation could be the presence of energy transfer phenomena between the tryptophans and the absorption bands due to the metals, overlapping the fluorescence emission. It is known [20] that energy can be transferred from a donor to an acceptor molecule over a distance R. The distance for 50% transfer is:

$$R_0^6 = 8.8 \times 10^{-25}\, \Phi_D\, k^2\, n^{-4}\, J_{AD},$$

where Φ_D is the donor fluorescence quantum yield, k^2 is an orientation factor, n is the refractive index of the intervening medium and J_{AD} is the overlap integral between the donor emission and the acceptor absorption.

In the present case the factor J_{AD} is much greater for the copper derivative than it is for cobalt (see fig. 5). Thus the different extent of the fluorescence quenching may be easily understood. The shift in the fluorescence maximum seen for the copper derivative could be interpreted as a different efficiency of transfer from the different tryptophans. Other conditions being equal a different efficiency of transfer could depend on the factor k^2. The commonly used figures for k^2 are either 0.425 for a slowly rotating pair of acceptor and donor or 0.667 for fast rotating species [21].

However in the core of a protein either species (donor and/or acceptor) could be prevented from rotation during the lifetime of the excited state of the donor. This would explain why strong absorption bands, as seen for iodide or azide derivatives, do not cause strong fluorescence quenching and would also account for the detection of spectroscopically different tryptophans.

A strong argument against the energy transfer mechanism comes from the observation that the mercury derivative shows a great fluorescence quenching in the absence of any absorption band overlapping the emission of tryptophan. This finding is similar to those previously reported for azurin [3]. At least in this case modifications due to metal coordination rather than long range interactions seem to be involved. Other observations are in line with this hypothesis. It is known that, in human carbonic anhydrase C, two or three tryptophans are within 10 Å of the metal site [6], i.e., at a distance compatible with exchange interaction [21]. Galley and Stryer [8] found that in bovine carbonic anhydrase at least one tryptophan is located very near to the zinc atom. The mercuric ion is known from X-ray crystallography to be displaced 1 Å respect to the position normally occupied by zinc. This may result in a strain of the amino acid side chains nearby.

The quenching effect of iodide as a function of concentration seems to offer additional evidence for the presence of different tryptophans in the protein. In fact all of the carbonic anhydrases tested show a biphasic quenching effect (fig. 7). This behaviour can be ascribed to the occurrence of static and dynamic mechanisms of quenching [22]. The effect at low iodide concentrations can be clearly ascribed to the former mechanisms for the copper and cobalt derivatives. In the case of apocarbonic anhydrase the presence of two straight lines with different slopes might suggest either a similar mechanism or the presence of tryptophans which interact with iodide at lower rates.

At the highest iodide concentrations used an identical residual fluorescence is always observed indicating that some tryptophans are not at all affected by iodide either by long range or by short range interactions.

Acknowledgement

The authors wish to thank Mr. Paolo Gerosa and Mr. Mario Sanchioni for skilful technical assistance.

References

[1] S.S. Lehrer, J. Biol. Chem. 244 (1969) 3613.
[2] A. Finazzi Agrò, G. Rotilio, L. Avigliano, P. Guerrieri, V. Boffi and B. Mondovì, Biochemistry 9 (1970) 2009.
[3] A. Finazzi Agrò, C. Giovagnoli, L. Avigliano, G. Rotilio and B. Mondovì, Eur. J. Biochem. 34 (1973) 20.
[4] L. Morpurgo, A. Finazzi Agrò, G. Rotilio and B. Mondovì, Biochim. Biophys. Acta 271 (1972) 292.
[5] K. Nagami, Biochem. Biophys. Res. Commun. 51 (1973) 364.
[6] S. Lindskog, L.E. Henderson, K.K. Kannan, A. Liljas, P.O. Hyman and B. Strandberg, in: The enzymes, Vol. 5, ed. P.D. Boyer (Academic Press, New York, 1971) p. 587.
[7] J.M. Brewer, T.E. Spencer and R.B. Ashworth, Biochim. Biophys. Acta 168 (1968) 359.
[8] W.C. Galley and L. Stryer, Proc. Natl. Acad. Sci. U.S. 60 (1968) 108.
[9] J.M. McCord and I. Fridovich, J. Biol. Chem. 244 (1969) 6049.
[10] S. Lindskog and B.G. Malmström, J. Biol. Chem. 237 (1962) 1129.
[11] Y. Pocker and J.T. Stone, Biochemistry 6 (1967) 668.
[12] S. Lindskog, Structure and Bonding 8 (1970) 153.
[13] J.M. Longworth in: Excited states of proteins and nucleic acids, eds. R.F. Steiner and I. Weinryb (MacMillan, New York, 1971) p. 319.
[14] S.R. Anderson, M. Brunori and G. Weber, Biochemistry 9 (1970) 4723.
[15] S. Lindskog and A. Nilsson, Biochim. Biophys. Acta 295 (1973) 117.
[16] R.S. Becker, Theory and interpretation of fluorescence and phosphorescence (Wiley Interscience, New York, 1969) p. 190.
[17] J.E. Coleman, Biochemistry 4 (1965) 2744.
[18] J.E. Coleman and R.V. Coleman, J. Biol. Chem. 247 (1972) 4718.
[19] J.S. Taylor and J.E. Coleman, J. Biol. Chem. 246 (1971) 7058.
[20] Th. Förster, Modern quantum chemistry, Istanbul Lectures (Academic Press, New York, 1966).
[21] J. Eisinger, B. Feuer and A.A. Lamola, Biochemistry 8 (1969) 3908.
[22] B. Arrio, F. Rodier, C. Boisson and C. Vernotte, Biochem. Biophys. Res. Commun. 39 (1970) 589.

BIOPHYSICAL CHEMISTRY 2 (1974) 158–163. © NORTH-HOLLAND PUBLISHING COMPANY

STACKING INTERACTIONS OF ETHIDIUM BROMIDE BOUND TO A POLYPHOSPHATE AND PHAGE DNA IN SITU

G. LÖBER

Akademie der Wissenschaften der DDR, Forschungszentrum für Molekarbiologie und Medizin, Zentralinstitut für Mikrobiologie und experimentelle Therapie Jena, Abteilung Biophysikochemie, 69 Jena, DDR

J. KOUDELKA

Institute of Biophysics of the Czechoslovak Academy of Sciences, Brno, Czechoslovakia

and

E. SMÉKAL

Institute of Medical Physics of the University I.E. Purkyne, Brno, Czechoslovakia

Received 19 February 1974
Revised manuscript received 11 June 1974

Ethidium bromide forms spectroscopically detectable aggregates in aqueous solution and at a high dye concentration larger than 1×10^{-3} moles/ℓ. At moderate concentration in the order of 1×10^{-4} moles/ℓ the dye interacts with inorganic polyphosphate Graham salt and with phage sd DNA in situ by formation of stacking complexes. Maximal stacking was found at a phosphate to dye ratio, P/D, of approximately 1 for Graham salt and 1.5–2 for phages. In going to a higher P/D ratio Graham salt dye complex dissociates again and free dye reappears, while phage dye binding changes from stacking (type II complex) to intercalation (type I complex). Stacking is accompanied by a decrease and intercalation by an increase of relative fluorescence intensity with respect to free dye. However, both binding types lead to hypochromism and a red shift of the dye absorption band in the visible spectral region. Thus spectral behavior of ethidium aggregates deviate clearly from that known for other dyes, i.e., acridines.

1. Introduction

The trypanocidal dye ethidium bromide forms stable complexes with DNA [1, 2]. As consequences of the complex formation pronounced alterations in absorption [1] and fluorescence [2] spectra of the dye and hydrodynamic parameters of DNA [2] are observed. Similarities in the binding behavior with that of acridines put forward the idea that the binding of ethidium bromide occurs predominantly in form of type I complexes, i.e., by intercalation of the flat dye molecules between the base pairs of DNA. Strong indication for intercalation was given by the unwinding of supercoiled circular DNA induced by the dye [3–6]. However, acridines and ethidium differ in their abilities to be bound in stacked type II complexes at the DNA surface [7, 8, 10]. Binding of acridine orange in long stacks is favored at lower ratios of DNA-phosphates to dye molecules, P/D, at low ionic strengths [8], and water as a solvent [9]. In using an inorganic polyphosphate instead of DNA, type II binding takes place exclusively [10, 11]. It was also shown that the structural conditions of phage DNA in situ are more in favor of stacked binding of acridine orange, although a rather high ionic strength, 0.15 M NaCl, was used [12].

Obviously the tendency for outside binding of ethidium bromide is much weaker that that of acridine orange. From the shape of Scatchard isotherms as well as the ionic strength dependency of the binding of ethidium bromide with DNA [1] and double stranded RNA [13] a weaker outside binding process could be established besides intercalation. However, no pronounc spectral alterations induced by stacking were detectable. The results of a proton magnetic resonance study of the

interaction between ethidium bromide and several uracil derivatives, uridylyl(3'-5')uridine, and polyuridylic acid are in agreement with a stacked complex [14]. Therefore in this paper we ask whether a stacked complex of ethidium bromide may be formed and detected under suitable conditions, i.e., with the inorganic polyphosphate Graham salt in water solution or with phage DNA in its natural state.

2. Material and methods

Ethidium bromide from Serva, Heidelberg, was used without further purification. Graham salt (molecular weight ≈ 20 000, less branched) was a gift from the Institut fur anorganische Chemie der Akademie der Wissenschaften der DDR. Absorption spectra were recorded by means of the spectrophotometers Ultrascan (Hilger and Watts, London) and Specord (VEB Carl Zeiss, Jena). The apparatus for measuring the fluorescence spectra were Fluorispec SF100E, Baird Atomic and the modified model of spectrofluorimeter described earlier [15]. Fluorescence spectra were not corrected for the spectral distribution of both apparatus used. For the spectrophotometric investigation of the dye–polyphosphate complex, aqueous solutions of polyphosphate and dye were mixed. Dye concentration was kept constant to 8×10^{-5} mole/ℓ, while the polyphosphate concentration ranged from 0.002 to 0.04%, corresponding 2.54×10^{-4} and 5.08×10^{-3} mole phosphate/ℓ, respectively.

The experiments with bacteriophage were performed with phage sd, which was obtained from Professor A.S. Krivisky. Its properties were described elsewhere [16]. The spectrophotometric and fluorescence measurements were carried out after addition of small aliquots of purified concentrated phage to the dye diluted to $(10^{-4}-10^{-5})$ mole/ℓ. To make the conditions of polyphosphate and phage measurements comparable, the 10^{-3} M phosphate buffer pH 6.5 was used in all experiments with phage; however, no significant differences were observed in measurements at higher ionic strength. P/D ratio in these measurements was based on the initial phage DNA and dye concentrations.

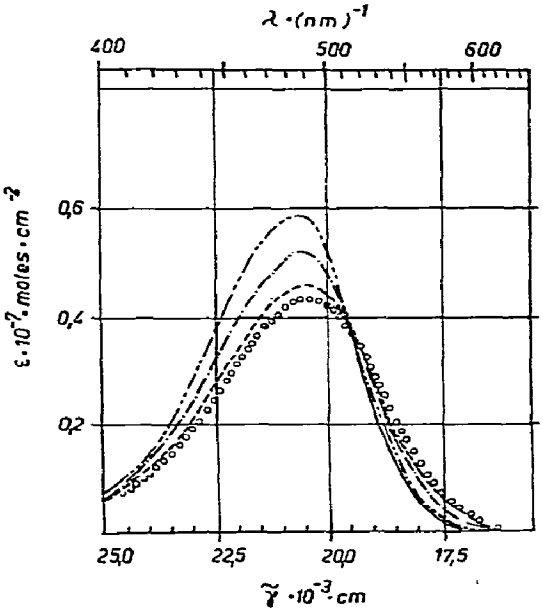


Fig. 1a. Changes in the absorption spectrum of ethidium bromide after addition of Graham salt; dye concentration 8×10^{-5} mole/ℓ; in water; (— · —) without and in the presence of high amounts Graham salt (1×10^{-3} mole/ℓ phosphate), (— — —) 2.5, (ooo) 5.1, (— · —) 25×10^{-5} mole/ℓ phosphate.

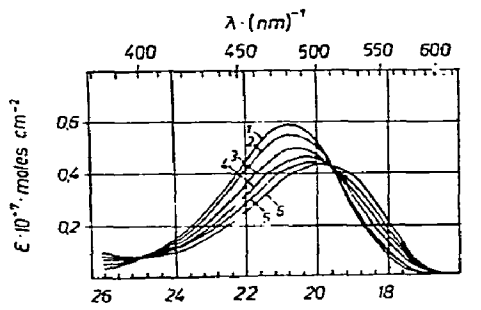


Fig. 1b. Changes in the absorption spectrum of ethidium bromide after addition of sd phages; curves correspond to different ratios of dye to DNA phosphates of phages, P/D; dye concentration 5×10^{-5} mole/ℓ; in 10^{-3}M phosphate buffer pH 6.5; 1: P/D = 0, 2: P/D = 0.4, 3: P/D = 0.8, 4: P/D = 1.2, 5: P/D = 1.6, 6: P/D = 2.8–5.2.

3. Results

Free ethidium bromide shows an absorption band in the visible region with a maximum at 485 nm. After addition of Graham salt up to a ratio P/D of approximately 1, the optical density of the absorption maximum decreased with parallel red shift of about 5 nm. At P/D > 1

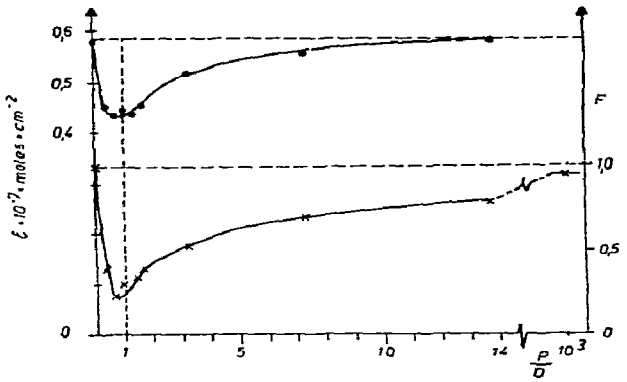


Fig. 2. Changes in the absorption at 485nm (●●●) and relative fluorescence intensity at 620nm (×××) of ethidium bromide in dependence on the ratio of Graham salt phosphates to dye, P/D; dye concentration 8×10^{-5} mole/ℓ; in water.

the optical density increased again and a blue shift of the maximum took place. Finally, the absorption band was similar to that typical for free dye (fig. 1a).

Similar results were observed with the phage. The optical density of ethidium bromide decreased to a minimum which was not sharp but rather flat, between P/D = 2–5; simultaneously there appeared a red shift of about 25 nm in the spectral maximum (fig. 1b). The further addition of the phage led to an increase of optical density of the red shifted band; not shown in fig. 1b however, this increase was influenced by the dye bound to phage DNA in the intercalated form.

Upon excitation with light of the wavelength 446 nm ethidium bromide shows a fluorescence emission with a maximum of the fluorescence band at 620 nm. After addition of Graham salt the fluorescence intensity decreased and at P/D = 1 its value was only 22% of that found in the absence of any polyphosphate. At P/D > 1, fluorescence intensity increased again by approximating the value found for free dye (fig. 2). The dye bound to phage particles revealed similar behavior. The fluorescence excited at 480 nm had a minimum 55% at P/D = 1.5–2, and was slightly changed compared with polyphosphate. However, the increase of P/D after further addition of phage was accompanied by an increase of fluorescence intensity over the value corresponding to the free dye (fig. 3). This is apparently due to the influence of dye bound in the intercalated form; the effect of pure stacked complex thus cannot be observed at higher P/D.

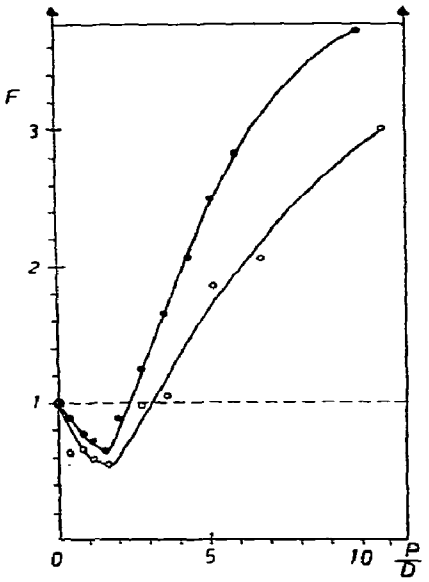


Fig. 3. Changes in relative fluorescence intensity of ethidium bromide at 620nm in dependence on the ratio of phage DNA phosphates to dye, P/D; the measurements at two different dye concentrations indicate that the effect is essentially the same. (○○○) 5×10^{-5} mole/ℓ; (●●●) 1×10^{-4} mole/ℓ in 10^{-3}M phosphate buffer pH 6.5.

4. Discussion

4.1. Formation of stacking complexes with Graham salt and phage sd DNA in situ

Ethidium bromide reveals at high concentrations spectral shifts and hypochromism, both indicating the formation of dye aggregates. Contrary to acridine orange and similar dyes, the shift of ethidium bromide is directed to the red (fig. 4), which might be interpreted as consequence of a different type of dye aggregate as in the case of acridine orange.

Similar red shifts are induced in the spectrum of ethidium bromide by DNA and were interpreted by Waring [1] as being due to intercalation process. Moreover we have observed red shifts, though smaller, after binding of Graham salt to ethidium bromide. In the latter case there is no possibility of intercalation and obviously the spectral effects in this complex will be due to the outside binding of isolated dyes or interac-

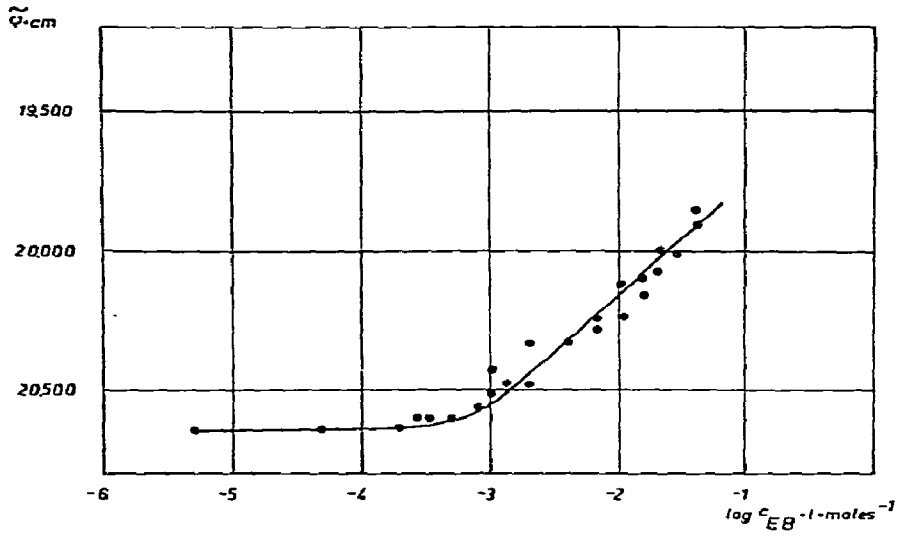


Fig. 4. Red shift observed in the absorption band of ethidium bromide with increasing dye concentration; in water.

tions of neighbouring bound dye molecules only. It is apparent that this red shift may be influenced by at least two different processes, by mutual dye–dye interactions and/or the intercalation process in the DNA–ethidium bromide complex. In an attempt to distinguish between these two possibilities we have focussed our attention on the differences between the binding of ethidium bromide to Graham salt and DNA, obvious from the experimental data:

(i) The red shift reported as due to the binding of ethidium bromide with Graham salt is 5 nm smaller than that for the DNA–ethidium complex.

(ii) The red shift found in the spectrum of the DNA-dye complex cannot be reverted after addition of high amounts of DNA. The opposite is true for the Graham salt–dye complex.

(iii) Binding of ethidium bromide with DNA is highly insensitive to the presence of salts in solution [17]. For this reason ethidium binding is a good tool for the measuring of sedimentation coefficients by means of the cesium chloride density gradient technique which needs high salt concentrations (4.5 M). On the contrary the binding of ethidium bromide to Graham salt is strongly suppressed already at moderate salt concentrations, e.g., in the presence of 0.01 M NaCl.

(iv) Fluorescence intensity in the presence of DNA is higher as compared with that of free dye [2], while a pronounced decrease is induced by the Graham salt.

Thus it can be concluded that, although the red shifts and hypochromicities in the absorption spectrum of ethidium bromide are similar when the dye was attached either to DNA or to Graham salt, the points (ii), (iii) and (iv) are in agreement with a stacking binding of dye molecules at the inorganic polyphosphate chain. In particular stacking decreases with increasing concentration of added salt, e.g., sodium chloride, and reached a maximum corresponding to a minimum in the plots of the optical density or fluorescence intensity versus P/D (fig. 2). This behavior which was observed also for the acridine orange–Graham salt complex should be mainly attributed to cooperativity of the binding process.

It has been shown earlier [12, 18] that the specific conformation of phage DNA in situ favors the surface stacking of the dye bound to such a structure. Even relatively weakly stacking dyes like proflavine reveal considerably higher stacking on phage T4 DNA in situ as compared with the isolated DNA from the same source [18]. Ethidium bromide bound at low concentration to phage sd DNA in situ shows also significant cooperativity expressed by changes in fluorescence intensity. The behavior of ethidium bromide bound to phage at low P/D may be considered as equivalent to that of dye bound to polyphosphate chain. However, the effects are not strictly comparable, as in the case of phage the inter-

calation of dye to DNA may interfere at higher P/D values. Contrary to polyphosphate, the stacking of ethidium bromide on phage is relatively stable even at higher ionic strength (of the order 0.1 M), which may be affected by the highly ordered conformation of phage DNA in situ.

4.2. Spectral properties of ethidium aggregates

Molecular aggregation in solution has been a subject of numerous investigations. Very often, the absorption spectrum of the aggregate is located at the shorter wavelength side of the monomeric peak [7, 19–24]. Besides Zanker's theory that the dimer peak is identical with the 0–1 vibrational transition in the electronic spectrum [25], the most common interpretation is given by Förster [26] and corresponds to the Davydov splitting [27] as consequence of an intermolecular interaction. While the long wavelength band is symmetry-forbidden the shorter one becomes allowed and corresponds to the typical aggregate spectrum. If for electrostatic or steric reasons an asymmetrical aggregate structure is preferred the forbidden transition becomes increasingly allowed [28, 29]. Recently a new approach for investigating interactions between dye molecules was given, where the dye monomers were treated by the one dimensional electron gas model for branched electron systems. Depending on the steric arrangement of dye molecules in the stacked aggregates, both short- and long-wavelength shifted spectra can be obtained [30, 31]. According to that theory, the latter seems to be favored if the dye molecules lie not completely parallel and if their planes are displaced towards a head to tail binding with an only partial overlap of the π–electron system. Such a case can not be excluded for ethidium, since the heterocyclic phenanthridine ring system carries asymmetrically located bulky phenyl and ethyl groups, which certainly produce some steric hindrance for the formation of symmetrical aggregates. According to the NMR studies done by Kreishman et al. [14] ethidium bromide forms parallel stacks in concentrated solution. However, the structures of the dye aggregates bound to polyphosphate or condensed DNA inside the phage are not necessarilly the same as those found in solution. This could be one reason for the fact that the magnitude of the red shifts found in these cases differ. Detailed data on this subject are lacking at present.

Acknowledgement

The authors are greatly indebted to Mrs. R. Klarner for her valuable technical assistance and to Dr. V. Kleinwachter for his critical advice during the preparation of this manuscript.

References

[1] M.J. Waring, J. Mol. Biol. 13 (1965) 269.
[2] J.B. Le Pecq and C. Paoletti, J. Mol. Biol. 25 (1967) 87.
[3] L.V. Crawford and M.J. Waring, J. Mol. Biol. 25 (1967) 23.
[4] L.V. Crawford and M.J. Waring, J. Gen. Virol. 1 (1967) 387.
[5] W. Bauer and J. Vinograd, J. Mol. Biol. 33 (1968) 141.
[6] M.J. Waring, J. Mol. Biol. 54 (1970) 247.
[7] A.R. Peacocke and J.N.H. Skerrett, Trans. Faraday Soc. 52 (1956) 261.
[8] A.L. Stone and D.F. Bradley, J. Amer. Chem. Soc. 83 (1961) 3627.
[9] G. Löber, V. Kleinwachter and H. Berg, Studia Biophysica 35 (1973) 29.
[10] D.F. Bradley and M.K. Wolf, Proc. Acad. Sci. USA 45 (1959) 944.
[11] G. Schwarz, Eur. J. Biochem. 12 (1970) 442.
[12] J. Koudelka, A.S. Krivisky and V.V. Esipova, Studia Biophysica 36/37 (1973) 407.
[13] R.J. Douthart, J.P. Burnett, F.W. Beasley and B.H. Frank, Biochemistry 12 (1973) 214.
[14] G.P. Kreishman, S.J. Chan and W. Bauer, J. Mol. Biol. 61 (1971) 45.
[15] E. Smékal, Chemické zvesti 20 (1966) 299 (in Czech).
[16] A.S. Krivisky, S.A. Tartakovsky and T.P. Chernik, in: Genetika Mikroorganizmov (Medetsina, Moscow, 1966) p. 144.
[17] W. Bauer and J. Vinograd, in: Progress in molecular and subcellular biology 2, Complexes of biologically active substances with nucleic acids and their modes of action, ed. F.E. Hahn (Springer Verlag, Berlin, Heidelberg, New York, 1971) p. 181.
[18] D.B. Dusenberg and R.B. Uretz, Biophys. J. 12 (1972) 1056.
[19] V. Zanker, Z. Phys. Chem. 199 (1952) 225.
[20] M.E. Lamm and D.M. Neville Jr., J. Phys. Chem. 69 (1965) 3872.
[21] R.W. Armstrong, T. Kurucsev and U.P. Strauss, J. Amer. Chem. Soc. 92 (1970) 3174.
[22] B.H. Robinson, A. Löffler and G. Schwarz, Trans. Faraday Soc. 69 (1973) 56.
[23] Y. Kubota and M. Miura, J. Sci. Hiroshima Univ. Ser. A-II 30 (1966) 49.
[24] R.E. Ballard and C.H. Park, J. Chem. Soc. (A) (1970) 1340.
[25] V. Zanker, Z. Physik. Chem. 200 (1952) 250.
[26] Th. Förster, Naturwissenschaften 33 (1946) 166.
[27] A.S. Davydov, J. Exp. Theoret. Physik (USSR) 18 (1948) 210.

[28] G. Scheibe and O. Wörz, Angew. Chem. 78 (1966) 304.
[29] K.K. Rohatgi and A.K. Mukhopadhyay, Photochem. Photobiol. 14 (1971) 551.
[30] V. Czikkely, G. Dreizler, H.D. Försterling, H. Kuhn and J. Sondermann, Z. Naturforsch. 24a (1969) 1821.
[31] V. Czikkely, H.D. Försterling and H. Kuhn, Chem. Phys. Letters 6 (1970) 207.

BIOPHYSICAL CHEMISTRY 2 (1974) 164–169. © NORTH-HOLLAND PUBLISHING COMPANY

VISCOELASTIC PROPERTIES OF LIGATION-INHIBITED FIBRIN CLOTS*

L.F. MOCKROS, W.W. ROBERTS and L. LORAND
Biomedical Engineering Center and Biochemistry Division of the Department of Chemistry, Northwestern University, Evanston, Illinois 60201, USA

Received 5 March 1974
Revised manuscript received 6 May 1974

1. Introduction

Fibrin, the main product of the thrombin-catalyzed hydrolysis of fibrinogen, forms the structural framework of blood clots:

$$n \text{ fibrinogen} \xrightarrow{\text{thrombin}} n \text{ fibrin} \rightleftharpoons (\text{fibrin})_n \text{ gel}.$$

The bonds holding this type of fibrin polymer together are readily broken by the addition of solutes such as 30% urea or 1% monochloroacetic acid. Irreversible covalent bonding between fibrin units ensues, however, in the course of normal clotting through the action of another enzyme (called fibrinoligase, activated fibrin stabilizing factor or Factor $XIII_a$):

$$(\text{fibrin})_n \text{ gel} \xrightarrow[Ca^{2+}]{\text{fibrinoligase}} \text{ligated } (\text{fibrin})_n \text{ gel}.$$

Ligation is brought about by a selective transmidation between a few γ-glutamyl and ϵ-lysine side chain residues of adjacent fibrin molecules (for a review, see [1]) and contributes to the structural rigidity of the network [2, 3]. Furthermore, the ligated gel can no longer be dispersed by urea or acid solutions.

Certain synthetic amines specifically inhibit ligation by competing against the ϵ-amino (donor) functional groups of lysine of fibrin and these compounds themselves become enzymatically inserted into the γ-glutaminyl (acceptor) sites of fibrin, thus blocking the process of normal ligation (see [4, 5]). Previous work [2, 3] indicated marked differences in mechanical rigidity between ligated and unligated clots. (A recent study [6], however, indicates little effect of ligation on storage moduli measured at high frequency.) The present study deals with the effects of the amine-type inhibitors on the physical characteristics of fibrin clots. In specific terms, it examines the viscoelastic properties of clots formed in the presence of fibrinoligase with and without synthetic amines added. Measurements were made by recording the response of clots to forced sinusoidal shear strain in a rheogoniometer under varying conditions of strain level, total ionic strength and oscillatory frequency.

2. Materials and methods

Except for one series that involved fresh citrated platelet-poor human plasma, all other clotting mixtures were derived from solutions of purified fibrinogen. The first step in preparing ligated clots with the purified components was to incubate fibrin stabilizing factor (factor XIII or FSF), thrombin, calcium chloride, and cysteine in 0.01 M NaCl and Trishydroxymethylaminomethane (Tris) at pH 7.5 for ten minutes, thereby activating FSF. Fibrinogen was then admixed by gently tumbling the tube to avoid any foaming. The final concentrations were 2.7 to 6.2 mg/ml for fibrinogen, four units per ml for fibrinoligase, one NIH unit per ml for thrombin, 2.4 mM $CaCl_2$, 3.4 mM cysteine, 0.05 M Tris buffer and the necessary sodium chloride to adjust total ionic strength to values between 0.09 and 0.23. All tests were conducted at 37°C and a pH of about 7.5.

* Address reprint requests to Professor L.F. Mockros, Department of Civil Engineering, Technological Institute, Northwestern University, Evanston, Illinois 60201.

The purified fibrinogen, fibrin, thrombin and fibrinoligase were prepared and assayed using the methods given by Lorand and Gotoh [7]. Freezedried human fibrinogen was obtained in 95% clottable form from Kabi, Stockholm. It was dissolved in 0.05 M Tris chloride, pH 7.5, and was dialyzed against the same overnight at 4°C. The 15 mg/ml fibrinogen stock solution was stored in 3 ml aliquots at −10°C. Activities of bovine thrombin and bovine fibrin stabilizing factor stock preparations were 300 NIH units/ml and 1000 "crosslinking" units/ml, respectively.

The clot forming techniques were essentially identical to those reported by Roberts et al. [3]. Immediately after mixing, the solutions were poured onto the plate portion of the cone-plate test section of a Model R17 Weissenberg Rheogoniometer. The cone was lowered into position and the strain transducer adjusted with the entire procedure taking less than one minute; overall clotting times were approximately six minutes. After coating the external surface of the gel with mineral oil (Nujol), the temperature control jacket was closed around the entire section and the solution was left undisturbed for about one hour. As previously reported [3], these clotting mixtures gradually stiffened over a period of about one hour and then maintained constant properties for two additional hours. After the one hour gelation period, the samples were tested for response to forced sinusoidal shear strain. Except for one series of experiments in which dependence on frequency was investigated, all testing was performed with a sinusoidal frequency of 0.03 Hz. The cone-plate section had a diameter of 7.5 cm and a 1.5° cone.

Stress–strain data were obtained by increasing peak strain in discrete steps up to a maximum of 30% and then decreasing it to the minimum value, all at 0.03 Hz. For studying dependence on test frequency, clots were subjected to forced sinusoidal strains at frequencies ranging from 0.01 to about 0.3 Hz. The latter tests were conducted with peak strains of 10%.

3. Results and discussion

The rheogoniometer records the forced sinusoidal motion of the plate and the sinusoidal shear stress that develops on the cone. The stress, τ, in phase with the peak strain, ϵ, is a measure of the elasticity of the gel and the phase shift, δ, between the peak strain and peak stress is a measure of its viscosity. The stress at peak strain divided by strain, is the shear storage, or rigidity, modulus, G', and the stress at zero strain divided by peak strain is the shear loss modulus, G''. The shear loss modulus divided by frequency is the dynamic viscosity. In the present study, the loss tangent, i.e., tan δ or the ratio of the loss modulus to storage modulus, is used as an index of energy dissipation during dynamic testing. In most experiments, plots of stress versus strain were non-linear, and the slope of the secant between the origin and the point on the curve at 10% strain, i.e., the storage modulus, was used in comparing elastic rigidity of various clots.

Fig. 1 shows the stress in phase with the peak strain versus the peak strain for clots formed in platelet poor human plasma. The addition of glycine ethylester [curves (b) and (c)] to the plasma at the time of recalcification caused the rigidity of the clot to be significantly reduced from that of the control (curve a). At 10% strain, this reduction in storage modulus

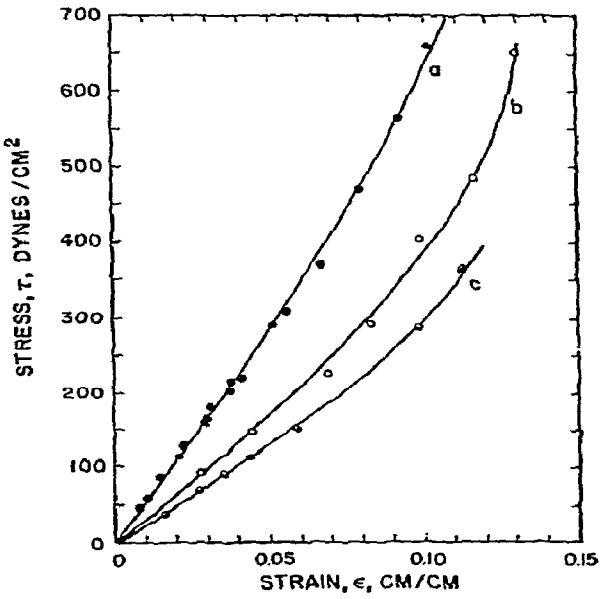


Fig. 1. Stress in phase with strain for clots obtained by recalcification of citrated human plasma. Clotting times were about 5 min. Curve (a) without glycine ethylester. Curves (b) and (c) with 25 and 50 mM glycine ethylester added, respectively.

amounted to 40% with 25 mM and to 52% with 50 mM glycine ethylester. Boyd and Stoner [8] measured electrical resistance changes in recalcified plasma and reported that the final clot showed 35% less resistance when formed in the presence of 75 mM glycine methylester than did an uninhibited clot. With 25 mM, however, the resistance changes were similar to that for uninhibited samples and with 65 and 70 mM the total change was only slightly less than control. Thus, mechanical rigidity of the final clots appears to be more sensitive to changes induced by ligation inhibitors than electrical resistance.

Figs. 2–7 pertain to clots formed in purified systems. Fig. 2 compares the dynamic stress–strain behavior of ligated and non-ligated clots with those obtained under ligating conditions in the presence of 15 mM glycine ethylester. Similar results were obtained when histamine was used for inhibiting ligation (fig. 3).

Both glycine ethylester and histamine are representative of a group of amines that have been extensively studied in a biochemical sense for their effects on the last step of blood clotting. These synthetic compounds are known, for example, to become covalently attached to fibrin, occupying sites which would be otherwise available for ligation between fibrin molecules [1, 4].

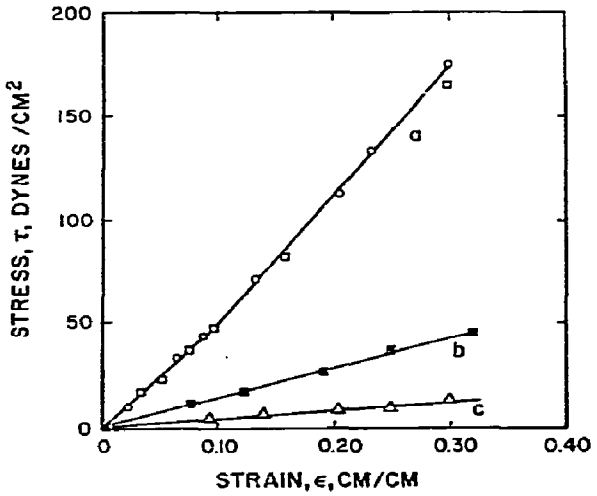


Fig. 2. Stress in phase with peak strain for clots derived from purified fibrinogen (6.2 mg/ml) solutions at μ 0.10. Curve (a), with fibrinoligase in the clotting mixture; curve (c) without fibrinoligase. Curve (b) as in (a) but with 15 mM glycine ethylester included.

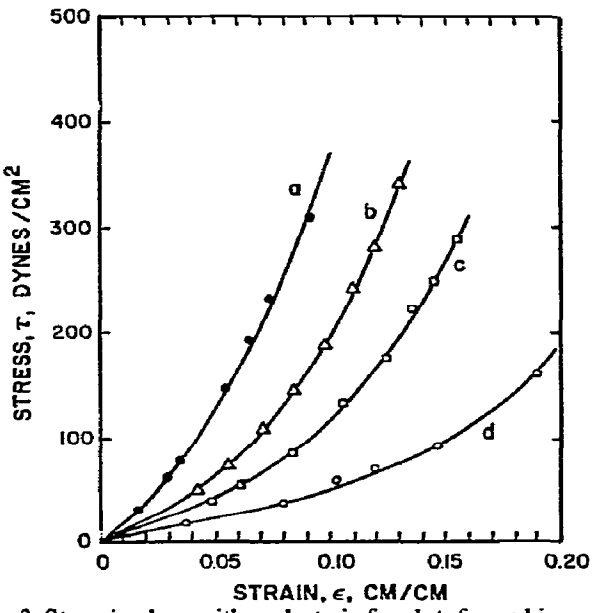


Fig. 3. Stress in phase with peak strain for clots formed in purified fibrinogen (3.8 mg/ml) solutions at μ 0.17. Curve (a), with fibrinoligase; curve (d) without this enzyme. Curves (b) and (c) as in (a) but including 10 and 20 mM histamine, respectively.

In general, they do not inhibit the gelation of fibrin; hence fibrin-to-fibrin contacts critical for gel formation are not interfered with. Fibrin exposed to fibrinoligase in the presence of amines yields a clot that is easily dispersed by chemical agents (e.g., 1% monochloroacetic acid) which dissolve unligated clots but are without such effect on ligated ones [9]. Furthermore, in contrast with the latter group, clots in which ligation has been inhibited by amines can be digested by fibrinolytic enzymes (e.g., urokinase plus plasminogen) just as readily as unligated fibrin clots [10, 11].

The results are given in figs. 1–3 indicate that this enhanced susceptibility to both dispersal and lysis correlates with a significant alteration of the viscoelastic properties of the clot structures. The effect of the inhibitors, however, is not a qualitative change in mechanical properties, but rather a quantitative change. The mechanical properties of the inhibited clots fall intermediate between those of ligated and unligated clots. A plot of storage moduli at 10% strain as a function of the concentration of inhibitor present during clot formation (fig. 4) shows a substantial reduction in clot rigidity which, at high enough concentration of the inhibitor, approaches the values found for unligated

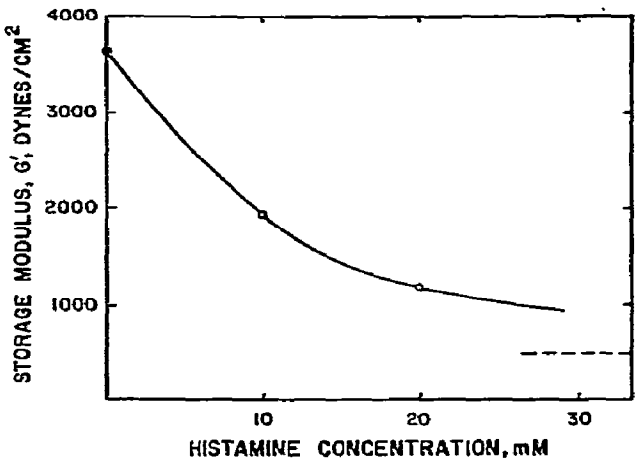


Fig. 4. Storage moduli at 10% strain as a function of concentration of histamine for data in fig. 3. The horizontal broken line represents the value obtained with fibrinoligase.

fibrin clots.

The storage moduli and loss tangents for inhibited clots are shown as a function of ionic strength in figs. 5 and 6 and compared thereon with those of previously reported [3] ligated and unligated clots. Since changing ionic strength affects the rate of clotting of fibrinogen with thrombin, the concentration of the latter was adjusted so as to maintain a uniform clotting time of about six minutes in all tests. Figure 5 indicates that fibrin exposed to fibrinoligase in the presence of histamine yields gels that are more compliant at all ionic strengths than their counterparts without histamine, and the higher the histamine concentration the more the moduli approach the values obtained for unligated fibrin clots. With 10 mM of the inhibitor the peak rigidity, as with uninhibited ligated clots, is at about $\mu = 0.17$. Under certain conditions (e.g., $\mu = 0.19$), histamine (10 mM) caused a reduction in storage modulus by as much as 90% of the difference between ligated and unligated clots (fig. 5), yet it increased the loss tangent by only 35% of the difference (fig. 6). A few fibrin-to-fibrin covalent links are known to form even in the presence of inhibitors such as histamine, leading to oligomerically ligated fibrin units [12, 1, 5]. These protein links are apparently sufficient for maintenance of an elastic

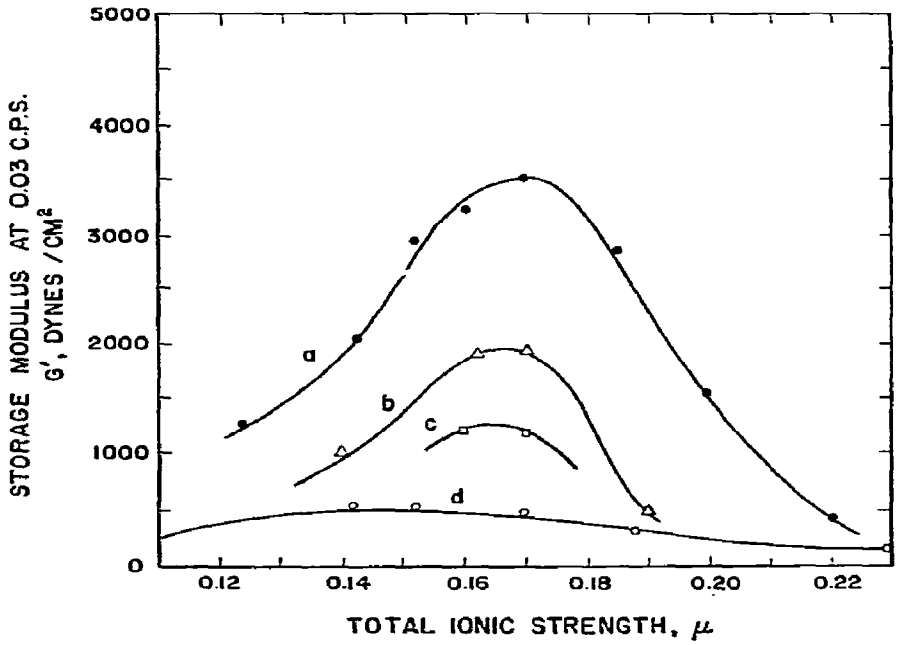


Fig. 5. Storage moduli at 10% strain as a function of ionic strength for clots formed (a) in the presence and (d) in the absence of fibrinoligase in purified fibrinogen solutions (as in fig. 3). Curves (b) and (c) represent clots formed in the presence of the ligase but with 10 and 20 mM histamine added, respectively.

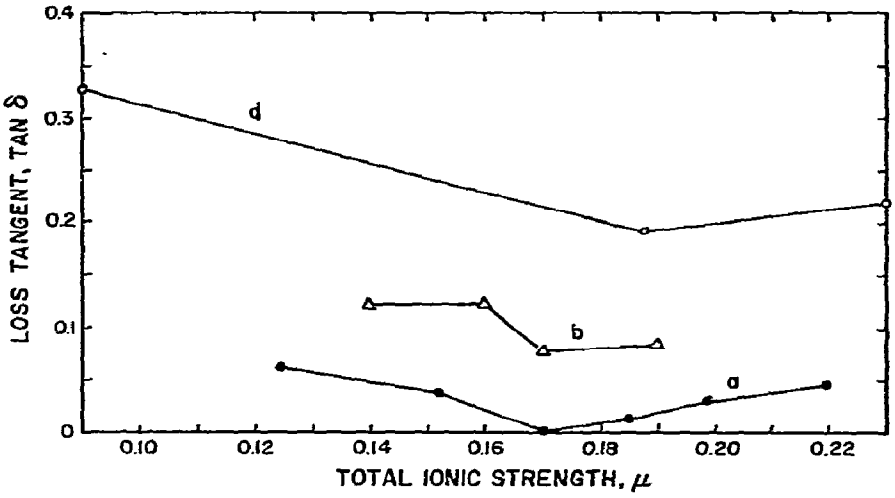


Fig. 6. Loss tangents for curves (a), (b) and (d) shown in fig. 5, as a function of ionic strength.

structure that dissipates only about one-third as much energy as an unligated clot but is nevertheless almost totally as compliant.

Figure 7 shows the dependence of storage moduli on the test frequency. As with previously reported [3] ligated and unligated clots, the moduli are virtually independent of frequency for $0.01 < \nu < 0.3$ Hz.

In conclusion, these findings indicate that the presence of inhibitory amines during ligation results in formation of clot structures (both in plasma and in purified clotting systems) with viscoelastic shear properties not unlike those of ligated and unligated clots: i.e.

(i) stress–strain relations are nonlinear, being more stiff at higher strains and showing a tendency to a constant tangent modulus at strains greater than 10 to 20%;

(ii) the storage modulus and loss tangent are dependent on total ionic strength, with a peak stiffness and minimum dissipation at about 0.17; and

(iii) the storage modulus is virtually independent of test frequency below one Hz.

Thus, the presence of the inhibitors does not alter many of the qualitative aspects of the mechanical properties (notwithstanding the major affect on quantitative values) and the overall design of the clot network appears to be unaffected by covalent modification of fibrin by the amines; i.e., fibrin-to-fibrin contact sites for network formation seemingly have been not interfered with. In a quantitative sense, under conditions of ligation the presence of amines caused formation of clots with viscoelastic properties intermediate between ligated and unligated structures. Increasing the concentration of inhibitory amine seemed to bring measured values for storage modulus and loss tangent closer to those found in unligated clots. The effect was particularly noticeable in terms of the greatly reduced storage modulus. The structural elements of ligated, ligation-inhibited and unligated clots do not

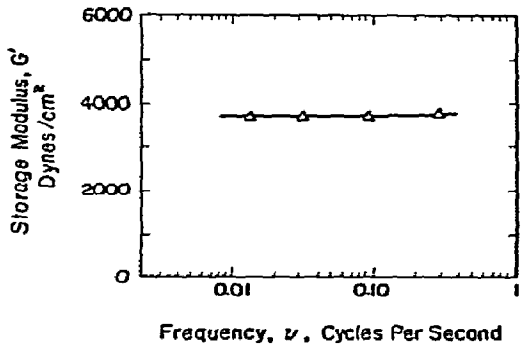


Fig. 7. Storage modulus at 10% peak strain for a fibrin clot partially inhibited by histamine. The clots were formed in the presence of fibrinoligase and with 4.8 mg/ml fibrinogen, μ 0.19, and 5 mM histamine. These clots were approximately 60 to 70% soluble in 1% MCA or urea.

have relaxation times within the frequency range tested, as indicated by the relatively flat frequency response of storage modulus. The effect of the inhibitors on the covalent bonds has a relaxation time outside of the range tested. Clots should be examined at higher and lower frequencies to more precisely examine the specificity of these inhibiting amines.

Acknowledgement

This work was supported by grants from the National Institutes of Health (HL-02212, HL-16346, GM-00874 and GM-15418). L. Lorand is the recipient of a U.S. Public Health Service Research Career Program Award.

References

[1] L. Lorand, Ann. N.Y. Acad. Sci. 202 (1972) 6.
[2] J.D. Ferry, M. Miller and S. Shulman, Archives Biochem. Biophys. 34 (1951) 424.
[3] W.W. Roberts, L. Lorand and L.F. Mockros, Biorheology 10 (1973) 29.
[4] L. Lorand, D. Chenoweth and A. Gray, Ann. N.Y. Acad. Sci. 202 (1972) 155.
[5] L. Lorand and J.L.G. Nilsson, in: Drug design, Vol. 3, ed. A.J. Arines (Academic Press, New York, 1972). p. 415.
[6] W.W. Roberts, O. Kramer, R.W. Rosser, F.H.M. Nestler, J.D. Ferry, Biophys. Chem. 1 (1974) 152.
[7] L. Lorand and T. Gotoh, in "Proteolytic Enzymes" Vol. 19, "Methods in Enzymology", pp. 770 (1970).
[8] T.H. Boyd III and G.E. Stoner, Thrombosis Research 3 (1973) 209.
[9] L. Lorand, N.G. Rule, H.H. Ong, R. Furlanetto, A. Jacobsen, J. Downey, N. Oner and J. Bruner-Lorand, Biochemistry 7 (1968) 1214.
[10] L. Lorand and A. Jacobsen, Nature 195 (1962) 911.
[11] L. Lorand, J. Bruner-Lorand and T.R.E. Pilkington, Nature 210 (1966) 1273.
[12] L. Lorand, Thromb. Diath. Haemorrh. Suppl. 39 (1970) 75.
[13] J.D. Ferry and P.R. Morrison, J. Am. Chem. Soc. 69 (1947) 388.
[14] M. Kaibara, Biorheology 10 (1973) 61.

BIOPHYSICAL CHEMISTRY 2 (1974) 170–174. © NORTH-HOLLAND PUBLISHING COMPANY

DETERMINATION OF THE EQUILIBRIUM CONSTANTS OF SELF-ASSOCIATING PROTEIN SYSTEMS. X. EVALUATION OF THE WEIGHT FRACTION OF MONOMER FROM THE DIFFUSION COEFFICIENT AS A FUNCTION OF CONCENTRATION*

Paul W. CHUN

Department of Biochemistry, College of Arts and Sciences, University of Florida, Gainesville, Florida 32610, USA

Received 15 January 1974

A simplified procedure for determining the mode of association and weight fraction of monomer of a self-associating protein system based on the average diffusion coefficient as a function of concentration is described. This procedure is applicable to cases of monomer-*n*-mer, three species or indefinite association.

1. Introduction

A number of papers have appeared in recent years describing methods of analyzing self-associating protein systems. The examination of ultracentrifugal transport boundary and boundary shapes permits quantitative analysis of polymerizing systems [1–6]. It has also been used as a diagnostic tool for recognition of the mode of association in such systems. The most widely used methods of analysis of self-associating protein systems are sedimentation equilibrium measurements, on which much has been published, molecular sieve chromatography [7,8], countercurrent distribution [9,10], and electrophoresis [11,12].

Several numerical methods for the analysis of Lamm's transport equation [13] have been reported that are capable of dealing with concentration dependent sedimentation and diffusion [4,14,15].

A number of numerical models based on Vink's finite-difference approximation of Fick's second law have been proposed to simulate the diffusion of an ideal case [4,16]. Cox [14] has elaborated on the Vink method to encompass a system in which $\bar{D}$, the average diffusion coefficient as defined by Steiner [17], varies with local solute concentration. The resulting computer simulation may be applied to a rapidly polymerizing system by compartmentalization of the ultracentrifuge cells, assigning the mean solute concentration of each. Both sedimentation and diffusion are related to the total solute concentration of each compartment by the relations $D_i = D_1/i^{1/3}$ and $S_i = S_1 i^{2/3}$ respectively [18].

In simulating sedimentation in a rapidly polymerizing system during high speed ultracentrifugation runs, the variation of the association constants with position in the cell is assumed to be due solely to concentration dependence, i.e. $(\partial K_i/\partial X)_c$ must be zero [8,15]. However, in cases of pressure dependent self-association, this quantity may not, in fact, be zero [8,15]. Earlier data simulation methods have also been limited to a consideration of monomer-*n*-mer association.

Our primary goal is to simplify the expression of the relationship between $\bar{D}$ and C in order to accurately deduce the stoichiometry of the self-associating solute. A procedure for determination of the average diffusion coefficient, $\bar{D}$, as a function of concentration for self-associating systems is described, in which the weight fraction of monomer may be determined from a plot of $\bar{D}$ versus C. Application of our method to cases of monomer-*n*-mer, monomer-*n*-mer-*l*-mer and indefinite association is outlined.

* This work was supported by National Science Foundation Grant GB 28223 and in part by General Research Support, College of Medicine, University of Florida.

2. Enumeration of basic quantities and determination of stoichiometry of the self-associating solute

Fick's second law of diffusion [22] for the ith interacting species may be expressed as

$$\partial C_i/\partial t = D_i(\partial^2 C_i/\partial X^2), \quad i = 1, \ldots n. \tag{1}$$

The total concentration of the self-associating solute is given by

$$C = \sum_i C_i \quad \text{where} \quad C_i = K_i C_1^i. \tag{2}$$

Thus, eq. (1) can be rewritten as

$$\frac{\partial}{\partial t}\left(\sum_i C_i\right) = \frac{\partial}{\partial X}\left(\sum_i D_i \frac{\partial C_i}{\partial X}\right). \tag{3}$$

Solving for partial differentials with respect to monomer concentration C_1 of eq. (2)

$$\frac{\partial C_i}{\partial X} = iK_i C_1^{i-1}\frac{\partial C_1}{\partial X}, \text{ where } \left(\frac{\partial K_i}{\partial X}\right)_c = 0 \text{ for all } i\text{th species.}$$

Letting the average diffusion coefficient [17] be represented by

$$\bar{D}_{(c)} \approx \left(\sum_i D_i \frac{\partial C_i}{\partial X}\right)$$

$$= \left(\sum_i D_i iK_i C_1^{i-1}\right) / \left(\sum_i iK_i C_1^{i-1}\right). \tag{4}$$

Rearrangement of eq. (4) gives

$$\sum_i i(\bar{D} - D_i)K_i C_1^i = 0.$$

Hence, from eqs. (2), (3) and (4),

$$\frac{\partial C}{\partial t} = \frac{\partial}{\partial X}\left(\bar{D}\frac{\partial C}{\partial X}\right). \tag{5}$$

Differentiating with respect to x, and substituting $y = \partial C/\partial X$, eq. (5) becomes

$$\frac{\partial y}{\partial t} = \frac{\partial^2}{\partial X^2}(\bar{D}y). \tag{6}$$

The numerical expression for eq. (6) may be writte as

$$\left(\frac{\Delta y}{\Delta t}\right)_x = \left\{\frac{y_{t+\Delta t} - y_t}{\Delta t}\right\}$$

$$= \left\{\frac{(\bar{D}y)_{x+\Delta x} - 2(\bar{D}y)_x + (\bar{D}y)_{x-\Delta x}}{\Delta x^2}\right\}_t. \tag{7}$$

Using a synthetic boundary cell in low speed sedimentation runs, where $dx/dt \to 0$, the cell is partitioned into two parts, pure solvent and solution, at t_0. At some time t, we observe a spreading of the boundary due to diffusion. In order to evaluate $\bar{D}$, the concentration gradient curve is divided into numerous frame from x_0 to x_i. $(\bar{D})_{x_i,t}$ may be computed for all x_i using the general expression

$$(\bar{D})_{x_i,t} = \left\{\frac{(y_{t+\Delta t} - y_t)_{x_{i-1}}(\Delta X^2/\Delta t) + 2(\bar{D}y)_{x_{i-1},t} - (\bar{D}y)_{x_{i-2}}}{y_{t,x_i}}\right. \tag{8}$$

Hence, at the radial distance $x = x_0$, eq. (8) becomes

$$(\bar{D})_{x_1,t} = \frac{y_{t+\Delta t,x_0}}{y_{t,x_1}}\left(\frac{\Delta X^2}{\Delta t}\right). \tag{9a}$$

Similarly, at $x = x_1$

$$(\bar{D})_{x_2,t} = \left\{\frac{(y_{t+\Delta t} - y_t)_{x_1}(\Delta X^2/\Delta t) + 2(\bar{D}y)_{x_1,t}}{y_{t,x_2}}\right\} \tag{9b}$$

where $(\bar{D}y)_{x_1,t}$ is known from eq. (9a), and $(\bar{D}y)_{x_1-\Delta} = (\bar{D}y)_{x_0,t} = 0$. $(\bar{D})_{x_i,t}$ may be similarly obtained for all x_i using the general expression (8). This expression may be applied to free boundary diffusion experiments as well as in a synthetic boundary run.

The concentration at any given radial distance x_i is calculated from

$$C = \int_{x_0}^{x}\left(\frac{dC}{dx}\right)dx. \tag{10}$$

Thus, computer calculations of eqs. (8) and (10) may be used to generate the curve of $\bar{D}$ versus C. Based on this curve, we generate a new weight average quantity $\bar{D}_w$, which may be expressed as

$$\bar{D}_w = \frac{1}{C}\int_0^C \bar{D}dC = \frac{1}{C}\sum_i D_i C_i = \sum_i D_i f_i. \tag{11}$$

The values of f_i are the weight fractions of ith-mer, where $\Sigma_i f_i = 1$. It is also possible to generate a Z-average quantity

$$\bar{D}_z = \frac{1}{C^2}\int_0^C C\bar{D}_w\,dC \qquad (12)$$

which may be useful in cases where three or four species are in chemical equilibrium, but is more difficult to evaluate.

Basic equations given to this point will suffice to determine the equilibrium constant and weight fraction of monomer when as many as three species are involved in chemical equilibrium.

Case (i) $\quad qP_i \rightleftharpoons rP_n, \quad n > 1.$

The expressions for evaluation of the parameters which follow are arranged in matrix form, which is easily adaptable to computer analysis and applicable to a variety of model systems.

When two species are involved in monomer-n-mer association, the equilibrium constant and weight fraction of monomer may be evaluated from the expressions

$$\begin{aligned} C &= C_1 + K_n C_1^n \\ C\bar{D}_w &= C_1 D_1 + D_n K_n C_1^n \\ 0 &= (\bar{D}-D_1)C_1 + n(\bar{D}-D_n)K_n C_1^n. \end{aligned} \qquad (13)$$

By determinants [23], the solution to equation set (13) is given by

$$\Delta = \begin{vmatrix} 1 & 1 & 0 \\ D_1 & 0 & 1 \\ \bar{D}-D_1 & n\bar{D} & -n \end{vmatrix} = (n-1)(D_1-\bar{D}),$$

$$C_1 = \Delta_1/\Delta, \quad \Delta_1 = \begin{vmatrix} C & 1 & 0 \\ C\bar{D}_w & 0 & 1 \\ 0 & nD & -n \end{vmatrix} = nC(\bar{D}_w-\bar{D}),$$

$$C_1^n K_n = \Delta_2/\Delta, \quad \Delta_2 = \begin{vmatrix} 1 & C & 0 \\ D_1 & C\bar{D}_w & 1 \\ \bar{D}-D_1 & 0 & -n \end{vmatrix} = nC(D_1-\bar{D}_w) + (\bar{D}-D_1)C,$$

$$K_n C_1^n D_n = \Delta_3/\Delta, \quad \Delta_3 = \begin{vmatrix} 1 & 1 & C \\ D_1 & 0 & C\bar{D}_w \\ \bar{D}-D_1 & n\bar{D} & 0 \end{vmatrix} = C\bar{D}_w(\bar{D}-D_1) + nC\bar{D}(D_1-\bar{D}_w).$$

In the case of monomer-n-mer association, it is not necessary to assume $D_i = D_1/i^{1/3}$. D_1 is obtained by extrapolation of $\bar{D}$ versus C, as C approaches zero.

In terms of the weight fraction of monomer, the following equations may be set up:

$$\begin{aligned} 1 &= f_1 + f_n \\ \bar{D}_w &= D_1 f_1 + D_n f_n \\ 0 &= (\bar{D}-D_1)f_1 + n\bar{D}f_n - nD_n f_n. \end{aligned} \qquad (14)$$

By determinants, the unknown parameters, f_1, f_n and D_n, can be solved as follows:

$$f_1 = \Delta_1/\Delta, \ \Delta_1 = n(\bar{D}_w-\bar{D}),$$

$$f_n = \Delta_2/\Delta, \ \Delta_2 = \begin{vmatrix} 1 & 1 & 0 \\ D_1 & \bar{D}_w & 1 \\ \bar{D}-D_1 & 0 & -n \end{vmatrix} = n(D_1-\bar{D}_w)-(D_1-\bar{D}),$$

$$f_n D_n = \Delta_3/\Delta, \ \Delta_3 = \begin{vmatrix} 1 & 1 & 0 \\ D_1 & 0 & \bar{D}_w \\ \bar{D}-D_1 & n\bar{D} & 0 \end{vmatrix} = n\bar{D}(D_1-\bar{D}_w) - \bar{D}_w(D_1-\bar{D}),$$

$$K_n = Cf_n/[Cf_1]^n.$$

It is also possible to determine the stoichiometry of monomer-n-mer association without setting up a matrix, by solving either of two sets of simultaneous equations:

$$C = C_1 + K_n C_1^n \qquad 1 = f_1 + f_n$$

or

$$C\bar{D}_w = D_1 C_1 + D_n K_n C_1^n \qquad \bar{D}_w = D_1 f_1 + D_n f_n$$

where $\bar{D}_w = D_1 f_1 + D_n(1-f_1) = (D_1-D_n)f_1 + D_n$.
The weight fraction of the monomer and equilibrium constants are evaluated from the expressions:

$$f_1 = (\bar{D}_w-D_n)/(D_1-D_n), \ f_n = (1-f_1)$$

$$K_n = C_n/C_1^n.$$

In order to determine the unknown D_n, one of two sets of simultaneous equations must be solved.

$$C = C_1 + C_n \qquad \text{or} \quad 1 = f_1 + f_n$$
$$C\bar{D}_w = C_1 D_1 + D_n C_n \qquad \bar{D}_w = D_1 f_1 + D_n f_n$$
$$\bar{D} = (D_1 C_1 + nD_n C_n)/(C_1 + nC_n) \qquad \bar{D}(f_1 + nf_n) = D_1 f_1 + nD_n f_n.$$

Elimination of $(D_n f_n)$ yields either

$$n\bar{D}_w - \bar{D}(f_1 + nf_n) = (n-1)D_1 f_1$$
or $$n\bar{D}_w = (n-1)(D_1 - \bar{D})f_1 + n\bar{D}.$$

Thus, f_1, f_n and D_n are evaluated as follows:

$$f_1 = n(\bar{D}_w - \bar{D})/(n-1)(D_1 - \bar{D}),$$
$$f_n = (1 - f_1) = \{n(D_1 - \bar{D}_w) - (D_1 - \bar{D})/(n-1)(D_1 - \bar{D})\},$$
$$D_n = (\bar{D}_w - D_1 f_1)/f_n$$
$$= \{n\bar{D}(D_1 - \bar{D}_w) - \bar{D}_w(D_1 - \bar{D})/n(D_1 - \bar{D}_w) - (D_1 - \bar{D})\}$$

Case (ii) $\quad qP_1 \rightleftharpoons SP_m + rP_n, \quad n > m > 1.$

When three species are involved in a chemical equilibrium, the following equations are solved simultaneously:

$$1 = f_1 + f_m + f_n$$
$$\bar{D}_w = D_1 f_1 + D_m f_m + D_n f_n$$
$$0 = (\bar{D} - D_1)f_1 + m(\bar{D} - D_m)f_m + n(\bar{D} - D_n)f_n$$

or

$$C = C_1 + C_m + C_n$$
$$C\bar{D}_w = C_1 D_1 + C_m D_m + C_n D_n$$
$$0 = (\bar{D} - D_1)C_1 + m(\bar{D} - D_m)C_m + n(\bar{D} - D_n)C_n. \qquad (15)$$

Applying matrix transformation,

$$f_1 = \Delta_1/\Delta, \quad f_m = \Delta_m/\Delta, \quad f_n = \Delta_n/\Delta.$$

Similarly $C_1 = \bar{\Delta}_1/\bar{\Delta}$, $C_m = \bar{\Delta}_2/\bar{\Delta}$ and $C_n = \bar{\Delta}_3/\bar{\Delta}$;

$$\Delta = \begin{vmatrix} 1 & 1 & 1 \\ D_1 & D_m & D_n \\ (D_1 - \bar{D}) & m(D_m - \bar{D}) & n(D_n - \bar{D}) \end{vmatrix}, \quad \bar{\Delta} = \Delta$$

$$\Delta_1 = \begin{vmatrix} 1 & 1 & 1 \\ \bar{D}_w & D_m & D_n \\ 0 & m(D_m - \bar{D}) & n(Dn - \bar{D}) \end{vmatrix} \quad \bar{\Delta}_1 = \begin{vmatrix} C & 1 & 1 \\ C\bar{D}_w & D_m & D_n \\ 0 & m(\bar{D} - D_m) & n(\bar{D} - D_n) \end{vmatrix}$$

$$\Delta_m = \begin{vmatrix} 1 & 1 & 1 \\ D_1 & \bar{D}_w & D_n \\ (D_1 - \bar{D}) & 0 & n(D_n - \bar{D}) \end{vmatrix} \quad \bar{\Delta}_2 = \begin{vmatrix} 1 & C & 1 \\ D_1 & C\bar{D}_w & D_n \\ (\bar{D} - D_1) & 0 & n(\bar{D} - D_n) \end{vmatrix}$$

$$\Delta_n = \begin{vmatrix} 1 & 1 & 1 \\ D_1 & D_m & \bar{D}_w \\ D_1 - \bar{D} & m(D_m - \bar{D}) & 0 \end{vmatrix} \quad \bar{\Delta}_3 = \begin{vmatrix} 1 & 1 & C \\ D_1 & D_m & C\bar{D}_w \\ (\bar{D} - D_1) & m(\bar{D} - D_m) & 0 \end{vmatrix}.$$

Having determined the values of f_i, the equilibrium constants may be evaluated from eq. (16)

$$K_i = f_i/f_1 C_1^{i-1}. \qquad (16)$$

Case (iii) Indefinite association

The methods to be used in the theoretical consideration of indefinite association are identical with the procedure outlined in part III [24–26] of this series and by Adams [27,28]. The quantity $kC < 1$, where k is the intrinsic equilibrium constant. By our procedure, it is possible to formulate the weight average diffusion coefficient as well as a new function for describing the convergence of the series as applied to the weight fraction in cases of indefinite association.

The total concentration, C, can be expressed as

$$C_i = ik^{i-1}C_1^i$$
$$C = \sum_i C_i = C_1/(1 - kC_1)^2. \qquad (17)$$

The weight average diffusion coefficient, $\bar{D}_w$ of eq. (11), becomes

$$\bar{D}_w = \sum_i D_i f_i = f_1 \sum_i D_i i(kC_1)^{i-1}$$
$$= f_1 \sum_i iD_i(1 - \sqrt{f_1})^{i-1}. \qquad (18)$$

Eq. (18) can be solved for C_1 and the intrinsic equilibrium constant k can be evaluated from $kC_1 = 1 - \sqrt{f_1}$.

Eq. (18) is the most useful function to be derived by this method. In order to generate the convergence of the series, we assume $D_i = D_1/i^{1/3}$. Substitution into eq. (18) yields

$$\bar{D}_w = f_1 D_1 \sum_i i^{2/3}(1-\sqrt{f_1})^{i-1}$$

$$= f_1 D_1 \{1 + \sum_{i=2}^{\infty} i^{2/3}(1-\sqrt{f_1})^{i-1}\}. \quad (19)$$

Letting $\lambda = 1-\sqrt{f_1}$, where $0 < \lambda < 1$, then eq. (19) becomes

$$\bar{D}_w/D_1 = f_1 \sum_{i=1}^{\infty} i^{2/3}\lambda^{i-1} \quad (20)$$

where $\theta = \bar{D}_w/D_1 \leqslant 1$.

The convergence of the series can be checked by the ratio test as follows:

$$\lim_{i\to\infty} \frac{(i+1)^{2/3}\lambda^i}{i^{2/3}\lambda^{i-1}} = \lim_{i\to\infty} \left(\frac{i+1}{i}\right)^{2/3} \lambda \simeq \lambda < 1.$$

Plotting θ as a function of $\lambda, 0 < \lambda < 1$, the resulting weight fraction data can be readily compared with values obtained from other transport experiments. Eq. (18) is analogous to our expression for the partition coefficient as a function of concentration for indefinite association [24,26].

Application of this simplified theoretical procedure for evaluation of the weight fraction of monomer based on $\bar{D}$ versus C to various self-associating protein systems will be described in detail in a succeeding paper.

References

[1] G.A. Gilbert, Discussions Faraday Soc. 20 (1955) 68.
[2] G.A. Gilbert, Proc. Roy. Soc. London, Ser. A 276 (1963) 354.
[3] A. Fujita, Mathematical theory of sedimentation analysis (Academic Press, New York, 1962).
[4] D.J. Cox, Arch. Biochem. Biophys. 112 (1965) 249.
[5] D.J. Cox, Arch. Biochem. Biophys. 142 (1971) 514.
[6] J.R. Cann and W.B. Goad, Science 170 (1970) 441.
[7] J.K. Zimmerman and G.K. Ackers, J. Biol. Chem. 65 (1961) 1761.
[8] J.K. Zimmerman, D.J. Cox and G.K. Ackers, J. Biol. Chem. 246 (1971) 4242.
[9] J.L. Bethune and G. Kegeles, J. Phys. Chem. 65 (1961) 1761.
[10] J.L. Bethune, J. Phys. Chem. 74 (1970) 3837.
[11] J.R. Cann and W.B. Goad, Science 170 (1970) 441.
[12] J.R. Cann, Interacting macromolecules (Academic Press, New York, 1970).
[13] O. Lamm, Arkin. Mat. Astron. Fysik. 21B (1929) 2.
[14] M. Dishon, G.H. Weiss and D.A. Yphantis, Biopolymers 4 (1966) 449, 457.
[15] D.J. Cox, Arch. Biochem. Biophys. 129 (1969) 106.
[16] H. Vink, Acta Chem. Scand. 18 (1964) 409.
[17] R.F. Steiner, Arch. Biochem. Biophys. 49 (1954) 400.
[18] H.K. Schachman, Ultracentrifugation in biochemistry (Academic Press, 1959).
[19] G. Kegeles, L. Rhodes and J.L. Bethune, Proc. Natl. Acad. Sci. 58 (1967) 45.
[20] L.F. TenEyck and W. Kauzman. Proc. Natl. Acad. Sci. 58 (1967) 888.
[21] R. Josephs and W.F. Harrington, Proc. Natl. Acad. Sci. 58 (1967) 1587.
[22] L.J. Gosting, Adv. Prot. Chem. 11 (1956) 429.
[23] L.D. Harris, Numerical methods using Fortran (Columbus, Ohio, Charles E. Merrile Book, 1964) p. 149.
[24] P.W. Chun and S.J. Kim, Biochemistry 8 (1969) 1633.
[25] P.W. Chun and S.J. Kim, Biochemistry 9 (1970) 1957.
[26] P.W. Chun, S.J. Kim, C.A. Stanley and G.K. Ackers, Biochemistry 8 (1969) 1625.
[27] E.T. Adams Jr., Biochemistry 4 (1965) 1646.
[28] E.T. Adams Jr., Biochemistry 4 (1965) 1655.

PHYSICAL CHEMICAL STUDIES OF SHORT-CHAIN LECITHIN HOMOLOGUES. IV. A SIMPLE MODEL FOR THE INFLUENCE OF SALT AND THE ALKYL CHAIN LENGTH ON THE MICELLAR SIZE

R.J.M. TAUSK and J.Th.G. OVERBEEK
Van 't Hoff Laboratory, State University, Utrecht, The Netherlands

Received 21 February 1974

A simplified association model for micellisation is presented. In this model two features are incorporated: (a) There is an optimum for the change of the standard free energy per monomer upon micellisation at a certain association number. (b) At higher association numbers this free energy change becomes constant. The resulting equations for the dependence of the average micellar weight on the concentration are used to explain the experimentally observed effects of a salting-out agent (NaCl) and of the alkyl chain length of dihexanoyl-, diheptanoyl- and dioctanoyl-lecithin.

1. Introduction

In a previous paper, part II of the series [1], we found that the micellar size of dihexanoyllecithin (diC_6-) increased only slightly with the lecithin concentration, whereas the concentration dependence of the diheptanoyllecithin micellar size was more pronounced. In part III [2] we saw that the diC_8- micellar weight increased very steeply with the micellar concentration. We also noted that a salting-out agent (NaCl) increased the steepness of the micellar weight-concentration curve. In this paper we explain these phenomena semiquantitatively with the help of the multiple equilibrium model [3–5]. More specifically we worked out a modified open association model, based upon the work of Mukerjee [5].

2. Association model

2.1. Equations

One of the characteristic properties of many aqueous micellar solutions is the absence of appreciable amounts of aggregates with very low association numbers (i), except for some cases where the presence of dimers has been suggested [6]. This means that the association constants (k_i) for low values of i are relatively small. At infinite dilution k_i is defined by

$$k_i = C_i/(C_{i-1}C_1); \qquad i = 2, 3, \ldots \tag{1}$$

where C_i equals the molar concentration of the i-mer. At higher concentrations eq. (1) still holds if the activity coefficient f_i of each micellar species (and of the monomers) is given by [1, 2]

$$\ln f_i = M_i(B_1 C + B_2 C^2 + \ldots) . \tag{2}$$

B_1 and B_2 are constants. C is the total solute concentration. It depends on the behaviour of k_i as a function of i whether the micellar size distribution will be wide or narrow. If the association constants for high i are all comparable in value the distribution will be wide and the average micellar size will increase with the micellar concentration. In the "open association model" k_i is assumed to be independent of i. This implies that the standard free energy change of micellisation per monomer is independent of the association number. Such a behaviour can indeed be expected for large non-ionic micelles, where the shape strongly departs from the spherical. For smaller micelles we would expect k_i to depend on i: k_i will probably increase with i up to a

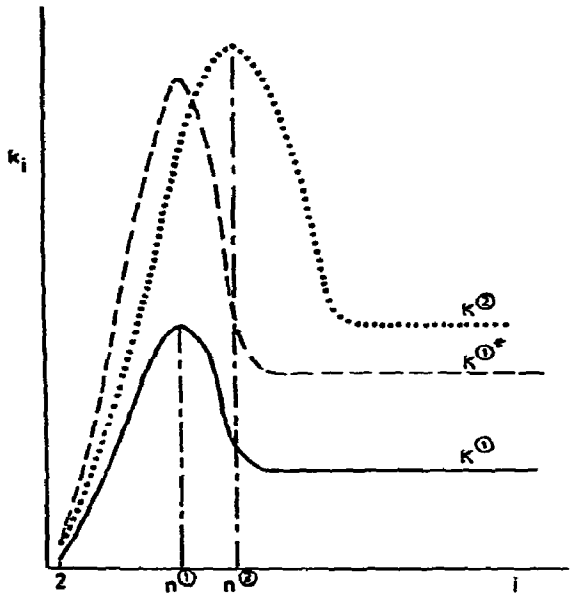


Fig. 1. A schematic picture of the dependence of the association constant k_i on the association number i. The fully drawn line represents the dependence for homologue 1 in salt free solutions. After addition of a salting-out agent the broken line (– – –) is obtained. The dotted line (· · ·) represents the dependence in salt free solutions for a higher homologue.

certain value of i, where energetically favourable micelles are formed. In an extreme model we might visualize the smallest possible micelle to be a sphere with little hydrocarbon–water contact. These micelles may further grow to disks, oblate or prolate ellipsoids or cylinders if the surfactant concentration is increased. k_i might have a pronounced maximum at a certain value of i, where we assume a transition from "small" to " large" micelles. We will denote this association number by n. For nonionic surfactants, such as our zwitterionic lecithins, we may assume the value for n to be determined primarily by geometrical parameters of the monomer molecule.

In fig. 1 a general picture of the dependence of k_i on the association number is presented.

In the following derivations a sharp transition between the small and the large micelles (where all association constants are taken to be equal) is assumed. This modified open association model results in

$$K_n = C_n/(C_1)^n = \prod_{i=2}^{n} k_i \tag{3}$$

and

$$K = C_{n+j}/(C_{n+j-1}C_1). \tag{4}$$

We now assume the concentrations of the micelles with $i < n$ to be negligible, that is we assume all $k_i\,(i<n)$ to be small and k_n to be very large so that $K_n = \Pi_{i=2}^{n} k_i$ obtains a suitable finite value.

The equivalent micellar concentration $E-C_1$ (micellar concentration expressed in amounts monomer per unit volume) and the weight average micellar association number N_w are found from

$$E - C_1 = \sum_{i=2}^{\infty} iC_i = \sum_{i=n+1}^{\infty} iC_i + nC_n \tag{5}$$

and

$$N_w = \frac{\Sigma_{i=2}^{\infty} i^2 C_i}{E - C_1} = \frac{\Sigma_{i=n+1}^{\infty} i^2 C_i + n^2 C_n}{E - C_1}. \tag{6}$$

Using eq. (4) and solving the resulting binomial series, in analogy to Mukerjee's procedure [5], we obtain

$$E - C_1 = C_n\left(\frac{n}{1-X} + \frac{X}{(1-X)^2}\right) \tag{7}$$

and

$$N_w = n + \frac{X}{1-X} + \frac{X}{(1-X)^2[n + X/(1-X)]} \tag{8}$$

where $X = KC_1$. (9)

At high concentrations in a polydisperse micellar system the following approximation will be valid: $X = 1-\partial$ with ∂ approaching zero as the concentration increases.

Using this approximation for $\partial \ll 1/n$ and combining eqs. (3), (7) and (8) we find

$$\begin{aligned} N_w &= 2(K^{n-1}/K_n)^{1/2}[(E-C_1)/C_1]^{1/2} \\ &= 2(K/K_1)^{(n-1)/2}(c_m/c_1)^{1/2}, \end{aligned} \tag{10}$$

where c_m equals the total micellar concentration in mass per unit volume and c_1 is the monomer concentration ($\approx$ CMC). K_1 is the geometric average of the

association constants for the small micelles

$$K_1 = \left(\prod_{i=2}^{n} k_i\right)^{1/(n-1)} \qquad (11)$$

Eq. (10) is analogous to Mukerjee's [5] eq. (26); only the proportionality factor is different: Mukerjee explicitly used $n = 2$.

2.2. Salt effects

The main influences of added electrolytes on the association properties of nonionic detergents originate from salting-out and salting-in effects [7, 8]. If n is mainly determined by geometrical factors it should be reasonably independent of the salt concentration. In this case we must look for possible effects of the salt on K/K_1. One may expect that the net effect of addition of salt is due to salting-out of the hydrocarbon part of the free monomer molecule (effects on the micelles cancel each other to a great extent in the calculation of the association constants), leading to an increase of the standard free energy of micellisation per monomer which is independent of the micellar size. This results in an increase of all association constants k_i by the same factor f as shown in fig. 1 (broken line).

$$k_i^* = k_i f \quad \text{(for all values of } i \geq 2) \qquad (12)$$

and also

$$K_1^* = K_1 f. \qquad (13)$$

If this is correct eq. (10) shows that the weight average micellar weight at a given value of c_m/c_1 is independent of the salt concentration. The monomer concentration c_1^* ($\approx$ CMC*) will of course be lowered by a factor f with respect to c_1 (in salt free solutions).

2.3. Influence of the hydrocarbon chain length

Geometrical factors will undoubtedly lead to an increase of n with increasing chain length. K and K_1 will also increase. The dependence of K/K_1 on the chain length is, however, more complicated.

The area per molecule measured at the surface of the hydrocarbon core of densely packed spherical micelles with a diameter proportional to the chain length is independent of the chain length. In larger elongated micelles of the same packing density and diameter the area per molecule will be smaller than in the case of spherical micelles. Therefore the packing of the parts of the chain close to the head groups will be more constrained (smaller number of possible configurations) for large micelles than for small ones. On elongating the chains this effect will become relatively less important, leading to an increase of K/K_1 with increasing chain length (see dotted curve in fig. 1).

For ionic surfactants the repulsive forces are thought to reside mainly in the polar parts, which extend away from the hydrocarbon core surface. The area per head group, measured at some distance outside the core, in small densely packed spherical micelles decreases on elongation of the alkyl chain length. The repulsive forces will therefore increase with the chain length. The area per head group in elongated micelles will be less dependent on the chain length. K/K_1 will therefore increase for ionic surfactants. For zwitterionic micelles the situation is more complicated since depending on the orientation of the dipoles attractive or repulsive forces exist. A decrease in the area per head group changes the electrostatic interactions and the number of possible configurations of the polar parts. Probably the radius of curvature of the micellar surface is also very important. A general rule for the dependence of K/K_1 on the chain length is difficult to derive.

A slight increase of K/K_1 together with the increase in n will lead to a much steeper increase of N_w with $(c_m/c_1)^{1/2}$ for higher surfactant homologues.

3. Interpretation of the experimental data in terms of this association model

We will now apply this association model to the results of the micellar weight determinations given in part II and III of this series [1, 2]. In fig. 2 we have plotted the weight average association number of the three homologues (diC_6-, diC_7-, diC_8-) as a function of $(c_m/c_1)^{1/2}$. On the basis of these data, n, K and K_1 can in principal be determined. The accurate evaluation, especially of n and K_1 is hampered by the uncertainties in the thermodynamic nonideality and the difficulties of measuring at low micellar concentrations.

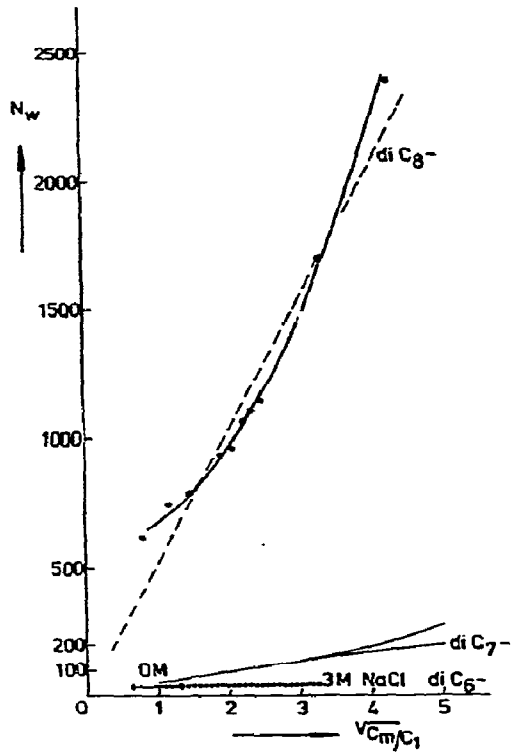


Fig. 2. The idealised weight average association number for three lecithin homologues as a function of the square root of the ratio of the micellar and monomer concentration. The data were taken from parts II and III of this series [1, 2]. The broken line for diC$_8$- was calculated from $N_w = 2.38 \times 10^7/526.5\ (c_m)^{1/2}$ (the first term from the curve fitting performed in part III [2]). The two lines for diC$_7$- originate from two micellar models (part II [1], fig. 15, curve I and II). The fully drawn line for diC$_6$- refers to NaCl free solutions while the dotted line refers to solutions containing 3M NaCl.

Dihexanoyllecithin. The weight average micellar weight increases slightly with the micellar concentration. The system is therefore relatively monodisperse and because $X = KC_1$ is too small compared to unity the approximate eq. (10) cannot be applied (a numerical value for X will be given later on). The parameters n, K and K_1 were therefore obtained by numerical curve fitting procedures (least squares) using eqs. (3), (7) and (8). The experimental data were first corrected for nonideality using the excluded volume of rigid non-interacting particles [1]. The geometrical model in which all micelles are assumed to be spheres (part II, model I, fig. 11) is incompatible with this association model (polydisperse system with k_i independent of i for $i > n$). We therefore used the data where the micelles were visualised as spherocylinders with little hydrocarbon–water contact. The two sets of values for the parameters n, K and K_1, given in table 1 (*a*) and (*b*), were calculated using outer radii of 15Å and 18Å respectively (part II, model II, figs. 13 and 14). From table 1 we also see that addition of 3M NaCl has virtually no influence on n and K/K_1 in accordance with our assumptions (section 2.2).

In NaCl free solutions the monomer concentration (≈CMC) is largely determined by K_1 and is around 7 mg/ml [1, 8]. With $K = 56$ ℓ mole^{-1} we find X to be 0.83 ($M = 471.5$). The standard free energy of micellisation per monomer (ΔG°) is in this case calculated from $-[RT(n-1)/n] \ln K_1$. For the higher homologues the monomer concentration rapidly approaches $1/K$ leading to $\Delta G^\circ = -RT \ln K$. Since K_1 is smaller than K we would expect the difference in ΔG° between diC$_7$- and diC$_6$- to be larger than the difference between successive higher homologues. This effect has indeed been observed (part I of this series, fig. 5) [8].

Diheptanoyllecithin. In our previous paper [1] we already saw that a plot of N_w versus $(c_m/c_1)^{1/2}$ was essentially independent of the salt concentration (part II, figs. 16 and 17). Using eqs. (3), (7) and (8) we can in principle find values for n, K and K_1, but many different combinations of values give virtually the same micellar weight-concentration dependence except for the very low concentration range ($c_m/c_1 \leqslant 1$) where the experimental accuracy is low. The data given in table 1 were obtained using the two micellar models (for the calculation of the excluded volume): (*c*) compact spherocylindrical micelles with radii of 19Å, which disregards the hydrocarbon–water interface (part II, model I, fig. 15, curve I) and (*d*) micelles with radii of 16Å and hydrocarbon cores (core radius 9.1Å) with as little water contact as possible (part II, model II, fig. 15, curve II). Especially in this latter case the range of applicable values n and K_1 is very large. The two limiting sets of data are given in table 1 (diC$_7$-*d*). The results from the micellar model with outer radii of 19Å and little hydrocarbon–water contact (core radius 9.1Å) are incompatible with the present association model, since the curve of N_w versus $(c_m/c_1)^{1/2}$ is curved upwards (part II, fig. 17). This

Table 1
Parameters of the association model for three lecithin homologues

Lecithin	NaCl conc. (mole ℓ^{-1})	K (ℓ mole^{-1})	K/K_1	n
diC_6- (*a*)	–	58	1.05 (± 0.02)	28.0 (∓ 0.4)
	3	332	1.055 (± 0.01)	27.2 (∓ 0.4)
diC_6- (*b*)	–	60	1.107 (± 0.01)	26.9 (∓ 0.5)
	3	337	1.09 (± 0.01)	26.2 (∓ 0.6)
diC_7- (*c*)	–	700	1.22 (± 0.01)	30.9 (∓ 1)
diC_7- (*d*)	–	700 {	> 1.25 < 679	< 29.7 > 2
diC_8-	–	4050 {	> 1.1 <66400	<117 > 2

The errors in K are about 5 to 10% and stem from the inaccuracy of the CMC determinations [1, 2, 8]. The errors in brackets in column 4 and 5 give the coupled ranges of acceptable values for K/K_1 and n.

effect may be due to the neglect of higher virial terms.

Dioctanoyllecithin. In this case eq. (10) is, for low values of n, a very good approximation of the combined eqs. (3), (7) and (8) and the range of applicable combinations of n and K_1 is therefore still larger. The two limiting sets are again given in table 1. Assuming for instance n to equal 40 or 30 we obtain K/K_1 to be 1.33 or 1.26 respectively. These values seem in the right order of magnitude as compared to the results from dihexanoyl- and diheptanoyllecithin.

4. Conclusions

The association model elaborated in this paper fits all our experimental observations regarding the influence of added salt and the chain length on the concentration dependence of the micellar weight of the lecithin homologues. Accurate determination of n from the theory is only possible if experiments are extended to micellar concentrations which are low in respect to the CMC, which was impossible for dioctanoyllecithin. Analysis on diheptanoyllecithin is hampered by the large influence of uncertainties in the thermodynamic nonideality corrections.

References

[1] R.J.M. Tausk, J. van Esch, J. Karmiggelt, G. Voordouw and J.Th.G. Overbeek, Biophys. Chem. 1 (1974) 184, see also Erratum, Biophys. Chem. 1 (1974) 396.
[2] R.J.M. Tausk, C. Oudshoorn and J.Th.G. Overbeek, Biophys. Chem. 2 (1974) 53.
[3] J.M. Corkill, J.F. Goodman, T. Walker and J. Wyer, Proc. Roy. Soc. A312 (1969) 243.
[4] J.G. Watterson and H.G. Elias, Kolloid Z.Z. Polym. 249 (1971) 1136.
[5] P. Mukerjee, J. Phys. Chem. 76 (1972) 565.
[6] P. Mukerjee, Adv. Coll. Interf. Sci. 1 (1967) 241.
[7] P. Mukerjee, J. Phys. Chem. 69 (1965) 4038.
[8] R.J.M. Tausk, J. Karmiggelt, C. Oudshoorn and J.Th.G. Overbeek, Biophys. Chem. 1 (1974) 175.

BIOPHYSICAL CHEMISTRY 2 (1974) 180–184. © NORTH-HOLLAND PUBLISHING COMPANY

RADIAL MIGRATION OF DNA MOLECULES IN CYLINDRICAL FLOW.

I. THEORY OF THE FREE-DRAINING MODEL

Richard H. SHAFER, Nora LAIKEN and Bruno H. ZIMM
Department of Chemistry, Revelle College,
University of California (San Diego), La Jolla, California 92037, USA

Received 16 May 1974

Inward radial migration of large DNA molecules undergoing concentric-cylinder shear flow has been previously observed in this laboratory during measurements of viscoelastic retardation times. In this paper a theoretical treatment of this effect is presented in the framework of the bead-spring model of polymer molecules. Equations of motion of the diffusion type are solved for the free-draining polymer in a solvent undergoing Couette flow. The results show an inward radial motion, essentially due to the curvilinear solvent flow field.

1. Introduction

Molecular weights of large DNA molecules have been recently determined by measuring the viscoelastic relaxation or recovery of solutions of such molecules from mechanical shear stress [1]. In these measurements, the solution is placed in the annular region between two concentric cylinders (the inner cylinder is actually a fully submerged rotor that floats in the solution). A magnetic field is used to rotate the inner cylinder, thereby creating a shear force that deforms or stretches the DNA molecules. When the field is turned off, the inner cylinder rotates in the opposite direction due to the recoil, or relaxation, of the previously stretched molecules. The molecular weight may be determined from the retardation times [2] which can be determined from the rotor motion as the molecules relax from their stretched configurations.

The phenomenon investigated in this and the following paper [6] was observed by Dr. Elliot Uhlenhopp in this laboratory while measuring retardation times of single-stranded DNA molecules from lysates of human lymphoblast cells. He noticed that if the rotor was removed from the solution after having been rotated for a long time by the magnetic field there was a highly viscoelastic liquid that surrounded, and stuck to, the rotor. This was not observed if the rotor was not rotated before being removed from the solution.

We show in this and the following paper that this effect can be theoretically predicted as the result of inward radial migration of DNA molecules due to the curvilinear shear flow in the concentric-cylinder apparatus. The large molecules move towards the inner cylinder, thus creating a concentrated and highly viscoelastic solution in the immediate region of the rotor.

In this paper, we treat the case of the free-draining polymer using the bead-spring model employed previously [2]. In the following paper we show that the non-draining polymer also develops an inward radial velocity that is highly dependent on the size, or molecular weight, of the polymer. We then discuss normal stress effects, and finally we discuss two applications presently being pursued experimentally in this laboratory:

1. The use of the molecular weight dependence of the radial velocity as a basis for a method to separate DNA molecules in solution according to size.

2. The study of normal stress differences as a method for determining the molecular weight of large DNA molecules in solution.

2. Calculation of inward radial motion in concentric-cylinder geometry

2.1. Basic assumptions

We consider steady Couette flow, in which the solution of interest is placed in the annular gap between two concentric cylinders. The inner cylinder has radius R_1 and the outer cylinder has radius R_2. The absolute value of the angular velocity of the inner cylinder is denoted by Ω. Let the inner cylinder rotate in the clockwise direction with angular velocity Ω rad/s (counter-clockwise rotation would be described by $-\Omega$ rad/s) while the outer cylinder remains stationary. The steady velocity field of the solvent, in the absence of any polymer molecules, is assumed to be, in cylindrical coordinates, r, θ, z, centered on the cylinders,

$$v_\theta = w(r), \quad v_r = v_z = 0,$$

with the boundary conditions

$$w(R_1) = \Omega \text{ (clockwise rotation)},$$

$$w(R_2) = 0.$$

The solvent is considered a continuum with each point moving at a constant circular speed $rw(r)$. In addition we assume the solvent to be a simple, incompressible newtonian fluid that satisfies the stress–strain relationship

$$\mathbf{T} = -p\mathbf{1} + 2\eta\mathbf{D}, \tag{1}$$

where $\mathbf{T}$ and $\mathbf{D}$ are the stress and rate-of-deformation tensors, respectively, $\mathbf{1}$ the unit tensor, p the thermodynamic pressure [$p = (-1/3)\,\mathrm{Tr}\,\mathbf{T}$], and η is the (constant) viscosity of the solvent. For this fluid, $w(r)$ is given by [3]

$$w(r) = \frac{\Omega R_1^2}{R_2^2 - R_1^2}\left(\frac{R_2^2}{r^2} - 1\right). \tag{2}$$

Following ref. [3], the shear rate, K, is given by

$$K(r) = |rw'(r)| = 2\Omega R_1^2 R_2^2/(R_2^2 - R_1^2)r^2. \tag{3}$$

We will always consider angular speeds, Ω, small enough so that centrifugal effects are negigible.

2.2. Description of coordinate system

The motion of a solute molecule in the annular gap is calculated with respect to a local cartesian coordinate system whose origin, O, is fixed at some radius R, as indicated in fig. 1.

The polymer molecule is assumed to occupy a small neighborhood surrounding the origin. The local coordinates of the point P, whose cylindrical coordiantes are (r, θ, z) in fig. 1, are

$$x = r\sin\theta, \quad y = r\cos\theta - R, \quad z = z. \tag{4}$$

Define a new variable s by the relation

$$s = r - R. \tag{5}$$

Since the magnitude of s is of the order of molecular dimensions,

$$s/R \ll 1. \tag{6}$$

We then have

$$x = (R + s)\sin\theta, \quad y = (R + s)\cos\theta - R, \tag{7}$$

and since θ is always small, the trigonometric functions can be expanded in their power series, retaining only the leading terms,

$$x \approx (R + s)\theta, \quad y \approx s. \tag{8}$$

For clockwise rotation of the inner cylinder, the local cartesian coordinates of the velocity of the solvent at the point P are

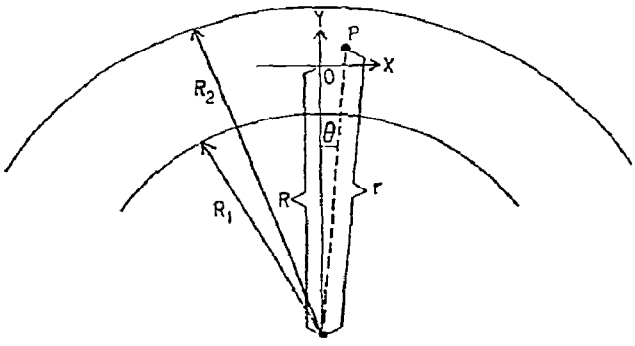


Fig. 1. Diagram of local cartesian coordinate system.

$$v_x = rw(r)\cos\theta \approx rw(r),$$
$$v_y = rw(r)\sin\theta = xw(r), \tag{9}$$
$$v_z = 0.$$

Further, $rw(r)$ can be written, for $s/R \ll 1$, as

$$rw(r) = \frac{\Omega R_1^2}{R_2^2 - R_1^2}\left[\frac{R_2^2}{R}\left(1 - \frac{s}{R} + \dots\right) - r\right] \tag{10}$$

$$\approx \frac{\Omega R_1^2}{R_2^2 - R_1^2}\left[R\left(\frac{R_2^2}{R^2} - 1\right) - s\left(\frac{R_2^2}{R^2} + 1\right)\right]. \tag{11}$$

Using eq. (8), we have

$$v_x = \gamma R - \gamma_1 y, \tag{12}$$

where

$$\gamma = \frac{\Omega R_1^2}{R_2^2 - R_1^2}\left(\frac{R_2^2}{R^2} - 1\right);$$
$$\gamma_1 = \frac{\Omega R_1^2}{R_2^2 - R_1^2}\left(\frac{R_2^2}{R^2} + 1\right). \tag{13}$$

Similarly, for v_y we obtain

$$v_y = \gamma x - \gamma_2 xy, \tag{14}$$

where

$$\gamma_2 = 2\Omega R_1^2 R_2^2/(R_2^2 - R_1^2)R^3. \tag{15}$$

The uperturbed solvent velocity field in the neighborhood of the molecule is summarized by

$$v_x = \gamma R - \gamma_1 y, \quad v_y = \gamma x - \gamma_2 xy, \quad v_z = 0. \tag{16}$$

2.3. Equations of motion and the bead-spring model

We consider an ensemble of non-interacting polymer molecules, i.e., a dilute solution. The bead-spring model for large, random-coil polymers is used, each polymer consisting of $N + 1$ beads connected by N hookean springs, each with a force constant $3kT/b^2$, where b is the root mean square length of a spring. All the interactions with the solvent occur at the beads, each of which has a frictional coefficient ρ.

The dynamics of such a system has been formulated in detail previously [2], so we will note the main results very briefly. The frictional force due to the motion of the beads with respect to the solvent is balanced by the sum of the spring forces and the "force" due to brownian motion. Thus, for the y-component of motion of the jth bead, we have

$$\rho(\dot{y}_j - v'_{yj}) = -k_B T\,\partial \ln\psi/\partial y_j - (3k_B T/b^2)(-y_{j+1} + 2y_j - y_{j-1}), \tag{17}$$

where $\dot{y}_j$ is the y-component of velocity of the jth bead, v'_{yj} the velocity the solvent would have at the position of the jth bead if that bead alone were absent, k_B is Boltzmann's constant and ψ is the distribution function due to brownian motion. Appropriate changes in eq. (17) must be made for $j = 0$ and $j = N$. We assume the Kirkwood–Riseman approximation [4] to the Oseen interaction tensor to give

$$v'_{yj} = v_{yj} + \sum_{j \neq k} T_{jk} F_{ky}, \tag{18}$$

where v_{yj} is the velocity of the unperturbed solvent, the force F_{ky} is either side of eq. (17) and

$$T_{jk} = 1/\{(6\pi^3)^{1/2}\eta b(|j - k|)^{1/2}\}; \tag{19}$$

η is the solvent viscosity.

The equations of motion are most compactly written in matrix form. We define the $N + 1$ dimensional column vectors $\boldsymbol{x}, \dot{\boldsymbol{x}}, \boldsymbol{v}_x$, $\partial/\partial\boldsymbol{x}$ and similarly for y and z, where

$$\boldsymbol{x} = \begin{pmatrix} x_0 \\ x_1 \\ x_2 \\ \vdots \\ x_N \end{pmatrix}, \text{ etc.}$$

The two matrices $\mathbf{H}$ and $\mathbf{A}$ are defined by

$$(\mathbf{H})_{ij} = \rho T_{ij}, \quad i \neq j; \quad (\mathbf{H})_{ii} = 1, \tag{20}$$

and

$$\mathbf{A} = \begin{pmatrix} 1 & -1 & 0 & 0 & 0 & \cdots \\ -1 & 2 & -1 & 0 & 0 & \cdots \\ 0 & -1 & 2 & -1 & 0 & \cdots \\ 0 & 0 & -1 & 2 & -1 & 0 \cdots \\ \cdot & \cdot & \cdot & \cdot & \cdot & \cdots \end{pmatrix} \tag{21}$$

The equation of motion in the y-direction is, from eq. (17)

$$\dot{y} = v_y - D\,\mathbf{H}\cdot(\partial/\partial y)\ln\psi - \sigma\,\mathbf{H}\cdot\mathbf{A}\,y, \tag{22}$$

where $D = k_B T/\rho$ and $\sigma = 3k_B T/b^2\rho$. Similar results hold for the x- and z-components.

We focus on the y-direction motion of the molecules as a whole, which is obtained by averaging eq. (22) over the distribution function ψ which can be calculated from eq. (17) of ref. [2]. As we are interested in the steady-state solution, we seek the average motion over the time-independent distribution function. If g denotes any dynamical variable, then the ensemble average of g is written as $\langle g\rangle$ and defined by

$$\langle g\rangle = \int g\,\psi\,\mathrm{d}x_0\,\mathrm{d}x_1 \ldots \mathrm{d}z_n. \tag{23}$$

The dynamical behavior is determined by transforming to a set of normal coordinates, discussed in detail previously [2]. Let the $N+1$ eigenvalues and eigenvectors of the matrix $\mathbf{H}\cdot\mathbf{A}$ be denoted by λ_k and α_k, respectively. The α_k form the $N+1$ column vectors of a matrix $\mathbf{\Omega}$ such that

$$\mathbf{\Omega}^{-1}\cdot\mathbf{H}\cdot\mathbf{A}\cdot\mathbf{\Omega} = \mathbf{\Lambda}, \tag{24}$$

where $\mathbf{\Lambda}$ is diagonal with elements λ_k. $\mathbf{A}$ is then diagonalized by the congruent transformation,

$$\mathbf{\Omega}^{\mathrm{T}}\cdot\mathbf{A}\cdot\mathbf{\Omega} = \mathbf{M}, \tag{25}$$

where $\mathbf{M}$ is diagonal with elements μ_k. Finally $\mathbf{H}$ is diagonalized by

$$\mathbf{\Omega}^{-1}\cdot\mathbf{H}\cdot(\mathbf{\Omega}^{-1})^{\mathrm{T}} = \mathbf{M}^{-1}\cdot\mathbf{\Lambda} = \mathbf{N}, \tag{26}$$

where $\mathbf{N}$ is diagonal with elements $\nu_k = \lambda_k/\mu_k$.

The normal coordinate transformation is then given by

$$\begin{aligned} &x = \mathbf{\Omega}\cdot\xi, \quad \xi = \mathbf{\Omega}^{-1}\cdot x, \\ &\partial/\partial x = (\mathbf{\Omega}^{-1})^{\mathrm{T}}\cdot\partial/\partial\xi, \quad \partial/\partial\xi = \mathbf{\Omega}^{\mathrm{T}}\cdot\partial/\partial x, \end{aligned} \tag{27}$$

and similarly for y, η and z, ζ. Applying this transformation to eq. (22) we obtain

$$\dot{\eta} = v_\eta - D\mathbf{N}\cdot(\partial/\partial\eta)\ln\psi - \sigma\mathbf{\Lambda}\cdot\eta, \tag{28}$$

where

$$v_\eta = \mathbf{\Omega}^{-1}\cdot v_y. \tag{29}$$

Let the row vectors of $\mathbf{\Omega}^{-1}$ be denoted by β_k^{T}. Then in the previous work [2] it was shown that the center of resistance (center of mass in the free-draining polymer) has the coordinates (x_{cr}, y_{cr}, z_{cr}) where

$$x_{cr} = N^{-1/2}\xi_0, \quad y_{cr} = N^{-1/2}\eta_0, \quad z_{cr} = N^{-1/2}\zeta_0. \tag{30}$$

Here $\xi_0 = \beta_0^{\mathrm{T}}\cdot x$, $\eta_0 = \beta_0^{\mathrm{T}}\cdot y$ and $\zeta_0 = \beta_0^{\mathrm{T}}\cdot z$. Hence the translational motion of the molecule as a whole, in the y-direction, is determined by the zeroth component of eq. (28). Since $\lambda_0 = 0$, we have

$$\dot{\eta}_0 = v_{\eta 0} - D\,\nu_0\,(\partial/\partial\eta_0)\ln\psi. \tag{31}$$

Furthermore, we place the center of resistance of the polymer at the origin of our coordinate system so that $\dot{y}_{cr}$, the velocity of the center of resistance in the y-direction, describes the radial motion of the whole molecule. Averaging eq. (31) over ψ and using eq. (30), we have

$$\langle\dot{y}_{cr}\rangle = N^{-1/2}\langle\dot{\eta}_0\rangle = N^{-1/2}\langle v_{\eta 0}\rangle. \tag{32}$$

Referring to eqs. (16) and (29) and using the fact that the center of resistance is at the origin, we can write eq. (32) as

$$\langle\dot{y}_{cr}\rangle = -N^{-1/2}\gamma_2\langle\beta_0^{\mathrm{T}}\cdot xy\rangle, \tag{33}$$

where

$$xy = \begin{pmatrix} x_0 y_0 \\ x_1 y_1 \\ \vdots \\ x_N y_N \end{pmatrix}$$

is a column vector.

In order to proceed further, we must obtain the eigenvalues λ_k and the eigenvectors α_k from the equation

$$\mathbf{H}\cdot\mathbf{A}\,\alpha_k = \lambda_k\,\alpha_k. \tag{34}$$

Following ref. [2], we convert from a discrete representation to a continuous one, by writing the lth component of the kth eigenvector as

$$\alpha_{kl} = (2/N)^{1/2}\,\alpha_k(s), \tag{35a}$$

and

$$\beta_{kl} = (2/N)^{1/2}\,\beta_k(s), \tag{35b}$$

where

$$s = 2l/N - 1. \tag{36}$$

The sum over k, Σ_k, becomes $\frac{1}{2}N\int_{-1}^{+1} ds$, and eqs. (35) become [5]

$$\alpha_k''(r) + h\int_{-1}^{+1} \alpha''(s)\,(|r-s|)^{-1/2}\,ds = -\tfrac{1}{4}N\lambda_k\,\alpha_k(r), \tag{37}$$

where

$$h = N^{1/2}\rho/(12\pi^3)^{1/2}\,b\eta\,, \tag{38}$$

with the boundary condition $\alpha_k'(\pm 1) = 0$.

We consider in this paper the case $h = 0$ which corresponds to the free-draining limit. In this case, $\beta_0(r) = 2^{-1/2}$ and we have

$$\beta_0 \cdot xy = (1/N)^{1/2}\sum_k\sum_l \xi_k\,\eta_l \int_{-1}^{+1} \alpha_k(r)\,\alpha_l(r)\,dr, \tag{39}$$

where we have used the continuous representation for $x = \Omega\cdot\xi$ and $y = \Omega\cdot\eta$ given by

$$x(r) = (2/N)^{1/2}\sum_k \alpha_k(r)\,\xi_k\,,$$
$$y(r) = (2/N)^{1/2}\sum_k \alpha_k(r)\,\eta_k\,. \tag{40}$$

Since the free-draining eigenfunctions form an orthonormal basis set, eq. (39) with (33) leads to

$$\langle\dot{y}_{cr}\rangle = -(1/N)\,\gamma_2\sum_k\langle\xi_k\,\eta_k\rangle\,, \tag{41}$$

where the average quantity,

$$\langle\xi_k\,\eta_k\rangle = J\int \xi_k\,\eta_k\,\psi\,d\xi_0\,d\xi_1\ldots d\zeta_N, \tag{42}$$

and J is the absolute value of the jacobian determinant of the transformation to normal coordinates. Recalling eq. (15), we note the dependence of $\langle\dot{y}_{cr}\rangle$ on the curvature of the apparatus.

In the following paper, the averages in eq. (41) are computed, the calculations are extended to the non-draining polymer, and the results and applications are more fully discussed.

Acknowledgements

The authors are grateful to the National Institutes of Health for support of this work through postdoctoral fellowships to N.L. and R.H.S. and Grant GM 11916 and to the American Cancer Society for aid through Grant # PF-873 to R.H.S.

References

[1] R.E. Chapman, Jr., L.C. Klotz, D.S. Thompson and B.H. Zimm, Macromolecules 2 (1969) 637; L.C. Klotz and B.H. Zimm, Macromolecules 5 (1972) 471; J. Mol. Biol. 72 (1972) 779.
[2] B.H. Zimm, J. Chem. Phys. 24 (1956) 269.
[3] B.D. Coleman, H. Markowitz and W. Noll, Viscometric flows of non-newtonian fluids (Springer-Verlag, New York, 1966).
[4] J.C. Kirkwood and J. Riseman, J. Chem. Phys. 16 (1948) 565.
[5] A revised version that takes more accurate account of the singularities in the matrix $\mathbf{H}\cdot\mathbf{A}$ is presented in: K. Osaki, Macromolecules 5 (1972) 141. For the two limits, $h = 0$ and $h \gg 1$, eq. (37) gives correct results.
[6] R.H. Shafer, Biophys. Chem. 2 (1974) 185–188.

BIOPHYSICAL CHEMISTRY 2 (1974) 185–188. © NORTH-HOLLAND PUBLISHING COMPANY

RADIAL MIGRATION OF DNA MOLECULES IN CYLINDRICAL FLOW.

II. THE NON-DRAINING MODEL AND POSSIBLE APPLICATION TO FRACTIONATION

Richard H. SHAFER
Department of Chemistry, Revelle College,
University of California (San Diego), La Jolla, California 92037, USA

Received 16 May 1974

The radial-migration calculation of the preceding paper is extended to the non-draining polymer. The results show an inward radial velocity that depends on the 5/2 power of the molecular weight, assuming gaussian statistics for the chain. This sensitivity to size serves as the basis for a method of separating DNA molecules in solution according to their size. Normal stress (Weissenberg) effects are also discussed.

1. Introduction

In the preceding paper [1], referred to as I hereafter, an expression for the radial velocity of a free-draining polymer undergoing shearing concentric-cylinder flow was derived. In this paper, we extend the calculation to the more realistic non-draining case and discuss normal stress effects. We propose a new method for separating DNA molecules in solution according to molecular weight and consider measuring normal stress differences as a means of determining molecular weight.

2. Calculation of radial migration

We start with eq. (33) of I, for the velocity of the center of resistance of the polymer molecule in the y-direction:

$$\langle \dot{y}_{cr} \rangle = -N^{-1/2} \gamma_2 \langle \beta_0^{\mathrm{T}} \cdot xy \rangle , \tag{1}$$

and consider the non-draining polymer, $h \gg 1$, where h is the draining parameter, defined in eq. (38) of I:

$$h = N^{1/2} \rho / (12\pi^3)^{1/2} b\eta . \tag{2}$$

In this case [2],

$$\beta_0(r) = \frac{\sqrt{2}\,\Gamma(5/4)}{\Gamma(1/2)\,\Gamma(3/4)} \frac{1}{(1-r^2)^{1/4}} , \tag{3}$$

where Γ is the gamma function, and

$$\beta_0^{\mathrm{T}} \cdot xy = \frac{2}{N^{1/2}} \frac{\Gamma(5/4)}{\Gamma(1/2)\,\Gamma(3/4)} \times \sum_k \sum_l \xi_k \eta_l \int_{-1}^{+1} \frac{\alpha_k(r)\,\alpha_l(r)}{(1-r^2)^{1/4}} \, \mathrm{d}r , \tag{4}$$

where the $\alpha_k(r)$ are the non-draining eigenfunctions. It will be shown later that the terms in eq. (4) with $k \neq l$ vanish upon taking the ensemble average with respect to the distribution function ψ, introduced in I. This gives the following expression for the radial velocity.

$$\langle \dot{y}_{cr} \rangle = \frac{-2\gamma_2}{N} \frac{\Gamma(5/4)}{\Gamma(3/4)\,\Gamma(1/2)} \times \sum_k \langle \xi_k \eta_k \rangle \int_{-1}^{+1} \frac{\alpha_k^2(r)}{(1-r^2)^{1/4}} \, \mathrm{d}r , \tag{5}$$

where $\langle \xi_k \eta_k \rangle$ is defined in eq. (42) of I.

The eigenfunctions, $\alpha_k(r)$, are expanded in a Fourier series, following Zimm et al. [3]

$$\alpha_k(r) = {}^k a_0 + \sum_{m=2}^{\infty} {}^k a_m \cos(\pi m r/2), \quad k \text{ and } m \text{ even},$$
$$\alpha_k(r) = \sum_{m=1}^{\infty} {}^k a_m \sin(\pi m r/2), \quad k \text{ and } m \text{ odd}. \tag{6}$$

The integrals in eq. (5) can all be evaluated analytically [4]. For example

$$\int_{-1}^{+1} \frac{\cos^2(\pi k r/2)}{(1-r^2)^{1/4}}\, dr \tag{7}$$
$$= \frac{1}{2}\left[\frac{\Gamma(1/2)\,\Gamma(3/4)}{\Gamma(5/4)} + \Gamma(3/4)\left(\frac{2\pi}{k}\right)^{1/4} J_{1/4}(\pi k)\right],$$

where $J_{1/4}$ is the Bessel function of the first kind of order 1/4.

Looking at both eq. (41) of I and eq. (5), we see that the radial motion is determined by the ensemble average of the normal coordinates, $\langle \xi_k \eta_k \rangle$. In order to evaluate these averages, the shear rate, K, is assumed to be constant over molecular dimensions, i.e., $K = K(R)$ is assumed to be independent of s. We may then replace the true distribution function ψ for Couette flow by the distribution function that describes simple shear (laminar) flow. The velocity field in simple shear flow is given by

$$v_x = Ky, \quad v_y = v_z = 0. \tag{8}$$

In this approximation, the required averages in steady flow are [2]

$$\langle \xi_k \eta_k \rangle = KD/2\mu_k \lambda_k \sigma^2, \quad k \neq 0,$$
$$\langle \xi_0 \eta_0 \rangle = 0, \quad \langle \xi_k \eta_l \rangle = 0, \quad k \neq l. \tag{9}$$

The factors appearing in eq. (9) are all defined in I.

Returning to the free-draining polymer, in which case $\mu_k = \lambda_k = \pi^2 k^2/N^2$, we obtain for the radial velocity

$$\langle \dot{y}_{cr} \rangle = -K \gamma_2 \rho b^4 N^3/1620\, k_B T. \tag{10}$$

For the non-draining polymer, $\lambda_k = (4h/N^2)\lambda'_k$, and λ'_k are tabulated in ref. [3]. The μ_k were calculated from eq. (10b) of ref. [3] and eq. (6) above. The Fourier series expansion in eq. (6) was carried out to $m = 7$, the required integrals computed analytically, and the final result is

$$\langle \dot{y}_{cr} \rangle = -0.00845\, \gamma_2 \eta K L^5/k_B T, \tag{11}$$

where $L = N^{1/2} b$ is the root mean square end-to-end length of the polymer molecule.

Using eqs. (3) and (15) of I, we obtain the relationship

$$\gamma_2 = K(R)/R. \tag{12}$$

Eqs. (10) and (11) can then be rewritten as

$$\langle \dot{y}_{cr} \rangle = \frac{-\rho b^4 N^3}{1620\, k_B T} \frac{K^2(R)}{R} \quad \text{(free-draining case)}, \tag{13}$$
$$= \frac{-0.00845\, \eta L^5}{k_B T} \frac{K^2(R)}{R} \quad \text{(non-draining case)}. \tag{14}$$

Thus in both cases the radial dependence is the same, and can be written as

$$K^2(R)/R = 4\Omega^2 R_1^4 R_2^4/(R_2^2 - R_1^2)^2 R^5. \tag{15}$$

and so

$$\langle \dot{y}_{cr} \rangle \propto \Omega^2/R^5. \tag{16}$$

Furthermore, in the non-draining case, since the molecular weight M is proportional to L^2 for this ideal gaussian chain, we have

$$\langle \dot{y}_{cr} \rangle \propto M^{5/2}. \tag{17}$$

Eq. (17) indicates that the radial velocity has a strong dependence on the molecular weight, or size, of the polymer molecule.

An average radial velocity, $\overline{\langle \dot{y}_{cr} \rangle}$, can be defined by averaging eq. (14) over the annular gap to give

$$\overline{\langle \dot{y}_{cr} \rangle} = -0.00563\, \Omega^2 R_1 R_2 \left[\frac{R_2^3 - R_1^3}{(R_2^2 - R_1^2)^3}\right] \frac{\eta L^5}{k_B T}. \tag{18}$$

As a sample calculation, consider an aqueous solution of DNA from *E. coli* with an estimated value for L of 1.2×10^{-3} cm [5]. With $R_1 = 2.3$ cm, $R_2 = 2.5$ cm, $\Omega = 2$ rad/s and at room temperature, the average radial velocity is $\overline{\langle \dot{y}_{cr} \rangle} = -3 \times 10^{-4}$ cm/s.

3. Radial pressure distribution ("Weissenberg effect")

When centrifugal effects are negligible, the pressure on the inner cylinder is greater than the pressure on the outer cylinder. Attributing this pressure gradient

in the fluid to the frictional force the polymer molecule exerts on the fluid as it moves towards the center, we can calculate the radial dependence of the pressure in the following manner: Consider a small surface element at some radius R and perpendicular to that radius, with area $R\,d\theta\,dz$. The number of molecules in a volume element including this surface element is $C_n R\,dR\,d\theta\,dz$ where C_n is the number density of molecules. The radial pressure, dP, exerted by these molecules is

$$dP = \bar{\rho} C_n \langle \dot{y}_{cr} \rangle dR\,, \tag{19}$$

where $\bar{\rho}$ is the translational frictional coefficient of the molecule as a whole. Again, we treat the two limiting classes of polymers:

1) *Free-draining polymer*: here, $\bar{\rho} = N\rho$ and eq. (41) of I becomes, with the aid of eq. (9),

$$\langle \dot{y}_{cr} \rangle = (-\gamma_2/N) \sum_k \langle \xi_k \eta_k \rangle$$

$$= [-2K^2(R) D/NR] \sum_k \tau_k^2\,, \tag{20}$$

where $\tau_k = 1/2\,\sigma\lambda_k$. Using the relationship [2]

$$\tau_k = M\eta[\eta]_0/R_g T \lambda_k (\Sigma_l\, 1/\lambda_l)\,, \tag{21}$$

where M is the molecular weight, $[\eta]_0$ the intrinsic viscosity in steady flow and R_g the gas constant, eq. (20) can be rewritten as

$$\langle \dot{y}_{cr} \rangle = (-2K^2 D S_2/R)\ (M\eta[\eta]_0/R_g T)^2, \tag{22}$$

where $S_2 = \Sigma_k \lambda_k^{-2}/(\Sigma_k \lambda_k^{-1})^2 = 0.4$ for the free-draining polymer [2]. Converting to concentration in g/cm^3, C_g, we get

$$R\,\partial P/\partial R = (-2C_g M S_2/R_g T)\,\eta^2 [\eta]_0^2 K^2. \tag{23}$$

2) *Non-draining polymer*: here, $\bar{\rho} = L\eta/0.192$ giving

$$R\,\partial P/\partial R = (-0.00845\,\eta^2 L^6 C_n/0.192\,k_B T)\,K^2. \tag{24}$$

Using the relationship [2]

$$[\eta]_0 = 2.84 \times 10^{23} L^3/M\,, \tag{25}$$

eq. (24) becomes

$$R\,\partial P/\partial R = (-0.198\,C_g M/R_g T)\,\eta^2 [\eta]_0^2 K^2. \tag{26}$$

It is interesting to compare these results with those obtained via the phenomenological, or constitutive equation approach (see refs. [6–8]). This method leads quite directly to the following expression for the radial pressure gradient in Couette flow:

$$R\,\partial P/\partial R = -\sigma_1\,, \tag{27}$$

where σ_1 is the first normal stress difference in the convention used in refs. [7] and [8], i.e., in Couette flow

$$\sigma_1 = T^{rr} - T^{\theta\theta}\,, \tag{28}$$

where T is the stress tensor. For simple fluids as defined by Coleman et al. [6], both σ_1 and the second normal stress difference, σ_2, are material properties independent of the particular type of flow and solely a function of the local shear rate (provided the flow is viscometric, which includes simple shear, Couette, cone-plate and other common flows). Hence σ_1 can be calculated from simple, laminar shear flow described in eq. (8),

$$\sigma_1 = T^{xx} - T^{yy}\,, \tag{29}$$

and applied to Couette flow. In the bead-spring model [2, 9],

$$\sigma_1 = (2S_2 MC_g/R_g T)\,\eta^2 [\eta]_0^2 K^2. \tag{30}$$

Comparison of eqs. (23), (27) and (30) shows complete agreement for the free-draining polymer between the radial-velocity approach and the constitutive equation approach. For the non-draining polymer [2], $S_2 = 0.206$ and so

$$\sigma_1 = (0.412\,C_g M/R_g T)\,\eta^2 [\eta]_0^2 K^2. \tag{31}$$

Comparison of eqs. (26), (27) and (31) indicates a disagreement by a factor of 2, approximately. A possible source of this discrepancy may be that the expression of the translational frictional coefficient, $\bar{\rho} = L\eta/0.192$, is not applicable to this situation. Further work is necessary to resolve this completely.

4. Applications

As previously remarked, eq. (17) shows that the radial velocity depends on the 5/2 power of the molecular weight. An even stronger dependence on molecular weight may be expected for real polymers whose dimensions are larger than those predicted by purely gaussian random flight statistics. This sensitivity to molecular weight suggests the possibility of

separating large DNA molecules from a solution of large and small molecules. For example, placing a lysate in a concentric cylinder apparatus and rotating the inner cylinder will result in the larger DNA molecules collecting around the inner cylinder, essentially removed from solution. One can then drain off the surrounding solution and redissolve the larger molecules in pure buffer solution.

We are also investigating the possibility of measuring normal stress differences as a means of determining molecular weight. One possible approach to such a measurement employs a cone-plate apparatus. Here the solution is placed in the gap between a cone and a flat plate, the cone rotating relative to the plate. The velocity field is then described in spherical coordinates, with the origin at the apex of the cone, by

$$V_\phi = W(\theta),\ V_r = V_\theta = 0. \tag{32}$$

If the angle of the gap, α, is less than 4°, the shear rate is essentially constant throughout the gap [6]. In such a flow, the radial variation of the $\theta\theta$ component of the stress tensor is [6, 7]

$$R\,\partial T^{\theta\theta}/\partial \ln R = \sigma_1 + 2\sigma_2\ , \tag{33}$$

where σ_1 and σ_2 are the first and second normal stress differences, respectively. In the bead-spring model, $\sigma_2 = 0$ and eq. (33) becomes

$$R\,\partial T^{\theta\theta}/\partial \ln R = (2\,C_g M S_2/R_g T)\,\eta^2\,[\eta]_0^2\,K^2. \tag{34}$$

Since K is a constant, a plot of $T^{\theta\theta}$ as a function of $\ln R$ should yield a straight line. Using an equation such as that derived by Crothers and Zimm [10] relating $[\eta]_0$ and M, the molecular weight can be obtained directly from the slope of this line.

Finally, we point out that the inward radial motion that develops in Couette flow (it will also occur in parallel-plate and cone-plate flow) will lead to a non-uniform distribution of polymer molecules in the solution. This non-uniformity may lead to changes in rheological properties as well as to secondary flows rendering the desired flow unstable. Such effects are probably insignificant in polymers of molecular weights on the order of 10^6 or less. In large polymers, most particularly in bacterial and eukaryotic chromosomal DNA, these effects are important.

Acknowledgement

The author thanks Professor Bruno H. Zimm for suggesting this problem and for many valuable discussions. This work was supported by a Postdoctoral Fellowship from NIH and Grant #PF-873 from the American Cancer Society.

References

[1] R.H. Shafer, N. Laiken and B.H. Zimm, Biophys. Chem. 2 (1974) 180–184.
[2] B.H. Zimm, J. Chem. Phys. 24 (1956) 269.
[3] B.H. Zimm, G.M. Roe and L.F. Epstein, J. Chem. Phys. 24 (1956) 279.
[4] E. Jahnke and F. Emde, Tables of functions, 4th Ed. (Dover, New York, 1945).
[5] J.B. Hays, M.E. Magar and B.H. Zimm, Biopolymers 8 (1969) 531.
[6] B.D. Coleman, H. Markowitz and W. Noll, Viscometric flows of non-newtonian fluids (Springer-Verlag, New York, 1966).
[7] A.S. Lodge, Elastic liquids (Academic Press, London and New York, 1964).
[8] J.D. Ferry, Viscoelastic properties of polymers, 2nd Ed. (Wiley, New York, 1970).
[9] H. Yamakawa, Modern theories of polymer solutions (Harper and Row, New York, 1971).
[10] D.M. Crothers and B.H. Zimm, J. Mol. Biol. 12 (1965) 525.

BIOPHYSICAL CHEMISTRY 2 (1974) 189–192. © NORTH-HOLLAND PUBLISHING COMPANY

HIGH PRESSURE STABILIZATION OF ACETYLCHOLINESTERASE SIZEOZYMES AGAINST THERMAL DENATURATION*

David B. MILLAR‡, Melba A. GRAFIUS‡, James R. WILD‡ and David A. PALMER‡
Naval Medical Research Institute, National Naval Medical Center, Bethesda, Maryland 20014, USA

Received 21 January 1974

We have investigated the effect of hydrostatic pressure on the thermal denaturation of multiple molecular weight forms of acetylcholinesterase (sizeozymes). Only the 7.4 S enzyme showed stabilization by pressure, the denaturation of the 11 S and 70 S forms was relatively unaffected by hydrostatic pressure below 2 000 psig. The 7.4 S enzyme denatures with apparent second order kinetics while the 11 S and 70 S enzyme denature with two apparent first order processes. The pressure stabilization and difference in denaturation kinetics of 7.4 S enzyme compared to 11 S and 70 S enzyme may be due to altered subunit conformation in the 7.4 S enzyme.

Acetylcholinesterase (acetylcholine hydrolase, E.C.3.1.1.7) is of fundamental importance in neural transmission. It is loosely bound to neurogenic membranes and exists in a variety of enzymatically active molecular sizes, 70–50 S, 18–14 S, 11–10 S and 7–8 S [1–3]. We are currently studying the physical and enzymatic properties of 7.4 S acetylcholinesterase [4] as compared to other sizeozymes. As a probe of these parameters in neurogenic membrane constituents pressure is little used but in principle can be very informative [5, 6]. We report here the effect of hydrostatic pressure upon the thermal stability of three acetylcholinesterase sizeozymes.

70 S enzyme was prepared from *Electrophorus electricus* according to Grafius et al. [7] and then further purified by an additional sucrose gradient sedimentation [2]. 11 S enzyme was prepared by incubating 3.5 ml of 70 S enzyme (100 units/ml, 1 unit = one nmole acetylcholine hydrolyzed per mg of protein per hour) with 1 mg of pancreatic trypsin (Calbiochem, crystalline, A grade) for 20 minutes at 20°C in toluene saturated standard buffer (0.015 M sodium phosphate, 0.1 M NaCl, pH 7.1) + 10% sucrose. The reaction was stopped by the addition of 2 mg of soybean trypsin inhibitor (Sigma Type 1-S, chromatographically pure) and 11 S enzyme then isolated by sucrose gradient sedimentation [2]. 7.4 S enzyme was prepared from frozen electric eel electroplax [4]. All enzyme preparations were exhaustively dialysed against standard buffer at 4°C. Thermal denaturation studies were carried out by diluting stock enzyme into prewarmed buffer and withdrawing aliquots with time. Aliquots were *immediately* assayed [8]. For high pressure studies, 0.1 ml aliquots of enzyme were placed in capillary tubes and then sealed with mineral oil. No air space abutted on the enzyme solution. The capillaries were then placed in stainless steel bombs filled with distilled water at the desired experimental temperatures. The sealed bombs, each with three capillaries, were immersed in a water bath and nitrogen gas pressure was applied to the water filled bomb through a hydrostatic reservoir. Hydrostatic pressure was used to avoid exotic effects of the "inert" gases [9]. After $2\frac{1}{2}$ min the bombs were pressurized. At the end of

* From the Bureau of Medicine and Surgery, Navy Department, Research Tasks MR041.06.01.0005A0CK and MR041.06.01.0021B9KL. The opinions or assertions contained herein are the private ones of the authors and are not to be construed as official or reflecting the views of the Navy Department or the naval service at large.
‡ Environmental Biosciences Department.
‡ Microbiology Department.

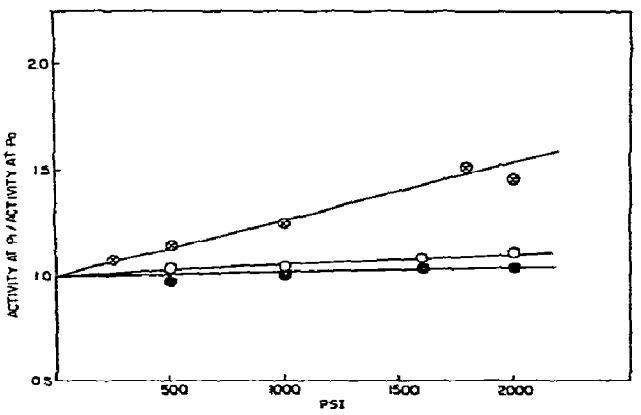


Fig. 1. Effect of hydrostatic pressure on the thermal denaturation of 7.4 S acetylcholinesterase (⊗); 11 S acetylcholinesterase (●); 70 S acetylcholinesterase (○). Po is atmospheric pressure. Pi is test pressure. Incubation at 42°C for thirty minutes.

30 min the bombs were carefully depressurized, the samples removed and again immediately assayed. Controls (Po) were treated in the same manner except at ambient pressure. All chemicals were of reagent grade quality or better.

For the preparations used here, thermal denaturation experiments at ambient pressure showed that thirty minutes at 42°C resulted in activity losses of 58.8% (s.d. ± 0.8) for 7.4 S enzyme, 48.8% (s.d. ± 3.7) for 11 S and 46.0% (s.d. ± 1.6) for 70 S enzyme. 0.1 mM benzethonium chloride, a protease inhibitor did not decrease this loss. Accordingly, thirty minutes at 42°C was selected as the denaturing period for the high pressure experiments. Fig. 1 shows that under these conditions hydrostatic pressure up to 2 000 psig barely influences the denaturation of 11 S or 70 S enzyme. 7.4 S enzyme however is quite sensitive showing a linear protection of activity with increasing pressure. In an attempt to understand the stabilization of the 7.4 S enzyme we investigated the kinetics of denaturation of the 7.4 S, 11 S and 70 S enzyme. Fig. 2 shows that for over a 95% loss of activity 7.4 S enzyme follows apparent second order kinetics with a k of 4.9×10^{-4}% act^{-1} t^{-1}. Apparent second order kinetics are exhibited from 42° to 50°. Fig. 3

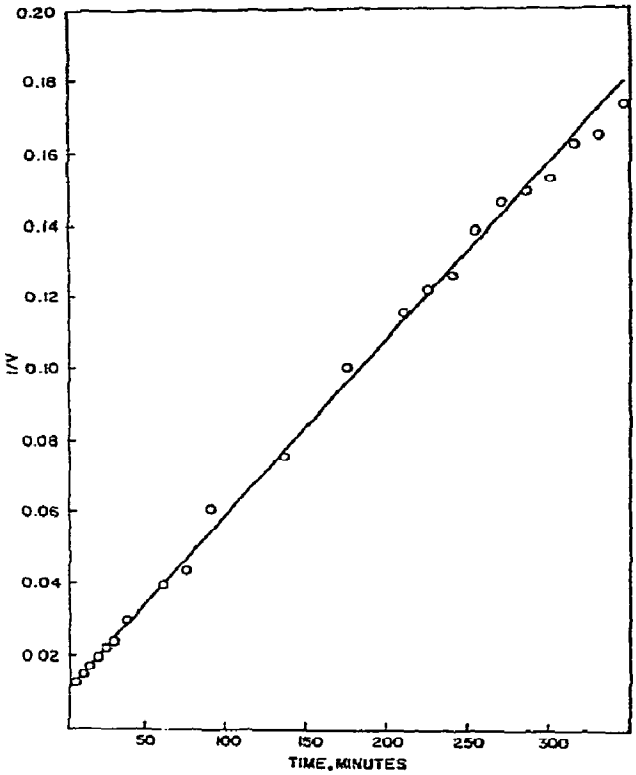


Fig. 2. Kinetics of denaturation of 7.4 S enzyme. Temperature = 42°C. V is percent original activity.

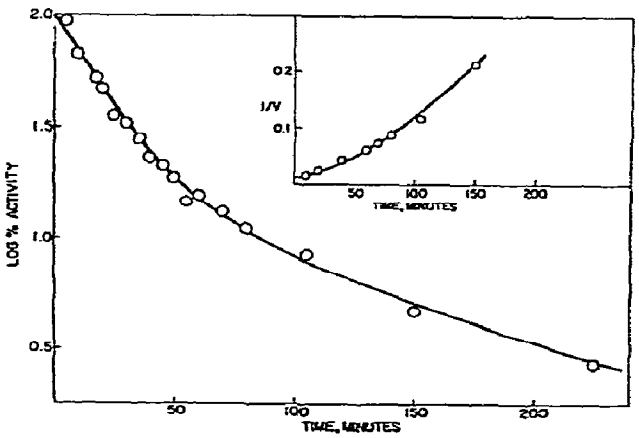


Fig. 3. Kinetics of denaturation of 11 S enzyme. Temperature = 42°C. V is percent original activity. The line showing the variation of log % original activity versus time is calculated. The results at 49°C were displayed since they illustrated the distinction in kinetics better than those at 42°C. See text.

demonstrates that 11 S enzyme does not follow second order kinetics or simple first order kinetics over a 90% loss of activity. An F test based on minimum sum of squares showed that the activity loss was best fitted by two apparent first order processes. Identical results were obtained with 70 S enzyme and Coleman and Eley [10] have observed a two first order denaturation for erythrocyte acetylcholinesterase. Assuming that each process is a one step denaturation the data was computer fitted by nonlinear regression analysis† to an equation of the form:

$$\% \text{ activity} = m_1 \exp(-k_1 t) + m_2 \exp(-k_2 t), \qquad (1)$$

where m_1 and m_2 are multipliers quantitating the percent activity loss given by process 1 and 2 respectively, k_1 and k_2 are the rate constants and t is time. The solid line in fig. 3 is calculated with eq. (1) and values of $m_1 = 85.6, m_2 = 19.3, k_1 = 0.0524$ min^{-1} and $k_2 = 0.0086$ min^{-1}. The difference in denaturation rate constants for m_1 and m_2 indicate target sites of different thermal sensitivity which affect the catalytic activity of the enzyme. Thermal studies for both 11 S and 70 S enzymes between 42 and 50°C show the ratio m_1/m_2 to increase from approximately 0.7 (± 0.2) at 42°C to 4.4 (± 0.3) at 50°C. The values of m_1 and m_2 therefore may be functions of a thermolabile protein conformation.

The differences in the kinetics of denaturation and pressure stabilization are most likely related to structural differences in the sizeozymes. In this regard, 7.4 S enzyme (molecular weight 134 000) is apparently derived from the 18 S and/or 14 S enzymes (molecular weight $\sim 1 \times 10^6 - 8 \times 10^5$ [11]), has two subunits of ~ 65 000 molecular weight, a specific activity about 1/100th that of crystalline 10.8 S enzyme and a K_m for acetylthiocholine of 1.34×10^{-4} M [4]. Using the previous techniques [4] we also determined the K_m of 11 S enzyme to be 2×10^{-4} M. The K_i for eserine is the same as for 11 S enzyme [4]. The Hill coefficients for both enzymes are about 1 with acetylthiocholine as substrate [4]. 11 S enzyme has a molecular weight of 260 000 [12,13] and 4 subunits of about 65 000–75 000 molecular weight [12,14]. The highly purified 14 S and 18 S enzymes have subunit weights of approximately 80 000–90 000 and (in lesser amounts) 60 000–65 000 [11,15]. From this data, there appears to be no a priori reason for the difference in denaturation kinetics. However, our observed differences could be due to a preexisting protease nick in 7.4 S enzyme. Such a nick might make for a less stable internal structure and for reaction paths which make the denaturation kinetics apparently second order. A looser subunit interaction might be revealed by the ΔV^* for the process by [5,6]

$$\Delta V^* = -2.303\, RT \log(kp_2/kp_1)/(p_2 - p_1), \qquad (2)$$

where R is the gas constant (0.082 ℓ atm/mole), T is the absolute temperature, kp_1 and kp_2 are the apparent second order rate constants of inactivation at pressures p_1 (1 atm) and p_2 (136 atm). To determine kp_2/kp_1 we assumed that the order of inactivation did not change between 1 atm and 136 atm. Since we expressed activity in percent of zero time value and we know the percentage activity left at thirty minutes at any pressure, kp_2/kp_1 is easily calculated. Such a calculation leads to a value of ΔV^* of 164 cm^3/mole. The complicated kinetics of 11 S and 70 S enzyme do not permit such an estimation. However, the relative lack of stabilization of these sizeozymes by pressure indicates that at 42°C the difference in volume between the inactive and active enzyme is apparently small. These results suggest that with the 11 S and 70 S sizeozyme, thermal inactivation at 42°C is due to events whose effects are confined to the active site. In contrast, with the 7.4 S enzyme activity loss is accompanied by a large volume expansion of the molecule suggesting the involvement of sizeable portions of the polypeptide chain. These results indicate sizeable structural differences in 7.4 S enzyme as compared to other sizeozymes. The temperature dependence of the properties of 7.4 S and 11 S or 18 S enzymes should reveal much about the interplay of subunit interactions and activity in this important enzyme.

† We are indebted to Dr. Louis Homer of this Institute for providing us with a very powerful fitting algorithm and for stimulating discussions concerning the statistical characteristics of the fitting process.

References

[1] M.A. Grafius and D.B. Millar, Biochim. Biophys. Acta 110 (1965) 540.
[2] M.A. Grafius and D.B. Millar, Biochemistry 6 (1967) 1034.
[3] J. Massoulié, F. Rieger and S. Bon, Eur. J. Biochem. 21 (1971) 542.
[4] D.B. Millar, M.A. Grafius, D.A. Palmer and G. Millar, Eur. J. Biochem. 37 (1973) 425.
[5] F.H. Johnson, H. Eyring and M.J. Polissar, in: The kinetic basis of molecular biology (Wiley, New York, 1954) p. 305.
[6] K. Suzuki and Y. Taniguchi, in: The effects of pressure on living organisms, S.E.B. Symposia 26 (Academic Press, New York, 1972) p. 103.
[7] M.A. Grafius, H.E. Bond and D.B. Millar, Eur. J. Biochem. 22 (1971) 382.
[8] G.L. Ellman, K.D. Courtney, V. Andres, Jr. and R.M. Featherstone, Biochem. Pharmacol. 7 (1961) 88.
[9] R.M. Featherston,e S. Hegeman and W. Settle, in: Underwater physiology, ed. C.J. Lamberton (Academic Press, New York, 1971).
[10] M.H. Coleman and D.D. Eley, Biochim. Biophys. Acta 67 (1963) 646.
[11] J.T. Powell, S. Bon, F. Rieger and J. Massoulié, FEBS Letters 36 (1973) 17.
[12] W. Leuzinger, M. Goldberg and E. Cauvin, J. Mol. Biol. 40 (1969) 217.
[13] D.B. Millar and M.A. Grafius, FEBS Letters 12 (1970) 61.
[14] J.D. Berman, Biochemistry 12 (1973) 1710.
[15] Y. Dudai, I. Silman, M. Shinitzky and S. Blumberg, Proc. Natl. Acad. Sci. USA 69 (1972) 2400.

BIOPHYSICAL CHEMISTRY 2 (1974) 193–195. © NORTH-HOLLAND PUBLISHING COMPANY

POLYNUCLEOTIDES XV. A COMMON ERROR IN THE PLOTTING OF CONTINUOUS VARIATION (MIXING CURVE) EXPERIMENTS*

Michael D. TOPAL and Jacques R. FRESCO
Department of Biochemical Sciences, Frick Chemical Laboratory, Princeton University, Princeton, New Jersey 08540, USA

Received 9 April 1974

The often employed practice of reporting continuous variation experiments with polynucleotides in terms of *relative* ultraviolet absorbance, to better portray the hypochromicity of the complex whose stoichiometry is under investigation, is shown to be incorrect. Ways in which this type of plot can lead to erroneous conclusions are discussed. It is concluded that plotting the *observed* absorbance measurements is the appropriate method for data analysis and presentation.

The continuous variation experiment (mixing curve) [1] is the established method for determining the stoichiometry of reaction between synthetic polynucleotides [2–4]. For this reason it is important to point out a common error in the way mixing curve data has often been reported [4–11]. In such titration experiments, the raw experimental data consists of absorbance (or some other property) at some fixed wavelength, A_{obs}, as a function of residue mole fraction, X_M (= $1-X_N$), of one of the two interacting polymers, N and M [3]. Since the property measured is one that varies linearly with the number of interacting base residues, the titration should result in straight line segments in a plot of A_{obs} versus X_M that intersect at a value(s) of X_M equal to the mole fraction of M residues in the complex(es) formed [1, 3].

Often, for convenience, data has been presented as a plot of A_{rel} versus X_M, where $A_{rel} = A_{obs}/A_{calc}$, and $A_{calc} = [X_M A_M + (1 - X_M)A_N]$, i.e., the absorbance expected where there is no polymer–polymer interaction. Thus, the plotting of A_{rel} versus X_M is equivalent to dividing the expected straight line segments in the plot of A_{obs} versus X_M by another straight line, A_{calc}. The resulting A_{rel} versus X_M plot has been used invariably to determine stoichiometry after the points have been fitted to a straight line, with apparent deviations from linearity attributed to experimental error. In fact, in general the A_{rel} plots should not produce straight line segments:

Given 2 straight lines having x in common

$$y_1 = m_1 x + b_1 \qquad \text{and} \qquad y_2 = m_2 x + b_2$$

their ratio,

$$y_1/y_2 = (m_1 x + b_1)/(m_2 x + b_2)$$

reduces to an equation for a straight line only under the following special conditions:

a) *When m_1 and/or m_2 is equal to zero*

Case 1: The slope of one of the lines is equal to zero; i.e. $m_2 = 0$, $m_1 \neq 0$†

$$y_1/y_2 = (m_1 x + b_1)/b_2 = (m_1/b_2)x + b_1/b_2$$ (a straight line of slope m_1/b_2 and y intercept b_1/b_2)

* The last paper in this series was: A.J. Lomant and J.R. Fresco, J. Mol. Biol. 77 (1973) 345.

† If $m_1 = 0$, $m_2 \neq 0$, then $1/(y_1/y_2)$ versus x gives a straight line of slope m_2/b_1 and y intercept b_2/b_1.

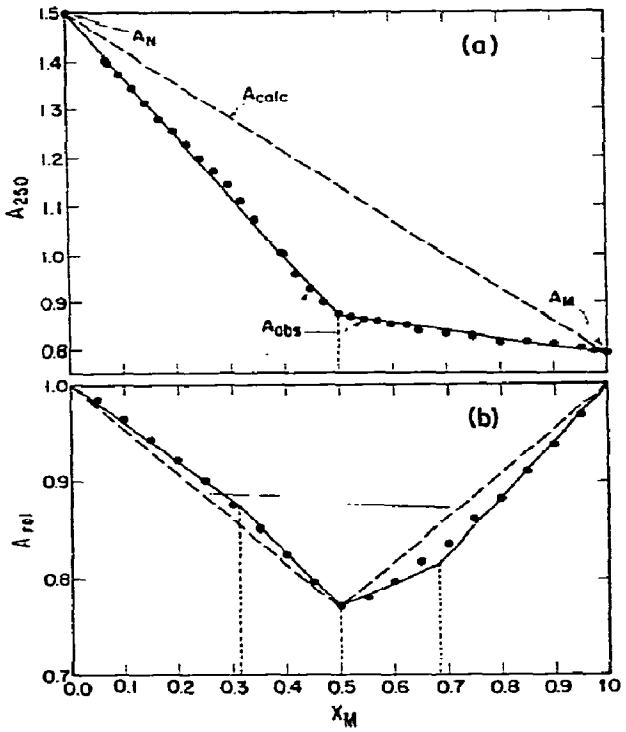


Fig. 1. Mixing curves for 2 interacting synthetic polynucleotides for which the stock solutions, $X_M = 0.0$ and $X_M = 1.0$, were of equimolar residue concentration. In (a) the data points indicate A_{obs} at 250 nm for mixtures of M and N, such that [N] + [M] is constant. The dashed line, A_{calc}, indicates the expected absorbance if there were no interaction. In (b), where A_{rel} is plotted, the data points were calculated using the straight line segments through the points in (a) and A_{calc}. The solid line segments in (b) represent an attempt to interpret equilibria that could give rise to the curvature indicated by these data points. The dashed line segments in (b) are arbitrary lines inserted to emphasize the deviation from linearity of the A_{rel} data points. Note that the plot in (a) indicates only one equilibrium complex at $X_M = 0.5$, whereas the plot in (b) suggests 2 additional equilibria.

Case 2: The slope of both of the lines is equal to zero; $m_1 = 0, m_2 = 0$
$y_1/y_2 = b_1/b_2$ (a straight line of slope 0, and y intercept b_1/b_2)

b) *When the x or y intercept of one or both of the lines is equal to zero*
Case 1: The y intercept of one of the lines is equal to zero; i.e. $b_1 = 0$[‡]
$y_1/y_2 = m_1 x/(m_2 x + b_2)$
$1/(y_1/y_2) = (b_2/m_1)(1/x) + m_2/m_1$ (a straight line of slope b_2/m_1 and y intercept m_2/m_1)
Case 2: The y intercept of both lines is equal to zero; $b_1 = b_2 = 0$
$y_1/y_2 = m_1 x/m_2 x = m_1/m_2$ (a straight line of slope 0 and y intercept m_1/m_2)
Note that the cases for x intercept = 0 give comparable results.

From these considerations, the curvature noticeable in some of the data reported in the literature is expected, and the straight lines imposed on such data are not justified. In those cases where no curvature is noticeable, it is due to the accidental use of conditions where $\epsilon_N \approx \epsilon_M$ (condition a, case 1 ($m_2 = 0$) above). In the general case where $\epsilon_N \not\approx \epsilon_M$, curvature is definitely noticeable (see for example fig. 1b), though it is absent in the A_{obs} versus X_M plot (fig. 1a). The amount of this curvature will be proportional to the difference between ϵ_N and ϵ_M. Fortunately, this difference was small in the literature examples cited, so that conclusions concerning stoichiometry were not affected. However, in the case shown in fig. 1, which is typical for many real situations, the difference between ϵ_N and ϵ_M is large. Incorrectly plotted as in fig. 1b (representing a replot of the straight line segments of fig. 1a in terms of A_{rel}), the data could easily be misinterpreted in terms of non-equilibrium three stranded complexes at $X_M = 0.33$ and 0.66; correct plotting avoids this possibility (fig. 1a). We have also performed continuous variation experiments in which the endpoint of the titration (mixture of maximum hypochromicity) would have

[‡] If $b_2 = 0, y_1/y_2$ versus $1/x$ gives a straight line of slope b_1/m_2 and y intercept m_1/m_2.

been artifactually located by the A_{rel} versus X_M plot.

It is concluded that A_{rel} values are not suitable for proper evaluation of mixing curve experiments and that presentation of the observed data remains the method of choice.

Acknowledgement

This work was supported by grants from the National Science Foundation (GB- 35595X1), the National Institutes of Health (GM-07654) and The American Heart Association. We are grateful to Mr. Martin A. Rice for fine technical assistance.

References

[1] P. Job, Ann. Chem. 9 (1928) 113.
[3] G. Felsenfeld and A. Rich, Biochim. Biophys. Acta 26 (1957) 457.
[3] G. Felsenfeld, Biochim. Biophys. Acta 29 (1958) 133.
[4] J.R. Fresco and B.M. Alberts, Proc. Natl. Acad. Sci. USA 46 (1960) 311.
[5] R.F. Steiner, J. Biol. Chem. 236 (1961) 842.
[6] M.N. Lipsett, L.A. Heppel and D.F. Bradley, J. Biol. Chem. 236 (1961) 857.
[7] E.K.F. Bautz and F.A. Bautz, Proc. Natl. Acad. Sci. USA 52 (1964) 1476.
[8] C.L. Stevens and G. Felsenfeld, Biopolymers 2 (1964) 293.
[9] R.D. Blake, J. Massoulie and J.R. Fresco, J. Mol. Biol. 30 (1967) 291.
[10] F.B. Howard, J. Frazier and H.T. Miles, J. Biol. Chem. 246 (1971) 7073.
[11] A.J. Lomant and J.R. Fresco, Biopolymers 12 (1973) 1889.

BIOPHYSICAL CHEMISTRY 2 (1974) 196. © NORTH-HOLLAND PUBLISHING COMPANY

ERRATUM

E. Bańkowski and W.M. Mitchell, Human procollagen I. An anionic tropocollagen precursor from skin fibroblasts in culture. Biophys. Chem. 1 (1973) 73–86.

Figures 2 and 3 on page 76 should be reversed.

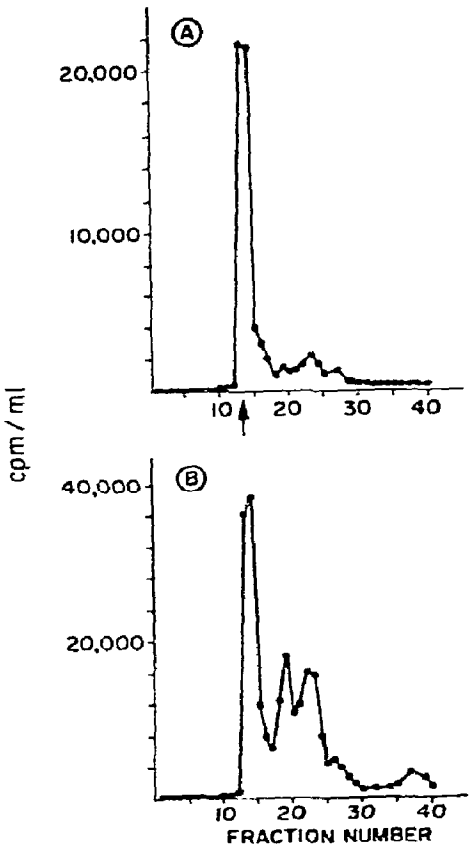


Fig. 2. Molecular sieve chromatography on agarose of human fibroblast culture fluid following extensive dialysis. A, serum free culture medium; B, serum containing culture medium.

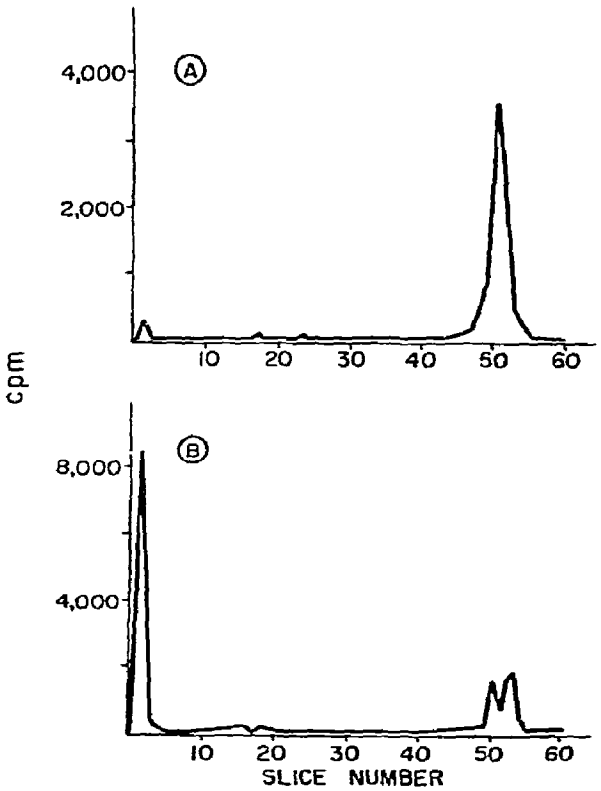


Fig. 3. Electrophoresis of human fibroblast culture fluid fo lowing extensive dialysis. A, serum free culture medium; E serum containing culture medium.

BIOPHYSICAL CHEMISTRY 2 (1974) 197–207. © NORTH-HOLLAND PUBLISHING COMPANY

THE EQUIVALENCE OF FLUCTUATION ANALYSIS AND CHEMICAL RELAXATION MEASUREMENTS: A KINETIC STUDY OF ION PORE FORMATION IN THIN LIPID MEMBRANES

H.P. ZINGSHEIM and E. NEHER

Max-Planck-Institut für biophysikalische Chemie (Karl-Friedrich-Bonhoeffer-Institut), D 34 Göttingen–Nikolausberg, Germany

Received 11 June 1974

(1) Autocorrelation measurements were made of the current fluctuations due to ion-conducting channels produced by gramicidin A in black lipid membranes.

(2) Relaxation experiments using a voltage jump were made on the same system.

(3) Reciprocal time constants were determined by both methods over a 10^8 fold range in membrane conductivity, starting from the single channel level.

(4) The mean squared amplitudes of the fluctuations were determined from the autocorrelation functions.

(5) The data were tentatively rationalized on the basis of a hypothetical dimerization reaction, assuming that gramicidin A dimers form conducting channels. The same forward rate constants are obtained, via (3), by both methods (1) and (2). The backward rate constant agrees excellently with direct measurements of the mean life time of a conducting channel.

(6) The unit channel conductance and – assuming again a dimerization – the equilibrium constant can be obtained from the fluctuation amplitude distribution.

1. Introduction

The determination of reaction rate constants in homogeneous systems by chemical relaxation methods has become a standard practice during the past decade [1]. The fluctuation dissipation theorem [2] indicates an alternative approach, which in principle should lead to equivalent results. The theorem relates the average time course of the decay of spontaneous microscopic fluctuations to the time course observed during equilibration after a small but macroscopic perturbation. The autocorrelation function of random concentration fluctuations arising from a simple process – i.e., a single reaction step – is an exponential, which has the same time constant as the relaxation response of the system. Only very few experimental attempts towards an application of this theorem for kinetic measurements in homogeneous systems have been reported [3, 4].

In the particular case of membranes one may regard the ionic currents as directly proportional to the number of ionic channels being created by a chemical transformation. On the basis of this assumption measurements of ion current noise have been introduced into membrane physiology [5] as an alternative to the traditional relaxation studies by the voltage clamp method [6]. Noise measurements have led to an estimate of the unit conductance step associated with the opening of an "Acetylcholine gate" at the neuromuscular junction [7, 8]. It was also claimed that the would allow one to decide between various models fo the action currents in nerve membranes [9–11].

Discrete, stepwise conductance changes, which represent the opening and closing of individual ionic channels, may be obtained in black lipid membranes. Such channels are produced by a number of polypeptides, the antibiotic gramicidin A presently being the best characterized ion channel former [12]. The random superposition of many single events leads to higher membrane conductance values. The current noise may be analyzed and the results be related to the properties of the unit channel.

We have chosen this model system for our study because it appears ideally suited for testing the validi

of fluctuation analysis. Incidentially, it may also serve as a unique illustration of the fluctuation dissipation theorem as applied to chemical reactions.

Bamberg and Läuger [13] have recently studied the kinetics of ion pore formation by gramicidin A with a relaxation technique (voltage clamp). The parameter, which was assumed to perturb the equilibrium between the channels and the nonconducting species is the voltage dependent membrane thickness [12, 14]. The authors analyzed their results on the basis of a hypothetical reaction scheme assuming a dimerization process as suggested by Urry et al. [15]. A further assumption is that only gramicidin A dimers form conducting channels and that every dimer is an ion pore.

The results of the present study show that the same rate constants are obtained by correlation analysis and by the relaxation technique. The analysis of the fluctuation amplitudes yields the value for the unit conductance step and, provided the assumption on the reaction mechanism is correct, the equilibrium constant of the reaction. The data of Bamberg and Läuger as well as those of our study do not contradict the dimerization scheme. Nevertheless, for the purpose of this investigation the question of the correct model was largely irrelevant. Our intention is not to present a full kinetic analysis of the ion channel formation by gramicidin A. The object is primarily the demonstration of the equivalence of both kinetic methods in a case which is sufficiently clear and where measurements are sufficiently sensitive to allow comparison of the statistical analysis with direct measurements of individual molecular events.

2. Experimental

2.1. Materials

The lipids used were dioleoyl-L-α-lecithin (Supelco), glyceryl monooleate (Sigma Chem. Co) and cholesterol (Sigma Chem. Co). Valine gramicidin A was a sample kindly provided by Dr. E. Grell from this institute.

n-Decane (reference substance for gas chromatography) was obtained from Merck. Ethanol was p.a. grade from Merck. KCl and NaCl were Suprapur grades from Merck. All chemicals were used without further purification. The water used was triple destilled (twice from alkaline and acid $KMNO_4$, respectively) and the salt solutions were equilibrated with *n*-decane and filtered prior to use.

2.2. Instrumentation and experimental procedure

Membranes were formed by conventional techniques [16] over 0.3–1.5 mm diameter openings of polypropylene vessels placed in a 30 ml outer container made of glass. The concentrations of the lipid solutions were approx.: Dioleoyl-L-α-lecithin, 20 mM; dioleoyl-L-α-lecithin : cholesterol, 20 : 20 mM; glyceryl-monooleate, 10 mM. Gramicidin A was added to the aqueous phase of the outer container in approx. 5 μl aliquots from 5×10^{-9}–5×10^{-6} M stock solutions in ethanol. Experiments were performed at room temperature (21–23°C).

Two sintered Ag–AgCl pellets were used as electrodes. The membrane current was measured with a standard feedback circuit employing a model 380 K operational amplifier from Function Modules Inc. This amplifier was selected on the basis of its subpicoampere specifications with respect to current noise and current drift, combined with low input capacitance and low input voltage noise. Membrane current noise measurements were performed at 100 mV applied potential. Relaxation experiments were performed using voltage steps from either 50 or 150 mV to the 100 mV level, supplied by a Hewlett–Packard Model 3310 A function generator. The bandwidth was limited to 100 Hz during single channel experiments (1 GΩ feedback resistor) and to 20 kHz during high conductance experiments (100 kΩ feedback resistor). The current signals were directly recorded on a strip chart recorder and an oscilloscope and simultaneously stored by an FM-magnetic tape recorder (Hewlett–Packard Model 3960) after passage through a high pass filter with a time constant of 13 s and a further step of amplification. For correlation analysis the current recordings were subsequently replayed at higher speeds into a "Fabritek" Model 1074 Instrument Computer (Nicolet Instruments Corporation) equipped with a Model SD-75 A auto/cross correlation digitizer.

As this instrument utilizes only one sample of the signal waveform per sweep, the same noise trace was replayed repeatedly (with varying starting points) until the autocorrelation function showed no significant improvement by doubling the number of sweeps

(512–1024 sweeps). The relaxation experiments, however, were made "on line" using the Fabritek instrument in the averaging mode, averaging from 2 to 16 relaxation responses.

All curves shown in this report are direct reproductions from the original results.

3. Analysis of experimental data

3.1. The autocorrelation function of unit conductance steps

The current signal at the single channel level represents a superposition of independent square pulses of varying duration. The autocorrelation function of such a signal is an exponential with a time constant equal to the mean duration of the pulses. This results from the following considerations:

(a) The autocorrelation function of superimposed independent signals is equal to the sum of the autocorrelation functions of the individual signals.

(b) The autocorrelation function of a random sequence of unit square pulses of fixed duration T is a symmetric triangular function centered at zero delay time and extending to $\pm T$.

(c) For a signal consisting of a random sequence of unit pulses possessing a distribution of durations, represented by $p(T) = p(0) \exp(-T/\tau_0)$ [12] one will obtain a distribution of triangular autocorrelation functions which, when superimposed according to (a), give rise to an exponential with a time constant τ_0.

At higher levels of conductance, individual pulses cannot be resolved. The above consideration is invalid, because the individual events may no longer be regarded as independent. The autocorrelation function is, however, still an exponential, provided the fluctuations arise from a single process. The time constant depends on the actual nature of the interaction [10].

3.2. The dependence of the time constants on the membrane conductance

The reciprocal values of the time constants $1/\tau$ (s^{-1}) as obtained by either fluctuation analysis or relaxation measurements were plotted versus the square root of the specific membrane conductivity $\bar{\lambda}$ (Ω^{-1} cm^{-2}). This was done for ease of comparison with the results of Bamberg and Läuger [13]. The described manner of plotting the data follows from a hypothetical reaction scheme, involving a dimerization reaction [13]:

$$A + A \underset{k_d}{\overset{k_r}{\rightleftarrows}} A_2 , \tag{1}$$

where A represents monomer and A_2 dimer. k_r and k_d are the forward and backward rate constants, respectively.

$$N = N_1 + 2N_2 , \tag{2}$$

where N (Mol cm^{-2}) is the total molar concentration of gramicidin A molecules in the membrane. N_1 and N_2 are the respective concentrations of monomers and dimers. The solution of the linearized rate equation is an exponential with a time constant [1]

$$1/\tau = k_d + 4 k_r N_1 . \tag{3}$$

By virtue of the law of mass action and the fact that the superposition of N_2 single channels leads to an average conductivity

$$\bar{\lambda} = N_L N_2 \Lambda \tag{4}$$

one obtains

$$1/\tau = k_d + 4\sqrt{k_d k_r / N_L \Lambda}\sqrt{\bar{\lambda}} , \tag{5}$$

where N_L is Avogadro's number and Λ (Ω^{-1}) the unit channel conductance.

3.3. Fluctuation amplitudes

Let $\Phi(0)$ and $\Phi(\infty)$ be the values of the autocorrelation function at zero and infinite delay time respectively. It follows from the definition of the autocorrelation function that $\Phi(0)$ is equal to the mean squared amplitude and $\Phi(\infty)$ is equal to the square of the mean amplitude [17]. Due to (4), $\Phi(0) - \Phi(\infty)$ is proportional to $\overline{N_2^2} - \bar{N}_2^2 = c_{N_2}^2$, the variance of the distribution of the dimer concentration around the average concentration $\bar{N}_2$. In our measurements $\Phi(\infty)$ was usually zero, because the dc component of the current signal was removed by a high pass filter. $\Phi(0) - \Phi(\infty)$ was measured in units of (membrane current)^2 and σ_I^2 denotes this quantity. Moreover, it is evident that the relationship *

* For footnote see next page.

$\sigma^2_{N_2}/\bar{N}_2 = 1/N_L$ or $\sigma^2_\lambda/\bar{\lambda} = \Lambda$

should be valid for independent channels [18]. Generally this will be true only for very low conductivity values close to the single channel level. At higher conductivities, $\sigma^2_\lambda/\bar{\lambda}$ should decrease by a factor depending on the actual nature of the interdependence between the channels. Following again the hypothesis of a simple dimerization reaction, one obtains:

$$\frac{\sigma^2_\lambda}{\bar{\lambda}} = \Lambda \frac{\sqrt{N_L/K\Lambda}\sqrt{\bar{\lambda}}}{4\bar{\lambda}/\Lambda + \sqrt{N_L/K\Lambda}\sqrt{\bar{\lambda}}} \quad . \tag{6a}$$

This follows from $\sigma^2_{N_2} = kT/(\mathrm{d}^2G/\mathrm{d}N_2^2)$, where G is the Helmholtz free energy of the reaction, k the Boltzmann constant and T the absolute temperature [19]. $K = k_r/k_d$ represents the equilibrium constant. G is expanded into a Taylor series around the equilibrium value in the usual way, including also second order terms. Together with the equilibrium condition $\mathrm{d}G/\mathrm{d}N_2 = 0$, with eqs. (2) and (4) this procedure yields eq. (6a).

A plot of $\bar{\lambda}/\sigma^2_\lambda$ versus $\sqrt{\bar{\lambda}}$ should yield a straight line due to

$$\bar{\lambda}/\sigma^2_\lambda = 1/\Lambda + 4\sqrt{K/N_L\Lambda^3}\sqrt{\bar{\lambda}} \,. \tag{6b}$$

4. Results

4.1. Unit channel conductance

Fig. 1 shows examples of unit channel recordings obtained with dioleoyl-L-α-lecithin membranes.

Below we summarize the unit channel conductance values Λ (at 100 mV) for the membrane systems investigated in this study (table 1). Our values were obtained from histograms of current amplitudes, measured by an A/D converter connected to a PDP-11/20 digital computer. The most frequent value is given. If the occasionally occurring small conductance channels (see fig. 1) are included, the average unit channel conductance differs from the most frequent value by less than 10%.

Any distinction between integral and differential conductance definitions is irrelevant for this study, as the unit channel conductance of gramicidin A is practically ohmic in 1 M salt solutions at potentials up to 200 mV [12].

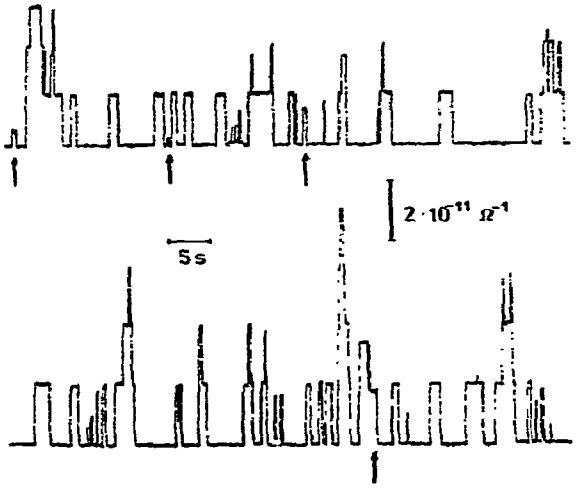


Fig. 1. Recordings of unit conductance steps produced by gramicidin A in black lipid membranes formed from dioleoyl-L-α-lecithin in *n*-decane.

Upper trace: at 1 M NaCl; lower trace: at 1 M KCl. The arrows point towards infrequently occurring conductance steps of nonuniform magnitude.

Table 1

Membrane lipid in *n*-decane	Unit channel conductance $10^{11}\,\Lambda\,(\Omega^{-1})$	
	1 M KCl	1 M NaCl
dioleoyl-L-α-lecithin [a]	1.95	1.65
dioleoyl-L-α-lecithin + cholesterol [a]	2.3	
glyceryl monooleate [b]	4.1	

[a] This study.

[b] Data by Hladky and Haydon [12]. The value of this study agrees within ± 5%.

* The normalization used is as follows: σ^2_λ is obtained from σ^2_I by dividing this value by the membrane area and the square of the applied potential. The validity of this procedure becomes evident, if the operation is looked upon as the superposition of the contributions of many independent membranes, so that the area adds up to 1 cm^2. (The variance of the sum of independent processes is equal to the sum of the variances.) Thus, σ^2_λ has the dimension $\Omega^{-2}\,cm^{-2}$.

4.2. The dissociation rate constant of ion channel formation by gramicidin A

As long as the assumption is correct that there exists only a single, exclusively conducting species (the dimer) the interpretation of the mean channel life time is immediately evident. It equals the backward rate constant k_d of the reaction leading to the conducting channel.

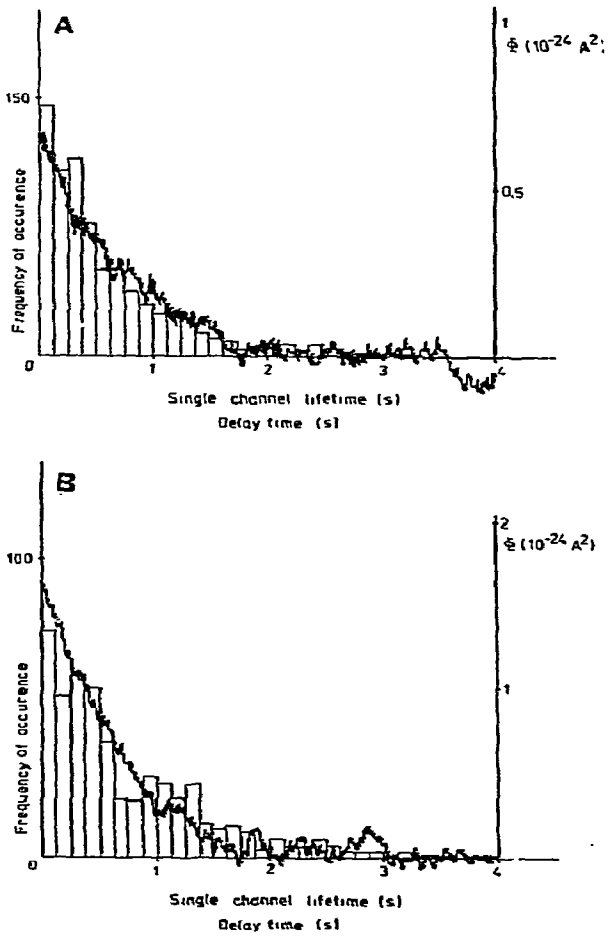


Fig. 2. Histograms of single channel lifetimes. The autocorrelation functions obtained from the same experiments are superimposed; (a) at 1 M NaCl, (b) at 1 M KCl.

Fig. 2a shows a life time histogram obtained by manual measurement of 800 recorded single channels in dioleoyl-L-α-lecithin membranes at 1 M NaCl. The appropriately scaled histogram is superimposed on a direct reproduction of the autocorrelation function obtained from the same experiment. From the histogram $k_d = 1.52 \pm 0.05\ s^{-1}$. The autocorrelation function yields $k_d = 1.56 \pm 0.08\ s^{-1}$.

The analogous information for 1 M KCl is presented in fig. 2b, with $k_d = 1.32 \pm 0.05\ s^{-1}$ from the histogram (300 channels) and $k_d = 1.28 \pm 0.08\ s^{-1}$ from the autocorrelation function.

The corresponding values at 1 M KCl (by autocorrelation only) for glyceryl monooleate are $k_d = 2.45 \pm 0.07\ s^{-1}$ and for dioleoyl-L-α-lecithin plus cholesterol $k_d = 2.2 \pm 0.1\ s^{-1}$.

4.3. The dependence of the time constants on the membrane conductivity

4.3.1. Dioleoyl-L-α-lecithin membranes

At higher conductivity levels individual single channels can no longer be resolved. However, it is still possible to obtain reliable autocorrelation functions. Their time constants τ are, within experimental error, equal to the time constants of the relaxation responses at the same conductivity. Furthermore, it is evident that any conductivity dependence of $1/\tau$, if extrapolated to zero conductivity (the single channel level) should yield k_d for either method. The results presented in fig. 3 have been plotted in the manner described earlier. For a summarization of the numerical results see table 2.

4.3.2. Other lipids

Correlation analysis of the conductivity dependence of the time constants was also applied to black lipid membranes formed at 1 M KCl from glyceryl monooleate and 1:1 mixtures of dioleoyl-L-α-lecithin and cholesterol. In contrast to dioleoyl-L-α-lecithin membranes no statistically significant variation of $1/\tau$ with $\sqrt{\lambda}$ was observed for glyceryl monooleate membranes (fig. 4a) over the same conductance range. A small variation may be deduced from the considerably scattered data in the case of the mixed lipid membranes (fig. 4b).

Table 2
Summary of the numerical results

Experimental conditions			Analysis of time constants							Analysis of fluctuation amplitudes for hypothet. dimerization	
			2nd order				3rd order				
membrane lipid	method	cation (1M)	k_d (s^{-1})	$10^{-13}k_r$ (M^{-1} cm^2 s^{-1})	r_{xy}	$10^{-13}K$ (M^{-1} cm^2)	k_d (s^{-1})	$10^{-26}k_r$ (M^{-2} cm^4 s^{-1})	r_{xy}	$10^{11}\Lambda$ (Ω^{-1})	$10^{-13}K$ (M^{-1} cm^2)
D.L.	single channel life time histogram	Na^+	1.52			not applicable					
		K^+	1.32								
	single channel autocorrelation	Na^+	1.56			not applicable					
		K^+	1.28								
	conductivity dependence, autocorrelation	Na^+	1.5	7.0	0.957	4.7	1.7	2.7	0.951	1.6	16
		K^+	1.4	2.5	0.896	1.9	1.5	0.7	0.880	2.1	1.7
	conductivity dependence, relaxation	Na^+	1.3	6.2	0.930	4.7	1.6	2.8	0.930		
		K^+	1.8	2.9	0.982	1.6	1.9	0.8	0.931		
	conductivity dependence, relaxation, by Bamberg and Läuger [13]	Na^+ a)	1.6	22	0.964	14	2.1	14	0.960		
		b)	1.4	88	0.992	63	2.1	120	0.989		
GMO	single channel autocorrelation	K^+	2.45			not applicable					
	conductivity dependence, autocorrelation	K^+	2.4	<0.1		<0.1	not investigated			4.4	<0.1
D.L. + Ch	single channel autocorrelation	K^+	2.20			not applicable					
	conductivity dependence, autocorrelation	K^+	2.2	0.5	0.428	0.2	not investigated			2.6	2.8

Abbreviations: D.L.: Dioleoyl-L-α-lecithin; GMO: Glyceryl monooleate; Ch: Cholesterol.
r_{xy}: Correlation coefficient of the linear regression.
a) 125 mV, data corrected for $\Lambda = 1.65 \times 10^{-11}\ \Omega^{-1}$.
b) 205 mV, data corrected for $\Lambda = 1.65 \times 10^{-11}\ \Omega^{-1}$.

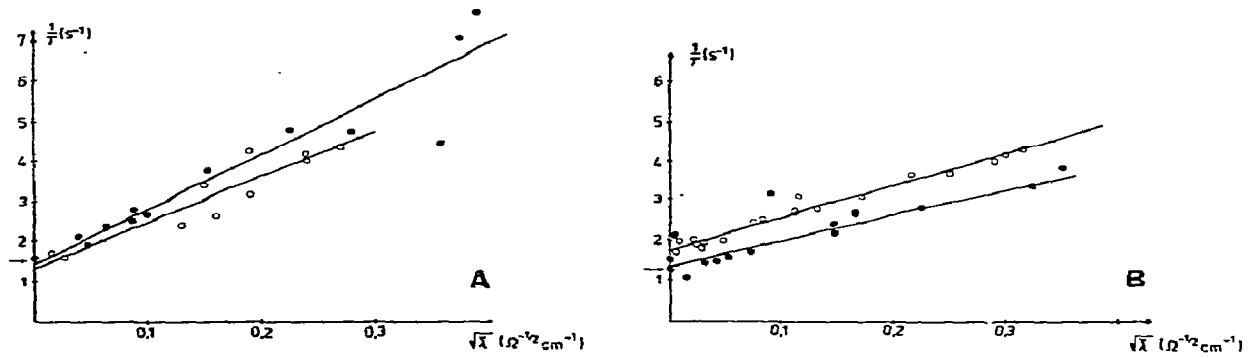


Fig. 3. Dependence of the reciprocal time constants on membrane conductivity. $1/\tau$ is plotted versus $\sqrt{\lambda}$ (see text). (•) Correlation analysis, (○) relaxation experiment. (a) At 1 M NaCl, (b) at 1 M KCl. The arrows indicate the values obtained from single channel measurements.

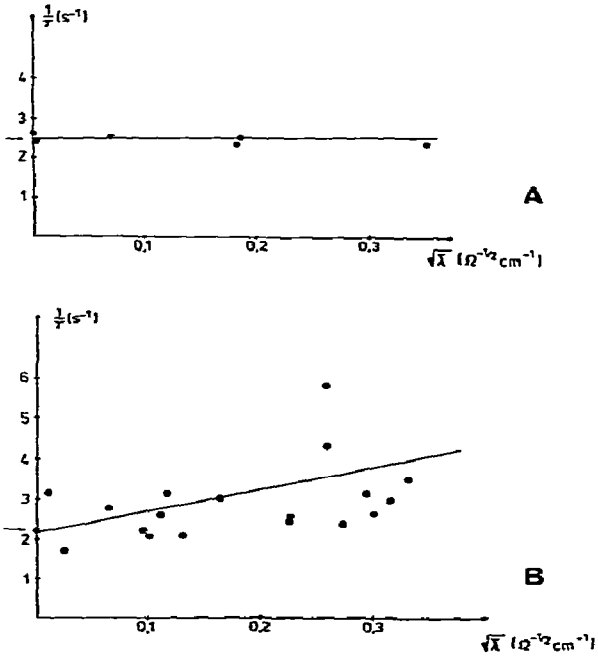


Fig. 4. As fig. 3, 1 M KCl, correlation analysis only. (a) Black lipid membranes formed from glyceryl monooleate in *n*-decane; (b) from 1:1 dioleoyl-L-α-lecithin + cholesterol in *n*-decane. The arrows indicate the values obtained at the single channel level.

4.4. Slow fluctuations

Slow current fluctuations introduced additional time constants $> 10\,\tau$. Correspondingly, inclined base lines of the autocorrelation functions were observed frequently. The slow current fluctuations result from at least two undesired effects:

(a) Lateral convection in the membrane, combined with an inhomogeneous gramicidin A distribution over the membrane and the adjacent bulk liquid interfaces.

(b) A combination of (a) plus capacitive transients upon the fusion of solvent lenses with the torus [16] produces large instantaneous current excursions proportional to the size of the lenses.

The slow fluctuations showed amplitudes up to 10 times the normal current fluctuation amplitudes. Even so, this means that at high levels of conductivity the membrane current was constant to within 1 part in at least 10^4 over time periods of the order of 10 s. For an example, see fig. 5. The slow fluctuations not only interfered with our measurements, they also completely masked any expected contributions by lateral diffusion of gramicidin A in the plane of very small membranes (10 μm diameter). High pass filters were used to suppress the undesired components. As a rule data were rejected, whenever the filter time constant had to be smaller than $10\,\tau$. Nevertheless, we frequently had to put up with inclined baselines. The slow fluctuations were nearly absent in dioleoyl-L-α-lecithin + cholesterol membranes and most pronounced

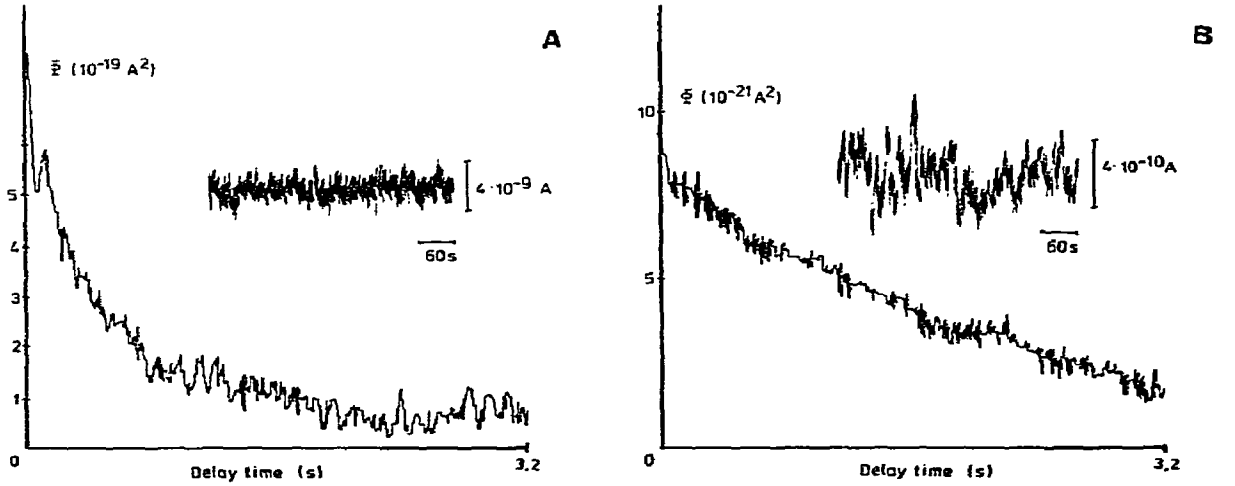


Fig. 5. Examples of autocorrelation functions obtained from glyceryl monooleate membranes in 1 M KCl. In both cases a high pass filter with a time constant of 13 sec was used. The inserts show strip chart recordings of the actual noise traces (the amplified ac component of the membrane conductivity) from which the autocorrelation functions were obtained; (a) in the absence of slow fluctuations, (b) in the presence of slow fluctuations. This is a typical example for data which were rejected.

in glyceryl monooleate membranes. Lateral convection could be minimized by restricting the amount of lipid solution around the hole in the polypropylene vessel to a minimum.

4.5. Amplitude analysis

Fig. 6 shows the experimental results for dioleoyl-L-α-lecithin membranes in 1 M KCl and for glyceryl monooleate membranes in 1 M KCl. The data are plotted according to eq. (6b). The solid lines represent the expected result when K is calculated from the kinetic parameters (figs. 3b, 4a). For the remaining two types of membrane, namely dioleoyl-L-α-lecithin in 1 M NaCl and dioleoyl-L-α-lecithin + cholesterol in 1 M KCl agreement with eq. (6) is poor. Although the plots are linear and for low conductivity values $\sigma_\lambda^2/\bar{\lambda}$ equals Λ within $<10\%$, the K values are higher than those calculated from the kinetic data. The numerical results are also summarized in table 2.

5. Discussion

Although we have already pointed out a number of assumptions which must be made in order to analyze the experimental results, there remain three further points:

(a) The channels are independent at the unit conductance level. This was already investigated by Hladky and Haydon [12], who showed that the frequency of occurrence of 0, 1, 2, ... etc., simultaneous-

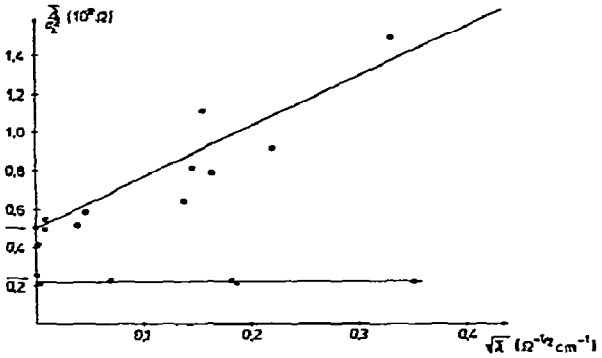


Fig. 6. Dependence of $\bar{\lambda}/\sigma_\lambda^2$ on $\sqrt{\bar{\lambda}}$ (see text). Upper part: Dioleoyl-L-α-lecithin membranes in 1 M KCl. Lower part: Glyceryl monooleate membranes in 1 M KCl. The arrows indicate the reciprocal values of the unit channel conductances.

ly open channels is described by a Poisson distribution.

(b) The autocorrelation function arises from a single process, provided slow fluctuations, which represent convective motions in the membrane, are absent. Pure diffusion in our system is sufficiently slow and may be neglected: for a membrane diameter of 0.1–1 mm and an assumed upper limit of 10^{-8} cm^2 s^{-1} for the lateral diffusion coefficient of gramicidin the time constants due to diffusion would be of the order of hours. Thus, there is only an extremely small probability that an existing channel is terminated by diffusion out of the membrane into the torus.

(c) The rate of association is not diffusion limited. This was shown by Bamberg and Läuger [13].

As figs. 3, 4, and table 2 show, the results ($1/\tau$, k_r, k_d) obtained by a relaxation method and by statistical analysis of the membrane current noise are in good agreement. Moreover, the particularly beneficial feature of the studied model system lies in the possibility of independently obtaining two important parameters, namely the backward rate constant k_d and the unit channel conductance Λ by direct measurements. Thus, for low conductance values we may also compare $1/k_d$ with the mean channel lifetime and $\sigma_\lambda^2/\bar{\lambda}$ with Λ (see also table 2). Again, there is excellent agreement.

At low levels of conductivity ($\leqslant 10^{-4}\ \Omega^{-1}$ cm^{-2}) both k_d and Λ may be measured within ± 10%. At this level of conductance the channels may be regarded as independent. Less than 2% of the gramicidin molecules in the membrane form conducting channels. On the other hand, at a membrane conductance of $10^{-1}\ \Omega^{-1}$ cm^{-2} approx. 40% of the gramicidin molecules form channels. (Values for dioleoyl-L-α-lecithin membranes at 1 M KCl.)

The comparison of our results (k_r) for dioleoyl-L-α-lecithin membranes in 1 M NaCl with the results of Bamberg and Läuger [13] shows agreement only within a factor of 2–3, even if the latter results are recalculated for the correct value of Λ (see table 2). (The authors assumed $\Lambda = 2.4 \times 10^{-11}\ \Omega^{-1}$. This is the value for glyceryl monooleate membranes in 1 M NaCl [12]. The correction reduces their k_r by approx. 30%.) There are at least two possible explanations based on experimental observations:

(a) Frequently, and almost exclusively for dioleoyl-L-α-lecithin membranes in 1 M NaCl, erratic current bursts were observed. They were strongly voltage dependent and much larger and faster than the normal current fluctuations due to gramicidin A or alamethicin [20]. Under these conditions the time constants were shortened by a factor of 2–5 in both correlation and relaxation measurements. The nature of this contamination is not clear. An inorganic precipitate is suggested by the partial success due to filtering of the salt solutions as opposed to roasting of the NaCl.

(b) If the gramicidin A, which spreads at the oil water and membrane water interfaces [21, 22], is not homogeneously distributed over the plane of the membrane, the specific membrane conductivity $\bar{\lambda}$ will always be underestimated. This leads to an overestimation of k_r. Correspondingly, we observed abnormally short time constants whenever the conductivity was still rising steeply after gramicidin A had been added to a membrane which previously had given normal results. The effect is potentially more serious with larger membranes. Large membranes are needed in relaxation studies for reasons pointed out by Bamberg and Läuger [13].

The poor agreement of $\sigma_\lambda^2/\bar{\lambda}$ with the prediction by eq. (6) at high conductivity values for dioleoyl-L-α-lecithin membranes in 1 M NaCl may also be caused by these effects. On the other hand the large scatter of the time constants from dioleoyl-L-α-lecithin-cholesterol membranes most likely reflects small differences in membrane thickness, due to slight variations in membrane composition. It is known that k_d depends strongly on the membrane thickness [12].

Generally, a most important factor influencing the reproducibility of the measurements was the age of the membranes. It is very difficult to obtain truly equilibrated black lecithin membranes of a well defined, minimum thickness [16]. No problems in this respect are encountered with the glyceryl-monooleate membranes, which reach their equilibrium thickness within a few seconds after drainage [16, 14].

Although the ion pore properties of the gramicidin A induced membrane conductance have been thoroughly characterized [12, 23], the mechanism of pore formation has not yet been established unequivocally. The dimerization reaction used in rationalizing the kinetic data must be regarded as hypothetical as long as other alternatives have not been excluded. Even the order of the reaction is difficult to obtain from the presently available data. A linear regression analysis of our data

points and of those published by Bamberg and Läuger shows that the data fit a 3rd order trimolecular reaction just as well (see table 2). The only reliable kinetic clue that the 2nd order is more likely comes from comparing the k_d values (obtained by extrapolation of concentration dependence of the time constants) with the independently obtained values (from single channel measurements). Agreement is poor for 3rd order. This comparison was not possible for Bamberg and Läuger, though, because the mean single channel life time was not known to them.

The above reservations also apply to the interpretation of the fluctuation amplitudes at higher conductivity levels.

The same assumption concerning the reaction scheme had to be made again for the derivation of eq. (6). Moreover, the equilibrium constant K in eq. (6) presently cannot be obtained from independent measurements of the concentrations of the nonconducting species in the membrane. The presence of a second, slow time constant in the autocorrelation function (due to the described slow fluctuations) affected the accuracy of the amplitude analysis more than that of the time constants. As slow fluctuations were nearly absent in the membranes formed from dioleoyl-L-α-lecithin + cholesterol the amplitude analysis on this system is more reliable than the kinetic analysis. The opposite is true for pure dioleoyl-L-α-lecithin membranes.

We conclude that measurements of the ion current noise in membranes can be at least as reliable as relaxation studies. Due to their essentially two-dimensional geometry, membranes (and interfaces) are inherently well adapted to the main requirement for fluctuation analysis, namely that the number of observed events be sufficiently small. Apart from the practical advantage of obtaining kinetic and equilibrium information whenever the membrane current is measured, a further important advantage of fluctuation measurements lies in the fact that the system need not be perturbed. The choice of suitable perturbing parameters is rather restricted if fast membrane transport processes are to be investigated. In the case of black lipid membranes the reported method eliminates disturbing capacitive transients due to torus relaxations and makes kinetic measurements feasible, which would otherwise be impossible [24].

In our study the concentration fluctuations frequently were of the same order of magnitude as the average concentrations. Nevertheless, we observed many artifacts of which the most important examples have been discussed. The experience gained by this work at first sight seems pertinent only to a rather special type of membrane conductance which transduces concentration fluctuations into electrical noise. Many of the difficulties are, however, caused by the properties of the black lipid membrane [16]. The problems will therefore reappear in the expected attempts to apply correlation analysis to processes (diffusion, binding) measured by optical transducers, i.e., fluorescent probes.

Acknowledgement

We are particularly grateful to Dr. K. Gnädig and Dr. J. Hendrix for drawing our attention to the concept of correlation analysis and for many helpful discussions. We are also indebted to Dr. K.H. Tews for the computer program used in obtaining our amplitude histograms.

References

[1] M. Eigen and L. DeMaeyer, Relaxation methods, in: Techniques of organic chemistry, ed. A. Weissberger (Interscience, New York, 1963) Vol. VIII, p. 895.
[2] H.B. Callen and R.F. Greene, Phys. Rev. 86 (1952) 702; R.F. Greene and H.B. Callen, Phys. Rev. 88 (1952) 1387.
[3] G. Feher and M. Weissman, Proc. Natl. Acad. Sci. USA 70 (1973) 870.
[4] D. Madge, E. Elson and W.W. Webb, Phys. Rev. Letters 29 (1972) 705.
[5] A.A. Verveen and H.E. Derksen, Proc. IEEE 56 (1968) 906.
[6] K.S. Cole, Membranes, ions and impulses (University of California Press, Berkeley and Los Angeles, 1968).
[7] B. Katz and R. Miledi, J. Physiol. 224 (1972) 665.
[8] C.R. Anderson and C.F. Stevens, J. Physiol. 235 (1973) 655.
[9] H.M. Fishman, Proc. Natl. Acad. Sci. USA 70 (1973) 876.
[10] Y. Chen and T.L. Hill, Biophys. J. 13 (1973) 1276.
[11] C.F. Stevens, Biophys. J. 12 (1972) 1028.
[12] S.B. Hladky and D.A. Haydon, Nature 225 (1970) 451; Biochim. Biophys. Acta 274 (1972) 294.
[13] E. Bamberg and P. Läuger, J. Membrane Biol. 11 (1973) 177.

[14] D.M. Andrews, E.D. Manev and A.D. Haydon, Special Discussions Faraday Soc. no. 1 (1970) 46.
[15] D.W. Urry, Proc. Natl. Acad. Sci. USA 68 (1971) 672; D.W. Urry, M.C. Goodall, J.D. Glickson and D.F. Mayers, Proc. Natl. Acad. Sci. USA 68 (1971) 1907.
[16] D.A. Haydon, R. Fettiplace, L.G.M. Gordon, S.B. Hladky, J. Requena and H.P. Zingsheim, in: Methods in membrane biology, ed. E. Korn (Plenum Press, New York, in press).
[17] H. Dern and J.B. Walsh, in: Physical techniques in biological research, ed. W.L. Nastuk, (Academic Press, New York and London, 1963) Vol. VI, p. 99.
[18] S.O. Rice, Bell Syst. Techn. J. 23 (1944) 282.
[19] L.D. Landau and E.M. Lifshitz, Statistical physics (Pergamon Press, London, 1958) 350.
[20] L.G.M. Gordon and D.A. Haydon, Biochim. Biophys. Acta 255 (1972) 1014.
[21] D.A. Haydon and S.B. Hladky, Quart. Rev. Biophys. 5 (1972) 187.
[22] G. Kemp, K.A. Jacobsen and C.E. Wenner, Biochim. Biophys. Acta 255 (1972) 493.
[23] V.B. Myers and D.A. Haydon, Biochim. Biophys. Acta 274 (1972) 313.
[24] E. Neher, Asymmetric Membranes Resulting from Fusion of Two Black Lipid Bilayers, Biochim. Biophys. Acta, in press.

BIOPHYSICAL CHEMISTRY 2 (1974) 208–217. © NORTH-HOLLAND PUBLISHING COMPANY

RHEOLOGY OF FIBRIN CLOTS. II. LINEAR VISCOELASTIC BEHAVIOR IN SHEAR CREEP

Christian GERTH, Wesley W. ROBERTS and John D. FERRY
Department of Chemistry and Rheology Research Center, University of Wisconsin, Madison, Wisconsin 53706, USA

Received 28 May 1974

Creep of human fibrin clots in small shearing deformations has been studied over a time scale from 20 to 10^4 s. Most clots were prepared by the action of thrombin on purified fibrinogen, under various conditions of pH and ionic strength to produce networks with either coarse or fine structure, and with or without ligation by calcium ion and fibrinoligase. Combination of data with previous results on dynamic viscoelastic properties provided a description of viscoelastic behavior over seven logarithmic decades of time or frequency scale. Fine, unligated clots showed very little creep over most of this range. Coarse, unligated clots showed substantial creep but this was suppressed by ligation. It is postulated that the basic fibril element formed by polymerization of fibrin units remains intact under stress but that, in coarse clots, some slippage of these elements within aggregated bundles occurs unless they are secured by α–α ligation. The elastic modulus (in a time scale of seconds) is proportional to the 1.5 power of fibrin concentration in unligated clots (the magnitude for fine clots being somewhat smaller than for coarse) and to the 2.3 power for coarse, ligated clots. Creep behavior with different shear strain magnitudes (up to 0.2) and tests of creep recovery by the Boltzmann superposition principle show strict adherence to linear viscoelastic behavior, indicating no basic structural changes during the experiments, provided the structure is fully developed before strain is imposed. If progressive ligation continues in the strained state, subsequent creep recovery is incomplete. Clots formed with ancrod instead of thrombin show a smaller modulus and much more extensive creep.

1. Introduction

There has been renewed interest in study of the mechanical properties of fibrin clots to seek additional clues for unanswered problems in the mechanism of their formation from fibrinogen [1] and their detailed structure. Recent reports include measurements of dynamic viscoelastic properties [2–4] and of elastic modulus corresponding to a time scale, presumably, of a few seconds or minutes [5]. Differences between clots with coarse and fine structures, and between those with and without ligation by fibrinoligase, are of particular interest. In the fine clots, there is little lateral aggregation of the primary fibrillar structures which are postulated to have twice the cross-section area of the fibrinogen units [1, 6, 7]; in the coarse clots there is extensive aggregation to form fibers hundreds of Å in diameter.

Dynamic viscoelastic measurements in the frequency range from 0.01 to 160 Hz [3] show comparatively little dependence of modulus on frequency, though there are distinct differences between coarse and fine clots; there is little viscoelastic relaxation in the corresponding range of time scale (10^{-3} to 6 s). The present study explores linear viscoelastic behavior in a much longer time scale range, from 20 to 10^4 s, by measurements of shear creep and creep recovery in small deformations, thus extending the effective scale to 7 logarithmic decades. Time-dependent processes are more evident at longer times, especially in coarse, unligated clots.

2. Materials

The sources and methods of processing of purified fibrinogen (human), thrombin (bovine), and fibrin stabilizing factor (FSF, human) were the same as in

the first paper of this series. We are indebted to Professor L. Lorand and Mr. A.J. Gray for the FSF and for purified bovine thrombin which was used in a few experiments, and also for gel electrophoresis analysis of polypeptide chain subunit patterns which was made on a few clots to determine the extent of α–α and γ–γ ligation [8].

Determinations of the clottability of the fibrinogen by several methods gave values from 90% and 95%. (This statement, omitted in typesetting, also applies to Paper I of this series [3].)

Calcium chloride and FSF were added to the clotting mixture in amounts as specified below when ligation was desired. Presence or absence of ligation was always tested by absence of dissolution in alkaline urea or 1% monochloracetic acid, and in certain cases by gel electrophoresis analysis.

A few clots were formed with the snake venom ancrod instead of thrombin; we are indebted to Dr. Joseph F. Donahoe of the Abbott Laboratories for this material (Venacil).

As before [3], an aliquot of each clotting mixture was allowed to clot in a spectrophotometer cell and the opacity was measured at 6000 Å (at the same time that viscoelastic measurements were begun) as a gauge of coarseness. The clots described as coarse (usually formed at pH 7.5, ionic strength (μ) 0.15 of which 0.10 was sodium chloride and 0.5 tris buffer) had opacities in the range from 0.7 to 1.1 cm^{-1}, measured with an optical path length of 0.2 cm; the opacities of $> 2\ cm^{-1}$ previously reported for similar clots [3] were in error because of too large a path length. The clots described as fine (usually formed at pH 8.5, ionic strength 0.45 of which 0.40 was sodium chloride and 0.05 tris buffer) had opacities in the range from 0.01 to 0.05 cm^{-1}, measured with a path length of 1 cm.

3. Method

The torsion apparatus of Plazek et al. [9] was used for torsion of a cylindrical sample, formed by clotting in situ between two circular plates of 2 in. diameter separated usually by 1 mm. Surface tension retained the solution until clotting; clotting times were from 3 to 10 min. The lower, fixed plate was surrounded by Teflon ring with a well which was filled after clotting with mineral oil to seal the open edge of the clot against evaporation. The upper plate, suspended from a fine wire, was subjected to a torque at the beginning of an experiment by rotating the top of the wire. Since the rotation of the top was usually at least 60° and the rotation of the plate (upper surface of the clot) less than 0.1°, the torque was constant within less than 0.2% during an experiment. The rotation of the plate was followed by deflection of a light beam from a mirror rigidly attached to it. The displacement was usually followed by manual adjustment of a pair of opposed photocells mounted on a micrometer, with an optical lever of 315 in. [10]. For short time periods, automatic recording was used; the light source was a helium–neon laser and reflection from two fixed mirrors increased the path length to about 24 m.; a Honeywell–Brown recorder with two opposing photocells was used to track the beam and provide linear plots of displacement against time. The maximum shear strain was usually less than 0.04. Although the strain was inhomogeneous (greatest at the sample periphery), tests at different strains and of Boltzmann superposition in recovery (as shown below) verified linear viscoelastic behavior, so the creep compliance $J(t)$ in cm^2/dyne was calculated from the torque and angular displacement by the simple formula appropriate to linear behavior [9]. Measurements were made at the ambient temperature of 22.5 ± 0.5°C, after lapse of at least 3 hours from the moment of clotting to provide for complete development of the clot structure [5, 11].

4. Results

4.1. Characteristics of creep

Creep curves for four different types of clots with approximately the same fibrin concentration are plotted logarithmically in fig. 1; the conditions of clotting and some numerical data are listed in table 1. The fine unligated clot undergoes relatively little creep in a period of two hours. The coarse unligated clot has a smaller initial compliance (higher modulus) but creeps much more at longer times. Ligation of the coarse clot decreases the compliance (increased modulus as reported by other investigators [2, 4, 5]) and almost eliminates the creep at longer times. The latter

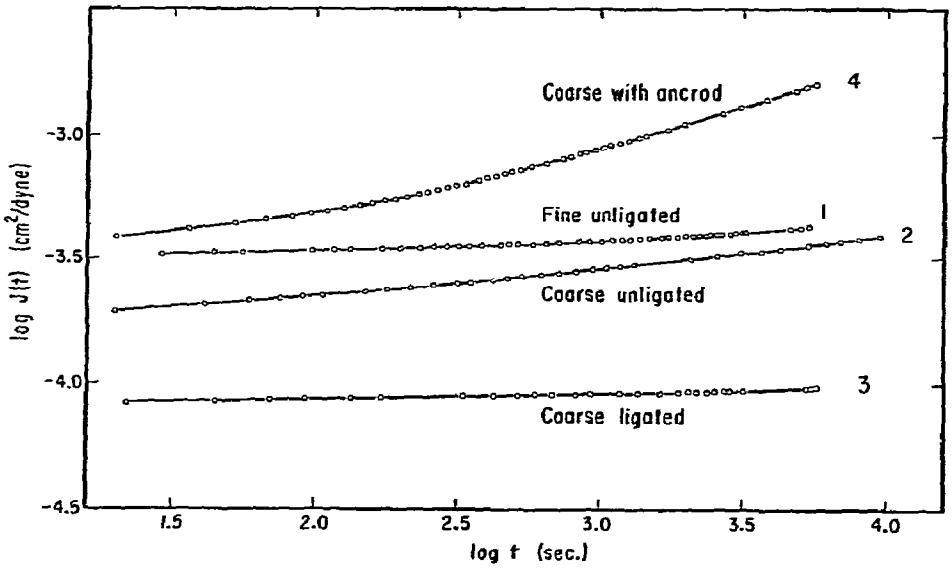


Fig. 1. Creep curves for four different types of clots; conditions are given in table 1.

behavior is consistent with the effect of ligation on stress relaxation which can be inferred from a much earlier study [12]. The clot formed with ancrod has a much larger compliance and more extensive creep than the others.

4.2. Combination of creep with dynamic viscoelastic measurements and calculation of relaxation spectrum

Since the slopes of curves 1 and 2 in fig. 1 are so small, the creep compliance can be very simply converted to the dynamic storage modulus as a function of frequency; to a close approximation, $\log G'(\omega) = -\log J(t)$, with the radian frequency ω corresponding to $1/t$ [13]. The results are combined in fig. 2 with storage modulus data measured previously in the frequency range from 0.01 to 160 Hz on coarse and fine unligated clots prepared under closely similar conditions [3]. The fibrin concentrations were not exactly the same, and different preparations of fibrinogen have been found previously to be poorly reproducible, so the data calculated from creep have been arbitrarily adjusted in magnitude ($\Delta \log G' = \pm 0.15$) where the two methods overlap. The data match well in slope and describe the viscoelastic behavior over 7 logarithmic decades of frequency scale.

Table 1
Data for comparison of types of clots (fig. 1)

Curve no.	Fibrin conc. (g/ℓ)	Thrombin or ancrod (u/ml)	pH	μ	Initial [a] strain	$-\log J(t)$ initial [a] (cm^2/dyne)	$d \log J(t)/d \log t$ initial [a]
1	10.5	T 0.04	8.5	0.45	0.017	3.48	0.03
2	10.1	T 0.34	7.5	0.15	0.042	3.72	0.10
3	8.5	T 0.05 [b]	7.5	0.15	0.017	4.08	0.02
4	8.8	A 0.43	7.5	0.15	0.020	3.41	0.13

[a] Measured 20 to 30 s after imposition of torque.
[b] With 0.0032 M Ca^{2+} and FSF 0.005 mg/mL

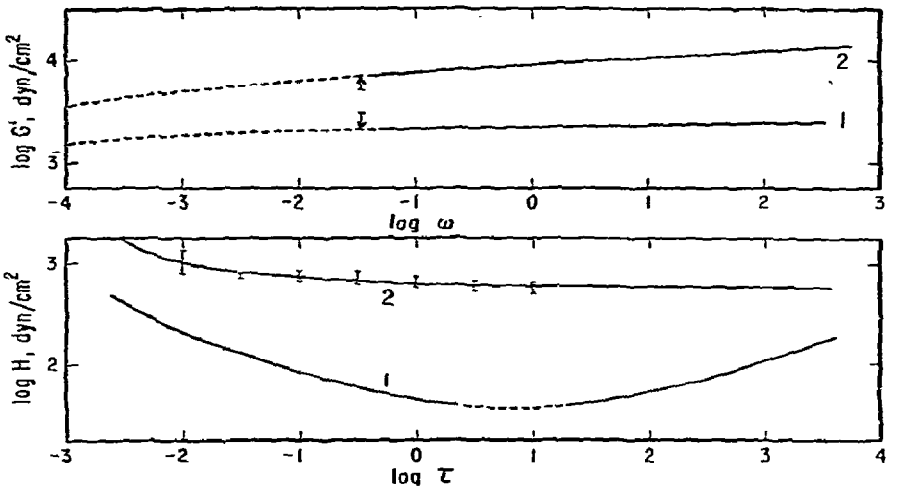


Fig. 2. Storage shear modulus G' of unligated fine (1) and coarse (2) clots plotted logarithmically against radian frequency; solid curves measured directly (ref. [3]), dashed curves converted from fig. 1. Below, relaxation spectra H of the two clots. Vertical bars connect separate calculations from G' and G''.

The relaxation spectrum H has been calculated from G' (also from G'' for the coarse clot) by first approximation formulas [13] and is also plotted in fig. 2. The spectra are very broad, and that for the fine clot goes through a shallow minimum. The relaxation strength for the coarse clot is higher than that of the fine by about an order of magnitude.

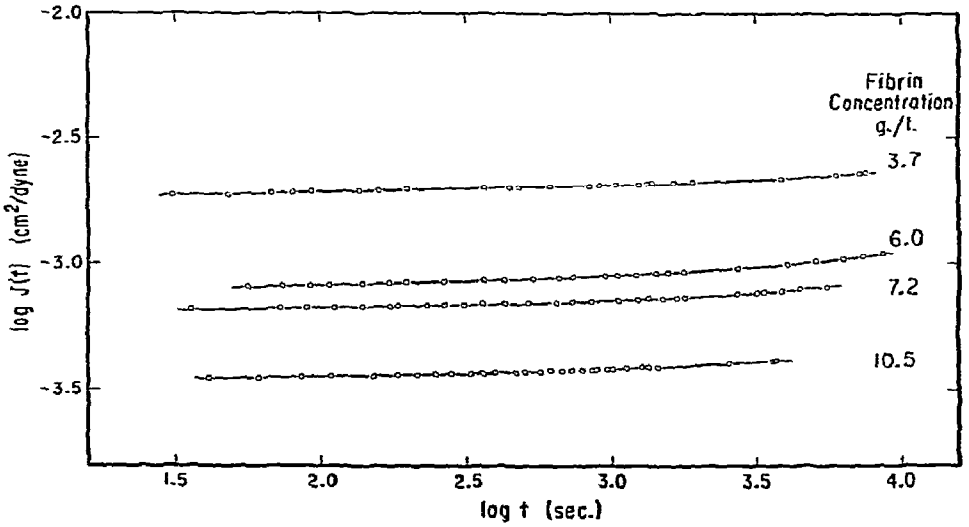


Fig. 3. Creep curves for fine, unligated clots at 4 different fibrin concentrations as shown; pH 8.4 to 8.5, μ 0.45, thrombin 0.36 to 0.40 u/ml, initial strain about 0.02.

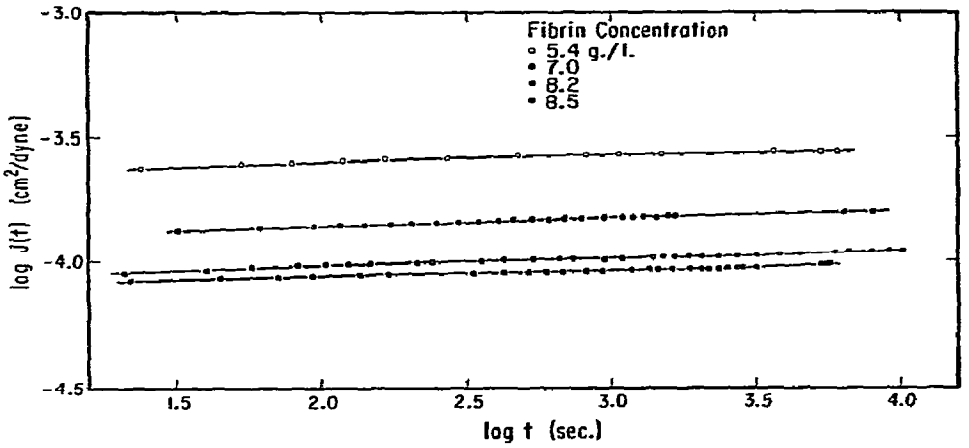


Fig. 4. Creep curves for coarse, ligated clots at 4 different fibrin concentrations as shown; pH 7.5, μ 0.15, thrombin 0.04 to 0.07 u/ml, Ca^{2+} 0.0032M, FSF 0.005 mg/ml, initial strain about 0.02.

4.3. Dependence on fibrin concentration

Logarithmic creep curves for fine, unligated clots with different fibrin concentrations are shown in fig. 3, and for coarse, ligated clots in fig. 4. In each case the slopes are closely similar at different concentrations.

Table 2
Initial compliances of various clots (20 to 30 s after imposition of torque)

F' gen Stock	pH	μ	Ligation	Fibrin conc. (g/ℓ)	Thrombin or ancrod (u/ml)	$-\log J(t)$
N- 7	7.5	0.15	no	3.0	T 0.25	3.07
N- 7	7.5	0.15	no	3.0	T 0.23	2.84
N- 7	7.5	0.15	no	5.5	T 0.20	3.39
N- 8	7.5	0.15	no a)	5.7	T 0.25	3.70
N- 8	7.5	0.15	no	8.5	T 0.07	3.27
N- 7	7.5	0.15	yes	5.3	T 0.09	3.64
N- 8	7.5	0.15	yes	5.4	T 0.05	3.62
N- 8	7.5	0.15	yes	7.0	T 0.04	3.88
N- 8	7.5	0.15	yes	8.2	T 0.07	4.04
N- 8	7.5	0.15	yes	8.2	T 0.07	4.17
N- 8	7.5	0.15	yes	8.7	T 0.05	4.07
R	8.5	0.45	no	8.2	T 0.53	3.27
R	8.5	0.45	no	9.4	T 0.53	3.23
F- 9	8.5	0.45	no	8.7	T 0.40	3.23
F-10	8.5	0.45	no	8.7	T 0.40	3.29
G-10	8.5	0.45	no	3.7	T 0.38	2.73
G-10	8.5	0.45	no a)	6.0	T 0.36	3.09
G-10	8.5	0.45	no	7.2	T 0.40	3.19
N- 9	7.5	0.15	no	8.8	A 0.43	3.41
N- 9	7.5	0.15	no	9.1	A 0.55	3.58
R	8.5	0.45	no	9.4	A	2.85
R	8.5	0.45	no	9.4	A	2.59

a) Absence of ligation confirmed by gel electrophoresis analysis.

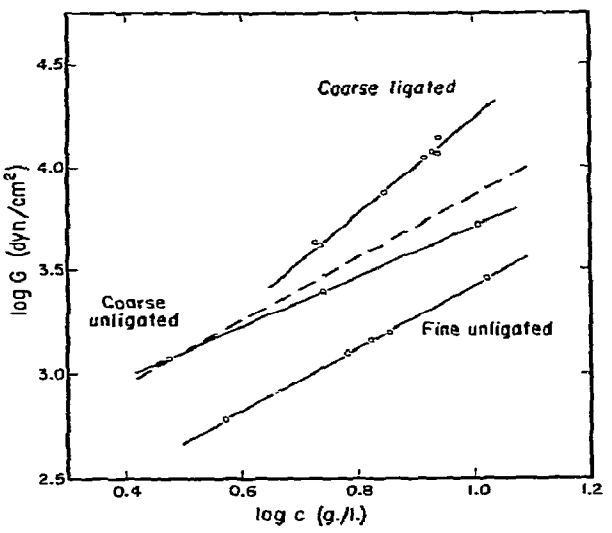


Fig. 5. Modulus corresponding to about 20 s, plotted logarithmically against fibrin concentration for three types of clots. Dashed line: data from ref. [3].

Values of the initial compliance, i.e., corresponding to 20 to 30 s after imposition of stress, for these and other clots formed under various conditions are listed in table 2. The corresponding initial modulus (reciprocal of compliance, and corresponding to G' near the center of the frequency range in fig. 2) is plotted logarithmically against fibrin concentration in fig. 5. The moduli of the unligated clots, both coarse and fine, are proportional approximately to the 1.5 power of concentration. (The limited data for coarse unligated shown here give a somewhat smaller slope, but earlier data [3, 11] correspond to 1.5.) For the coarse ligated clots, however, the modulus is proportional to the 2.3 power of concentration. The higher exponent is consistent with earlier measurements of Roberts et al. [2]. Fine, ligated clots will be investigated subsequently with determination of both α–α and γ–γ ligation (see Discussion below). Ligation increases the modulus, as observed by others [2, 4, 5], though this effect was not prominent in the fragmentary results of the first paper of this series [3].

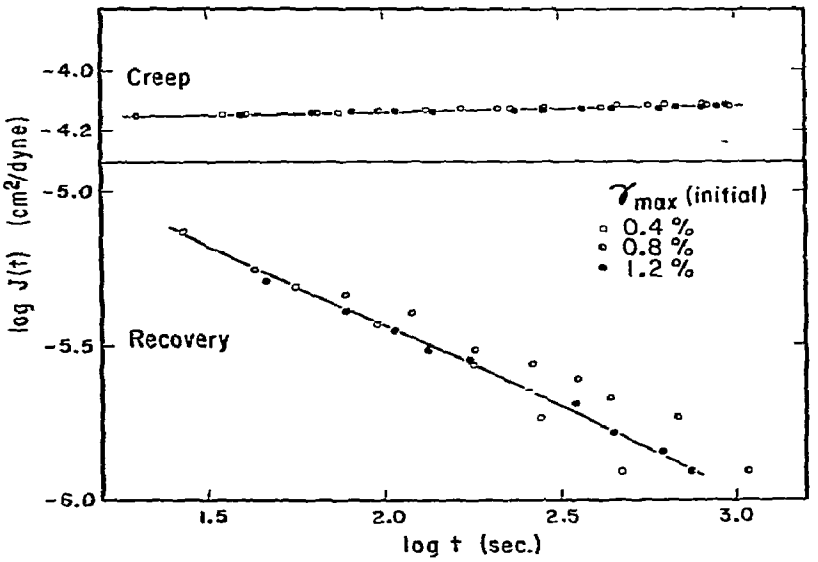


Fig. 6. Creep compliance and creep recovery compliance of a coarse, ligated clot at three strain magnitudes as shown; fibrin 8.6 g/ℓ, pH 7.4, μ 0.15, thrombin 0.05 u/ml, Ca^{2+} 0.0032M, FSF 0.005 mg/ml.

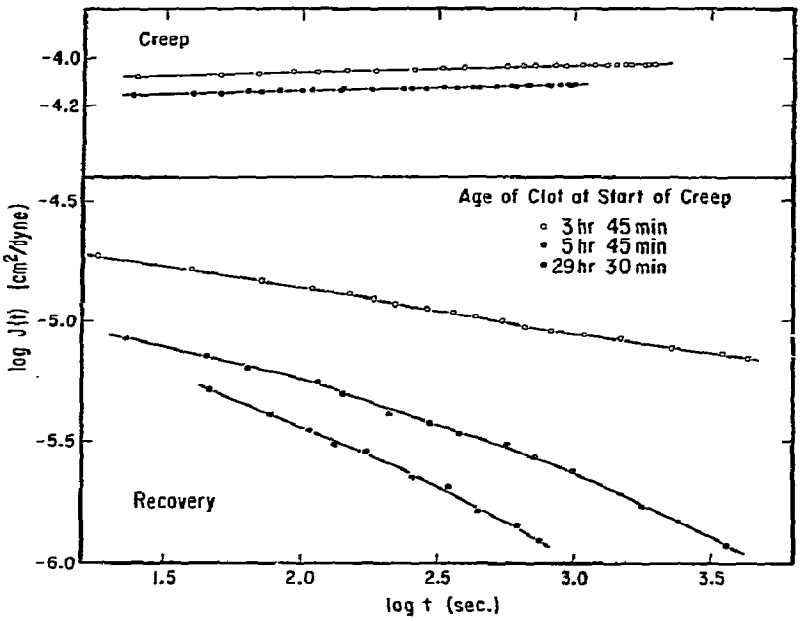


Fig. 7. Creep compliance and creep recovery compliance of a coarse, ligated clot; creep experiment begun at three different elapsed times since clot formation. Conditions same as for fig. 6.

4.4. Creep and recovery: effect of strain and age of clot, test of Boltzmann superposition principle

Creep recovery measurements were made by rotating the top of the torsion wire back to the position corresponding to zero torque and following the decrease of strain with time. Examples are shown in fig. 6 for a coarse, ligated clot which had aged for one day before these measurements, with three different magnitudes of initial strain. First, the compliance during the creep is independent of strain magnitude, showing linear viscoelastic behavior within this range of small strains ($\leqslant 0.012$). The compliance during creep recovery is also independent of strain magnitude; the points are scattered because the strains measured in recovery are very small. Thus, after 10^3 s, the recovery is more than 98% complete and a linear instead of a logarithmic plot would be close to the abscissa axis.

For a coarse, ligated clot measured after a shorter lapse of time since clotting, however, both creep and creep recovery were different from those of a well-aged clot. In fig. 7, it is evident that the compliance during creep is smaller after 4 h than after 6 h, corresponding to a stiffer structure. The recovery curves are entirely different, the recovery being much more nearly complete after 6 h. From 6 to 29 h, there is no perceptible change in the creep curve but the extent and speed of recovery are increased. In view of the recent work of Hermans and collaborators [5], these differences may be attributed to progressive ligation of α chains; the increased modulus associated with ligation appears to be associated with α–α rather than γ–γ linkages. When the creep experiment begins 4 h after clotting, the bonds introduced gradually after that point tend to link the structure in its *strained state*. Hence, after release of stress, the sample does not return to its original shape but rather approaches a state of ease in which the bonds formed before and after the creep experiment began are pulling in opposite directions. (Such behavior has been investigated previously for other cross-linked systems with very different structures, viz., gelatin gels [14] and rubbers [15].) For the fully aged clot, all the bonds are presumably formed before the creep experiment begins and none are formed in the strained state, so

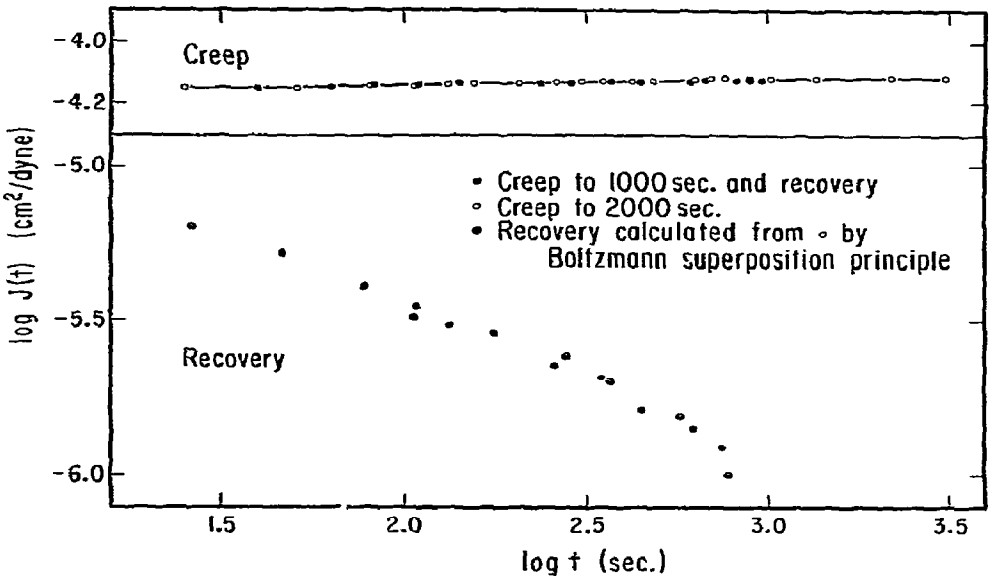


Fig. 8. Creep compliance and creep recovery compliance for a coarse, ligated clot with test of Boltzmann superposition principle. Conditions same as for fig. 6.

subsequent recovery is nearly complete.

A severe test of linearity in viscoelastic behavior is application of the Boltzmann superposition principle to predict the creep recovery from the creep. It should be given [16] by

$$J_r(t) = J(t) - J(t - t_1), \qquad (1)$$

where t_1 is the time the stress was removed, $J(t)$ is the creep compliance that would have been measured at time t if the stress had not been removed, and $J(t - t_1)$ is the creep compliance corresponding to the time point $t - t_1$. Two experiments are required, one with recovery starting at t_1 and another with continued creep to the maximum time for which recovery is to be calculated. An example is given in fig. 8 for a coarse, ligated clot; the agreement with observed and calculated values is very good. Similar agreement is observed in fig. 9 for a fine, unligated clot. This linear viscoelastic behavior implies that the material could be modelled by a combination of linear springs and dashpots whose parameters do not change during the duration of the experiments; there is no fundamental change in the structure associated with either strain or aging. For the creep after 3 h 45 min in fig. 7, by contrast, the Boltzmann superposition fails completely because of structural changes during the experiment.

5. Discussion

A theory has been proposed by Sternstein [17] for the elastic modulus for a random two-dimensional fibrous structure; from it one can infer that for a three-dimensional structure as well, the modulus will depend on the number of fibrous elements (proportional to the number of branch points [5]), and the stiffness of the fibrous elements in various deformations by extension, bending, and relative rotations of the elements at their junctions. The higher modulus of the coarse clots may be attributed to greater stiffness of the larger constituent fibers outweighing the smaller number of fibers per unit volume. The increased modulus of coarse clots with ligation is probably attributable to increased stiffening; the change in concentration dependence from an exponent of 1.5 to 2.3 may provide a clue to the nature of the stiffening in that the exponent is expected to increase with increasing rotational stiffness at junctions rela-

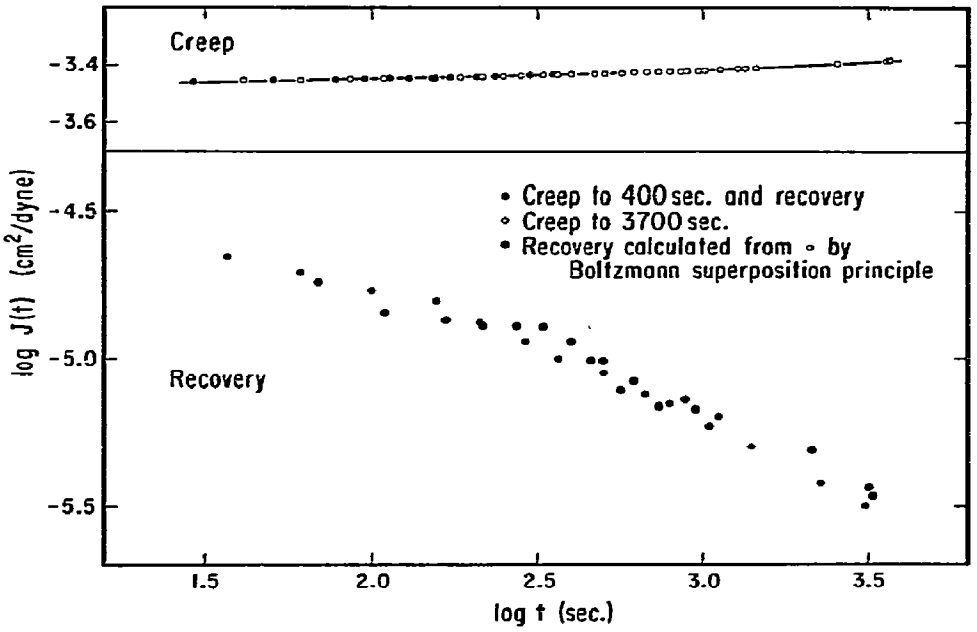


Fig. 9. Creep compliance and creep recovery compliance for a fine, unligated clot with test of Botzmann superposition principle. Fibrin 10.5 g/ℓ, pH 8.5, μ 0.45, thrombin 0.40 u/ml, initial strain 0.017.

tive to extensional stiffness [18].

It is an attractive postulate that the γ–γ ligations bind fibrin monomer units into protofibrils with twice the cross-section area of the monomer and the staggered overlapping arrangement proposed for intermediate fibrin polymers [7], while the α–α ligations bind such protofibrils together in the lateral aggregations which occur in coarse clots [1]. Then the modulus increase produced by α–α ligation may be regarded an effect of strengthening the coherence of these lateral aggregations, which should indeed affect rotational and flexural more than extensional stiffness.

In the same framework, the creep which is most prominent in coarse, unligated clots can be attributed to slippage of the protofibrils within the aggregated bundles. It is largely absent in the fine clots because they have very little lateral aggregation; it is suppressed in the ligated coarse clots by the α–α ligations which prevent slippage.

It is not clear at present how the lower modulus and much more prominent creep of clots formed with ancrod are associated with structural differences occasioned by the inability of this enzyme to release the B fibrinopeptide. Further experiments are in progress to probe clues to the detailed structures of clots of various types.

Acknowledgement

This work was supported in part by Grant HL-13760 from the National Institutes of Health. We are much indebted to Professor L. Lorand and Mr. A.J. Gray, Jr., of Northwestern University for their advice, help, and cooperation in various aspects of these studies, and to Mr. F.H.M. Nestler for help with preparation and characterization of the proteins.

References

[1] R.F. Doolittle, Adv. Protein Chem. 27 (1973) 1.
[2] W.W. Roberts, L. Lorand and L.F. Mockros, Biorheology 10 (1973) 29.
[3] W.W. Roberts, O. Kramer, R.W. Rosser, F.H.M. Nestler and J.D. Ferry, Biophys. Chem. 1 (1974) 152.

[4] L.F. Mockros, W.W. Roberts, and L. Lorand, Biophys. Chem. 2 (1974) 164.
[5] L.L. Shen, R.P. McDonagh, J. McDonagh and J. Hermans, Jr., Biochem. Biophys. Res. Comm. 56 (1974) 793.
[6] J.D. Ferry, Proc. Nat. Acad. Sci. U.S. 38 (1952) 566.
[7] J.D. Ferry, S. Katz and I. Tinoco, J. Polymer Sci. 12 (1954) 509.
[8] P. McKee, P. Matlock and R.L. Hill, Proc. Nat. Acad. Sci. U.S. 66 (1970) 738.
[9] D.J. Plazek, M.N. Vrancken and J.W. Berge, Trans. Soc. Rheol. 2 (1958) 39.
[10] R.A. Dickie and J.D. Ferry, J. Phys. Chem. 70 (1966) 2594.
[11] J.D. Ferry and P.R. Morrison, J. Am. Chem. Soc. 69 (1947) 388.
[12] J.D. Ferry, M. Miller and S. Shulman, Arch. Biochem. Biophys. 34 (1951) 424.
[13] J.D. Ferry, Vicoelastic properties of polymers, 2nd Ed. (Wiley, New York, 1970) Ch. 4.
[14] M. Miller, J.D. Ferry, F.W. Schremp and J.E. Eldridge, J. Phys. Colloid Chem. 55 (1951) 1387.
[15] P.J. Flory, Trans. Faraday Soc. 56 (1960) 722.
[16] Reference [13] p. 20.
[17] S.S. Sternstein, in: Cellulose and cellulose derivatives, Vol. 5, eds. N. Bikales and L. Segal (Wiley, New York, 1971) p. 649.
[18] S.S. Sternstein, personal communication.

BIOPHYSICAL CHEMISTRY 2 (1974) 218–230. ©NORTH-HOLLAND PUBLISHING COMPANY

DIELECTRIC INCREMENT AND DIELECTRIC DISPERSION OF SOLUTIONS CONTAINING SIMPLE CHARGED LINEAR MACROMOLECULES

I. THEORY

F. VAN DER TOUW and M. MANDEL

Gorlaeus Laboratoria der Rijksuniversiteit Leiden, afdeling Fysische Chemie III, Leiden, The Netherlands

Received 18 April 1974
Revised manuscript received 13 August 1974

A theory is derived for the static and frequency dependent value of the electric permittivity for model systems representing a solution of a macromolecule bearing a large number of identical charges. The polyion is represented either as a charged rigid rod (A) or as a sequence of charged rodlike subunits in an arbitrary but fixed configuration (B) and it is assumed that a certain fraction of the counterions is closely associated to the macromolecule. The dielectric properties are described in terms of fluctuations in the distribution of the associated counterions along the polyion. These fluctuations can occur locally between potential barriers marking the ends of the subunits (if considered) but can also extend over the whole molecule. Neglecting correlations between different associated counterions expressions for the static value of the dielectric increment are obtained which reveal its dependence on the fraction of bound ions, on the charge of the counterions and on the length of the molecule for model A or the radius of gyration for model B. The dynamic behaviour of A is distinguishable from that of B as the former will present one single dispersion curve of the frequency dependent electric permittivity while the latter may give rise to two different dispersion regions. This will be the case if both the exchange between bound and free ions and the rotation of the complete molecule are relatively slow in comparison to the local bound counterion density fluctuations and if these fluctuations occur on a much shorter time scale than the ion density fluctuations extending over the complete macromolecule.

1. Introduction

Dielectric properties of solutions of charged macromolecules, both natural and synthetic, have been extensively studied as it is expected that the dielectric behaviour may yield information on molecular dimensions and geometry, charge distribution, binding phenomena, etc. Recent reviews can be found in the articles by Block and North [1] and by Schwarz [2]. For aqueous solutions of highly charged macromolecules bearing only one kind of charged groups such as simple synthetic polyelectrolytes, charged polypeptides and DNA (at neutral pH) the dielectric properties are often interpreted in terms of a large induced dipole moment resulting from the deformation by the electric field of the ionic atmosphere, particularly that part containing the so-called bound counterions. Several theoretical approaches based on a rigid rodlike model for the polyion gave expressions for the static dielectric increment due to the dissolved polyelectrolyte [3, 6] and discussed the dielectric dispersion in terms of the relaxation of the perturbed ionic atmosphere [3, 4, 6]. A spherical model for the polyion was also used [7]. These theories always predict a single dispersion curve with a molecular weight dependent relaxation time in agreement with experimental observations at frequencies below 1 MHz [8–11]. These results suggested the existence of a second dispersion region at higher frequencies which was observed already in an early stage [12]. A systematic investigation by Sachs et al. [13] of the dielectric behaviour of polystyrenesulphonic acid and polyacrylic acid in the frequency region between 1 and 100 MHz and by Allen et al. [14] for carboxymethylcellulose confirmed the existence of this second dispersion region characterized by a molecular weight independent relaxation time. Results

obtained by Minakata and Imai [15] and in our laboratory [16] over a wide frequency region demonstrated the existence of both dispersion regions for several synthetic polyelectrolytes, poly-glutamic acid and DNA. For the rodlike alfalfa mosaic virus particle (at neutral pH where it is essentially negatively charged) only one single dispersion curve was observed however between 10 kHz and 100 MHz and the experimental results were found to be in fair agreement with the earlier theoretical predictions [17]. It has been suggested that the higher frequency dispersion region found for many polyelectrolytes should be ascribed to a Maxwell–Wagner effect but this cannot explain why a rigid charged particle, such as the alfalfa mosaic virus, only presents a single dispersion region. Also in general a Maxwell–Wagner effect will be characterized by a relaxation time which will depend on the molecular geometry and dimensions.

Recently we have proposed [16] that the existence of two dispersion regions may be connected to deviations from the rigid rodlike conformation of most flexible charged polyelectrolytes.

In the present paper we shall derive theoretical expressions for the static dielectric increment and the dielectric dispersion for solutions of large, highly charged particles. Only simple polyelectrolytes will be considered, the case of polyampholytes being excluded. The charged particles will be represented either as rigid rods or as rigid sequences of rodlike subunits of arbitrary but fixed conformation. In both cases the deformation of the ionic atmosphere due to the so-called bound counterions will be taken into account as well as the exchange between bound and free counterions and the orientation of the charged particles. It will be shown that for the non-rodlike polyelectrolytes two distinct dispersion regions may be expected in agreement with the experimental facts. In subsequent papers experimental results obtained with several charged macromolecules in aquous solutions will be discussed in terms of this theoretical approach.

2. General considerations concerning the models used

In the present calculation we shall use for the description of the dielectric properties of a solution of charged polyelectrolytes two models for the polyion. In a macromolecule of large dimensions a great number of conformations may occur due to the flexibility of the chain which is, however, strongly affected by the repulsion of the fixed charges on the polyion. Properties which are determined essentially by short sequences of monomeric units along the chain can be derived from a rigid rod model. This is the case for many thermodynamic properties, e.g., ion binding [18, 19]. For others where the macromolecular dimensions play a first order role, such as viscosity and light scattering, it is necessary however to consider deviations from the rigid rod representation explicitely. As this seems also to be the case for the dielectric properties of some charged polyelectrolytes [16] we shall derive expressions based on two models in which the macromolecular chain is represented either as a *rigid rod* or as a *sequence of identical rigid rodlike subunits*. In the latter case the subunits, defined by a reasonable number of monomers of the order of several tens, will be treated as occurring in a given time independent configuration.

We shall consider only salt-free solutions of polyelectrolytes sufficiently diluted to neglect interactions between polyions. For such solutions most properties can be derived additively from the properties of a subvolume V_s of the system [18] ($V_s = V/N_M$, where V is the total volume of the system and N_M the number of macromolecules) containing one single polyion of charge $-Z_0$ and its N counterions of charge ze ($Nz - Z_0 = 0$) with e the positive unit charge, Z_0 the number of unit charges on the negatively charged polyion and z the number of unit charges on the positively charged counterion. As electroneutrality has to be assumed in V_s the total dipole moment of the charge distribution due to the polyion and its counterions can be defined with respect to an arbitrary origin which for convenience will be chosen in the center of mass of the polyion.

In polyelectrolyte solutions strong interactions occur between the polyion and its counterions and the behaviour of such solutions deviates considerably from the behaviour of solutions of simple electrolytes containing an identical number of charged units. This is essentially due to the fact that in the former the charged units which are connected into macromolecular chains cannot diffuse freely through the total available volume as is the case for the latter. An exact theoretical treatment of polyelectrolyte solutions, taking into account the distribution of the ionic charges

of both the polyions and the small ions, is very difficult. Therefore more simple descriptions for the charge distribution are often used. For many properties the so-called two-phases model [19] has been found to yield a satisfactory description of the behaviour of polyelectrolyte solutions and will also be used presently. In this model a certain average fraction $\bar{f}$ of all counterions are considered to be bound so strongly to the polyion that their ability of free translation through the system is lost and they are part of the macromolecular phase. The other counterions of average fraction $(1-\bar{f})$ are treated if they were without specific interactions with the polyion of *reduced charge* $-e(Z_0-\bar{f}Nz)$. In fact in the two-phases model all specific interactions are accounted for through $\bar{f}$. Therefore in this model the solution of the partially screened-off polyion and the free counterions behave "ideally" and can be treated as a solution of simple electrolytes. The latter have been found to show no appreciable deviations of their dielectric behaviour at low concentrations with respect to the solvent. The specific and large dielectric effects observed with polyelectrolyte solutions must thus, according to the two-phases model, be determined essentially by the macromolecular phase containing the polyion and the bound counterions distributed along the macromolecular chain.

In what follows we shall derive expressions for the static dielectric increment of the polyelectrolyte solution and its frequency dependence based on the polarization of the macromolecule and its bound counterions, within the framework of the two models considered. We shall neglect the contribution to this polarization arising from the permanent dipole moment of the macromolecule itself. This is justified by the fact that for uncharged linear macromolecules the dielectric increments are negligibly small compared to those of charged ones. As pointed out before only the case of simple polyelectrolytes bearing one kind of charged (or chargeable) groups will be considered. Thus effects due to chemical relaxation as introduced by Schwarz [2, 20, 21] will not be included. In the theoretical treatment a certain number of simplifying assumptions will be introduced. The most important one will consist in the neglect of the correlation between bound counterions as was done in an earlier stage [4]. The influence of these interactions have been studied for the rodlike model by McTague and Gibbs [5], Minakata and Imai [15], Oosawa [6], Schurr [22] and recently by Warashina and Minakata [23]. It follows particularly from the last three papers that taking into account only the interactions between the bound counterions but neglecting other interaction effects or corrections for other simplifying assumptions may lead to overestimation of the deviations from the more simple theory. The theoretical analysis becomes far too intricate to be handled properly if most of the simplifying assumptions are dropped. Therefore the bound counterion interaction effect has not been included in our present treatment.

3. The polyion as a rigid rod

Let us represent the macromolecule as an infinitely thin rigid rod of length L with Z_0 identical charged $-e$ equally spaced along the rod. In this unidimensional model the *bound counterions* of charge ze each are characterized by a given equilibrium distribution along the axial direction. If the rod is assumed to be of infinite length the axial equilibrium distribution in the absence of any external perturbation will be uniform. For a rod of finite length L the equilibrium distribution will deviate from uniformity towards the ends but it may be assumed that these end-effects are negligibly small for rods of sufficiently large dimensions.

The position of the center of mass of the polyion and its orientation (defined by the orientation of the unit vector $\boldsymbol{l}_L$ in the axial direction of the rod) are defined with respect to an external coordinate system (X, Y, Z). An internal unidimensional reference frame parallel to $\boldsymbol{l}_L$ is introduced, the origin coinciding with the center of mass of the polyion. In this internal reference frame the position of the fixed charges on the rod are given by ρ_i and of the bound counterions by $\boldsymbol{r}_i(\rho_i = \rho_i \boldsymbol{l}_L$ and $\boldsymbol{r}_i = r_i \boldsymbol{l}_L)$.

The equilibrium distribution of the bound counterions is perturbed by the application of an external electric field. Let us assume that if an uniform average field $E(t)$ is established in the total system the uniform field acting on the polyion and its bound counterions may be represented by $E^P(t)$. If the system is isotropic E and E^P are parallel to the unit vector $\boldsymbol{l}_e$ in the direction of the external field. The contributing $\Delta H(t)$ to the hamiltonian of V_s arising from the polyion and its counterions can be represented by

$$\Delta H(t) = \Delta H^0(t) - ze \sum_{i=1}^{N} f_i(t)\, r_i(t) \cdot E^p(t) + e \sum_{j=1}^{Z_0} \rho_i \cdot E^p(t) = \Delta H^0(t) - ze \sum_{i=1}^{N} f_i(t)\, r_i(t) \cdot E^p(t)\,. \tag{1}$$

Here $\Delta H^0(t)$ stand for the contribution in the absence of the field. It has been assumed that the interactions between polyion, counterions and the solvent are unaffected by the *small* field applied and that the only contribution due to this field arises from the dipole moment of the charge distribution due to the fixed charges on the polyion and the charges on the bound counterions. The contribution arising from the permanent dipole moment and the free counterions in the presence of E have thus been neglected. The contribution of the bound counterions is written as a sum over *all* counterions ($1 \leqslant i \leqslant N$) but binding is taken into account through an ionic binding factor f_i which can have only two values: $f_i(t) = 1$ if ion i may be considered bound at the moment t and $f_i(t) = 0$ if ion i is free. Furthermore due to the symmetric distribution of the fixed charges on the rod the following condition is satisfied,

$$\sum_{j=1}^{Z_0} \rho_j = \left(\sum_{j=1}^{Z_0} \rho_j \right) I_L = 0\,, \tag{2}$$

which was already introduced into (1). The total time dependent dipole moment of the polyion and its bound counterions is given by

$$m(t) = ze \sum_{i=1}^{N} f_i(t)\, r_i(t)\, I_L(t)\,, \tag{3}$$

where again condition (2) has been used.

In what follows a certain number of assumptions will be used: (1) no interactions between small ions are taken into account (i.e., correlations between small ions are neglected); (2) there is no correlation between the distribution of the counterions and the configuration of the rod representing the polyion, all interactions between the polyion and its counterions being taken into account only through the binding factors; (3) the binding factors themselves are not correlated to the distribution of the counterions along the rod and the configuration of the rod. Furthermore no remanent polarization arising from the polyion and its bound counterions will be considered so that $(\Delta P_0)_{E^p=0} = 0$. It then follows that

$$\langle m(0) \rangle_0 = ze \sum_{i=1}^{N} \langle f_i(0)\, r_i(0)\, I_L(0) \rangle_0 = 0. \tag{4}$$

Here the brackets $\langle \ldots \rangle_0$ stand for an ensemble average with the *time independent distribution function in the absence of the field* which is proportional to $\exp(-\Delta H^0/kT)$. This average has to be performed over all possible configurations of the counterions (at constant configuration of the polyion) and all configurations of the polyion itself. As according to the assumption there is no correlation between $f_i(0)$ and $r_i(0)\, I_L(0)$, the average fraction of bound ions $\bar{f}$ may be defined by

$$\bar{f}N = \sum_{i=1}^{N} \langle f_i(0) \rangle_0\,, \tag{5}$$

and it follows from (4) that the following condition holds:

$$\langle r_i(0)\, I_L(0) \rangle_0 = \langle r_i(0) \rangle_0 \langle I_L(0) \rangle_0 = 0\,. \tag{6}$$

As the average distribution of counterions in the absence of the field has been assumed to be uniform and all orientations of the rod are equally probable under the same conditions (due to the neglect of polyion interactions) both quantities on the r.h.s. of (6) are equal to zero separately.

It is possible to derive an expression for the static value ΔP_s of the additional polarization arising from the bound ions and the polyion. As it is assumed that the electrostatic interactions between solvent and macromolecule may be neglected ΔP_s will represent the total change in polarization of the whole system. In the linear approximation with respect to the field ΔP_s will be given by

$$\Delta P_s = [(ze)^2 C_M/kT] \left\langle \left[I_e \cdot \sum_{i=1}^{N} f_i(0)\, r_i(0)\, I_L(0) \right]^2 \right\rangle_0 E_s^p , \tag{7}$$

where E_s^p stands for the static value of the effective field acting on the macromolecule, and C_M for the number of polyions per unit volume ($C_M = V_s^{-1}$). Using the assumptions introduced explicitely above the expression for ΔP_s can be put into the following form:

$$\Delta P_s = [(ze)^2 C_M/kT] \sum_{i=1}^{N} \sum_{j=1}^{N} [I_e \cdot \langle f_i(0) f_j(0)\rangle_0 \langle r_i(0)\, r_j(0)\rangle_0 \langle I_L(0)\, I_L(0)\rangle_0 \cdot I_e]\, E_s^p . \tag{8}$$

As $\langle r_i(0)\, r_j(0)\rangle_0 = \langle r_i^2(0)\rangle_0 \delta^{ij}$, $f_i(0) = f_i^2(0)$ and $\langle I_L I_L\rangle_0 = \frac{1}{3}\mathbf{U}$, with δ^{ij} the Kronecker delta and $\mathbf{U}$ the unit tensor of second rank, (8) may be transformed into

$$\Delta P_s = [(ze)^2 C_M/3kT] \tfrac{1}{12} \bar{f} N L^2 E_s^p . \tag{9}$$

Here use has been made of the fact that $\langle r_i^2(0)\rangle_0 = \frac{1}{12}L^2$ which follows from the uniform distribution of the counterions in the absence of the field (as can be calculated either by considering that the distribution can occur continuously over the total length L or over discrete sites equally spaced along the rod). From (9) an expression can be derived for the static dielectric increment $\Delta\epsilon_s$ of the polyelectrolyte solution with respect to the electric permittivity of the solvent.

$$\Delta\epsilon_s = \Delta P_s \cdot E_s/\epsilon_0 E_s^2 = [(ze)^2 C_M \bar{f} N L^2/36\, kT\epsilon_0]\gamma , \tag{10}$$

where $\gamma = (E^p/E_s)$ and ϵ_0 is the electric permittivity in vacuo (practical, rationalized units are used throughout). This expression is in agreement with previously derived expressions for polyions which can be represented as rigid rods [4], neglecting bound counterions interactions.

The additional time dependent polarization $\Delta P(t)$ of the system arising from polyions and counterions may be represented in the following way

$$\Delta P(t) = \int_{-\infty}^{\infty} \phi(t')\, E^p(t-t')\, dt' , \tag{11}$$

where $\phi(t)$ is the scalar response function which, in the linear approximation, can be expressed as follows in terms of molecular parameters using Kubo's theory [24]:

$$\phi(t) = -\frac{(ze)^2 C_M}{kT} \frac{\partial}{\partial t} \langle [I_e \cdot m(0)]\, [m(t) \cdot I_e]\rangle_0$$

$$= -\frac{(ze)^2 C_M}{kT} \frac{\partial}{\partial t} \left\langle \left[I_e \cdot \sum_{i=1}^{N} f_i(0)\, r_i(0)\, I_L(0) \right] \left[\sum_{j=1}^{N} f_j(t)\, r_j(t)\, I_L(t) \cdot I_e \right] \right\rangle_0 . \tag{12}$$

Fourier transformation of (11) yields a relation between the frequency dependent polarization $\Delta P(\omega)$ and the frequency dependent electric susceptibility $\Delta\chi(\omega)$, where ω stands for the circular frequency of the applied field.

$$\Delta P(\omega) = \Delta\chi^*(\omega)\, E^p(\omega) , \tag{13}$$

$$\Delta\chi^*(\omega) = \int_0^{\infty} e^{-i\omega t} \phi(t)\, dt . \tag{14}$$

The susceptibility is related to the frequency dependent dielectric increment $\Delta\epsilon^*(\omega)$:

$$\Delta\chi^*(\omega)\, E^p(\omega) = \epsilon_0 \Delta\epsilon^*(\omega)\, E(\omega) . \tag{15}$$

Combining eqs. (13) and (15) yields the following expression for the time dependent dielectric increment of the

solution, assuming $E^{\mathrm{p}}(\omega)/E(\omega) = E_{\mathrm{s}}^{\mathrm{p}}/E_{\mathrm{s}} = \gamma$.

$$\Delta\epsilon^*(\omega) = (\gamma/\epsilon_0) \int_0^\infty \mathrm{e}^{-i\omega t}\, \phi(t)\, \mathrm{d}t\,. \tag{16}$$

The frequency dependence is entirely determined through the Fourier transform of the response function as defined by (12). If the same procedure is applied to (12) as used for obtaining (8) from (7) the following expression is found for the response function.

$$\phi(t) = -\frac{(ze)^2 C_{\mathrm{M}}}{kT} \frac{\partial}{\partial t}\left[\sum_{i=1}^{N} \langle f_i(0)\, f_i(t)\rangle_0 \langle r_i(0)\, r_i(t)\rangle_0 \langle \boldsymbol{l}_{\mathrm{e}} \cdot \boldsymbol{l}_{\mathrm{L}}(0)\, \boldsymbol{l}_{\mathrm{L}}(t) \cdot \boldsymbol{l}_{\mathrm{e}}\rangle_0 \right]. \tag{17}$$

Here use has been made of the fact that $\langle r_i(0)\, r_j(t)\rangle_0 = \langle r_i(0)\, r_i(t)\rangle_0\, \delta^{ij}$ and has the same value for any ion which can fluctuate along the macromolecular rod.

The response function as given by (17) can also be written as the time derivative of a normalized decay function $\Gamma(t)$

$$\phi(t) = -\frac{(ze)^2 C_{\mathrm{M}}}{kT}\left[\frac{\partial}{\partial t}\Gamma(t)\right] \left\langle \left[\boldsymbol{l}_{\mathrm{e}} \cdot \sum_{i=1}^{N} f_i(0)\, r_i(0)\, \boldsymbol{l}_{\mathrm{L}}(0) \right]^2 \right\rangle_0, \tag{18}$$

$$\Gamma(t) = \frac{\langle [\boldsymbol{l}_{\mathrm{e}} \cdot \boldsymbol{m}(0)]\, [\boldsymbol{m}(t) \cdot \boldsymbol{l}_{\mathrm{e}}]\rangle_0}{\langle [\boldsymbol{l}_{\mathrm{e}} \cdot \boldsymbol{m}(0)]\, [\boldsymbol{m}(0) \cdot \boldsymbol{l}_{\mathrm{e}}]\rangle_0} = \frac{[\Sigma_{i=1}^{N} \langle f_i(0)\, f_i(t)\rangle_0] \langle r_i(0)\, r_i(t)\rangle_0 \langle \boldsymbol{l}_{\mathrm{e}} \cdot \boldsymbol{l}_{\mathrm{L}}(0)\, \boldsymbol{l}_{\mathrm{L}}(t) \cdot \boldsymbol{l}_{\mathrm{e}}\rangle_0}{[\Sigma_{i=1}^{N} \langle f_i(0)\, f_i(0)\rangle_0] \langle r_i(0)\, r_i(0)\rangle_0 \langle \boldsymbol{l}_{\mathrm{e}} \cdot \boldsymbol{l}_{\mathrm{L}}(0)\, \boldsymbol{l}_{\mathrm{L}}(0) \cdot \boldsymbol{l}_{\mathrm{e}}\rangle_0}. \tag{19}$$

It can be seen that the decay function $\Gamma(t)$ is a product of three independent decay functions, one for the fluctuations in the number of bound counterions, one characteristic for the fluctuations of the counterions along the rod and finally a decay function for the orientational fluctuations of the rod with respect to the direction of the external field. If all three decay functions may be represented by exponentials with respect to time with three characteristic relaxation times τ_{f}, τ_{c} and τ_{r} respectively, then $\Gamma(t)$ will also be an exponential function leading, together with (9), (11), (12) and (16) to the following expression for the frequency dependent dielectric increment.

$$\Delta\epsilon^*(\omega) = \Delta\epsilon_{\mathrm{s}}\, (1 + i\omega t)^{-\mathrm{i}}, \tag{20}$$

$$\tau^{-1} = \tau_{\mathrm{f}}^{-1} + \tau_{\mathrm{c}}^{-1} + \tau_{\mathrm{r}}^{-1}\,. \tag{21}$$

It follows from (20) and (14) that the amplitude of the dielectric dispersion due to the rigid rod and its bound counterions is entirely determined by the dipole moment resulting from the perturbation of the bound ions distribution in the presence of an electric field. The relaxation time of this dispersion, here assumed of the Debye-type, is however not solely dependent on fluctuations in the bound ions distribution but also contains contributions from the orientational motion of the polyion and from the exchange mechanism between bound and free ions. Only if the three relaxation times τ_{f}, τ_{c} and τ_{r} are differing significantly in order of magnitude will the relaxation time of the dielectric dispersion according to (21) be determined essentially by the fastest mechanism, i.e., the mechanism which has the shortest relaxation time.

4. The polyion as a sequence of rigid rods

The average conformation of the polyion here considered is a sequence of p subunits represented by infinitely thin rigid rods of equal length b, each of which is in a fixed time-independent relative orientation with respect to its preceding neighbouring subunit. The existence of "breaks" in the average conformation of the macromolecule leading to a non-linear sequence of rigid subunits will perturb the equipotentials along which the bound counterions move and will give rise to potential barriers between neighbouring subunits. This implies that bound counter-

ions can move freely along each subunit but can cross over from one subunit to a neighbouring one only by overcoming this potential barrier. This means that a fluctuation in the bound counterions distribution relaxes towards the equilibrium distribution in two steps which will be assumed to be independent; (a) a process characterized by a relaxation time τ_b leads to an uniform distribution of the bound counterions along each subunit leaving unaffected the number of bound counterions on each subunit; (b) a relatively slower process equilibrates the number of bound counterions along the different subunits leading to an uniform distribution of the counterions along the whole molecule. This process is characterized by a relaxation time τ_q which must be larger than τ_b as it is assumed that the diffusion velocity from one subunit to a neighbouring one is opposed by the potential barrier. Of course no detailed information about this potential barrier is available if the solution for the electric potential around the polyion in the given conformation in not known explicitely.

This model is assumed to reflect the behaviour of bound ions fluctuating along a flexible macromolecular chain. It may be assumed for such a molecular system that the bound ions will be characterized by two different diffusion times. The short-time fluctuations occur over distances of only a limited number of monomeric units as local potential barriers may arise due to the flexibility of the chain. Fluctuations over the complete macromolecular domain refer to a much longer time scale.

Each macromolecule will be given an internal reference frame x, y, z the origin of which coincides with its center of mass. The three directions represented by the unit vectors $\boldsymbol{I}_x, \boldsymbol{I}_y$ and $\boldsymbol{I}_z$ correspond to the three principal axes of the polyion, one of which will be parallel to the end-to-end vector in the case of a rather stretched macromolecule. The orientation of the macromolecule with respect to the external reference frame X, Y, Z (the origin of which is taken identical to the one of the internal reference frame as translational motion of the polyelectrolyte is not taken into account) is completely determined by the orientation of these unit vectors with respect to the external reference frame. Each subunit α will be characterized by three parameters in the internal coordinate system: its orientation $\boldsymbol{I}_{b,\alpha}$, the distance q_α of its midpoint (assumed to be the center of mass of the subunit) to the center of mass of the polyion and the unit vector $\boldsymbol{I}_\alpha$ in the direction pointing from the center of mass of the polyion to the midpoint of unit α. From the definiton of the center of mass it follows

$$\sum_{\alpha=1}^{p} q_\alpha \boldsymbol{I}_\alpha = \sum_{\alpha=1}^{p} q_\alpha = 0 . \tag{22}$$

On each subunit there are Z_0/p equal fixed charges assumed to be equally spaced along its axis with coordinates $\rho_{\alpha,j}$ in the internal reference frame. The following condition holds:

$$\sum_{\alpha=1}^{p} \sum_{j=1}^{Z_0/p} \rho_{\alpha,j} = \sum_{\alpha=1}^{p} q_\alpha = 0 . \tag{23}$$

The position r_i of a given counterion along the polyelectrolyte chain is given by

$$r_i = \sum_{\alpha=1}^{p} g_i^{(\alpha)} [q_\alpha \boldsymbol{I}_\alpha + s_i^{(\alpha)} \boldsymbol{I}_{b,\alpha}] . \tag{24}$$

Here $s_i^{(\alpha)}$ indicates the position of ion i with respect to the midpoint of subunit α if the ion is on this subunit. The occupation factor $g_i^{(\alpha)}$ is equal to unity if ion i is on the subunit α and zero under all other circumstances. Clearly the following condition must be satisfied:

$$\sum_{\alpha=1}^{p} g_i^{(\alpha)}(t) = 1 . \tag{25}$$

A radius of gyration R_g of the polyion may be defined by

$$R_g = \left(p^{-1} \sum_{\alpha=1}^{p} q_\alpha \cdot q_\alpha \right)^{1/2} = \left(p^{-1} \sum_{\alpha=1}^{p} q_\alpha^2 \right)^{1/2} , \tag{26}$$

but in this definition the finite dimensions of the subunits are not taken into account.

The total time dependent moment of the polyion and its bound counterions as well as the hamiltonian ΔH arising from an electric field are given analogously to (3) and (1) by the following expressions:

$$m(t) = ze \sum_{i=1}^{N} f_i(t)\, r_i(t) = ze \sum_{i=1}^{N} f_i(t) \sum_{(\sigma)} \sum_{\alpha=1}^{p} g_i^{(\alpha)}(t)\,[q_\alpha (l_\alpha \cdot l_\sigma) + s_i^{(\alpha)}(t)\,(l_{b,\alpha} \cdot l_\sigma)]\, l_\sigma \,, \tag{27}$$

$$\Delta H(t) = \Delta H^0(t) - ze \sum_{i=1}^{N} f_i(t) \sum_{(\sigma)} \sum_{\alpha=1}^{p} g_i^{(\alpha)}(t)\,[q_\alpha (l_\alpha \cdot l_\sigma) + s_i^{(\alpha)}(t)\,(l_{b,\alpha} \cdot l_\sigma)]\, l_\sigma \cdot E^{p}(t) \,. \tag{28}$$

Here the orientation of the vectors l_α and $l_{b,\alpha}$ have been expressed with respect to the external reference frame through the unit vectors l_σ (with $\sigma = x, y$ or z). The static polarization ΔP_s can be obtained from a generalization of (7) and is given by

$$\Delta P_s = \frac{(ze)^2 C_M E_s^p}{kT} \left\langle \left\{ l_e \cdot \sum_{i=1}^{N} f_i(0) \sum_{(\sigma)} l_\sigma \sum_{\alpha=1}^{p} g_i^{(\alpha)}(0)\,[q_\alpha (l_\alpha \cdot l_\sigma) + s_i^{(\alpha)}(0)\,(l_{b,\alpha} \cdot l_\sigma)] \right\}^2 \right\rangle_0 \,. \tag{29}$$

It can be transformed using the assumptions of the preceding section together with an additional assumption about the absence of correlation between the distribution of bound counterions on a given subunit and the distribution along all possible subunits. These assumptions transform (29) into the following expression

$$\Delta P_s = \Delta P_{s,1} + \Delta P_{s,2} \,, \tag{30}$$

$$\Delta P_{s,1} = \frac{(ze)^2 C_M E_s^p}{kT} \left\{ \sum_{i=1}^{N} \langle f_i^2(0) \rangle_0 \sum_{(\sigma)} \left[\langle l_e \cdot l_\sigma(0)\, l_\sigma(0) \cdot l_e \rangle_0 \right.\right.$$

$$\left.\left. \times \sum_{\alpha=1}^{p} \langle l_\sigma \cdot q_\alpha\, g_i^{(\alpha)}(0)\, g_i^{(\alpha)}(0)\, q_\alpha \cdot l_\sigma \rangle_0 \right] \right\} = \frac{(ze)^2 C_M E_s^p N \bar{f}}{3kT} R_g^2 \,, \tag{31}$$

$$\Delta P_{s,2} = \frac{(ze)^2 C_M E_s^p}{kT} \left\{ \sum_{i=1}^{N} \langle f_i^2(0) \rangle_0 \sum_{(\sigma)} \left[\langle l_e \cdot l_\sigma(0)\, l_\sigma(0) \cdot l_e \rangle_0 \right.\right.$$

$$\left.\left. \times \sum_{\alpha=1}^{p} \langle l_\sigma \cdot l_{b,\alpha} s_i^{(\alpha)}(0)\, g_i^{(\alpha)}(0)\, g_i^{(\alpha)}(0)\, s_i^{(\alpha)}(0)\, l_{b,\alpha} \cdot l_\sigma \rangle_0 \right] \right\} = \frac{(ze)^2 C_M E_s^p N \bar{f}}{3\,kT} \frac{b^2}{12} \,. \tag{32}$$

Here explicite use has been made of the following relations

$$\langle g_i^{(\alpha)}(0) \rangle_0 = \langle [g_i^{(\alpha)}(0)]^2 \rangle_0 = p^{-1}, \qquad \langle g_i^{(\alpha)}(0)\, s_i^{(\alpha)}(0) \rangle_0 = 0,$$

$$\langle [g_i^{(\alpha)}(0)\, s_i^{(\alpha)}(0)]^2 \rangle_0 = \langle [g_i^{(\alpha)}(0)]^2 \rangle_0 \langle [s_i^{(\alpha)}(0)]^2 \rangle_0 = (b/12p) \,,$$

which follow from the simplifying assumptions. The static polarization ΔP_s thus contains two independent contributions; the first one $\Delta P_{s,1}$ depends on the average dimensions of the complete polyion through R_g, the second one $\Delta P_{s,2}$ on the dimensions b of the subunits. Note that in the particular case where all subunits are aligned R_g^2 is given by $R_g^2 = (p^2 b^2 - b^2)/12$ and (30) becomes identical to (9) as $p^2 b^2 = L^2$.

From (30) the following expression can be derived for the static dielectric increment $\Delta\epsilon_s$ of the polyelectrolyte solution with respect to the electric permittivity of the solvent.

$$\Delta\epsilon_s = [(ze)^2 C_M \bar{f} N \gamma / 36\, kT\, \epsilon_0]\, (12\, R_g^2 + b^2) = \Delta\epsilon_{s,1} + \Delta\epsilon_{s,2} \,. \tag{33}$$

The response function of the time dependent polarization $\Delta P(t)$ for this model can be written analogously to (12) as

$$\phi(t) = -\frac{(ze)^2 C_M}{kT}\frac{\partial}{\partial t}\left\{ l_e \cdot \left\langle \sum_{i=1}\sum_{j=1} f_i(0) f_j(t)\, r_i(0)\, r_j(t) \right\rangle_0 \cdot l_e \right\}$$

$$= -\frac{(ze)^2 C_M}{kT}\frac{\partial}{\partial t}\left\{ \left\langle \sum_{i=1}\sum_{j=1} f_i(0) f_j(t) \right\rangle_0 \langle l_e \cdot r_i(0)\, r_j(t) \cdot l_e \rangle_0 \right\}. \tag{34}$$

Introducing (24) and expressing again the vectors l_α and $l_{b,\alpha}$ through their components along the unit vectors l_σ ($\sigma = x, y$ or z) the response function (34) can be simplified into the following expression using all the assumptions mentioned.

$$\phi(t) = -\frac{(ze)^2 C_M}{kT}\frac{\partial}{\partial t}\left\{ \left\langle \sum_{i=1}^{N} f_i(0) f_i(t) \right\rangle_0 \sum_{(\sigma)} \sum_{\alpha,\beta=1}^{p} \langle l_\sigma \cdot l_\alpha q_\alpha\, g_i^{(\alpha)}(0)\, g_i^{(\beta)}(t)\, q_\beta l_\beta \cdot l_\sigma \rangle_0 \langle l_e \cdot l_\sigma(0)\, l_\sigma(t) \cdot l_e \rangle_0 \right.$$

$$\left. + \left\langle \sum_{i=1}^{N} f_i(0) f_i(t) \right\rangle_0 \sum_{(\sigma)} \sum_{\alpha=1}^{p} \langle l_\sigma \cdot l_{b,\alpha}\, s_i^{(\alpha)}(0)\, g_i^{(\alpha)}(0)\, g_i^{(\alpha)}(t)\, s_i^{(\alpha)}(t)\, l_{b,\alpha} \cdot l_\sigma \rangle_0 \langle l_e \cdot l_\sigma(0)\, l_\sigma(t) \cdot l_e \rangle_0 \right\}. \tag{35}$$

This response function contains two independent contributions each of which is composed of three components along the principal axes of the polyion. The frequency dependent susceptibility $\Delta\chi^*(\omega)$ defined according to (14) can be put into the following form

$$\Delta\chi^*(\omega) = \sum_{(\sigma)} \Delta\chi^*_{1,\sigma}(\omega) + \sum_{(\sigma)} \Delta\chi^*_{2,\sigma}(\omega), \tag{36}$$

$$\Delta\chi^*_{1,\sigma}(\omega) = -\frac{(ze)^2 C_M \gamma}{kT}\left[\sum_{i=1}^{N} \langle f_i^2(0) \rangle_0 \sum_{\alpha=1}^{p} \langle l_\sigma \cdot l_\alpha\, q_\alpha\, g_i^{(\alpha)}(0)\, g_i^{(\alpha)}(0)\, q_\alpha\, l_\alpha \cdot l_\sigma \rangle_0 \right.$$

$$\left. \times \langle l_e \cdot l_\sigma(0)\, l_\sigma(0) \cdot l_e \rangle_0 \right] \int_0^\infty e^{-i\omega t} \frac{\partial \Gamma_{1,\sigma}}{\partial t}\, dt, \tag{37}$$

$$\Delta\chi^*_{2,\sigma}(\omega) = -\frac{(ze)^2 C_M \gamma}{kT}\left[\sum_{i=1}^{N} \langle f_i^2(0) \rangle_0 \sum_{\alpha=1}^{p} \langle l_\sigma \cdot l_{b,\alpha}\, s_i^{(\alpha)}(0)\, g_i^{(\alpha)}(0)\, g_i^{(\alpha)}(0)\, s_i^{(\alpha)}(0)\, l_{b,\alpha} \cdot l_\sigma \rangle_0 \right.$$

$$\left. \times \langle l_e \cdot l_\sigma(0)\, l_\sigma(0) \cdot l_e \rangle_0 \right] \int_0^\infty e^{-i\omega t} \frac{\partial \Gamma_{2,\sigma}}{\partial t}\, dt. \tag{38}$$

Here six independent decay functions $\Gamma_{1,\sigma}$ and $\Gamma_{2,\sigma}$ have been introduced the three first of which describe the decay of the polarization $\Delta P_{s,1}$ whereas the three others describe the decay of the polarization $\Delta P_{s,2}$. They are defined by the following equations:

$$\Gamma_{1,\sigma} = \frac{\langle \Sigma_{i=1}^{N} f_i(0) f_i(t) \rangle_0}{\langle \Sigma_{i=1}^{N} f_i^2(0) \rangle_0} \cdot \frac{\Sigma_{\alpha,\beta=1}^{p} (l_\sigma \cdot l_\alpha)(l_\sigma \cdot l_\beta) \langle q_\alpha g_i^{(\alpha)}(0)\, g_i^{(\beta)}(t)\, q_\beta \rangle_0}{\Sigma_{\alpha=1}^{p} (l_\sigma \cdot l_\alpha)^2 \langle \sigma_z^2 [g_i^{(\alpha)}(0)]^2 \rangle_0} \cdot \frac{\langle l_e \cdot l_\sigma(0)\, l_\sigma(t) \cdot l_e \rangle_0}{\langle l_e \cdot l_\sigma(0)\, l_\sigma(0) \cdot l_e \rangle_0} = \Gamma_f \Gamma_{q,\sigma} \Gamma_{r,\sigma}, \tag{39}$$

$$\Gamma_{2,\sigma} = \frac{\langle \Sigma_{i=1}^{N} f_i(0) f_i(t) \rangle_0}{\langle \Sigma_{i=1}^{N} f_i^2(0) \rangle_0} \cdot \frac{\langle s_i^{(\alpha)}(0)\, g_i^{(\alpha)}(0)\, g_i^{(\alpha)}(t)\, s_i^{(\alpha)}(t) \rangle_0}{\langle [s_i^{(\alpha)}(0)]^2 [g_i^{(\alpha)}(0)]^2 \rangle_0} \cdot \frac{\langle l_e \cdot l_\sigma(0)\, l_\sigma(t) \cdot l_e \rangle_0}{\langle l_e \cdot l_\sigma(0)\, l_\sigma(0) \cdot l_e \rangle_0} = \Gamma_f \Gamma_b \Gamma_{r,\sigma}. \tag{40}$$

Use has been made of the fact that within this model the scalar products $l_\sigma \cdot l_\alpha$ and $l_\sigma \cdot l_{b,\alpha}$ are constant and the average quantities $\langle [s_i^{(\alpha)}(0)]^2 [g_i^{(\alpha)}(0)]^2 \rangle_0$ and $\langle s_i^{(\alpha)}(0)\, g_i^{(\alpha)}(0)\, g_i^{(\alpha)}(t)\, s_i^{(\alpha)}(t) \rangle_0$ are independent of α.

It follows from (39) and (40) that each of these decay functions can be written as a product of three independent decay functions one of which describes the decay of the fluctuations in the distribution between bound and free counterions (Γ_f) and another the decay of the orientational fluctuations of the principal axes σ of the polyion ($\Gamma_{r,\sigma}$). Furthermore $\Gamma_{1,\sigma}$ contains the contribution $\Gamma_{q,\sigma}$ of the decay of the fluctuations in the distribution of bound ions between different subunits whereas $\Gamma_{2,\sigma}$ has a contribution Γ_b characteristic for the decay of the fluctuations in the bound counterions distribution on a given subunit.

If the decay functions are assumed to be exponentials with respect to time, the frequency dependent dielectric increment of the polyelectrolyte solution obeys the following equation describing the superposition of six Debye-like dispersion curves each of which is characterized by the relaxation time $\tau_{1,\sigma}$ or $\tau_{2,\sigma}$ of the decay function $\Gamma_{1,\sigma}$ and $\Gamma_{2,\sigma}$ respectively.

$$\Delta\epsilon^*(\omega) = \sum_{(\sigma)} [(\Delta\epsilon_{s,1})_\sigma/(1 + i\omega\tau_{1,\sigma}) + (\Delta\epsilon_{s,2})_\sigma/(1 + i\omega\tau_{2,\sigma})] , \tag{41}$$

$$(\Delta\epsilon_{s,1})_\sigma = [(ze)^2 C_M N\bar{f}\gamma/3kT]\ (1/p) \sum_{\alpha=1}^{p} \langle (I_\sigma \cdot I_\alpha)\, q_\alpha^2 \rangle_0 , \tag{42}$$

$$(\Delta\epsilon_{s,2})_\sigma = [(ze)^2 C_M N\bar{f}\gamma/36kT]\ (b^2/p) \sum_{\alpha=1}^{p} \langle (I_\sigma \cdot I_{b,\alpha})^2 \rangle_0 . \tag{43}$$

Note that of course the following conditions are satisfied

$$\sum_{(\sigma)} (\Delta\epsilon_{s,1})_\sigma = \Delta\epsilon_{s,1}, \qquad \sum_{(\sigma)} (\Delta\epsilon_{s,2})_\sigma = \Delta\epsilon_{s,2} , \tag{44}$$

where $\Delta\epsilon_{s,1}$ and $\Delta\epsilon_{s,2}$ are defined by (33). The relaxation times $\tau_{1,\sigma}$ and $\tau_{2,\sigma}$ will be related to the relaxation times τ_f, $\tau_{r,\sigma}$, $\tau_{q,\sigma}$ and τ_b characteristic for the decay functions Γ_f, $\Gamma_{r,\sigma}$, $\Gamma_{q,\sigma}$ and Γ_b respectively through the eqs. (45) and (46) which follow from (39) and (40):

$$(\tau_{1,\sigma})^{-1} = (\tau_f)^{-1} + (\tau_{r,\sigma})^{-1} + (\tau_{q,\sigma})^{-1} , \tag{45}$$

$$(\tau_{2,\sigma})^{-1} = (\tau_f)^{-1} + (\tau_{r,\sigma})^{-1} + (\tau_b)^{-1} . \tag{46}$$

It may be seen from (41) that the dispersion curve of the dielectric increment may be very complicated indeed as different dispersion regions may overlap considerably. It may become somewhat simpler if the different mechanisms contributing to the relaxation times $\tau_{1,\sigma}$ and $\tau_{2,\sigma}$ are characterized by rates of decay of different order of magnitude. This will be discussed below. Note that from the preceding relations it follows that in the limit $p \to 1, b \to L$ the equation for the dielectric dispersion of a rodlike polyion, as derived in section 3, are recovered.

This limit implies the disappearance of the potenital barriers opposing the fluctuations of the bound counterions. Of course if the subunits are only aligned but the potential barrier between subunits are maintained, eq. (41) does not become identical to (20) although the static value $\Delta\epsilon_s$ according to (33) becomes equal to (9). This latter case is not very realistic because the potential barriers are thought to be related to the flexibility of the chain.

In this model based on a non-linear sequence of rigid subunits the diffusion of the bound counterions along a given subunit must always occur on a much shorter time-scale than the mechanism which tends to equalize the distribution of the bound counterions between different subunits. Therefore $\tau_b \ll \tau_{q,\sigma} \approx \tau_q$. If the former also proceeds by a mechanism which is much faster than the one responsible for the exchange between bound and free counterions and the rotational diffusion of the complete polyion, the following conditions also will be satisfied: $\tau_b \ll \tau_f, \tau_b \ll \tau_{r,\sigma}, \tau_{2,\sigma} = \tau_2 \ll \tau_{1,\sigma}$. In this particular case two separate dispersion regions will be found according to the equation

$$\Delta\epsilon^*(\omega) = \sum_{(\sigma)} [(\Delta\epsilon_{s,1})_\sigma/(1 + i\omega\tau_{1,\sigma}) + \Delta\epsilon_{s,2}/(1 + i\omega\tau_b)] . \tag{47}$$

The lower frequency part, which will not overlap with the higher frequency part of the dispersion curve characterized by τ_b, may still contain three independent contributions characterized by $\tau_{1,\sigma}$. Different possibilities may be considered. If the exchange mechanism between bound and free counterions has the highest rate of decay as compared to the two others characterized by $\tau_{q,\sigma}$ and $\tau_{r,\sigma}$ then only one singie relaxation curve is observed at the lower frequency end of the dispersion curve:

$$\Delta\epsilon^*(\omega) = \Delta\epsilon_{s,1}/(1 + i\omega\tau_f) + \Delta\epsilon_{s,2}/(1 + \omega\tau_b) . \tag{47a}$$

If the rotational diffusion or the mechanism which tends to equaliz. the distribution of bound counterions between the different subunits have faster rates of decay as compared to the mechanism characterized by τ_f then the lower frequency end of the dispersion curve will consist of the superposition of three independent relaxation curves according to (47) with $\tau_{1,\sigma}$ essentially determined by $\tau_{r,\sigma}$, $\tau_{q,\sigma}$ or both. The amplitude of each of these relaxation curves, defined by (42) will depend on the geometry of the polyion and may be of significantly different orders of magnitude.

Another possibility to be considered is that $\tau_f \ll \tau_b$, $\tau_f \ll \tau_{r,\sigma}$. It then follows that $\tau_{1,\sigma} \approx \tau_{2,\sigma} \approx \tau_f$ and one single dispersion curve will be observed:

$$\Delta\epsilon^*(\omega) = \Delta\epsilon_s/(1 + i\omega\tau_f) . \tag{48}$$

In case the rotational diffusion is the fastest mechanism as compared to all others, it is to be expected that the dispersion curve will obey the following equations consisting of three relaxation curves, the amplitude and relaxation time of each being determined directly by the geometry of the macromolecule:

$$\Delta\epsilon^*(\omega) = \sum_{(\sigma)} [(\Delta\epsilon_{s,1})_\sigma + (\Delta\epsilon_{s,2})_\sigma]/(1 + i\omega\tau_{r,\sigma}) . \tag{49}$$

5. Discussion

Before discussing in more details the results obtained in the theoretical analysis of sections 3 and 4 it is necessary to emphasize that this analysis was based on an oversimplified model for the charged macromolecule. It is however not to be excluded that the essential conclusions which will be drawn in this work remain valid at least qualitatively although the expressions obtained here may differ from those which would result from more sophisticated models. This presumption is based on the comparison of the expression for the static electric permittivity of polyelectrolyte solutions as found by the very simple theory for rigid rodlike polyions [4] and by the more complicated one in which electrostatic repulsion between the bound counterions along the polyelectrolyte chain are taken into account [6]. Not only do both theories yield expressions for the static dielectric increment which agree qualitatively but it has been shown that the experimental data obtained with a truly rodlike charged particle can be interpreted satisfactorily even in a semi-quantitative way by the former [17]. Furthermore it is also evident that by releasing one or more simplifying assumptions introduced here the analysis of the relaxation behaviour will become increasingly difficult and may obscure at least partially some of the essential features which are apparent in the more simple treatment.

It is also important to note that in the models used presently the charge of the polyions $-Z_0$ has been taken constant. This implies that the models are strictly spoken only applicable to charged macromolecules which behave like strong polyelectrolytes. For weak polyacids or polybases the charge distribution of the polyions will also be a fluctuating quantity. Under experimental conditions where the exchange of protons may be assumed to be much slower than all the other mechanisms considered here, the treatment given in the present paper may still apply but it is not to be excluded that an additional dispersion may be observed at very low frequencies due the fluctuating charge distribution of the polyion. This would also imply that the static dielectric increment $\Delta\epsilon_s$ derived here is not the true equilibrium value for weak polyelectrolytes which could contain a contribution

arising from the charge of the polyion (as well as a contribution due to the permanent dipole moment which has also be neglected throughout). It may be estimated [2] that, e.q., for weak polyacids at pH = 6 or higher the exchange of protons is too low to give rise to a dispersion situated in the frequency region above 1 kHz so that the dispersion regions observed at these frequencies will correspond to the ones discussed in the present treatment. At lower pH however the situation may be more complicated.

The most important conclusion that can be drawn from the theoretical analysis given in section 3 and 4 is that rodlike and non-rodlike polyions will differ much more by their frequency dependent dielectric dispersion than by the static dielectric increment to which they give rise. In fact the latter will be quite analogous for both kinds of polyions showing an identical dependence on such factors as the valency and number of bound counterions and the ratio γ between the effective field acting on the macromolecule and the Maxwell field in the system. The only difference arises from the geometrical factor which depends on the dimensions of the average conformation considered. For the rodlike polyion this factor is according to (10) given by $L^2/12$ whereas for the non-rodlike one it is $(12\,R_g^2 + b^2)/12$ as follows from (33). Solutions of rodlike polyions on the other hand will give rise to a simple dispersion curve (20) but non-rodlike polyions will in general exhibit a dispersion behaviour of more complicated features. As pointed out already in the preceding section solutions of non-rodlike polyions may show under certain circumstances two distinct relaxation regions in the dielectric dispersion as is observed experimentally with aqueous solutions of some charged macromolecules with not negligible flexibility.

The results presented here indicate that the static dielectric increment of polyelectrolyte solutions alone does not allow discrimination between rodlike and non-rodlike polyions. This is due to the uncertainty about the ratio γ which is very difficult to calculate theoretically (and for sake of simplicity is generally assumed to be of the order of unity) and the difficulty to assess a value to $\bar{f}$, although the latter may be estimated from independent measurements. Calculated values of the geometrical factor may therefore be rather unreliable. This is even more true as interactions between bound counterions, not taken into account in (10) and (33) will tend to decrease the value of $\Delta\epsilon_s$ with respect to its ideal value, as shown by the work of McTague and Gibbs [5] and Oosawa [6]. It is also to be expected that the same effect will result from polyion–polyion interactions in not extremely diluted solutions. This may explain why in the past equations analogous to (10) have been found to be in fair agreement with experimental data obtained from solutions containing rather flexible, synthetic polyelectrolytes.

As mentioned already in section 3 and 4 prediction of the relaxation behaviour of polyions and subsequent analysis of an experimental dispersion curve necessitated assessment of the order of magnitude for the different relaxation times which may play a role. For some of these theoretical expressions or estimates are available, e.g., τ_c or τ_b [6, 25], τ_r or $\tau_{r,\sigma}$ [26–28] and τ_f [29], although numerical evaluation can only be based on estimation of certain quantities which are not known accurately. For $\tau_{q,\sigma}$ no such expression has been derived yet. The analysis of a dispersion curve may be greatly facilitated however by considering the molecular weight dependence of these relaxation times, particularly for macromolecules of rather stretched average conformation. It may be inferred that τ_r, $\tau_{r,\sigma}$, τ_c and $\tau_{q,\sigma}$ will be size dependent and thus will increase with molecular weight. On the other hand for polyelectrolytes with sufficiently large molecular weight τ_f and τ_b will probably not depend on this quantity. In case the exchange mechanism between bound and free counterions is the fastest as compared to all others, both rodlike and non-rodlike polyions will be characterized by one single dispersion curve with a molecular weight independent relaxation time as follows from (20) and (48). In case the rotational diffusion is the fastest, discrimination between both kinds of polyions is also impossible [see (20) and (49)] except in the case where the rotational diffusion gives rise to distinguishable features in the dispersion curve for a non-rodlike polyion. (Note that if the rodlike polyion deviates considerably from the infinitely thin model considered here these features also could appear in the dispersion curve. The relaxation time will be molecular weight dependent however as will also be the case for a rodlike polyion for which $\tau \approx \tau_c$.)

The existence of two separated relaxation regions must in general be attributed to non-rodlike polyions. If the higher frequency part has a relaxation time which is molecular weight independent but the lower not, this points to a dispersion curve as given by (47) whereas molecular weight independence of both relaxation times would point to (47a). Should several relaxation mechanisms contribute simultaneously to $\tau_{1,\sigma}$ and $\tau_{2,\sigma}$ however the overall

shape of the dispersion curve may become very intricate indeed and the molecular weight dependence completely obscured.

In subsequent papers we shall apply this theoretical analysis to experimental results obtained in this laboratory with different types of charged macromolecules.

References

[1] H. Block and A.M. North, Adv. Mol. Rel. Proc. 1 (1970) 309.
[2] G. Schwarz, in: Dielectric and related molecular processes, Vol. 1 (The Chemical Society, London, 1972) ch. 6.
[3] G. Schwarz, Z. Physik 145 (1956) 563.
[4] M. Mandel, Mol. Phys. 4 (1961) 489.
[5] J.P. McTague and Gibbs, J. Chem. Phys. 44 (1966) 4245.
[6] F. Oosawa, Biopolymers 9 (1970) 677.
[7] G. Schwarz, J. Phys. Chem. 66 (1962) 2636.
[8] M. Mandel and A. Jenard, Trans. Faraday Soc. 59 (1963) 2158, 2170.
[9] F. van der Touw and M. Mandel, Book of Abstracts of the IUPAC Symposium on Macromolecules (Leiden 1970) Vol. I, p. 375.
[10] S. Takashima, J. Mol. Biol. 7 (1963) 455.
[11] S. Takashima, Biopolymers 5 (1967) 889.
[12] H.M. Dintzis, J.L. Oncley and R.M. Fuoss, Proc. Natl. Acad. Sci. US 40 (1954) 62.
[13] S.B. Sachs, A. Raziel, H. Eisenberg and A. Katchalsky, Trans. Faraday Soc. 65 (1969) 77.
[14] D.J. Allen, S.M. Neale and P.J.T. Tait, J. Polymer Sci. A2 10 (1972) 433.
[15] A. Minakata and N. Imai, Biopolymers 11 (1972) 329, 347.
[16] M. Mandel and F. van der Touw, in: Polyelectrolytes, ed. E. Sélégmi (Reidel, Dordrecht, 1974) p. 285.
[17] F. van der Touw, J.W.H. Briedé and M. Mandel, Biopolymers 12 (1973) 111.
[18] A. Katchalsky, Pure Appl. Chem. 26 (1971) 327.
[19] F. Oosawa, Polyelectrolytes (Marcel Dekker, New York, 1971).
[20] G. Schwarz, J. Phys. Chem. 12 (1967) 4021.
[21] G. Williams, Adv. Mol. Rel. Proc. 1 (1970) 409.
[22] J.M. Schurr, Biopolymers 10 (1971) 1371.
[23] A. Warashina and A. Minakata, J. Chem. Phys. 58 (1973) 4743.
[24] R. Kubo, Lectures Theoret. Phys. (Boulder) 1 (1959) 120.
[25] G. Wyllie, in: Dielectric and related molecular processes, Vol. 1 (The chemical Society, London, 1972) ch. 2.
[26] F. Perrin, J. Phys. Radium 5 (1934) 497.
[27] J.M. Burgers, Second report on viscosity and plasticity (North Holland, Amsterdam, 1938).
[28] R. Ullman, Macromolecules 2 (1969) 27.
[29] S. Lifson and J.L. Jackson, J. Chem. Phys. 36 (1962) 2410.

BIOPHYSICAL CHEMISTRY 2 (1974) 231–241. © NORTH-HOLLAND PUBLISHING COMPANY

DIELECTRIC INCREMENT AND DIELECTRIC DISPERSION OF SOLUTIONS CONTAINING SIMPLE CHARGED LINEAR MACROMOLECULES

II. EXPERIMENTAL RESULTS WITH SYNTHETIC POLYELECTROLYTES

F. VAN DER TOUW and M. MANDEL

Gorlaeus Laboratoria der Rijksuniversiteit Leiden, afdeling Fysische Chemie III, Leiden, The Netherlands

Received 18 April 1974
Revised manuscript received 13 August 1974

The electric permittivity of aqueous solutions of different synthetic polyelectrolytes have been measured as a function of frequency in the range 5 kHz up to 100 MHz in the absence of added salt. Solutions of polymethacrylic acid and polyacrylic acid of different degrees of polymerization, both partially neutralized with NaOH, were investigated as well as solutions of Na-polystyrenesulphonate at different concentrations.

For all systems a dispersion profile with two separated dispersion regions was obtained with a molecular weight dependent value of the static electric permittivity. The low frequency dispersion region was found to be characterized by a molecular weight dependent mean relaxation time while for the high frequency dispersion region both the mean relaxation time and the dielectric increment are molecular weight independent. It is shown that the reciprocal values of the specific increments and of the relaxation times depend linearly on the macromolecular concentration. Extrapolation of the corresponding quantities to infinite dilution was found to be possible. A comparison of these extrapolated values with calculated ones according to the previously derived theory also applicable to flexible macromolecules establishes that this theory describes satisfactorily the dielectric behaviour of the systems investigated.

The conclusion is reached that the high frequency dispersion and relaxation can be attributed to fluctuations in the distribution of bound counterions along limited parts of the macromolecule. The relaxation time of the low frequency dispersion region seems to be essentially determined by the rotation of the complete molecule and the static electric permittivity can be explained in terms of fluctuations in the counterion density extending over the whole macromolecule.

1. Introduction

In the preceding paper [1] (to be indicated as part I) a theoretical analysis has been presented of the dielectric properties of solutions of simple polyelectrolytes which may be represented either by a rigid rod or a rigid sequence of rodlike subunits in as far as their average conformation is concerned and which carry a constant number of identical charged sites.

Using a very simple model calculation it has been shown that the two kinds of polyions will in general be characterized by a different relaxational behaviour as revealed by the dielectric dispersion.

In particular a rodlike polyion is expected to yield a simple dispersion curve with a relaxation time which may be molecular weight dependent in case the relaxation mechanism is essentially determined by the (exponential) decay of fluctuations in the bound counterions distribution along the rod or the orientational fluctuations of the complete polyion. Such a behaviour has already been found for the rigid elongated particle of the Alfalfa Mosaic virus in aqueous solutions [2].

More flexible polyelectrolytes should behave in a different way as follows from the model calculations on a polyion represented as a rigid sequence of rodlike subunits. Here in general more dispersion regions are expected each of which will be characterized by a different relaxation time.

It is the purpose of the present paper to present some experimental results obtained with aqueous saltless solutions of different synthetic polyelectrolytes

and to discuss these results in terms of the theory which has been developed [1]. The measurements were performed over a broad frequency interval (2.5 kHz to 100 MHz) using special measuring techniques developed in this laboratory.

2. Experimental

2.1. Materials

The polyelectrolytes used in this investigation are poly(styrenesulphonic acid) (PSS) and poly-(acrylic acid) (PAA) and poly-(methacrylic acid) (PMA). The PAA and PMA samples were obtained by radical polymerization of the corresponding monomers and fractionation of the product [3]. The degree of polymerization DP of the different fractions was for PAA: DP = 640, DP = 1530 and DP = 7500. PSS was prepared as the potassium salt by polymerization of the K-styrenesulphonate in aqueous solution using as initiator a mixture of $K_2S_2O_8$ and $KHSO_3$ [4, 5]. The polymer is precipitated by pouring the reaction mixture in ethanol. After filtration, washing and drying the polyelectrolyte is redissolved in water, dialyzed and transformed into the acid form using a cation exchange resin. Two samples were prepared starting from different amounts of initiator; the degree of polymerization was found to be DP = 500 and DP = 15 000 respectively. All molecular weights were determined viscosimetrically.

Saltless solutions were prepared by dissolving the polyacids in conductance water and neutralizing to the chosen degree of neutralization α by adding known amounts of NaOH 0.1 M prepared from fixanal or Merck ampullae (with the usual precautions to avoid contamination by carbonate). Solutions of PSS were completely neutralized, solutions of PAA and PMA up to $\alpha = 0.40$ (pH $\approx$ 6.4).

2.2. Measuring method

The electric permittivity was measured in the frequency range 5 kHz–100 MHz using two different bridge techniques. In the low frequency range (5 kHz –500 kHz) a modified Schering bridge, originally described by Mandel and Jung [6] for measurements of capacitances shunted by low resistances was constructed in the laboratory. The original design was improved in order to increase the sensitivity as will be described elsewhere [7]. The bridge was used in conjunction with a Rohde and Schwarz tunable amplifier and RC oscillator. The measuring cell containing the polyelectrolyte solution was essentially a condensor with plane, parallel platinum plates with variable spacing.

This cell was developed to correct in an adequate way for the frequency dependent electrode effects (electrode polarization) by expanding the measured capacitance as a polynomial in the inverse of the distance between the electrodes.

This method, described in details elsewhere [8], has been found to yield more reliable values for the electric permittivity of conducting solutions as compared to the more conventional ones. In particular it takes also into account deviations with respect to the ideal behaviour of a plane condensor. These deviations interfere with the electrode effects at frequencies below 100 kHz and maygive rise to large errors in the electric permittivity. The accuracy on ϵ' depends therefore largely on the frequency and the conductivity of the system.

At frequencies above 50 kHz ϵ' could be determined with an accuracy of 0.3 or better for the systems investigated. At lower frequencies this value increases with decreasing frequencies due to the increasing importance of the electrode effects. The measurements have always been limited at the lower frequency end in such a way that the correction of the electrode effects never exceeds the contribution of the polarization of the system itself [8]. Under these circumstances the error on ϵ' of the lowest frequencies never exceeds two units. (In some of the figures representing the experimental results the error on ϵ' has been represented.)

The high frequency results (0.7 MHz–100 MHz) were obtained with a commercial bridge (Boonton RX Meter), with internal generator and detector. A coaxial cell with variable cell constant (variable height of liquid column) was used. Three sources of error have been taken into account in the method developed to determine the electric permittivity of conducting liquids in this frequency range, as will be published in a separate paper [9]:

(a) the contribution of parasitic effects in the not adjustable branches of the bridge;

(b) the influence of the connection between bridge and measuring cell;

(c) the necessity to represent the electric field by an electromagnetic wave inside the liquid in the cell at the higher frequencies.

The accuracy on ϵ' above 2 MHz is 0.5 or better. At lower frequencies where the sensitivity of the equipment decreases this value is generally somewhat larger but does not exceed one unit.

In the whole frequency range considered only the real part of the complex electric permittivity, ϵ', was measured. The imaginary part ϵ'' leads to a small increase in the dc conductivity for these ionic solutions. In the low frequency range the change in the conductivity with frequency was hardly detectable with the experimental set-up. The measured high frequency conductivity shows an increase with frequency, consistent with the decrease of ϵ', but too small to yield values for ϵ'' with the same accuracy as ϵ'.

3. Results

The electric permittivity of all solutions investigated shows as function of the frequency two well defined dispersion regions. Therefore the experimental results for a given solution at a given concentration were fitted with a computerized weighted least-squares procedure to the following analytical function

$$\epsilon' = \epsilon_\infty + \tfrac{1}{2}\Delta\epsilon_1\left(1 - \frac{\sinh \beta_1 x_1}{\cosh \beta_1 x_1 + \cos \tfrac{1}{2}\pi\beta_1}\right) + \tfrac{1}{2}\Delta\epsilon_2\left(1 - \frac{\sinh \beta_2 x_2}{\cosh \beta_2 x_2 + \cos \tfrac{1}{2}\pi\beta_2}\right), \quad (1)$$

which corresponds to a superposition of two dispersion curves according to the formula proposed by Cole and Cole [10]. Here $x_i = \ln(2\pi f \tau_i)$, with f the frequency and τ_i the mean relaxation time of dispersion region i, β_i is the Cole–Cole parameter characteristic for the distribution of relaxation times in dispersion region i ($0 \leq \beta_i \leq 1$, with $\beta_i = 1$ in case the dispersion region i may be represented by a Debye relaxation curve with one single relaxation time), and ϵ_∞ is the extrapolated electric permittivity at the high frequency end of the complete dispersion curve. The amplitudes of both dispersion regions are given by $\Delta\epsilon_1 = \epsilon_s - \epsilon_2$ and $\Delta\epsilon_2 = \epsilon_2 - \epsilon_\infty$ respectively where ϵ_s stands for the extrapolated value of ϵ' at the low frequency end of the dispersion curve so that $\Delta\epsilon_s = \epsilon_s - \epsilon_w$ represents the static dielectric increment of the solution with respect to the electric permittivity of the solvent ϵ_s.

Equation (1) contains 7 adjustable parameters which implies that rather large standard deviations on these parameters are to be expected by a least squares fit. As it has been found previously that the Cole–Cole parameter β for the low and high frequency region are nearly equal [11, 13, 15] a reduction of the number of parameters was achieved by putting $\beta_1 = \beta_2 = \beta$. It was further found that fitting with a floating β yielded a value for all the systems investigated around 0.7 with deviations smaller than 0.1 and that fitting with a fixed value of $\beta = 0.7$ did not increase significantly the standard deviation of the experimental points with respect to the calculated curve which remains of the same order of magnitude as the average experimental error on ϵ'. Therefore a good fit with better standard deviations on the other adjustable parameters was obtained with $\beta_1 = \beta_2 = 0.7$. The experimental results for some solutions together with the calculated curve according to (1) are represented in figs. 1, 2 and 3.

The extrapolated value of the electric permittivity to high frequencies ϵ_∞ was found in all cases to be equal to the static electric permittivity of pure water ϵ_w within experimental error (± 0.5). For some systems this constant value for ϵ' was already reached within the frequency range available. For others it has been checked by independent measurements at higher frequencies (< 500 MHz) using a transmissionline set-up, that $\epsilon_\infty = \epsilon_w$ indeed. Therefore $\Delta\epsilon_s = \Delta\epsilon_1 + \Delta\epsilon_2$. This proves that no further dispersion region due to the polyelectrolyte is to be expected at higher frequencies than explored in this work. The parameters describing the dielectric behaviour of all solutions as resulting from the curve fitting procedure are collected in table 1. The inaccuracy on $\Delta\epsilon_2$ and τ_2 can be estimated to amount to 0.5–1.0 units and 10–20% respectively.

The accuracy on $\Delta\epsilon_s$ and τ_1 depends strongly on the DP. For lower values of DP where $\Delta\epsilon_s$ is generally below 40 and the critical frequency of the lower dispersion region falls well within the frequency domain explored, the inaccuracy on $\Delta\epsilon_s$ is about 1 to 2 units and on τ_1 about 20%. It decreases however considerably for higher DP and may reach a value of 5 to 10% on $\Delta\epsilon_s$ and 20 to 50% on τ_1. Also if under certain con-

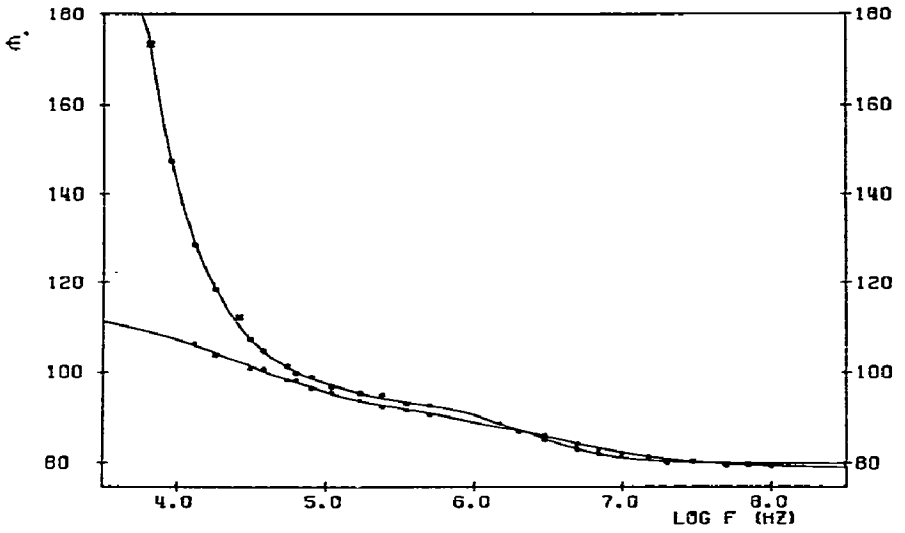


Fig. 1. Electric permittivity as function of frequency: (▲) PSS–Na^+, DP = 500, $C_p = 1.5 \times 10^{-3}$ monomol ℓ^{-1}; (●) PSS–Na^+, DP = 4.8×10^4, $C_p = 1.1 \times 10^{-3}$ monomol ℓ^{-1}.

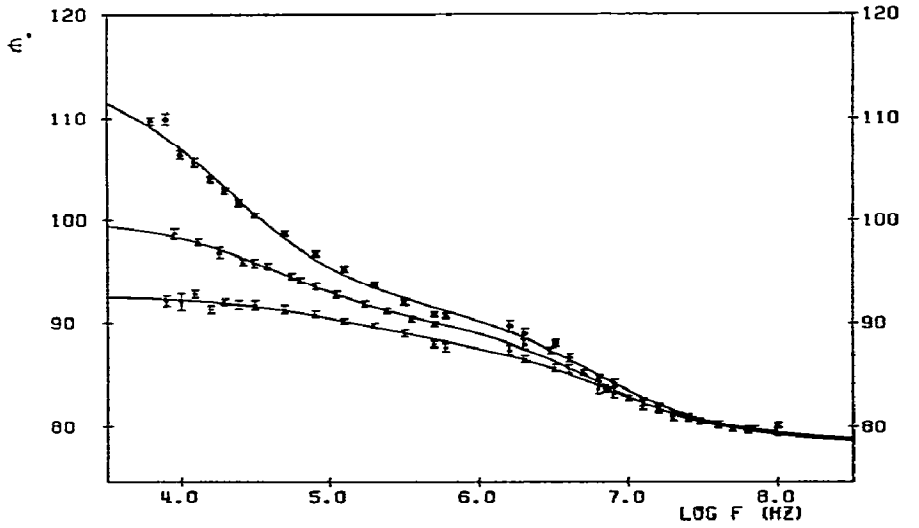


Fig. 2. Electric permittivity as function of frequency: PAA, $\alpha = 0.4$, $C_p = 5.2 \times 10^{-3}$ monomol ℓ^{-1}, DP = 640(+), 1530(▲), 7500(●).

ditions $\Delta\epsilon_2$ or $\Delta\epsilon_s$ are smaller than 5 units, the inaccuracy on the relaxation times increases to 20–50%. This estimation of the errors in the final results corresponds to a mean value of the standard deviation in the calculated parameters according to (1) with $\beta = 0.7$.

The data obtained with PSS and PAA reveal that the high frequency dispersion region is characterized by a molecular weight independent relaxation time τ_2 in agreement with the conclusions of Sachs et al. [11] on results with poly-(vinylsulphonic acid) (PVS) and Allen et al. [12] with carboxymethylcellulose in

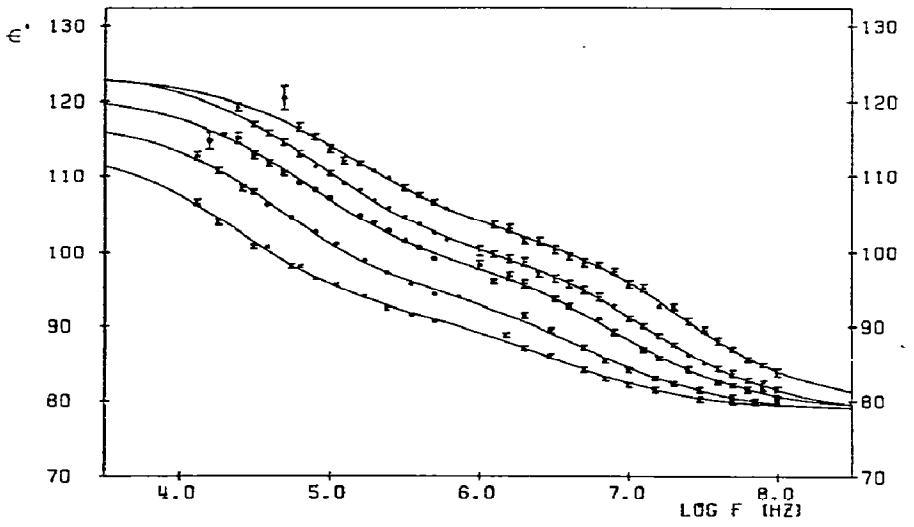


Fig. 3. Electric permittivity as function of frequency: PSS–Na^+; DP = 500; $C_p = 1.5 \times 10^{-3}$ (×), 3.0×10^{-3} (♦), 6.0×10^{-3} (●), 10×10^{-3} (+), 20×10^{-3} (▲) monomol ℓ^{-1}.

the same frequency region. The low frequency dispersion region of PSS and PAA has a relaxation time τ_1 which increases with molecular weight in agreement with earlier results of Mandel and Jenard [13] with PMA and Takashima [14] with DNA. Note that for the highest degrees of polymerization used in the present investigation τ_1 is so large that a significant part of the lower dispersion region falls outside our frequency range and the extrapolation to $f = 0$ must be considered with proper care. The results obtained with PMA of one single DP and one single concentration are in good agreement with previous results obtained with the same polyelectrolyte at frequencies below 1 MHz [13].

In the case of PSS five different concentrations have been investigated for the lower molecular weight sample. As can be seen from table 1 the relaxation times τ_1 and τ_2 decrease with increasing macromolecular concentration as do also the specific increments $(\Delta\epsilon_s/C_p)$ and $(\Delta\epsilon_2/C_p)$, with C_p the polyelectrolyte concentration expressed in moles monomer per liter. This is in contrast to results obtained with the rigid rodlike charged particle Alfalfa Mosaic virus for which the specific increment $(\Delta\epsilon_s/C)$ was found to be practically independent of concentration [2].

Table 1

Sample	C_p (monomol/ℓ)	α	DP	$\Delta\epsilon_s$	$\Delta\epsilon_2$	$\tau_1 \times 10^6$ (s)	$\tau_2 \times 10^8$ (s)
PSS	1.1×10^{-3}	1	48000	(4000) [a]	12.9	(400) [a]	6.9
PSS	1.5×10^{-3}	1	500	35.4	12.3	6.3	4.8
PSS	3.0×10^{-3}	1	500	39.4	15.4	3.6	2.9
PSS	6.0×10^{-3}	1	500	42.5	19.6	2.5	1.8
PSS	10.0×10^{-3}	1	500	45.8	21.7	2.0	1.2
PSS	20.0×10^{-3}	1	500	44.2	23.5	1.2	0.7
PAA	5.2×10^{-3}	0.4	640	14.2	9.6	1.3	2.0
PAA	5.2×10^{-3}	0.4	1530	21.8	11.7	3.6	2.6
PAA	5.2×10^{-3}	0.4	7500	36.4	13.0	8.0	2.8
PMA	5.2×10^{-3}	0.4	1050	33.5	11.7	8.0	2.5

[a] Values between parentheses are unreliable (see text).

4. Discussion

For all three synthetic polyelectrolytes investigated two distinct dispersion regions have been observed, the lower frequency one being characterized by an average relaxation time which is molecular weight dependent, the other by an average relaxation time which seems to be independent of the size of the macromolecule. As follows from the discussion in part I this is to be expected for simple polyelectrolytes *if the average conformation cannot be represented by a rigid rod and the high frequency dispersion region has a relaxation time which is essentially determined by fluctuations of the bound counterions along the rigid subunits.* For a more quantitative discussion of the effects observed it should be emphasized that the theoretical expressions derived in part I are strictly valid only at infinite dilution. In the solutions investigated the concentration are still too large to be assimilated to infinite dilution. This follows from the concentration dependence of the specific increments and relaxation times with concentration and is in agreement with previous observations on aqueous solutions of synthetic polyelectrolytes in the same concentration range [11, 13, 15]. Although the influence of finite concentration on the dielectric behaviour may from a theoretical point of view be very involved (particularly as a certain number of assumptions used explicitely in the derivations of part I become less valid with increasing concentration) as a first approximation we shall take into consideration only the influence of concentration on a certain number of molecular parameters appearing in the theoretical expressions for the dielectric increments and relaxation times as derived in part I.

Neglecting at the moment the problem of the existence of a certain distribution of relaxation times as revealed by the deviation of each single dispersion curve from a simple Debye-like one, which will be discussed here-after, it follows from the theory that the dielectric increments are given by the following equations [see I, eqs. (33), (41)–(44), (47)]:

$$\Delta\epsilon_s = [(ze)^2 \bar{f} N\gamma/36\, kT\epsilon_0]\ (12R_g^2 + b^2)C_M, \qquad (2)$$

$$\Delta\epsilon_2 = [(ze)^2 \bar{f} N\gamma/36\, kT\epsilon_0]\, b^2 C_M. \qquad (3)$$

Here R_g and b stand for the radius of gyration and the length of the rodlike subunit respectively, N is the total number of counterions per polyelectrolyte molecule, $\bar{f}$ the average fraction of counterions bound to the polyion, ze the charge of a counterion, ϵ_0 the absolute permittivity of free space and γ the ratio of the effective field acting on the polyion to the average field in the system. The concentration C_M of the macromolecule is expressed in number of polyions per *unit volume*. Therefore $NC_M = 1000\, \alpha N_{Av} C_p$ where N_{Av} stands for Avogadro's constant. It may be inferred that the concentration will affect $\bar{f}$, the average dimensions of the macromolecule as characterized by R_g and its flexibility. This last property of the polyelectrolyte chain enters the equations through the length b of the rigid subunits which characterize the average nonrodlike conformation of the macromolecule. If it is assumed that the strongest effect arising with increasing concentration stems from the influence of polyion–polyion interactions on the average conformation of the polyelectrolyte it is expected that both $\Delta\epsilon_s/C_p$ and $\Delta\epsilon_2/C_p$ will decrease with increasing concentration. In fact it is well known from, e.g., viscosity studies that a polyelectrolyte in aqueous solution tends to a more stretched and rigid conformation upon dilution. This decrease of the specific increments with increasing concentration has been observed indeed with PSS in the present investigation and was also found by Mandel and Jenard [13] for $\Delta\epsilon_s$ with PMA, by Sachs et al. [11] for $\Delta\epsilon_2$ with PVS and by Minakata and Imai [15] for $\Delta\epsilon_s$ and $\Delta\epsilon_2$ with PAA.

We have found that the concentration effect on the specific increments can be described by the following empirical equations

$$\Delta\epsilon_s/C_p = (\Delta\epsilon_s/C_p)_0/(1 + B_s C_p), \qquad (4)$$

$$\Delta\epsilon_2/C_p = (\Delta\epsilon_2/C_p)_0/(1 + B_2 C_p), \qquad (5)$$

where $(\Delta\epsilon_s/C_p)_0$ and $(\Delta\epsilon_2/C_p)_0$ stand for the value of the specific increments extrapolated to infinite dilution. These empirical equations follow from the fact that in the concentration range considered a plot of $(\Delta\epsilon_s/C_p)^{-1}$ or $(\Delta\epsilon_2/C_p)^{-1}$ against C_p yields straight lines, as can be seen from figs. 4, 5, 6 and 7. In table 2 are collected the values of the extrapolated increments and of the "interaction parameters" B_s and B_2 according to (4) and (5) for the results of the present in-

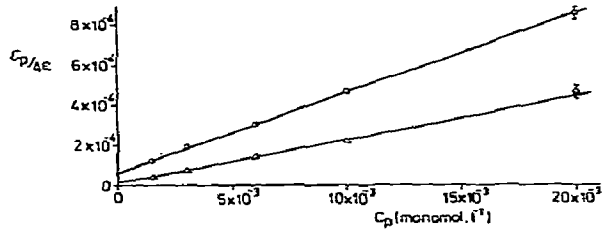


Fig. 4. $C_p/\Delta\epsilon_S$ (△) and $C_p/\Delta\epsilon_2$ (○) against C_p for PSS–Na^+.

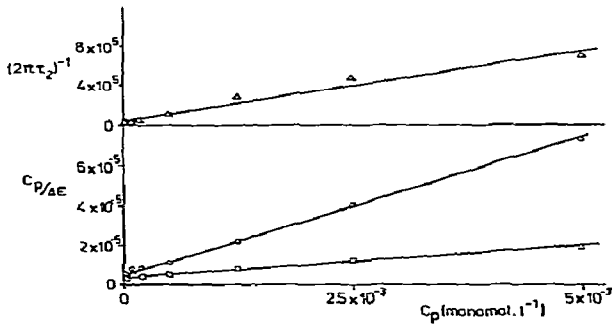


Fig. 5. Results of Minakata et al. [15] for PAA–$(Bu)_4N^+$; $C_p/\Delta\epsilon_S$ (□), $C_p/\Delta\epsilon_2$ (○) and $(2\pi\tau_2)^{-1}$ (△) against C_p.

vestigation with PSS and for some results taken from the literature. It is interesting to note that the values of B_S or B_2 for the different systems are of the same order of magnitude which lends good credit to the empirical method proposed here for extrapolation to infinite dilution.

The specific increments $(\Delta\epsilon_S/C_p)_0$ and $(\Delta\epsilon_2/C_p)_0$ may be interpreted according to eq. (2) and (3) respectively. In these expressions four parameters ap-

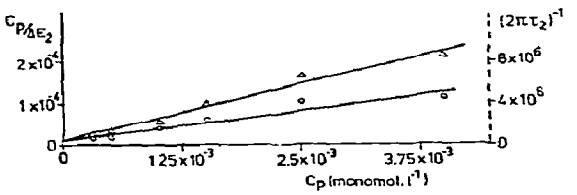


Fig. 6. Results of Sachs et al. [11] for PVS–Na^+; $C_p/\Delta\epsilon_2$ (△) and $(2\pi\tau_2)^{-1}$ (○) against C_p.

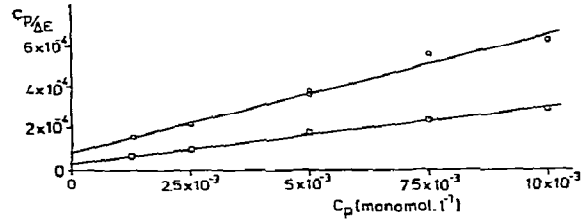


Fig. 7. Results of Mandel and Jenard [13] for PAA–Na^+, K^+; $C_p/\Delta\epsilon_S$ (□) and $C_p/\Delta\epsilon_2$ (○) against C_p.

pear: R_g, b, $\bar{f}$ and γ. The last one is very difficult to evaluate theoretically and no method is available for its experimental determination. It is usually assumed that γ does not differ too much from unity so that we may put $\gamma \approx 1$ in a first approximation. The average fraction $\bar{f}$ of bound counterions has been estimated for different polyelectrolyte systems using thermodynamic or transport properties [16]. Although no perfect agreement is reached between the estimates obtained by different methods the order of magnitude of $\bar{f}$ may be considered to be well established. The estimates for $\bar{f}$ which appear in table 2 are either experimental values taken from literature or established

Table 2

Sample	PSS	PMA [13]	PMA [13]	PAA [15]	PVS [11]
DP, α	500, 1	700, 1	5200, 1	1000–2000, 1	500, 1
Counterion	Na^+	Na^+	Na^+, K^+	$(Bu)_4N^+$	Na^+
$B_S\times10^{-3}$ (monomol^{-1} ℓ)	1.7 ±0.4	0.9 ±0.2	0.6±0.1	0.7±0.1	–
$B_2\times10^{-3}$ (monomol^{-1} ℓ)	0.60±0.05	0.7 ±0.2	1.0±0.1	2.4±0.2	$3<B_2<15$
$(\Delta\epsilon_S/C_p)_0\times10^{-5}$(monomol^{-1} ℓ)	0.9 ±0.2	0.34±0.06	1.4±0.2	2.4±0.3	–
$(\Delta\epsilon_S/C_p)_0\times10^{-4}$(monomol^{-1} ℓ)	1.5 ±0.1	1.3 ±0.4	2.0±0.4	18 ±2	$5<(\Delta\epsilon_2/C_p)_0<30$
$\bar{f}$	0.7	0.6	0.6	0.8	0.7
$(\bar{L}^2)_0^{1/2}$ (nm)	104 ±12	69 ±6	140 ±10	159 ±10	–
b_0 (nm)	42.6 ±1.4	42 ±6	53 ±5	138 ±7	$80<b_0<190$

from results obtained with analogous systems. From the values of the specific increments at infinite dilution it is now possible to evaluate R_g and b according to (4) and (5). Note that in an infinitely diluted system even a flexible polyelectrolyte will exhibit a rather stretched average conformation. According to the model used in part I, if the subunits of length b would be perfectly aligned the radius of gyration would be related to the overall length of the polyion through the equation $R_g^2 = (L^2 - b^2)/12$. Therefore it may be assumed that in an infinitely diluted solution of a flexible polyelectrolyte $(12R_g^2 + b^2)$ is a measure of the average square end-to-end distance $(\overline{L^2})$. In table 2 calculated values of $(\overline{L^2})_0^{1/2}$ and b_0 according to (4) and (5) are given.

The values of the dielectric increments taken from the literature may be somewhat less accurate as compared to the values in the present investigation. This is due to the fact that in the former the fitting of the dispersion curve to an equation analogous to (1) was performed graphically only and the low frequency electric permittivities are less reliable than in our case in view of the methods used for correcting electrode effects. It may be concluded that from eqs. (4) and (5) reasonable values for $(\overline{L^2})_0^{1/2}$ and b_0 may be obtained. Taking into account the extreme simplicity of the model used in part I these equations probably describe quite satisfactorily the dielectric increments of both dispersion regions observed with aqueous solutions of flexible polyelectrolytes at infinite dilution.

Quite interesting is the finding that for our low molecular weight PSS the value of $(\overline{L^2})_0^{1/2}$ should be not too different from the value of L for a fully stretched polyion estimated on a contribution of 0.2–0.25 nm per monomeric unit. Also remarkable is the fact that the flexibility of a polyelectrolyte chain at infinite dilution increases with increasing molecular weight. This may be inferred from the value of the ratio $(\overline{L^2})_0^{1/2}/b_0$ for PMA at two different DP (taken from the same series of measurements). An analogous conclusion could be drawn from our results on PAA of different DP but at the same finite concentration (see table 1) if, in a rough approximation it is assumed that $B_2 \approx B_s$ leading to $\Delta\epsilon_s/\Delta\epsilon_2 \approx (\overline{L^2})_0^{1/2}/b_0^2$. This increase in flexibility with molecular weight at infinite dilution may be expected intuitively.

As pointed out before the finding that τ_2 is molecular weight independent but τ_1 not, is according to the theory developed in part I an indication that the high frequency relaxation mechanism is essentially determined by the fluctuations in the bound counterions distribution along the *subunits*. Expressions for the relaxation time corresponding to such a mechanism have been derived by Oosawa [17] and Wyllie [18] by solving the unidimensional diffusion equation using a Fourier expansion. Comparing the expressions obtained by each author for the the lowest mode, which practically determines the relaxation behaviour, they are found to differ only through a numerical constant (in case interactions between the diffusing ions are neglected) as a result of a different choice of the boundary conditions. As the boundary conditions used by the latter author seem to fit better into the model proposed in part I we have prefered for τ_2 the expression which follows from Wyllie's calculations.

$$\tau_2 = \tau_b = b^2/\pi^2 u k T. \tag{6}$$

Here u stands for the mobility of the bound counterion moving along the rigid subunit of length b. If τ_2 is calculated for an infinitely diluted solution of PSS, (DP is 500) using (6) with for b_0 the value derived from the specific increment $(\Delta\epsilon_2/C_p)_0$ as given in table 2 and for u the mobility u_0 of a Na^+ ion in an infinitely diluted electrolyte solution ($u_0 = 3.1\times10^{11}$ m s^{-1} N^{-1}) a value of 1.5×10^{-7} s is found. In fig. 8 a plot of $(\tau_2)^{-1}$ versus C_p using values of τ_2 from table 1 shows a linear relationship analogously to what was found for $\Delta\epsilon_2/C_p$.

$$\tau_2 = (\tau_2)_0/(1 + B'_2 C_p), \tag{7}$$

with $(\tau_2)_0 = 0.9\times10^{-7}$ s. In view of the simplicity of the model the agreement with the value calculated from (6) is satisfactory. It is interesting that $B'_2 = (0.61 \pm 0.12)\times10^3$ monomol ℓ^{-1} is equal to B_2, which is given in table 2. This may indicate that the empirical equations (2), (3) and (7) all reflect the change of the macromolecular dimensions with increasing concentration due to polyion–polyion interactions. The data for PAA and PVS taken from the literature also obey eq. (7) as can be seen from figs. 5 and 6 where $f_{c,2} = (2\pi\tau_2)^{-1}$ has been plotted against C_p. It should be noted that from the extrapolated

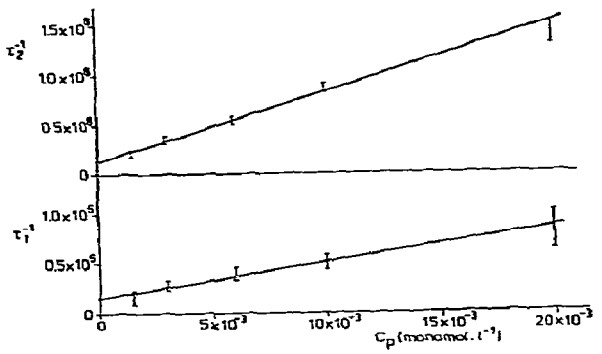


Fig. 8. τ_1^{-1} and τ_2^{-1} against C_p for PSS–Na^+, DP = 500.

values $(\tau_2)_0$ for PVS (DP = 500) and u_0 a value of $b_0 = 70 \pm 25$ nm may be calculated using (6) and for PAA a value of $b_0 = 130 \pm 40$ nm. These values are in good agreement with the values of b_0 obtained from the extrapolated values of the specific increments $\Delta\epsilon_2/C_p$ (see table 2). This shows that the interpretation of the high-frequency dispersion in terms of (6) and (7), is consistent with the theory developed in part I.

As far as the low-frequency dispersion is concerned it has already been emphasized that the interpretation of the average relaxation time is much more difficult. From the molecular weight dependence of this relaxation time it may be concluded, according to theory, that the relaxation mechanism is determined by the rotational diffusion of the polyion as a whole or by the axial diffusion of the bound counterions along the complete polyelectrolyte chain or by both simultaneously. Here again an important effect of finite concentration on the relaxation times is to be expected as in both cases the overall dimensions of the polyion and frictional coefficients play an important role. For PSS (DP = 500) the concentration dependence of τ_1 could be expressed by a relationship analogous to (7) (see fig. 8) with $(\tau_1)_0 = 7 \times 10^{-6}$ s and $B_s' = (0.22 \pm 0.05) \times 10^3$ ℓ monomol^{-1}. Note that this value is considerably smaller than B_s, B_2 and B_2' From the discrepancy between B_s and B_s' it may be concluded that the intermolecular interaction affects the relaxation time of the low frequency dispersion not only through the average dimensions as in a good approximation is the case for $\Delta\epsilon_s$, $\Delta\epsilon_2$ and τ_2.

In the case of an infinitely diluted solution where the polyion is in an extended conformation the orientational relaxation time τ_r may be evaluated using the formulae developed for the rotational diffusion coefficient of cylindrical particles [19–21]. For such particles in an ideal solution without interactions the following equation holds for the rotational relaxation time τ_r for rotations about the short axis which give the largest contribution to the electric polarization.

$$\tau_r = \pi\eta_s L^3/6kT[\ln(2L/d) + K]. \quad (8)$$

Here L represents the length of the cylinder, d its diameter (corresponding to the short axis), η_s the solvent viscosity and K is a constant which varies slightly from one author to another but is of the order of -0.5. If 0.2 nm $< d <$ 1 nm and $L = 104 \pm 12$ nm, eq. (8) yields for τ_r a value between 1.5×10^{-5} s and 4.5×10^{-5} s. This value should be compared to the value of τ_1 for PSS (DP = 500) extrapolated to infinite dilution, $(\tau_1)_0 = 7 \times 10^{-6}$ s. The discrepancy between τ_1 and τ_r could be attributed to the fact that τ_1 may also contain a contribution of the relaxation mechanism due to the axial diffusion of bound counterions from one subunit to another for which no theoretical expression for the relaxation time τ_q is available yet. Therefore from the experimental results it cannot be concluded unambiguously that the low frequency relaxation mechanism is determined only by the rotation of the polyion. However, the order of magnitude of τ_r as compared to $(\tau_1)_0$ justifies the assumption that rotational relaxation strongly contributes to the mechanism. The dielectric behaviour of PMA in the low frequency dispersion region is quite analogous to that of PSS, as follows from the results of Mandel and Jenard [13]. For a sample of comparable DP and analogous concentrations, values of τ_1 of the same order of magnitude as for PSS(DP = 500) but somewhat smaller have been found, leading also to a lower value for $(\tau_1)_0$ in agreement with the fact that for the former $(\overline{L^2})_0^{1/2}$ is also slightly smaller than for the latter. Here again the relaxation time τ_1 is found to decrease with increasing concentration for $10^{-3} < C_p < 7 \times 10^{-3}$ monomole ℓ$^{-1}$. On the contrary the results of Minakata and Imai [15] for PAA do not show this concentration effect in a conclusive way. Their relaxation time for a DP situated between 1000 and 2000 is about 10^{-4} s which again would be of the same order of magnitude as the value of τ_r cal-

culated according to (8) taking into account a value of $L = 160$ nm (see table 2). It is interesting to note that in the present investigation for a sample of PAA (DP = 1530) at $C_p = 5 \times 10^{-3}$ monomole ℓ^{-1} but at a degree of ionization $\alpha = 0.4$ the value of τ_1 was practically a factor 30 smaller than the relaxation time found by Minakata and Imai under comparable conditions but $\alpha = 1$. If it is assumed that the larger value of τ_1 at $\alpha = 1.0$ as compared to $\alpha = 0.4$ is only due to the expansion of the polyion (i.e., to the influence of $(\overline{L^2})^{1/2}$ on τ_2), then for $\Delta\epsilon_s$ a value ten times larger than in the present investigation would be predicted according to (2) for the system investigated by Minakata and Imai*.

In fact the latter found a $\Delta\epsilon_s = 268$ at $C_p = 5 \times 10^{-3}$ monomole ℓ^{-1}, which as compared to our $\Delta\epsilon_s = 22$ is in good agreement with this rough evaluation. This again confirms that τ_1 for these flexible polyelectrolytes is to a large extent determined by the orientational relaxation time of the polyion. Of course at the present stage it is not yet possible to ascertain whether or not the other relaxation mechanism which gives rise to a molecular weight dependent relaxation time contributes to τ_1. It should also be pointed out that with increasing molecular weight τ_r may reach values which could be of comparable order of magnitude as or even larger than the relaxation time τ_f due to the exchange mechanism between bound and free counterions. Should this be the case the molecular weight dependence of τ_1 is expected to level off at large values of DP. This seems to be the case for PMA according to the results of Mandel and Jenard [13]. However as the influence of the concentration on τ_1 for the same set of systems has not been investigated this conclusion should be considered with proper care.

There still remains to be discussed the problem of the existence of a certain distribution of relaxation times for both dispersion regions. In as far as the lower frequency dispersion region is concerned it has already been pointed out in part I that in general a complicated dispersion behaviour is to be expected, which may give rise to deviations with respect to the simple Debye curve. Furthermore the following specific factors may eventually contribute to a real distribution of relaxation times: the heterodispersity of the samples investigated and the possibility that different conformations close to the average conformation contribute separately to the relaxation mechanism. The second of these may also be partially responsible for the distribution of relaxation times observed in the high frequency dispersion region through a certain distribution in the lengths b of the subunits. Also in as far as this dispersion region is concerned it should not be excluded that the bound ions move along a given subunit in different "layers" characterized by different values of b and of u. It is very difficult in the present stage of the theory to take these possibilities into account explicitely. Finally it should be emphasized that the possibility to fit the experimental results of different synthetic polyelectrolytes both in the low and the high frequency region to a Cole–Cole curve with the same value for β should not be interpreted too readily as pointing to the same origin for the distribution of relaxation times in all cases considered. More likely it proves that the least-squares fitting procedure as applied to our experimental results does not allow to discriminate between small differences in this factor.

* As we are only interested in the order of magnitude the influence of a small difference of f for the counterions involved is neglected.

Acknowledgement

These investigations have been carried out under the auspices of the Netherlands Foundation for Chemical Research (SON) and with financial aid from the Netherlands Organization for the Advancement of Pure Research (ZWO).

References

[1] F. van der Touw and M. Mandel, Biophys. Chem. 2 (1974) 218.
[2] F. van der Touw, J.W.H. Briedé and M. Mandel, Biopolymers 12 (1973) 111.
[3] M. Mandel and J.C. Leyte, J. Polymer Sci. A2 (1964) 2883.
[4] R.H. Wiley, N.R. Smith and C.C. Ketterer, J. Am. Chem. Soc. 76 (1954) 720;
R.H. Wiley and S.F. Reed, Jr., J. Am. Chem. Soc. 78 (1956) 2171.
[5] R. van Wijk, private communication.
[6] M. Mandel and P. Jung, Bull. Soc. Chim. Belg. 61 (1952) 553.

[7] F. van der Touw, W.M. van Beek and M. Mandel, to be published.
[8] F. van der Touw and M. Mandel, Trans. Faraday Soc. 67 (1971) 1336, 1343.
[9] W.M. van Beek, F. van der Touw and M. Mandel, in preparation.
[10] K.S. Cole and R.H. Cole, J. Chem. Phys. 9 (1941) 341.
[11] S.B. Sachs, A. Raziel, H. Eisenberg and A. Katchalsky, Trans. Faraday Soc. 65 (1969) 77.
[12] D.J. Allen, S.M. Neale and P.J.T. Tait, J. Polymer Sci. A2 (1972) 433.
[13] M. Mandel and A. Jenard, Trans. Faraday Soc., 59 (1963) 2158, 2170.
[14] S. Takashima, J. Mol. Biol. 7 (1963) 455.
[15] A. Minakata and N. Imai, Biopolymers 11 (1972) 329.
[16] A. Katachalsky, Pure Applied Chem. 26 (1971) 3, 4.
[17] F. Oosawa, Biopolymers 9 (1970) 67.
[18] G. Wyllie, in: Dielectric and related molecular processes, Vol. I, ed. M. Davies (The Chemical Society, 1972) ch. 2.
[19] F. Perrin, J. Phys. Radium 5 (1934) 497.
[20] J.M. Burgers, Second Report on Viscosity and Plasticity (1938).
[21] R. Ullman, Macromolecules 2 (1969) 27.

BIOPHYSICAL CHEMISTRY 2 (1974) 242–254. © NORTH-HOLLAND PUBLISHING COMPANY

DIELECTRIC PROPERTIES OF POLY-L-GLUTAMIC ACID IN SALT-FREE AQUEOUS SOLUTIONS

G. MULLER*, F. VAN DER TOUW, S. ZWOLLE and M. MANDEL
Gorlaeus Laboratoria der Rijksuniversiteit Leiden, Afdeling Fysische Chemie III, Leiden, The Netherlands

Received 18 April 1974
Revised manuscript received 13 August 1974

The electric permittivity of poly-L-glutamic acid (PGA) in salt-free aqueous solutions was measured in the frequency range 2.5 kHz – 100 MHz at different concentrations and degrees of ionization. Two samples of different molecular weight were investigated. The experimental results could under most circumstances be described by a superposition of two dispersion curves of the Cole–Cole type. The low-frequency dielectric parameters were strongly molecular weight dependent, the high-frequency ones not. Strong concentration effects were observed resulting in increasing specific dielectric increments and relaxation times with decreasing concentration. Using the theory proposed by Van der Touw and Mandel to interpret the experimental results these concentration effects could be ascribed to the influence of the polyion interactions on the average dimensions and the rigidity of the polyelectrolyte chains. The change in the total dielectric increment and low-frequency relaxation time with degree of ionization correctly reflects the helix–coil transition of PGA occurring in the region $\alpha = 0.3–0.5$. The effect of counterion size and charge on the dielectric behaviour was also found to be consistent with the theoretical model.

1. Introduction

Synthetic polypeptides in solution can serve as useful models of proteins and for this reason they have been extensively studied during the recent years. It is now well established that polypeptides can exist in both rigid, rod-like helical conformations and in more coil-like ones. The equilibrium helix–coil can be shifted to favor either the helical or the random coil conformation, e.g., by changing temperature, pH, solvent, etc. The helix to coil transition of polypeptides has been investigated by many different techniques such as ultrasonic absorption [1–3], temperature jump [4, 5], nuclear magnetic resonance [6, 7] or dielectric dispersion [8–11].

The dielectric properties of polypeptides in organic solvents have been extensively studied [12–14]. Poly-γ-benzyl-L-glutamate has been the poly-α-amino-acid ester chosen for most investigations and it has been shown to have a large electric dipole along the helical axis. The dipole contribution to the static value of the dielectric permittivity (which is solvent dependent) is consistent with an orientational polarization of a rod-like structure. There are only few dielectric studies however on polyaminoacids in aqueous solution. Takashima [15] studied the dielectric dispersion of polyglutamic acid (PGA) as a function of pH in the frequency range 1 kHz–1 MHz and found that the dielectric increments are larger for the coiled state than for the helical one while the relaxation times have about the same values. An interesting observation made by this author is that there are minima in both the relaxation time and the dielectric increment in function of the degree of ionization around the transition range. The experimental results were interpreted by assuming the PGA has the larger dipole moment in the coil form than in the helix form. It was also found that the simple Maxwell–Wagner theory [16] cannot be used to explain the experimental results. Kumazaki and Sugai [17] studied the dielectric dispersion of poly-L-lysine and its various salts between 1 kHz and

* On leave of absence from Université de Rouen, Faculté des Sciences, Laboratoire de Chimie Macromoléculaire (Directeur: Prof. E. Sélégny), 76130 Mont-Saint-Aignan, France.

1 MHz. They found that the dielectric relaxation of PLL–HCl in the frequency range lower than 100 kHz may be considered to be originated from movements of counter-ions while in the frequency region higher than 100 kHz the dielectric dispersion was thought to be due to a Maxwell–Wagner–Sillars effect. No peculiar behaviour during the transition was observed. It should be noted that both Takashima and Kumazaki's results should be considered with proper care in view of the somewhat doubtful electrode polarization correction used and method by which the dielectric parameters were determined.

We have studied the dielectric behaviour of salt-free aqueous solutions of PGA over the frequency range 2.5 kHz – 100 MHz. The influence of ionization, molecular weight, concentration and nature of counter-ions on the dielectric permittivity and the relaxation time of PGA has been investigated. Particular care was taken to study if the transition occurring during the ionization is detectable by dielectric measurements.

2. Experimental

2.1. Material and solutions

Two samples of PGA were used in this investigation. The first was purchased from KEK (sample 1, acid form, DP = 620) and the other from Sigma (sample 2, sodium salt, DP = 308). The solutions were prepared in the following way. The solutions of sample 1 were prepared up to a certain degree of ionization by dissolving PGA in dilute NaOH solution followed by an extensive dialysis against distilled water to obtain solutions without extra salt. The solution of sample 2 were prepared by flowing solutions of the sodium salt of the polyacid through an ion-exchange resin column and neutralization thereafter by addition of NaOH. The pH of solutions was measured just before measurements and all the solutions were kept in polyethylene bottles. The measurements were performed at $t = 22.1°C$ under an atmosphere of nitrogen to avoid interaction with carbon dioxyde. All the concentrations are expressed in g/ℓ.

2.2. Measuring method

The dielectric permittivity was measured in the frequency range 2.5 kHz – 100 MHz by use of bridge techniques. In the low-frequency part (2.5–500 kHz) a specially designed bridge was employed for measuring capacitances of condensers shunted by a low resistance [18]. A method has already been described for the determination of the electric permittivity of highly conducting liquids below 1 MHz with a measuring cell consisting of a plane parallel plate condenser with variable electrode spacing [19]. The electrode effects (due to the impedance of the diffuse double layer at the electrodes) and the edge effects (due to the perturbation of the uniform electric field near the edges of the plates) are taken into account in the expressions for the total capacitance and conductance of the cell. The high-frequency measurements (1–100 MHz) were performed with a Schering impedance bridge RX Meter type 250, manufactured by Boonton-Radio Corp., and a coaxial cell with variable electrode length. This special construction is necessary for the correction of the parasitic effects arising from the cell connections to the bridge and effects caused by the fact that the dimensions of the cell are no longer negligible compared to the wavelength of the electromagnetic wave. The details on the high-frequency measuring method will be described in a subsequent paper [20].

Only the value of the real part of the frequency dependent complex permittivity ϵ' could be determined. The imaginary part ϵ'' was within experimental accuracy completely determined by the conductivity σ of the solutions (cf. [36b]). The experimental values of ϵ' were fitted by a weighted least-squares fitting procedure to the following analytical expression for two separated dispersion regions, each one being described by the dispersion relation proposed by Cole and Cole [21]:

$$\epsilon' = \epsilon_\infty + \tfrac{1}{2}\Delta\epsilon_1\left(1 - \frac{\sinh\beta x_1}{\cosh\beta x_1 + \cos\tfrac{1}{2}\beta\pi}\right) + \tfrac{1}{2}\Delta\epsilon_2\left(1 - \frac{\sinh\beta x_2}{\cosh\beta x_2 + \cos\tfrac{1}{2}\beta\pi}\right). \quad (1)$$

Here $x_1 = \ln(2\pi f\tau_1)$, $x_2 = \ln(2\pi f\tau_2)$ and β is the Cole–Cole parameter ($0 < \beta < 1$).

The dispersion regions are characterized by mean

relaxation times τ_1 and τ_2 and dielectric increments $\Delta\epsilon_1 = \epsilon_s - \epsilon_2$ and $\Delta\epsilon_2 = \epsilon_2 - \epsilon_\infty$. ϵ_s and ϵ_∞ are the extrapolated electric permittivities at the low- and the high-frequency end of the dispersion curve. The extrapolation of the experimental results at $f = 0$ yields the static electric permittivity ϵ_s of the solution or the dielectric increment $\Delta\epsilon_s = \epsilon_s - \epsilon_w$, where ϵ_w is the electric permittivity of water (experimentally it is always found that $\epsilon_\infty = \epsilon_{water}$). Both dispersion regions cannot be described by a simple Debye curve (with $\beta = 1$) which indicates for both regions the existence of a distribution of relaxation times. It was attempted to separate the whole dispersion curve into two curves both of them satisfying the Cole–Cole formula with a Cole parameter $0.5 < \beta < 1$. Following the same procedure as described previously by Van der Touw and Mandel [36b] it was found that all curves could be fitted by a superposition of two Cole–Cole functions with the same value $\beta = 0.80$, leading to the best standard deviations of the fitting procedure. Therefore all results given here were fitted by a curve with $\beta = 0.80$. In some cases [particularly for the lowest concentrations in the case of the low molecular weight PGA under helix form (table 3)], it was very difficult to discriminate in the complete dispersion curve two separated regions owing to the low values of the dielectric increments. Therefore in such cases it seemed more appropriate to define the whole dispersion curve with one mean relaxation time.

The accuracy on the increments $\Delta\epsilon_2$ and $\Delta\epsilon_s$ are estimated to be about 0.5 unit for $\Delta\epsilon_2$ and between 1 and 2 units for $\Delta\epsilon_s$. The accuracy of the relaxation times is around 10% as long as the corresponding increments are not smaller than 5. (See ref. [36b].)

3. Experimental results

3.1. Dependence of dielectric parameters on the degree of ionization

The effect of the ionization was studied on salt-free aqueous solutions of PGA neutralized with sodium hydroxyde (DP = 620, C_p = 0.13 g/ℓ = 10^{-3} monomole/ℓ).

In a large range of ionization, the dielectric dispersion profile of PGA can be described by two well separated dispersions according to relation (1), one with a lower critical frequency in the range 10^4–10^5 Hz whereas the high critical frequency is observed in the region 10^6–10^7 Hz. Figure 1 shows a dispersion pattern of Na–PGA in the coil form. The experimental results are summarized in table 1.

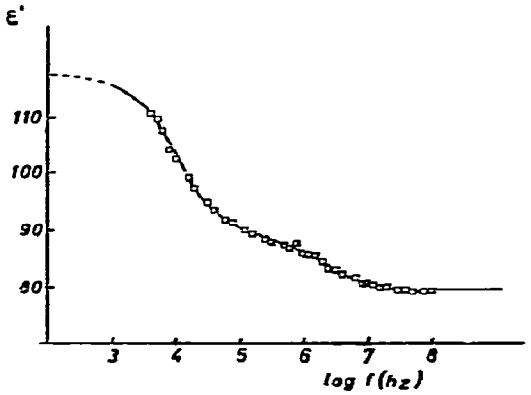


Fig. 1. Electric permittivity ϵ' as a function of the frequency f for PGA–Na (DP = 620, C_p = 0.13 gℓ^{-1}, degree of ionization = 0.9). The drawn curve is the calculated dispersion curve according to the Cole–Cole formula (1) with the help of the least-squares procedures.

Table 1
Dependence of dielectric parameters of PGA on the degree of ionization (PGA–Na, DP = 620, C_p = 0.13 g/ℓ).

Degree of ionization	pH	$\Delta\epsilon_s$	$\Delta\epsilon_2$	$\tau_1 \times 10^6$ s	$\tau_2 \times 10^7$ s
0.09	4.90	8.4	4.7	14.1	3.6
0.11	5.00	9.4	3.9	4.5	2.2
0.13	5.10	8.6	4.9	4.0	2.2
0.20	5.50	11.1	4.1	3.2	1.4
0.23	5.70	12.2	5.0	5.6	1.7
0.27	6.0	13.4	5.1	6.3	1.3
0.39	6.25	15.6	6.2	5.6	1.1
0.44	6.30	25.5	8.1	7.9	1.0
0.46	6.35	23.5	6.9	10.0	1.3
0.51	6.50	31.1	9.5	12.6	1.3
0.55	6.55	27.0	7.5	11.2	1.1
0.60	6.75	31.5	10.6	12.6	1.0
0.75	7.25	32.1	9.9	11.2	1.0
0.79	7.35	33.3	8.9	11.2	0.8
0.85	7.60	30.7	10.1	8.9	1.0
0.90	8.10	30.6	8.8	8.9	0.6
1.0	9.20	32.5	10.6	8.9	0.5
	9.50	31.3	9.2	8.9	0.5

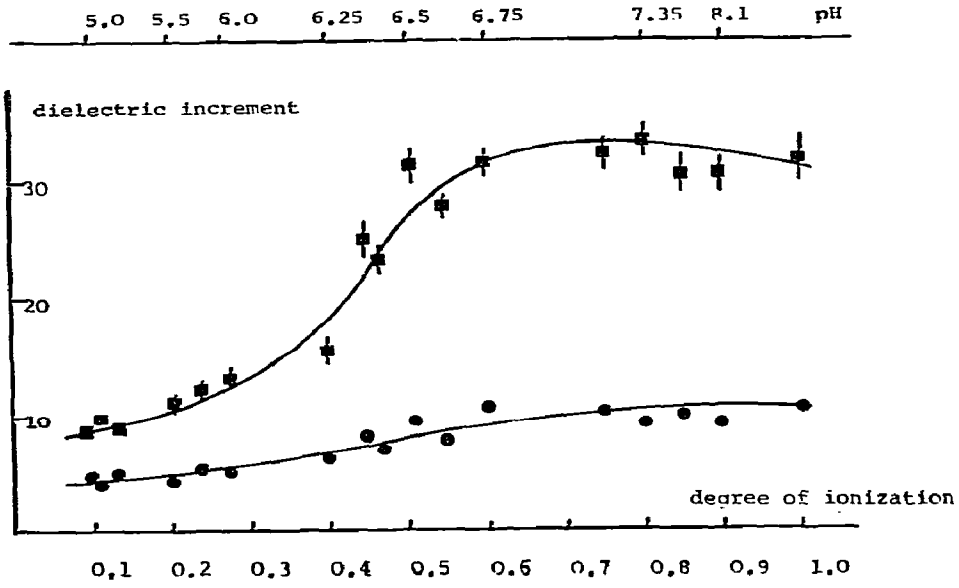


Fig. 2. Dependence of the dielectric increment $\Delta\epsilon_S$ (■) and $\Delta\epsilon_2$ (●) on the degree of ionization α for PGA–Na: DP = 620, C_p = 0.13 g/ℓ.

The values reported in table 1 clearly show that $\Delta\epsilon_s$, and at a lesser extent $\Delta\epsilon_2$, increase during the neutralization of carboxylic groups. The molecular conformation of PGA at various degrees of neutralization has been well clarified by potentiometric titration and other methods [22–24]. It is well known that PGA undergoes a conformational change during the neutralization and a helix to coil transition clearly appears during the titration of a 10^{-3} M PGA solution around $\alpha = 0.3$–0.4. The values below pH = 5 must be considered with proper care due to agregation [25]. In the region of the α values corresponding to the transition a change in the slope $\Delta\epsilon$ versus α is observed (fig. 2). The reduced viscosity is also found to increase from helix to coil form (table 2).

With the exception of the initial high value of τ_1 for pH below 5, the first relaxation time also increases during the transition as shown in fig. 3. The second re-

Table 2
Reduced viscosity of PGA (DP = 308, $C_p = 10^{-3}$ mole/ℓ) as a function of the degree of ionization (α)

α	0	0.1	0.2	0.3	0.4	0.5	0.7	0.9
η_{sp}/C_p (dl/g).	0.17	0.60	1.8	3.0	4.5	5.2	6.4	6.1

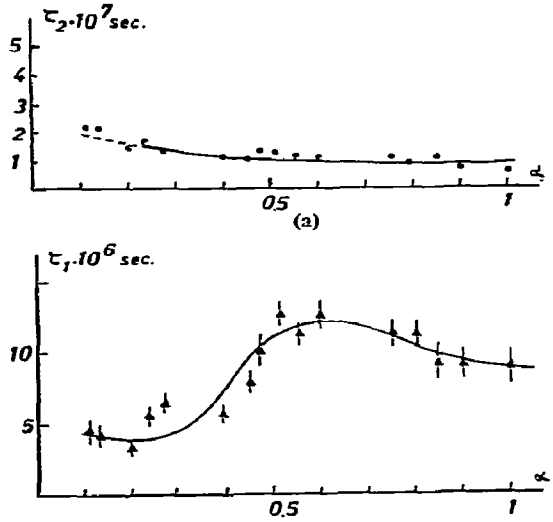


Fig. 3 Variation of the high-frequency relaxation time τ_2(●) and the low-frequency relaxation time τ_1(▲) with α for PGA–Na: DP = 620, C_p = 0.13 g/ℓ.

Table 3
Effect of concentration on dielectric parameters of PGA (DP = 308)

C_p (g/ℓ)	η_{sp}/C_p (dl/g)	$\Delta\epsilon_s$	$\Delta\epsilon_2$	$\Delta\epsilon_s/C_p$ (ℓ/g)	$\Delta\epsilon_2/C_p$ (ℓ/g)	$\tau_1 \times 10^6$ (s)	$\tau_2 \times 10^7$ (s)
PGA–Na, coil form (α = 0.9)							
0.75	3.9	20	13.7	27	18	1.3	0.18
0.375	4.7	15	9.8	40	26	1.6	0.23
0.15	6.5	10	7.5	67	50	1.8	0.40
0.075	7.4	7	5.0	93	67	3.2	1.0
0.037	8.1	4.5	2.8	120	75	3.6	1.5
PGA–Na, helix form (α = 0.2)							
0.75	1.05	6.9	5.0	9.2	6.7	2.0	0.2
0.30 [a]	1.7	3.1		10.3			$\tau = 2.2 \times 10^{-7}$ s
0.15 [a]	1.9	2.6		17.3			$\tau = 3.6 \times 10^{-7}$ s

[a] For C_p = 0.30 and 0.15 g/ℓ, it is not possible to separate the complete dispersion curve in two parts, as discussed above. On the other hand, for C_p = 0.75 g/ℓ the dispersion curve can better be fitted with two dispersion regions than with a single one; if it is described with only one dispersion the following values are found: $\Delta\epsilon_s$ = 5.5, $\Delta\epsilon_s/C_p$ = 7.3 ℓ/g and $\tau = 0.35 \times 10^{-7}$ s.

laxation time τ_2 is slightly decreasing from low to high α values. No minimum in $\Delta\epsilon_s$ or τ_1 in the transition region has been observed however, in contrast to what Takashima has found [15].

3.2. Effects of concentration on dielectric parameters of PGA

The measurements were carried out at several concentrations for each sample of PGA. In a very large range of concentration, there exist two well separated dispersion regions for PGA in the coil-like form as usually observed for solutions of flexible macromoles [26]. The experimental results are reported in tables 3 and 4, for PGA (DP = 308) and PGA (DP = 620) respectively.

As shown in fig. 4 the concentration dependence of the dielectric increment is non linear and both the reduced increments $\Delta\epsilon_s/C_p$ and $\Delta\epsilon_2/C_p$ are function of the polymer concentration C_p. For the helix form, the reduced increment is found to be less dependent on the concentration as for the coil form. It should also be mentioned that the relaxation time τ_2 of the higher frequency dispersion region is practically independent of the molecular weight in contrast to the relaxation time τ_1 of the lower frequency region (fig. 5).

Table 4
Effect of concentration on dielectric parameters of PGA (DP = 620). PGA–Na coil form (α = 0.9)

C_p (g/ℓ)	η_{sp}/C_p (dl/g)	$\Delta\epsilon_s$	$\Delta\epsilon_2$	$\Delta\epsilon_s/C_p$ (ℓ/g)	$\Delta\epsilon_2/C_p$ (ℓ/g)	$\tau_1 \times 10^6$ (s)	$\tau_2 \times 10^7$ (s)
0.56	11.7	33.4	14.4	60	26	2.2	0.2
0.39	14.2	33.7	14.4	87	37	3.6	0.3
0.28	15.3	28.2	11.5	100	41	2.2	0.3
0.21	16.6	26.0	11.3	126	50	5.0	0.6
0.16	18.1	31.0	11.0	192	68	5.0	0.5
0.13	19.2	31.0	9.0	230	77	8.9	0.6
0.11	20.0	25.0	7.8	220	70	6.3	1.4
0.10	20.0	25.0	10.0	240	97	11.2	1.6
0.07	20.8	21.0	7.7	308	112	12.6	1.4
0.03	–	8.9	3.6	317	130	11.2	3.1

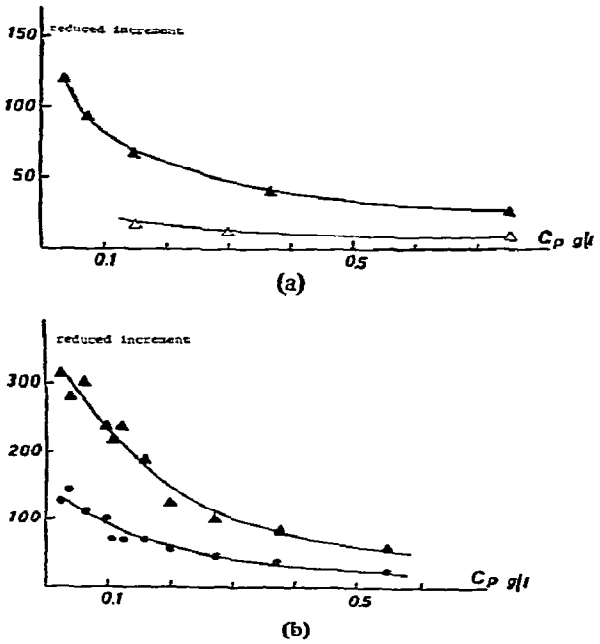


Fig. 4. Concentration dependence on the reduced increment.
Upper curve: variation of $\Delta\epsilon_s/C_p$ in function of the concentration for PGA–Na, DP=308 in the coil form (▲) and the helix form (△).
Lower curve: variation of $\Delta\epsilon_s/C_p$ (▲) and $\Delta\epsilon_2/C_p$ (●) in function of the concentration for PGA–Na: DP = 620, coil form.

3.3. Ionic specificity

We have investigated (at fixed concentration C_p = 0.13 g/ℓ) the dependence of dielectric dispersion on the nature of the counter-ion (Na^+, $(CH_3)_4N^+$, $(nC_4H_9)_4N^+$ and mixtures Na^+/Ba^{2+}). The experimental results are given in tables 5 and 6.

Table 5
Dependence of dielectric parameters on monovalent counter-ion type (PGA, DP = 308, α = 0.9, C_p = 0.13 g/ℓ)

	Counterion		
	Na^+	$(CH_3)_4N^+$	$(nC_4H_9)_4N^+$
η_{sp}/C_p (dl/g)	6.5	5.7	9.1
$\Delta\epsilon_s$	10.4	10.2	17.8
$\Delta\epsilon_2$	7.5	7.5	13.1
$\tau_1 \times 10^6$ (s)	1.8	1.3	1.8
$\tau_2 \times 10^7$ (s)	0.4	0.5	1.05

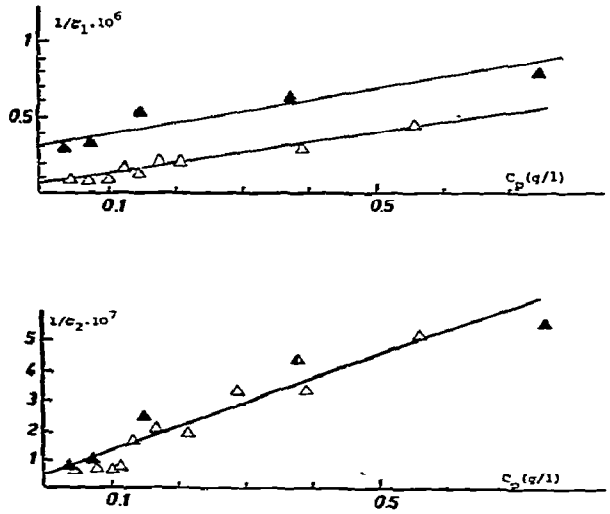


Fig. 5. Effect of the molecular weight and concentration on the low-frequency relaxation time τ_1 and on the high-frequency relaxation time τ_2 for PGA–Na in the coil form: (▲) PGA, DP = 308; (△) PGA, DP = 620.

As shown in table 5 there is no significant difference between $(CH_3)_4N^+$ and Na^+ in as far as the dielectric parameters of PGA are concerned whereas larger dielectric increments and an increase of the high-frequency relaxation time are found in the presence of the bulky quaternary ammonium ion $(C_4H_9)_4N^+$. This difference of the behaviour of PGA in the presence of both types of counterions is also observed in the reduced viscosity and the potentiometric titration, as shown in fig. 6.

The results of dielectric measurements obtained with mixtures of mono- and divalent counter-ions are reported in table 6.

As shown in fig. 7, for PGA neutralized by a mixture of Na^+ and Ba^{2+} counter-ions the dielectric increment $\Delta\epsilon_s$ is found to be highest in the intermediate value of the mixing ratio (20% of Ba^{2+}) afterwhat it sharply decreases as the fraction of divalent ions exceeds 30%. In contrast $\Delta\epsilon_2$ only changes very slowly at low Ba^{2+}/Na^+ ratios but definitively decreases after 20%. The specific viscosity is found to decrease monotonously with increasing mixing ratio Ba^{2+}/Na^+.

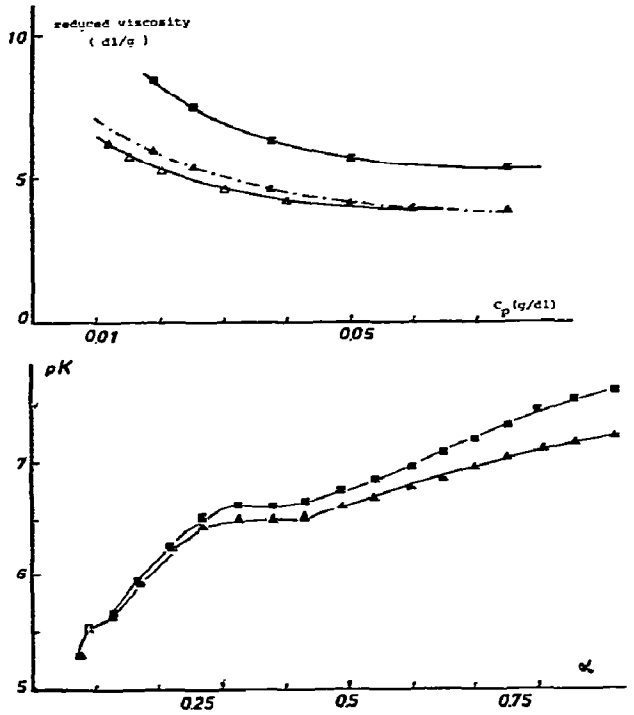


Fig. 6. Reduced viscosity of PGA (DP = 308, $\alpha = 0.9$) in the presence of monovalent counterions (■) $(nC_4H_9)_4N^+$, (▲) Na^+ and (△) $(CH_3)_4N^+$ and potentiometric titration of 0.001 M PGA neutralized with tetrabutylammonium hydroxyde (□) and sodium hydroxyde (▲).

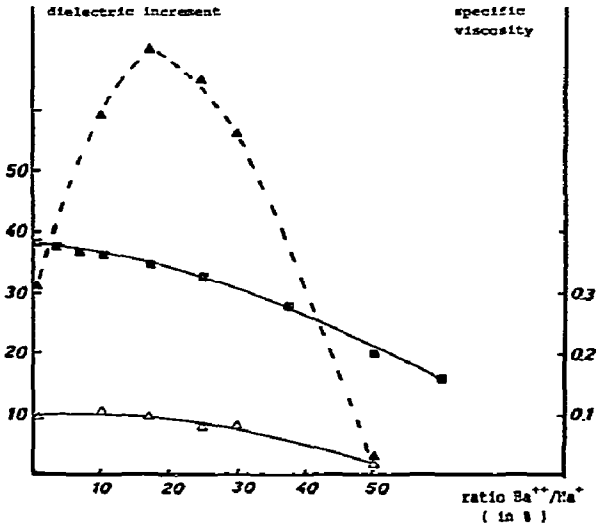


Fig. 7. Low-frequency dielectric increment $\Delta\epsilon_S$ (▲) and high-frequency dielectric increment $\Delta\epsilon_2$ (△) as a function of counterion ratio for PGA (DP = 620, $C_p = 0.13$ g/ℓ, $\alpha = 0.9$) neutralized by a mixture of NaOH and $Ba(OH)_2$. (■) specific viscosity in function of the mixing ratio.

4. Discussion

Different models have been proposed to interpret the dielectric behaviour of polypeptides. The experimental results found with proteins (often at their isoelectric point) were explained in terms of orientational polarization [27–29]. Kirkwood and Shumaker [30] suggested that fluctuations in the distribution of protons might give rise to the dielectric effects. In the case of synthetic polyelectrolytes the dielectric behaviour is generally explained in terms of the polarization of the ionic atmosphere [31–35]. The corresponding theories are based on a rigid rod model for the polyion and different approaches have been used by Schwarz [32], Mandel [33], McTague and Gibbs [35] and Oosawa [34]. In general synthetic polyelectrolytes are more or less flexible and therefore

Table 6
Dielectric dispersion of PGA neutralized with a mixture of mono- and divalent ions (PGA, DP = 620, $\alpha = 0.9$, $C_p = 0.13$ g/ℓ)

	Ratio Ba^{2+}/Na^+ (in % of equivalents)						
	0	10	17	25	30	37.5	50
$\Delta\epsilon_S$	31	60	71	65	56	4.2	2.8
$\Delta\epsilon_2$	9	11	10	7.7	8.5	2.0	1.4
$\tau_1 \times 10^6$ (s)	8.9	14	18	12.6	10.0	–	–
$\tau_2 \times 10^7$ (s)	0.6	0.6	0.9	0.8	1.0	–	–
η_{sp}	0.39	0.36	0.35	0.33	0.30	0.20	0.18

a new theory was proposed by Van der Touw and Mandel [36a]. The polyion is represented as a sequence of rigid rodlike subunits in a given configuration along which counterions "bound" to the polyelectrolyte can move. In this discussion we shall investigate if this theory can also be used to explain the results obtained with PGA.

The theory proposed by van der Touw and Mandel predicts two separated dispersion regions if the rigid subunits of the macromolecule are separated by energy barriers in as far as the diffusion of bound counterions along the polyelectrolyte chain is concerned and if the diffusional relaxation for the counterion motion along each subunit is much faster than the relaxation due to the orientational or deformational relaxation of the macromolecule as a whole as well as the relaxation due to the exchange between "bound" and free counterions. The total dielectric increment due to the perturbation of the "bound" counterions distribution along the chain is given by

$$\Delta\epsilon_s = (ze)^2 C_p \gamma \bar{n} \overline{L^2}/36 kT\epsilon_0, \qquad (2)$$

where ϵ_0 is the electric permittivity in vacuo, γ is the ratio of the effective field acting on the polyion and the Maxwell field in the system, C_p is the macromolecular concentration (expressed in the number of polyions per unit volume), $\bar{n}$ represents the average number of "bound" counterions per polyion ($\bar{n} = \bar{f}Z/z$ where Z is the number of elementary charges e fixed on the polyion, z the number of elementary charges per counterion and $\bar{f}$ the average fraction of "bound" counterions). The increment depends on the average dimensions of the polyelectrolyte through $\overline{L^2}$ which is a quantity related to the average square length [36] (for a completely rodlike molecule of total length L the same relation holds). The amplitude of the high-frequency dispersion $\Delta\epsilon_2$ is given by an expression analogous to eq. (2) in which $\overline{L^2}$ is replaced by the square of the length b of each subunit. The relaxation time τ_2 corresponding to this high frequency dispersion region, which is determined by the diffusion process of "bound" counterions along each subunit, is given by

$$\tau_2 = b^2/\pi^2 kTu, \qquad (3)$$

where u is the mobility of the counterions along the subunit. For the low frequency dispersion region it has been shown that the corresponding relaxation time τ_1 can be determined by the fluctuations in the "bound" counterions distribution over the complete macromolecule, the orientational motion of the polyion and the exchange mechanism between "bound" and free counterions.

From τ_2 an estimate of b can be made from (3) using an assumption for u. From the ratio of $\Delta\epsilon_s$ and $\Delta\epsilon_2$ the ratio $\overline{L^2}/b^2$ may be determined and thus also an estimate for $\overline{L^2}$:

$$\Delta\epsilon_s/\Delta\epsilon_2 = \overline{L^2}/b^2. \qquad (4)$$

The properties of the high frequency dispersion region have been explained by some authors in terms of a Maxwell–Wagner effect combined or not with surface conductivity [37]. In general it is not possible however to give a consistent quantitative explanation in terms of the latter model although qualitatively some of the experimental observations can be understood by it [17, 38–41].

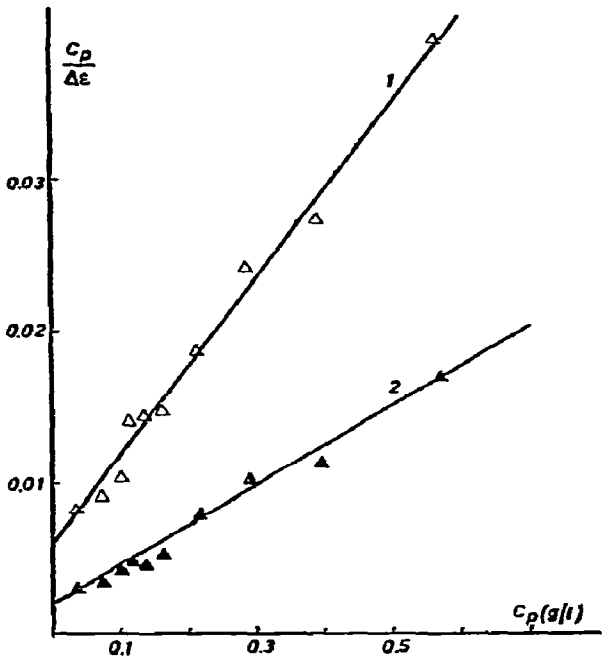


Fig. 8. Dependence of the reciprocal reduced increments $C_p/\Delta\epsilon_2$ (1) and $C_p/\Delta\epsilon_s$ (2) on the polymer concentration C_p for PGA–Na, DP=620, in the coil-like form ($\alpha = 0.9$).

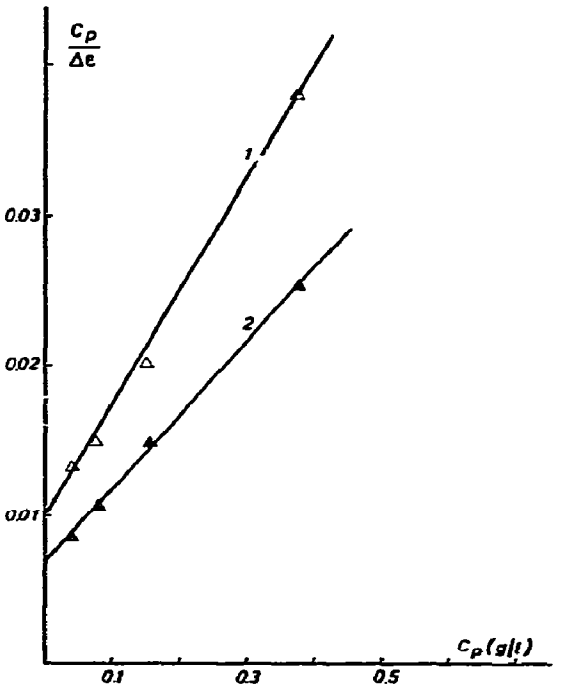


Fig. 9. Dependence of the reciprocal reduced increments $C_p/\Delta\epsilon_2$ (1) and $C_p/\Delta\epsilon_s$ (2) on the polymer concentration C_p for PGA–Na, DP = 308, in the coil-like form ($\alpha \approx 0.9$).

4.1. Concentration and molecular weight dependence

In order to investigate if the Van der Touw and Mandel theory applies to the results obtained with PGA it is necessary to extrapolate the dielectric quantities derived form experiment to zero concentration as the theory is valid only for systems at infinite dilution. From figs. 8 and 9 it can be seen that the reciprocal values of the specific increments depend linearly on the concentration both for PGA (DP = 620) and PGA (DP = 308). Extrapolation to infinite dilution then yields the following values for the specific increments of PGA at $\alpha = 0.9$ (coil-like conformation):

$$(\Delta\epsilon_s/C_p)_{C_p\to 0} = 500\ \ell g^{-1} \quad (DP = 620),$$
$$= 143\ \ell g^{-1} \quad (DP = 308),$$
$$(\Delta\epsilon_2/C_p)_{C_p\to 0} = 167\ \ell g^{-1} \quad (DP = 620),$$
$$= 100\ \ell g^{-1} \quad (DP = 308).$$

The value of the fraction of "bound" ions for PGA has been determined by measurements of the transference number [42]. Using the value at $\alpha = 0.9$ found in this way ($\bar{f} = 0.45$), b and $(\overline{L^2})^{1/2}$ can be calculated using (2) and the analogous expression for $\Delta\epsilon_2$, assuming $\gamma = 1$. The following values are then found:

DP = 620: $b = 670$ Å, $(\overline{L^2})^{1/2} = 1160$ Å,

DP = 308: $b = 519$ Å, $(\overline{L^2})^{1/2} = 620$ Å.

Note that these values only should be regarded as orders of magnitudes as nothing can be said about the exact value of γ which however may be estimated not to differ too much from unity. The small difference in the values of b for the two molecular weights is probably due to the fact that these molecular weights are rather low. The values of $(\overline{L^2})^{1/2}$ seem to be of the right order of magnitude as compared to the theoretical lengths for a completely stretched chain. From (3) the values of τ_2 can be calculated using the values of b found hereabove and assuming that the mobility u of the "bound" counterions along the subunits can be put equal to the mobility u_0 of the counterion in an ordinary electrolyte solution. This yields the following:

DP = 620: $\tau_2 = 3.6 \times 10^{-7}$ s,

DP = 308: $\tau_2 = 2.2 \times 10^{-7}$ s.

If the data collected in tables 3 and 4 are extrapolated to infinite dilution in a linear plot of $1/\tau_2$ against C_p (see fig. 5), values in good agreement with the former are found. It is thus confirmed that the mobility of the counterions moving on an equipotential surface along the rigid subunits of the polyelectrolyte does not differ significantly from the mobility of free ions. If it is now assumed that $u = u_0$ at all concentrations investigated the concentration dependence of τ_2 can be fully ascribed to the concentration dependence of b. Values of b calculated from (3) using this assumption, collected in table 7, are found to be practically independent of the molecular weight and to decrease with increasing concentration. The latter is also true for the values of $(\overline{L^2})^{1/2}$ calculated with the help of eq. (4). This is consistent with an expansion of the macromolecule upon dilution as is also revealed by

Table 7
Average dimensions of PGA in function of the concentration C_p (degree of ionization = 0.9)

DP		C_p (g/ℓ)							
		0.75	0.375	0.15	0.075	0.037			
308	b (Å)	155	175	230	355	445			
	$(\overline{L^2})^{1/2}$ (Å)	185	215	270	420	550			
		C_p (g/ℓ)							
		0.56	0.39	0.28	0.21	0.16	0.13	0.11	0.10
620	b (Å)	175	200	200	280	250	280	420	410
	$(\overline{L^2})^{1/2}$ (Å)	265	305	310	425	420	520	740	700

viscosity measurements (table 3). From the change of the specific increments with concentration and molecular weight M (see figs. 8 and 9) it can be concluded that the value of b and $(\overline{L^2})^{1/2}$ should converge with increasing dilution and decreasing M. It may be expected that from a certain value of M downwards PGA will behave as a rigid rod at infinite dilution.

The concentration dependence of the reduced increment is probably primarily determined by the effect of polyion–polyion interactions on the dimensions of the polyelectrolyte molecule. It was shown already that the reduced increments for the coil form of PGA more rapidly decrease with increasing concentration than for the helix form (see fig. 4). This is in agreement with the assumption that the helix form is more rigid than the coil-like form. As b is related to the rigidity of the chain it could be possible that for the helix form b and $(\overline{L^2})^{1/2}$ are of the same order of magnitude thus justifying the fact that for the helical form of PGA only one dispersion region could be detected at the lower concentrations. From a value of $\tau_2 = 3 \times 10^{-7}$ s (average value at low concentration, see table 3) the estimate for $b = (\overline{L^2})^{1/2}$ is 600 Å which is reasonable for PGA (DP = 308).

It was pointed out that τ_1 according the theoretical calculation can be determined by three processes: the exchange between "bound" and free counterions, the diffusion of ions along the complete chain and the orientation or deformation of the macromolecule as a whole. Provided one of these three mechanisms proceeds much faster than the others its relaxation time will determine essentially τ_1. As the relaxation time τ_1 has been found to be strongly molecular weight dependent, in agreement with measurements on other polyelectrolytes, the exchange process can be ruled out as the determining mechanism for τ_1.

The value of the orientational relaxation time can be estimated if the molecule is assumed to be a rigid rod at infinite dilution. The rotational relaxation time τ_{rot} for a cylinder of length L and diameter d is given by

$$\tau_{rot} = \pi \eta_s L^3 / 6kT[\ln(2L/d) + K] , \qquad (5)$$

where η_s is the viscosity of the solvent (0.95×10^{-2} g cm^{-1} s^{-1}) and K is a constant which, according to different authors, may range from -0.3 to -0.8 [43–45]. Using for L the values of $(\overline{L^2})^{1/2}$ calculated for PGA in the coil form at infinite dilution and for d an estimate of 12 Å the following values for τ_{rot} are then found:

DP = 620: $\tau_{rot} = 4 \times 10^{-5}$ s,

DP = 308: $\tau_{rot} = 7 \times 10^{-6}$ s.

These values are of the same order of magnitude as the extrapolated values of τ_1 at infinite dilution for PGA, $\alpha = 0.9$:

DP = 620: $(\tau_1)_{C_p \to 0} = 2.5 \times 10^{-5}$ s,

DP = 308: $(\tau_1)_{C_p \to 0} = 3.3 \times 10^{-6}$ s.

It thus may be concluded that the orientational relaxation of the macromolecule will contribute to τ_1. As no estimate can be made about the value of the counterion distribution relaxation time as long as nothing quantitative can be said about the potential barriers opposing the crossing of the counterions from one subunit to a neigbouring one, no conclusion can be reached whether the latter contributes to τ_1 or not.

4.2. Effect of ionization on the dielectric parameters

Starting this discussion it should be pointed out that all measurements with variable α were performed at one single concentration and no extrapolation to infinite dilution was possible. Therefore concentration effects as discussed previously may obscure partially the variation of the dielectric parameters with α. The latter is interesting in view of the conformational transition which from other experimental evidence is known to occur in the ionization range 0.3–0.5 [22–24].

In fig. 3 the dependence of τ_1 and τ_2 on α has been represented. In the region of α between 0.3 and 0.5 a sharp increase in τ_1 is observed in contrast to τ_2. It was already concluded that τ_1 must be related to the rotational relaxation time of the polyion and perhaps also to the counterion distribution relaxation time both of which are directly related to the overall dimensions of the macromolecule. As the conformational transition is accompanied by an increase in the average dimensions of PGA the observed increase of τ_1 in the transition region probably reflects this effect. The value of τ_2 remains practically constant over the complete range of degree of ionization except at low values of α where it is difficult to determine because of the small increments in electric permittivity observed under these circumstances. This would indicate that b does not change much in course of the ionization probably also as a result of the increasing polyion-polyion interactions with increasing α. This is confirmed by the slow and monotously increase in $\Delta\epsilon_2$ with α which may be attributed primarily to the increase of $\bar{f}$. The variation of $\Delta\epsilon_s$ with α reflects both the sudden change in the average dimension of the polyion in the transition region and the change of $\bar{f}$ with α.

From the ratio $\Delta\epsilon_2/\tau_2$ the value of $\bar{f}$ can be calculated using the assumptions $u = u_0$ and $\gamma = 1$. In fig.

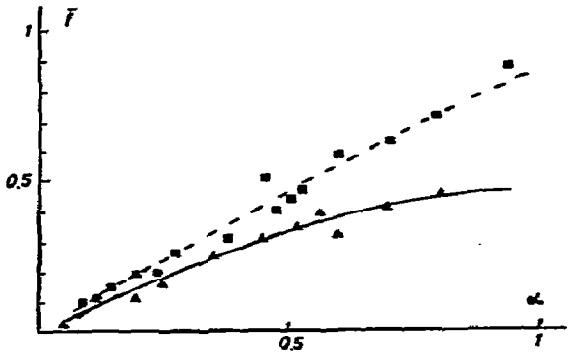


Fig. 10. Average fraction $\bar{f}$ of bound counterions in function of the degree of ionization α calculated from dielectric measurements (■) and measured from transference number (▲) (from ref. [42]).

10 these values of $\bar{f}$ are plotted against α; in the same figure experimental values of $\bar{f}$ obtained from transference number measurements [42] are also represented. It can be seen that the latter are systematically smaller than the former. This may be due to the assumptions used in the calculation of $\bar{f}$ from the dielectric parameters, particularly $\gamma = 1$. It is certainly not to be excluded that γ may be larger than unity attaining values of the order of 2. On the other hand the influence of the finite concentration on $\bar{f}$ calculated with the help of equations derived for infinite diluted solutions should not be negligible. Finally it is not to be excluded that a different fraction of "bound" counterions contribute to the transference numbers and to dielectric properties.

4.3. Ion specificity

As was already pointed out there is a significant difference in the dielectric, viscosimetric and potentionmetric properties of PGA in the presence of Na^+ or $(CH_3)_4N^+$ and $(C_4H_9)_4N^+$. From viscosimetric results (see fig. 6) it could be concluded that the polyion in the presence of $(C_4H_9)_4N^+$ is in a more extended conformation than in the presence of the two other counterions. Possibly this is due to the smaller screening effect of the bulky $(C_4H_9)_4N^+$ which cannot approach the polyelectrolyte chain as close as Na^+ or $(CH_3)_4N^+$. The same conclusion can

be reached from the potentiometric titration curves which reveal that the apparent pK for the system PGA–$(C_4H_9)_4N^+$ is larger than for PGA–Na. The dielectric results are too fragmentary to allow a more detailed interpretation but are consistent with the influence of $(C_4H_9)_4N^+$ on the average conformation of the polyion.

The influence of the ratio Ba^{2+}/Na^+ on $\Delta\epsilon_s$, as shown in fig. 7, can qualitatively be understood in terms of the charge effect due to the replacement of monovalent Na^+ by divalent Ba^{2+} in the ionic atmosphere of the polyelectrolyte and a conformational effect reflecting the decrease of the average dimension of PGA with increasing Ba concentration as also observed in the specific viscosity. The former effect gives rise to an increase of $\Delta\epsilon_s$ the latter to a decrease explaining the appearance of the maximum. It is remarkable that for $\Delta\epsilon_2$ no such maximum is apparent. Although here again no detailed analysis of the dielectric parameters can be given it may be pointed out that it is not impossible that the divalent cations are so strongly bound to PGA that they do not give rise to fluctuations in the distribution of counterions along the subunits on a time scale of the order of magnitude of 10^{-7} to 10^{-8} s.

5. Conclusions

The dielectric properties of polyglutamic acid, as found in the present investigation, can be interpreted in terms of the theory proposed by Van der Touw and Mandel [36]. This theory predicts the existence of two dispersion regions of the electric permittivity which under most circumstances have been observed for PGA. The assumption that the high-frequency relaxation time τ_2 is determined by a diffusion process of the "bound" counterions along rigid subunits of the macromolecule was consistent with the observed experimental facts. It was also found that at infinite dilution the mobility of the counterions along the subunits does not differ significantly from the mobility of ions free in solution. The low-frequency relaxation time τ_1 was found to be dependent on the average macromolecular dimensions and thus to be due either to orientation of or to a diffusion process along the complete macromolecule or both.

The effect of polyelectrolyte concentration on the apparent dimensions of the polyion and its subunits, as calculated from τ_2 and the ratio $\Delta\epsilon_s/\Delta\epsilon_2$ could be explained in terms of polyion–polyion interactions.

The marked increase both in $\Delta\epsilon_s$ and τ_1 at degrees of ionization around $\alpha = 0.4$ can be directly related to the conformational helix–coil transition known to occur for PGA in this region. No minimum in $\Delta\epsilon_s$ and τ_1 was found here contrary to the observations by Takashima [15].

The effect of counterion size the charge on $\Delta\epsilon_s$ also is in qualitative agreement with the predictions of the theory. The results are too fragmentary however to allow a more quantitative interpretation.

No attempt has been made to discuss the interaction between bound counterions along the polymer chain, as introduced by Oosawa for a rodlike model of the polyelectrolyte. It is our feeling that the effects due to these repulsions are difficult to separate from other effects that have been neglected in the theory. In the present stage the importance of the former cannot be estimated anyway, as long as there is no independent determination available for the molecular parameters involved.

Acknowledgement

One of us (G.M.) wishes to thank the Centre National de la Recherche Scientifique (C.N.R.S.), the Netherlands Organization for the Advancement of Pure Science (Z.W.O.) and the North Atlantic Treatise Organization (N.A.T.O.) for grants which have made possible his stay in the Netherlands.

References

[1] T.K. Saksena, R. Michels and R. Zana, J. Chem. Phys. 65 (1968) 597.
[2] G.G. Hammes and R.B. Roberts, J. Am. Chem. Soc. 91 (1969) 1812.
[3] G. Schwarz, J. Mol. Biol. 11 (1965) 64.
[4] R. Lumry, R. Legare and W.G. Miller, Biopolymers 2 (1964) 484.
[5] E. Hamori and H.A. Scheraga, J. Phys. Chem. 71 (1967) 4147.
[6] J. Ferretti, Chem. Comm. (1967) 1030.
[7] J.L. Markley, D.H. Meadows and O. Jardetsky, J. Mol. Biol. 27 (1967) 25.
[8] A. Wada, Chem. Phys. Letters 8 (1971) 211.

[9] A Wada, T. Tanaka and H. Kihara, Biopolymers 11 (1972) 587.
[10] G. Schwarz and J. Seelig, Biopolymers 6 (1969) 1263.
[11] E. Marchal, Biopolymers 10 (1971) 417.
[12] A. Wada, J. Chem. Phys. 29 (1958) 674.
[13] A. Wada, Bull. Chem. Soc. Japan 33 (1960) 822.
[14] E. Marchal and J. Marchal, J. Chim. Phys. 64 (1967) 1607.
[15] S. Takashima, Biopolymers 1 (1963) 171.
[16] J.S. Maxwell, A treatise on electricity and magnetism, Vol. II (Oxford, 1892);
K. Wagner, Ann. Phys. 40 (1913) 817.
[17] M. Kumazaki and S. Sugai, J. Phys. Soc. Japan 32 (1972) 785.
[18] M. Mandel and P. Jung, Bull. Soc. Chim. Belg. 61 (1952) 533.
[19] F. van der Touw and M. Mandel, Trans. Faraday Soc. 67 (1971) 1336, 1343.
[20] W.M. van Beek, F. van der Touw and M. Mandel, in preparation.
[21] K.S. Cole and R.H. Cole, J. Chem. Phys. 9 (1941) 341.
[22] A. Wada, J. Mol. Phys. 3 (1960) 409.
[23] M. Nagasawa and A. Holtzer, J. Am. Chem. Soc. 86 (1964) 538.
[24] A. Ciferri, D. Puett, L. Rajagh and J. Hermans, Biopolymers 6 (1968) 1019.
[25] A.B. Zezin, N.F. Bakeev, V.P. Merzlov, L.A. Sheldina and P.V. Kozlov, Biofizika 10(2) (1965) 207.
[26] M. Mandel and F. van der Touw, in: Polyelectrolytes, ed. E. Sélégny (Reidel, Dordrecht, 1974) p. 285.
[27] J.L. Oncley, J. Am. Chem. Soc. 60 (1938) 1115; Chem. Rev. 30 (1942) 433.
[28] S. Takashima, Arch. Biochem. Biophys. 77 (1958) 454; J. Polym. Sci. 56 (1962) 257; A1 (1963) 2791; J. Phys. Chem. 69 (1965)2281.
[29] P. Moser, P.G. Squire and C.T. O'Konski, J. Phys. Chem. 70 (1966) 744.
[30] J.G. Kirkwood and J.B. Shumaker, Proc. Natl. Acad. Sci. (U.S.) 38 (1952) 855.
[31] G. Schwarz, Z. Physik 145 (1956) 563; 19 (1959) 286.
[32] G. Schwarz, J. Phys. Chem. 66 (1962) 2636.
[33] M. Mandel, Mol. Phys. 4 (1961) 489.
[34] F. Oosawa, Biopolymers 9 (1970) 677.
[35] J.P. McTague and J.H. Gibbs, J. Chem. Phys. 44 (1966) 4295.
[36] a. F. van der Touw and M. Mandel, Biophys. Chem. 2 (1974) 218.
[36] b. F. van der Touw and M. Mandel. Biophys. Chem. 2 (1974) 231.
[37] C.T. O'Konski, J. Phys. Chem. 64 (1960) 605.
[38] M. Mandel and A. Jenard, Trans. Faraday Soc. 12 (1962) 257.
[39] S.B. Sachs, A. Raziel, H. Eisenberg and A. Katchalsky, Trans. Faraday Soc. 65 (1969) 77.
[40] A. Minakata and N. Imai, Biopolymers 11 (1972) 329; A. Minakata, ibid. 11 (1972) 1567.
[41] D.J. Allen, S.M. Neale and P.J.T. Tait, J. Polym Sci. A2 10 (1972) 433.
[42] S. Sugai and K. Nitta, Biopolymers 7 (1969) 495.
[43] F. Perrin, J. Phys. Res. 5 (1934) 497.
[44] J.M. Burgers, Second Report on Viscosity and Plasticity (North-Holland, Amsterdam, 1938).
[45] R. Ullmann, Macromolecules 2 (1969) 27.

BIOPHYSICAL CHEMISTRY 2 (1974) 255–263. © NORTH-HOLLAND PUBLISHING COMPANY

DIFFUSION CONTROLLED REACTION RATES IN SPHEROIDAL GEOMETRY. APPLICATION TO REPRESSOR–OPERATOR ASSOCIATION AND MEMBRANE BOUND ENZYMES

Peter H. RICHTER and Manfred EIGEN

Max-Planck-Institut fur biophysikalische Chemie, Göttingen–Nikolausberg, Am Fassberg, Germany

Received 31 March 1974

The von Smoluchowski–Debye formulae for diffusion controlled reaction rates are extended to the more general case of spheroidal geometry. Their application to the association of repressor and operator is thoroughly discussed in the light of recent experiments on the lac system by Riggs et al. The conclusions suggest that the surprisingly high association rate is not essentially due to electrostatic attraction but rather to unspecific binding of repressor to nonoperator DNA with subsequent diffusion along the chain.

1. Introduction

The association rate of the E. coli lac repressor with its operator has been found to be unusually high [1]. The well known von Smoluchowski formula for diffusion controlled reaction rates [2] does not seem to account for the observed rate constants, and long range electrostatic forces have been invoked in order to explain the experimental results [1]. Undoubtedly there is an attraction between the negatively charged phosphate groups of the DNA chain and positive charges on the repressor molecule; the effect of shielding of this particular interaction is clearly seen when the ionic strength is increased by adding KCl. However, from general experience as well as from theoretical considerations one would expect this effect to be more pronounced in the dissociation rather than in the association rate – in contrast to the experimental findings [1]. Therefore, it is necessary to look for a more satisfying explanation of the observed phenomena. We shall present here a model in which unspecific binding to any part of the DNA is assumed together with subsequent diffusion along the chain. The possibility of unspecific repressor binding to non operator DNA has been demonstrated in recent investigations [3–6].

The model of repressor molecules diffusing along the DNA has already been discussed very briefly by Riggs et al. [1]; however, without going into any detailed theoretical treatment they reject it on what we feel to be rather superficial arguments. The purpose of the present paper is to perform a quantitative analysis of the model and show that it may well account for the experimental findings.

The basic method of our treatment is the same as in von Smoluchowski's [2] and many subsequent works, i.e., we calculate the steady state diffusion flux of repressor particles into an operator sink (which in our particular case, due to the possibility of linear diffusion along the DNA, is more extended than the actual binding site). The representation of the operator region as a sink for repressor molecules has two aspects: physically it means that every encounter leads to a binding reaction, and this is precisely what is called a diffusion controlled process; the mathematical implication is that the initial situation of no reaction product present is maintained through all times and thus becomes describable as a well defined stationary solution of the diffusion equation.

There have been numerous applications of this idea to the reaction between spherical molecules, including the effects of electrostatic interaction and Debye–Hückel screening [7–11]. However, we are not aware of any calculation for rod or disc shaped target molecules. We fill this gap in section 3 of the present paper. Yet, the difficulty with, e.g., DNA-like long macromolecules is not entirely a mathematical one. It is well known that an infinitely long chain would be too powerful a sink as to allow for a nontrivial steady state so-

lution. Therefore, when considering the whole DNA molecule as a possible target for the repressor we have to take into account an effective finite length of that part of DNA which may contribute to the repressor–operator binding. The following section is largely devoted to a discussion of that length. In addition, for the sake of a more general applicability of our reasoning we shall as well investigate the analogous questions for two dimensional systems, i.e., membranes. The general idea that reduction of dimensionality may effectively enhance reaction rates has already been exposed in a very stimulating article by Adam and Delbrück [12].

Finally, in section 4, we shall compare our theoretical results with kinetic measurements and show that there is good consistency. As a test for our picture we propose kinetic investigation of operator containing DNA fragments shorter than the natural cut-off length.

2a. Effective range of the operator along the DNA

Starting from the two observations that

(i) nonspecific electrostatic forces between DNA phosphate groups and positive charges on the repressor aid the highly specific operator–repressor binding [1], and

(ii) there is an appreciable binding between nonoperator DNA and the repressor [3–6],

we think it worthwhile considering in detail the following model. Repressor molecules diffuse through the solution and are trapped unspecifically each time they encounter a piece of DNA:

$$R + DNA \underset{k_{diss}}{\overset{k_{ass}}{\rightleftharpoons}} R\text{–}DNA \qquad (1)$$

Due to the relatively short lifetime of the unspecific R – DNA complex, equilibrium is rapidly reached as compared to repressor–operator binding – an assumption that has successfully been employed by Lin and Riggs [5] in their rate competition experiments. Now during that lifetime, which on the average is $1/k_{diss}$, the repressor is allowed to diffuse along the DNA chain, with a "one dimensional" diffusion constant D_1 which may be considerably smaller than the constant D_3 for three-dimensional diffusion in solution. Nevertheless, the repressor's chance to find the operator and bind to it may increase because diffusion in one dimension is much more efficient in reaching a target than it is in three. Since the distance covered by diffusion is of the order of $\sqrt{D_1/k_{diss}}$ we may say that the extension of the sink that is to represent the operator in our von Smoluchowski-type calculation is $\sim \sqrt{D_1/k_{diss}}$ on both sides of the operator.

The statement can be made somewhat more precise by taking into account the stochastic nature of the diffusion process, viz. its distribution function. For that purpose, let us think of a particle which at time $t = 0$ is located at x_0 and subsequently diffuses along the x axis; whenever it reaches the point $x = 0$ (the site of the operator) it is assumed to be absorbed. What is its probability of being absorbed until time t? The answer can be found in textbooks, e.g., in ref. [13]:

$$p(x_0, t) = \operatorname{erfc}(x_0/2\sqrt{D_1 t}), \qquad (2)$$

where erfc is the complementary error function, $\operatorname{erfc} x = (2/\sqrt{\pi})\int_x^\infty \exp(-t^2)\mathrm{d}t$. If there is a homogeneous initial distribution along the x axis, with ρ particles per unit length, the total number of absorbed particles, at time t, is

$$\int_0^\infty \rho p(x_0, t)\mathrm{d}x_0 = (2/\sqrt{\pi})\sqrt{D_1 t}\cdot\rho. \qquad (3)$$

Hence the effective range A of the operator is

$$A = (2/\sqrt{\pi})\sqrt{D_1/k_{diss}} \qquad (4)$$

in both directions along the DNA.

In the next section we shall calculate how many encounters per unit time will occur between repressor molecules and DNA pieces of length $2A$. Before doing so, however, we have to find out the range of applicability of this picture. Obviously A has to exceed l_{rep}, the DNA chain length covered by the repressor, otherwise diffusion along the chain would not be of much help. Likewise, A must be smaller than the total length l of DNA; if not, l instead of A would be the characteristic length limiting the extent of the operator sink. A chain length dependence should therefore be observable in the range $l \lesssim A$.

2b. Extended range of membrane bound enzymes

An analogous two dimensional situation is met in

connection with binding of substrate to membrane bound enzymes [12]. In this case, if unspecific binding $M + S \rightleftharpoons MS$ to the membrane is possible together with diffusion along the surface, the effective sink for substrate molecules is a disc of radius $A \sim \sqrt{D_2/k_{diss}}$. For sufficiently large D_2 or small k_{diss} the association rate may therefore be enhanced by orders of magnitude.

Again, a more precise examination of A would yield an additional factor which here depends somewhat on the actual ratio between A itself and the radius r_E of the enzyme. However, Adam and Delbrück [12] have shown that this factor is only very smoothly decreasing, from 1.1 to 0.4, with A/r_E growing from 10 to 10^6. In view of the various other approximative features of our model we may thus safely neglect this factor altogether.

The applicability of the above arguments is restricted in the same way as it was in the one dimensional case. For $A \lesssim r_E$, i.e., small diffusion constants D_2 and/or high dissociation rates k_{diss}, no enhancement of the association rate will result. If on the other hand, A exceeds the radius r_M of the total membrane, r_M has to replace A in the subsequent formulae; a characteristic dependence of the association rate on the membrane's size will then become observable.

3. Diffusion controlled reaction rates in spheroidal geometries

The repressor–operator problem as formulated in the preceding section requires a von Smoluchowski theory for long cylindrical targets. The membrane bound enzymes, on the other hand, involve flat disc-shaped geometries. We shall treat both configurations as limiting cases of the more general situation of spheroidal surfaces of encounter. These are obtained by rotating and ellipse about a diameter; depending upon whether the rotation occurs about the major or the minor axis, the spheroids are called prolate or oblate. A long cylinder may well be represented by a long prolate spheroid whereas an oblate spheroid should be good enough an approximation to our membrane disc.

If the repressor molecules are taken to be spherical a spheroidal surface of encounter does not exactly imply that the target itself is spheroidal although it is very nearly so. Consequently the target's electrostatic potential, acting on the repressor molecule, is not exactly spheroidal either. However, since the effects of non-ideal shape and nonuniform distribution of charges on the molecules are anyway much more pronounced we may safely assume that the spheroidal surface of encounter be an equipotential surface of the field generated by the charges on the target.

The calculations are then straightforward. The basic set of equations is provided by the continuity equation for the repressor particle density

$$\partial n/\partial t + \operatorname{div} \boldsymbol{j} = 0 \tag{5}$$

and the usual relation between particle flux $\boldsymbol{j}$ and its driving forces

$$\boldsymbol{j} = -D_3 [\operatorname{grad} n + (n/kT) \operatorname{grad} U]. \tag{6}$$

U is the electrostatic energy of the repressor molecule in the target's potential, D_3 the diffusion constant in three dimensions.

Due to the spheroidal geometry the quantities appearing in the above equations depend on only one of the three spheroidal coordinates, usually denoted by ξ (see appendix). If $\xi = \xi_0$ characterizes the surface of encounter the boundary conditions may be formulated in analogy to the spherical problem, treated in a previous paper [8].

For the forward reaction (association), since only the nonassociated particles are to be taken into account

$$\begin{array}{lll} n = 0 & & \xi = \xi_0 \\ & \text{for} & \\ n = n_\infty & & \xi \to \infty. \end{array} \tag{7}$$

For the back reaction (dissociation) only the associated particles have to be considered so that

$$\begin{array}{lll} n = n_0 & & \xi = \xi_0 \\ & \text{for} & \\ n = 0 & & \xi \to \infty, \end{array} \tag{8}$$

where n_0 corresponds to one particle per target volume.

Furthermore, since at the steady state $\operatorname{div} \boldsymbol{j} = 0$ outside the surface of encounter the total flux I into any surface $\xi = \text{const.}$ ($\xi \geqslant \xi_0$),

$$I = -\int_{(\xi)} \boldsymbol{j} \cdot \mathrm{d}^2 \boldsymbol{r}, \tag{9}$$

is a constant. It will be determined eventually by adjust-

ing the general solution (13) to the appropriate boundary conditions. In fact, I is essentially the reaction rate we want to calculate. In the case of association,

$$k_{\rightarrow} = I_{\rightarrow}/n_{\infty}. \tag{10}$$

Since chemists like to measure $k_{\rightarrow}$ in units of $M^{-1}s^{-1}$, they have to multiply the right hand side by a factor $N/1000$ if $I_{\rightarrow}/n_{\infty}$ is given in $cm^3\ s^{-1}$, N being Avogadro's number. The dissociation rate $k_{\leftarrow}$ is simply the negative of the corresponding flux $I_{\leftarrow}$:

$$k_{\leftarrow} = -I_{\leftarrow}. \tag{11}$$

Evaluating eqs. (5), (6), and (9) for I yields

$$I = 2\pi D_3 a[\xi^2 \overset{-}{(+)} 1]\left(\frac{\partial n}{\partial \xi} + \frac{n}{kT}\frac{\partial U}{\partial \xi}\right) \tag{12}$$

for prolate (oblate) spheroids, a being the interfocal distance of their basic ellipses. This first order differential equation is readily integrated to give

$$n(\xi) = \frac{I}{2\pi D_3 a}\exp[-U(\xi)/kT]\int^{\xi}\frac{\exp(U/kT)}{\xi^2 \overset{-}{(+)} 1}\,d\xi. \tag{13}$$

Taking into account the boundary conditions (7), (8) we get

$$I_{\rightarrow} = \frac{2\pi D_3 a n_{\infty}}{\int_{\xi_0}^{\infty}\exp(U/kT)[\xi^2 \overset{-}{(+)} 1]^{-1}\,d\xi} \tag{14}$$

for the association and

$$I_{\leftarrow} = -(n_0/n_{\infty})\exp(U_0/kT)\,I_{\rightarrow} \tag{15}$$

for the dissociation reaction.

The integration in eq. (14) can easily be carried out if U itself, like $n(\xi)$, satisfies Laplace's equation outside the spheroid. This is the case for very low concentration of electrolyte where there is no charge distribution outside the spheroid and thus Debye–Hückel screening does not yet take place. We have then

$$[\xi^2 \overset{-}{(+)} 1]\,dU/d\xi = \text{const.}, \tag{16}$$

which leads to

$$I_{\rightarrow} = \frac{4\pi D_3 a n_{\infty}}{\ln[(\xi_0+1)/(\xi_0-1)]}\,\frac{U_0}{kT[\exp(U_0/kT)-1]} \tag{17}$$

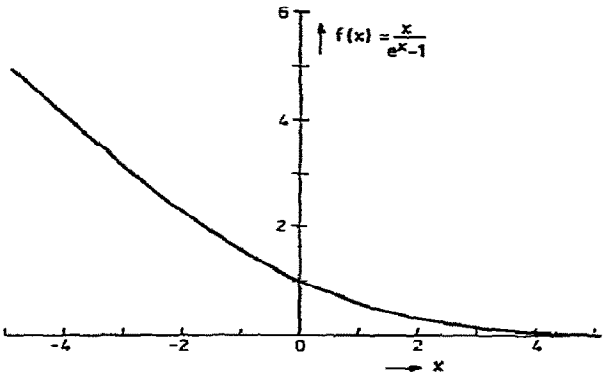


Fig. 1. The dependence of the association rate on an electrostatic potential $x \equiv U_0/kT$. The rate enhancement is linear in x for attractive potential; the rate decreases exponentially with x for repulsive electric forces.

for prolate and

$$I_{\rightarrow} = \frac{4\pi D_3 a n_{\infty}}{\pi - 2\arctan\xi_0}\,\frac{U_0}{kT[\exp(U_0/kT)-1]} \tag{18}$$

for oblate spheroids.

Let us first discuss the electrostatic factor

$$[\exp(U_0/kT)-1]^{-1}U_0/kT.$$

It is one for vanishing charges, and for arbitrary $U_0/$

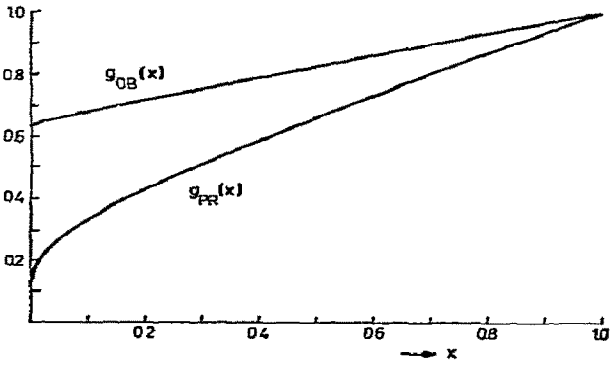


Fig. 2. The dependence of the association rate on the ratio $x \equiv B/A$ of the minor to the major axes of the spheroids. An extremely flat disc ($g_{OB}(x)$ for $x \to 0$) is still $2/\pi \approx 64\%$ as effective a sink as a sphere of radius A. For a thin rod, the geometric factor $g_{PR}(x)$ decreases as $1/\log(2/x)$.

can be taken from fig. 1. The potential energy U_0 may be expressed in terms of the total charges q_D on the target DNA and q_R on the repressor (or q_M and q_S for membrane and substrate respectively):

$$U_0 = \frac{q_D q_R}{4\pi a \epsilon} \times \begin{cases} \ln[(\xi_0 + 1)/(\xi_0 - 1)] & \text{(prolate)} \\ \pi - 2\arctan \xi_0 & \text{(oblate)} \end{cases} \quad (19)$$

(ϵ is the dielectric constant of the medium).

We shall now concentrate on the reaction rates $I_{\rightarrow}^{(0)}$ without electrostatic forces. It seems appropriate at this stage to leave the spheroidal coordinates and introduce the major and minor half axes A and B of the basic ellipses. This yields

$$I_{\rightarrow}^{(0)} = 4\pi D_3 A n_\infty g(B/A), \quad (20)$$

where $g(B/A)$ is a geometrical factor being

$$g(x) = \frac{2\sqrt{1-x^2}}{\ln[(1+\sqrt{1-x^2})/(1-\sqrt{1-x^2})]} =: g_{PR}(x) \quad (21)$$

for prolate and

$$g(x) = \frac{\sqrt{1-x^2}}{\pi/2 - \arctan(x/\sqrt{1-x^2})} =: g_{OB}(x) \quad (22)$$

for oblate spheroids. In both cases, $g(x)$ tends to 1 for $x \to 1$ thus reproducing the well known results for spherically symmetrical particles [2, 7, 8]. The functions g_{PR} and g_{OB} are shown in fig. 2.

The actual physical situations we referred to in section 2 involved the limiting cases of a long cylinder and of a flat disc. We shall now give the explicit final results for these particular geometries. It is convenient to express the electrostatic influence in terms of Bjerrum's length b [14],

$$b = -q_D q_R / 4\pi\epsilon kT, \quad (23)$$

which is something like an effective range of the Coulomb forces at temperature T, positive or negative according to whether the forces are attracting or repelling.

The association rate for the repressor trapped by a DNA cylinder of length $2A$ and radius B is

$$k_{\rightarrow} = 4\pi D_3 \frac{-b}{\exp[-(b/A)\ln(2A/B)] - 1}. \quad (24)$$

In the case of very strong electrostatic effects,

$$|b| \gg \frac{A}{\ln(2A/B)}, \quad (25)$$

the geometric factors nearly cancel:

$$k_{\rightarrow} \approx 4\pi D_3 |b| \times \times \begin{cases} 1 & \text{(attraction)} \\ \exp[-(|b|/A)\ln(2A/B)] & \text{(repulsion).} \end{cases} \quad (26)$$

On the other hand, the geometry dominates if the electric forces are small:

$$k_{\rightarrow} \approx 4\pi D_3 \frac{A}{\ln(2A/B)} \left(1 + \frac{b}{2A} \ln \frac{2A}{B}\right). \quad (27)$$

It is interesting to note that a cigar-shaped ellipsoid is almost as efficient a sink as a sphere with diameter equal to the long axis; this is because the logarithm in eq. (27) does not alter the order of magnitude.

The sink associated with a membrane bound enzyme, in our model, is represented by one side of an oblate spheroid. At first sight, a complication arises due to the fact that the presence of the rest of the membrane reduces the space available for the substrate's diffusion; we assume a plane membrane so that the remaining space is a half space. Now in accordance with our general picture there is equilibrium between the non sink part of the membrane and the substrate; the solution (13) is therefore not affected by the introduction of this membrane. The rate of association with one side of a membrane disc of radius A is thus

$$k_{\rightarrow} = 4\pi D_3 \frac{-b}{\exp(-\pi b/A) - 1}. \quad (28)$$

(If both sides of the membrane are involved in the enzyme–substrate association, then of course, this rate constant has to be doubled.)

In the limit of strong electrostatic effects we get

$$k_{\rightarrow} = 4\pi D_3 |b| \times \begin{cases} 1 & \text{(attraction)} \\ \exp(-\pi|b|/A) & \text{(repulsion)} \end{cases} \quad (29)$$

whereas for dominating geometry

$$k_{\rightarrow} = 4\pi D_3 \frac{A}{\pi} \left(1 + \frac{\pi}{2} \frac{b}{A}\right). \quad (30)$$

As expected, the thickness of the spheroid does not play any role in the extreme case.

In conclusion of this theoretical section we should like to comment on the possibility of including Debye–Hückel screening into our formulae. Eqs. (14) and (15) are still valid; however, the potential U does no longer satisfy the simple eq. (16). Instead, a Poisson equation holds with a charge distribution outside the target spheroid which may be derived by application of Boltzmann's principle. The same arguments that lead to the famous Debye–Hückel equation in the case of spherical geometry [15] give the following equation for U if spheroidal symmetry is assumed:

$$\frac{\partial}{\partial\xi}[\xi^2 \overline{(+)}1] \frac{\partial U}{\partial\xi} = (\tfrac{1}{2}a\kappa)^2 [\xi^2 \overline{(+)}\tfrac{1}{3}] U. \qquad (31)$$

κ is the conventional reciprocal Debye–Hückel length,

$$\kappa^2 = \sum_i n_i q_i^2/\epsilon kT. \qquad (32)$$

The solution of eq. (31) is not generally obtainable in terms of elementary functions as in the case of spherical symmetry [15]. Only in some limiting zones can we give an analytic expression. Thus, with $\xi \to \infty$, $\frac{1}{2}a\xi = r$ we effectively restore spherical geometry to get the classical result $U \propto e^{-\kappa r}/r$. In the neighborhood of a long cylinder, $\xi \approx 1$, $\xi - 1 \approx 2r^2/a^2$, $\kappa r \ll 1$, we get

$$U \propto -iH_0^{(1)}(i\sqrt{\tfrac{2}{3}}\,\kappa r) = (2/\pi)(\ln \kappa r/1.375 + \ldots) \qquad (33)$$

where $H_0^{(1)}$ is a Hankel function; it is reasonable that the cylinder's length a does not appear to a first approximation.

Unfortunately, since eq. (31) cannot be integrated on the whole range $\xi_0 \leqslant \xi < \infty$ we are not able to perform the integration in eq. (14). Therefore the effect of Debye–Hückel screening, at this stage, can only qualitatively be discussed.

4. Comparison with experiments

In the preceding section we presented a theoretical treatment of diffusion controlled association and dissociation of electrically charged macromolecules in spheroidal geometry – thereby filling a gap that was mentioned by Riggs et al. [1]. In section 2, on the other hand, we estimated the effective size of the "molecules" to be considered here so that we are now in the position to give a quantitative description of the repressor–operator association in terms of our model.

Unfortunately, we are not aware of any measurement of D_1; k_{diss} was estimated by Rigler [16], on the basis of T-jump relaxation data, to be $\sim 5\ s^{-1}$ for ionic strength $I = 0.14$ and calf thymus DNA. From the very marked dependence of the unspecific dissociation constant $K_{RD} = k_{diss}/k_{ass}$ on ionic strength [5] one may infer a value $k_{diss} \sim 0.1\ s^{-1}$ for the low ionic strengths of Riggs et al. [1]. Therefore, with $D_1 \lesssim 10^{-7}\ cm^2 s^{-1}$ we expect $A \lesssim 10^{-3}$ cm. It seems, however, reasonable to assume a markedly reduced mobility for the unspecifically bound repressor, and a diffusion constant as low as $D \approx 10^{-11}\ cm^2 s^{-1}$ would leave us with $A \approx 10^{-5}$ cm which is still a very appreciable extension of the operator sink. Actually, one need not be too pessimistic with respect to D_1; if the unspecific binding between repressor and DNA is mainly due to electrostatic attraction, diffusion along the chain is expected to be much less hindered than it is in a perpendicular direction. This has been shown for the diffusion of alkali ions along DNA and polyphosphate strands [17]. For the present discussion, however, as long as there are no better data on either D_1 or k_{diss} we must use D_1/k_{diss} as an adjustable parameter.

As a first approach, let us neglect electrostatic effects. Then eq. (26) gives

$$k_{\rightarrow} = 8\sqrt{\pi}D_3 \frac{\sqrt{D_1/k_{diss}}}{\ln(4\sqrt{D_1/k_{diss}}/\sqrt{\pi}B)}. \qquad (34)$$

Using $D_3 \approx 5 \times 10^{-7}\ cm^2 s^{-1}$ and $B \approx 10^{-7}$ cm we get $(2/\sqrt{\pi})\sqrt{D_1/k_{diss}} = 10^{-5}$ cm = 1000 Å from the experimental value of $k_{\rightarrow} = 7 \times 10^9\ M^{-1}\ s^{-1}$ [1]. This is a very reasonable length, well consistent with our estimate. The effective trap for the repressor would thus have a length which extends the actual binding site by a factor of about 20. The surprisingly high association rate is therefore basically understood without even taking into account electrostatic forces.

We must, however, comment on their effect as well. First, let us critisize the arguments of Riggs et al. [1]. Within the framework of their picture, taking $q_D q_R \approx -10$ as determined from the dependence on ionic strength, the Bjerrum length would be about 70 Å. Consequently, the highest possible association rate, with no ions present for shielding, would be given by eq. (28):

$k_- \approx 2.6 \times 10^9\ M^{-1}\ s^{-1}$. The experimental values at low ionic strength, instead, definitely exceed $10^{10}\ M^{-1}s^{-1}$ and seem to approach $10^{11}\ M^{-1}s^{-1}$ at vanishing ion concentration. Actually, the ionic strengths chosen were relatively high [1], $1/\kappa$ being always less than ~ 30 Å. Bjerrum's length should therefore effectively be replaced by Debye–Hückel's which makes the expectation for k_- even lower. In conclusion, our quantitative analysis reveals that electrostatic attraction by a small operator binding site cannot be the essential rate enhancing mechanism.

On the other hand, we can readily account for the marked dependence of the association rate on ionic strength on the basis of our model. First of all, let us recall the general experience – whenever electrostatic attraction plays a role – that dissociation rates are much more sensitive to changes of ionic strength than recombination rates. Qualitatively, this may be seen from eqs. (15) and (18), with the effective potential being reduced by increasing ionic strength. Therefore, the observed strong decrease of k_- with growing ion concentration is as unusual as its high absolute value. Now, according to our theory k_- is intimately connected with the (unspecific) dissociation constant k_{diss}; this yields a very natural explanation for the electrostatic effects because k_{diss} is expected to be strongly dependent on the ionic strength. Indeed, Lin and Riggs [5] have shown that the dissociation constant K_{RD} for unspecific binding rises by a factor 400 within the range $0.03 \leqslant I \leqslant 0.20$ of ionic strength. A minor part of this is certainly due to a decrease in the association rate because of shielding, but undoubtedly the overwhelming contribution stems from an enhancement in k_{diss}, a factor 100 being a reasonable guess. As a consequence, the effective length $\sqrt{D_1/k_{diss}}$ of the repressor trap would shrink by a factor 1/10. The actual decrease in k_- according to Riggs et al. [1] is 1/40 over this range, the remaining 1/4 again being ascribable to a reduced association due to screening. We cannot hope to give any more rigorous account of this screening because even in the case of spherical symmetry only the case $b \ll 1/\kappa$ could be dealt with adequately [11]. The estimates show, however, that our picture gives a very satisfactory explanation to all the quantitative aspects of repressor–operator binding some of them being rather surprising at the first glance.

A crucial test for our view would be an investigation of the binding properties of fragmented operator DNA. As stated in section 2 the chain length l should be inserted for A in eq. (24) if $l \lesssim (2/\sqrt{\pi})\sqrt{D_1/k_{diss}}$. According to the results of the present discussion a marked decrease in the association rate is expected for fragments of molecular weight less than ~ 10^5 (at low ionic strength). The negative outcome of experiments with molecular weights ~ 10^6, mentioned by Riggs et al. [1] and put forward as an argument against this model does not affect it at all. Future work has to be awaited for; our analysis provides a basis for the quantitative aspects of its design.

5. Concluding remarks

The idea that reduction of dimensionality in diffusion processes may enhance reaction rates [12] has been combined with von Smoluchowski-type calculations of recombination rates in spheroidal geometry. The results have been demonstrated to account for the unusual properties of the lac repressor–operator association, namely its high rate as well as its strong dependence on ionic strength. Clearly we only considered a somewhat idealized model and did not take into account, e.g., a possible folding of the DNA. It can be assumed, however, that this would not change the order of magnitude of the calculated reaction rates: on the one hand, at least at low ionic strength, the curvature of DNA strands should not be very pronounced because of electrostatic repulsion of the phosphate groups; on the other hand, the repressor's diffusion along the chain should not be affected by a slight bending. A little reduction of the association rate, with increasing ionic strength, might result from the effective shortening of the operator sink due to DNA folding.

The aim of our paper was not, in the first place, to describe the in vivo situation of the repressor–operator interaction but rather to explain the findings of the in vitro studies of Riggs et al. [1]. Nevertheless, it is reasonable to assume that similar rate enhancing mechanisms play an important role in vivo. In particular, this should be true for the case of membrane bound enzymes, ribosomes, or mitochondria. Whenever there exists an unspecific affinity of the membrane for the respective substrate molecules, a rate enhancement may be expected due to diffusion on that membrane. This would complement the idea put forward by Goldman and Katchalski [18] that consecutive reactions might be

accelerated by fixing the corresponding enzymes to the same membrane. According to our picture, a single enzyme mediated reaction could already be speeded up by embedding the enzyme into a membrane. The fundamental difference between our arguments and those of Goldman and Katchalski is that we look for a possible enhancement of the basic association rates whereas they consider them as given. Both aspects should be combined to explain the high advantage obtained by embedding enzymes into membranes.

Our suggestions allow for a straight forward experimental test: a decrease in the association rate should be observed with DNA (membrane) fragments smaller than the effective range of the operator (enzyme).

Appendix: Spheroidal coordinates

Since the notation is not unique throughout the standard textbooks we have to present the definitions adopted in this paper.

(i) *Prolate spheroidal coordinates* [19]. An ellipse with foci located at $x = y = 0$, $z = \pm\frac{1}{2}a$ is rotated about the z axis. Let x, y, z be any point on the resulting prolate spheroid,

$$r_{1,2} = \sqrt{(z \pm \tfrac{1}{2}a)^2 + x^2 + y^2}$$

its distances to the two foci. Then $\xi = (r_1 + r_2)/a$ is a constant along the spheroid, its possible values being $1 \leqslant \xi < \infty$. $\xi = 1$ characterizes the line connecting the foci, $\xi \to \infty$ describes spheroids with approximately spherical shape. The second spheroidal coordinate, $\eta = (r_1 - r_2)/a$, $-1 \leqslant \eta \leqslant 1$, each characterizes one sheet of a hyperboloid of revolution, $\eta = \pm 1$ being the z axis in the range $z > \frac{1}{2}a$, $z < -\frac{1}{2}a$ respectively, $\eta = 0$ the x, y plane. The third coordinate, $\varphi = \arctan y/x$, $0 \leqslant \varphi < 2\pi$, is the angle of rotation about the z axis.

The major half axis is $A = \frac{1}{2}a\xi$, the minor half axis $B = \frac{1}{2}a\sqrt{\xi^2 - 1}$. The surface element on a spheroid $\xi =$ const. is

$$|\mathrm{d}^2 r| = (\tfrac{1}{2}a)^2\sqrt{(\xi^2 - 1)(\xi^2 - \eta^2)}\,\mathrm{d}\eta\,\mathrm{d}\varphi$$

the volume element

$$\mathrm{d}^3 r = (\tfrac{1}{2}a)^3(\xi^2 - \eta^2)\mathrm{d}\xi\,\mathrm{d}\eta\,\mathrm{d}\varphi.$$

The ξ-component of the gradient is

$$(\nabla\psi)_\xi = \frac{2}{a}\sqrt{\frac{\xi^2 - 1}{\xi^2 - \eta^2}}\,\frac{\partial\psi}{\partial\xi}.$$

The Laplacian of a function ψ which only depends on ξ is the following:

$$\nabla^2\psi(\xi) = \frac{\psi}{a^2(\xi^2 - \eta^2)}\,\frac{\partial}{\partial\xi}(\xi^2 - 1)\,\frac{\partial\psi}{\partial\xi}.$$

Note that this depends on η via the metric coefficients.

(ii) *Oblate spheroidal coordinates.* This time we deviate from Morse and Feshbach [19] in that we continue to let the interfocal distance be a (and not $2a$). The axis of rotation is again chosen to be the z axis, but here it coincides with the minor axis of the generating ellipse. The foci thus form a circle of radius $\frac{1}{2}a$ in the x, y plane. The spheroidal coordinates ξ, η, φ have similar though not exactly equal geometric interpretation. Their ranges are $0 \leqslant \xi < \infty$, $-1 \leqslant \eta \leqslant 1$, $0 \leqslant \varphi < 2\pi$. The major half axis is $A = \frac{1}{2}a\sqrt{\xi^2 + 1}$, the minor half axis $B = \frac{1}{2}a\xi$.

All the other formulae we need may be obtained from those for prolate spheroids by making the following changes:

$$\xi^2 - 1 \to \xi^2 + 1,\ \xi^2 - \eta^2 \to \xi^2 + \eta^2.$$

References

[1] A.D. Riggs, S. Bourgeois and M. Cohn, J. Mol. Biol. 53 (1970) 401.
[2] M. von Smoluchowski, Physik. Z. 17 (1916) 557, 585; Z. Physik. Chem. 92 (1917) 129.
[3] S.Lin and A.D. Riggs, Nature 228 (1970) 1184.
[4] S. Lin and A.D. Riggs, Biochem. Biophys. Res. Commun. 45 (1971) 1542.
[5] S. Lin and A.D. Riggs, J. Mol. Biol. 72 (1972) 671.
[6] A.D. Riggs, S.Lin and R.D. Wells, Proc. Natl. Acad. Sci. USA 69 (1972) 761.
[7] P. Debye, Trans. Electrochem. Soc. 82 (1942) 265.
[8] M. Eigen, Z. Phys. Chem. N.F. 1 (1954) 176.
[9] R.A. Alberty and G.G. Hammes, J. Phys. Chem. 62 (1958) 154; 63 (1959) 274.
[10] K.S. Schmitz and J.M. Schurr, J. Phys. Chem. 76 (1972) 534.
[11] M. Eigen, W. Kruse, G. Maass and L. de Maeyer, Progr. Reaction Kin. 2 (1964) 286.
[12] G. Adam and M. Delbrück, in: Structural chemistry and molecular biology, eds. A. Rich and N. Davidson (Freeman, San Francisco, 1968).

[13] L.D. Landau and E.M. Lifshitz, Fluid mechanics (Pergamon Press, Oxford, 1959) ch. VI.
[14] N. Bjerrum, Kgl. Danske Videnskab. Selskab. Mat. Fys. Medd. 9 (1926) 7.
[15] P. Debye and E. Hückel, Physik. Z. 24 (1923) 185.
[16] R. Rigler, private communication.
[17] M. Eigen and G. Schwarz, in: Electrolytes, ed. B. Pesce (Pergamon Press, Oxford, 1962).
[18] R. Goldman and E. Katchalski, J. Theor. Biol. 32 (1971) 243.
[19] P.M. Morse and H. Feshbach, Methods of theoretical physics II (Mc Graw-Hill, New York, 1953) ch. 10.3.

BIOPHYSICAL CHEMISTRY 2 (1974) 264–268. © NORTH-HOLLAND PUBLISHING COMPANY

THE DISSOCIATION-RATE DEPENDENT ELECTROCHEMICAL REDUCTION OF VALINOMYCIN COMPLEXES OF MONOVALENT IONS

M. BŘEZINA, A. HOFMANOVÁ-MATĚJKOVÁ and J. KORYTA
J. Heyrovský Institute of Physical Chemistry and Electrochemistry, Czechoslovak Academy of Sciences, Opletalova 25, 110 00 Prague, Czechoslovakia

Received 14 November 1973
Revised manuscript received 1 February 1974

The polarographic reduction of valinomycin complexes of alkali metal and thallium (I) ions takes place via dissociation of the complex while the free metal ions are reduced. The stability constants determined from the half-wave potentials and the dissociation-rate constants determined from the polarographic limiting currents show a distinct ion-specificity. The values for the thallium (I) complex lie outside the sequence based on crystallographic ionic radii.

1. Introduction

Valinomycin [1] is a typical example of macrocyclic ion carriers which uncouple oxidative phosphorylation in mitochondria [2, 3], enabling the alkali metal cations to penetrate their membranes, increase the conductivity of artificial lipid bilayer membranes [4] and induce bi-ionic potentials at these membranes [5]. All these effects have an ion-specific character. The ion specificity is due to varying stability of alkali-metal ion complexes of the carriers [6–8]. The ion-specific rate of complex formation may also play a role in the process of alkali-metal ion transport through the membranes [9].

Of the complexes of macrocyclic ion-carriers, the monovalent-ion complexes of cyclic polyethers ('crowns') and the ammonium complex of nonactin are the only ones whose polarographic reduction has so far been reported [10,11]. With the exception of the ammonium complex the 'crown' complexes give reversible polarographic waves from the half-wave potentials of which stability constants can be determined. The electroreduction of valinomycin complexes of alkali metal and thallium (I) ions in acetonitrile is reported in this paper. During the reduction the limiting currents are controlled by the dissociation rates of the complexes thus enabling both the dissociation-rate and the stability constants of these complexes to be determined. Kinetics of complexation of alkali metal ions by valinomycin have also been studied by Funck et al. using ultrasonic absorption [12] in methanolic medium. Because of difficulties encountered in polarographic work with methanol (see section 2) acetonitrile was used as electrolyte solvent in our experiments.

2. Materials and methods

The polarographic method is suitable for determination of the stability constants of metal ion complexes provided that the activities of metal ions and of metal dissolved in the amalgam obey the Nernst equation, during reduction of the complex at the dropping mercury electrode (see refs. [13] pp. 211–234, and [14] pp. 147–152). If the equilibrium between the free and the complexed metal ions, which is disturbed by reduction of the free metal ions, cannot be re-established during the drop-life of the electrode, so-called kinetic limiting currents are observed, which are controlled by the rate of dissociation of the complex [15].

The polarograms were recorded on a Model OH-102 Polarograph (Radelkis, Budapest, Hungary) using a three-electrode system. The usual mercury dropping electrode was used as a test electrode, an Ag/AgCl elec-

Table 1
Limiting currents and half-wave potentials

Metal ion	Valinomycin conc. (mM)	I_k/I_d [a]	$\Delta E_{1/2}$ [b] (mV)	Drop-time (s)
K^+	0.23[c]	0.396	111	1.5
	0.63	0.233	141	1.41
	0.96	0.19	163	1.39
Rb^+	0.22[c]	0.43	123	1.6
	0.60	0.224	151	1.5
Cs^+	0.43	0.807	120	1.71
	0.60	0.755	137	1.6
Tl^+	0.22[c]	0.853	103	2.4
	0.60	0.698	131	1.6

a) Ratio of the limiting current in the presence of valinomycin (I_k) to the computed limiting diffusion current of the complex (I_d).
b) Difference in the half-wave potentials of the free metal ions and of the complexes.
c) Data not used for calculation of k_{32} or K_{MV} since condition (ii) is not fulfilled.

trode in sat. M tetramethylammonium chloride as a reference and a platinum wire as a counterelectrode. Since alkali metal ions are reduced at rather negative potentials, extremely pure solvents are required (since most trace impurities would be reduced before the alkali metals). Acetonitrile from LOBA-Chemie (Vienna, Austria) 'Austranal' was used after purification by azeotropic distillation with ethanol. Unfortunately high purity methanol (e.g., Merck Uvasol) has not so far proven suitable for polarographic experiments even after careful purification. Tetrabutylammonium perchlorate, made in this Institute, was used at a concentration of 25 mM as a base electrolyte. The alkali metal ion concentration was 0.2 mM. Solutions were de-aerated with pure argon.

3. Results and discussion

On addition of valinomycin to potassium, rubidium, cesium or thallium (I) ion solutions in acetonitrile the limiting polarographic currents of these ions decreased strongly while the half-wave potentials shifted to more negative values (see table 1). The decrease in limiting currents was considerably larger than would correspond to the decrease of the diffusion coefficient of the ion caused by complexation. At higher valinomycin concentrations the limiting current was almost independent of the hydrostatic pressure of the mercury column indicating that it was controlled by chemical reaction rather than by diffusion alone (see [14] p. 345).

In the case of valinomycin–alkali metal ion complexes it is impossible that the complex would be reduced by an electron transfer to the ion inside of the macrocyclic cavity since – besides other reasons – the resulting zero-valent species would immediately reduce the ligand itself thus regenerating metal ion which is again reducible. Hence dissociation of the complex with subsequent reduction of the free metal ion is the only possible explanation of the experimental facts.

Assuming the establishment of a steady state between diffusion and the chemical reactions in the neighbourhood of the electrode [16,17], the transport process to the electrode is described by the differential equation

$$D_M(d^2c_M/dx^2) + k_b(c_{MV} - K_{MV}\,c_V\,c_M) = 0, \qquad (1)$$

where c_M, c_V and c_{MV} are the concentrations of free metal ions, of valinomycin and of complexed metal ions, respectively, D_M is the diffusion coefficient of the free metal ion, k_b is the dissociation rate constant and K_{MV} is the stability constant of the complex and x is the distance from the surface of the electrode. It is assumed that the metal ion-to-valinomycin ratio in the complex is 1:1 [18,19,20].

Funck et al. [12] assumed that the formation of the valinomycin–metal ion complex is a two step process with an associate between valinomycin and the partially desolvated cation $V.M^+(solv.)$ as an intermediate

$$V + M^+(solv.) \underset{k_{21}}{\overset{k_{12}}{\rightleftharpoons}} V.M^+(solv.) \underset{k_{32}}{\overset{k_{23}}{\rightleftharpoons}} VM^+. \qquad (2)$$

The formation of this intermediate is probably a very fast reaction the rate-determining step being a ligand conformation change which occurs during the stepwise substitution of solvent molecules from the cation [12]. Under these conditions $k_{21} \gg k_{23}$ and

$$k_b = \frac{k_{21}\,k_{32}}{k_{21} + k_{23}} \approx k_{32}. \qquad (3)$$

The quantities c_{MV} and c_V in eq. (1) can be considered constant under the following conditions:

(i) The average kinetic limiting current I_k is sufficiently smaller than the average diffusion current of the complex I_d computed by means of the Ilkovič equation (see e.g. [13] p. 34, or [14] p. 82) assuming that the diffusion coefficient of all complexes $D_{MV} = 5.9 \times 10^{-6}$ cm^{2}s^{-1}. This value is based on the assumed value of the Stokes radius of the potassium complex 8.5 Å estimated from the dimensions of the cylindrical K^+-complex with a height of 12 Å and base radius of 7.5 Å [20].

(ii) Valinomycin is present in sufficient excess; practically at least $c_V \geq 4\,(I_k/I_d)c_{MV}$ if most of the metal cations are bound in the complex. Then the solution of the above differential equation for the boundary condition of the limiting current

$$x = 0, \qquad c_M = 0 \tag{4}$$

gives the expression for the limiting current density ([15] p. 298),

$$j_k = F D_M (\mathrm{d}c_M/\mathrm{d}x)_{x=0} = F c_{MV} (k_b D_M / K_{MV} c_V)^{1/2}, \tag{5}$$

where F is the Faraday constant.

The average kinetic current is then given by the expression

$$I_k = j_k \bar{A}, \tag{6}$$

where $\bar{A}$ is the average area of the dropping electrode

$$\bar{A} = 0.51\, m^{2/3}\, t_1^{2/3}. \tag{7}$$

Here m is the flow rate of mercury in g s^{-1} and t_1 the drop-time.

If condition (i) does not hold, then a correction must be made for the diffusion of the complex, which is expressed by the equation ([15] p. 299),

$$\frac{I_k}{I_d - I_k} = 0.886 \left(\frac{k_b t_1}{K_{MV} c_V} \frac{D_M}{D_{MV}} \right)^{1/2}. \tag{8}$$

The stability constant K_{MV}, which is necessary for the evaluation of the rate constant k_b, has been determined from the difference $E_{1/2}$ between the half-wave potentials for the free metal ion and the half-wave potential for the complex [21]

$$E_{1/2} = (RT/F) \ln (K_{MV} c_V) + (RT/F) \ln (I_k/I_d). \tag{9}$$

In fig. 1 the values of the dissociation rate constants $k_b = k_{32}$ are compared with values of Funck et al. [12] measured in methanol. Fig. 2 shows the values of the

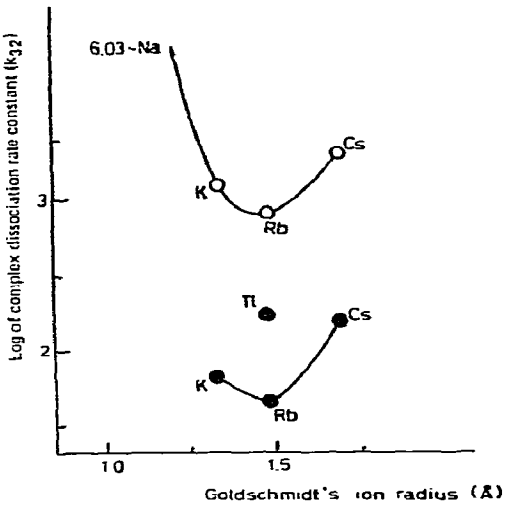


Fig. 1. (●) Values of the present paper – acetonitrile. (○) Values of Funck et al. [12] – methanol.

stability constants for acetonitrile. Sodium ions form a weak complex with valinomycin so that neither a kinetic current nor a shift of the half-wave potential was observed. However it was possible to determine the stability constant of the sodium complex K_{NaV} from the shift of the half-wave potential of the Tl (I)-

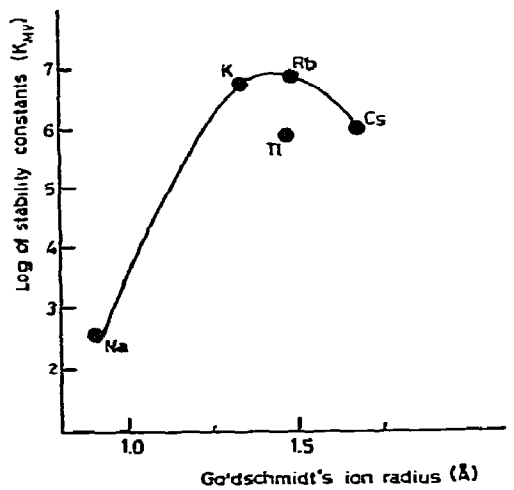


Fig. 2. Stability constants of monovalent ion complexes of valinomycin in acetonitrile.

complex wave at a large excess of sodium ions where most of the valinomycin (except that complexed with thallium) was bound in the sodium complex. Under these conditions, the concentration of free valinomycin is given by equation

$$c_V = (\bar{c}_V - \bar{c}_{Tl})/(\bar{c}_{Na} - \bar{c}_V + \bar{c}_{Tl})K_{NaV} , \quad (10)$$

where $\bar{c}_V$, $\bar{c}_{Tl}$ and $\bar{c}_{Na}$ are the overall concentrations of valinomycin, thallium and sodium, respectively. Inserting eq. (10) into eq. (9) results in the equation for the difference between the half-wave potential of the free Tl (I) wave and of the Tl (I)-complex in the presence of excess Na^+ (in the present experiments between 3 and 15 mM),

$$\Delta E_{1/2} = (RT/F) \ln [(K_{MV}/K_{NaV})(\bar{c}_V - \bar{c}_{Tl}) / (\bar{c}_{Na} - \bar{c}_V + \bar{c}_{Tl})] + (RT/F) \ln (I_k/I_d). \quad (11)$$

The rate as well as the stability constants show an analogous ion specificity in both acetonitrile and methanol. Since both these solvents have almost equal dielectric constants, the difference in the formation rate as well as stability cannot be explained by a Born-type effect. The Gibbs free energies of solvation of the free alkali metal cations seems not to be much different in methanol and acetonitrile [22]. Thus larger stability of the complexes in acetonitrile is most probably caused by their stronger solvation in acetonitrile in comparison with methanol.

If the intermediate $V.M^+$ (solv.) is solvated in the similar way in acetonitrile and in methanol we can expect that the difference between the complex formation in methanol and acetonitrile is mainly connected with the second step of (2) where the stronger solvation of the complex in acetonitrile is the cause of the decrease of the complex dissociation rate.

The Tl (I)-ion, which has a non-'noble-gas' structure, obviously lies out of sequence of both the reaction-rate and the stability constants as functions of ion radius for both methanol [12] and acetonitrile. This anomalous behaviour can be explained by the nature of its interaction with solvent molecules and with the macrocyclic ligand. This interaction is not fully electrostatic as in the case of alkali metal ions but the overlapping of electron clouds of the cation and of the binding groups of these molecules also takes place (cf. [23]). Obviously, this interaction of Tl^+ is stronger with the solvent molecules than with valinomycin. The overall result is a comparatively weaker complex with a higher dissociation rate.

Acknowledgement

We are indebted to Professor Yu.A. Ovchinnikov for the gift of valinomycin.

References

[1] H. Brockmann and G. Schmidt-Kastner, Chem. Ber. 88 (1955) 57.
[2] H.A. Lardy, D. Johnson and W.C. McMurray, Arch. Biochem. Biophys. 84 (1958) 587.
[3] M. Höfer and B.C. Pressman, Biochem. 5 (1966) 3919.
[4] A.A. Lev and E.P. Buzhinskii, Tsitologiya 9 (1967) 106.
[5] P. Mueller and D.O. Rudin, Biochem. Biophys. Res. Commun. 26 (1967) 398.
[6] D.C. Tosteson, D.C. Cook, T.E. Andreoli and M. Tiefenberg, J. Gen. Physiol. 50 (1967) 2513.
[7] G. Szabo, G. Eisenman and S. Ciani, J. Membrane Biol. 1 (1969) 346.
[8] M.M. Shemyakin, Yu.A. Ovchinnikov, V.T. Ivanov, V.K. Antonov, E.J. Vinogradova, A.M. Shkrob, G.G. Malenkov, A.V. Yevstratov, I.A. Laine, J.I. Melnik and I.D. Ryabova, J. Membrane Biol. 1 (1969) 402.
[9] P. Läuger, Science 178 (1972) 24.
[10] J. Koryta and M.L. Mittal, J. Electroanal. Chem. 36 (1972) App. 14.
[11] K. Angelis, M. Březina and J. Koryta, J. Electroanal. Chem. 45 (1973) 504.
[12] T. Funck, F. Eggers and E. Grell, Chimia 26 (1972) 637.
[13] I.M. Kolthoff and J.J. Lingane, Polarography (Interscience, New York, 1952).
[14] J. Heyrovský and J. Kůta, Principles of polarography (Academic Press, New York, 1965).
[15] J. Koryta, in: Advances in electrochemistry and electrochemical engineering, eds. P. Delahay and C.W. Tobias Vol. 6 (Interscience, New York, 1967) Chap. 3.
[16] K. Wiesner, Chem. Listy 41 (1947) 6.
[17] J. Koutecký and R. Brdička, Coll. Czech. Chem. Commun. 12 (1947) 337.
[18] B.C. Pressman, E.J. Harris, W.S. Jagger and J.H. Johnson, Proc. Nat. Acad. Sci. USA 58 (1967) 1949.
[19] M.M. Shemyakin, Yu.A. Ovchinnikov, V.T. Ivanov, V.K. Antonov, A.M. Shkrob, I.I. Mikhaleva, A.V. Yevstratov and G.G. Malenkov, Biochem. Biophys. Res. Commun. 29 (1967) 834.
[20] M. Pinkerton, L.K. Steinrauf and P. Dawkins, Biochem. Biophys. Res. Commun. 35 (1969) 512.
[21] J. Koryta, in: Progress in polarography, Vol. 1, eds. P. Zuman and I.M. Kolthoff (Interscience, New York, 1962) pp. 292–293.

[22] B. Case and R. Parsons, Trans. Faraday Soc. 63 (1967) 1224.

[23] G. Eisenman and S.J. Krasne, in: MTP International Review of Science, Biochemistry Series, Vol. 2, ed. C.F. Fox (Butterworths, London, 1973).

BIOPHYSICAL CHEMISTRY 2 (1974) 269–272 © NORTH-HOLLAND PUBLISHING COMPANY

EFFECT OF POLYELECTROLYTES ON THE KINETICS OF IONIC REACTIONS. III. HYDROLYSIS OF PYROPHOSPHATE IN POLY-(ETHYLENEIMINE) SOLUTIONS

D. TURYN, E. BAUMGARTNER‡ and R. FERNÁNDEZ-PRINI
Departamento de Fisicoquímica, Facultad de Farmacia y Bioquímica, Universidad de Buenos Aires, Junín 956, Buenos Aires, Argentina

Received 19 November 1973

The effect of the weak polyelectrolyte poly-(ethyleneimine) on the rate of hydrolysis of pyrophosphate has been studied as a function of pH at 70°C. Inhibition by the macroions was observed at pH ≥ 2, the inhibition becomes stronger as pH increases. At pH > 7 the hydrolysis in the presence of polyions becomes undetectable. Addition of NaCl to the solutions reduces the inhibitory effect of the polyelectrolyte.

Electrostatic interactions between macroions and substrate ions cause the observed inhibition, therefore this is another manifestation of the polyelectrolyte effect due to the large charge density on the polycations.

1. Introduction

In the course of the study of the effect of polyelectrolytes on the rate of ionic reactions, we have undertaken the study of the kinetics of pyrophosphate hydrolysis in the presence of polycations. The substrate was chosen because its study extends our current work on the decomposition of organic phosphate esters in polyelectrolyte solutions [1, 2]. Furthermore, there are evidences [3] that an excess of free amino groups in hardtissue collagen bears a relation to the process of crystallization of calcium phosphate. It seemed interesting to test the possible influence of the free amino groups of a macroion on the rate of pyrophosphate hydrolysis as one possible explanation of the observed behaviour, this can be assessed employing a relatively simple synthetic polycation like poly-(ethyleneimine) (PEI), which is a weak polyelectrolyte having free amino groups in basic solutions.

In spite of previous work [4–6] on the hydrolysis of pyrophosphate in water, its mechanism is not conclusively established. The fact that the substrate may exist in five different charged states, according to the pH of the solution, complicates very much the interpretation of the kinetic data. In polyelectrolyte solutions the system is even more complicated and it is not possible at present to offer a quantitative and detailed description of the effect of PEI upon the hydrolysis of pyrophosphate. It was observed that PEI inhibits the hydrolysis of the substrate, which becomes undetectable above pH 7. In the absence of macroions the hydrolysis is not observed to occur at pH > 10 (70°C). Added NaCl reduces the magnitude of the observed polyelectrolyte effect.

In more alkaline solutions (pH > 8.5) a different reaction between substrate and PEI seems to occur.

2. Experimental

The methods usually employed to determine phosphate in the presence of pyrophosphate were found to fail in solutions containing polyelectrolytes. A modification of the method described by Wirth [7] for the determination of small amounts of pyrophosphate in the presence of orthophosphate (up to a hundred times more PO_4^{3-} than $P_2O_7^{4-}$) was adopted in this work.

The method is based on the fact that pyrophosphate complexes Fe(III) ions. Hence, if pyrophosphate ions are added to solutions containing Fe(III) and SCN^- ions, there will be competition between $P_2O_7^{4-}$ and SCN^- for the Fe(III) ions and the optical absorp-

‡ Career Investigator of the Consejo Nacional de Investigaciones Científicas y Técnicas (Rep. Argentina).

tion at 470 nm due to the ferric-thiocyanate complex decreases.

The concentrations of the reagents employed, were standardized to the following values. Solutions having no PEI: $[Fe(III)] = 3.6 \times 10^{-5}$ molar, $[SCN^-] = 0.13$ molar; solutions containing PEI: $[Fe(III)] = 5.3 \times 10^{-5}$ molar, $[SCN^-] = 0.052$ molar. In all cases the pH of the solutions was fixed to a value of 2 with HNO_3. Under these conditions the percentual optical transmission was found to vary linearly with the concentration of pyrophosphate in PEI solutions up to 3.8×10^{-5} molar.

Unfortunately, it was not possible to find suitable experimental conditions for the determination of pyrophosphate in solutions containing poly-(vinylbenzyltrimethylammonium chloride). Consequently the effect of this strong polycation could not be studied.

Mallinckrodt (A.R.) $Na_4P_2O_7.10\,H_2O$ was employed as the substrate, PEI was Polymine P (B.D.H.) having a molecular weight of 40000. In the kinetic runs the concentration of pyrophosphate was 1.88×10^{-3} molar and the concentration of PEI was 4.8×10^{-2} monomoles/ℓ (the molecular weight of PEI monomer was taken to be 59 g [2]).

The kinetic runs were carried out at 70°C (± 0.1°C) and the pH was fixed by adding the necessary amount of HCl to the PEI solutions [2] since the weak polyelectrolyte has buffer capacity. In the absence of PEI appropriate buffers were employed. The hydrolysis of pyrophosphate was followed by withdrawing aliquots at various times and keeping them in alkaline solutions having such a pH that no further decomposition of pyrophosphate was observed to occur within a month. The optical density of the aliquots corresponding to a given run were all measured within a period of one hour to reduce experimental error. The reactions followed up to three half-lives were strictly first-order in pyrophosphate.

The solutions corresponding to kinetic runs at pH > 8.5 became yellowish after a week. In these solutions the analytical method of pyrophosphate determination did not work. The optical absorption of the solutions at 400 nm was found to increase with pH until pH = 9.6 and to increase with PEI concentration. It may be suspected that this behaviour involves a reaction between the substrate and the free amino groups of PEI, because a 10 % of the primary amino groups of PEI appeared blocked according to the test with ninhydrine.

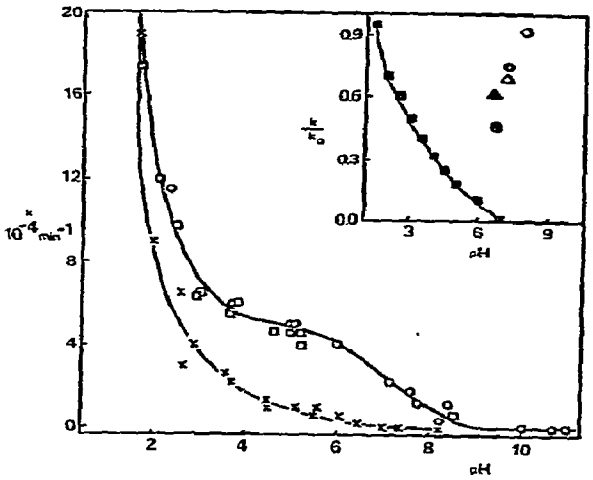


Fig. 1. Rate of hydrolysis of sodium pyrophosphate at 70°C in aqueous solutions of PEI (×), and in water: (○) present work, (□) results from ref. [5].

Insert: k/k_0 against pH at various NaCl concentrations. [NaCl] = 0.0 molar (■); 0.1 molar (●); 0.3 molar (▲); 0.5 molar (△); 0.7 molar (○); and 1.0 molar (○). The limit of precision of the measured rate constants is approximately 5×10^{-6} min^{-1}.

Furthermore, dialysis indicated that approximately 5–6 % of PO_4^{3-} corresponding to complete hydrolysis of the substrate was retained by the polyion.

3. Results and discussion

Fig. 1 shows the pH profile of the first-order rate constant for the hydrolysis of pyrophosphate at 70°C in the absence and in the presence of PEI in the solutions. Some of the results obtained by Campbell and Kilpatrick [5] are also represented in this figure. They may be seen to agree in general with our results, considering their measurements were carried out at 69.4°C and in solutions having a different ionic strength.

Our results also confirm the observation of Campbell and Kilpatrick [5] that the rate of hydrolysis decreases more slowly with pH in the range 3 to 5. The data of Mitra et al. [6] also agree with this observation but their rate constants are significantly smaller than those plotted in fig. 1.

It is quite clear from the data in fig. 1 that PEI strongly inhibits the hydrolysis of pyrophosphate at

pH > 2. The insert in fig. 1 depicts the change in the ratio k/k_0 (k_0 = first-order rate constant without polyelectrolyte) with pH and reproduces the data of five runs carried out with PEI and various concentrations of NaCl.

The fact that NaCl reduces the effect of PEI indicates that electrostatic interactions between macroion and substrate cause the inhibition observed in the presence of PEI. In very acid solutions (pH < 2), k/k_0 is close to unity because at such pH the added HCl acts in the same way as NaCl, that is, it shields the charges on the macroion; furthermore, at these pH values pyrophosphate has a very small charge (between −1 and 0), reducing considerably the possibility of close electrostatic interaction between substrate and macroion. From pH > 2.0, k/k_0 decreases until pH 7, where the hydrolysis was undetectable even after seven days (the maximum value that k could have at that pH is 5×10^{-6} min^{-1}).

Previous work on the decomposition of *p*-nitrophenyl phosphate [1,2] in the presence of PEI showed that the free amino groups in the polyion acted at pH > 6 as nucleophilic reagents upon the substrate concentrated in its vicinity. This is apparently not the case in pyrophosphate solutions containing PEI up to pH 7; nucleophilic attack by the ionogenic groups of the polyelectrolyte would increase the rate of pyrophosphate decomposition, this was not observed when pH ≤ 7. However, the yellow colour appearing at pH > 8.5 may be due to nucleophilic attack of the substrate by PEI as suggested above. Thus, it may be concluded that the effect of polycations with free amino groups upon the hydrolysis of pyrophosphate does not explain the crystallization of calcium phosphate in hard-tissue collagen at least in solutions having a pH around 7.

The mechanisms usually proposed [4–6] to explain the hydrolysis of pyrophosphate in water are bimolecular attacks on $H_{4-i}P_2O_7^{-i}$ ($i = 0, 1, 2, 3, 4$) by H_3O^+ and by water. It is very difficult to distinguish between them because as the pH changes the fraction of the various $H_{4-i}P_2O_7^{-i}$ species also changes. Consequently both reaction mechanisms will show a pH dependent first-order rate constant. We do not consider that it has been proved so far that one of these bimolecular mechanisms does not contribute to the hydrolysis of the substrate. The possible contribution to the observed rate of hydrolysis of a truly unimolecular mechanism similar to that operating in the hydrolysis of organic phosphate esters [8] cannot be completely ruled out on the same grounds.

The observed reduction of the rate of hydrolysis of pyrophosphate by PEI may be qualitatively explained taking account of the electrostatic interactions between macroions and mobile ions. The H_3O^+ ions will be repelled from the neighbourhood of the chain. This microscopic heterogeneity affects the apparent dissociation constants of the successive $H_{4-i}P_2O_7^{-i}$ acids, this type of effect has been observed with organic acids in polyelectrolyte solutions [9]. Thus, at any measured pH value, the equilibrium concentration of the more basic $H_{4-i}P_2O_7^{-i}$ species will increase near the chain of PEI, while the more acidic species will have a smaller concentration in those regions. Since according to fig. 1 in the absence of polyions the more basic species are less reactive, the presence of PEI will appear to inhibit the hydrolysis of pyrophosphate.

According to the idea of counterion condensation of the polyions postulated by Manning [10], the species having $i = 1$ will compete with the Cl^- counterions for positions close to the charged chain (in fact at finite concentrations there will be a continous distribution of counterions). When $i \geq 2$, multicharged substrate species will condense on the macroion preferentially to Cl^- counterions, and the effect of PEI would reach a maximum.

It would have been interesting to extend our observations to solutions of a strong cationic polyelectrolyte like poly-(vinylbenzyltrimethyl ammonium chloride) in which case there is no possibility of reaction between the substrate and free amino groups. The comparison of the pH-rate constant profiles for pyrophosphate in PEI solutions to that in strong polyelectrolyte solutions would have allowed us to verify whether the inhibition is of electrostatic nature. Unfortunately, this was not possible because the analytical method employed in PEI solutions is not applicable to solutions containing that polycation, as already mentioned.

Acknowledgement

The authors thank the Consejo Nacional de Investigaciones Científicas y Técnicas (Rep. Argentina) and the Universidad de Buenos Aires for financial support.

References

[1] R. Fernández-Prini and D. Turyn, Chem. Commun. (1972) 1013.
[2] R. Fernández-Prini and D. Turyn, J. Chem. Soc. Faraday I 69 (1973) 1326.
[3] C.C. Solomons and J.T. Irving, Biochem. J. 68 (1958) 499.
[4] J.P. Crowther and A.E.R. Westman, Canad. J. Chem. 32 (1954) 42;
J.D. McGilvery and J.P. Crowther, Canad. J. Chem. 32 (1954) 174.
[5] D.O. Campbell and M.L. Kilpatrick, J. Amer. Chem. Soc. 76 (1954) 893.
[6] R.P. Mitra, H.C. Malhotra and D.V.S. Jain, Trans. Faraday Soc. 62 (1966) 173.
[7] H.E. Wirth, Ind. Eng. Chem., Anal. Ed. 14 (1942) 722.
[8] A.J. Kirby and A.G. Varvoglis, J. Amer. Chem. Soc. 89 (1967) 415.
[9] E. Baumgartner, R. Fernández-Prini and D. Turyn, J. Chem. Soc. Faraday I 70 (1974) 1518.
[10] G.S. Manning, Ann. Rev. Phys. Chem. 23 (1972) 117.

BIOPHYSICAL CHEMISTRY 2 (1974) 273–277. © NORTH-HOLLAND PUBLISHING COMPANY

STUDY OF EXCITON INTERACTIONS IN SOME PYRIMIDINE DINUCLEOTIE IN AQUEOUS SOLUTION BY MEANS OF ABSORPTION SPECTROSCOPY

D.E. JOYCE and T. KURUCSEV
Department of Physical and Inorganic Chemistry,
The University of Adelaide, Adelaide, 5001 South Australia

Received 1 August 1974

The near ultraviolet absorption spectra of CpC, TpT and UpU in aqueous solution have been measured and pared with the corresponding spectra of C, T and U. The differences in shapes of the spectral envelopes betwee monomeric and dimeric species have been interpreted in terms of exciton coupling between the bases. The larg differences were observed for the pair CpC/C in neutral solution and these were analysed by the use of vibroni coupling theory. Parameters characteristic of the relative conformation of and the rate of energy transfer betw the bases in CpC were derived.

1. Introduction

Interactions between degenerate transition moments may affect the shape of absorption spectral envelopes [1]. Such exciton interactions may also induce optical activity provided that the arrangement of the coupled chromophores is non-enantiomorphic and non-racemic [2].

We have reported recently spectral studies on associating heterocyclic bases in aqueous solution [3, 4] where the differences between the spectra of the coupled and non-coupled species are small, although clearly discernible. Analysis of the spectral differences led to information, of possible biological relevance, concerning the resonance transfer of singlet electronic excitation between the molecules.

The work presented here is concerned with the nature and extent of exciton interactions in some pyrimidine dinucleotides in aqueous solution. We wish to compare our results, obtained by means of absorption spectroscopy, with conclusions reached from circular dichroism measurements in these systems [5–9]. Our purpose is primarily to provide an unequivocal test of the method and assumptions involved in the use of absorption spectroscopy as a tool in the study of exciton interactions which is applicable to both optically active and inactive systems.

2. Experimental

The following materials were purchased ma Chemical Co. and used without further tion: C, cytidine (lot 10C-1190); T, thymi 92C-2530); U, uridine (lot 12C-1210); Cp((3′-5′)cytidine (lot 12C-3090); TpT, thym (3′-5′)thymidine (lot 81C-7020) and UpU, (3′-5′)uridine (lot 53C-2790).

Solutions of U, UpU, T and TpT were p by dissolving appropriate quantities of con water; the solutions were of pH 5.2. Neutr (pH 6.9 at 20°C) of C and of CpC were pr the use of cacodylic acid–sodium cacodyl system [10], while their acidic solution of was obtained by the addition of perchloric the materials dissolved in water.

All spectra were measured at 20 ± 1°C PMQ II manual spectrophotometer. The st viation in transmittance of the instrument to be $\sigma_T = 0.13\%$ [11]. The absorbances, this work were all within the range $0.7 > A$ Accordingly, the relative standard deviatio absorbances was always less than 0.5% and dard deviation of the logarithmic differenc to be described later was $\sigma_{\Delta \log I} \leq 0.004$.

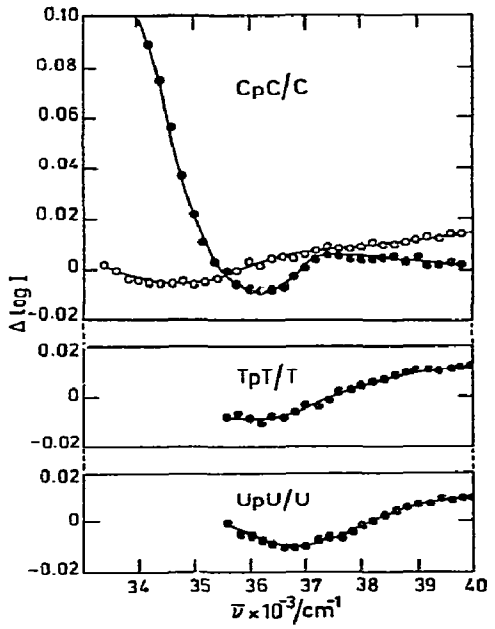


Fig. 1. Logarithmic difference spectra for the pairs CpC/C in neutral solution (filled circles), CpC/C in acidic solution (empty circles) and for TpT/T and UpU/U at pH 5.2.

3. Results

Previously published comparative near ultraviolet spectra of solutions of dinucleotides and of their monomeric analogues show up the major changes as differences in the intensities of the absorption envelopes, although shape changes in the spectra as a result of base–base interactions have been observed and attributed to exciton splitting [12–14].

Separation of the two effects of intensity and of shape differences between dinucleotide and nucleoside spectra has been achieved in this work by consideration of the ratios of corresponding intensities or, more appropriately, the logarithms of such ratios. In fig. 1 we show the logarithmic difference spectra of the three pairs of substances considered; the pair CpC/C has been studied both in neutral solution (filled circles) and in acidic solution (empty circles). In the figures shown the logarithmic difference at any wavenumber is defined as

$$\Delta \log I = \log I_{\mathrm{NpN}} - \log I_{\mathrm{N}},$$

where I_{NpN} and I_{N} stand for dinucleotide and nucleoside absorptivities, respectively, normalised to equal peak intensities.

4. Discussion

4.1. Qualitative interpretation of data

The logarithmic difference spectrum corresponding to a slight blue shift would be a monotonic, slowly increasing function of the wavenumber. Three of the curves shown in fig. 1, those for the pairs TpT/T, UpU/U and CpC/C in acidic solution approximate such a function. However, the deviations from monotonic increase indicate the existence of small differences between the shapes of the relevant spectra as well. In contrast to the above three curves, that showing the logarithmic difference spectrum of the CpC/C pair in neutral solution leaves no doubt as to the existence of significant shape differences between the spectral envelopes of CpC and C.

The results obtained corroborate the conclusions of previous circular dichroism studies concerning "stacking" interactions in dinucleotides. Thus it has been suggested that at 20°C in aqueous solution a small but finite fraction of the bases are stacked both in UpU [8] and in TpT [9]. This agrees with the weak exciton coupling reflected in the small but finite differences in shape observed between the dinucleotide and nucleoside spectra in these instances. Similarly, the very pronounced difference in the spectral properties of the CpC/C pair in acidic compared with neutral solution parallels the conclusion that the bases in neutral solution of CpC are stacked, while the extent of the stacking decreases drastically when the bases become charged [5–7].

Further quantitative discussion of the results will be restricted to CpC in neutral solution. In this system the degenerate exciton interactions between the cytosine moieties manifest themselves with sufficient magnitude to render the spectrum amenable to analysis by vibronic coupling theory.

4.2. CpC in neutral solution; preliminary considerations

Vibronic coupling theory, at its present stage of development [15–17] is subject to a number of restric-

tions. For the system considered here two of the most relevant are that analysis must be confined to a single non-degenerate transition of the monomer species and that the transition should correspond to a single vibronic progression.

Self consistent field molecular orbital calculations with configuration interaction have been carried out on cytosine recently by all-valence-electron [18] and by π-electron [19] methods. On the bases of such studies, the near ultraviolet absorption peak of cytosine may be assigned to a single in-plane (π^*, π) transition, centred near 35 000 cm^{-1}. Such an assignment is supported by the dichroic spectra of cytosine and cytidine in stretched poly(vinyl alcohol) films [20]. However, inspection of the dichroic spectra reveals the onset of an overlap of this transition with a higher energy transition near 38 000 cm^{-1}. This conclusion is also supported by fluorescence polarisation studies on cytidine-5'-monophosphate [14]. One may thus assert that the first restriction referred to above is satisfied by the CpC/C system provided that quantitative discussion is restricted to the wavenumber region preceding 38 000 cm^{-1}.

The significance and validity of the second assumption concerning the description of the absorption envelope in terms of a single vibronic progression has been discussed before [21–24]. The procedure [3, 25] consists of fitting the absorption envelope of the monomeric species to a vibronic progression characterised by five parameters:

(i) the position of the (0, 0) band $\bar{\nu}_{00}$,
(ii) the intensity of the (0, 0) band, I_{00},
(iii) a constant separation between successive bands, $\Delta\bar{\nu}$,
(iv) a constant gaussian bandwidth for each band, b_g, and
(v) the ratio of (1, 0) to (0, 0) band intensities, X.

The fitting of the experimental points to such a model may be performed by non-linear least squares methods and, in this way, "best values" and confidence limits for the five parameters may be obtained.

The fitting of the spectrum of cytidine, considered as the monomer species in this instance, to the model of a single vibronic progression was carried out in accordance with the procedure referred to above with one modification: the value of $\Delta\bar{\nu}$ was fixed at 1245 cm^{-1}. This value represents the strongest Raman spectral peak characteristic of the cytosine nucleus [26] and may be assumed, therefore, to correspond to the dominant, totally symmetric vibrational mode. The "best fit" curve is compared with the experimental spectrum of cytidine in neutral solution in fig. 2; the origins and relative intensities of the individual bands are also indicated in this figure.

4.3. Exciton coupling parameters

The method of calculating vibronically coupled dimer spectra has been described before [15, 25]. In this instance the parameters $\Delta\bar{\nu}$, $\bar{\nu}_{00}$, b_g and X were fixed at the values determined from the spectrum of cytidine. The experimental spectrum of CpC was fitted by adjusting in the calculated spectrum the following three parameters: an angle ϑ, related to the angle between the interacting transition moments, the exciton coupling energy, E, and a spectral shift parameter, $\delta\bar{\nu}$. The last of these parameters represents a shift, usually a red shift, of the coupled spectrum relative to the monomer spectrum attributed to coulombic interactions between the chromophores.

The fitting of the experimental spectrum has been greatly facilitated by certain properties of the logarithmic difference spectrum. First, the *position* of

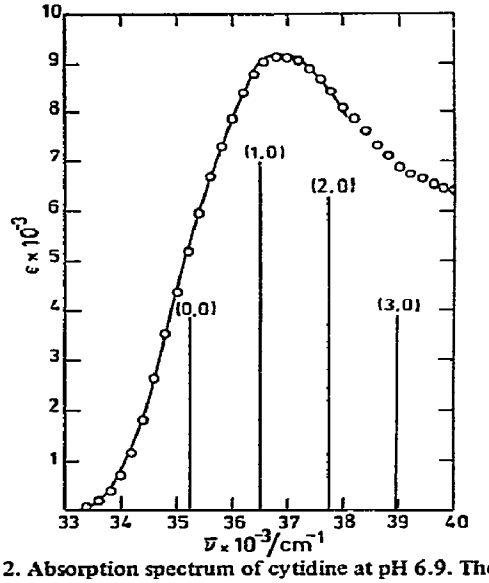


Fig. 2. Absorption spectrum of cytidine at pH 6.9. The experimental spectrum is shown by the circles and fitted spectrum by the full line; the individual bands and their relative intensities are indicated.

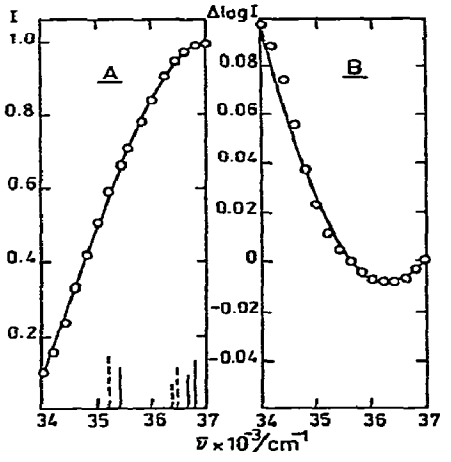


Fig. 3. Comparison between "best fit" calculated and experimental spectra. In each case calculated spectra are shown as full lines and experimental spectra as circles.

(A) Spectrum of CpC. The position and relative intensities of vibronically coupled bands are indicated; full lines: plus series; broken lines: minus series.

(B) Logarithmic difference spectrum.

the minimum of the calculated $\Delta \log I$ versus $\bar{\nu}$ curve was found to be virtually independent of the value chosen for E and for $\delta\bar{\nu}$ and the experimental minimum shown in fig. 1, was well reproduced by an angle of $\theta = 75°$. At this value of θ the *shape* of the calculated logarithmic spectrum was found, in turn, to be very sensitive to the choice of the energy parameter, E, but not so much to the value of $\delta\bar{\nu}$, while the *position* of the curve relative to the Y-axis depended strongly on the value of the spectral shift parameter, $\delta\bar{\nu}$.

In fig. 3 the "best fit" CpC and logarithmic difference spectra are shown. The values of the "best fit" parameters and the corresponding confidence limits estimated from considering the precision of the data are as follows:

$$\theta = 75 \pm 3°,$$

$$E/hc = 375 \pm 25\ \text{cm}^{-1},$$

$$\delta\bar{\nu} = 40 \pm 10\ \text{cm}^{-1}, \quad \text{(red shift)}.$$

The first of the above parameters is related to the molecular conformation of CpC in neutral solution. Johnson et al. [27] obtained poor agreement between calculated and experimental CD spectra of CpC in neutral solution when the molecular conformation was assumed to correspond to the B-form of DNA; however, conformations that increased the angle between the bases well above 36° gave much improved results. Our results concerning θ, insufficient on their own to provide definitive information on molecular conformation of CpC, do lend support to the conclusions of the above workers.

The magnitude of the second derived parameter, E, the exciton coupling, corresponds to a transfer rate [1] of about $10^{14}\ \text{s}^{-1}$. Even if one allowed for the relatively short lifetimes, of the order of 10^{-11} s, of singlet excited states for mononucleotides [28], the above transfer rate would enable up to 1000 transfers of excitation energy to occur during the lifetime of the lowest energy singlet excited state between cytosine moieties at room temperature.

5. Conclusions

We have been able to show that meaningful exciton interaction parameters may be obtained by the use of absorption spectroscopy in systems where the magnitude of such interactions lead to small changes in the shapes of spectral envelopes. The results agree with previous conclusions based on CD measurements on the molecular conformation in aqueous solution of the dinucleotides studies. Absorption spectroscopy, not restricted to optically active systems may be rated, therefore, as a valuable tool in studies concerned with molecular conformation and/or energy transfer between chromophores.

References

[1] Th. Förster, in: Modern quantum chemistry, Vol. 3, ed. O. Sinagoglu (Academic Press, New York, 1965) pp. 93–137.
[2] I. Tinoco, Advan. Chem. Phys. 4 (1962) 113–160.
[3] J.N. Kikkert, G.R. Kelly and T. Kurucsev, Biopolymers 12 (1973) 1459–1477.
[4] G.R. Kelly and T. Kurucsev, Biopolymers 13 (1974) 769–778.
[5] M.M. Warshaw and I. Tinoco, J. Mol. Biol. 13 (1965) 54–64.

[6] M.M. Warshaw and I. Tinoco, J. Mol. Biol. 20 (1966) 29–38.
[7] J. Brahms, J.C. Maurizot and A.M. Michelson, J. Mol. Biol. 25 (1967) 465–480.
[8] J. Brahms, J.C. Maurizot and A.M. Michelson, J. Mol. Biol. 25 (1967) 481–495.
[9] C.R. Cantor, H.H. Warshaw and H. Shapiro, Biopolymers 9 (1970) 1059–1077.
[10] C. Long, E.J. King and W.M. Sperry, eds., Biochemists' handbook (E. & F.N. Spon Ltd., London, 1961).
[11] L.P. Gianneschi and T. Kurucsev, J.C.S. Faraday II 70 (1974) 1334–1342.
[12] A.A. Lamola and J. Eisinger, Proc. Natl. Acad. Sci. U.S. 59 (1968) 46–51.
[13] D.J. Browne, J. Eisinger and N.J. Leonard, J. Amer. Chem. Soc. 90 (1968) 7302–7323.
[14] P.R. Callis, Chem. Phys. Letters 19 (1973) 551–555.
[15] R.L. Fulton and M. Gouterman, J. Chem. Phys. 41 (1964) 2280–2286.
[16] A. Witkowski, in: Modern quantum chemistry, ed. O. Sinagoglu, Vol. 3 (Academic Press, New York, 1965) pp. 161–175.
[17] M.Z. Zgierski, J. Chem. Phys. 59 (1973) 1052–1053, 3319–3322.
[18] W. Hug and I. Tinoco, J. Amer. Chem. Soc. 95 (1973) 2803–2813.
[19] M.L. Bailey, Theoret. Chim. Acta 16 (1970) 309–315.
[20] A.F. Fucaloro and L.S. Forster, J. Amer. Chem. Soc. 93 (1971) 6443–6448.
[21] D.P. Craig, J. Chem. Soc. (1950) 2146–2151.
[22] E.F. McCoy and I.G. Ross, Austr. J. Chem. 15 (1962) 573–590.
[23] V.P. Klochkov and V.L. Bogdanov, Opt. Spektrosk. 29 (1970) 852–867 [Opt. Spectrosc. 29 (1970) 458–461].
[24] V.P. Klochkov and V.L. Bogdanov, Opt. Spektrosk. 34 (1973) 46–51 [Opt. Spectrosc. 34 (1973) 25–28].
[25] M.E. Gál, G.R. Kelly and T. Kurucsev, J.C.S. Faraday II 69 (1973) 395–402.
[26] R.C. Lord and G.J. Thomas, Spectrochim. Acta 23A (1967) 2551–2591.
[27] W.C. Johnson, M.S. Itzkowitz and I. Tinoco, Biopolymers 11 (1972) 225–234.
[28] A. Lamola, Pure Appl. Chem. 34 (1973) 281–303.

BIOPHYSICAL CHEMISTRY 2 (1974) 278–289. © NORTH-HOLLAND PUBLISHING COMPANY

EXPERIMENTAL STUDIES OF THERMAL DENATURATION OF THE Na–DNA SYSTEM WITH RESPECT TO MANNING'S MODEL

Marie-Agnès RIX-MONTEL, Henri GRASSI and Dane VASILESCU
Laboratoire de Biophysique, U.E.R.D.M., Université de Nice, Parc Valrose, 06034 Nice-Cedex, France

Received 4 March 1974
Revised manuscript received 15 May 1974

The sodium and chloride activity coefficients in DNA solution were measured by selective electrodes. These experiments were performed for native and thermally denatured DNA. The ratio of activities in helix and coil states were compared with those given by Manning's model. These results are in good agreement with the theoretical values.

We also compare the experimental values of the charge parameter ξ of DNA in the helix (ξ_h) and coil (ξ_c) configurations with the theoretical parameters appearing in Manning's model and which have been adjusted to correspond with the known conformation of the molecule. From this comparison, we deduce the change of enthalpy $(\Delta H)_{T_m}$ at the temperature of denaturation (T_m) of DNA.

The value of $(\Delta H)_{T_m}$ thus calculated is smaller than the theoretical value and comparable with that observed experimentally by Privalov et al.

1. Introduction

Several experimental investigations have been devoted to the study of the interaction of metallic cations with DNA in solution. The results were generally interpreted as a function of various models based on the Poisson–Boltzmann equation [1–6]. The recent investigations of Manning [7–11] on the limiting laws and counterion condensation in polyelectrolyte solutions appear to provide a better understanding of the behaviour of the DNA poly-anion in the presence of the sodium counterion.

The present laboratory study of thermal transconformation by various techniques (selective electrodes [12], dielectric studies [13], noise studies [14]), revealed an increase in the activity of the sodium counterion during the helix–coil transition. The systematic study of the behaviour of the Na^+–DNA system was intensified by potentiometric measurements by means of electrodes selective to Na^+ and Cl^- ions, in order to compare results with the model suggested by Manning. This was carried out in a concentration range of DNA and added salt in excess, for which the electrodes provide workable results.

We shall also deduce the values of the charge parameter, ξ, corresponding to the helix and coil configurations. These values will then be discussed in the light of the known conformation of DNA, particularly for the configuration in the form coil.

2. Manning's model

2.1. Notations

The fundamental parameter employed by Manning and most other authors is ξ defined by

$$\xi = e^2 / 4\pi\epsilon_0\epsilon'_r kTb \qquad (1)$$

(in the rationalized MKSA system), where b is the distance between two phosphate sites projected on the axis of the double helix, ϵ_0 is the permittivity of the vacuum, ϵ'_r is the relative permittivity of the solvent. For $\xi > 1$ unstable systems are involved and the counterions must condense along the polyion in order to reduce ξ to its limiting value $\xi = 1$. This limiting value corresponds to the critical charge ensuring the stability of the polyion; b is then equal to 7.155 Å which is

the Landau length of the classic theory concerning 1–1 electrolytes in solution.

Let n_1 be the molar concentration of the counterion and n_2 the molar concentration of the co-ion; then $n_1 = n_e + n_s$ and $n_2 = n_s$ where n_s is the molar concentration of the monovalent salt added to the polyelectrolyte and $n_e = PN_p/V$ is the molar concentration of the ionized sites of the polyion (with N_p the number of polyions in solution, P the number of charged groups per polyion, V the total volume). The activities of the counterion a_1 and the co-ion a_2 are given by

$$a_1 = \gamma_1 n_1, \qquad a_2 = \gamma_2 n_2,$$

where γ_i is the activity coefficient. According to Manning's theory the activity coefficients of the counterion and co-ion are given respectively by

$$\gamma_1 = \frac{\xi^{-1}X + 1}{X + 1} \exp\left(-\frac{1}{2}\frac{\xi^{-1}X}{\xi^{-1}X + 2}\right), \tag{2}$$

and

$$\gamma_2 = \exp\left(-\frac{1}{2}\frac{\xi^{-1}X}{\xi^{-1}X + 2}\right), \tag{3}$$

with $X = n_e/n_s$.

2.2. Experimental parameters

In the case of DNA in solution in NaCl, consider the two extreme conformations: the native state (or helix, noted h) and the denatured state (or coil, noted c). Introducing the parameters ξ_c and ξ_h for the coil and helix state respectively, Manning obtains the following expressions for the ratio of the activity coefficients in both states

$$\left(\frac{\gamma^h_{Na^+}}{\gamma^c_{Na^+}}\right)_{theor.} = \frac{1 + \xi_h^{-1}X}{1 + \xi_c^{-1}X} \exp\left(\frac{\eta X}{(2 + \xi_c^{-1}X)(2 + \xi_h^{-1}X)}\right), \tag{4}$$

$$\left(\frac{\gamma^h_{Cl^-}}{\gamma^c_{Cl^-}}\right)_{theor.} = \exp\left(\frac{\eta X}{(2 + \xi_c^{-1}X)(2 + \xi_h^{-1}X)}\right), \tag{5}$$

with $\eta = (\xi_c^{-1} - \xi_h^{-1})$. According to Manning $\xi_c = 1$, $\xi_h = 4.2$ and thus $\eta = 0.76$.

It is also possible to introduce the theoretical extent of binding ψ_{th} as proposed by Archer et al. [15]:

$$\psi_{th} = (n_1 - [Na^+]_e)/n_e. \tag{6}$$

Here $[Na^+]_e$ is the active concentration as measured by the electrode and may be defined by

$$a_1 = \gamma^c_s [Na^+]_e = \gamma_1 n_1, \tag{7}$$

since the effective concentration $[Na^+]_e$ corresponds to the concentration of Na^+ in a pure NaCl solution which exhibits the same activity as Na^+ in the polyelectrolyte solution [18]. For sufficiently low concentrations of NaCl we may put the activity coefficient γ^c_s of the counterions in a pure salt solution with concentration n_s equal to unity ans thus find

$$\psi_{th} = (n_1 - a_{Na^+})/n_e = (1 + X^{-1})(1 - \gamma_1). \tag{8}$$

The difference in theoretical extent of binding $\Delta\psi_{th}$ between the coil and helix state may be defined using (7) and (8)

$$\Delta\psi_{th} = (a^c_{Na^+} - a^h_{Na^+})/n_e = (1 + X^{-1})(\gamma^c_{Na^+} - \gamma^h_{Na^+}), \tag{9}$$

where $a^c_{Na^+}$ and $a^h_{Na^+}$ are the activity of the Na^+ ions for the system in the coil and helix state respectively. We can observe that in Liquori and coworkers' [16,17] investigations $\Delta\psi_{th}$ is noted $\Delta\gamma_{Na^+}$.

It is possible to obtain the activity of the free ions in the solution, a_{Na^+} and a_{Cl^-}, by potentiometric measurements with the help of selective electrodes. Consequently, the following may be written for the helix and coil states:

$$\frac{\gamma^h_{Na^+}}{\gamma^c_{Na^+}} = \frac{a^h_{Na^+}}{a^c_{Na^+}} \qquad \text{and} \qquad \frac{\gamma^h_{Cl^-}}{\gamma^c_{Cl^-}} = \frac{a^h_{Cl^-}}{a^c_{Cl^-}}.$$

By determining the ratio of our activity measurements in natural and thermally denaturated solution of DNA, we obtain the ratio of activity coefficients γ defined by Manning, enabling us to compare our experimental values with theoretical predictions based on Manning's model.

3. Experimental measurements

3.1. Experimental apparatus and problems

3.1.1. Measurement device

The employed technique involved a potentiometric

measurement providing the activity of free ions in solution. In order to do this, electrodes were employed which were selective to various types of ions, together with the corresponding reference electrodes. The employed electrodes are summarized below:

Sodium:	Beckman No. 39 278	Ref. No.	39 170
	Orion No. 94-11-A	Ref. No.	90-02
	Corning No. 476 210	Ref. No.	476 002
Chloride:	Beckman No. 39 048	Ref. No.	39 170
	Orion No. 94-17-A	Ref. No.	90 01

These electrodes were connected to a Cary 31 high input impedance electrometer fitted with a special head for potentiometric measurements. In order to increase its sensitivity we employed an opposition method allowing a full-scale reading of 10 mV.

This opposition was effected by means of an AOIP P 12 R potentiometer supplied with AOIP ZS stabilized power supply. The signals were recorded on a Graphispot recorder, on which 1 mV corresponded to 2.5 cm. The solutions analysed were thermostat-controlled at 0.05°C by a Haake thermostat. The electrodes were precalibrated in three standard solutions of known concentration. The measurement procedure has been decribed in a preceding paper [12].

3.1.2. Monitoring of test solutions

For each DNA solution, we have measured the concentration of ionisable sites by spectrophotometry at 2600 Å, by considering that the molecular weight of a nucleotide unit of sodium salt is 331. The hyperchrome effect was checked by spectrophotometry during thermal denaturation, and a mean percentage of 35 % made it clear that the DNA employed was highly polymerized. The calf thymus and E. Coli DNA employed was obtained from the Centre de Biophysique Moléculaire at Orléans and the Centre de Recherche sur les Macromolécules at Strasbourg.The test solutions were prepared with supra pure Merck NaCl dissolved in water which was freshly double-distilled in quartz.

3.1.3. Experimental limits of this method

The accuracy of results is limited by several factors, the major ones being the following:
– uncertainty concerning the Nernst slope of the electrodes,
– electrode drift,
– reproductibility of measurements, and
– possible influence of foreign ions liable to interfere with the sodium.

These factors were accounted for as follows:
– Calibration of the electrode led to a mean slope falling between two extreme values. This slope permitted calculation of the activity of the unknown solution to be measured, itself falling between two extreme values (fig. 1).
– When the equilibrium potential of the electrode is reached (at the end of a more or less extended time lapse), drift was observed. We selected the potential value such that the drift was less than 0.5 mV in 15 min.
– It was also observed that the prior treatment of the electrode exerted an effect on its behaviour. Therefore, it appeared indispensable to calibrate the electrode before each measurement. Furthermore, the electrodes

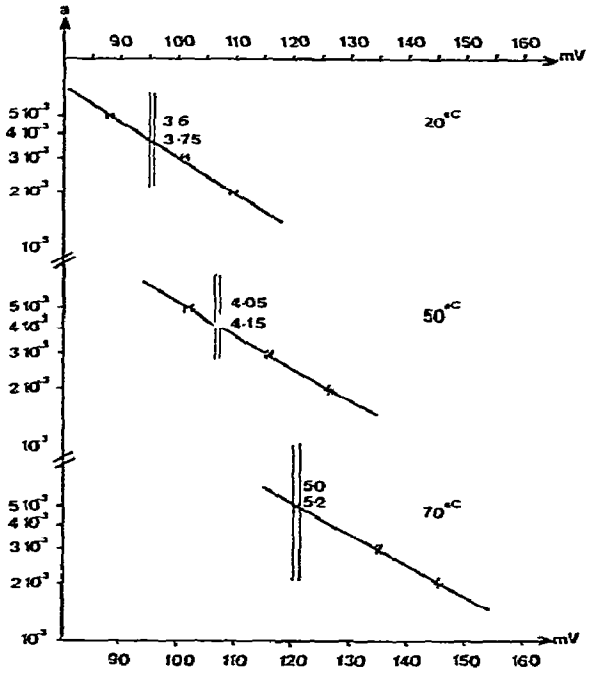


Fig. 1. Electrode calibration line. For three standard solutions of NaCl, activity a_{Na^+} was measured with an uncertainty of 1 mV plotted on the figure. The unknown activity was deduced by interpolation.

Table 1
Difference between activity coefficients of chloride in helix and coil states (for symbols, see text). For values of ϵ which are small with respect to 1, Manning's model indicates that the activity coefficient of the chloride ion in the helix state approaches that calculated for the coil state

DNA	DNA conc. (g/ℓ)	n_e	n_s	X	ϵ
V. 378	0.375	1.133×10^{-3}	5×10^{-3}	0.227	0.038
E. Coli 6	0.343	1.036×10^{-3}	2×10^{-3}	0.513	0.073
V. 378	0.4	1.2×10^{-3}	2×10^{-3}	0.6	0.082
E. Coli 6	0.47	1.42×10^{-3}	2×10^{-3}	0.71	0.092
E. Coli 6	0.62	1.873×10^{-3}	2×10^{-3}	0.936	0.109
E. Coli 6	0.4	1.2×10^{-3}	10^{-3}	1.2	0.125
V. 7	0.73	2.205×10^{-3}	10^{-3}	2.205	0.158

selective to sodium ions were sensitive to other ions. In this respect, Corning indicated the following selectivity ratios:

At pH 7: $Na^+ / K^+ = 1000$
$Ag^+ / Na^+ = 1500$
$Na^+ / Li^+ = 250$
$Na^+ / NH_4^+ = 3000.$

Finally, it is also necessary to verify the condition $pH \geqslant pNa + 3$, so that for solutions in which the Na^+ activity is about 10^{-3} M, the $pH \geqslant 6$. Since our solution has a mean pH of 6.5, the latter condition was always satisfied.

3.2. Results

3.2.1. Chloride co-ion

During the denaturation of DNA, no variation in Cl^- concentration was observed, allowing for accurate measurements [19]. According to Manning's theory, $(\gamma^h_{Cl^-}/\gamma^c_{Cl^-})$ is given by (5) and may be written $\approx 1-\epsilon$, provided that

$$\epsilon = \eta X/(2 + \xi_c^{-1} X)(2 + \xi_h^{-1} X)$$

is small.

The values of ϵ calculated for some experimental points are given in table 1. This table shows that Manning's model correctly predicts that the value of $\gamma^c_{Cl^-}$ approaches that of $\gamma^h_{Cl^-}$ for the Cl^- co-ion in our measurement range.

3.2.2. Sodium counterion

The activity of the free sodium ion in the solution was measured for the native state of DNA at 20°C ($a^h_{Na^+}$) and for the denatured state at 70°C ($a^c_{Na^+}$). As it turned out, for the NaCl concentrations employed, the T_m of DNA occurred at about 52°C.

From this, we deduced the activity coefficient ratio of the sodium ion in the helix and coil states of DNA.

This ratio was then compared to the theoretical ratio of Manning's model; the results are shown in table 2. The theoretical curve $(\gamma^h_{Na^+}/\gamma^c_{Na^+})_{theor.}$ was plotted (fig. 2) as a function of the parameter X [eq. (3)]. The experimental values were observed to scatter around the theoretical curve. However, two points P_1 and P_2 fell outside this pattern, one by 20 % and the second by 30 %. In both cases, it may be observed that the DNA concentration is high and the added salt concentration is low. This high concentration of DNA may be the cause of a masking effect giving rise to a misleading reading of the electrode potential. Moreover, in order to confirm the theoretical conditions of Manning's model, it is necessary to employ a large excess of salt, which was certainly not the case for the two points in question, particularly for P_2. This work was thus limited to DNA concentrations ranging from 0.8 to 0.3 g/ℓ in order to avoid this masking effect and also to detect the ejection of sodium ions with sufficient sensitivity.

Figure 3 shows the results of our measurements using X as a parameter in order to better display the relative influence of n_e and n_s.

Table 2
Comparison between experimental and theoretical ratios $\gamma^h_{Na^+}/\gamma^c_{Na^+}$ (for symbols, see text); $a^c_{Na^+}$ measured at 70°C. $(\gamma_h/\gamma_c)_{exp}$ = ratio of activity coefficients of sodium corresponding to the helix and coil states of DNA, obtained from the corresponding ratio of activities measured by selective electrodes

DNA	DNA conc. (g/ℓ)	n_e	n_s	X	$a^h_{Na^+}$	$a^c_{Na^+}$	$(\gamma_h/\gamma_c)_{exp}$	$(\gamma_h/\gamma_c)_{th}$
V. 378	0.375	1.133×10^{-3}	5×10^{-3}	0.227	4.7×10^{-3}	5.2×10^{-3}	0.904	0.892
V. 11	0.325	0.982×10^{-3}	3×10^{-3}	0.327	2.9×10^{-3}	3.6×10^{-3}	0.805	0.855
					2.9×10^{-3}	3.7×10^{-3}	0.784	
					3×10^{-3}	3.6×10^{-3}	0.833	
					3×10^{-3}	3.7×10^{-3}	0.812	
E. Coli 6	0.343	1.036×10^{-3}	2×10^{-3}	0.518	2.1×10^{-3}	2.45×10^{-3}	0.857	0.796
						2.5×10^{-3}	0.84	
V. 11	0.8	2.417×10^{-3}	4.5×10^{-3}	0.537	4.7×10^{-3}	5.1×10^{-3}	0.922	0.796
					4.8×10^{-3}	5.1×10^{-3}	0.941	
V. 378	0.4	1.2×10^{-3}	2×10^{-3}	0.6	2×10^{-3}	2.5×10^{-3}	0.80	0.775
E. Coli 6	0.47	1.42×10^{-3}	2×10^{-3}	0.71	2.2×10^{-3}	2.6×10^{-3}	0.846	0.749
						2.65×10^{-3}	0.830	
V. 11	0.77	2.326×10^{-3}	3×10^{-3}	0.775	3.6×10^{-3}	5×10^{-3}	0.72	0.735
					3.7×10^{-3}	5×10^{-3}	0.74	
E. Coli 6	0.62	1.873×10^{-3}	2×10^{-3}	0.936	2.2×10^{-3}	2.8×10^{-3}	0.786	0.704
					2.3×10^{-3}		0.821	
V. 7	0.375	1.133×10^{-3}	10^{-3}	1.133	1.2×10^{-3}	1.65×10^{-3}	0.727	0.672
						1.7×10^{-3}	0.706	
E. Coli 6	0.4	1.2×10^{-3}	10^{-3}	1.2	1.2×10^{-3}	1.76×10^{-3}	0.68	0.662
V. 378	0.8	2.417×10^{-3}	2×10^{-3}	1.208	2.3×10^{-3}	2.9×10^{-3}	0.793	0.661
V. 7	0.73	2.205×10^{-3}	10^{-3}	2.205	1.49×10^{-3}	2.02×10^{-3}	0.737	0.557

4. Discussion

4.1. Calculation of ξ_h and ξ_c from the experimental results

According to (9) we have:

$$\gamma^c_{Na^+} - \gamma^h_{Na^+} = (\Delta a_{Na^+}/n_e)[1/(1+X^{-1})].$$

The difference $\Delta a_{Na^+} = a^c_{Na^+} - a^h_{Na^+}$ is known experimentally for each given value of X. From the ratio and the difference of $\gamma^c_{Na^+}$ and $\gamma^h_{Na^+}$ we can deduce their values, which are shown in table 3. We then substitute these experimentally obtained values into the expression for γ_i in Manning's theory as given by eq. (2). We can thus calculate, independently of each other, the values of ξ_h and ξ_c corresponding to our experiments. These values are shown in table 4.

The values of ξ_h and ξ_c thus obtained fall into two groups and we may take the average values:

$$\langle \xi_h \rangle = 5.3 \quad \text{i.e.} \quad \langle \xi_h^{-1} \rangle = 0.18$$

$$\langle \xi_c \rangle = 1.6 \quad \langle \xi_c^{-1} \rangle = 0.61.$$

This result enables us to calculate the value of a fundamental parameter, η:

$$\eta = \xi_c^{-1} - \xi_h^{-1} = 0.43.$$

Using the parameter ξ, given by (1) it is now easy to calculate the average distance b between consecutive phosphate sites for both the helix and loose-coil configurations.

$$b = \frac{e^2}{4\pi\epsilon_0\epsilon'_r kT\xi} = \frac{l}{\xi}$$

where $l = 1.669 \times 10^{-5}/\epsilon'_r T$ is the Landau length for

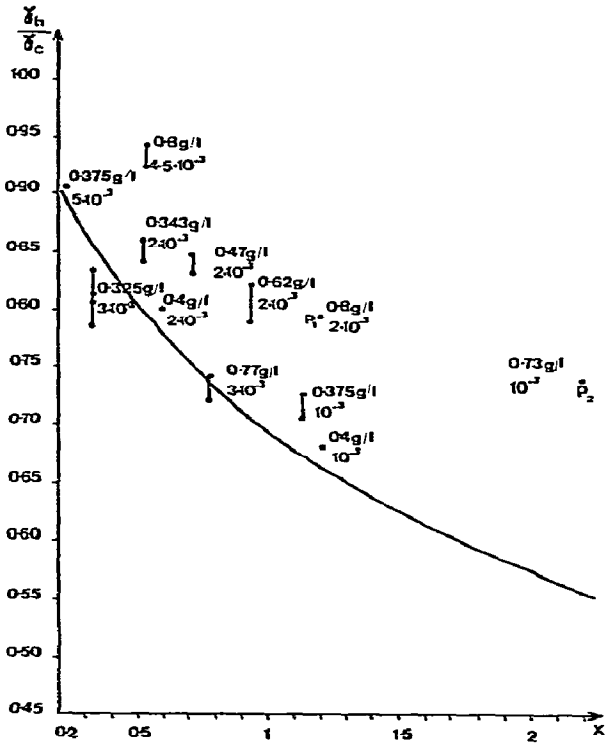


Fig. 2. $\gamma^{h}_{Na^+}/\gamma^{c}_{Na^+}$ as a function of X. The solid curve represents the theoretical ratio given by Manning's model. The dots represent the experimental values obtained by means of the electrodes.

the 1–1 electrolyte and ϵ'_r is the permittivity of the solvent (taken equal to the permittivity of water) [20].

At 25°C: $\epsilon'_r = 78.3$, therefore $b = 7.15\,\xi^{-1}$ Å, $\langle b_h \rangle = 1.3$ Å

At 70°C: $\epsilon'_r = 63.82$, therefore $b = 7.62\,\xi^{-1}$ Å, $\langle b_c \rangle = 4.68$ Å

The average value $\langle b_c \rangle = 4.7$ Å is smaller than the theoretical value 7.1 Å chosen by Manning and seems more realistic for DNA in the coil configuration. Manning assumed that at high temperatures, the two strands of DNA are completely separated and that each strand is fully stretched out and linear, so that b_c should have its maximum value. We may suppose, however, that even above 70°C, the strands of DNA are only partially unwound and exist in the form of a zig-zag.

The average value for $\langle b_h \rangle = 1.3$ Å, on the other hand, is slightly less than the minimum acceptable value of 1.7 Å. This latter value corresponds to the projection on the axis of the double helix of the distance between two phosphate sites. This distance is equal to 3.36 Å for *each of the two strands separately*.

This configuration is that of DNA type B and corresponds to the system Na^+ DNA in solution [21].

It seems, therefore, more reasonable to assume $b_h = 1.7$ Å and to choose the corresponding value $\xi_h = 4.2$, the value also chosen by Manning.

4.2. Calculation of ξ_c with $\xi_h = 4.2$

Having chosen $\xi_h = 4.2$, it is interesting to re-calculate ξ_c using a single experimental value – the ratio $(\gamma^{h}_{Na^+}/\gamma^{c}_{Na^+})_{exp}$. Substituting this value in the theoretical expression for this ratio, eq. (4) we obtain the values for ξ_c which are listed in table 5. The average value of ξ_c is $\langle \xi_c \rangle = 1.26$, giving

$\langle b_c \rangle = 6.08$ Å.

We thus see that even using the value for ξ_h given by Manning, the average value for b_c remains smaller than 7.1 Å, the length of the helix separating two phosphate sites on the same strand.

4.3. Calculation of ξ during the thermal transconformation

We use the same argument ($\xi_h = 4.2$) to study the evolution of ξ during the process of thermal denaturation. We have, therefore, measured the activity of the ion Na^+ at different temperatures during the transition helix–coil. The values of the ratio $\gamma_{Na^+}(T)/\gamma^{c}_{Na^+}$ thus obtained, and hence the corresponding values for $\xi(T)$ are shown in table 6.

In fig. 4 we plot, as a function of temperature, the variation of $\xi(T)$ and in fig. 5 the corresponding values of $b(T)$ for several solutions of DNA. In fig. 6 the curves for the optical density of the same solutions measured at 2600 Å are plotted.

We may note that the value $\langle b_c \rangle = 6.5$ Å measured for dilute solutions (0.37 g/ℓ) is a little greater than the value $\langle b_c \rangle = 6.08$ Å calculated in section 4.2 and approaches the value 7.1 Å chosen by Manning.

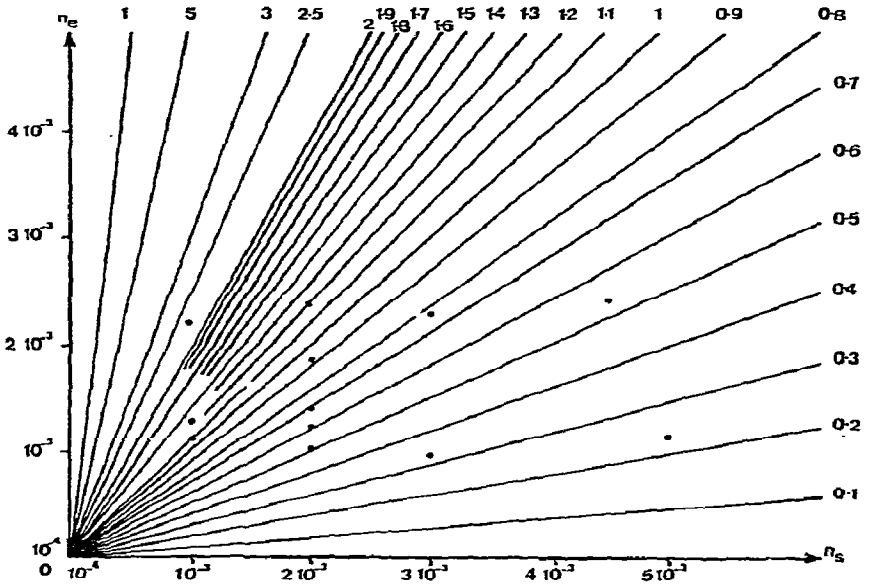


Fig. 3. Experimental points in space (n_e, n_s), with X as a parameter.

Table 3
Activity coefficients in helix and coil states ($\gamma^h_{Na^+}$ and $\gamma^c_{Na^+}$) obtained from our experiments (for symbols, see text)

DNA	Δa_{Na^+}	n_e	$\Delta\psi$	X^{-1}	$(\gamma^c_{Na^+} - \gamma^h_{Na^+})_{exp}$	$\gamma^c_{Na^+}$	$\gamma^h_{Na^+}$
V. 378	0.5×10^{-3}	1.133×10^{-3}	0.442	4.405	0.0817	0.851	0.769
V. 11	0.7×10^{-3}	0.982×10^{-3}	0.713	3.058	0.1757	0.901	0.725
	0.8×10^{-3}		0.814		0.2006	0.929	0.728
	0.6×10^{-3}		0.611		0.1505	0.901	0.750
	0.7×10^{-3}		0.713		0.1757	0.934	0.759
E. Coli 6	0.35×10^{-3}	1.036×10^{-3}	0.338	1.930	0.1153	0.812	0.696
	0.4×10^{-3}		0.386		0.1317	0.823	0.691
V. 11	0.4×10^{-3}	2.417×10^{-3}	0.165	1.862	0.0576	0.738	0.681
	0.3×10^{-3}		0.124		0.0433	0.734	0.691
V. 378	0.5×10^{-3}	1.2×10^{-3}	0.416	1.667	0.156	0.78	0.624
E. Coli 6	0.4×10^{-3}	1.42×10^{-3}	0.282	1.408	0.117	0.759	0.643
	0.45×10^{-3}		0.317		0.1316	0.774	0.642
V. 11	1.4×10^{-3}	2.326×10^{-3}	0.602	1.290	0.263	0.939	0.676
	1.3×10^{-3}		0.559		0.2441	0.939	0.695
E. Coli 6	0.6×10^{-3}	1.873×10^{-3}	0.320	1.068	0.1547	0.723	0.568
	0.5×10^{-3}		0.267		0.1291	0.721	0.592
V. 7	0.45×10^{-3}	1.133×10^{-3}	0.397	0.883	0.2108	0.772	0.561
	0.5×10^{-3}		0.441		0.2342	0.797	0.562
E. Coli 6	0.56×10^{-3}	1.2×10^{-3}	0.466	0.833	0.2542	0.794	0.540
V. 378	0.6×10^{-3}	2.417×10^{-3}	0.248	0.828	0.1357	0.656	0.520
V. 7	0.53×10^{-3}	2.205×10^{-3}	0.240	0.453	0.1651	0.627	0.463

Table 4
ξ_h and ξ_c parameters obtained from some of our experiments

DNA	X	γ^h_{Na+}	ξ_h^{-1}	ξ_h	γ^c_{Na+}	ξ_c^{-1}	ξ_c
E. Coli 6	0.518	0.696	0.1544	6.475	0.812	0.618	1.619
		0.691	0.1255	7.969	0.823	0.676	1.48
V. 11	0.537	0.681	0.112	8.95	0.738	0.335	2.983
		0.691	0.149	6.712	0.734	0.326	3.068
E. Coli 6	0.71	0.643	0.190	5.259	0.759	0.547	1.829
		0.642	0.183	5.461	0.774	0.634	1.578
V. 11	0.775	0.676	0.316	3.163	0.939	1.238	0.807
		0.695	0.413	2.422	0.939	1.238	0.807
E. Coli 6	0.936	0.568	0.139	7.20	0.723	0.598	1.671
		0.592	0.214	4.68	0.721	0.598	1.671
V. 7	1.133	0.561	0.238	4.196	0.772	0.821	1.219
		0.562	0.238	4.196	0.797	0.891	1.121
E. Coli 6	1.2	0.540	0.217	4.616	0.794	0.9	1.11
V. 378	1.208	0.520	0.166	6.04	0.656	0.521	1.917
V. 7	2.205	0.463	0.305	3.243	0.627	0.676	1.480

Table 5
ξ_c calculated from Manning's expression [eq. (4)] where $\gamma^h_{Na+}/\gamma^c_{Na+}$ is given by our experimental results and $\xi_h = 4.2$

DNA	X	$(\gamma^h_{Na+}/\gamma^c_{Na+})_{exp}$	ξ_c^{-1}	ξ_c
V. 378	0.227	0.904	0.915	1.092
V. 11	0.327	0.805	1.36	0.735
		0.784	1.49	0.671
		0.833	1.16	0.862
		0.812	1.31	0.763
E. Coli 6	0.518	0.857	0.745	1.342
		0.84	0.818	1.222
V. 11	0.537	0.922	0.485	2.062
		0.941	0.42	2.38
V. 378	0.6	0.80	0.915	1.092
E. Coli 6	0.71	0.846	0.665	1.5037
		0.830	0.73	1.370
V. 11	0.775	0.72	1.098	0.910
		0.74	1.01	0.990
E. Coli 6	0.936	0.786	0.75	1.33
		0.821	0.645	1.55
V. 7	1.133	0.727	0.855	1.170
		0.706	0.925	1.081
E. Coli 6	1.2	0.68	0.985	1.015
V. 378	1.208	0.793	0.647	1.54
V. 7	2.205	0.737	0.61	1.639

However, the value $\langle b_c \rangle = 4.68$ Å measured for a more concentrated solution of DNA (0.7 g/ℓ) is considerably smaller. This fact seems to indicate that the model holds only for very dilute solutions of DNA, as was predicted by Manning.

Lastly it is interesting to note the variation of b as a function of the temperature is well correlated with the picture of thermal denaturation that is obtained from the variation of the optical density at the absorption maximum.

4.4. Study of the enthalpy change close to T_m

In ref. [11] Manning gives the following expression for the change of enthalpy close to T_m:

$$\Delta H(T_m) = 1.15\, RT_m^2\, (\mathrm{d}T/\mathrm{d}\log m_{Na+})^{-1}\eta,$$

where m_{Na+} is the counter-ion concentration, and points out a discrepancy between his theoretical predictions and the values measured experimentally by Privalov et al. [22] at 337 K. He states that in order to obtain an agreement, the parameter η would have the value $\eta = 0.31$.

We have repeated these calculations for 325 K, (corresponding to our T_m) using the value $\mathrm{d}T/\mathrm{d}\log m_{Na+} = 18$ chosen by Manning. We find, according to theory,

Table 6
ξ_C and b_C as functions of temperature from eq. (4) and (1) where $\gamma^h_{Na^+}/\gamma_{Na^+}$ is given by our experimental results at different temperatures, $\xi_h = 4.2$, $b = l\xi^{-1}$, where $l = 1.669 \times 10^{-5}/\epsilon'_r(T)T$ is the Landau length

DNA	X	T(°C)	γ_h/γ	ξ	DO	ϵ'_r	l	b
V. 378	0.227	20 → 40	1	4.2	0.75	78.33	25°: 7.15	1.702
						73.15	40°: 7.29	1.736
		50	0.995	4.0	0.77	69.89	7.39	1.85
		60	0.953	1.818	0.88	66.78	7.51	4.13
		65	0.928	1.333	0.95	65.28	7.56	5.67
		70	0.911	1.163	1.0	63.82	7.62	6.55
		> 70	0.904	1.092	1.04	62.38	75°: 7.69	7.04
						60.98	80°: 7.75	7.09
V. 7	1.133	20 → 45	1	4.2	0.72	78.33	25°: 7.15	1.70
						73.15	40°: 7.29	1.736
		50	0.923	2.564	0.84	69.89	7.39	2.88
		55	0.857	1.96	0.93	68.32	7.45	3.80
		60	0.774	1.235	0.97	66.78	7.51	6.08
		> 70	0.706	1.081	1.01	63.82	70°: 7.62	7.05
						60.98	80°: 7.75	7.17
V. 7	2.205	20 → 40	1	4.2	1.46	78.33	25°: 7.15	1.702
						73.15	40°: 7.29	1.736
		45	0.898	2.778	1.55	71.50	7.34	2.64
		50	0.814	2.105	1.70	69.89	7.39	3.51
		55	0.772	1.852	1.82	68.32	7.45	4.02
		60	0.749	1.695	1.87	66.78	7.51	4.43
		> 70	0.737	1.639	1.90	63.82	70°: 7.62	4.65
						60.98	80°: 7.75	4.73

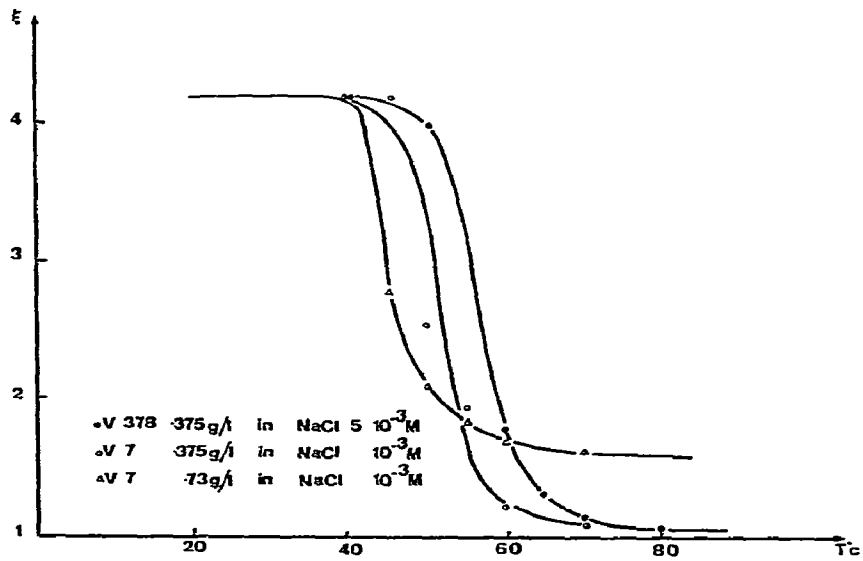


Fig. 4. ξ as a function of T with $\xi_h = 4.2$.

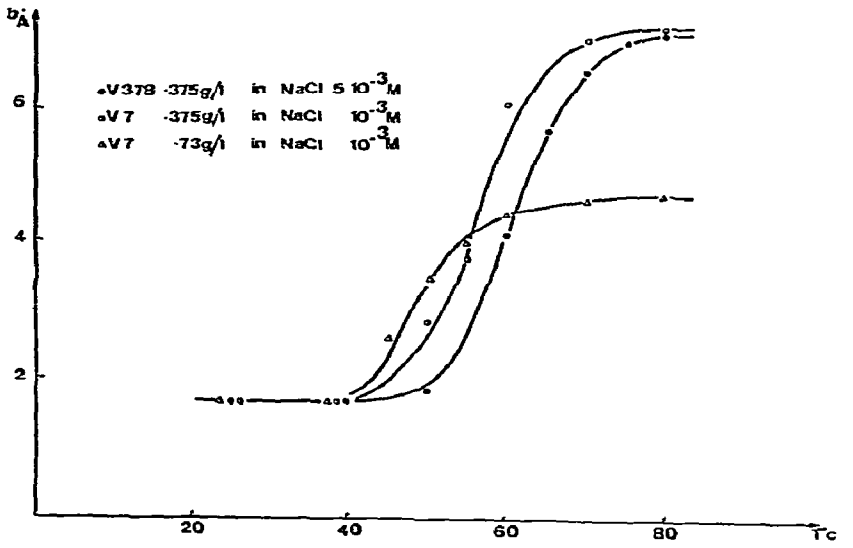


Fig. 5. b as a function of T with $\xi_h = 4.2$ and $b = \xi^{-1} l$.

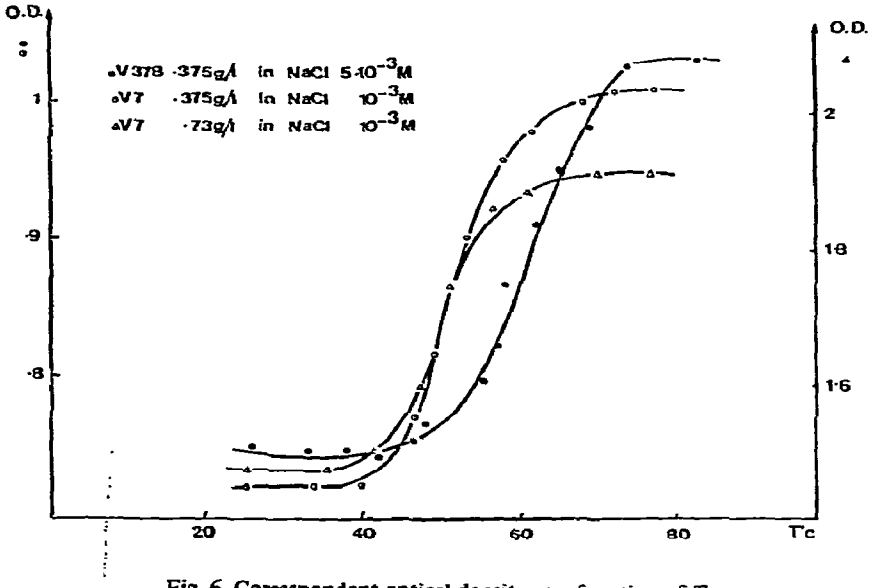


Fig. 6. Correspondent optical density as a function of T.

$\eta = 0.76$, $\Delta H = 10.2$ kcal (mole base)$^{-1}$.

From the experimental results of Privalov et al. [22]

$\Delta H = 4.5$ kcal (mole base)$^{-1}$,

leading to

$\eta = 0.335$.

Taking the value η_{av} obtained in section 4.2 from inde-

pendent calculations of ξ_h and ξ_c we obtain

$\eta = 0.43$,
leading to
$\Delta H = 5.77$ kcal (molebase)$^{-1}$.

Finally taking the value η_{av} obtained in section 4.3 from the values $\xi_h = 4.2$, $\xi_c = 1.26$, we find

$\eta = 0.55$,
leading to
$\Delta H = 7.4$ kcal (mole base)$^{-1}$.

We see that if we take the value of η calculated from our experimental results (sections 4.2 and 4.3) we obtain a theoretical value for ΔH which is closer to the value observed by Privalov et al. [22]. This observation lessens the 'discrepancy' pointed out by Manning.

5. Conclusion

This investigation shows that for DNA solutions at concentrations in agreement with the hypotheses of Manning, and with the limits imposed by measurements carried out with the help of selective electrodes, the experimental results are in good agreement with the laws proposed by this author.

First of all it may be stated that for the two helix and coil conformations of DNA, the interaction of the Na^+ counterion is correctly predicted. The ejection of the cation after crossing T_m is measurable thanks to the ratio $\gamma^h_{Na^+}/\gamma^c_{Na^+}$, which is directly connected to the structural parameter η.

We have also been able to determine, in a semi-empirical way, the values of the parameter ξ which is fundamental for describing the state of DNA. We note that the various values are grouped, but that the average value of $\langle \xi_h \rangle$ leads to a value for b_h which is a little smaller than the acceptable limit for the double helix of DNA in form B.

We have studied the distance between ionised sites on the helix as a function of temperature taking the theoretical value of $\xi_h = 4.2$ as a starting point. This leads an average value for ξ_c in the coil configuration of $\langle \xi_c \rangle = 1.26$ from which we have deduced a new value for η and for the change of the enthalpy during thermal denaturation. This latter value is considerably smaller than the original theoretical one, and is comparable with, though still greater than the value found from the calorimetric measurements of Privalov et al. [22].

These facts seem to indicate that the process of thermal denaturation can be explained, in terms of the conformation, by starting from a configuration of double helix type B which is transformed into a coil where the two strands are more or less unwound ($b_c < 7.1$ Å). This transformation is accompanied by the ejection of the counter ion.

This picture of the thermal transconformation of DNA is in agreement with the results of recent investigations by Schmitz and Schurr [23] using the technique of inelastic light scattering.

Acknowledgement

The authors acknowledge their thanks to Madame Sadron of the 'Centre de Biophysique Moléculaire' at Orléans and Monsieur Daune of the 'Centre de Recherche sur les Macromolécules' at Strasbourg, who kindly provided the DNA employed in this study. The authors also express their gratitude to Dr. G.S. Manning for the fruitful discussions that they held with him. They express their thanks to G.M. Searby for his help in translating this manuscript.

This work was sponsored by the DRME contract No. 73/406, and partly by the CNRS RCP No. 195.

References

[1] L. Kotin and M. Nagasawa, J. Chem. Phys. 36 (1962) 873.
[2] L. Kotin, J. Mol. Biol. 7 (1963) 309.
[3] S. Lifson and A. Katchalsky, J. Polym. Sci. 13 (1964) 43.
[4] A. Katchalsky, Z. Alexandrowicz and O. Kedem, in Chemical physics of ionic solutions, eds. B.E. Conway and R.G. Baraadas (Wiley, New York, 1966) p. 295.
[5] F. Oosawa, Biopolymers 6 (1968) 145.
[6] M. Daune, Biopolymers 7 (1969) 659.
[7] G.S. Manning, J. Chem. Phys. 51 (1969) 924.
[8] G.S. Manning, J. Chem. Phys. 51 (1969) 934.
[9] G.S. Manning, J. Chem. Phys. 51 (1969) 3249.
[10] G.S. Manning, Biopolymers 9 (1970) 1543.
[11] G.S. Manning, Biopolymers 11 (1972) 937.
[12] D. Vasilescu and M.A. Rix, Biochim. Biophys. Acta 199 (1970) 553.
[13] H. Grassi and D. Vasilescu, Biopolymers 10 (1971) 1543.
[14] D. Vasilescu, M. Teboul, H. Kranck and B. Camous, Biopolymers 12 (1973) 341.

[15] B.G. Archer, C.L. Craney and H. Krakauer, Biopolymers 11 (1972) 781.
[16] F. Ascoli, C. Botre, A.M. Liquori, J. Mol. Biol. 3 (1961) 202.
[17] A.M. Liquori, F. Ascoli, C. Botre, V. Crescenzi and A. Mele, J. Polym. Sci. XL (1959) 169.
[18] G.S. Manning, personal communication.
[19] D. Vasilescu, M.A. Rix-Montel and H. Grassi, C.R. Acad. Sci. Paris D 273 (1971) 1154.
[20] Handbook of Chemistry and Physics, ed. R.C. Weast (Chemical Rubber Co., Ohio, 1971) p. E. 67.
[21] R. Langridge, D.A. Marwin, W.E. Seeds, H.R. Wilson, W.C. Hooper, M.H.F. Wilkins and L.D. Hamilton, J. Mol. Biol. 2 (1960) 38.
[22] P.L. Privalov, O.B. Ptitsyn and T.M. Birshtein, Biopolymers 8 (1969) 559.
[23] K.S. Schmitz and J.M. Schurr, Biopolymers 12 (1973) 1543.

BIOPHYSICAL CHEMISTRY 2 (1974) 290–295. © NORTH-HOLLAND PUBLISHING COMPANY

THE ORDERED STRUCTURE OF THE ENCEPHALITOGENIC PROTEIN FROM NORMAL HUMAN MYELIN

M.A. MOSCARELLO, E. KATONA, A.W. NEUMANN and R.M. EPAND
Research Institute, The Hospital for Sick Children, Toronto, Department of Mechanical Engineering, University of Toronto, Toronto, and the Department of Chemistry, University of Guelph, Guelph, Canada

The conformation of the encephalitogenic protein isolated from normal human myelin has been studied by circular dichroism and surface tension techniques. The findings support the conclusion that this protein has a highly ordered structure in solution, with little α-helical or β structure. Conformational changes were observed at extremes of pH. Heating at high or low pH values had the effect of inducing more structure as determined by circular dichroism. Surface tension measurements showed a low temperature conformational change at low pH and a high temperature conformational change at high pH. At other pH values the structure appeared to be stable.

1. Introduction

The encephalitogenic basic protein of myelin is one of the major protein components in the membrane. Injection of a few micrograms into a susceptible animal produces an autoimmune encephalomyelitis [1]. The protein can be readily extracted from myelin [2] and purified. Intensive chemical studies have culminated in the elucidation of the complete amino acid sequence [3,4] and the importance of the single tryptophan residue at position 116 for biological activity has been demonstrated [5].

A number of interesting observations have been made concerning the relationship between secondary structure and the encephalitogenic activity of this protein. The biological activity is reported stable to heating, autoclaving, ultrasonic vibrations, treatment with trichloracetic acid [6] and urea [5]. It was concluded from these studies that secondary structure played no role in the ability of the protein to elicit experimental autoimmune encephalomyelitis.

Until recently it has been assumed that the protein was devoid of ordered structure and existed in a largely open conformation in the isolated state [7,8]. However, recent experiments have shown that it has a nonrandom structure in solution. On the basis of viscosity, sedimentation velocity, low angle X-ray scattering and electron microscopy, a prolate ellipsoid model was proposed for the shape of this protein with approximate dimensions of 15 × 150 Å [15]. The present work provides additional evidence from circular dichroism and surface tension measurements that this protein forms a specific stable conformation over a wide range of pH and temperature. Thermal transitions are observed only at extremes of pH.

2. Materials and methods

Myelin basic protein was prepared by the method of Lowden et al. [2]. For optical measurements the concentration varied from 0.21–0.29 mg protein/ml as measured by the Lowry method [9]. The measurements were made on a Cary, Model 61 spectropolarimeter, calibrated according to the values given by Cassim and Yang [10]. The temperature of the sample was controlled by means of a thermostable cell holder attached to a circulating constant temperature bath. A mean residue weight of 108.5 was calculated from the amino acid composition [11,12].

The surface tension was determined by a modified Wilhelmy technique utilizing a Cahn electrobalance and a temperature scanning device [13]. For each run 5 ml of a protein solution containing 0.8 mg/ml in 0.2M phosphate buffer at the appropriate pH was placed in the glass cup. The adsorption of the protein

from the bulk solution into the liquid vapor interface is a slow process. Equilibration started immediately at 18–20° and continued for 16–17 h at this temperature. After this time the change of surface tension due to further adsorption of the protein molecules in the air–water interface was of the order of 0.003 erg/cm^2 min. Surface tension was recorded with continuous heating of the solution at a rate of 0.45°/min. The corresponding change in surface tension was of the order of 0.05 erg/cm^2 min and hence, so large that the adsorption effects mentioned above may be neglected.

3. Results

3.1. Circular dichroism

In fig. 1 are shown the spectra, from 250–190 nm, of the encephalitogenic protein at pH values of 1.68, 11.3 and 12.1. Each solution was scanned over the whole temperature range. Only the spectra at 25° and 85° are shown. At pH 1.68 and 25° $[\theta]$ is very low at 222 nm, indicating little or no helical component. Below this wavelength a rapid increase in the magnitude of $[\theta]$ was observed reaching a maximum at 200 nm. When heated to 85°, the magnitude of $[\theta]$ at 200 nm decreased representing a decrease in random structure.

The spectrum at pH 11.3 and 25° showed little evidence of structure throughout the scan with low values of $[\theta]$. Heating to 85° decreased the magnitude of the ellipticity at 200 nm.

At pH 12.1, the maximum ellipticity was shifted from 200 to 205 nm, with some evidence of helical structure at 222 nm. Heating to 85° decreased the magnitude of $[\theta]$ at 205 nm as was observed also at pH 1.68; a small increase was observed at 222 nm indicating an increase in structure at the higher temperature.

In fig. 2, the $[\theta]_{222}$ values are plotted as a function of temperature. The extent of the change of CD was largest at extremes of pH, i.e., 1.68 and 12.2 and less at 11.4.

When the peptide concentration was increased by 10-fold, the results were similar although there were some quantitative differences (fig. 3).

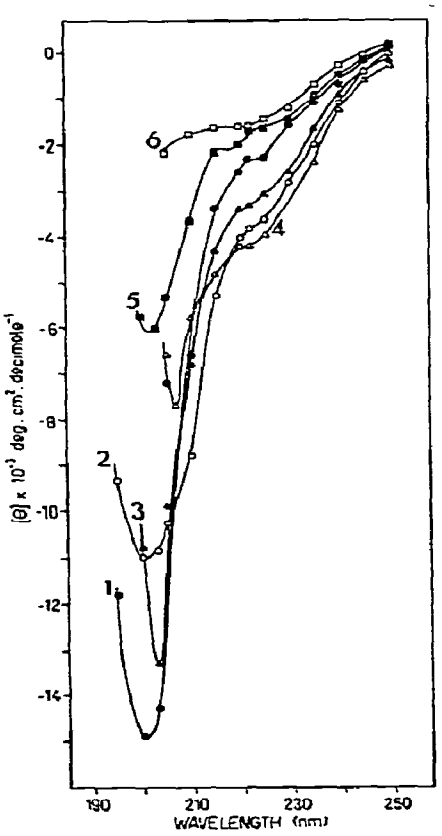


Fig. 1. Circular dichroism of the encephalitogenic protein from normal human myelin at pH 1.68, 11.3 and 12.1; curves 1 and 2, pH 1.68, 25° and 85° respectively; curves 3 and 4, pH 12.1, 25° and 85° respectively; curves 5 and 6, pH 11.3 at 25° and 85° respectively.

3.2. Surface tension

3.2.1. Adsorption

Equilibration of the system for 16–17 h was carried out routinely until the change of surface tension due to further adsorption was negligible compared with the subsequent change due to heating. The change in surface tension during this time is shown in fig. 4 which represents an actual recorder output. During the first 4–6 h the surface tension decreased rapidly

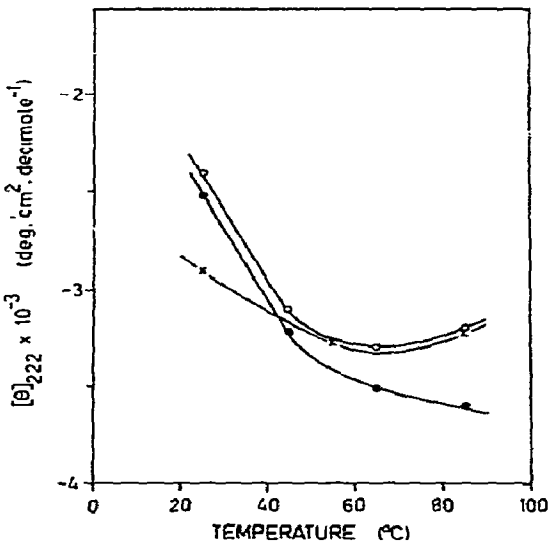


Fig. 2. Ellipticity $[\theta]_{222}$ as a function of temperature. pH 1.68 (•–•); pH 12.1 (o–o); pH 11.3 (x–x).

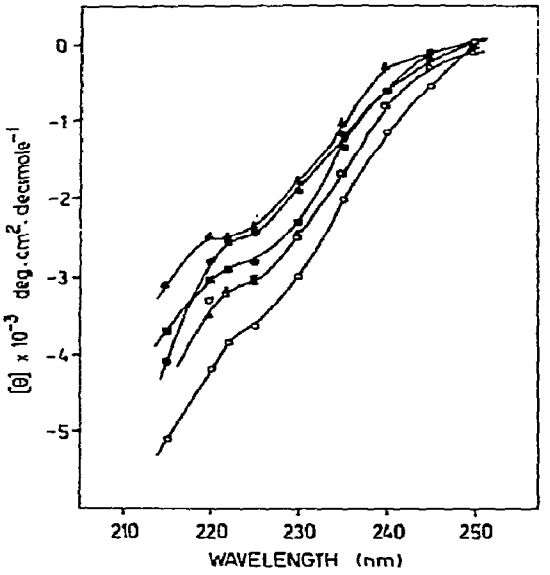


Fig. 3. Circular dichroism of the encephalitogenic protein from normal human myelin. pH 1.68, 25°, (•–•), pH 1.68, 85° (o–o); pH 12.1, 25° (▲–▲), pH 12.1, 85° (△–△); pH 11.3, 25° (■–■), pH 11.3, 85° (□–□).

indicating adsorption of the protein at the solution–air interface and thereafter, more slowly. Thus, at the concentrations used in this work the basic protein readily adsorbed at the air–water interface. At very low concentrations (2 μg/ml) Demel et al. [18] reported that it was not appreciably adsorbed at the surface.

3.2.2. Temperature scanning surface tension

The recorder outputs for the temperature scans are reproduced in fig. 5a→f at different pH values from 2.23 → 12.5. As explained previously [13] we expect a linear decrease in surface tension with increasing temperature if there are no conformational changes. Changes of the slope of the γ_{LV} versus T curves indicate such transitions. The scans in fig. 5 thus reveal a number of conformational changes. The values for the surface tension and temperature at which the changes occur are given in table 1. The first transition was observed at low temperatures. The transition was

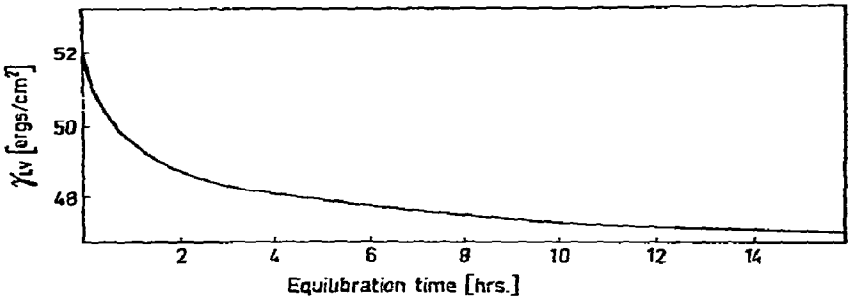


Fig. 4. The change in surface tension (γ_{LV}) with time of equilibration for the encephalitogenic protein from normal human myelin.

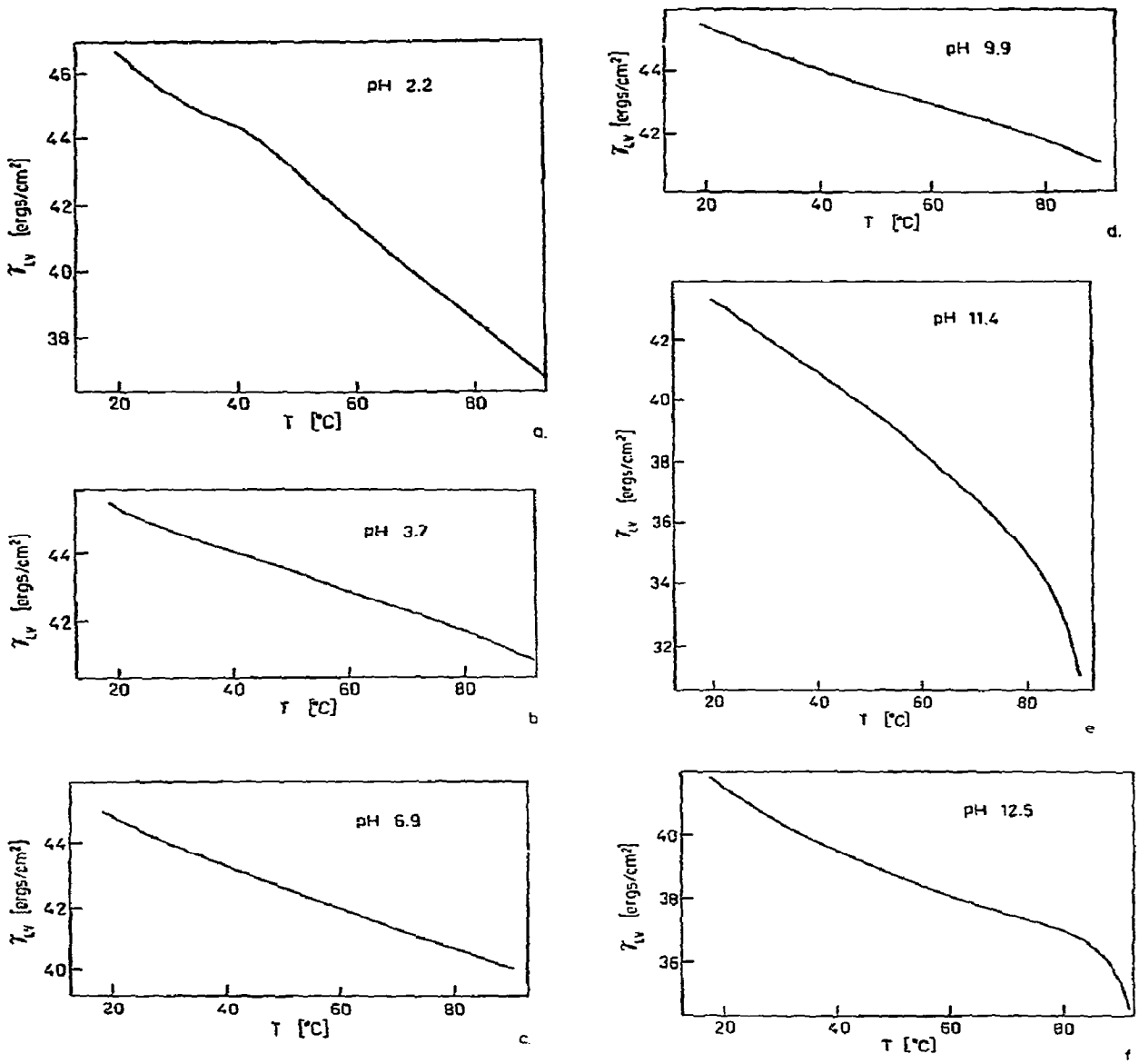


Fig. 5. Change in surface tension (γ_{LV}) with increasing temperature at pH values of 2.2, 3.7, 6.9, 9.9, 11.4 and 12.5.

small or absent at all pH values, exept at low pH (2.23) where a large phase transition was observed. Transitons II and III were small and only observed at low and high pH values. Transition IV observed at high temperatures (about 80°) was not observed at low pH but was pronounced at pH 11.40 and 12. The two major transitions, the one at low temperature (I) and the one at high temperature (IV) were observed at low and high pH values respectively. The protein at the end of each run was recovered from solution. When compared to freshly isolated protein on polyarcylamide gels, identical mobilities were observed. There-

Table 1
Conformational changes at different pH values for myelin basic protein

pH	Surface tension [a]	Transitions							
		I		II		III		IV	
		T°	γ	T°	γ	T°	γ	T°	γ
2.23	46.1	31	44.6	44	43.7	61	40.9	–	–
3.66	45.3	27	44.8	–	–	–	–	79	41.7
6.90	44.8	–	–	–	–	–	–	79	40.8
9.90	45.3	34	44.4	–	–	–	–	77	42.1
11.40	43.4	–	–	51	39.8	–	–	84	34.8
12.50	41.6	37	39.3	–	–	–	–	87	36.7

[a] Surface tension (erg/cm^2) after 16 h equilibration, immediately prior to start of temperature program.

fore, the heating at various pH values did not chemically alter the protein.

4. Discussion

Until recently [15] myelin basic protein has been assumed to be largely devoid of an ordered structure [7,8]. This conclusion was based on the high intrinsic viscosity and the optical rotary properties of this protein.

Because the molecule has a large number of basic residues (arginine, histidine, lysine) it was thought to be ideal for interacting with the phosphoryl groups of phospholipids. That it does interact with phospholipids has been demonstrated [16–18]. The "open" conformation and a large number of basic residues gave support to the theory that it was probably on the external surface of the myelin membrane.

Roboz-Einstein et al. [19] showed that the basic protein was an excellent substrate for a neural acid proteinase. A theory of myelin breakdown was advanced [19,20] whereby this protein in open conformation, interacting on the surface of myelin with phosphoryl groups, could be readily hydrolysed by a brain proteinase. The resulting fragments could subsequently lead to the development of an autoimmune disease. Therefore, we thought it was of considerable importance to determine if indeed any structure was present in the molecule. The intrinsic viscosity and optical-rotary data mentioned above [7,8] are also consistent with a highly ordered protein having a specific tertiary structure which is asymmetrical and relatively devoid of α-helical or β-structures. On the basis of viscosity, sedimentation velocity, low angle X-ray scattering and electron microscopy, the protein has been shown to be a prolate ellipsoid, 15 X 150 Å [15]. The experiments presented in this communication support this conclusion. Both circular dichroism and surface tension studies have shown that conformational changes occur predominantly at extremes of pH. The circular dichroism data showed that heating to 85° at extremes of pH induced more structure as determined by the increase in the magnitude of $[\theta]_{222}$, as well as the decrease in the magnitude of ellipticity at 200–205 nm. Since extremes of pH are known to denature proteins [14], some "loosening" of the structure appears to be necessary prior to the thermal phase transitions.

Surface tension studies showed few and minor transitions at intermediate pH values. However, a marked low temperature transition was observed at pH 2.23 and a marked high temperature transition at pH 11–12. The decrease in surface tension at 20° with increasing pH (table 1) is brought about by an increase in concentration in the surface at higher pH values. This is probably due to a decrease in charge of the basic groups as the pK is approached. The lowest value of the surface tension is observed at pH 12.50 due to the high pK of 12–13 reported by some authors for this protein [21].

We conclude therefore, that the basic protein from myelin is a highly structured molecule. Its position in the architecture of the myelin membrane is not yet clear. However, it appears from other studies [21] that

it is not found on the surface of the membrane.

Acknowledgement

Financial support from the Medical Research Council of Canada and the Multiple Sclerosis Society of Canada is gratefully acknowledged.

References

[1] Y. Oshiro and E.H. Eylar, Arch. Biochem. Biophys. 138 (1970) 392.
[2] I.A. Lowden, M.A. Moscarello and R. Morecky, Can. J. Biochem. Physiol. 44 (1966) 567.
[3] E.H. Eylar, S. Brostoff, G. Hashim, J. Caccam and P. Burnet, J. Biol. Chem. 246 (1971) 5770.
[4] P.R. Carnegie, Nature 229 (1971) 25.
[5] E.H. Eylar, Ann. N.Y. Acad. Sci. 195 (1972) 481.
[6] E. Roboz-Einstein, in: Handbook of neurochemistry, Vol. 7 (Plenum Press, New York, 1972).
[7] E.H. Eylar and M. Thompson, Arch. Biochem. Biophys. 129 (1969) 468.
[8] L.P. Choa and E.R. Einstein, J. Neurochem. 17 (1970) 1121.
[9] O.H. Lowry, N.J. Rosebrough, A.L. Farr and R.J. Randall, J. Biol. Chem. 193 (1951) 265.
[10] J.Y. Cassim and J.T. Yang, Biochemistry 8 (1969) 1947.
[11] E.H. Eylar, Proc. Nat. Acad. Sci. USA 67 (1970) 1425.
[12] P.R. Carnegie, Nature 223 (1969) 958.
[13] A.W. Neumann, M.A. Moscarello and R.M. Epand, Biopolymers 12 (1973) 1945.
[14] J. Steinhardt and S. Beychok, in: The proteins, Vol. II (Academic Press, New York, 1964).
[15] R.M. Epand, M.A. Moscarello, B. Zierenberg and W.J. Vail, Biochemistry 13 (1974) 1264.
[16] J.S. Anthony and M.A. Moscarello, Biochem. Biophys. Acta 243 (1971) 419.
[17] F.B. Palmer and R.M.C. Dawson, Biochem. J. 111 (1969) 637.
[18] R.A. Demel, Y. London, W.S.M. Guerts Van Kessel, F.G.A. Vossenberg and L.L.M. Van Deenen, Biochim. Biophys. Acta 311 (1973) 507.
[19] E.R. Einstein, J. Csejtey, R.B. Dalal, C.W.M. Adams, O.B. Bayliss and J.F. Hallpike, J. Neurochem. 19 (1972) 653.
[20] E.R. Einstein, K.B. Dalal and J. Csejtey, J. Neurol. Sci. 11 (1970) 109.
[21] C.W. Adams and M. Leibowitz, in: Research on multiple sclerosis (Charles C. Thomas, U.S.A., 1972) p. 68.

BIOPHYSICAL CHEMISTRY 2 (1974) 296–299. © NORTH-HOLLAND PUBLISHING COMPANY

A GENERAL FORMULATION OF THE FREE ENERGY OF INTERACTION IN COOPERATIVE LIGAND BINDING: APPLICATION TO HEMOGLOBIN

Allen P. MINTON and H.A. SAROFF

Laboratory of Biophysical Chemistry, National Institute of Arthritis, Metabolism, and Digestive Diseases, National Institutes of Health, Bethesda, Maryland 20014, USA

Received 5 June 1974

A general method for calculating the change in free energy of cooperative interaction upon partial or complete liganding of a protein containing an arbitrary number of binding sites is presented. This method is used to estimate the change in free energy of interaction upon oxygenation of hemoglobin under physiological conditions, which is compared to the internal energy change upon binding oxygen to the non-interacting binding site.

1. Introduction

In 1935 Pauling [1] proposed that the characteristic shape of the oxygen saturation curve of hemoglobin was due to stabilizing interactions between liganded hemes that were not present between unliganded hemes. The concept of ligand-dependent interactions between hemes (or, more generally, ligand binding sites) introduced by Pauling has provided the thermodynamic basis for most of the subsequent models of cooperative ligand binding in proteins [2]. An attempt has been made to calculate the change in the free energy of interaction upon liganding of a protein with an arbitrary number of equivalent binding sites, without reference to the mechanism of the ligand binding process [3]. This attempt did not, however, yield the quantity which was sought, but rather the difference between changes in the free energy of interaction upon liganding the first and last binding sites [4].

In the following section we shall derive a completely general expression for the change in free energy of interaction upon either partial or complete liganding of a protein containing an arbitrary number of binding sites (not necessarily equivalent). This expression may be evaluated from the equilibrium ligand saturation curves for the intact protein and an ensemble of non-interacting binding sites (or suitable approximation thereto), without recourse to curve-fitting or other extensive computation. In section 3 we shall utilize the relation derived, together with experimental data in the literature, to calculate the change in free energy of interaction upon oxygenation of hemoglobin under physiological conditions. It will be shown that under these conditions, the change in free energy of interaction amounts to approximately eleven per cent of the change in internal energy upon binding oxygen to the corresponding number of non-interacting binding sites.

2. Free energy relations

Consider a system at constant temperature and pressure, containing n_s moles of binding sites in a condensed phase, n_X^b moles of bound ligand X and n_X^f moles of free gaseous ligand X. If the total amount of X is constant, then at equilibrium

$$dG_c/dn_X^b = dG_g/dn_X^f, \tag{1}$$

where G_c is the Gibbs free energy of the condensed phase and G_g is that of the gaseous phase. We define the fractional saturation of binding sites $y \equiv n_X^b/n_s$. If gaseous X is assumed to behave ideally, then it follows from eq. (1) that

$$dG_c = n_s(G_X^0 + RT \ln x)dy, \tag{2}$$

where G_X^0 is the standard state free energy of gaseous

X, R is the molar gas constant, T the absolute temperature and x the concentration or partial pressure of gaseous X. The change in free energy of the condensed phase upon increasing ligand saturation from y_1 to y_2 is therefore

$$G_c|_{y_1}^{y_2} \equiv \int_{G_c(y_1)}^{G_c(y_2)} dG_c = n_s\{(y_2-y_1)G_X^0 + RT\int_{y_1}^{y_2} \ln x\, dy\} \quad (3)$$

Consider now two systems, 1 and 2, with the same number of binding sites. The difference between $G_c|_{y_1}^{y_2}$ for the two systems is

$$(G_c^{(2)} - G_c^{(1)})|_{y_1}^{y_2} = n_s RT \int_{y_1}^{y_2} (\ln x^{(2)} - \ln x^{(1)})dy. \quad (4)$$

If, in addition, it is specified that system 2 is identical to system 1 except for the presence of cooperative interactions between the binding sites in system 2 which are absent in system 1, then the changes in intrinsic free energy arising from liganding of the two sets of binding sites will be equal, and $(G_c^{(2)} - G_c^{(1)})|_{y_1}^{y_2}$ will be equal to $G^I|_{y_1}^{y_2}$, the change in free energy of cooperative interaction in system 2 between the saturation levels y_1 and y_2. The total integral free energy of interaction, defined to be equal to the change in free energy of interaction upon complete saturation of the binding sites of system 2, is then

$$G^I|_0^1 = n_s RT \int_0^1 (\ln x^{(2)} - \ln x^{(1)})dy. \quad (5)$$

According to eq. (4), evaluation of $G^I|_{y_1}^{y_2}$ requires explicit consideration of the ligand binding properties of *two* systems, the interacting system and the non-interacting reference system. In fig. 1 are shown three possible relationships between the equilibrium saturation curves of the reference system (dashed line) and the interacting system (solid line). The 'cooperativity' (i.e., shape of the saturation curve) of the interacting system is the same for all three cases. The magnitude of the integral on the right hand side of eq. (5) is equal to the area bounded by the dashed and solid curves in a given plot, and the sign of the integral is determined by whether $\ln x^{(2)}$ is greater or less than $\ln x^{(1)}$ for a given range of y. In fig. 1a $G^I|_0^1$ is positive and in fig. 1c it is negative. In fig. 1b $G^I|_0^{0.5}$ is positive, but $G^I|_{0.5}^1$ is negative and of equal magnitude, so that $G^I|_0^1$, the total integral free energy of interaction, is zero. This figure provides a graphic illustration that no relationship between 'cooperativity' and the free energy of interaction can be established without taking into account the ligand binding properties of the non-interacting binding site, a point which we have stressed elsewhere [4].

3. Application to hemoglobin

In a biologically functioning system the concentra-

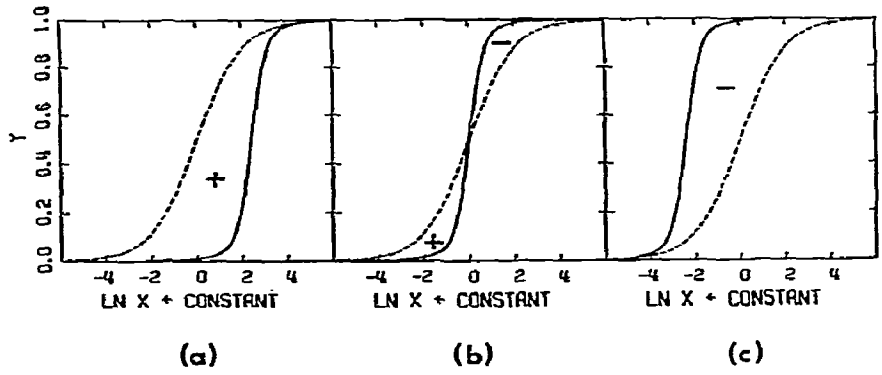


Fig. 1. Three possible relationships between the equilibrium saturation curve of the interacting system (solid line) and that of the non-interacting reference system (dashed line). See text for interpretation.

tion of ligand may vary broadly but is always finite; The ligand-binding protein is seldom fully saturated or deprived of ligand. Therefore the entire free energy of interaction is not ordinarily manifested in a physiological process, but only that part of it which comes into play between levels of ligand saturation corresponding to experimentally defined limits of free ligand concentration. We may rewrite eq. (4) to obtain the average change in free energy of interaction per binding site between the saturation limits y_1 and y_2:

$$\bar{G}^{\mathrm{I}}|_{y_1}^{y_2} \equiv (1/n_s)G^{\mathrm{I}}|_{y_1}^{y_2} = 2.303RT\int_{y_1}^{y_2}(\log x^{(2)} - \log x^{(1)})\,dy \qquad (6)$$

By substituting p, the partial pressure of gaseous oxygen in equilibrium with hemoglobin of saturation y, for x, we may use eq. (6) to estimate the change in free energy of interaction upon oxygenation of hemoglobin under physiological conditions. The physiological limits of saturation are taken to be approximately 0.05 and 0.95 [5]. Although these values are not precise, the results to be obtained are not qualitatively dependent upon the exact values of the limiting saturations. Since one cannot measure the saturation curve of hemoglobin with its cooperative interactions 'switched off', we shall employ myoglobin and the isolated α-chain of hemoglobin, both of which bind oxygen noncooperatively, as approximate models for the noninteracting binding sites of hemoglobin. Oxygen binding measurements have been performed on the isolated α-chains [6–8] and myoglobin [9] at a sufficient number of temperatures to permit the affinity constant for each of these species to be reliably estimated at 37°. In fig. 2 are plotted the oxygen binding curves at 37° of myoglobin, isolated α-chains, and blood at pH 7.4 [10]. According to eq. (6), $\bar{G}^{\mathrm{I}}|_{0.05}^{0.95}$ is approximately equal to 2.303 RT times the area enclosed by the saturation curves for blood and either α-chains or myoglobin, and the horizontal (dashed) lines $y = 0.05$ and $y = 0.95$. Upon graphical integration using a planimeter we find that $\bar{G}^{\mathrm{I}}|_{0.05}^{0.95} = (2.15 \pm 0.1)RT$, or 1340 cal/mol at 37°.

It is of interest to compare the magnitude of the free energy of interaction to the internal energy of the chemical bond linking the oxygen molecule to the binding site, which is by definition equal to the internal energy change ΔE of the reaction

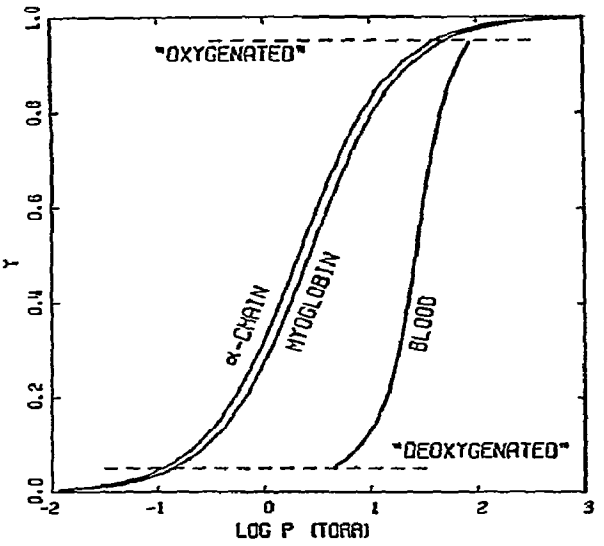


Fig. 2. Equilibrium saturation curves of isolated α-chains, myoglobin, and hemoglobin in blood (pH 7.4) at 37°. The curve for blood is truncated at $y = 0.05$ and $y = 0.95$.

$$\text{site} + O_2(g) \rightleftarrows \text{site} \cdot O_2.$$

ΔE is related to the standard state free energy change ΔG^0 of the reaction at constant temperature and pressure by

$$\Delta G^0 = \Delta E - T\Delta S^0 + p\Delta V, \qquad (7)$$

where ΔS^0 is the standard state entropy change, p is the pressure, and ΔV the volume change accompanying the reaction. According to the ideal gas approximation $p\Delta V = RT\Delta n$, where Δn is the change in moles of gas. Since $\Delta n = -1$ for each mole of the above reaction,

$$\Delta E = \Delta G^0 + T\Delta S^0 + RT. \qquad (8)$$

ΔG^0 is equal to $RT \ln p_{50}$, where p_{50} is the partial pressure of gaseous oxygen in equilibrium with half-saturated binding sites. ΔS^0 may be determined from the temperature dependence of ΔG^0. Assuming that both of these quantities may be estimated by taking the mean of the values calculated for the oxygenation reactions of myoglobin and α-chains, we obtain $\Delta G^0 \approx (0.86 \pm 0.1)RT$, $\Delta S^0 \approx (24.4 \pm 2)RT$, and $\Delta E \approx (-22.5 \pm 2.1)RT$. The average change in internal energy

of oxygen binding per non-interacting binding site upon increasing saturation from 0.05 to 0.95, denoted by $\bar{E}|_{0.05}^{0.95}$, is simply 0.9 ΔE, or $(-20.2 \pm 1.9)RT$. We observe that the value of $\bar{G}^{I}|_{0.05}^{0.95}$, which is positive, amounts to about eleven per cent of the value of $\bar{E}|_{0.05}^{0.95}$, which is negative.

The analysis presented here indicates that the steepening of the saturation curve of hemoglobin, relative to that of an ensemble of non-interacting binding sites (e.g., myoglobin, α-chains), results from a free energy of interaction which increases with, but which is not proportional to, the degree of saturation. It is obvious that the energy required to achieve this relative destabilization represents the utilization of a small fraction of the large energy yield of the reaction between ligand and binding site, energy which would otherwise be non-functionally dissipated into the molecular environment.

In conclusion, an entirely general method for the evaluation of changes in the free energy of interaction and the total integral free energy of interaction in an ensemble of binding sites has been presented. This method has been used to evaluate $\bar{G}^{I}|_{0.05}^{0.95}$ upon oxygenation of hemoglobin under physiological conditions. Using oxygen binding curves of blood at temperatures slightly below and/or above 37° in addition to that at 37°, the method presented here could be used to evaluate the enthalpic and entropic contributions to $\bar{G}^{I}|_{y_1}^{y_2}$ as well.

Acknowledgement

We thank Dr. T.L. Hill for critically reading the initial draft of this report.

References

[1] L. Pauling, Proc. Nat. Acad. Sci. U.S. 21 (1935) 186.
[2] H.A. Saroff and W.T. Yap, Biopolymers 11 (1972) 957.
[3] J. Wyman, Advan. Protein Chem. 19 (1964) 223.
[4] H.A. Saroff and A.P. Minton, Science 175 (1972) 1253.
[5] Handbook of respiration, eds. D.S. Dittmer and R.M. Grebe (W.B. Saunders, Philadelphia, 1958) p. 4.
[6] E.C. DeRenzo, C. Ioppolo, G. Amiconi, E. Antonini and J. Wyman, J. Biol. Chem. 242 (1967) 4850.
[7] I. Tyuma, R. Benesch and R.E. Benesch, Biochemistry 5 (1966) 2957.
[8] I. Tyuma, S. Shimizu and K. Imai, Biochem. Res. Commun. 43 (1971) 423.
[9] A. Rossi-Fanelli and E. Antonini, Arch. Biochem. Biophys. 77 (1958) 478.
[10] Handbook of respiration, eds. D.S. Dittmer and R.M. Grebe (W.B. Saunders, Philadelphia, 1958) p. 77.

BIOPHYSICAL CHEMISTRY 2 (1974) 301–315. © NORTH-HOLLAND PUBLISHING COMPANY

OPTICAL AND ELECTRO-OPTICAL PROPERTIES OF THE COMPLEXES OF DIBUTYLPROFLAVINE WITH DNA AND NUCLEOHISTONE

José BONTEMPS, Claude HOUSSIER and Eugène FREDERICQ
Laboratoire de Chimie Physique, Université de Liège au Sart-Tilman, B-4000 Liège, Belgium

Received 2 August 1974

A number of optical and electro-optical measurements showed that the binding of dibutylproflavine to calf thymus DNA and nucleohistone in 1 mM NaCl could be resolved on the basis of two external and orientated bound species, whose binding parameters have been determined by a spectrophotometric method.

The absorption and the electric dichroism properties were found to show up additivity of contributions from the two bound species. The orientation of the long axis of the strongly bound molecules of species I appeared close to the inclination of the DNA grooves, while that of species II differed by about ten degrees.

A spatial proximity of the two binding sites was suggested by the dependence of the circular dichroism signals, the fluorescence quantum yield and the emission anisotropy on the degree of binding. The mobility of the first bound dibutylproflavine molecules was similar to that of the intercalated proflavine molecules, but lower in nucleohistone as compared to DNA.

1. Introduction

In the studies of the complexes of various acridine dyes with different natural and synthetic nucleic acids by indirect methods, such as visible absorption and fluorescence, opposite conclusions have been drawn as regards the base-specificity of the binding process [1–13].

The theoretical binding curves derived by several authors [14–16] were found useful to resolve this important controversy. In the case of some acridine dyes, such as proflavine [15], acridine orange [15, 17], quinacrine [18] and of the phenanthridine drug, ethidium bromide [16, 18, 19], the binding results with DNA have been satisfactorily fitted, in the intercalation range, by a theoretical model of interaction in which both A–T and G–C pairs can serve as identical potential binding sites. In other binding results analyzed according to the classical Scatchard equation, a stoichiometry of about one dye molecule per four or five phosphate groups has been observed [3, 5, 20–22]. These data are also in agreement with the model of exclusion of the adjacent binding site, without base-specificity. Competition experiments, followed by indirect methods, also showed the identity of the binding sites on DNA for ethidium bromide, quinacrine, proflavine and methylene blue [5, 20, 22]. Although the intercalation of these planar dyes into DNA occurs at random, their fluorescence intensity depends differently upon the base composition of the binding site [2, 5, 6, 9, 11, 13, 23–25].

Contrary to these cases, a sharp binding specificity for the G–C pairs has been observed with actinomycin D [26], while dibutylproflavine seems to bind preferentially to the A–T pairs of DNA [27]. The requirements for this behaviour are partly known for the former, which intercalates into the base pairs of DNA, but to a lesser extent compared to the planar acridine dyes listed above [28]. On the contrary, dibutylproflavine is thought to form an outside-complex with DNA, the structural basis of which remains uncertain [27].

As noticed by Müller et al. [27], such specific compounds are of possible use for the selective staining of particular regions of the chromosomes observed by the fluorescence banding techniques ([29]; for a recent review of the field, see ref. [30]). Some interesting results, compared to those observed with more widely used fluorochromes, have already been obtained on chromosomes of different species with dibutylproflavine [31]. In view of the lack of a clear physico-chemical background for these characteristic fluorescence patterns, we

have examined some optical (visible absorption, fluorescence polarization and intensity, circular dichroism) and electro-optical (electric dichroism and electric birefringence) properties of the complexes of dibutylproflavine with calf thymus DNA and nucleohistone at low ionic strength. The behaviour of this dye will be compared to that reported for some intercalative dyes, among which the unsubstituted proflavine. Several distinctive features have already been evidenced by other authors at higher ionic strength [27, 32–33].

2. Materials and methods

2.1. Samples

The preparation and characterization of DNA [17] and nucleohistone [34] from calf thymus have been already described. The nucleohistone was prepared in a gel-form, but used in a soluble form by stirring the diluted gel with a glass propeller during 2-4 hours in the cold room (t = 5 °C, concentration: 0.5 mg DNA per ml). The concentrations of the DNA and nucleohistone solutions were calculated from their absorbance at 260 nm, using the molar extinction coefficient per mononucleotide residue: ϵ = 6450 and 6700 M^{-1} cm^{-1}, respectively. All solutions were made in pure water or in 1 mM NaCl, unbuffered but adjusted to pH 6.5 by NaOH.

Dibutylproflavine (3,6-diamino-2,7-di-t-butyl acridine) was kindly given by Dr. W. Müller (Stöckheim). The concentrations of the free dibutylproflavine solutions were determined spectrophotometrically, using ϵ = 34900 M^{-1} cm^{-1} at λ = 453 nm. This value, determined by Müller et al. [27] in a phosphate-saline buffer (pH 7.0), was found unchanged when the dye was dissolved in pure water or in 1 mM to 0.2 M NaCl solutions at pH 6.5. Proflavine hemisulfate was obtained from the British Drug House and was used without further purification. The concentration of the solutions was calculated using the molar extinction coefficient ϵ = 41000 M^{-1} cm^{-1} at λ = 444 nm.

2.2. Absorption spectrophotometry

The absorption spectra were recorded on a Zeiss RPQ 20A spectrophotometer and the precise absorbances were measured on a Shimadzu QV-50 spectrophotometer, using in the reference cell a macromolecular solution at the same concentration as in the complex. The experiments were carried out at two different total dye concentrations, $D_1 = 2.30 \times 10^{-5}$ and $D_2 = 1.41 \times 10^{-5}$ M. The binding degree, r, is defined per phosphate group.

2.3. Fluorescence intensity and polarization

The fluorescence apparatus and the calculation of (ϕ_{app}/ϕ_f), the ratio of the quantum yields, and of μ_{app}, the emission anisotropy, have been previously described [17]. The subscripts app and f denote quantities relative to the complex solution and to the free dye, respectively. For proflavine and dibutylproflavine, the excitation wavelengths were 453 and 477 nm, and the emission wavelengths were 510 and 520 nm, respectively.

2.4. Film dichroism

The preparation of the polyvinylalcohol films, the measurements and calculations of the dichroism were identical to those described by Houssier et al. [19].

2.5. Circular dichroism

The circular dichroism spectra were recorded on a Jasco ORD/CD/UV-5 instrument at constant dye concentration, using cells of path lengths of 1 or 2 cm. The results of fig. 1D and 1E are presented as the measured absorbance difference, $\Delta A = A_l - A_r$, for the left and right circularly polarized components of the incident light, divided by the total dye concentration, D.

2.6. Viscosity

The viscosity of the sonicated DNA-proflavine and dibutylproflavine complexes in 0.1 M NaCl were determined with an Ostwald viscometer of low gradient, at 25 °C. The experiments were performed at constant DNA concentration (0.02 mg ml^{-1}), by addition of microvolumes of a concentrated dye solution, directly in the viscometer. The results are presented according to the Cohen and Eisenberg representation, i.e., $([\eta]/[\eta]_0)^{1/3}$ [35].

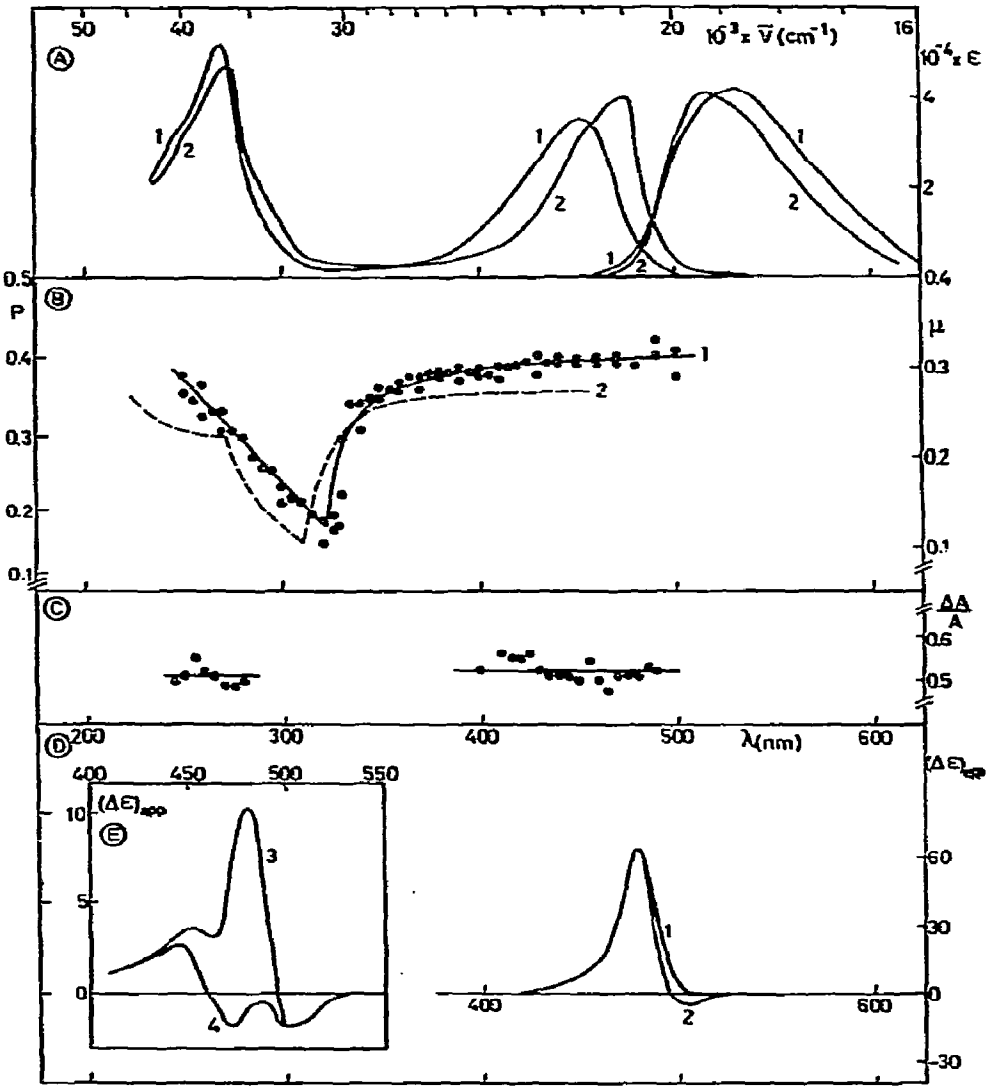


Fig. 1. Optical properties of dibutylproflavine and of its complexes with calf thymus DNA in 1 mM NaCl.

Part A: Absorption and fluorescence emission spectra. Curve 1: free dye; curve 2: bound dye ($P/D \approx 20$, at $D = 2.30 \times 10^{-5}$ M); the molar extinction coefficient, ϵ, is expressed in (M^{-1} cm^{-1}) units; the corrected fluorescence spectra have been normalized to the same arbitrary intensity at $\lambda_{em} = 520$ nm ($\lambda_{ex} = 477$ nm).

Part B: Fluorescence polarization spectra. Curve 1: dibutylproflavine in 90% (v/v) glycerol–water at $\lambda_{em} = 520$ nm; the results obtained by Weill and Calvin [38] with proflavine have been redrawn for comparison; p and μ denote the degree of polarization and the emission anisotropy, respectively, as defined in ref. [17].

Part C: Linear dichroism spectrum of a stretched polyvinylalcohol film dyed with dibutylproflavine. The reduced dichroism, $\Delta A/A$, is equal to the linear dichroism, $\Delta A = A_{\parallel} - A_{\perp}$, divided by the absorbance at random, calculated from $A = (A_{\parallel} + 2A_{\perp})/3$.

Part D and insert fig. E: circular dichroism spectra of the complexes with DNA. Curves 1 to 4 for P/D = 15.4, 8.8 (main fig.), 1.34 and 0.77 (insert fig.), respectively at $D = 2.30 \times 10^{-5}$ M. $(\Delta\epsilon)_{app}$ is defined in section 2.5. P/D is the mononucleotide to dye molar ratio.

2.7. Electric dichroism

The electro-optical measurements were performed by the technique previously described [17, 19, 36, 37]. For these experiments, we sonicated the macromolecular samples. Indeed, the native samples showed aggregation phenomena resulting in the formation of very viscous solutions which made the electro-optical measurements impossible. Sonication of DNA or nucleohistone (with a Mullard-60 W ultrasonic generator, during 10–15 min at 20 kHz, t below 10°C) does not modify their binding properties with respect to intercalative dyes [19, 37].

3. Results and discussion

3.1. Some electronic absorption properties of dibutylproflavine

Fig. 1 summarizes several optical properties of dibutylproflavine which may bring information about the assignment of the absorption bands and the polarization direction of their transition moments.

The fluorescence polarization spectrum of the dye in glycerol–water (90% v/v) is found very similar to that reported by Weill and Calvin [38] for proflavine and acridine orange (fig. 1B). It shows that the transition in the wavelength range of 310–320 nm has its moment nearly perpendicular to that of the first singlet–singlet transition absorbing in the region of 350 to 500 nm. Due to the important overlapping with the ultraviolet absorption band, the angle between these transitions cannot be estimated from the emission anisotropies, using eq. (2) of ref. [19]. As in the case of proflavine [39, 40], the main ultraviolet and visible transition moments are parallel and polarized along the long axis of the molecule, as evidenced by the film dichroism results (fig. 1C). The lower $\Delta A/A$ values compared to those reported for ethidium bromide [19] show a lower degree of orientation of the molecules by stretching. The measurements in the region of 300 to 400 nm were found very inaccurate because of the low molar extinction coefficient of dibutylproflavine in this wavelength range. We were unable to prepare films at higher dye concentration because of the too small quantities of dye available.

The fluorescence polarization spectra of dibutylproflavine bound to DNA or to nucleohistone (not shown in the figure) are similar in shape to that of the dye in glycerol (fig. 1B).

3.2. Binding parameters in 1 mM NaCl

Referring to the work of Müller et al. [27], dibutylproflavine binds to DNA at an ionic strength of 0.2 by two external processes, which have been distinguished by their thermal difference spectra and relaxation times in T-jump experiments (see insert fig. 5). The major binding process, denoted 2 by these authors and I by us by analogy with the intercalative process [18], has the slowest relaxation time and its binding parameters with poly[d(A–T)] have been characterized by a theoretical model with the exclusion of two adjacent base pairs. The existence of two processes has not been considered in the analysis of the binding curve at lower ionic strength (0.01 M phosphate buffer, pH 5.5) [33].

By working at low salt concentration, i.e., 1 mM NaCl, we expect the second binding process (process II) to become more important, if it is determined by electrostatic interactions. We shall calculate the binding parameters of both processes by different treatments of the spectrophotometric results, some of them having been previously described [18].

Typical spectra observed for the free (curve 1 with λ_{max} at 453 nm) and bound (curve 2 with λ_{max} at 472 nm and a shoulder around 450 nm) dibutylproflavine to DNA in 1 mM NaCl are shown in fig. 1A. At high P/D values, the differential spectra show positive (peak) and negative (trough) maxima at $\lambda = 477$ and 435 nm, respectively. The modification of shape of the bound-dye spectrum, already noticed by Müller et al. [27], was also well displayed in the apparent spectra of the complexes in 1 mM NaCl (not shown in the figure): in the region of 490–500 nm, the spectra for the intermediate P/D values (2 to 10) intercept the curve for $P/D = 100$. Such a behaviour was not observed at high ionic strength, i.e. 0.1 M NaCl. In both media, 0.1 and 0.001 M NaCl, no constant isosbestic point was observed, except at extremely high P/D values ($P/D > 50$).

The changes in the absorption coefficients at the wavelengths of maximum hypochromism ($\lambda = 435$ nm) and hyperchromism ($\lambda = 477$ nm) are quantitatively depicted in fig. 2, for the complexes with DNA and nucleohistone in 1 mM NaCl. The two representations adopted illustrate the method of Terada and Miyake [41]

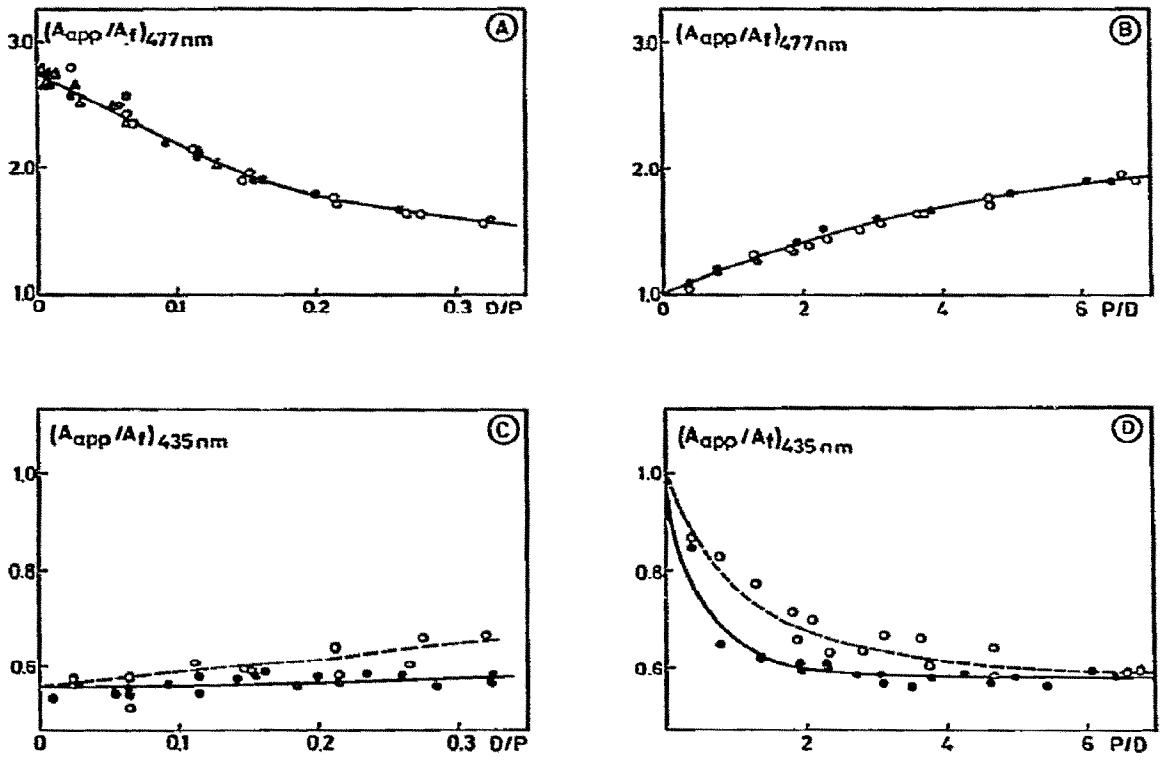


Fig. 2. Spectrophotometric titrations of the complexes of dibutylproflavine with DNA (filled symbols) and nucleohistone (open symbols) in 1 mM NaCl, at two different total dye concentrations: $D_1 = 2.30 \times 10^{-5}$ M (● and ○) and $D_2 = 1.41 \times 10^{-5}$ M (▲ and △).

The absorbances of the complex solutions, A_{app}, are divided by that of the dye alone, A_f, and plotted versus D/P (parts A and C) and P/D (parts B and D) at two wavelengths, $\lambda = 435$ and 477 nm, according to Terada and Miyake [41].

for the spectrophotometric determination of the binding parameters.

In the absence of an isosbestic point, the binding curves may be derived from spectrophotometric measurements assuming the existence of two bound species (I and II), the binding process of the second one being highly cooperative [37, 42–45]. The procedure however requires the determination of two limiting spectra: the spectrum of species I, predominant at high P/D ratios and obtained by an extrapolation method at infinite macromolecular concentration, as previously discussed [18], while that of species II is determined by the extrapolation to $D^{-1} = 0$ of the plot of ϵ_{app} versus D^{-1}, at a given low P/D value [42–44]. The results for the complexes with DNA are given in table 1. The spectrum of species II appears intermediate between that of species I and that of the free dye at high wavelengths, with a maximum around 460 nm, and very similar to that of species I at short wavelengths (not shown in the figure, but clearly depicted by the results at $\lambda = 435$ and 477 nm of table 1).

Table 1
Molar extinction coefficients ($\times 10^{-3}$ M^{-1} cm^{-1}) of free (f) dibutylproflavine and bound (b) species I and II to calf thymus DNA in 1 mM NaCl. ϵ_b^I and ϵ_b^{II} were determined according to Bontemps and Fredericq [18] and Schwarz et al. [43, 44], respectively

λ(nm)	ϵ_f	ϵ_b^{II}	ϵ_b^I
435	27.9	15.2	15.4
453	34.9	–	–
460	–	23.5	–
477	13.7	21.0	37.7

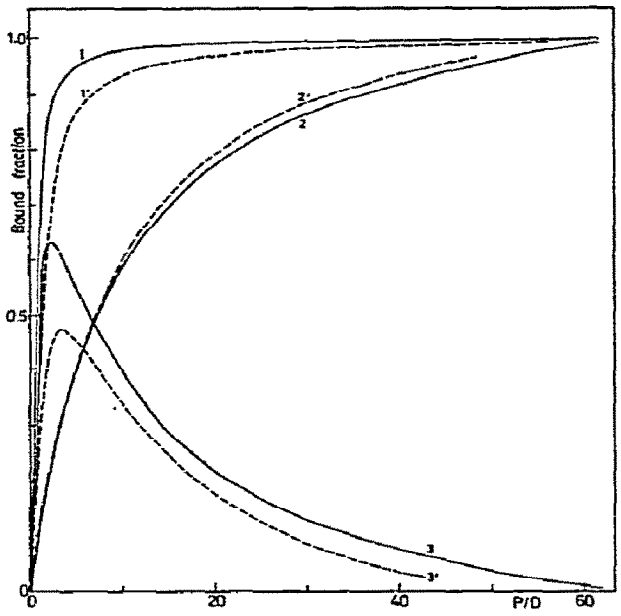


Fig. 3. Binding curves of dibutylproflavine complexes with DNA (filled curves) and nucleohistone (dashed curves) in 1 mM NaCl, at a constant total dye concentration equal to 2.30×10^{-5} M.

The curves 1, 2 and 3 refer to the total bound fraction, $(1-\alpha)_{tot}$, and to the bound fractions relative to processes I, $(1-\alpha)_I$, and II, $(1-\alpha)_{II}$, respectively.

Instead of using the property of some isosbestic points, as described by Dourlent and Helene [45], the calculations of the bound fractions were realized by working at two wavelengths ($\lambda = 435$ and 477 nm), using relationships similar to those presented by the latter authors. The binding parameters of process I were determined in this way (table 2b): a linear Scatchard plot was observed for P/D values ranging from 100 to 10, at $D = 2.30 \times 10^{-5}$ M. The binding curves, at D constant, relative to this process are presented in fig. 3: curves 2 and 2' for DNA and nucleohistone respectively. Below $P/D = 10$, the calculations yielded values of the bound fraction, $(1-\alpha)_I$, lower than those expected from the Langmuir isotherm determined from the results at high P/D values. These discrepancies of the method may possibly result from the existence of a third bound species.

The similarity of the values of ϵ_b^I and ϵ_b^{II} at $\lambda = 435$ nm allows a simple estimation of the whole binding curve, using the method of Terada and Miyake [41]. This treatment yields the binding parameters, K and N, relative to the sum of processes I and II (table 2a). These complete binding curves are marked 1 and 1' in fig. 3 for DNA and nucleohistone, respectively. The curves 3 and 3', relative to species II, were then calculated by simple difference: $(1-\alpha)_{II} = (1-\alpha)_{tot} - (1-\alpha)_I$. They present a maximum at low P/D values.

Table 2
Binding parameters of the complexes of dibutylproflavine with calf thymus DNA and nucleohistone in 1 mM NaCl, derived from spectrophotometric experiments. The binding constants are expressed in (10^{-5} M^{-1}) units

Process	DNA	Nucleohistone
a. Whole process	$K = 2.1$ $N = 1.0$	$K = 1.1$ $N = 0.67$
b. Process I	$k_I = 22$ $n_I = 0.11$	$k_I = 7.7$ $n_I = 0.11$
c. Process II (at large r_{II} values)	$k_{II} = 2.3$ $n_{II} = 0.89$	$k_{II} = 1.3$ $n_{II} = 0.56$

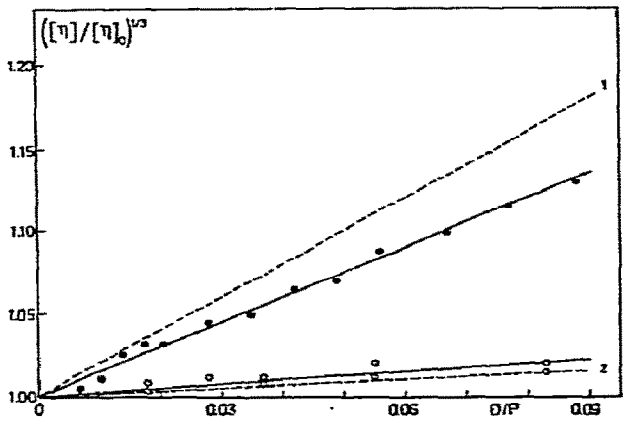


Fig. 4. Variation of $([\eta]/[\eta]_0)^{1/3}$ as a function of D/P for the complexes of dibutylproflavine (o) and proflavine (•) with sonicated DNA in 0.1 M NaCl at 25°C (see section 2.6). Line 1 illustrates the theoretical dependence of the contour length with r assuming that the intercalation of each dye molecule increases the length of the DNA helix of 3.4 A; line 2: results obtained by Festy et al. [48] with hydroxystilbamidine.

The values of K and N are related to those of the components by:

$$N = n_I + n_{II}, \quad (1)$$

$$K = k_I k_{II}/(k_I + k_{II}), \quad (2)$$

valid if the two constitutive Langmuir processes are characterized by similar binding constants, k_I and k_{II}.

Thus, the parameters k_{II} and n_{II} may be easily determined using the values of k_I and n_I listed in table 2b. This quantitative approach of process II is only valid at high r_{II} values ($r_{II} > 0.2$–0.3). Indeed, the Scatchard plots relative to the curves 3 and 3′ of fig. 4 for DNA and nucleohistone, present maxima around $r_{II} = 0.1$–0.2.

Our value of $n_I = 0.11$, obtained for the complexes with DNA and nucleohistone in 1 mM NaCl, is in perfect agreement with that reported by Dalgleish et al. [33] for DNA at a 0.01 ionic strength ($n = 0.113$). When comparing our spectrophotometric determination with the Scatchard plot derived by the equilibrium dialysis method, the value of $n_I = 0.11$ corresponds to the extrapolation at $r/m = 0$ of the "hysterisis" branch of the isotherms presented by Müller et al. [27]. This may be due to the mode of preparation of the complexes we have used: an aliquot of a concentrated dye solution was added to the saline solution containing the macromolecule at variable concentration. Consequently, the binding degree, r, is great in the upper part of the tube and is then reduced by mixing.

3.3. Viscosity of the complexes in 0.1 M NaCl

Since the hydrodynamic properties of DNA are not modified by the external binding process (process II) of dyes such as proflavine and acridine orange [15, 46, 47], we have measured the variation of the viscosity of DNA upon binding of dibutylproflavine in 0.1 M NaCl, i.e., at a salt concentration where process I is supposed to be preponderant, and compared the results to those obtained with proflavine.

As seen in fig. 4, dibutylproflavine weakly enhances the intrinsic viscosity of DNA, to a similar extent as hydroxystilbamidine (line 2), which is believed not to be intercalated [48].

The slope obtained in the Cohen–Eisenberg representation is 0.3 ± 0.1 for dibutylproflavine, as compared to 1.52 ± 0.07 for proflavine. Precipitates in the viscometer were observed with dibutylproflavine at D/P values higher than 0.09.

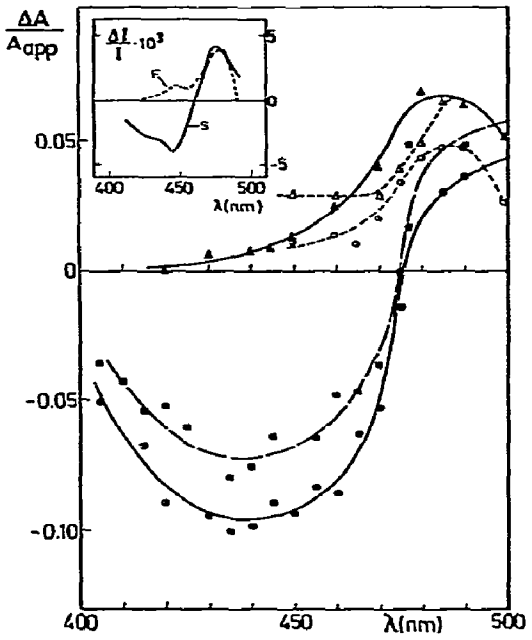


Fig. 5. Main fig.: Apparent linear dichroism spectra of the complexes of dibutylproflavine with sonicated DNA (•, ▪ and ▲ for $P/D \approx 20$, 10 and 2, respectively) and sonicated nucleohistone (0 and △ for $P/D \approx 20$ and 2, respectively), at $D = 2.30 \times 10^{-5}$ M. Pulses of 0.1 ms duration, at a field strength of 13 kV cm^{-1}, were applied to the solutions.

Insert fig.: Thermal difference spectra obtained by Müller et al. [27] with calf thymus DNA, in a phosphate-saline buffer at pH 7.0 (0.2 ionic strength). F and S refer to the fast and slow relaxation. Binding ratio, $r = 0.025$.

3.4. Electric dichroism and birefringence

3.4.1. Reduced electric dichroism spectra

As a first step of this study, we have measured the reduced electric dichroism spectrum in the main visible band of the complexes of the dye with DNA and nucleohistone, at various P/D values, using electric pulses of 0.1–0.2 ms (fig. 5).

Complexes with DNA. At high P/D ratios (20 and 10), i.e., when process I is the most important (see curve 2 of fig. 3), the apparent reduced dichroism spectra, $\Delta A/A_{app}$ versus λ (where A_{app} refers to the absorbance of the complex solution), present two distinctive regions differing in sign and magnitude: a region of negative dichroism (with a maximum around 440 nm) centered

on the short wavelength side of the absorption band of the dye (fig. 1A) and a region of low positive dichroism situated on the long wavelength side of the band.

At a low P/D value ($P/D \approx 2$), i.e., as $(1-\alpha)_{II}$ reaches its maximum value (see curve 3 of fig. 3), only low positive values are observed: the apparent maximum is located in the region of 480 to 490 nm. This spectral region also showed particularities in the absorption spectra.

These two types of spectrum may be compared to the thermal differential spectra reported by Müller et al. [27] and redrawn in the insert fig. 5. The comparison suggests that the positive dichroism values correspond to process II (faster relaxation time: F), while the negative values are generated by the molecules bound by process I (slower relaxation times: S), both species being characterized by a different position of their absorption spectrum. Moreover, this important similarity led us to think that a dichroism effect due to the orientation of the particles in the field used for the T-jump experiments, could have been actually measured by Müller et al. Indeed, for very low dichroism values, the reduced dichroism, $\Delta A/A$, is proportional to the change of light intensity, $\Delta I/I$ [49]. In this case, the relaxation time, τ_2, would be that relative to the relaxation of the DNA molecule and this would explain why its value is similar to that obtained by the study of the decay of the birefringence.

Complexes with nucleohistone. Similar experiments were carried out with nucleohistone: only positive values ranging from 0.01 to 0.06 were measured in the region of 450 to 490 nm, for $P/D = 20$ and 2.

The reduced dichroism values measured here are nearly an order of magnitude lower compared to the negative values (−0.5 to −0.6) observed by the same method with intercalative dyes [17, 19, 28, 36, 37]. It should be noticed that Müller et al. [27] did not observe any sharp dichroism effect on fibers of the DNA–dibutylproflavine complexes.

We also made the following observations. The presence of dibutylproflavine does not prevent the intercalation of acridine orange and does not modify the electro-optical properties of DNA (birefringence and relaxation) (table 3). The constancy of the relaxation times (table 3b) is in perfect agreement with the low increase of the intrinsic viscosity (fig. 4). The measurements of the birefringence of the complexes clearly demonstrate that the orientation of the dibutylproflavine–DNA complexes is similar to that of the macromolecule alone.

Table 3

Part a: Reduced dichroism of an acridine orange–DNA complex in 1 mM NaCl in the presence of dibutylproflavine. The value given in parentheses was calculated by replacing A_{app} by the absorbance of the complex with acridine orange alone. Field strength: 13 kV cm^{-1}, pulse duration: 0.1 ms

Dye	D(×10^5 M)	P/D	$(\Delta A/A_{app})_{510\,nm}$
Dibutylproflavine	2.3	9.9	≈0
Acridine orange	1.9	12	−0.54
Both dyes	2.3 and 1.9	≈10	−0.48 (−0.56)

Part b: Electro-optical properties of DNA (concentration: 25 mg dl^{-1}) in the presence of increasing amounts of dibutylproflavine. Field strength: 13 kV cm^{-1}, pulse duration: 0.5 ms. The birefringence was measured at λ = 550 nm

P/D	Birefringence (× 10^7)	Mean relaxation time (μs)
0	−10.0 ± 0.3	21 ± 2
50	−9.6 ± 0.4	18 ± 2
20	−9.7 ± 0.3	19 ± 1
10	−9.7 ± 0.3	17 ± 3

3.4.2. Dependence of the reduced dichroism upon the extent of binding

The dependence of the reduced dichroism value upon the macromolecular concentration was examined in a series of experiments at constant total dye concentration, and at three wavelengths (λ = 435, 477 and 490 nm in fig. 6).

At all three wavelengths, for the complexes with DNA (fig. 6A) and nucleohistone (fig. 6B), the shape of the curves was similar. Some reversals of sign are observed: from negative to positive values as the binding increases, at high P/D values (40 and 30 for DNA and nucleohistone at λ = 477 and 435 nm, respectively) or at low P/D value (3 for DNA at λ = 435 nm). Compared to fig. 5, small negative dichroism values are observed at λ = 435 nm for the complexes with nucleohistone, but for larger P/D values.

The shape of these curves agrees with the above de-

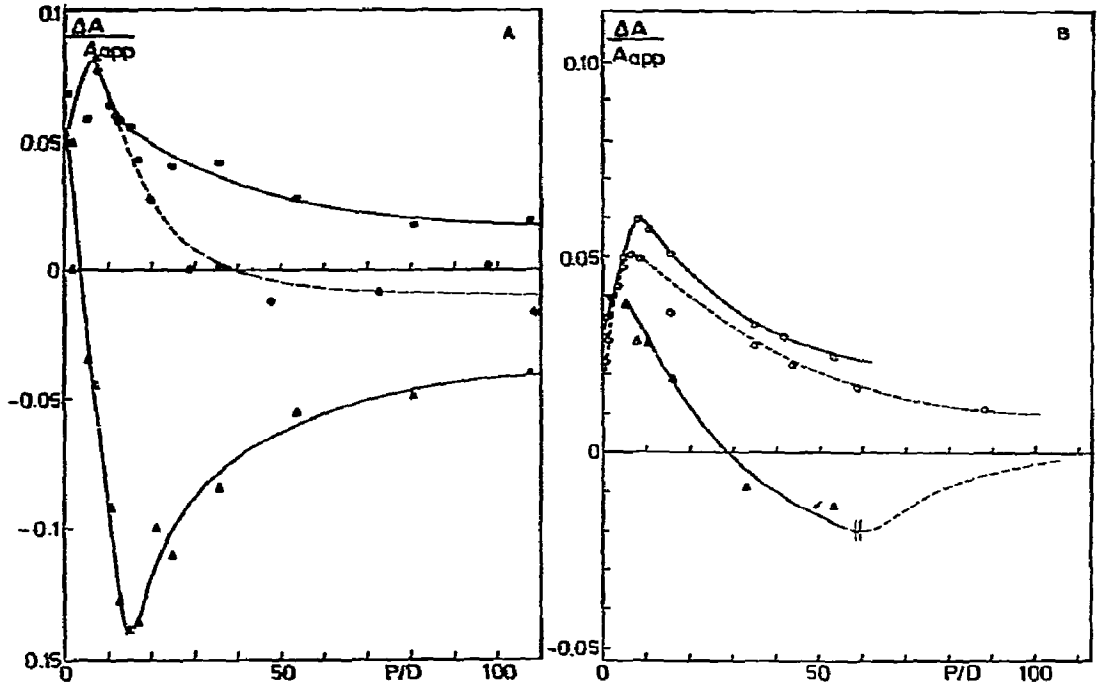


Fig. 6. Apparent linear dichroism as a function of P/D, at $D = 2.30 \times 10^{-5}$ M, of the complexes of dibutylproflavine with sonicated DNA (filled symbols, part A), and sonicated nucleohistone (open symbols, part B) at different wavelengths: $\lambda = 435$ (▲,△), 477 (◆,◇) and 490 (■,□) nm. Same experimental conditions as in fig. 5.

termination of the binding parameters (fig. 3) assuming negative values of the reduced dichroism for bound species I and positive ones for bound species II. If we consider that the reduced dichroism values observed in the case of the intercalative dyes (−0.5 to −0.6) correspond to an orientation of the long axis of these dye molecules perfectly parallel to the DNA base pairs, the observed values with dibutylproflavine correspond to angles of 60–70° and below 50° for processes I and II, respectively. These values have to be compared to the inclination of the DNA grooves, which is found equal to 57° taking 33.6 Å for the pitch and 20 Å for the diameter of the double helix. In the complexes with nucleohistone, bound species I forms a lower angle compared to the complexes with DNA, while species II is similarly orientated. The differences observed in the orientation of species I in the two macromolecules could simply reflect the distortion of the DNA helical conformation by the histones or a direct influence of these proteins on the binding site of the dye.

3.5. *Induced circular dichroism*

In agreement with Dalgleish et al. [33], the free dye did not show any optical activity in any of its ultraviolet or visible bands. When fully bound to DNA, i.e., $(1-\alpha)_{tot}$ higher than 0.97, dibutylproflavine showed the typical circular dichroism spectrum displayed in fig. 1D (curve 1), with a maximum at $\lambda = 477$ nm, corresponding to the peak of the differential spectra (section 3.2). The positive signal presents a less asymmetrical shape than its corresponding absorption band (fig. 1A). For P/D values higher than 20, at $D = 2.30 \times 10^{-5}$ M, an isoelliptic point was observed in the region of 460 nm. Its position differs by about 10 nm from the value reported by Dalgleish et al. [33]. This isoelliptic point disappeared as P/D decreased and important modifications of the shape of the spectrum were observed.

Below $P/D \approx 10$ (curve 2), a negative contribution centered at 500–510 nm is present without strongly affecting the magnitude and the shape of the main posi-

tive band. This negative band has its maximum amplitude at low *P/D* values (curves 3 and 4 in insert fig. 1E). If these results are compared to those described in the previous sections 3.2 and 3.4 for the same spectral range, we can attribute this negative band to species II. The high amplitude of the positive band at 480 nm possibly masks a lower positive contribution below 490 nm. In a 0.01 M phosphate buffer at pH 5.5, the positive band at 500–510 nm was previously detected at a value of *r* equal to 0.074 [33].

For *P/D* values lower than 5, the shorter wavelength side of the circular dichroism spectrum presents a shoulder, then a maximum in the region of 450 nm (curve 3). As *P/D* is still decreased, this part of the spectrum displays an "excitonic" shape with a zero value at $\lambda = 460$ nm (curve 4). At this moment, it must be noticed that the amplitude of the signals is considerably reduced, so that the peaks at $\lambda = 445$, 470, 500–510 nm were too low for accurate measurements. The excitonic band could result from stacked molecules of process III, which do not contribute to the electric dichroism.

The results of the calculations in terms of the molar dichroism of the total bound dye, $(\Delta\epsilon_b)_{tot}$ are given in fig. 7A for the measurements at $\lambda = 477$ nm. In this figure, only the free dye contribution has been subtracted: $(\Delta\epsilon_b)_{tot}$ is plotted as a function of the whole binding ratio, $r_{tot} = r_I + r_{II}$. For the two macromolecules, as r_{tot} goes to zero, the curves are practically identical and seem to extrapolate on the $\Delta\epsilon_b$-axis at a value different from zero, which was also observed for the complexes with DNA at higher ionic strength [33].

In order to determine the mechanism responsible for the variation of the optical activity with the degree of binding, we have first assumed that the band attributed to process II, at $\lambda = 500$–510 nm, does not contribute to the measurements at $\lambda = 477$ nm. Consequently, it is possible to relate the optical activity to the degree of binding of the first bound species (fig. 7B). In this way, our results with DNA in 1 mM NaCl (filled circles) satisfactorily agree, except at low binding, with those reported by Dalgleish et al. [33] in a 0.01 M phosphate buffer, at pH 5.5 (dashed curve). A similar negligible effect of the ionic strength has already been reported for ethidium bromide–DNA complexes (positive band at $\lambda = 308$ nm) [19].

The shape of the curves of fig. 7B cannot be explained by simple mechanisms including a single bound

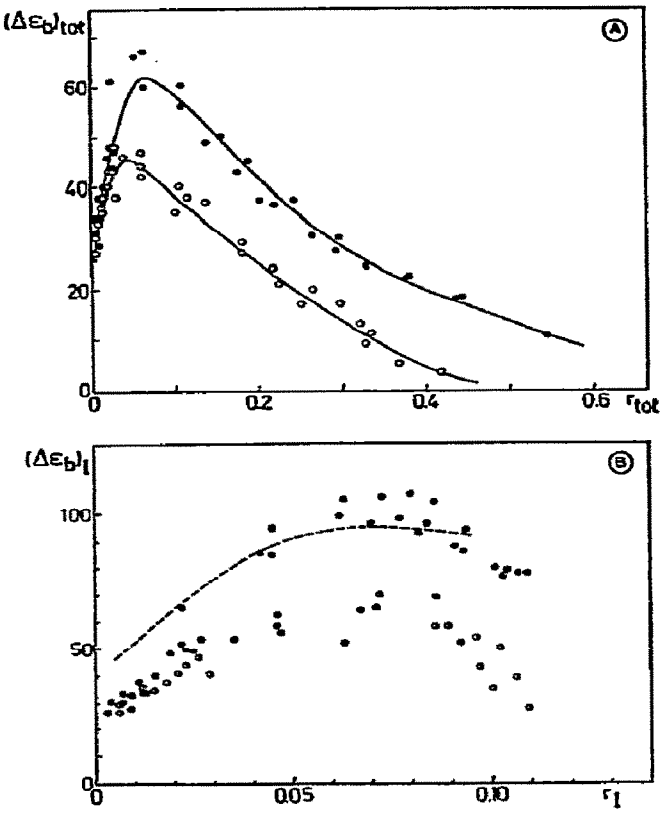


Fig. 7. Circular dichroism of bound dibutylproflavine in the main visible transition ($\lambda = 477$ nm) as a function of the binding degree of the whole process, r_{tot}, (part A) and of process I, r_I (part B). Filled and open symbols refer to DNA and nucleohistone, respectively. The dashed curve was taken from Dalgleish et al. [33], at an ionic strength of 0.01 M.

species, for instance an r_I^2 dependence, resulting from non-degenerated exciton interactions between the transition moments of dye molecules bound in neighbouring sites. However, such interactions could occur between the bound molecules of two different processes, and consequently should vary linearly with $(1-\alpha)_I(1-\alpha)_{II}$, the product of the bound fractions, available from section 2.2. This is indeed observed (fig. 8) for the complexes with DNA, as well as with nucleohistone.

3.6. Fluorescence quantum yield and anisotropy

First, let us consider the fluorescence parameters of the first bound molecule (extrapolation to *D/P* or *r* equal to zero), i.e. $(\phi_{app}/\phi_f)_{lim.}$ and μ_{app}^{lim}, according to

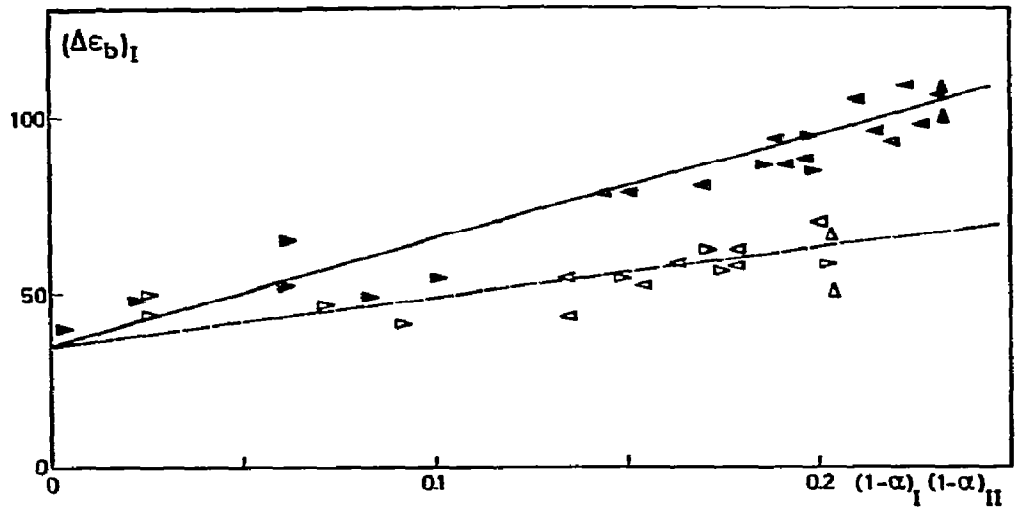


Fig. 8. Non-degenerated exciton interactions at $\lambda = 477$ nm between the bound molecules of both processes for the complexes of DNA (filled symbols) and nucleohistone (open symbols) in 1 mM NaCl. The quantity $(1-\alpha)_I\,(1-\alpha)_{II}$ was calculated from the binding results of fig. 3 and table 2. The orientation of the triangles refer to the rising part (▷), the maximum (△) and the decreasing part (◁) of the curves of $(\Delta\epsilon)_{b,I}$ or $(1-\alpha)_I(1-\alpha)_{II}$ versus r_I.

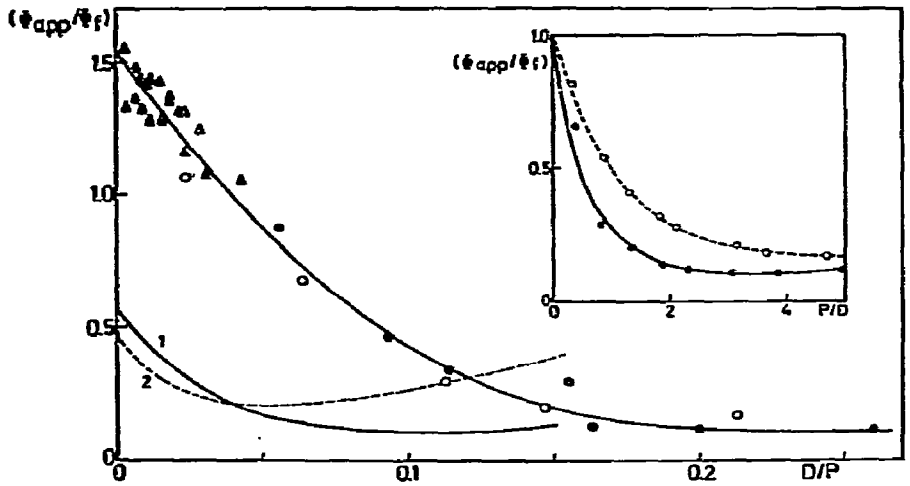


Fig. 9. Dependence of (ϕ_{app}/ϕ_f) upon D/P (main fig.) and P/D (insert fig.) for the complexes of dibutylproflavine with DNA (• and ▲ for $D = 2.30$ and 1.41×10^{-5} M, respectively), and nucleohistone (○ and △) in 1 mM NaCl, at $\lambda_{ex} = 477$ nm and $\lambda_{em} = 520$ nm. The comparison with the proflavine–DNA and proflavine–nucleohistone complexes in the same medium is given by curves 1 and 2, at $\lambda_{ex} = 453$ nm, $\lambda_{em} = 510$ nm and $D = 1.0 \times 10^{-5}$ M.

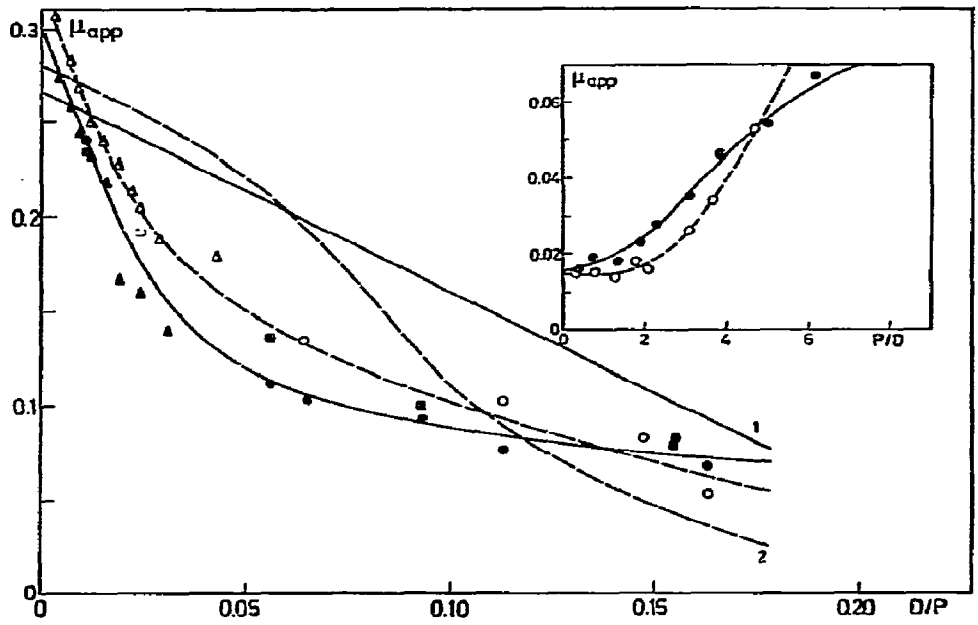


Fig. 10. Dependence of μ_{app} upon D/P (main fig.) and P/D (insert fig.) for the complexes of dibutylproflavine with DNA and nucleohistone compared to proflavine in 1 mM NaCl. Same symbols and experimental conditions as in fig. 9 except for ▪: dibutylproflavine–DNA complexes in 0.1 M NaCl.

our previous notations [18] (figs. 9 and 10, table 4).

Upon binding to calf thymus DNA or nucleohistone, the quantum yield of dibutylproflavine is increased by a factor 1.5, while that of proflavine is reduced. For the latter dye, the quenching is more important when the dye is bound to nucleohistone (curve 2 below curve 1 at low D/P in fig. 9). An enhancement of the dibutylproflavine fluorescence was also observed with M. luteus and Cl. perfringens DNA, the effect being proportional to the A–T content [27]. However, the magnitude of the dependence of the quantum yield on the base composition of DNA appears much lower than that reported for proflavine, acriflavine or quinacrine (earlier works listed in refs. [18] and [25]).

Table 4
Comparison between the fluorescence properties of the first bound dibutylproflavine and proflavine molecule on calf thymus DNA and nucleohistone. The experimental conditions are given in section 2.3

	DNA		Nucleohistone	
Dye	$(\phi_{app}/\phi_f)_{lim}$	μ_{app}^{lim}	$(\phi_{app}/\phi_f)_{lim}$	μ_{app}^{lim}
Dibutylproflavine	1.5	0.300	1.5	0.330
Proflavine	0.5 – 0.6	0.265	0.4 – 0.5	0.280

As regards the limiting value of the anisotropy, proflavine and its dibutyl derivative behave similarly. The high value of this fluorescence parameter indicates that the first dibutylproflavine molecules are as rigidly bound to the macromolecule as the first intercalated proflavine molecules are. A higher value of μ_{app}^{lim} is observed in nucleohistone compared to DNA, the interpretation of which has been previously reported [18, 50]. On a given macromolecule, μ_{app}^{lim} is somewhat higher with dibutylproflavine than with proflavine, but the difference is comparable in magnitude to that measured in glycerol (fig. 1B).

The variation of (ϕ_{app}/ϕ_f) as D/P increases is found identical for DNA and nucleohistone in the range of D/P values up to 0.15 (main fig. 9), but different at high binding ratios (insert, fig. 9). The latter behaviour simply reflects the difference in free-dye concentration for the two macromolecules at the same P/D value. The

reduction of fluorescence intensity as the binding increases could not be explained by a dimerization reaction of the bound dye, as shown in the case of acridine orange [17]. Indeed, the calculation of a dimerization constant was found impossible. The quenching process appeared always more efficient than that predicted by (i) nearest neighbour interactions between bound molecules of process I [8] or (ii) between molecules of both processes [19]. Consequently, in addition to mechanisms (i) and (ii), we must consider a heterogeneity of the fluorescence response with the base composition of the binding sites. Due to the high specificity of this dye for the A–T base pairs [27], it is likely that the A–T-rich regions of calf thymus DNA are first occupied at low r_I values, and that the base composition of the following strong binding sites is richer in G–C base pairs.

With increasing binding, the depolarization from the limiting value is more rapid with dibutylproflavine compared to proflavine (main fig. 10). We attribute these differences to the lower degree of organization of the fluorescent molecules of process I with dibutylproflavine, which increases the rate of transfer depolarization, in addition to the depolarization resulting from the reduction of quantum yield.

4. General discussion

4.1. Complexes with DNA

Confirming the results of Müller et al. [27] at high ionic strength, the complexes of dibutylproflavine with DNA at low ionic strength may be described by the existence of, at least, two binding processes differing in binding constant by an order of magnitude ($k_I/k_{II} \approx 9.6$). Both processes differentiate by their physicochemical properties: the absorption and the electric dichroism measurements (sections 3.2 and 3.4) show an additivity of contributions, while the fluorescence and circular dichroism studies (sections 3.5 and 3.6) bring evidence of interaction between the different bound species.

4.1.1. Process I

The stronger process follows a Langmuir-type binding isotherm, characterized by $k_I = 22 \times 10^5\ M^{-1}$ and $n_I = 0.11$. An interpretation of this relatively low number of binding sites has been proposed by Müller et al. [27]: the binding of a dibutylproflavine molecule excludes two adjacent binding sites and requires the presence of, at least, one A–T base pair. This important base-specificity has been recently confirmed by staining experiments of chromosome regions of known composition [31].

The optical properties of the first bound molecule may be summarized and interpreted as follows:

(i) The main visible absorption band is red-shifted by about $0.9 \times 10^3\ cm^{-1}$ and the fluorescence quantum yield is slightly enhanced. The former change is typically observed with the intercalative dyes, while the latter occurs with only some of them, such as ethidium bromide and acridine orange [5, 17, 18, 25, 38]. However, a non-intercalating molecule, pinacyanol, also displays an important red shift in the presence of calf thymus DNA [51]. A common interpretation for these observations has been suggested by Löber et al. [52]: the change of the hydrated state of the dye molecule is sufficient to explain the spectral effects.

(ii) The bound molecules present a high fluorescence anisotropy and an intrinsic optical activity (main positive band in the region of 480 nm). This indicates that the bound chromophores are rigidly hold in an asymmetric arrangement, which implies a close proximity with the DNA hydrophobic regions.

(iii) The long axis of the dibutylproflavine molecule is orientated at a mean angle of 60–70° with respect to the molecular axis of DNA, which is close to the inclination of the sugar-phosphate backbone.

As the binding increases, some of these optical properties are modified, mainly by interactions with the molecules of process II (fluorescence parameters and circular dichroism), while the conformation of DNA is practically unaffected, as revealed by the measurements of intrinsic viscosity, electric birefringence and relaxation times.

An "external" model of interaction with the insertion of the dye into the major groove of DNA is thought to take into account all the above observations.

4.1.2. Process II

This process is characterized by a high cooperativity, comparable to that detected by the same spectrophotometric approach with proflavine [37, 42–45]. It contains a high number of available binding sites ($n_{II} \approx 0.89$) which approaches the number of phosphate groups. This complex seems to be mainly stabilized by attractive

forces between the bound molecules themselves, since it was also formed at higher ionic strength [27, 33].

It has the following optical and electro-optical properties:

(i) An absorption spectrum with a maximum at λ = 460 nm, which manifests in the tail of the apparent spectra of the complexes at low *P/D* values (λ above 490 nm).

(ii) A negative band in circular dichroism, centered around 500–510 nm.

(iii) A positive electric reduced dichroism.

(iv) A cancelled fluorescence quantum yield.

While the absorption and the electric dichroism properties of species II contribute by simple additivity to the measurements, these bound molecules seem to interact strongly with the firstly bound molecules of process I, as revealed by the analysis of the dependence of the fluorescence intensity and of the circular dichroism signals of species I on the degree of binding.

These molecules are orientated at a mean angle of 50° with respect to the DNA axis. This value only differs by about 10 to 20° from that estimated for species I, so that one could imagine that a stacking of the molecules (species II) occurs next to the bound species I. These considerations predict the same base-specificity for both binding processes.

These results confirm by a different approach a general mechanism involved in dye-nucleic acids complexes, previously evidenced from binding and fluorescence studies [18], i.e., the spatial proximity of the different kinds of binding sites.

4.2. Complexes with nucleohistone

By comparing the binding results obtained with DNA and nucleohistone at the same ionic strength, it appears that the presence of histones mainly lowers the binding strength of process I ($k_{I,nucl.}/k_{I,DNA} = 0.35$), without affecting the number of primary binding sites, while both parameters of process II are similarly reduced in the nucleoprotein ($k_{II,nucl.}/k_{II,DNA} = 0.57$ and $n_{II,nucl.}/n_{II,DNA} = 0.63$). General discussions of this problem have been recently published [18, 53]. In the case of the base-specific dyes, such as actinomycin D [26] and dibutylproflavine [27], we must add that a part of the modification of the binding parameters could be due to a difference of base composition of the accessible part of DNA in nucleohistone, which is thought to be richer in G–C base pairs than the constitutive DNA [18, 54].

As regards the optical properties (absorption, fluorescence intensity and induced Cotton effect) of the first bound molecules of process I, as well as their variations with increasing r_I, they are found identical to those observed with DNA, except for the limiting value of the emission anisotropy and for the absolute value of the electric reduced dichroism. The first binding sites of the dye in nucleohistone are thus found structurally different compared to DNA, i.e., the reactive DNA in nucleohistone is probably structurally altered, in agreement, for instance, with a superhelical distortion.

No distinctive properties of the process II appear in nucleohistone compared to DNA.

Acknowledgement

This work was supported jointly by the Institut pour l'Encouragement de la Recherche Scientifique dans l'Industrie et l'Agriculture and by the Fonds de la Recherche Fondamentale Collective. The authors thank Miss. J. Linet for her excellent technical assistance and Mr. X. Emonds-Alt for carrying out some of the electro-optical measurements.

References

[1] A.R. Peacocke and J.N.H. Skerrett, Trans. Faraday Soc. 67 (1956) 261.
[2] R.V. Tubbs, W.E.Ditmars and Q. Van Winkle, J. Mol. Biol. 9 (1964) 545.
[3] M.J. Waring, J. Mol. Biol. 13 (1965) 269.
[4] G. Weill, Biopolymers 3 (1965) 567.
[5] J.B. LePecq and C. Paoletti, J. Mol. Biol. 27 (1967) 87.
[6] L.M. Chan and Q. Van Winkle, J. Mol. Biol. 40 (1969) 491.
[7] S.N. Cohen and K.L. Yielding, J. Biol. Chem. 240 (1965) 3123.
[8] N.F. Ellerton and I. Isenberg, Biopolymers 8 (1969) 769.
[9] J.C. Thomes, G. Weill and M. Daune, Biopolymers 8 (1969) 647.
[10] R. Bidet and J. Chambron, Ann. Phys. Biol. Med. 1 (1970) 1.
[11] L.M. Chan and J.A. McCarter, Biochim. Biophys. Acta 204 (1970) 252.
[12] R. Bidet, J. Chambron and G. Weill, Biopolymers 10 (1971) 225.
[13] U. Pachmann and R. Rigler, Exp. Cell Res. 72 (1972) 602.
[14] D.M. Crothers, Biopolymers 6 (1968) 575.

[15] R.W. Armstrong, T. Kurucsev and U.P. Strauss, J. Amer. Chem. Soc. 92 (1970) 3174.
[16] W. Bauer and J. Vinograd, J. Mol. Biol. 47 (1970) 419.
[17] E. Fredericq and C. Houssier, Biopolymers 11 (1972) 2281.
[18] J. Bontemps and E. Fredericq, Biophys. Chem. 2 (1974) 1.
[19] C. Houssier, B. Hardly and E. Fredericq, Biopolymers 13 (1974) 1141.
[20] N.B. Kurnick and I.E. Radcliffe, J. Lab. Clin. Med. 60 (1962) 669.
[21] D.S. Drummond, V.F.W. Simpson-Gildemeister and A.R. Peacocke, Biopolymers 3 (1965) 135.
[22] C.M. Lee, C.T. Chang and J.G. Wetmur, Biopolymers 12 (1973) 1099.
[23] J. Ramstein and M. Leng, Biochim. Biophys. Acta 281 (1972) 18.
[24] N. Weisblum and P.L. De Haseth, Proc. Nat. Acad. Sci. U.S. 69 (1972) 629.
[25] J.P. Schreiber and M.P. Daune, J. Mol. Biol. 83 (1974) 487.
[26] W. Müller and D.M. Crothers, J. Mol. Biol. 35 (1968) 251.
[27] W. Müller, D.M. Crothers and M.J. Waring, Eur. J. Biochem. 39 (1973) 223.
[28] M. Gellert, C.E. Smith, D. Neville and G. Felsenfeld, J. Mol. Biol. 11 (1965) 445.
[29] T. Caspersson, L. Zech, E.J. Modest, G.E. Foley, U. Wagh, and E. Simonsson, Exp. Cell Res. 58 (1968) 128.
[30] Chromosome identification, Proc. Nobel Symp. 23, eds. T. Caspersson and L. Zech (Academic Press, New York, and Nobel Foundation, Stockholm, 1973).
[31] C. Distèche and J. Bontemps, I.R.C.S. (International Research Communication System) 2 (1974) 1376; Chromosoma (Berlin) 47 (1974) 263.
[32] W. Müller and D.M. Crothers, Studia Biophysica 24 (1970) 279.
[33] D.G. Dalgleish, M.C. Fey and A.R. Peacocke, Biopolymers 11 (1972) 2415.
[34] E. Fredericq, Biochim. Biophys. Acta 55 (1962) 300.
[35] G. Cohen and H. Eisenberg, Biopolymers 4 (1966) 429.
[36] C. Houssier and E. Fredericq, Biochim. Biophys. Acta 120 (1966) 113.
[37] J. Ramstein, C. Houssier and M. Leng, Biochim. Biophys. Acta 335 (1973) 54.
[38] G. Weill and M. Calvin, Biopolymers 1 (1963) 401.
[39] V. Zanker, Z. Physik. Chem. (Frankfurt) 2 (1954) 52.
[40] L.I. Ingrahm and H. Johansen, Arch. Biochem. Biophys. 132 (1969) 205.
[41] H. Terada and K. Miyake, Kolloïd-Z.Z. Polym. 251 (1973) 139.
[42] G.Schwarz, Eur. J. Biochem. 12 (1970) 442.
[43] G. Schwarz, K. Klose and W. Balthasar, Eur. J. Biochem. 12 (1970) 454.
[44] G. Schwarz and W. Balthasar, Eur. J. Biochem. 12 (1970) 461.
[45] M. Dourlent and C. Hélène, Eur. J. Biochem. 23 (1971) 86.
[46] G. Cohen and H. Eisenberg, Biopolymers 8 (1969) 45.
[47] D.E.V. Schmechel and D.M. Crothers, Biopolymers 10 (1971) 465.
[48] B. Festy, J. Poisson and C. Paoletti, FEBS Letters 17 (1971) 321.
[49] K. Sauer and M. Calvin, J. Mol. Biol. 4 (1962) 451.
[50] L.M. Angerer, S. Georghiou and E.N. Moudrianakis, Biochemistry 13 (1974) 321.
[51] M. Kodama, Y. Takashira and C. Nagata, Biochim. Biophys. Acta 129 (1966) 638.
[52] G. Löber, H. Schütz and V. Kleinwächter, Biopolymers 11 (1972) 2439.
[53] P.F. Lurquin, Chem.-Biol. Interactions 8 (1974) 303.
[54] E.F. Minyat, O.F. Borisova, M.V. Vol'kenstein and G.P. Georgiev, Molekulyarnaya Biologiya (English Transl.) 4 (1970) 291–301.
[55] D.G. Dalgleish, E. Dingsøyr and A.R. Peacocke, Biopolymers 12 (1973) 445.

BIOPHYSICAL CHEMISTRY 2 (1974) 316–326. © NORTH-HOLLAND PUBLISHING COMPANY

ALIGNMENT OF ANILINONAPHTHALENE-SULFONATE AND RELATED FLUORESCENT PROBE MOLECULES IN SQUID AXON MEMBRANE AND IN SYNTHETIC POLYMERS

I. TASAKI, K. SISCO and A. WARASHINA

Laboratory of Neurobiology, National Institute of Mental Health, Bethesda, Maryland 20014, USA and Marine Biological Laboratory, Woods Hole, Massachusetts 02543, USA

Received 26 April 1974
Revised manuscript received August 1974

As a fluorescent probe for the squid axon membrane, the behavior of 1-anilinonaphthalene-8-sulfonate (1,8-ANS) was found to be very different from that of its positional isomer, 2,6-ANS, or of the methylated derivative, 2,6-TNS. The degree of polarization of the fluorescent light contributing to a transient intensity reduction during nerve excitation was larger than about 0.7 for both 2,6-ANS and 2,6-TNS, while the corresponding value for 1,8-ANS in a squid axon was about 0.35.

The physicochemical basis of this difference was investigated by measuring the fluorescence polarization of these probe molecules incorporated into poly(vinyl alcohol) sheets. In a stretched sheet of this synthetic polymer, 1,8-ANS showed poor alignment, while the 2,6-derivatives were highly oriented with their transition moments aligned approximately in the direction of stretching. Based on these findings, the experimental results obtained from squid axons were interpreted as an indication of the existence, at or near the membrane, of a longitudinally oriented macromolecular structure, bringing about a high degree of alignment of 2,6-ANS or 2,6-TNS molecules.

It is clear that, as a probe for fluorescence polarization studies of macromolecular structures, 2,6-TNS is far superior to 1,8-ANS.

1. Introduction

Various isomers and derivatives of anilinonaphthalene-sulfonate have been used by many investigators as fluorescent probes to study conformational states of biological macromolecules [1–5]. When injected into squid giant axons, these molecules fluoresce intensely. Electric stimulation of an axon labelled internally with one of these probe molecules is known to bring about a small change in the intensity of the fluorescent light [6,7]. This change is associated with a distinct shift of the emission spectrum, which has been interpreted as an indication of a change in the polarity of the medium in the immediate vicinity of the probe molecules [8]. It was recognized in an early stage of investigation with 2-p-toluidinylnaphthalene-6-sulfonate (2,6-TNS) that the portion of the fluorescent light contributing to the intensity change during the process of nerve excitation is high polarized [7].

The present study deals with the polarization properties of fluorescence of 2,6-TNS, 2,6- and 1,8-anilinonaphthalene-sulfonate (2,6-ANS and 1,8-ANS) introduced into squid giant axons as compared with the behavior of these molecules incorporated into synthetic polymers. It was shown that the two positional isomers of ANS behave very differently in squid giant axons, the behavior of 2,6-ANS being quite similar to that of 2,6-TNS. In order to elucidate the physicochemical basis of the differences between 2,6-TNS, 2,6-ANS and 1,8-ANS, studies were carried out on the properties of the emitted fluorescent light from the molecules embedded in stretched sheets of synthetic polymers. By improving the method described by Nishijima *et al.* [9] and by McGraw [10], it was possible to estimate the directions of the transition moments relative to the orientation axis of the molecules in a highly ordered polymer layer. The data obtained from squid giant axons were interpreted on the basis of these results as strongly suggesting that the quaternary

structure of the macromolecules at or near the inner surface of the squid axon membrane is highly ordered, so that linear probe molecules have almost unique orientation with respect to the long axis of the axon.

2. Methods

Giant axons used in the present study were taken from squid available at the Marine Biological Laboratory in Woods Hole, Mass. The standard injection technique was used to introduce fluorescent probes into the axon interior. The optical setup used is illustrated diagrammatically in fig. 1A, and was essentially the same as that previously described [8]. The light from the source (a 200 W xenon–mercury lamp) was converted into approximately parallel beams of polarized light of 365 ± 5 nm wavelength by inserting quartz lenses, a heat filter, an interference filter (purchased from Infrared Industry) and a polarizer (Polaroid HNP'B) between the light source and the axon. The emitted light was detected with a photomultiplier (RCA 4463) after passing through an analyzer (Polaroid HN38) and a secondary filter (Kodak Wratten 2A or 2C). A hemispherical lens was used to increase the fluorescent light reaching the photomultiplier; this lens did not introduce any artifact into the determination of polarization of the emitted light. The temperature of the axons under study was maintained at about 6°C. A computer of average transients was used to record the small changes in the extrinsic fluorescence intensity of squid giant axons during nerve excitation.

Fluorescence polarization properties of the probe molecules in synthetic polymers were examined with a Leitz polarizing microscope (Orthoplux Pol). The light source for this study was also a 200 W xenon–mercury lamp illuminating the sheet of polymer on the microscope stage from above at 45°, as shown diagrammatically in fig. 1B. Just as in the experiments with squid giant axons, a heat filter, an interference filter and a polarizer were inserted in the light pathway. The emitted light was collected with an accurately centered objective lens (2.5 X) and its intensity was measured with a photomultiplier tube (RCA 4463) through a secondary filter (Kodak Wratten 2A). The intensity of the fluorescent light was measured as a function of the angle of rotation of the microscope

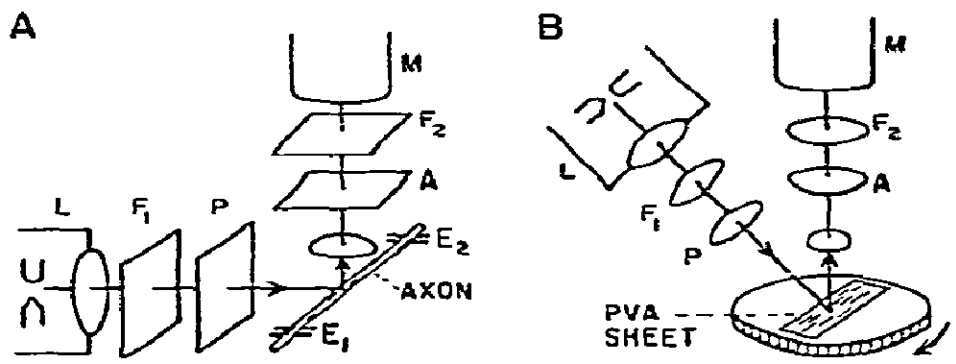


Fig. 1. Schematic diagrams of the experimental setup used to examine the polarization properties of fluorescent probes incorporated into squid giant axons (A) and into sheets of synthetic polymers (B). L represents a light source; F_1, primary filter; P, polarizer; E, electrodes for stimulation and for monitoring the action potentials of the axon; A, analyzer; F_2, secondary filter; M, multiplier phototube.

stage to which a labelled sheet of polymer was fixed. The microscope stage was rotated either manually or with a synchronous motor at a rate of about 3 s per revolution. The same microscope was used to determine the absorbance of the dye molecules incorporated into polymer sheets; in this case an incandescent light (100 W quartz iodine lamp) was used as the light source.

The method of aligning probe molecules in synthetic polymers was similar to that employed by Nishijima et al. [9]. It was pointed out by McGraw [11] that there is a shortcoming in this method, due to the high birefringence of a stretched sheet of polymer. In this method, the fluorescent molecules were incorporated into a sheet of polyvinyl alcohol (abbreviated as PVA) and then the sheet was stretched at a high temperature. Under these conditions, the fluorescent molecules are embedded deep inside a highly birefringent layer of polymer, creating a distortion of the polarization properties of both the incident and emitted light. This distortion can be demonstrated by placing a stretched dye-free PVA sheet above an unstretched PVA sheet containing randomly oriented dye molecules; under these conditions a measurement of polarization of the emitted light gives rise to a false impression that the dye molecules are partially oriented. An experimental study of the birefringence effect has shown, however, that the error due to this effect is not significant under the present experimental conditions. The probable error is about 15% of the maximum value of the portion of the fluorescent light deriving from randomly oriented probe molecules. The

emission from the fraction of probe molecules with a high degree of alignment is not affected by this effect to any significant degree. Since only a small fraction of the total probe molecules in stretched PVA sheets is randomly oriented, the error caused by the birefringence effect is expected to be negligible.

In most of the present studies, the following modified method was employed to incorporate fluorescent probes into polymer sheets. Poly(vinyl alcohol) was purchased from Baker Chemical Co. An aqueous solution of PVA (5 g per 100 ml) was cast in a 3 mm deep rectangular plastic container with a glass bottom and was dried overnight in an oven kept at about 45°C. The thickness of the sheet prepared by this technique was roughly 0.1 mm. Next, a drop of an aqueous solution of PVA containing probe molecules at a concentration between 0.1 and 0.5 mM, was placed on the surface of a dried PVA sheet and the solution was smeared by sliding the edge of a glass plate along the surface. Finally, the sheet was stretched in hot air (87–90°C) with a special device constructed in this laboratory, increasing the length of the stained PVA strip by a factor of 4 to 5.

When polarized emission of fluorescence from probe molecules in the sheet was examined, the smeared surface of the sheet was facing upward on the stage of the polarizing microscope. In experiments in which the transmission of polarized light through a sheet was examined, the smeared sheet was placed facing downward and the analyzer in the microscope tube was removed from the light path. Under these conditions, probe molecules are located near the surface of a PVA sheet and the major portion of the underlying birefringent material was not expected to affect the subsequent optical measurements. Aggregation and crystal formation of the probe molecules in the superficial layer of the PVA sheet, which could be detected by the appearance of the fluorescence excitation spectrum of crystalline 2,6-TNS, did not take place to any significant degree, probably because of the high rate of the drying process. The thickness of a single smeared layer of an aqueous solution of PVA was estimated to be roughly 1/100 mm.

3. Results

3.1. Polarization of fluorescence signals of axons labelled with TNS and ANS

Small changes in the extrinsic fluorescence intensity associated with the process of nerve excitation were examined in squid giant axons using the technique described under Methods. When an axon labelled internally with 2,6-TNS was exposed to a polarized light of 365 nm with its electric vector parallel to the long axis of the axon, a transient reduction in the fluorescence intensity (i.e., a negative fluorescence signal) was observed on stimulation of the axon. In this case, the portion of the light contributing to the signal was highly polarized with its electric vector oriented in the same direction as that of the incident light. With the polarizing axis of the analyzer oriented parallel to the axon, a distinct fluorescent signal was observed; but, when the analyzer was rotated through 90° under the same excitation conditions otherwise, only a record of random noise was obtained (fig. 2).

The degree of polarization, P, is defined formally as

$$P = \frac{I_{\parallel} - I_{\perp}}{I_{\parallel} + I_{\perp}},$$

where $I_{\parallel}$ and $I_{\perp}$ represent the amplitudes of the fluorescence signal observed with the analyzer axis parallel and perpendicular, respectively, to the direction of the electric vector of the incident light. The value of P for this type of 2,6-TNS signal was found to be greater than about 0.7, its accuracy being limited by the relatively high level of random noise. These results conform to previous findings [12].

The present study was directed toward gaining quantitative information concerning the difference in behavior between 2,6-ANS and 1,8-ANS in axons. In fig. 2 and table 1, the positions of the polarizer (P) or analyzer (A) were indicated by the symbols "parallel" and "perpendicular" which signify that the electric vector of the light transmitted through the Polaroid sheet was parallel and perpendicular, respectively, to the long axis of the axon. It is seen in the figure that, with the polarizer in the parallel direction, no significant signal above the noise level was observed from axons internally labelled with

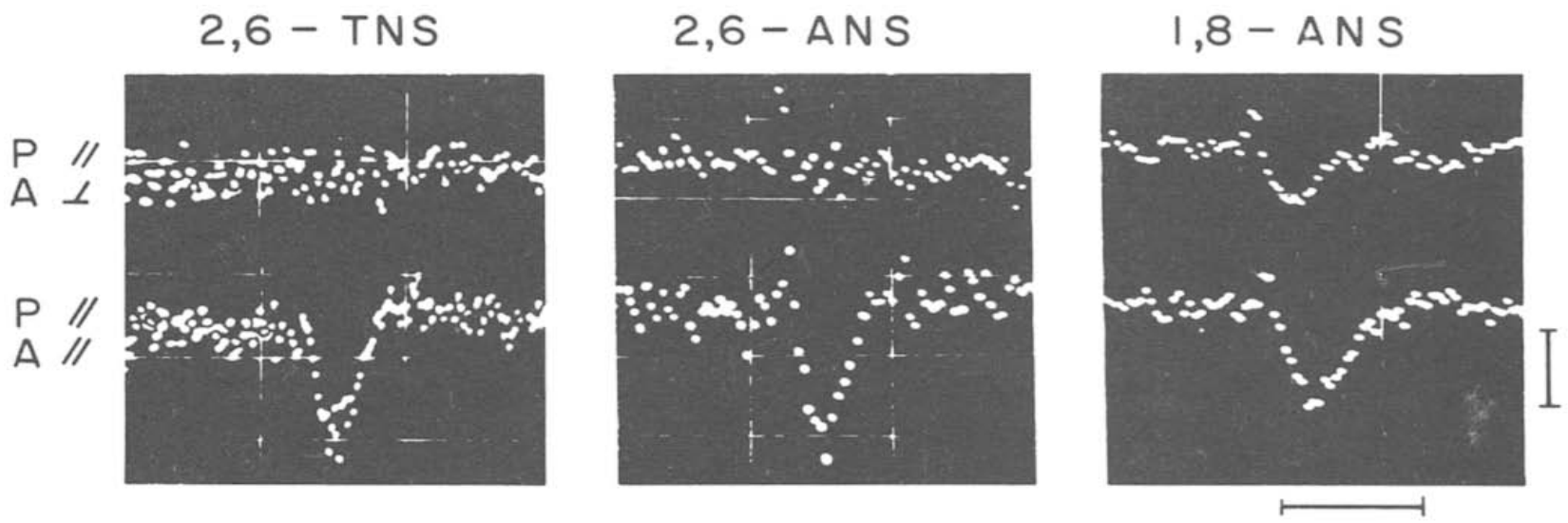


Fig. 2. Computer records showing a transient decrease in the intensity of fluorescence deriving from squid giant axons internally labelled with three different probes of anilinonaphthalene derivatives. P and A indicate the axes of the polarizer and analyzer relative to the longitudinal axis of the axon used. Two records in each column were taken from one and the same axon under the same illuminating and recording conditions. For the lower records, one vertical division represents 4.3×10^{-5} times the intensity at rest for 2,6-TNS, 3.4×10^{-5} times for 2,6-ANS and 8×10^{-5} times for 1,8-ANS. Each horizontal division represents approximately 7.8 ms.

2,6-ANS when the analyzer was in the perpendicular orientation. This sharply contrasts with the results obtained with 1,8-ANS in which clear signals were present under both the "parallel–parallel" and "parallel–perpendicular" conditions.

The upper row of table 1 shows the relative sizes of the fluorescence signals in axons labelled with 2,6-ANS at various combinations of orientations of the polarizer and the analyzer. The lower row shows the relative sizes of signals obtained using 1,8-ANS under similar conditions. A formal calculation of P

Table 1
Relative sizes of the fluorescence signals of squid giant axons labelled internally with 2,6-ANS (top), as compared with those of axons with 1,8-ANS internally (bottom). The polarizing axes of the polarizer (P) and the analyzer (A) relative to the long axis of the axons are indicated. The signal amplitudes (i.e., the changes, ΔI, in intensity) are expressed as values relative to that observed under the P-parallel and A-parallel conditions. The standard deviations of these values for 1,8-ANS were 0.01 (2nd and 3rd columns) and 0.03 (4th column). The standard deviation for 2,6-ANS (4th column) was 0.16. The data for 2,6-ANS were derived from the results of measurements on 22 axons; the data for 1,8-ANS from 11 axons. The asterisk indicates that the sign of the signal was positive (opposite to others)

	$P_{\parallel}, A_{\parallel}$	$P_{\parallel}, A_{\perp}$	$P_{\perp}, A_{\parallel}$	$P_{\perp}, P_{\perp}$
2,6-ANS (1)	<0.15	<0.17	0.25^{*}	
1,8-ANS (1)	0.48	0.24	0.23	

for 1,8-ANS observed with the electric vector of the incident light parallel to the long axis of the axon yielded a value of approximately 0.35. The corresponding value for 2,6-ANS was larger than about 0.74. These results clearly indicated that there is a significant difference in polarization behavior between 1,8-ANS and its 2,6-isomer.

3.2. Fluorescence polarization of probe molecules in stretched PVA sheets

In the following measurements, the axis of the polarizer (which determines the electric vector of the incident light of 365 nm wavelength) was parallel to the surface of the PVA sheet and the axis of the analyzer was either parallel or perpendicular to the axis of the polarizer. The intensity of the fluorescent light from PVA sheets containing probe molecules was measured as a function of the angle through which the sheet was rotated in the plane normal to the direction of light detection (see fig. 1B).

Fluorescent probe molecules incorporated into a layer of unstretched PVA sheet are randomly oriented. This can be shown by demonstrating that the intensity of the fluorescent light is practically independent of the angle of rotation of the PVA sheet (see fig. 3A). The degree of polarization, P, of 2,6-TNS in an unstretched PVA sheet was found to vary with the concentration of 2,6-TNS in the sheet. P was found to be

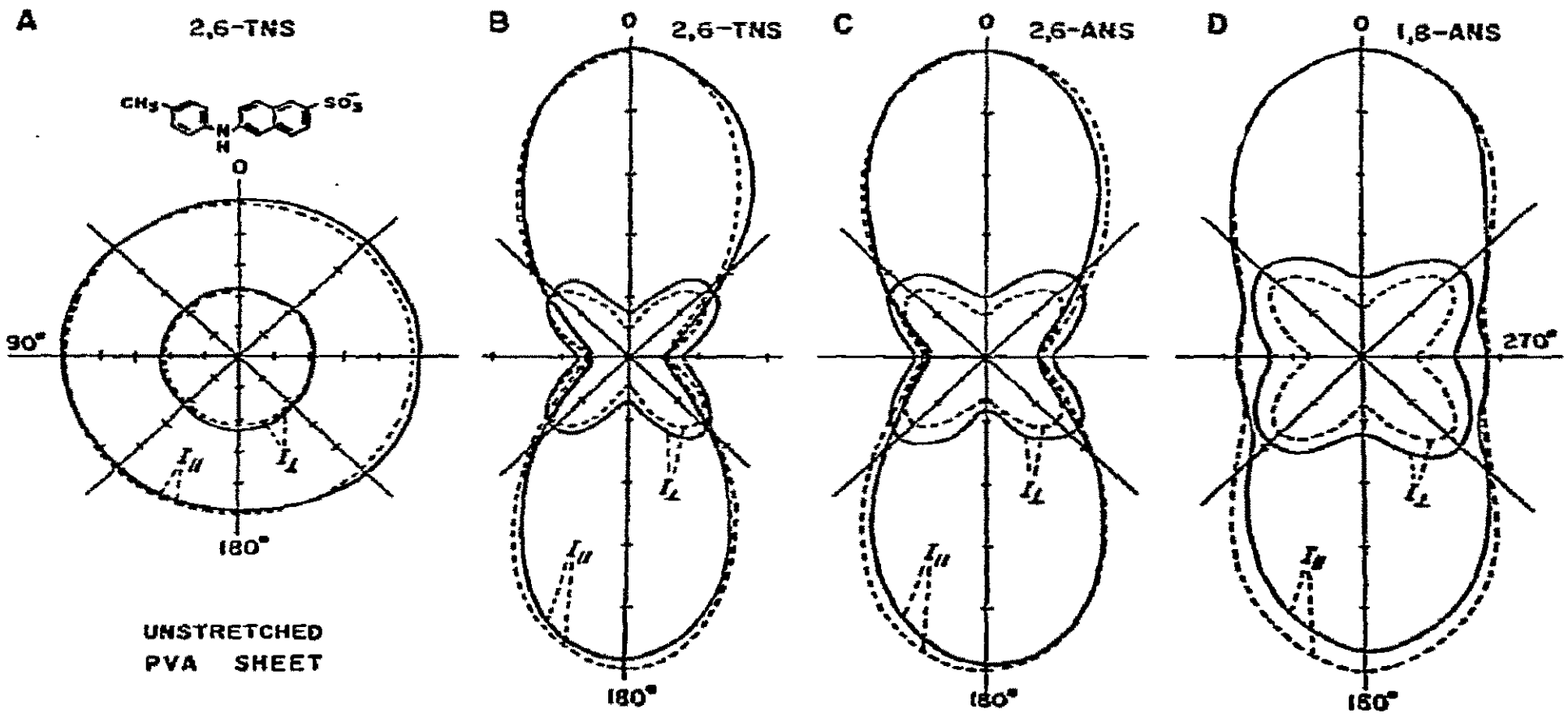


Fig. 3. The dependence of the intensity of fluorescent light from sheets of poly(vinyl alcohol) containing three kinds of probe molecules upon the angle of rotation of the sheets. The experimental setup illustrated in fig. 1B, was used to obtain the observed values shown by the continuous lines. The direction of the polarizing axis of the analyzer relative to that of the polarizer is indicated. The broken lines show the results of calculation by introducing $\alpha = 15°$, $\beta = -10°$ for 2,6-TNS and 2,6-ANS, and $\alpha = 12.5°$ and $\beta = 12.5°$ for 1,8-ANS into eqs. (12) and (13). The following correction terms were used: for an unstretched sheet containing 2,6-TNS (extreme left), $a = 0$ and $b = 0$; for a stretched sheet labelled with 2,6-TNS, $a = 0.7$ and $b = 0.6$; for 2,6-ANS, $a = 0.6$ and $b = 0.4$; for 1,8-ANS, $a = 0.4$ and $b = 0.4$.

approximately 0.37 in the range of probe concentration less than 0.1 mM in the original PVA solution. At concentrations higher than about 0.15 mM, there was a slight fall in the value of P.

As has been stated under Methods, a high degree of orientation of 2,6-TNS molecules in the superficial layer of a PVA sheet was created by smearing a PVA solution containing 0.1–0.5 mM probe molecules and subsequently stretching the sheet at a draw ratio of about 4.5. (The probe-to-polymer gram-ratio in this superficial layer is between 1:1600 and 1:320.) An example of the results of fluorescence polarization measurements on such stretched sheets stained with 2,6-TNS is shown in fig. 3B. As can be seen in the figure, the intensity of the observed fluorescent light varied to a great extent with the angle of rotation of the stretched PVA sheet. A maximum of the intensity was reached when the stretching direction coincided with the polarizing axes of the polarizer and the analyzer. The intensity reached a minimum when the sheet was rotated through 90° from this parallel condition. The ratio of the maximum to the minimum in intensity varied in the range between 7 and 9 under these conditions (P being between 0.75 and 0.80). This value was found to be very insensitive to a large variation in the 2,6-TNS concentration in the smeared layer of the PVA sheet. When the analyzer axis was at a right angle to the polarizer axis, maxima of the intensity were encountered when the stretching direction was at 45° to both the analyzer and polarizer. Qualitatively, these results are similar to those reported previously by Nishijima et al. [9] and by McGraw [10, 11].

Diagram C shows an example of the results obtained with 2,6-ANS. These results are very similar to those for 2,6-TNS. The ratio of the maximum to the minimum of the intensities observed under the parallel condition was found to be between 6 and 7 and was slightly smaller than the corresponding value for 2,6-TNS. The results obtained with 1,8-ANS were considerably different from those obtained with 2,6-derivatives (see diagram D). The angular dependence

of the light intensity was less marked in this case; the maximum-to-minimum ratio under these conditions was between 3 and 4.

By using a slightly different arrangement (see Methods), it was found that light absorption was strongest when the stretching direction of the PVA sheet containing 2,6-TNS in its superficial layer was parallel to the electric vector of the light beam used for measurement. The ratio of this maximum of absorbance to its minimum (at 90°) was in most cases between 2.5 and 4. In this connection, it is important to note that the accuracy of these measurements is quite limited as compared with that for fluorescence measurements. These measurements involve determination of differences between two comparable quantities, producing relatively large uncertainties in the results obtained. The dichroic ratio for 2,6-ANS in stretched PVA sheets was estimated to be between 1.5 and 3. The corresponding value for 1,8-ANS was between 1.5 and 2. Here again, it was found that the alignment of 1,8-ANS in stretched PVA sheets is far more imperfect than that of 2,6-derivatives.

Very similar results were obtained by using PVA sheets prepared by Nishijima's original method, namely with stretched PVA sheets prepared by drying an aqueous solution of PVA to which probe molecules were added at a concentration of about 20 μM and by subsequent stretching.

4. Discussion

It is known that the two aromatic rings of the 2,6-TNS molecule are not exactly coplanar [13, 14]. Since these rings carry side-groups (methyl and sulfonate) at the positions opposite to the amino group, the molecular orientation axis which tends to align the molecule in the direction of stretching of a PVA sheet is considered to be close to the straight line connecting the two side-groups of the molecule. Absorption and emission of polarized light by such a complex organic molecule can be described, within certain limits, by a classical model in which the molecule is represented by absorbing and emitting oscillators associated with definite vector directions with respect to the molecular coordinates (see Feofilov, ref. [15]). The optical behavior of 2,6-TNS in a stretched PVA sheet can then be described formally by specifying the following two angles:

α: the angle of the absorbing vector with axis OM,
β: the angle of the emitting vector with axis OM,

where OM represents the molecular orientation axis. The difference between these two angles, $(\alpha-\beta)$, is known to vary with the wavelength of the absorbed light.

The value of $(\alpha-\beta)$ for 2,6-TNS can be estimated by measuring the degree of polarization, P, in glycerol at low temperatures (see, e.g., p. 112 in Feofilov [15]). By extrapolating the observed value of P to $(T/\eta) = 0$, where T is the absolute temperature and η the viscosity, the value of $(\alpha-\beta)$ for 2,6-TNS at the excitation wavelength of 365 nm was estimated to be approximately 25°. This value is quite consistent with that estimated from the value of P (approximately 0.39) described previously by McClure and Edelman [2]. This value also agrees with the results of our measurements for 2,6-TNS incorporated randomly into a solid (non-shrinking) polymer, Bipax.

The separate values of α and β can be estimated from the measurements of the angular dependence of the absorbance and the intensity of fluorescence of stretched PVA sheets containing probe molecules (see fig. 3). The mathematical formulae described in the appendix were used to evaluate α and β. In the case of 2,6-TNS, the best agreement between the calculated and the observed values of the absorbance and the fluorescence intensity was obtained when α was chosen to be approximately 15° and β to be approximately −10°. (The difficulties involved in this evaluation are discussed in the appendix.) The broken lines in fig. 2 were obtained by introducing these values into eqs. (12) and (13). The agreement between the observed and calculated values is considered fair.

The best estimates of α and β for 2,6-ANS by the same technique are not very different from those for 2,6-TNS. A slight difference in the degree of alignment between these two 2,6-derivatives (compare fig. 3B with 3C) may be attributed to a slight increase in the randomly oriented fraction of 2,6-ANS molecules in the PVA sheet. The behavior of 1,8-ANS molecules in stretched PVA under the same experimental conditions was found to differ from that of 2,6-derivatives to a considerable extent. In this case, as much as 60% of the probe molecules in the sheet can be regarded as being randomly oriented. (The difference

between α and β for 1,8-ANS was almost the same as that of 2,6-derivatives.) The following two factors contributing to this difference between 1,8- and 2,6-ANS may be adduced.

(i) In 2,6-ANS molecules there is a more-or-less clear-cut long axis which tends to align the naphthalene ring along the stretched direction of a polymer layer, while 1,8-ANS molecules do not have a clear long axis.

(ii) The absorption spectrum of 1,8-ANS is known to be very different from that of 2,6-ANS or 2,6-TNS. Recent studies by Suzuki et al. [16] indicate that the lowest-energy absorption band of 1-amino-naphthalene (or α-naphthylamine) corresponds to two types of electronic transitions. These two bands are more-or-less distinct in 2-aminonaphthalene (or β-naphthylamine). The pattern of light absorption by 2,6-ANS is very similar to that of 2-aminonaphthalene, while the absorption bands of 1,8-ANS are quite comparable to those of 1-aminonaphthalene. (There is an increasing red-shift in the absorption bands with an increasing extent of substitution.) It is reasonable, therefore, to consider the angle α between the absorption oscillator and the molecular orientation axis as a quantity not well defined in the case of 1,8-ANS.

On the basis of these findings, the difference in behavior between 1,8- and 2,6-ANS in squid giant axons (see fig. 2) can now be interpreted. Squid axons labelled internally with 2,6-TNS or 2,6-ANS were shown to produce fluorescence signals which represent a transient reduction in highly polarized fluorescent light. In all probability, the probe molecules contributing to production of these signals are aligned inside the axons with their orientation axis along the long axis of the axon. During the action potential, the emission spectrum of these probe molecules is shifted and the quantum yield is slightly reduced [7]. Neither a simple fluorescence quenching nor a simple increased Brownian motion of the probe molecules can explain the process of production of these signals [8]. It seems impossible to attribute the voltage-dependence of these fluorescence signals (Davila et al. [17]) to a direct effect of changes in the electric field in the axon membrane, because the emitting oscillators of the 2,6-TNS molecules are shown to be oriented parallel to the surface of the axon, namely, in the direction roughly perpendicular to the direction of the electric field.

[It was pointed out by Prof. Akira Watanabe of the Tokyo Medical and Dental University (personal communication) that a two-dimensionally random distribution of 2,6-TNS molecules on the surface of the axon could produce a high degree of polarization. A decrease in the quantum yield of such molecules on the cylindrical membrane surface could explain the process of production of 2,6-TNS fluorescence signals. Mainly for the following two reasons, it is very unlikely that this mechanism of production of 2,6-TNS fluorescence signals is in operation. (i) When an angle of 25° between the absorbing and emitting oscillators is introduced in calculation of the polarization of 2,6-TNS fluorescence from a cylindrical surface, it is found that P does not exceed 0.5; the observed value of P for 2,6-TNS signals is higher than about 0.7. (ii) 2,6-TNS is an amphipathic molecule with a negative charge; it appears improbable that such a molecule stays randomly on the surface of a lipid layer (or a globular protein molecule) with its long axis parallel to the surface (see below).]

A high degree of alignment of these 2,6-derivatives of anilinonaphthalene-sulfonate may be considered as evidence for the existence of a highly ordered macromolecular structure at or near the membrane. The conformation of this structure is such that the 2,6-derivative probe molecule can have almost unique orientation in this structure while the 1,8-derivative is poorly aligned just as in the stretched PVA sheets. It is probable that the threadlike elements described by Metuzals and Izzard [19] is the structure which brings about a high degree of alignment of 2,6-TNS and 2,6-ANS at and near the squid axon membrane. The immobility of the 2,6-derivatives in the membrane structure does not indicate that the environment of these probe molecules in the axon is a continuous, rigid phase. A recent study of the effects of heavy water on the fluorescence of 2,6-TNS in axons (Carbone et al. [18]) strongly suggests the partial accessibility of H_2O molecules to the 2,6-TNS binding sites in or near the axon membrane (see also ref. [8]).

The difference in polarization properties between 1,8-ANS and 2,6-TNS appears to be more marked in squid axons than in stretched PVA sheets. To explain the origin of the positive fluorescence signals seen under the "perpendicular perpendicular" conditions (see table 1), it has been suggested that there is

more than one type of binding site for 2,6-TNS in a squid axon [12]. The distribution of 1,8-ANS in the axon appears to be different qualitatively from that of 2,6-derivatives (see table 1). To clarify these aspects of the difference between these two positional isomers of ANS, much more study is required.

Acknowledgement

We wish to thank Mrs. Karen Pettigrew for her assistance in writing the computer program for our mathematical analysis. We especially want to thank Dr. G.E. McGraw for his very helpful comments concerning our polymer studies.

Appendix

A.1. Orientation of probe molecules in stretched PVA sheet

When a thin sheet of polyvinyl alcohol (PVA) is stretched, a circle drawn on the surface of the sheet changes into an elipse elongated in the direction of stretching (see fig. 4). The points fixed to the material below the circle are expected to be displaced in a similar manner. Since the density of a PVA sheet (approximately 1.33) remained approximately the same by stretching, an increase in the length of the sheet will be accompanied by a decrease in the width and the thickness. Let n denote the ratio of the final to the initial length. The width is found to decrease approximately by a factor of $\sqrt{n}$ under these circumstances.

The displacement of radius OR of the circle (see diagram A in fig. 4) to the final position OQ is described by the following formula (see ref. [17]):

$$\tan\omega = n^{-3/2}\tan\rho \qquad (1)$$

where ρ is angle ROZ and ω angle QOZ. (Note that $\tan\rho = n\tan\sigma$ and $\tan\sigma = n^{1/2}\tan\omega$, where σ represents angle SOZ.) Regarding ρ as a function of ω, differentiation of eq. (1) yields

$$d\omega/d\rho = n^{3/2}[1-(1-n^{-3})\cos^2\omega]. \qquad (2)$$

Now it may be argued that eq. (2) describes the effect of stretching of the PVA sheet on the distribution of fluorescent probe molecules in the sheet. It is assumed that the distribution of these molecules is random initially and that all the molecules with their long axes oriented in the range between ρ and $(\rho+d\rho)$ initially are brought by stretching into the range between ω and $(\omega+d\omega)$. The probe molecules in the sheet should be displaced in this manner if they have a strong tendency to imitate the orientation of the polymer chains. In this case, $d\omega/d\rho$ corresponds to the ratio of the density of the molecules in the range of $d\rho$ initially to that in the range of $d\omega$ finally. When $n \approx 4.5$ as in the present studies, $1 \gg n^{-3}$. Therefore, the density of the molecules oriented in the direction of stretching ($\omega = 0$) becomes extremely large. In other words, the angular distribution of probe molecules with a long axis may be given approximately by a delta function.

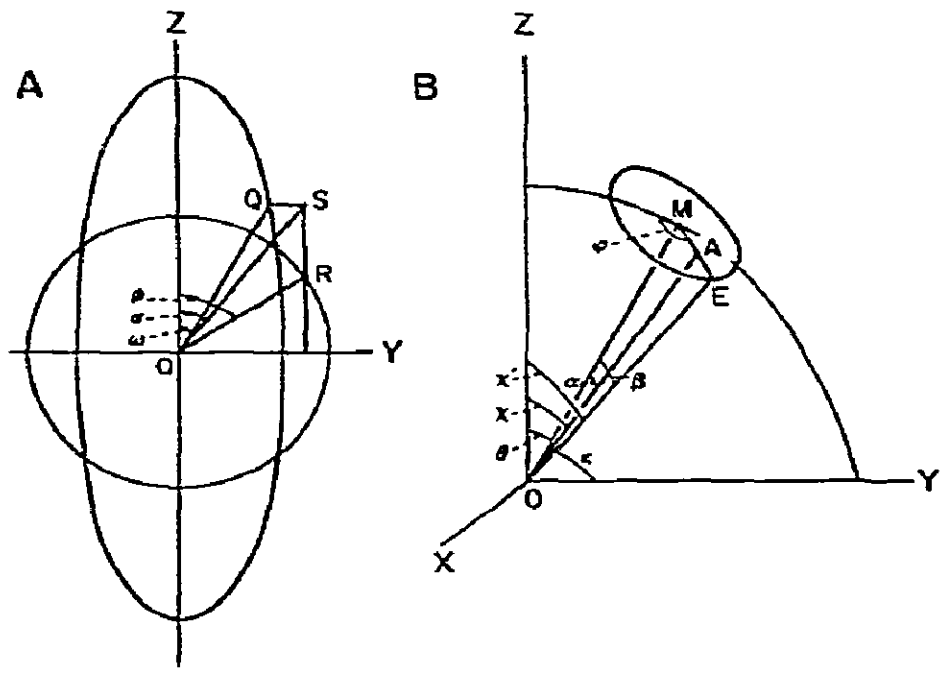


Fig. 4. (A) Diagram illustrating the effect of stretching of a polymer sheet upon the distribution of the probe molecules with a long axis in the sheet; see text. (B) Diagram showing the spatial relationship of the direction of the electric vector of the exciting light beam (OZ) to the molecular orientation axis (OM), the absorbing oscillator (OA) and the emitting oscillator (OE) of a fluorescent probe molecule. See text.

Tanizaki and Kubodera [17] treated the case in which the probe molecules are distributed randomly in three dimensional space before stretching. In this case, the angular distribution of long probe molecules in a stretched sheet is given by

$$f(\omega) = N\sin\omega[1-(1-n^{-3})\cos^2\omega]^{-3/2}, \qquad (3)$$

where N is the normalization constant, ω being the angle between the direction of stretching and the

molecular orientation axis in three dimensional space. Since preparation of a PVA sheet involves an enormous reduction in its thickness by drying, the dye molecules in the sheet cannot be oriented randomly in three dimensional space.

It is known that a stretched PVA sheet consists of two kinds of zones, crystalline and amorphous (see, e.g., refs. [9, 11]). Therefore a real PVA sheet is not expected to bring about perfect alignment of the probe molecules in the sheet.

A.2. Absorption and emission of light by fluorescent molecules in polymer sheets

In a complex organic molecule, the transition moment of the molecule does not in general coincide with the long axis of the molecule. Even when the molecular orientation axis is aligned perfectly along the direction of stretching, therefore, the absorbing or emitting oscillators are not expected to be all aligned in the same direction. In the following treatment, it is assumed that the three unit vectors fixed to the fluorescent probe molecule, the molecular orientation axis OM, the absorbing oscillator OA and the emitting oscialltor OE, are all in one plane.

Diagram B in fig. 4 shows the spatial relationship of these three unit vectors relative to the direction of the electric vector of the incident light, OZ. The surface of the stretched polymer sheet containing perfectly aligned probe molecules is parallel to plane YZ. The direction of the stretching of the sheet makes angle θ with axis OZ. Since nothing is known about the spatial orientation of the molecular plane reiative to the direction of stretching, this orientation is assumed to be completely random. Under these circumstances, the probability of absorption of the incident light by a single probe molecule is proportional to $\cos^2\chi$, where χ is the angle which OA makes with axis OZ. This angle is related to θ and φ (i.e., the angle between the molecular plane and plane YZ) by the following relationship:

$$\cos\chi = \cos\theta\cos\alpha + \sin\theta\sin\alpha\cos\varphi. \tag{4}$$

The absorbance $\epsilon(\theta)$ of light polarized in the direction OZ is proportional to the value of $\cos^2\chi$ averaged over φ namely by

$$\epsilon(\theta) \propto \cos^2\theta\cos^2\alpha + \tfrac{1}{2}\sin^2\theta\sin^2\alpha. \tag{5}$$

The intensity of the fluorescent light detected with the analyzer parallel to the direction of polarization of the incident light (OZ), $I_\parallel$, is given by the value of $\cos^2\chi\cos^2\chi'$ averaged over φ, where χ' is the angle of the emitting oscillator (OE) with the analyzer axis (OZ). Angle χ' is related to θ, β, and φ by

$$\cos\chi' = \cos\theta\cos\beta + \sin\theta\sin\beta\cos\varphi. \tag{7}$$

Averaging of $\cos^2\chi\cos^2\chi'$ leads to the following formula:

$$I_\parallel = K(A\cos^4\theta + B\sin^4\theta + C\cos^2\theta\sin^2\theta) \tag{8}$$

where K is a proportionality constant,

$$A = \cos^2\alpha\cos^2\beta, \quad B = \tfrac{3}{8}\sin^2\alpha\sin^2\beta,$$

and

$$C = \tfrac{1}{4}\sin 2\alpha\sin 2\beta + \tfrac{1}{2}\sin^2(\alpha+\beta).$$

Similarly, the intensity of the fluorescent light observed with the polarizer parallel to OZ and the analyzer parallel to OY (namely perpendicular to OZ), $I_\perp$, is proportional to the average value of $\cos^2\chi\cos^2\kappa$, where κ is the angle between OE and OY and satisfies the relationship

$$\cos\kappa = \cos(\tfrac{1}{2}\pi-\theta)\cos\beta + \sin(\tfrac{1}{2}\pi-\theta)\sin\beta\cos(\pi-\varphi). \tag{9}$$

A straightforward calculation leads to the following formula:

$$I_\perp = D\cos^4\theta + E\sin^4\theta + F\sin^2\theta\cos^2\theta, \tag{10}$$

where

$$D = \tfrac{1}{2}\cos^2\alpha\sin^2\beta,$$

$$E = \tfrac{1}{2}\sin^2\alpha\cos^2\beta,$$

$$F = A + B - \tfrac{1}{2}\sin 2\alpha\sin 2\beta.$$

These equations are extensions of the expressions described by Nishijima et al. [9]. In a special case where $\alpha = \beta = 0$, these equations reduce to those reported by the Japanese investigators.

A.3. The effect of imperfect alignment of probe molecules in polymer sheets

When the fluorescent probe molecules are not perfectly aligned in the polymer sheet, the expression describing light absorption and emission becomes very

complicated. The following treatment is limited to a case where the orientation axes of all the probe molecules are parallel to the surface of the sheet.

Let an even function of ω, $f(\omega)$, describe the angular distribution of the probe molecules in the sheet. When the orientation axis (OM) deviates from the direction of stretching of the sheet by angle ω, angle θ in expression for χ, χ' and κ in eqs. (4), (7) and (9) has to be replaced with $(\theta+\omega)$. In addition, the expressions for absorption and emission (5), (8) and (10), have to be integrated with respect to ω from $-\pi/2$ to $+\pi/2$. By carrying out this integration, the final equations describing the angular dependence of absorbance and of fluorescence intensities are

$$\epsilon \propto \tfrac{1}{2}(1+a\cos 2\theta)\cos^2\alpha + \tfrac{1}{4}(1-a\cos 2\theta)\sin^2\alpha, \quad (11)$$

$$I_{\parallel} = K[A(\tfrac{3}{8}+\tfrac{1}{2}a\cos 2\theta+\tfrac{1}{8}b\cos 4\theta) + B(\tfrac{3}{8}-\tfrac{1}{2}a\cos 2\theta+\tfrac{1}{8}b\cos 4\theta)+C(\tfrac{1}{8}-\tfrac{1}{8}b\cos 4\theta)], \quad (12)$$

and

$$I_{\perp} = K[D(\tfrac{3}{8}+\tfrac{1}{2}a\cos 2\theta+\tfrac{1}{8}b\cos 4\theta) + E(\tfrac{3}{8}-\tfrac{1}{2}a\cos 2\theta+\tfrac{1}{8}b\cos 4\theta)+F(\tfrac{1}{8}-\tfrac{1}{8}b\cos 4\theta)], \quad (13)$$

where a and b are the correction factors required to take care of imperfection of alignment of probe molecules in the sheet and defined by

$$a = \int f(\omega)\cos 2\omega\, d\omega,$$

and

$$b = \int f(\omega)\cos 4\omega\, d\omega.$$

Coefficients $A, B, \ldots, F$ have the same significance as before. The special case where $a = b = 1$ represents the situation in which the alignment is perfect and eqs. (11), (12) and (13) reduce to (5), (8) and (10). The case where $a = b = 0$ represents the situation where the distribution of the probe molecules is completely random. In real polymer sheets, the alignment of the probe molecules must be between these two extreme cases. It is also interesting to note that the expression for $I_{\parallel}$ is invariant when α and β are interchanged, while for $I_{\perp}$, this is not the case. Therefore, the $I_{\perp}$ measurement should give us more information than the $I_{\parallel}$ measurement in the theoretical sense.

A.4. Evaluation of α and β for 2,6-TNS

The angular dependence of the absorbance and the fluorescence intensities determined by the experiments described under Results (fig. 3) is expected to yield useful information concerning the magnitude of α and β. The ratio of quantity D to E in eq. (10) represents the ratio of the fluorescence intensity measured at positions $\theta = 0$ and to that at $\theta = \frac{1}{2}\pi$. When the probe molecules are not aligned perfectly, however, the difference between the intensities at these two positions becomes very small. Nevertheless, the experimental results shown in fig. 4 indicate that, in probe molecules under study, angle α is approximately equal to or slightly larger than angle β. In the range of α and β smaller than 30°, the fluorescent light intensity $I_{\parallel}$ observed at $\theta = 90°$ relative to that at $\theta = 0$ yields direct information as to the magnitude of the correction factors a and b.

Keeping these aspects of the mathematical expressions in mind, extensive numerical calculations of these eqs. (11), (12) and (13) were carried out. [For this calculation, an Electronic Calculator (Wang 600–14) was utilized.] The results of the calculation were presented on a polar coordinate system at the same relative scale as those obtained experimentally. By comparing the curves obtained by calculation with the observed curves, the values of α and β for 2,6-TNS were estimated to be roughly 15° and −10°, respectively.

The corresponding values for 2,6-ANS and 1,8-ANS were estimated in a similar fashion. With 1,8-ANS, however, the correction factors, a and b, were found to be far smaller than unity, indicating that a large portion of these probe molecules are irregularly oriented in the PVA sheet. Furthermore, a satisfactory agreement between the observed and calculated values of fluorescence intensity could not be obtained by adjusting the four parameters, α, β, a and b.

The conclusions reached from these mathematical analyses are as follows: (i) The degree of alignment in stretched PVA sheets decreases in the order: 2,6-TNS > 2,6-ANS > 1,8-ANS. (ii) The disagreement between the observed and calculated values of fluorescence intensity increases in the same order. This disagreement which cannot be taken care of by lowering of a and b may be attributed at least partly to the complexity of the absorption band of 1,8-ANS (see Discussion).

Nevertheless, the present studies clearly indicate that as a probe for fluorescence polarization analyses of macromolecular structures 1,8-ANS has several undesirable aspects. In contrast the results obtained with 2,6-derivatives (2,6-TNS in particular) was found to be more amenable to physicochemical interpretations than those obtained with 1,8-ANS.

References

[1] R. Anderson and G. Weber, Biochemistry 8 (1967) 371.
[2] O. McClure and G.M. Edelman, Biochemistry 5 (1966) 1908.
[3] L. Brand and J.R. Gohlke, Ann. Rev. Biochem. 41 (1972) 843–868.
[4] J. Vanderkooi and A. Martonosi, Arch. Biochem. Biophys. 133 (1969) 153.
[5] K. Radda and J. Vanderkooi, Biochem. Biophys. Acta 265 (1972) 509.
[6] I. Tasaki, A. Watanabe, R. Sandlin and L. Carnay, Proc. Nat. Acad. Sci. 61 (1968) 882.
[7] I. Tasaki, A. Watanabe and M. Hallett, Proc. Nat. Acad. Sci. 68 (1971) 938.
[8] I. Tasaki, E. Carbone, K. Sisco and I. Singer, Biochim. Biophys. Acta 323 (1973) 220.
[9] Y. Nishijima, Y. Onogi and T. Asai, J. Polym. Sci. C 15 (1966) 237.
[10] G.E. McGraw, J. Polym. Sci. A-2 (1970) 1323.
[11] G.E. McGraw, in: Structure and properties of polymer films, eds. R.W. Lenz and R.S. Stein (Plenum, New York, 1970).
[12] I. Tasaki, M. Hallett and E. Carbone, J. Membrane Biol. 11 (1973) 353.
[13] A. Cammerman and L.H. Jensen, J. Amer. Chem. Soc. 92 (1970) 4200.
[14] E.M. Kosower and K. Tanizawa, Chem. Phys. Letters 16 (1972) 419.
[15] P.P. Feofilov, The physical basis of polarized emission (Consultants Bureau, New York, 1961).
[16] S. Suzuki, T. Fujii and H. Baba, J. Mol. Spectrscopy 47 (1973) 243.
[17] H.V. Davila, L.B. Cohen, B.M. Salzberg and B.B. Shrivastav, J. Membrane Biol. 15 (1974) 29.
[18] E. Carbone, K. Sisco and A. Warashina, J. Membrane Biol, in press.
[19] J. Metuzals and C.S. Izzard, J. Cell Biol. 43 (1969) 456.
[20] Y. Tanizaki and S. Kubodera, J. Mol. Spectroscopy 24 (1967) 1.

BIOPHYSICAL CHEMISTRY 2 (1974) 327–337. © NORTH-HOLLAND PUBLISHING COMPANY

ENERGY TRANSFER IN THE PHOTOSYNTHETIC UNIT

I. The concept of independent units for photosystem II analyzed by flash yields for dichlorophenolindophenol reduction*‡

Shmuel MALKIN

Department of Biochemistry, The Weizmann Institute of Science, Rehovot, Israel

Received 15 May 1974

The problem of the interconnection of photosynthetic units is dealt with. Flash yield results together with quantum yield measurements of DCPIP reduction in isolated chloroplasts indicate that photosynthetic units of PS-II are essentially independent and probably morphological entities. This is shown by the exponential dependence of the flash yield on the flash intensity and a high quantum yield of excitation trapping. Deviation from exponentiality observed in some samples is explained in terms of energy transfer between the units when they are densely packed.

1. Introduction

The photosynthetic unit is defined as the minimal structure that performs the task of charge separation required for the reactions of photosynthesis. Essentially it includes at least the pigment system and the reaction center. It could also include the whole electron transport system and even the elements that perform the task of phosphorylation and related processes. However, it seems that this involves much larger structures processing the products of many reaction centers [1]. Hence, it is instructive to define a photosynthetic unit in the minimal sense and to discuss later the type of cooperation between several units which make the larger structures. According to Duysens [2] "the unit consists of a reaction center and those chlorophyll molecules that have the highest probability of transferring excitation energy to this reaction center when all reaction centers are in the trapping state".

Still, even with this limited definition, we encounter the question whether this definition represents indeed a separate (although complex) molecular entity, composed of a pigment aggregate plus a reaction center, which performs independently of the other similar entities [2–7]. It is conceivable, as an alternative, that the reaction centers are spread in a uniformly large matrix of pigments so that excitation absorbed in any part of the system can visit regions including many reaction centers, the only limitation being the lifetime of the excitation [5–9] (uniform pigment matrix model)*. There are also models which keep the concept of the independent smaller units but which allow a certain fraction of excitation transfer between the units [9–13]. Such intermediate models assume the validity of the independent unit model but suppose that the units are sufficiently close to make resonance transfer of energy between them relatively important. Otherwise these models may serve as an approximation to lifetime limitation. This is because in the uniform pigment matrix concept the average distance that an excitation can travel is limited by its life time and could be confined to a region containing one or few reactions centers only. These models were developed to a high degree of

* Part of the work was started during a stay in the Davy Faraday Laboratory, The Royal Institution, 21 Albemarle St. London, Great Britain. This stay was supported by EMBO.

‡ *Abbreviations*: DCPIP – 2.6 dichlorophenolindophenol. PS-I, PS-II = photosystems I and II respectively.

* This model has several names coined by several authors. Thus Robinson [4] refers to it as the "lake" model, Tumerman [5] calls it "multicenteral". Other people refer to it as the "statistical" model.

sophistication by Clayton [9], who considered pigment domains (super units) which contain any number of reaction centers, and by Lavorel and Joliot who considered the formation of groups of fluorescent units [13].

Experimentally there are several approaches to the problem. All methods are based in principle on the possibility to vary the proportion of the active reaction centers and to check various responses as a function of this variable. The most direct way to vary the state of the reaction center is to use the transition caused by (relatively strong) actinic light from the "open" (active: ready for reaction) to "closed" (charged: after the primary reaction) form which is reversed in a dark reaction. The most unambiguous answer came from fluorescence lifetime measurements versus fluorescence yield, the last parameter being varied in a direct response to the proportion of "closed" reaction centers. In the separate units model one expects to find nonlinear dependence between average lifetime and yield (contrary to the standard formula) but linear dependence for the uniform pigment matrix model, which is indeed what was found ([6] cf. also [14]).

Other experiments treat fluorescence induction data (reflecting the kinetics of "open" → "closed" form of the reaction center) to show a certain probability (~ 0.5) of energy transfer between the (assumed in first approximation) independent units [10, 11]. Another approach was to measure directly the macroscopic quantum yield of electron transport reactions versus the proportion of active centers [10–12]. In this case the variability of active reaction centers was achieved by changing the intensity of a background light [12] and it was assayed by the yield of oxygen obtained by saturating flashes. Again the results of such experiments suggest a certain probability (~ 0.5) of energy transfer between the "independent" units.

All these experiments may be subjected to various sorts of criticism. Fundamentally the fluorescence may depend on several parameters. The fluorescence induction does not reflect a simple conversion of reaction centers but perhaps a more complicated phenomenon [15, 16] or even several parallel phenomena [17] and until we understand it in full detail we cannot trust the conclusions about energy-transfer suggested from the kinetics. The oxygen yield experiments were performed before the concept of the charge accumulating S-states was developed [18], and hence we cannot be sure about the contribution of this factor.

The only experimental evidence for the concept of the continuous pigment aggregate is the fluorescence lifetime measurements mentioned above [6]. However, we feel that this concept is of such fundamental importance to deserve a systematic study of it by all kinds of approaches which we have at our disposal, including critical improvements of experiments carried out before. Also during experiments we arrived at the conclusion that in different samples and reaction media the energy transfer parameters change considerably and require a careful systematic study.

1.1. Flash yield versus flash intensity

A possible different approach to the problem which is relatively free from the above criticism is to analyze accurately flash yield versus flash intensity curves. The flash time should be short enough for only one electron transfer act to occur per reaction center during the flash times. We express the absorbed light intensity of the flash in units of photons, n. The number of reaction centers is r. The two extreme models of independent units or the uniform pigment matrix with infinite range of energy-transfer give very definite answers for the flash yield $Y(n)$, as a function of n [7].

1.2. Uniform pigment matrix model

Each photon creates one unit of excitation. The ultimate fate of the excitation is to be dissipated at the reaction center, either causing the desired photochemistry with a quantum yield ϕ, or being converted to heat by radiationless transition at the reaction centers. We ignore at the moment fluorescence and radiationless transition in the pigment system. A "closed" reaction center behaves as if it does not exist from the point of view of the excitation. For a number of photons, n, less than r/ϕ each excitation will finally arrive at an open reaction center and cause a reaction with a probability ϕ. The flash yield is therefore given by $Y(n) = \phi n$. However, the maximal flash yield cannot exceed the number of reaction centers. Therefore, for $n \geqslant r/\phi$, $Y(n)$ must be equal to r.

1.3. Independent units model

The distribution of photons between the units is random. The chance that a particular photon will hit a

particular unit is $1/r$ and the chance that it will not hit that unit is $1 - 1/r$. The probability function for m photons hitting a unit when the total number of photons is n is given by the binomial expression:

$$\frac{n!}{(n-m)!m!}\left(\frac{1}{r}\right)^m\left(1-\frac{1}{r}\right)^{n-m}.$$

Since r and n are very large numbers indeed (order of magnitude the same as the number of molecules) we can approximate the above expression by

$$\frac{1}{m!}\left(\frac{n}{r}\right)^m e^{-n/r}, \quad \text{(provided } m \ll n\text{)}.$$

Again we introduce a quantum yield ϕ for a successful reaction at the reaction center. For a unit hit by m photons the chance that a reaction will not occur is $(1-\phi)^m$ and the chance that the reaction will occur is $1-(1-\phi)^m$. The flash yield will be given therefore by the following expression:

$$Y(n) = r\sum_{m=1}^{\infty}\{1-(1-\phi)^m\}\frac{1}{m!}\left(\frac{n}{r}\right)^m e^{-n/r}.$$

After performing the sum this equation gives a rather simple result:

$$Y(n) = r(1-e^{-\phi n/r}).$$

To summarize: we get two different expressions for $Y(n)$. The continuous pigment system model gives:

$$\begin{aligned} Y(n) &= \phi n, \qquad (n < r/\phi), \\ &= Y_m = r, \quad (n > r/\phi). \end{aligned} \tag{1}$$

Y_m is the maximal yield.

The independent units model gives

$$Y(n) = r(1-e^{-\phi n/r}). \tag{2}$$

In both models the maximal yield Y_m is the same. The initial slope $(dY/dn)_{n=0}$ is also the same, as can be verified from the formulas.

Fig. 1 shows the difference between the predictions of the two models, as expected from eqs. (1) and (2). This approach is essentially the same as the one used in a recent work by Wang and Myers [7].

Earlier data [19–22] are difficult to analyze mainly

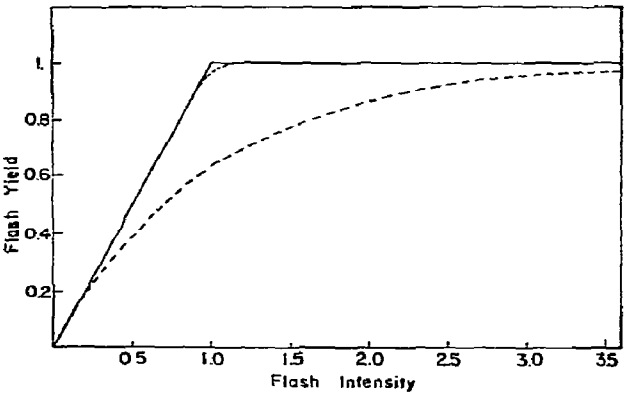


Fig. 1. Theoretical curves representing flash yields versus flash intensity for the independent units model (lower curve) and for the uniform pigment matrix model with infinite range of energy transfer (upper). To this curve a small correction is applied to allow for the experimental scatter in the flash intensity (cf. section 2).

because the main interest of the early work was to establish the maximum flash yield and to get an idea about turn-over times. Also the accuracy does not seem to be good enough, as a result of the long time needed for the measurement at that time. In spite of this there were specific claims that the form of $Y(n)$ versus n is exponential [20, 21] (cf. also [7] for a review) in accord with the independent unit model.

The recent work of Wang and Myers [7] intended to answer this question in view of the modern theories, by measuring the yield of a single flash. Unfortunately, no conclusive answer could be obtained from this work. This is mainly because the flash used was too weak to reach saturation. Hence the maximal flash yield Y_m is not given directly from the experiment but is treated as an adjustable parameter. The data nearly fit almost any of the models suggested in this work by adjusting parameters. The smallest standard deviation of the data from the calculated curves was obtained for either a model of separate units with an energy transfer probability of 30% (in the sense of Joliot et al. [10, 12]) or for completely separate domains with two reaction centers per domain (in the sense of Clayton [9]). However, the difference between the standard deviations for the different models does not seem to be significant.

The above experiments [7, 20, 21] may be further criticized for the following reasons:

(a) No particular attempt was made to make the light intensity uniform throughout the sample. To this end very dilute samples should have been used. Also, the flash light has a wide spectrum containing wavelengths for which the absorption of a single cell is considerable [23]. Thus different regions of the sample will "see" different light intensities and will give different contributions to the function $Y(n)$. The effect of this factor on the expected yield in the case of the uniform pigment matrix model would be to blur the point where the plot of yield changes its slope abruptly. The curve obtained will tend to be smoother and approach exponential-like behavior.

(b) The results obtained with an oxygen rate electrode [7] are uncertain to the extent that the linearity of the response with the oxygen evolution of such a system is difficult to ascertain, especially under flash conditions.

Our approach is to start with the simplest experimental system possible and get signals which are strictly proportional to the reaction extent. We used the DCPIP reduction by chloroplasts, which is undoubtedly a PS-II reaction (PS-I contribution is reversed quite rapidly [24]) and assayed it by very sensitive optical methods.

The presented results summarize the work done on many samples in a time of about a month. This was done in order to discover whether the pattern obtained is accidental or indeed represents a general trend.

2. Experimental

The most important point is to keep a homogeneous value of n over all the photosynthetic units present. It means that light absorption must be kept as low as possible, so that the light intensity will be uniform. To realize this point we filtered the flash light in such a way that only wavelengths corresponding to the absorption window in chloroplasts will be transmitted (approximately between 520 to 600 nm). This is achieved by using a Balzers K-4 broad band filter (Balzers, Liechtenstein). The best filter was made from a combination of two K-4 filters and a yellow cut-off > 520 nm filter (Schott OG 550). The transmission of these filters in relation to the chloroplasts absorption spectrum is shown in fig. 2. We used minimal concentration of chloroplasts corresponding to about 10% absorption.

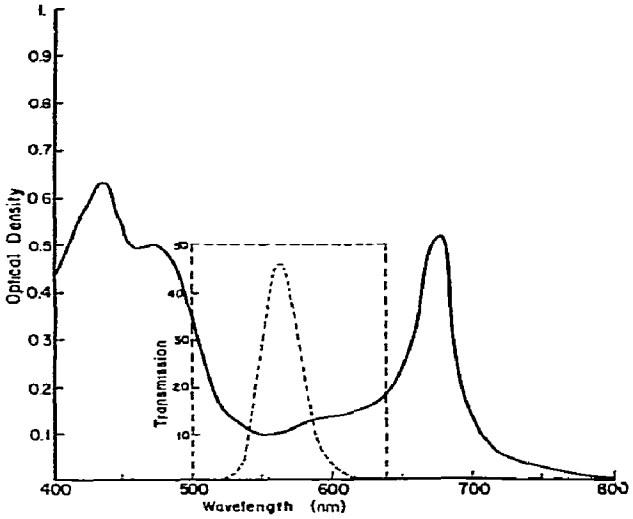


Fig. 2. Transmission spectrum (-----) of the combination of filters used for the experiments, in relation to the absorption spectrum (——) of the chloroplasts. Lettuce chloroplasts 15 μg chlorophyll/ml.

As a further trick a mirror was placed behind the cuvette reflecting back the flash light. For even 20% attenuation in the intensity over the cuvette optical pathlength the mirror causes a reversed attenuation and hence almost a homogeneous distribution of intensities (100% + 64% at the front; 80% + 80% at the rear).

A second point is to keep the flash intensity constant over many flashes. In order to get accurate results one must get a large signal. This requires integration of the results of many similar flashes. Our flash system utilizes a repetitive water-cooled xenon lamp (3F1 — made by ILC, Sunnyvale, California) which discharges a 18 μF condenser at 1 kV. This system was checked for intensity variations. The results of such check are represented in fig. 3 showing that over a series of 50 flashes about 60% gave intensities deviating within 3% of the average, about 30% deviated between 3 to 6%, while only about 10% deviated between 6 and 9% of the average. Larger deviations did not occur. It is possible to show that the effect of such distribution will produce only a negligible effect on the graphs of fig. 1 (fig. 1 — correction to the line representing the independent units response). The flash profile can be seen in fig. 4. Its half-time values is about 15 μs, the total time from firing to extinguishing (< 1%) is about 50 μs. The rate constants for electron transfer from the

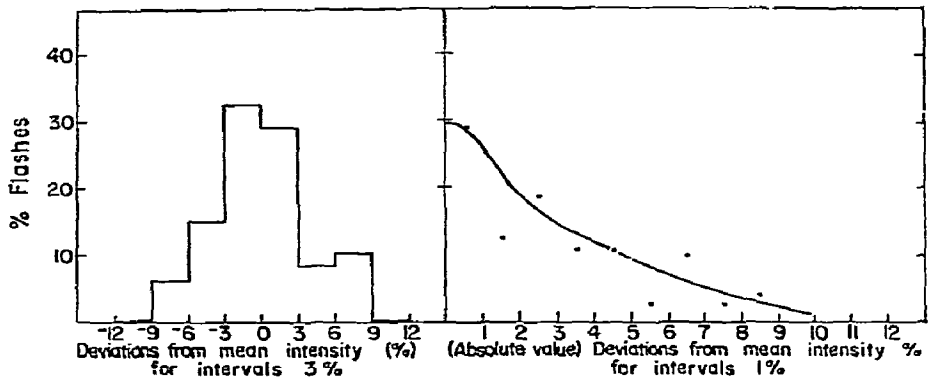


Fig. 3. Flash intensity distribution. A series of 50 flashes were given at a rate of 5 flashes/s. Scattered light from the flash was sensed by a photomultiplier and the signal was recorded with the help of a transient recorder (Biomation). Linearity was checked by neutral density filters.

reaction center are estimated [25] in the range of 1000 s^{-1}. Therefore, the contribution of two electron transfers during a flash must be less than 5% (taking the longer uncertainty in time), and is probably around 2% (taking the half-flash time).

The reaction was monitored in a dual-wavelength spectrophotometer (Aminco–Chance), capable of measuring small absorbance changes, and adapted to receive irradiation from a side window. 2 ml of the reaction mixture were placed in an ordinary optical cuvette. Series of about 20 to 40 flashes (in the small intensity range up to 100 flashes) were given at a rate of 3–5 flashes/s *. The flashes were counted by a scintillation counter triggered by a photoelectric cell place in the cuvette chamber. The flash yield is computed from the extent of the absorbance change at 610 nm relative to the change at 720 nm, divided by the number of flashes. A typical instrumental response of an experiment is shown in fig. 5.

It was necessary to ascertain that the extent of reaction is proportional to the number of flashes. This was checked by plotting the extent versus number of flashes, as shown in fig. 6. A linear plot was obtained. This test was performed for all samples tested. In very few cases there was a small extra (irreversible, or very slowly reversible) change which contributed to the extent in the first few flashes. In order to systematically eliminate such an effect the sample was flashed 4–5 times before the real measurement. After too many flashes a point was reached where the linearity ceased and the flash yield dropped. This is because we use a small amount of DCPIP which begins to be limiting as its depletion becomes considerable. We avoided this region. Flash yield data were supplemented by quantum yield determination in continuous light performed on the same sample. For this we used light from a projector which irradiated the same sample from a side opposite to the flash. The light was filtered by a B-11X type filter (band width 3 nm) from Baird-Atomic, Cambridge,

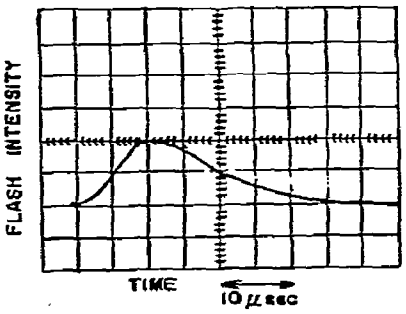


Fig. 4. Flash profile as seen on the oscilloscope. Time scale 5 μs/div.

* The dark time between the flashes (ca. 0.2–0.3 s) is quite long to ensure complete relaxation after each flash [19, 21, 22]. This point was checked i.. this work independently by observing that the flash yield was independent of the rate of flashing.

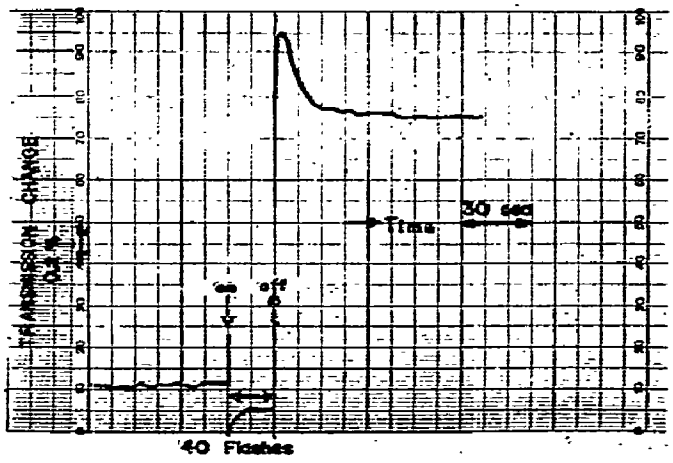


Fig. 5. Typical experimental record for DCPIP reduction. There is a change of light transmission after a series of flashes. (Lettuce chloroplasts 7.5 μg chlorophyll/ml, DCPIP 3 μM, NaCl 0.1 M, Hepes Buffer pH 7.8 5 mM, methyl ammonium chloride 3 mM). Full scale: 2% transmission. The overshoot is an experimental artifact. (During flashing the instrument is not responding.)

Mass., transmitting at 665 nm (cf. section 3). Light intensity was measured by a YSI radiometer (Yellow-Springs Instruments, Yellow Springs, Ohio). Special care was taken in constructing the optics so that the light is uniform (within 15%) over the irradiated surface. Light absorption was estimated with an integrating sphere photometer, using the same filter and sample.

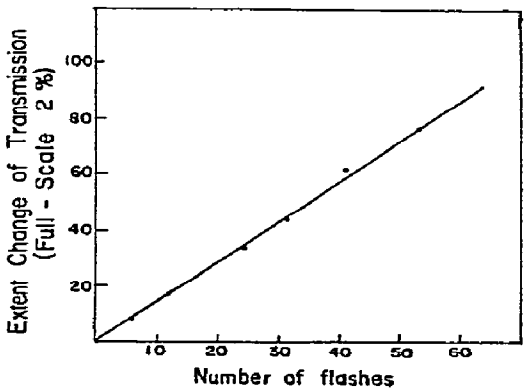


Fig. 6. A check that the extent of the transmission is proportional to the number of flashes. The same details as in fig. 5 but with different sample.

Quantum requirements were plotted against the light intensity and extrapolated to zero light intensity. The light intensity range for this plot was nearly limiting, so that the quantum requirement changes only a little and linearly, as expected. We estimate that the absolute quantum yield cannot deviate more than 10% from our value. Light intensity variations were achieved by using neutral density filters (Schott-NG type) carefully calibrated for each wavelength. Two kinds of sample were used: chloroplasts from pea (Pisum sativum var. Lincoln) and lettuce (Lactuca sativa var. romaine). These were prepared in a standard way [26], stored in a medium containing sucrose 0.2 M, sodium chloride 0.1 M, tricine pH 7 0.05 M, and human serum albumin 0.05%.

3. Results and discussion

Figure 7 represents the flash yield versus flash intensity for a few examples. Each point represents a fresh sample, since we preferred to renew the sample rather than to be in danger of DCPIP depletion. This in turn introduced some scatter of results, which we tried to minimize by careful pipetting and continually shaking the stocked chloroplasts. With our filter the flash yield at the highest intensity is about 80–90% of the maximum. In order to evaluate the maximal flash yield as an experimental parameter we also flashed the system with the cut-off filter > 520 nm alone. In this case complete saturation is achieved (fig. 7a), the flash yield stays remarkably constant until an attenuation of the intensity to about 12% is reached. Since the maximum flash yield represents the number of reaction centers and is independent of the type of model, we can use its value for the experiments with the nearly monochromatic filter.

In order to systematically check for exponentiality and estimate deviation from it a test point in the flash yield curve was chosen. This test point is defined by the value of n corresponding to the intercept of the tangent at $n = 0$ and the line $Y = Y_m$. A strictly exponential curve will give a value of Y/Y_m, at the test point, of $1-e^{-1} \approx 0.63$. The continuous pigment model gives a value of 1 at the test point. Any other intermediate model will give numbers between 0.63 and 1.

The results do not give a single general answer. On

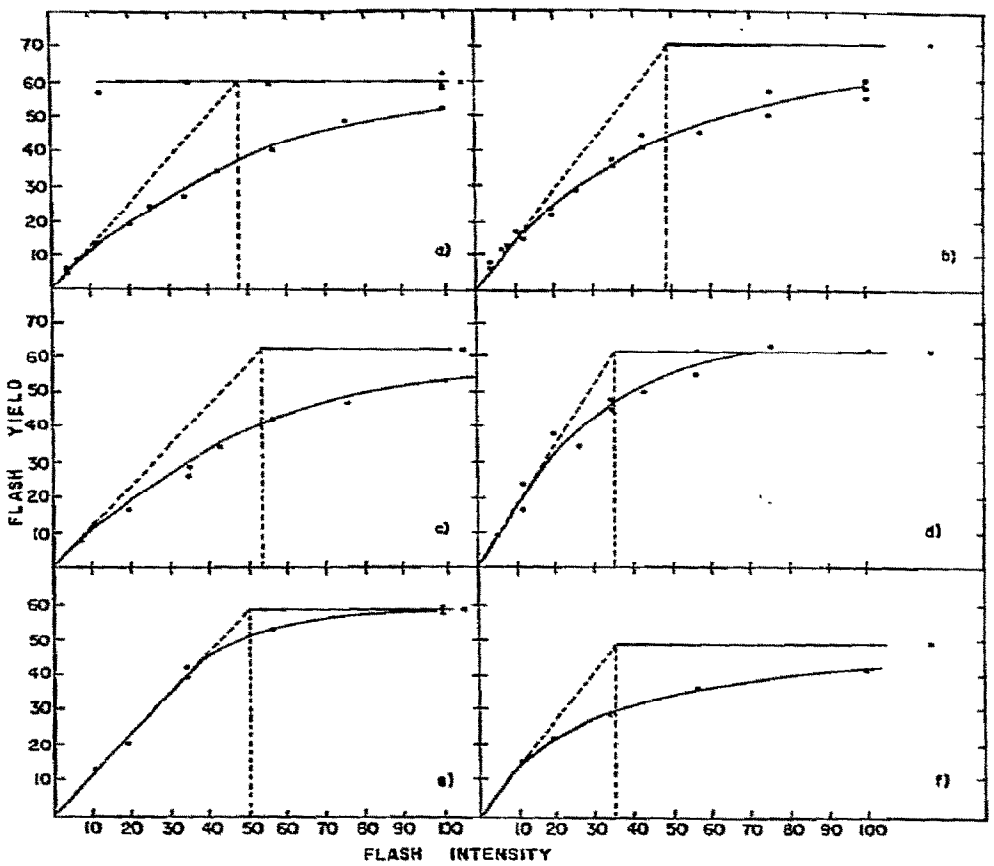


Fig. 7. Typical examples out of a larger number of experiments showing flash yield versus flash intensity. (a) Lettuce chloroplasts in the same reaction medium as in fig. 5. (b) Lettuce chloroplasts in a medium low in salt NaCl 0.01 M, Hepes pH 7.8 5 mM. (c) Lettuce chloroplasts in the same medium as in (a). (d) Pea chloroplasts in a medium as in fig. 5. (e) (Very green) pea chloroplasts in a medium as in fig. 5. (f) The same as (e), but after a few hours (approximately 5) of aging, Chloroplasts concentration in all experiments 10 μg chlorophyll/ml.
The ordinate is given as % of full-scale. Full-scale is 2% transmission for a–c and 1% for d–f. The flash yield is expressed as the transmission change per 30 flashes. In (a) the upper line represents flash yield curve with only a cut-off filter > 520 nm. This shows the maximal flash yield. In the other sections the upper line represents the mean value of several determinations at the maximal intensity with the cut-off filter. The values obtained are shown at the right extreme. Note that with the pea samples (d–e) saturation is achieved even with the monochromatic filter. The size of the PSU can be calculated taking the value of the maximal flash yield and the extinction coefficient for DCPIP at its peak absorption $2 \times 10^4\ M^{-1}\ cm^{-1}$ (10^4 equiv $e^{-1}\ cm^{-1}$). For a–c (lettuce) the typical result is 650 chlorophylls/unit while for d–f it is about twice as much.

the one hand we have three examples with clear exponential behavior (fig. 7a, b, c, and f). This is confirmed by the log $(Y_m - Y)$ versus flash intensity plot (fig. 8), and is supported by the numerical value interpolated for the flash yield at the test point. The examples a–c of fig. 7 give values Y/Y_m for this point of 0.61, 0.63, 0.65 respectively. On the other hand there are results quite close to a linear behaviour (fig. 7d, e: deviating only a little near the break point). The examples d and e of fig. 7 give a value Y/Y_m at the test point of 0.76, 0.87 respectively. The example f is for the same preparation of e but after aging for a few hours. It is exponential with a value 0.59 for Y/Y_m at the test point.

In order to make a unified picture we can start from the model of independent units on the one hand and imagine a smooth transition to the model of the uniform

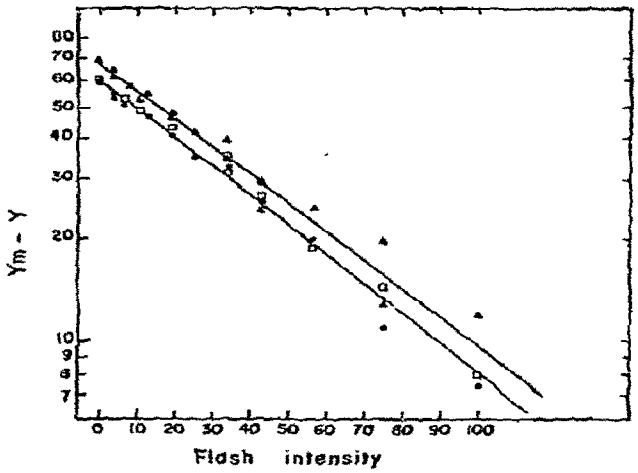


Fig. 8. Half log plots of the data from fig. 7a–c. (•) – a, (▲) – b, (□) – c. The plots for a and c are nearly identical so that they are represented by single line.

pigment matrix system. On the one extreme we may assume that when the concentration of the photosynthetic units is small, they will be far apart so that no excitation can be transferred between them. On the other extreme when the chloroplasts are loaded with photosynthetic units the units may be crowded and allow considerable excitation energy exchange. In this way we keep the concept of the unit as an entity in all circumstances.

On the other hand, we may start with the uniform pigment matrix model and assume in the extreme case an efficient energy transfer between all members with lifetime of the excitation long enough to visit effectively a large region containing many reaction centers. The transition to an (apparent) independent units model would be by decreasing the excitation lifetime of decreasing the efficiency of transfer, e.g., by considering samples with greater average distance between the pigments, or the presence of more parasite quenching centers; until at last the average lifetime is such that only one or less reaction centers may be visited on the average during the lifetime.

In order to make an intelligent choice between the above two alternative views, we have to consider the trapping efficiency. For this we will use the simplified formula given by Duysens [27, 28] (cf. appendix):

$$\Phi_{\text{trapping}} = \frac{\bar{p}T/N}{1 + \bar{p}T/N}, \tag{3}$$

where $\bar{p}$ is the average number of transfers during a lifetime considered without quenching in the reaction center ($\bar{p} = \tau/\tau_t$; $\tau \equiv$ lifetime, $\tau_t \equiv$ transfer time). T is the number of open centers and N the number of chlorophyll-a molecules.

Applying this formula to the uniform pigment matrix model, one can obtain an expression for the flash yield as follows:

$$-\frac{dT}{dt} = \phi\,\Phi_{\text{trapping}} I = \phi\,\frac{\bar{p}T/N}{1 + \bar{p}T/N}\,I \tag{4}$$

(ϕ is the quantum efficiency of a charge separation after successful trapping). This equation expresses the rate of disappearance of traps (i.e., conversion from "open" to "closed" form with a charge separation), as function of T, and I, the absorbed light intensity.

From (4) we get the following differential equation:

$$(N/\bar{p}T + 1)dT = -\phi\,dn \tag{5}$$

(considering that $n = \int I dt$) which for our flash will be integrated as follows:

$$(N/\bar{p})\ln(T/T_0) + (T - T_0) = -\phi n, \tag{6}$$

where T_0 is the initial number of reaction centers and n is the number of photons in the flash. The flash yield is $Y = T_0 - T$ and the maximal flash yield is $Y_m = T_0$. Hence eq. (6) can be expressed in terms of the flash yield as follows:

$$Y/Y_m - (N/\bar{p}T_0)\ln(1 - Y/Y_m) = \phi n/T_0. \tag{7}$$

This equation is the most general equation for the flash yield in the uniform pigment matrix model. It gives eq. (1) as a limit for very large $\bar{p}$. In this case, the second term on the l.h.s. will be small compared to the first term (except for values of Y very close to Y_m). On the other hand when $\bar{p}$ is small the first term may be neglected and we obtain an exponential behavior.

$$Y/Y_m \approx 1 - \exp(-\bar{p}\phi n/N). \tag{8}$$

From eq. (8) we conclude that also the uniform pigment matrix model can give rise to exponential behaviour of Y versus n, provided that $N/\bar{p}T_0$ is large which means that the efficiency of trapping is small.

In fig. 9 we plotted the theoretical flash yield versus

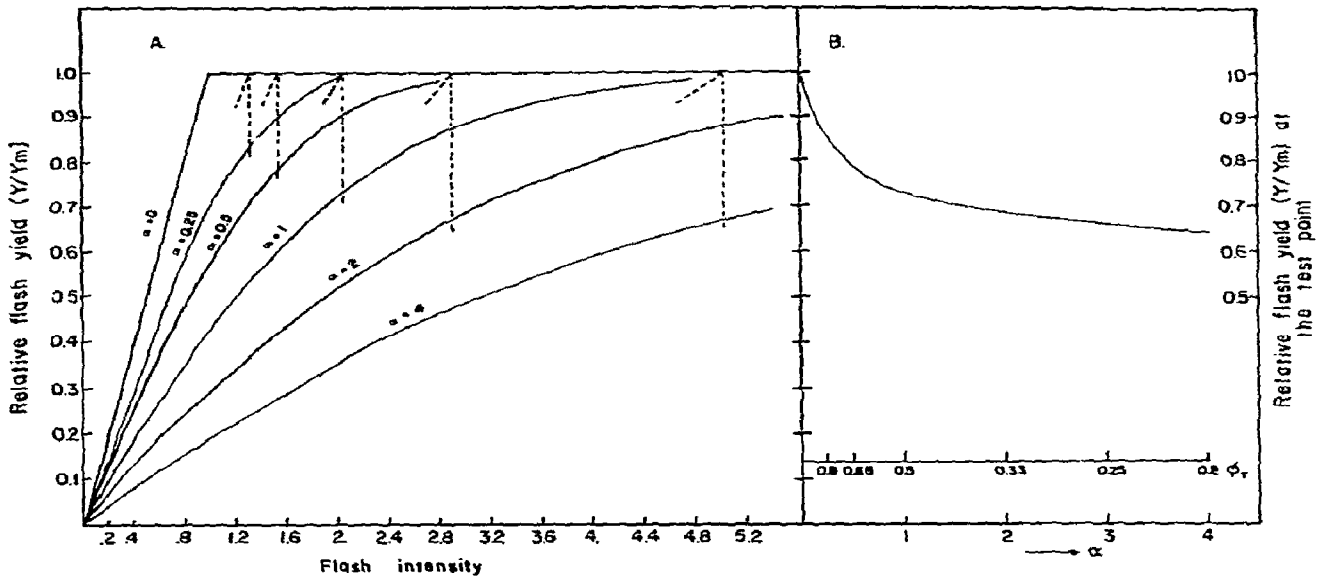


Fig. 9. (A) Theoretical plot of eq. (7), for the uniform pigment matrix model with various values of the parameter $\alpha = (\bar{p}T_0/N)^{-1}$. (B) The value of Y/Y_m at the test point calculated from the plot of fig. 9A, for different values of α.

$\phi n/T_0$ from eq. (7) for various values of the parameter $\alpha = N/\bar{p}T_0$. From these plots a value for Y/Y_m at the test point is calculated (fig. 9A). The quantum yield of trapping given by eq. (3) must also conform to the same value of $N/\bar{p}T_0$. This should be an adequate test for the continuous pigment model.

Measurements of quantum yield in limiting light conditions were therefore also performed. The quantum yield was measured at optimal conditions at a wavelength 665 nm. The reason to measure at this wavelength rather than at 560 nm (where the flash experiments were performed) is to approximate the quantum yield of $\Phi_{trapping}$ of eq. (3). At 560 nm there is an uncertainty in the factor of absorption into the carotenoids and the probability of energy transfer to the chlorophyll-a domain. The result at 665 nm must be corrected because of absorption into PS-I. For the general assumption of equal distribution of light between the two photosystems [29, 30] we get:

$\Phi_{trapping} \gtrsim 2 \times$ quantum yield at 640 nm.

Our quantum yield value was 0.4: hence $\Phi_{trapping} \gtrsim 0.8$ which should give (fig. 9B) a value of $\gtrsim 0.84$ for Y/Y_m at the test point while the actual value is close to 0.6 (cf. fig. 7a, b, c, f). A further check confirming the above estimation of $\Phi_{trapping}$, which is perhaps more direct, comes from considering the ratio F_{max} to F_0 in the fluorescence induction curves of the chloroplasts [3]. We have devised a method to estimate the quite considerable background fluorescence [31]. After subtracting the background fluorescence the ratio F_0/F_{max} is related [3] to $\Phi_{trapping}$ by $\Phi_{trapping} = 1 - F_0/F_{max}$. Our value for F_0/F_{max} is around 0.1 which gives $\Phi_{trapping} \approx 0.9$. ($N/\bar{p}T_0 \sim 0.11$ Y/Y_m (test point) $\approx$ 0.9.)

We therefore conclude that the exponential behaviour of Y together with the high $\Phi_{trapping}$ is not compatible with the uniform pigment matrix model. The exponential examples represent a case of independent units. The other examples probably represent then photosynthetic units with some interaction.

The plausibility of either concepts depends very much on personal taste and education. Thus Robinson [5] in his article refers to the uniform pigment matrix model (which he calls the "lake" model) as more ap-

pealing to the physicist. On the other hand from the point of view of biosynthesis it is perhaps much more plausible to think in terms of the following order of events: first a reaction center is synthesized and assembled and then pigments are assembled around it. At least during the first stages of biosynthesis the pigment systems around each reaction center will be separated from each other. Evidence for this point of view is missing, however. All existing data point to the fact that PS-II activity starts only after a lapse of time in which PS-I activity has been developed and a considerable fraction of chlorophyll has been synthesized [32, 33]. This shows by no means, however, that in PS-II the pigments are assembled before the reaction centers; it simply cannot give evidence for or against this point of view.

It is not the dynamics of the biosynthesis of PS-II but rather the comparison of the static situation in various photosynthetic organisms that gives some hint towards the concept of independent units. Schmid and Gaffron [34] showed that the size of the PSU is variable within the same species with a distribution of sizes from a very small value (300 chlorophylls per unit) to a very high value (5000 chlorophylls per unit). Wild [35] showed that in pale mutants it is the number of chlorophylls per reaction center rather than the number of photosynthetic units per cell which is reduced compared to wild types. It is clear that the average volume of a photosynthetic unit is quire variable while the distances between different reaction centers are much less so. If one does not accept that in these different circumstances the chlorophyll–chlorophyll distance is also variable the only choice is to assume the concept of a photosynthetic unit as a physical entity. The behaviour of samples e and f in fig. 7 is particularly interesting from this standpoint. The same sample e which showed a behaviour very close to the uniform pigment matrix model shows after a few hours of aging (f) different behaviour. Since the initial slopes are very nearly the same (meaning the same initial $\Phi_{trapping}$) the only explanation is in terms of a transition from a situation of strong interaction between photosynthetic units to another situation of negligible interaction between them. We cannot say at the moment what caused this change, or whether it is a general phenomenon.

The samples which behaved close to the uniform pigment matrix model (fig. 7d, e) were prepared from leaves of very deep green colour. Furthermore, the reaction mixture contained relatively high salt concentration. These two factors may help to establish conditions where the average distance between photosynthetic units is small and the interaction is large. The first factor means large relative concentration of chlorophyll. This is confirmed by noticing that the maximal flash yield per chlorophyll is about half compared to the lettuce samples (fig. 7a, b, c). The second factor means osmotic shrinkage. The samples prepared from lettuce fig. 7 (a, b, c) had relatively low chlorophyll concentration and behaved according to the independent units models.

We therefore suggest that the concept of a photosynthetic unit has a physical reality and that the approach, in a few cases, to a uniform pigment matrix model is a result of energy transfer interaction between the units which takes place when the units are sufficiently crowded. It is clear that the energy transfer factor p of Joliot et al. [10–12], cannot have any general significance, but it must vary.

One has to explain the results of fluorescence lifetime measurements [6] which hitherto were used to favor the concept of the uniform pigment matrix. It is, of course, possible that in the particular sample used the interaction between units was considerable. It is therefore planned to repeat the fluorescence lifetime experiments and to try and measure the fluorescence decay curve directly [36].

4. Conclusions

The response of flash yield versus flash intensity in many cases fits a model of independent photosynthetic units. The exceptions can be treated by allowing energy transfer between the units. This conclusion has to be confirmed by new measurements of fluorescence decay, and to be expanded by searching for the factors which control the interaction between the photosynthetic units.

Appendix: Derivation of eq. (3)

In view of our ignorance of the detailed structure of the photosynthetic unit we must not look for any formula derived by special models. Rather than we shall use the ratio T/N as giving a probability guide for the chain of

energy-transfer steps. Since the number of transfers during the excitation lifetime is quite large we can refer to one step of energy-transfer as an elementary process defining on the average a unit time scale. The probability of excitation decay during this time of transfer is given by τ_t/τ (τ_t = transfer time; τ = decay time), and the average number of transfers during a lifetime, $\bar{\rho}$, is the reciprocal τ/τ_t. The relative probability of a transfer to a reaction center is T/N compared to the probability of a transfer to a regular bulk pigment $1 - T/N$.

The probability of ρ transfers ending with trapping, is the product of

$$(1 - \tau_t/\tau)^\rho (1 - T/N)^\rho T/N.$$

The first factor is the probability that the system is still excited after ρ transfers, the second is the probability for ρ transfers in the bulk pigment, and the third is the probability for trapping. To find the total probability of trapping for any value of ρ we must sum this expression for ρ varying between 0 and ∞.

$$\Phi_{\text{trapping}} = \sum_{\rho=0}^{\infty} (1 - 1/\bar{\rho})^\rho (1 - T/N)^\rho T/N$$
$$= \frac{T/N}{1 - (1 - 1/\bar{\rho})(1 - T/N)}.$$

Since T/N and $1/\bar{\rho}$ are small numbers we can drop their product compared to any of them. Hence:

$$\Phi_{\text{trapping}} = \frac{T/N}{1/\bar{\rho} + T/N} = \frac{\bar{\rho}T/N}{1 + \bar{\rho}T/N}. \qquad \text{(Q.E.D.)}$$

References

[1] W. Junge and H.T. Witt, Z. Naturforsch 23B (1968) 244–254.
[2] L.N.M. Duysens, Brookhaven Symposia in Biology 19 (1966) 72–80.
[3] S. Malkin and B. Kok, Biochim. Biophys. Acta 126 (1966) 413–432.
[4] R.B. Park and N.G. Pon, J. Mol. Biol. 3 (1961) 1–10.
[5] G.W. Robinson, Brookhaven Symposia in Biology 19 (1966) 16–48.
[6] L.A. Tumerman and E.M. Sorokin, Mol. Biol. (English Transl.) 1 (1967) 527–535.
[7] R.T. Wang and J. Meyers, Photochem. Photobiol. 17 (1973) 321–332.
[8] W.J. Vredenberg and L.N.M. Duysens, Nature 197 (1963) 355.
[9] R.K. Clayton, J. Theor. Biol. 14 (1967) 173–186.
[10] P. Joliot and A. Joliot, Compt. Rend. 258 (1964) 4622–4625.
[11] P. Joliot, R. Delosme and A. Joliot, in: Currents of photosynthesis, eds. J.B. Thomas and J.C. Goodheer (Ad Donker, Rotterdam, 1966) pp. 359–366.
[12] P. Joliot, A. Joliot and B. Kok, Biochim. Biophys. Acta 153 (1958) 635–652.
[13] J. Lavorel and P. Joliot, Biophys. J 12 (1972) 815–831.
[14] A. Muller, R. Lumry and R.S. Walker, Photochem. Photo-, biol. 9 (1969) 113.
[15] W.L. Butler, J.W.M. Visser and H.M. Simons, Biochim. Biophys. Acta 292 (1973) 140–151.
[16] D. Mauzerall, Proc. Natl. Acad. Sci. US 69 (1972) 1358–1362.
[17] G.A. Den Haan, J.T. Warden and L.N.M. Duysens, Biochim. Biophys. Acta (1973) 120–125.
[18] B. Kok, B. Forbush and M. McGloin, Photochem. Photobiol. 11 (1970) 457–475.
[19] R. Emerson and W.J. Arnold, Gen. Physiol. 16 (1932) 191–205.
[20] H.I. Kohn, Nature 137 (1936) 706.
[21] B. Kok, Biochim. Biophys. Acta 21 (1956) 245–258.
[22] E. Rabinowitch, Photosynthesis (Interscience, New York, 1956) Vol. 1, part 2, ch. 34, pp. 1433–1484.
[23] L.N.M. Duysens and J. Huiskamp, cf. ref. [22] pp. 1863–1866.
[24] B. Kok, S. Malkin, O. Owens and B. Forbush, Brookhaven Symp. in Biology 19 (1966) 446–459.
[25] B. Forbush and B. Kok, Biochim. Biophys. Acta 162 (1968) 243–253.
[26] M. Avron, Biochim. Biophys. Acta 40 (1960) 257–272.
[27] L.N.M. Duysens, Transfer of excitation energy in photosynthesis, Thesis, Utrecht (1952).
[28] L.N.M. Duysens, Progress of Biophysics 14 (1964) 1–104.
[29] K. Sauer and R.B. Park, Biochemistry 4 (1965) 2791–2797.
[30] J. Kelly and K. Sauer, Biochemistry 4 (1965) 2798–2802.
[31] S. Malkin and Y. Siderer, Biochim. Biophys. Acta 363 (1974) 54–69.
[32] M. Plensicar and D.S. Bendall, in: Proc. II International Congress on Photosynthesis, Stresa, eds. G. Forti, M. Avron and A. Melandri (Junk, The Hague, 1971) pp. 2367–2374.
[33] N.K. Boardman, J.M. Anderson, A. Kahn, S.W. Thorne and T.E. Treffry, in: Autonomy and biogenesis of mitochondria and chloroplasts, eds. N.K. Boardman, A.W. Linnane and R.M. Smillie (North-Holland, Amsterdam, 1971) pp. 70–84.
[34] G.H. Schmid and H. Gaffron, in: Progress of photosynthesis research, Vol. II, ed. H. Metzner (Laupp, Tubingen, 1969) pp. 857–870.
[35] A. Wild, ref. [34] pp. 871–876.
[36] S. Malkin and C. Lewis, preliminary account of such experiments is in preparation.

BIOPHYSICAL CHEMISTRY 2 (1974) 338–344. © NORTH-HOLLAND PUBLISHING COMPANY

CONCERTED CHANGES IN AN ALLOSTERIC MACROMOLECULE

Alfredo COLOSIMO, Maurizio BRUNORI and Jeffries WYMAN

C.N.R. Center for Molecular Biology, Institutes of Biochemistry and Chemistry, University of Rome, and Regina Elena Institute for Cancer Research, Rome, Italy

Received 3 July 1974

This paper reports an analysis of the behaviour of allosteric macromolecules in the framework of the simple Monod–Wyman–Changeux model. The emphasis is on the analysis of the reciprocal influence of the various parameters which enter into the model, with particular reference to the relationship among a number of sites in the macromolecule and the Hill parameter n. This appears of interest for the behaviour of some of the extremely large respiratory proteins containing up to 100, or more, oxygen binding sites, where a very large value of n is often coupled with a relatively small value of the total interaction free energy.

Cooperative binding of a ligand by a macromolecule is conveniently described by a Hill plot in which $\ln [\bar{X}/(1-\bar{X})]$ is represented as a function of $\ln x$, where $\bar{X}$ is the fractional saturation of the macromolecule with ligand X and x is the ligand activity. Such a graph must always have an asymptote of unit slope at each end unless the interaction between the sites is infinite. The minimum value of the total interaction free energy realized per site in saturating the macromolecule with the ligand is then given by $RT\Delta \ln x$, where $\Delta \ln x$ is the horizontal distance between the asymptotes. Similarly and more generally, the minimum value of the interaction free energy realized in passing from *any* degree of saturation $\bar{X}_1$ to $\bar{X}_2$ is given by the horizontal distance between the lines of unit slope drawn through the two points $(\ln x_1, \ln [\bar{X}_1/(1-\bar{X}_1)])$ and $(\ln x_2, \ln [\bar{X}_2/(1-\bar{X}_2)])$. At the same time the point value of the interaction free energy at any degree of saturation is given by

$$[RT/\bar{X}(1-\bar{X})](1-1/n) = \Delta F_I ,$$

where n is the slope of the Hill plot at the point in question [1]. The earlier propositions just enunciated are obtained from this by integration; and it will be seen that whenever $n > 1$ anywhere, there must be positive (or stabilizing) interactions between sites, i.e., the system is cooperative. The parameter n can of course never exceed the number of sites, and when it is equal to the number of sites it means that the interaction free energy between the sites is infinite, i.e., that the sites are so strongly coupled that they all react simultaneously to give an nth order reaction. It should perhaps be pointed out that n is a statistical quantity and that even when n goes to infinity the point value of the interaction free energy is only

$$\Delta F_I = RT/\bar{X}(1-\bar{X}) .$$

Cooperativity in biological macromolecules is often the result of conformational (or allosteric) changes induced by the ligands; in other words, it is the expression of ligand-linked conformational equilibria. It is of interest to see how this shows up in the Hill plot, and what the actual behaviour of some of the very large macromolecules as represented in their Hill plots implies as to the underlying conformational changes. Of particular interest here are some of the extremely large respiratory proteins, containing up to 100 or more sites for oxygen, where a very large value of n is often coupled with a relatively small total interaction free energy, i.e., where the Hill plot shows a rather sharp upward bend or kink in the middle range of saturations associated with rather closely spaced asymptotes.

The two most commonly invoked allosteric models

are the Monod–Wyman–Changeux (M.W.C.) and the Koshland–Nemethy–Filmer (K.N.F.) models, both of which can be shown to be special cases of a more general parent model [2]. Of these, the M.W.C. (or concerted) model is the simplest and involves the smallest number of parameters (only 2). At the same time it offers the greatest possibility of a large but localized value of n coupled with a relatively small value of $\Delta F_{\mathrm{I,total}}$. It is this model, therefore, which we shall consider in what follows.

In the M.W.C. model [3] it is assumed that the macromolecule exists in only two forms (T and R), in each of which the ligand binding sites are all alike and independent. The binding polynomial (or generating function) for this model is given by

$$P = (1+x)^r + L_0(1+\alpha x)^r , \tag{1}$$

where r is the number of sites, the same in each of the two conformations; L_0 is the equilibrium constant for the $T \rightarrow R$ transition in the absence of ligand (i.e., $L_0 = R/T$, when $x = 0$), and α is the ratio of the binding constant K for a site in the R form to that of a site in the T form ($\alpha = K_R/K_T$).

In this model the value of $\bar{X}$, the fractional saturation of the macromolecule with ligand, is given by

$$\bar{X} = \frac{1}{r}\frac{\mathrm{d}\ln P}{\mathrm{d}\ln x} = \frac{1}{r}\frac{P'}{P} ,$$

where

$$P' = \frac{\mathrm{d}P}{\mathrm{d}\ln x} = r[(1+x)^{r-1}x + L_0(1+\alpha x)^{r-1}\alpha x] . \tag{2}$$

At the same time n is given by

$$n = \mathrm{d}\ln[\bar{X}/(1-\bar{X})]/\mathrm{d}\ln x = \frac{P''}{P'} - \frac{rP'-P''}{rP-P'} , \tag{3}$$

where

$$P'' = \mathrm{d}P'/\mathrm{d}\ln x$$

$$= P' + r(r-1)[(1+x)^{r-2}x^2 + L_0(1+\alpha x)^{r-2}\alpha^2 x^2] .$$

Eq. (3) may also be written as

$$n = (P''/P' - r\bar{X})/(1-\bar{X}) . \tag{4}$$

Further, the total apparent interaction energy is given by

$$\Delta F_{\mathrm{I,total}} = RT\ln c , \tag{5}$$

where

$$c = \frac{(1+L_0)(1+L_0\alpha^r)}{(1+L_0\alpha)(1+L_0\alpha^{r-1})} . \tag{5'}$$

In carrying out the analysis it is convenient to treat c and α as the independent variables and then, on the basis of (5'), to obtain L_0 by the relation

$$L_0 = (B \pm \sqrt{B^2-4A})/2A , \tag{6}$$

where

$$A = \alpha^r , \quad B = [1 - c(\alpha+\alpha^{r-1}) + \alpha^r]/(c-1) . \tag{6'}$$

These equations make it possible to calculate the Hill plot (or the corresponding binding curve, of the macromolecule for various sets of values of r, c, α, and L_0. What we are primarily interested in is of course the sharpness of the transition in relation to the spacing of the asymptotes, i.e., n in relation of $\Delta F_{\mathrm{I,total}}$ as given by c. As we shall see, for the sufficiently large values of r the transition can be extremely sharp for any value of $\Delta F_{\mathrm{I,total}}$, even a very small one, with the result that we run into something approaching a phase change. Although detailed calculations can be made very easily on the basis of the above equations with the aid of a computer, still, as a first step, it is convenient to get an analytical solution for the special case where we impose the conditions of symmetry of the binding curve. This brings the transition into the middle of the Hill plot, where $\bar{X} = \frac{1}{2}$; also it reduces the number of parameters to one (α) and greatly simplifies the equations.

The conditions of symmetry of the binding curve (or of the HIll plot, for they are the same) can be shown to be met provided only we set

$$L_0 = \alpha^{-r/2} . \tag{7}$$

For this value of L_0, the value of the median ligand activity, x_{m}, now equal to $x_{1/2}$ (for which $\bar{X} = \frac{1}{2}$), is given by

$$x_{\mathrm{m}} = x_{1/2} = \alpha^{-1/2} .$$

At the same time the equilibrium constant L for the $T \rightarrow R$ transition, which in the general case is given by

$$L = L_0\left(\frac{1+\alpha x}{1+x}\right)^r , \tag{8}$$

Table 1
Dependence of n_m on the number of binding sites, r, calculated from eq. (11) for two values of α

r	n_m	c	$\Delta F_{I,total}$ (cal)
a. $\alpha = 9$, $(1+\alpha)/(1+\alpha^{1/2})^2 = 0.625$			
4	1.75	7.5	1195
6	2.26	8.8	1290
8	3.76	9	1315
50	11.2	9	1315
100	24.0	9	1315
b. $\alpha = 100$, $(1+\alpha)/(1+\alpha^{1/2})^2 = 0.835$			
4	3.01	98	2700 #)
6	4.35	100	2730
8	5.69	100	2730
50	33.8	100	2730
100	70.0	100	2730

#) This corresponds very closely with the case of human hemoglobin, for which the binding curve is approximately, if not exactly, symmetrical (see Antonini and Brunori [4] for review); the result is an argument for the applicability of the concerted model to that molecule. The idea that symmetry of function might be associated with symmetry of structure was suggested many years ago [5].

becomes

$$L = \left(\frac{\alpha^{-1/2}+\alpha^{1/2}x}{1+x}\right)^r , \qquad (9)$$

and at the midpoint of the binding curve, where $x = \alpha^{-1/2}$, L is unity. At this point the value of n given by eq. (4) is

$$n \equiv n_m = 2[1 + (r-1)(1+\alpha)/(1+\alpha^{1/2})^2] - r . \qquad (10)$$

Furthermore

$$c = \frac{2+\alpha^{r/2}+\alpha^{-r/2}}{2+\alpha^{(r-2)/2}+\alpha^{-(r-2)/2}} . \qquad (11)$$

We adopt the convention that $\alpha > 1$, which means that $L_0 < 1$ *. It follows from (11) that for sufficiently large values of r, c becomes equal to α. Indeed for $\alpha = 10$ this is already approximately true even for $r = 4$. At the same time the expression $(1+\alpha)/(1+\alpha^{1/2})^2$ in the equation for n_m increases rather slowly from 0.625 to 1 as α goes from 9 to ∞. It is clear therefore that under conditions in which we are interested n_m will be linear in r regardless of the value of c (or $\Delta F_{I,total}$) and will increase without limit as r increases, with the result that the transition becomes a true phase change. This is brought out by the figures shown in table 1 (a and b). Another aspect of the situation is revealed in fig. 1, which shows how the value of n_m/r, i.e., the value of n_m, normalized with respect to its maximum value r, increases towards 1 as $\Delta F_{I,total}$ increases indefinitely. It will be seen that the curves for different values of $r \geq 4$ all lie close together and approach a common bounding curve as r gets bigger and bigger.

It is a simple matter, with the aid of a computer†, to construct full Hill plots for various cases. Such plots (up to $r = 36$) are shown in fig. 2. It is also a simple matter to construct Hill plots for more general cases where the constraint of symmetry is relaxed. Such plots are shown in fig. 3, where the transition (or switch over point, defined as the point where $R/T = L = 1$) is no longer centered at $\bar{X} = \frac{1}{2}$. It is interesting to see how, as we depart more and more from the condition of symmetry, the value of n, even at its greatest, decreases slowly but progressively while the region of high values of n moves farther and farther from the point $\bar{X} = \frac{1}{2}$, following the switch over point (where $L = 1$), and eventually comes to be outside the experimentally accessible range of saturation.

The chlorocruorin from the worm Spirographs spallanzanii, which has a molecular weight of ~2 500 000 and contains approximately 72 oxygen binding sites (hemes) per molecule, provides a good example of one of the larger respiratory proteins [6]. Its Hill plot, given in fig. 4, shows a maximum value of $n = 5$, which occurs at $\bar{X} \approx 0.64$, and a value of $\Delta F_{I,total} = 1800$ calories, corresponding to $c = 25$. A glance at fig. 1 shows that these results are incompatible with the assumption that the whole molecule with its 72 sites behaves like a simple M.W.C. model. If so, the value of $\Delta F_{I,total} = 1800$ cal would imply a value of $n_m/r = 0.45$ or $n_m \approx 72 \times 0.45 = 32.4$ as compared with the observed value of 5. We might, as the next simplest hypothesis, assume that the sites interact in independent constellations, each containing r sites.

* The opposite assumption would of course give the same results.

† Computations were made with a Hewlett Packard Model 9830A computer.

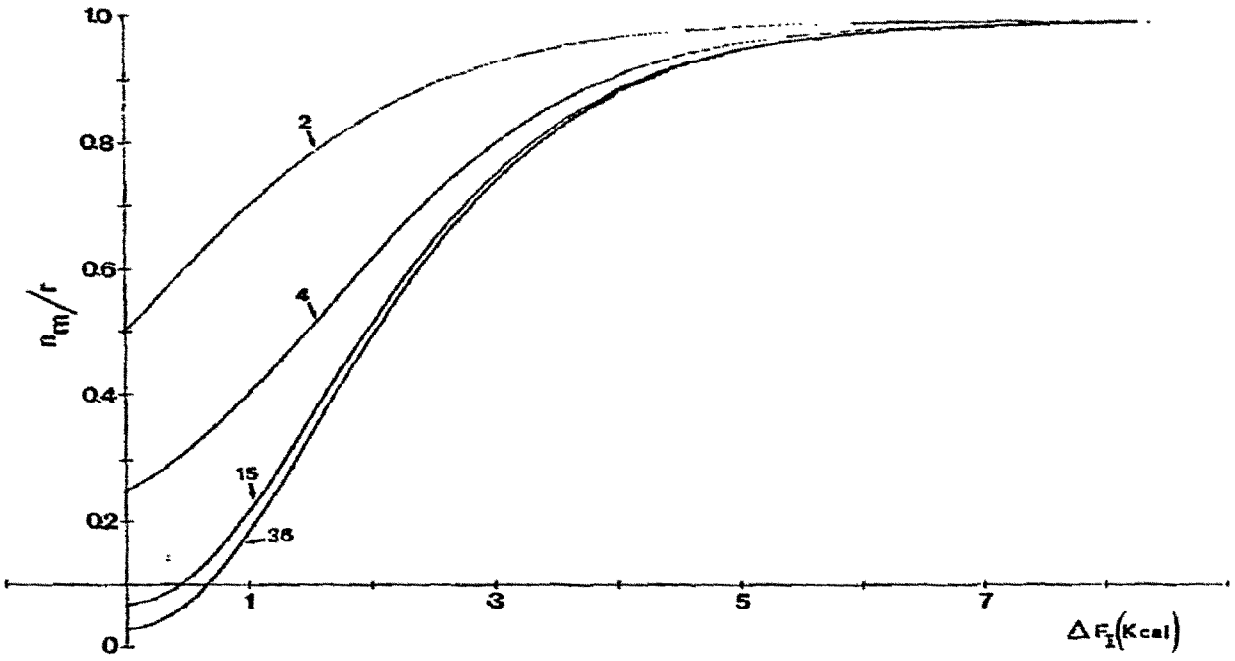


Fig. 1. Values of n normalized to its upper limit r (corresponding to $\Delta F_{I,total} \to \infty$), i.e., n_m/r as a function of $\Delta F_{I,total}$ (cal), for the different values of r shown on the curves. This is for the symmetrical case.

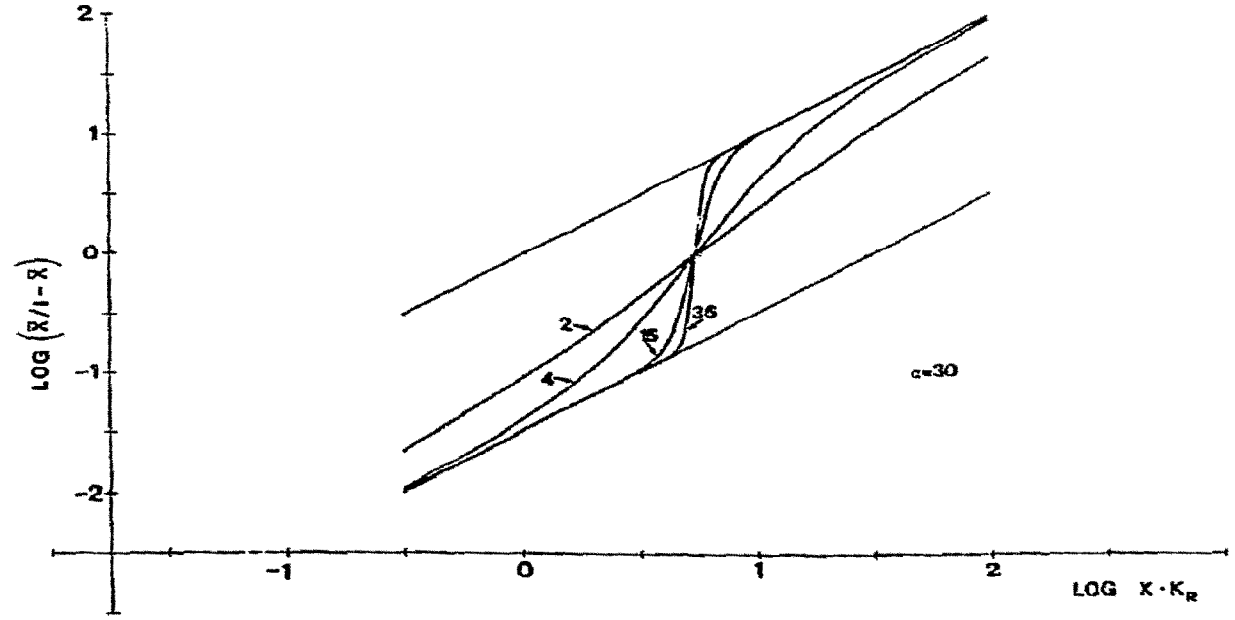


Fig. 2. Hill plots for the symmetrical case calculated for the constant $\alpha = K_R/K_T = 30$ for the different values of r shown on the curves. Except for $r = 2$, where $\Delta F_{I,total} = 1235$ cal, these curves all correspond to $\Delta F_{I,total} = 2000$ cal within 1 per cent.

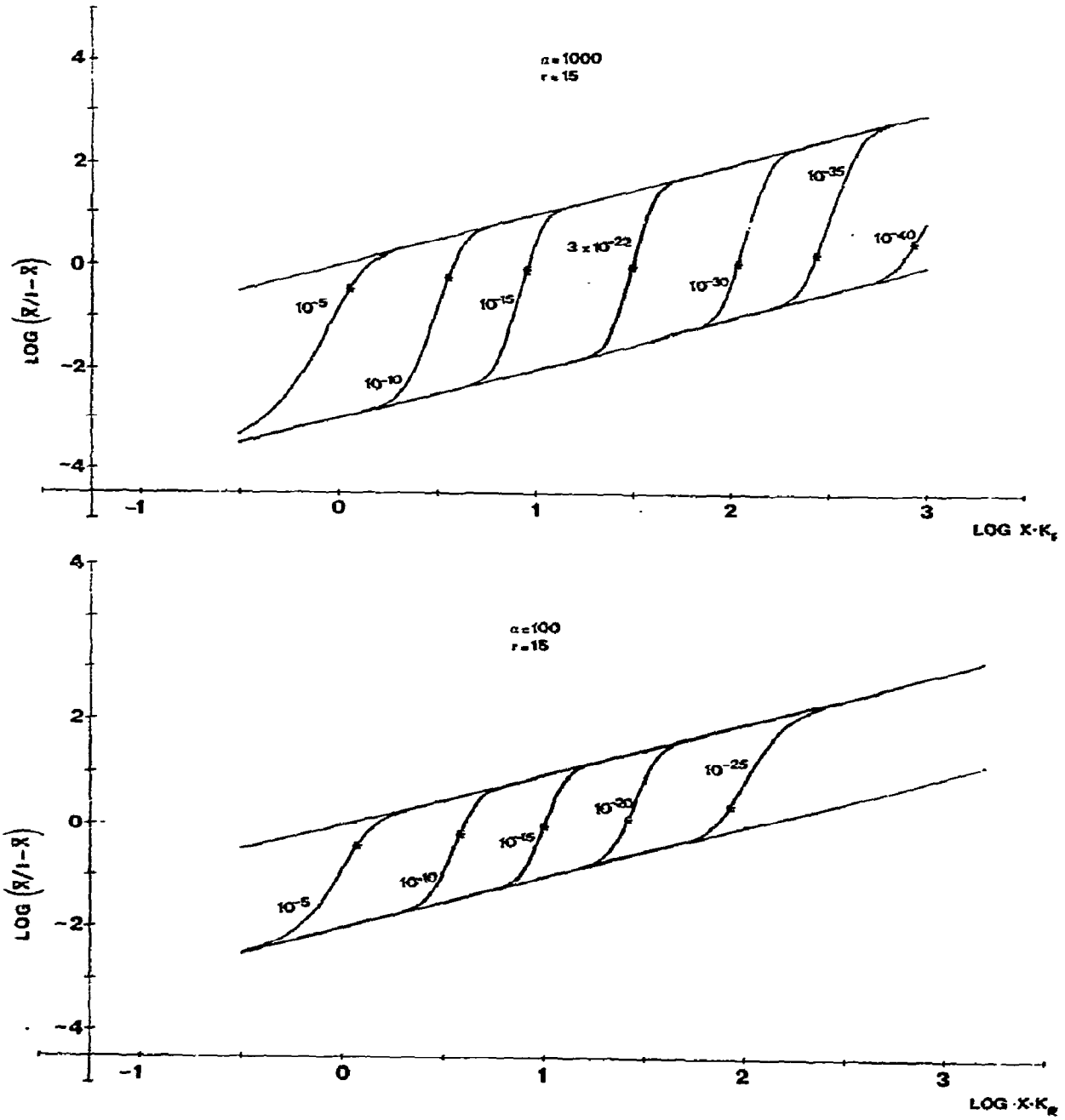


Fig. 3. Hill plots for the more general case where the symmetry condition is relaxed. $\alpha = 1000$ for top curves and $\alpha = 100$ for bottom curves. In both cases $r = 15$ and the values of L_0 are those shown on the curves. Asterisks indicate switch-over point. Here we have defined the switch over point as the point where the amounts of the T and R forms are equal. Alternatively we might have defined it as the point where the amounts of *ligand bound* by the T and R forms are equal. The two points are not the same. The former corresponds to $L = 1$, the latter to $Y_T = Y_R L$. The latter definition is more apposite to the analysis of kinetic experiments.

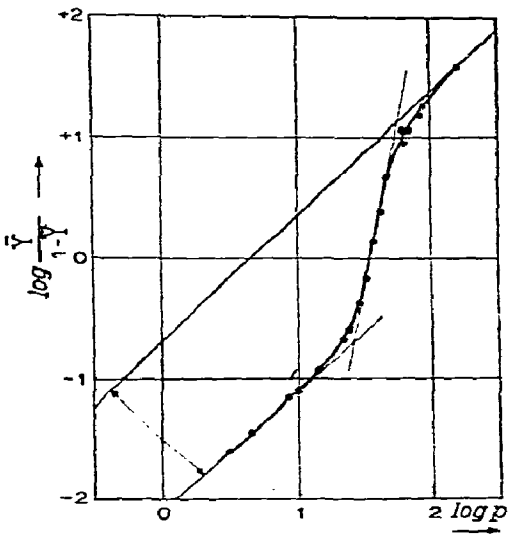


Fig. 4. Hill plot for oxygen binding by the blood of Spirographis spalanzanii at 20°C and pH 7 (from Antonini et al. [6]).

The value of n_m would then be the same as that for a constellation, and we could calculate the value of r, assuming the M.W.C. model to be applicable to each constellation, either with the aid of fig. 1 or, more directly, by rewriting eq. (10) in the form

$$r = (n_m + 2\lambda - 2)/(2\lambda - 1), \qquad (12)$$

where $\lambda = (1+\alpha)/(1+\alpha^{1/2})^2$. The answer is 10.

An alternative hypothesis would seem to be that the interactions involve all the sites, diminishing progressively in some manner with distance. A special case would be that of a number of small constellations of strongly interacting sites with secondary interactions between the different constellations – a kind of hierarchy of interactions. This is an idea which finds an echo in the complicated symmetrical structures revealed by electron microscopy [7].

Very similar considerations apply to an even larger molecule, namely the hemocyanin of Helix pomatia, whose molecular weight is of the order of 9×10^6 and which contains ~180 oxygen binding sites. Here the value of n_m is approximately 5. In this case it is found that when, in the absence of calcium, the molecular weight drops to (1/10)th of its full value, all cooperativity is lost although the (1/10)th subunits each still contain 18 sites [10]. It would seem that the integrity of the whole molecule is a condition of cooperativity.

It will be seen from this analysis that the M.W.C. model carries, buried within it, the prediction of a ligand linked phase change which is realized more and more completely as the number of sites increases indefinitely. That this is so should not be altogether surprising when it is realized that one of the primary features of the model is the exclusion of all mixed conformations; in applying the model we are in a sense treating the macromolecule as a crystal, and in this connection it is worth recalling that the liganded and unliganded derivatives of hemoglobin crystallize in different forms [8] which are also characterized by different solubilities [2]. The analysis given here may be compared with an earlier and rather different one [9], which, though physically somewhat unrealistic, is nevertheless suggestive in also predicting a phase change as the number of sites becomes infinite. Actually, although no completely sharp phase change has ever been observed, even in the case of the largest proteins studied, and although, as shown in the last paragraph, the simple M.W.C. model is not as such applicable to them, nevertheless data like those shown in fig. 4 often reveal a very sudden transition, or switch-over, which occurs within a limited critical range of liganding even when the total free energy of interaction is relatively small. At any rate, one thing is clear, and that is that the interactions responsible for the cooperativity in these giant molecules must radiate out to cover a large number of sites, almost certainly substantially larger than the minimum number calculated from eq. (12).

A grant from the National Science Foundation to Jeffries Wyman is gratefully acknowledged.

References

[1] J. Wyman, Advan. Prot. Chem. 19 (1964) 223.
[2] J. Wyman, Curr. Topics Cell Reg. 6 (1972) 209.
[3] J. Monod, J. Wyman and J.P. Changeux, J. Mol. Biol. 12 (1965) 88.
[4] E. Antonini and M. Brunori, Hemoglobin and myoglobin in their reactions with ligands, in: Frontiers of biology, Vol. 21 (North-Holland, Amsterdam, 1971).
[5] D.W. Allen, K.F. Guthe and J. Wyman, J. Biol. Chem. 187 (1950) 293.
[6] E. Antonini, A. Rossi-Fanelli and A. Caputo, Arch. Biochem. Biophys. 97 (1962) 336.

[7] D. Guerritore, M. Brunori, E. Antonini, J. Wyman and A. Rossi-Fanelli, J. Mol. Biol. 13 (1965) 234.
[8] M.F. Perutz, in: Barcroft Memorial Conference (Butterworths, London, 1949) p. 135.
[9] J. Wyman, J. Mol. Biol. 39 (1969) 523.
[10] R. van Driel, Biochemistry 12 (1973) 2696.

BIOPHYSICAL CHEMISTRY 2 (1974) 345–353. © NORTH-HOLLAND PUBLISHING COMPANY

THERMODYNAMIC EQUILIBRIUM IN REVERSIBLY INTERACTING RIBOSOMAL SYSTEMS OF E. COLI AND BAC. COAGULANS

C. GUERMANT, V.V. SHCHERBUKHIN and A.Ts. AVANESOV
Laboratory of Bioorganic Chemistry, Moscow State University, Moscow, USSR

Received 15 March 1974

The results which strongly confirm the existence of dynamic equilibrium 50S–30S ⇌ 50S + 30S in ribosomal systems of *E. coli* and *Bac. coagulans* are presented. A method has been devised which permitted to determine quantitatively the detailed composition of the reaction mixture of ribosomal subparticles and evaluate the equilibrium constant.

The analysis of equilibrium ribosomal systems of *E. coli* and *Bac. coagulans* at different temperatures allowed evaluation of appropriate thermodynamic parameters. In particular, the free energy of dissociation was shown to be higher in the case of thermophilic *Bac. coagulans* ribosomes.

1. Introduction

It has been shown that, after run-off, free 70S ribosomes may exist in solution [1–3]. However, analysis of end products of the translation process is complicated by the fact that an exchange of subunits between free ribosomes takes place [4]. Moreover, it is known that this exchange depends significantly on ionic conditions (concentration of Mg^{2+} and other ions) and temperature [5]. On the other hand, it has been shown that in the reaction mixture of purified subparticles, the level of association, i.e., the relative amount of 50S–30S couples, decreases upon dilution [6]. On the basis of this observation the hypothesis was suggested that there exists a dynamic equilibrium between ribosomes and subparticles. This idea was already used in interpreting many experimental results, besides, it would surely contribute to understanding the behaviour of ribosomes after termination of translation. All this makes it necessary to investigate quantitatively the equilibrium properties of the ribosomal system under different conditions.

In the present work we suggest a method that can be used for evaluation of the equilibrium constant and quantitative determination of the detailed composition of an equilibrium ribosomal system. The investigation of temperature dissociation of *E. coli* and *Bac. coagulans* ribosomes made also possible the evaluation of thermodynamic parameters which characterize the equilibrium between ribosomal subparticles and 50S–30S couples: 50S–30S ⇌ 50S + 30S.

2. Materials and methods

2.1. Cells and ribosomes

Cells of *E. coli* MRE 600 were grown and harvested. The ribosomes were prepared as described elsewhere [7, 8], and precipitated by adding 42 g $(NH_4)_2SO_4$ per 100 ml of the solution [9].

Cells of *Bac. coagulans* 8038 were grown at 55 °C with vigorous aeration of the solution containing per liter: 15 g casamino acids, 2 g K_2HPO_4, 3 g yeast extract, 5 g glucose, 5 g KNO_3, pH 7.4. The cells were harvested at the logarithmic phase of their growth. The ribosomes were prepared using conventional procedures described in refs. [7, 8].

2.2. Preparation of 50S and 30S subparticles

E. coli ribosomes precipitated by $(NH_4)_2SO_4$ were

collected by centrifugation for 20 min at 15 000 rpm, suspended in 10 mM Tris-HCl buffer, pH 7.5, with 500 mM NH_4Cl and 1 mM $MgCl_2$ and dialysed for 12 h at 4 °C against the same buffer.

Bac. coagulans ribosomes were collected by centrifugation for 20 min at 15 000 rpm and then suspended in 10 mM Tris-HCl, pH 7.5, 50 mM KCl and 20 mM $MgCl_2$, dialysed for 3 h against the same buffer and redialysed for 12 h at 4°C against 10 mM Tris-HCl, pH 7.5, 500 mM NH_4Cl and 3.5 mM $MgCl_2$. The two-stage dialysis was necessary to prevent partial unfolding of the 50S subparticles.

After dialysis, the suspensions were purified by centrifugation for 20 min at 15 000 rpm. As a result, the mixtures of 50S and 30S subparticles were prepared and separated by centrifugation through 15–30% linear sucrose gradients made up with the indicated buffers. The centrifugation was in an MSE B–XIV zonal rotor for 12 h at 4 °C, using the MSE SS-65 centrifuge. The subparticles were precipitated from the sucrose gradient fractions using $(NH_4)_2SO_4$ as described above, the Mg^{2+} concentration being adjusted to 10 mM.

Immediately before experiments the precipitates of 30S and 50S subparticles were salt-washed with $(NH_4)_2SO_4$, pelleted by centrifugation for 1 h at 20 000 rpm and dissolved in several ml of the standard buffer: 1 mM K_2HPO_4, 20 mM $MgCl_2$, 50 mM KCl, pH 7.5, and then dialysed against the same buffer for 12 h at 4 °C. After dialysis, the solutions were centrifuged for 20 min at 15 000 rpm to remove possible aggregates. The concentrations of the subparticles were determined by measuring the optical density at 260 nm with the assumption that $E^{1\%}_{260} = 150$. Molecular weights of 50S and 30S subparticles were assumed to be 0.9×10^6 and 1.8×10^6, respectively. Different samples prepared from the subparticles solutions as described in the legends were incubated under the above-mentioned conditions and then fixed by adding CH_2O–Mg^{2+} solution to the final concentrations of 4% and 20 mM, respectively [10].

2.3. Sedimentation analysis

The concentrations of the components in the ribosomal preparations after formaldehyde fixation were determined by sedimentation analysis in a Spinco model E analytical ultracentrifuge equipped with a photoelectric split-beam scanner, with absorption optics, multiplexer and monochromator. A sixplace AN-G rotor and double-sector cells were used.

3. Results

3.1. Some features of the composition of the E. coli ribosomal system

It should be noted that dimers and trimers of *E. coli* can appear in the homogeneous preparations of 30S and 50S subparticles after they have been precipitated with $(NH_4)_2SO_4$, resuspended and dialyzed. As a result, the preparations of the 30S and 50S subparticles were obtained whose components have the following sedimentation coefficients: 29S, 43S, 66S and 48S, 70S, 88S, respectively. Furthermore, in the course of separation a certain amount of purified subparticles loses the ability to associate, i.e., "defective" particles appear. Hence, it turns out that the four classic "components" revealed by sedimentation analysis of ribosomal systems, 30S, 50S, 70S and 100S, are, in fact, heterogeneous in composition. This considerably complicates the quantitative analysis of the ribosome association–dissociation reaction. Nevertheless, the understanding of the properties of particles which constitute the ribosomal system would make possible to introduce appropriate corrections into estimates of the concentrations of molecules which actually participate in the equilibrium.

To this end we studied the dependence of the relative amounts of dimers and trimers of *E. coli* ribosomal subparticles on the subparticles concentrations. The results are presented in table 1. As can be seen, dimers and trimers do not dissociate upon the decrease of the concentrations of 30S and 50S subparticles Thus, under these conditions (20 mM Mg^{2+}, 20 °C), the subparticles, dimers and trimers may be considered as a heterogeneous system of non-interacting components. This observation simplifies considerably the introduction of respective corrections for dimers and trimers in the studies of the equilibrium ribosomal system.

3.2. Dynamic equilibrium in the ribosomal system and evaluation of the relevant parameters

To evaluate the dynamic equilibrium constant, an

Table 1
Relative amounts of dimers and trimers at different concentrations of *E. coli* ribosomal subparticles (20 mM Mg^{2+}, 20°C)

Concentration of subparticles	Relative amount (%) of components in the solution of					
(A_{260} unit/ml)	50S subparticles			30S subparticles		
	50S	$(50S)_2$	$(50S)_3$	30S	$(30S)_2$	$(30S)_3$
1	89	7	4	62	18	20
2	87	9	4	64	21	15
3	87	9	3	57	22	21
6	87	11	2	60	22	18

experiment was carried out, in which ribosomal subparticles (1 A_{260} unit/ml, 20 mM Mg^{2+}, 20 °C) were mixed in different proportions. The mixtures were incubated at 20 °C for 30 min to ensure that the reaction had reached equilibrium, then fixed with CH_2O–Mg^{2+} solution and analysed by ultracentrifugation. The results are presented in fig. 1. If the subunits had not associated, i.e., had had an extremely high equilibrium constant, the dependence of the components (30S, 50S and 70S) concentrations on the initial concentration of 50S subparticles would have been linear [straight lines: $K \to \infty$ (fig. 1)]. However, experimental curves show that the subunits associate and that the nature of the change in 30S, 50S and 70S particles

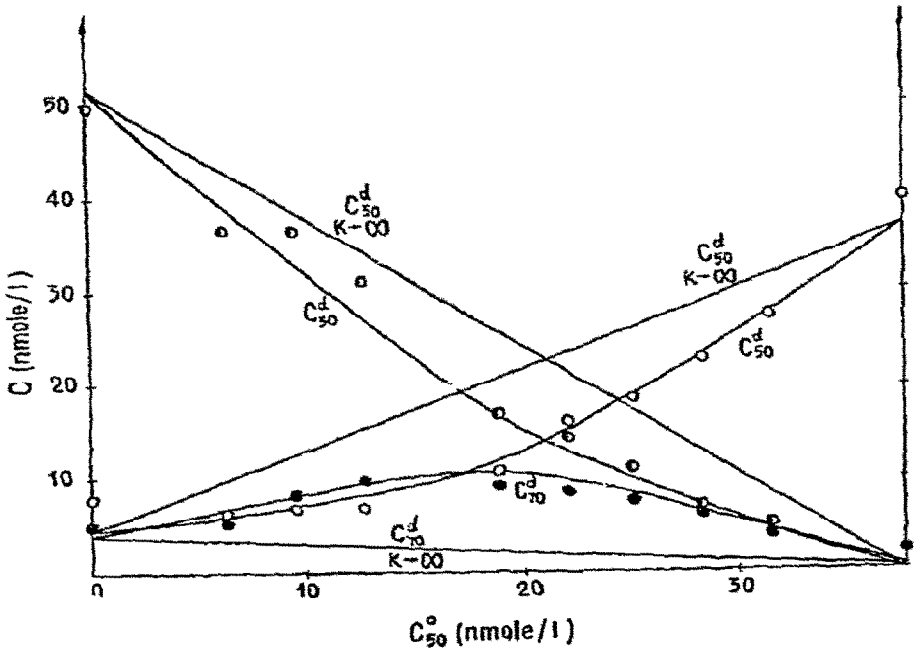


Fig. 1. The dependence of the equilibrium composition of the reaction mixture of *E. coli* ribosomal subparticles on the ratio of their initial concentrations.

Solutions of purified 30S and 50S subparticles (1 A_{260} unit/ml, 20 mM Mg^{2+}, 20°C) were mixed at different ratios (V_{30} + V_{50} = const. = 0.6 ml). After incubation for 30 min at 20°C, the mixtures were fixed by CH_2O–Mg^{2+} solution. The concentrations of the "components" were determined by analytical ultracentrifugation. Concentration of 30S "component": (–•–•–); concentration of 50S "component": (–o–o–); concentration of 70S "component": (–•–•–).

$C^d_{30,K\to\infty}$, $C^d_{50,K\to\infty}$ and $C^d_{70,K\to\infty}$ are the concentrations of the 30S, 50S and 70S "component" in the absence of the subparticles association. C^d_{30}, C^d_{50} and C^d_{70} are the theoretical dependences of 30S, 50S and 70S "components" concentration at the following values of the parameters: $\beta_{30} = 0.12$, $\gamma_{30} = 0.15$, $\beta_{50} = 0.02$, $\alpha_{30} = 0.31$, $\alpha_{50} = 0.57$, $K = 0.50 \times 10^{-9}$ mole/ℓ.

concentration corresponds to the stoichiometry of the association–dissociation reaction 50S–30S ⇌ 50S + 30S. It should also be noted that the concentration of particles with sedimentation coefficients around 70S has a distinct maximum which is in good agreement with the mass action law. Thus, our next step was to evaluate quantitatively the equilibrium constant and the constitution of the equilibrium ribosomal system based on the data of fig. 1. First, we would like to point out the following properties of ribosomal particles:

(1) Active subparticles and the molecules of formed 50S–30S associate are in the dynamic equilibrium [6].

$$50S–30S \rightleftharpoons 50S + 30S .$$

Let us assume that the fraction of active particles does not depend on concentration. Then, the amount of active 50S and 30S subparticles in the reaction mixture could be calculated by the following formulae:

$$C^a_{30} = \alpha_{30} C^0_{30} , \quad C^a_{50} = \alpha_{50} C^0_{50} ;$$

where

C^a_{30}, C^a_{50} are the concentrations of active 30S and 50S subparticles, respectively (mole/ℓ);

C^0_{30}, C^0_{50} are the initial concentrations of 30S and 50S subparticles in the reaction mixture (mole/ℓ);

α_{30}, α_{50} are the part of active 30S and 50S subparticles, respectively.

(2) Dimers and trimers of both subparticles do not participate directly in the reaction of association–dissociation and hence may be considered as "ballast". It was shown in section 3.1 that the relative amount of dimers and trimers does not depend on the concentration, i.e.,

$$C_{(30)_2} = \tfrac{1}{2}\beta_{30} C^0_{30} , \quad C_{(30)_3} = \tfrac{1}{3}\gamma_{30} C^0_{30} ;$$

$$C_{(50)_2} = \tfrac{1}{2}\beta_{50} C^0_{50} , \quad C_{(50)_3} = \tfrac{1}{3}\gamma_{50} C^0_{50} ;$$

where

$C_{(30)_2}$, $C_{(30)_3}$, $C_{(50)_2}$, $C_{(50)_3}$ are the concentrations of dimers and trimers of 30S and 50S subparticles, respectively (mole/ℓ);

β_{30}, γ_{30}, β_{50}, γ_{50} are the part of dimers and trimers of 30S and 50S subparticles, respectively.

(3) Sedimentation analysis of the ribosomal system reveals four "components" with sedimentation coefficients of about 30S, 50S, 70S and 100S. It should be kept in mind that the 50S "component" consists of 50S subparticles and dimers of 30S subparticles; the 70S "component" includes the 50S–30S associate, dimers of 50S subparticles and trimers of 30S subparticles; and the 100S "component" includes dimers of 50S–30S associate and trimers of 50S subparticles. In the experiment under consideration the amount of material sedimenting at 100S constitutes not more than 6%, and therefore the presence of the 100S component may be neglected in the equilibrium calculation.

So, the concentration of 30S, 50S and 70S "components" in the equilibrium mixture may be estimated by the following equations:

$$\begin{aligned} C^d_{70} &= \tfrac{1}{3}\gamma_{30} C^0_{30} + \tfrac{2}{3}\beta_{50} C^0_{50} + C^e_{70} , \\ C^d_{50} &= (1 - \beta_{50})\, C^0_{50} + \tfrac{1}{2}\beta_{30} C^0_{30} - C^e_{70} , \\ C^d_{30} &= (1 - \beta_{30} - \gamma_{30})\, C^0_{30} - C^e_{70} , \end{aligned} \tag{1}$$

where

$$C^e_{70} = \tfrac{1}{2}\left[(\alpha_{30} C^0_{30} + \alpha_{50} C^0_{50} + K) - \sqrt{(\alpha_{30} C^0_{30} + \alpha_{50} C^0_{50} + K)^2 - 4\alpha_{30} C^0_{30} \alpha_{50} C^0_{50}}\right] .$$

Here $K = C^e_{30} C^e_{50} / C^e_{70}$ is the equilibrium constant; and C^e_{30}, C^e_{50}, C^e_{70} are the equilibrium concentrations of 30S and 50S subparticles and 50S–30S associate, respectively (mole/ℓ).

The initial concentrations of 30S and 50S subparticles in this experiment are related to each other according to equations:

$$\begin{aligned} C^0_{30} &= C^*_{30}\, V_{30}/(V_{30} + V_{50}) , \\ C^0_{50} &= C^*_{50}\, V_{50}/(V_{30} + V_{50}) , \quad V_{30} + V_{50} = 0.6 \text{ ml} , \end{aligned} \tag{2}$$

where

C^*_{30}, C^*_{50} are the initial concentrations of 30S and 50S subparticles before mixing (mole/ℓ);

V_{30}, V_{50} are the volumes of the solutions of 30S and 50S subparticles being mixed (ml).

It is evident that the equations (1) are the nonlinear functions of the equilibrium constant and the fractions of active 30S and 50S subparticles, which makes the solution of the problem considerably more difficult. However, the fractions of dimers and trimers of 30S subparticles and dimers of 50S subparticles may be estimated accurately enough. For this purpose

we expand functions (1) in a Taylor series at the points $C^0_{50} = 0 (C^0_{30} = C^*_{30})$ and $C^0_{50} = C^*_{50}$ $(C^0_{30} = 0)$:

$$C^0_{30}\beta_{30} + C^0_{30}\gamma_{30} + C^0_{50}M - (C^0_{50})^2 Q = C^0_{30} - C^d_{30},$$

$$-\tfrac{1}{2} C^0_{30}\beta_{30} + C^0_{50}\beta_{50} + C^0_{50}M - (C^0_{50})^2 Q = C^0_{50} - C^d_{50},$$

$$\tfrac{1}{3} C^0_{30}\gamma_{30} + \tfrac{2}{3} C^0_{50}\beta_{50} + C^0_{50}M - (C^0_{50})^2 Q = C^d_{70},$$

for $C^0_{50} \geqslant 0$, and (3)

$$C^0_{30}\beta_{30} + C^0_{30}\gamma_{30} + C^0_{30}N - (C^0_{30})^2 R = C^0_{30} - C^d_{30},$$

$$-\tfrac{1}{2} C^0_{30}\beta_{30} + C^0_{50}\beta_{50} + C^0_{30}N - (C^0_{30})^2 R = C^0_{50} - C^d_{50},$$

$$\tfrac{1}{3} C^0_{30}\gamma_{30} + \tfrac{2}{3} C^0_{50}\beta_{50} + C^0_{30}N - (C^0_{30})^2 R = C^d_{70},$$

for $C^0_{30} \geqslant 0$; where M, N, Q, R are positive coefficients.

The values of β_{30}, γ_{30}, β_{50} and other coefficients of this expansion, which correspond to the experimental data of fig. 1, may be estimated from the least squares fit of eqs. (3) to the data, without taking the data at maximum association into consideration. The calculations gave the following values: $\beta_{30} = 0.12$, $\gamma_{30} = 0.15$, $\beta_{50} = 0.02$. This allowed to calculate the equilibrium concentration of the 50S–30S associate (open circles, fig. 2):

$$C^e_{70} = \frac{1}{3n} \sum_{i=1}^{n} [(C^d_{30,K\to\infty} - C^d_{30}) + (C^d_{50,K\to\infty} - C^d_{50}) + (C^d_{70} - C^d_{70,K\to\infty})]_i, \quad (4)$$

where
$C^d_{30,K\to\infty}$, $C^d_{50,K\to\infty}$, $C^d_{70,K\to\infty}$ are the concentrations of particles sedimenting at 30S, 50S and 70S, respectively, when no association of the subparticles occurs $(K \to \infty)$; and
n is the number of preparations studied at a given ratio of initial concentrations of the subparticles.

The values of $C^d_{30,K\to\infty}$, $C^d_{50,K\to\infty}$ and $C^d_{70,K\to\infty}$ may be calculated from the already known values of β_{30}, γ_{30} and β_{50} according to the following simple expressions:

$$C^d_{30,K\to\infty} = (1 - \beta_{30} - \gamma_{30}) C^0_{30},$$

$$C^d_{50,K\to\infty} = \tfrac{1}{2}\beta_{30} C^0_{30} + (1 - \beta_{50}) C^0_{50}, \quad (5)$$

$$C^d_{70,K\to\infty} = \tfrac{1}{3}\gamma_{30} C^0_{30} + \tfrac{2}{3}\beta_{50} C^0_{50}.$$

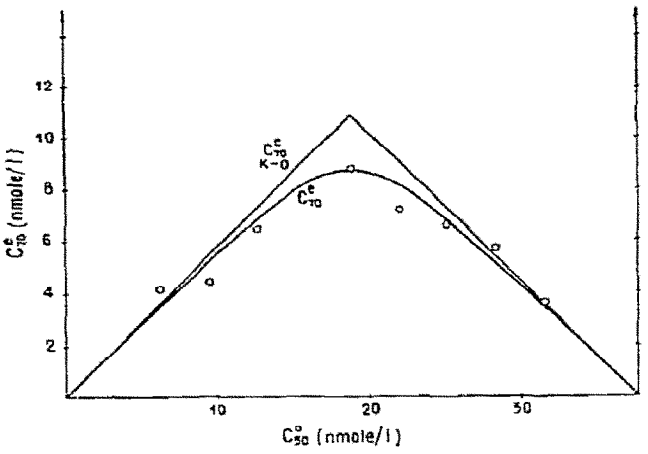


Fig. 2. The dependence of equilibrium concentration of 50S–30S associate on the ratio of initial concentrations of the subparticles.

The concentration of 50S–30S associate was calculated from the experimental data of fig. 1. C^e_{70} is the theoretical dependence of the concentration of 50S–30S associate at the following values of the parameters: $\alpha_{30} = 0.31$, $\alpha_{50} = 0.57$, $K = 0.50 \times 10^{-9}$ mole/ℓ.

$C^e_{70,K\to 0}$ is the concentration of 50S–30S associate under the condition of complete association.

Then, using the method of selected points for the data presented in fig. 2, the three following equations can be obtained:

$$(\alpha_{30} C^0_{30,i} - C^e_{70,i})(\alpha_{50} C^0_{50,i} - C^e_{70,i}) = K C^e_{70,i}, \quad (6)$$

with $i = 1, 2, 3$. The solution of this system of equations gave the following estimates of the fractions of active 30S and 50S subparticles and of the dynamic equilibrium constant: $\alpha_{30} = 0.31$, $\alpha_{50} = 0.57$, $K = 0.50 \times 10^{-9}$ mole/ℓ.

The theoretical curves (C^d_{30}, C^d_{50}, C^d_{70} and C^e_{70}) corresponding to the obtained values of α_{30}, β_{30}, γ_{30}, α_{50}, β_{50} and K are shown in figs. 1 and 2. One can see that the expectation, that a dynamic equilibrium exists in the ribosomal system, and the assumed properties of ribosomal particles are in good agreement with the experimental results. Thus, the quantitative approach developed in this section enables one to obtain satisfactory estimates of the main characteristics of the ribosomal system. Particularly, it was found that the fraction of active particles is not very large. This is especially true for 30S subparticles whose active fraction

is even twice smaller than that of 50S subparticles. The equilibrium constant under the conditions used (20 mM Mg^{2+}, 20°C) was found to be relatively small which implies that a considerable fraction of active subparticles whose initial concentration is smallest, is subject to association. This is well illustrated by fig. 2 which shows for comparison the concentration of 50S–30S associate $C^e_{70,K\to 0}$ versus the initial concentration of the subparticles under the conditions when the association is limited only by the lowest concentration of active 50S or 30S subparticles.

3.3. The effect of temperature on association–dissociation of ribosomes

3.3.1. Temperature dependence of the association

Preparation of reassociated *E. coli* and *Bac. coagulans* ribosomes (in the standard buffer) were incubated for 5 min at different temperatures and fixed by formaldehyde. The concentrations of components were determined by analytical ultracentrifugation at 20°C. As is evident from fig. 3, the concentration of associated subparticles gradually decreases with increase in the temperature until the ribosomes are completely dissociated.

However, a difference was found between the behaviour of *E. coli* and *Bac. coagulans* ribosomes. At 60°C all *E. coli* ribosomes are dissociated while *Bac. coagulans* ribosomes are dissociated only partially. It is worth-while to note the correlation between the higher temperature stability of the *Bac. coagulans* 50S–30S couple and the ability of this species to grow at elevated temperatures (55–60°C).

3.3.2. Reversibility

As in the previous experiment, samples were incubated for 5 min at elevated temperatures and then transferred to a water bath at 20°C. After further incubation for 30 min the mixtures were fixed and the concentrations of the components were measured as usual. The data obtained in the reversibility study are presented in table 2. The reversibility measure is taken to be the ratio between the fraction (by weight) of the associate and that in the control mixture at 20°C. The association level at 20°C is assumed to be 100%. The reaction becomes irreversible beyond 57°C for *E. coli* ribosome but the threshold temperature for *Bac. coagulans* ribosomes is as high as 63°C.

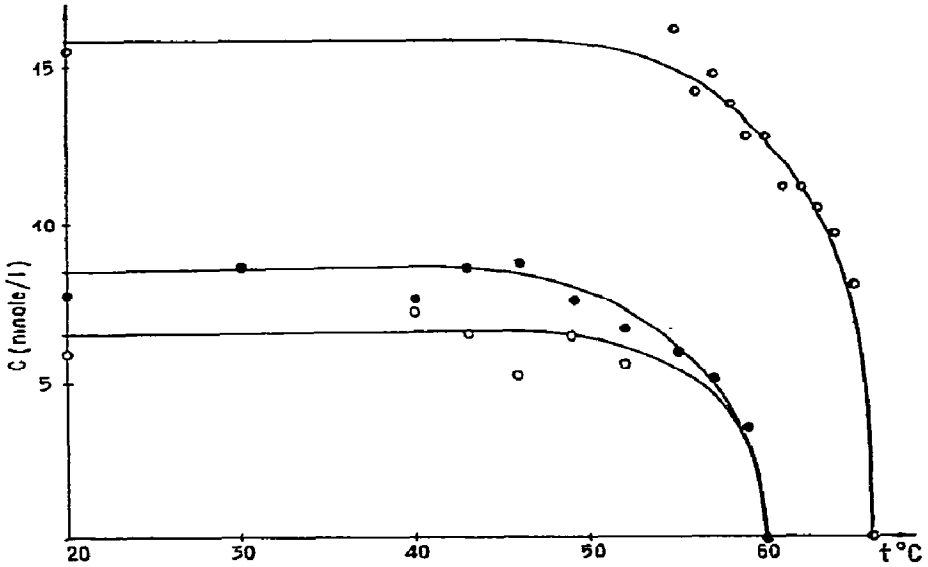


Fig. 3. The effect of temperature on the association of ribosomal subparticles.

After reassociation in buffer, containing 1 mM KH_2PO_4, 20 mM $MgCl_2$, 50 mM KCl, pH 7.5, 20°C, portions of ribosomes (1 A_{260} unit/ml) were incubated for 5 min at different temperatures and fixed by CH_2O to the final concentration of 4%. Equilibrium concentrations of 50S–30S associate (C^e_{70}) and its dimers (C^e_{100}) were determined by analytical ultracentrifugation with appropriate corrections for aggregation of the subparticles. Curve (–•–•–): C^e_{70} *Bac. coagulans*; curve (–o–o–): C^e_{70}; and curve (–•–•–): ($C^e_{70} + 2C^e_{100}$) of *E. coli* ribosomes.

Table 2
Reversibility of the association after heating. Samples of equimolar mixtures of ribosomal subparticles (1 A_{260} unit/ml, 20 mM Mg^{2+}) were incubated for 5 min at the indicated temperatures and then transferred to a water bath at 20°C. After incubation for 30 min the samples were fixed and analysed by ultracentrifugation. The ratio (in %) of the amount of the associate in the heated samples to that in the control sample kept at 20°C was considered as a measure of reversibility

Preparations of ribosomes	Reversibility after heating up to									
	20°	43°	52°	55°	57°	59°	60°	61°	63°	65°
E. coli	100	109	122	92	88	74	61	–	–	–
B. coagulans	100	–	–	104	96	100	–	93	88	63

It was previously shown that temperature-treatment of *Bac. stearothermophilus* ribosomes does not affect their synthetic activity *in vitro* under the conditions when the activity of *E. coli* ribosomes is rapidly lost [11]. It seems likely that, at extremely high temperatures, irreversible structural damage of ribosomes occurs which suppresses their biosynthetic activity and the ability to associate. In the temperature range where the structure and integrity of ribosomes remain intact, the association-dissociation reaction is reversible.

3.3.3. Stability of the ribosomal system during incubation at constant high temperature

In the experiments described in the previous section, the ribosomes were incubated for a relatively short period of time (5 min). We have also studied the effect of prolonged incubation at constant temperature. The preparations of *E. coli* and *Bac. coagulans* ribosomes were placed in a water bath at 52°C and 55°C, respectively, and then fixed at pre-set intervals. Fig. 4 shows that after 5 min incubation, a new equilibrium is established and further incubation does not induce additional dissociation.

Finally, from this set of experiments we can conclude that the position of equilibrium in the ribosomal system 50S–30S ⇌ 50S + 30S (with other factors being constant) is only determined by temperature (section 3.3.1) and does not depend on the incubation time (this section) or the previous treatment of the ribosomes (section 3.3.2).

3.4. Evaluation of thermodynamical parameters

The determination of thermodynamical parameters can be reduced to the measurement at different temperatures of the concentrations of the components which

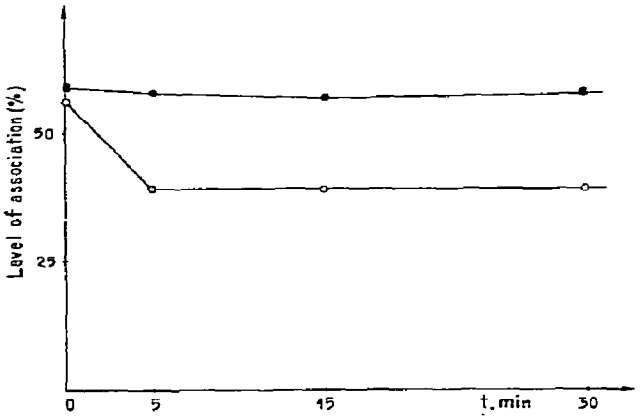


Fig. 4. The effect of incubation time at high temperature on the level of subparticle association.
Reassociated ribosomes of *E. coli* and *Bac. coagulans* (1 A_{260} unit/ml) were heated at 52°C and 55°C, respectively, in standard buffer containing 20 mM Mg^{2+}. At the indicated times CH_2O was added to final concentration 4%. Curve (–●–●–): *Bac. coagulans*; curve (–○–○–): *E. coli* ribosomes.

are actually involved in equilibrium. For this purpose, let us note that the concentration of 50S–30S associate and of its dimers within the plateau region of the temperature curve (fig. 3) is limited by the lowest concentration of the active 50S or 30S subparticles. This allows one to estimate the minimal fraction of active particles. On the other hand, the equilibrium constant ($K = C^e_{30}C^e_{50}/C^e_{70}$) is a symmetric function of the equilibrium concentration of the subparticles, hence, we will further consider two extremal cases only:

(1) when $\alpha_{30}C^0_{30} = \alpha_{50}C^0_{50} = (C^e_{70} + 2C^e_{100})_{plateau}$, or

(2) when $\alpha_{30}C^0_{30} = (C^e_{70} + 2C^e_{100})_{plateau}$, $\alpha_{50} = 1$.

Table 3
Thermodynamic parameters of the association–dissociation reaction of *E. coli* and *Bac. coagulans* ribosomes. The standard enthalpy (ΔH^0), entropy (ΔS^0) and free energy (ΔG^0) changes of ribosome dissociation were calculated from a van 't Hoff plot of $\ln K_{dissoc}$ versus $1/T$ for the data of fig. 3. The upper (lower) limit of all parameters was obtained on the assumption that the initial concentrations of active subparticles were equimolar (non-equimolar, respectively). Standard deviation in ΔG^0 evaluation did not exceed 0.1 kcal/mol

Ribosomes	ΔH^0	ΔS^0	ΔG^0 (kcal/mol)	
	(kcal/mol)	(e.u.)	57°C	59°C
Bac. coagulans	65.3–97.0	158–250	13.3–14.5	13.0–14.0
E. coli	50.4–77.5	116–196	12.1–12.9	11.8–12.5

The concentrations of the active 30S and 50S subparticles at equilibrium will be

$$C_{30}^{e} = \alpha_{30} C_{30}^{0} - (C_{70}^{e} + 2C_{100}^{e}),$$

$$C_{50}^{e} = \alpha_{50} C_{50}^{0} - (C_{70}^{e} + 2C_{100}^{e}),$$

respectively. Then, having calculated the equilibrium constant at different temperatures it is possible to determine from the plot of $\ln K$ versus $1/T$ the enthalpy, ΔH^0, and entropy, ΔS^0, and, hence, the change of the standard free energy ΔG^0.

The results presented in table 3 show that the thermal dissociation of *E. coli* and *Bac. coagulans* ribosomes is determined by different free energy values. Unfortunately, the precision of our measurements was not fine enough to decide whether enthalpic or entropic factors or both are the basis of this difference. Nevertheless, the estimations obtained of ΔH^0 and ΔS^0 for the association–dissociation reaction of *E. coli* and *Bac. coagulans* ribosomes have their own significance.

4. Discussion

It was shown earlier that 70S ribosomes undergo subunit exchange in each round of translation [4, 5]. It was also established that the association–dissociation reaction of purified ribosomes is governed by the law of mass action [6]. The dynamic equilibrium existing between ribosomal subparticles and 70S ribosomes may obviously influence the behaviour of ribosomes after the termination of translation. Therefore, a more detailed knowledge of the equilibrium and of its response to different factors would undoubtedly lead to a greater understanding of the ribosome function. However, the investigation of the association–dissociation reaction is complicated by the fact that the ribosomal preparations may contain particles which do not participate in the reaction. For instance, "defective" subparticles unable to associate may arise in the course of isolation and storage. Besides, as has been already noted, dimers and trimers are formed during storage of homogeneous preparations of 50S and 30S subparticles [12–14]. The results of table 1 confirm this tendency to aggregation of 50S and especially 30S subparticles. It was also found that aggregates of 50S and 30S subparticles sediment at 50S, 70S and 90S. Consequently, sedimentation analysis does not allow to distinguish the aggregates and "defective" particles from the classical constituents of the ribosomal system: 30S and 50S subparticles, 70S ribosomes and their 100S dimers.

Nevertheless, the method (described in section 3.2) which takes into consideration such an heterogeneity of the subparticles, enables one to evaluate the equilibrium constant of the association–dissociation reaction. The method consists in the determination of equilibrium concentrations of the components in non equimolar mixtures of the subparticles and subsequent calculations of relevant parameters. The investigation of *E. coli* ribosomes (20 mM Mg^{2+}, 20°C) has shown that:

(1) The idea that a dynamic equilibrium exists between ribosomal subparticles and the 50S–30S associate is in good agreement with the experimental data, namely the curves of the "components" concentration fit the stoichiometry of association–dissociation reactions and the law of mass action (fig. 1).

(2) Under the conditions used (20 mM Mg^{2+}, 20°C) the equilibrium is shifted to the association (fig. 2).

(3) The fraction of active 50S and, especially, 30S

subparticles is not large and constitutes 60% and 30%, respectively.

At elevated temperature, the equilibrium in the ribosomal systems of *E. coli* and *Bac. coagulans* is reversibly shifted to dissociation (fig. 3, table 2) and does not depend on the incubation time at constant temperature (fig. 4). The plateau in the curves of thermal dissociation of *E. coli* and *Bac. coagulans* ribosomes indicates that in this temperature range (20–40°C) the equilibrium is considerably shifted to association. This result confirms the conclusions made during the investigation of the equilibrium ribosomal system of *E. coli* at 20°C (section 3.2).

The investigation of the reversibility of the association–dissociation reaction has shown that, at extremely high temperature, the structure of ribosomes is irreversibly damaged with the resulting loss of their association ability (table 2). However, the irreversibility appears in thermophilic bacteria at more elevated temperatures. On the other hand, it is known that *Bac. stearothermophilus* 30S subparticles retain their biological activity *in vitro* after incubation for 5 min at 65°C while 30S subparticles of *E. coli* are inactivated under these conditions [15]. Thus, it is likely that there is a correlation between the ability of ribosomes to reassociate and their residual activity *in vitro* biosynthesis after temperature inactivation.

The results of section 3.3 allowed to evaluate thermodynamical parameters of association–dissociation reactions of *E. coli* and *Bac. coagulans* ribosomes (section 3.4). It turned out that, in the temperature range studied, the free energy of ribosome dissociation is higher in the case of thermophilic bacteria. However, the results did not allow to detect any difference between *E. coli* and *Bac. coagulans* in the enthalpy, ΔH^0, or entropy, ΔS^0. It is to be noted that our estimation of thermodynamical parameters for the *E. coli* ribosomal system is in good agreement with that obtained from a light-scattering study of the dissociation of *E. coli* ribosomes ($\Delta H^0 = 70$ kcal/mol, $\Delta S^0 = 120$ e.u.) [16], despite the different conditions of the two studies. Based on the above data it was suggested that subunits undergo structural changes upon association [16]. Such conformational changes in both ribosomal subparticles were then directly established by circular dichroism measurements of ribosomes and their isolated subunits [17].

In conclusion, the results of the present work suggest that the interconversion of the active ribosomal subparticles and 50S–30S couples is governed by the laws of thermodynamic equilibrium. That is, the equilibrium composition of the ribosomal system depends solely on the final conditions according to the mass action law and is not affected by incubation time under given conditions or by the previous evolution of the system. This fact could play a decisive role in the studies of the effects of different factors which are thought to interact with free 70S ribosomes or their subparticles. In such a case, the quantitative approach reported in this paper to the equilibrium studies of the ribosomal system may prove useful.

Acknowledgements

The authors would like to thank Professor A.S. Spirin for his interest in this work and for many valuable suggestions and comments. We gratefully acknowledge the assistance of Dr. R. Maribona in the initial phases of the experimental work on this project.

References

[1] R.E. Kohler, E.Z. Ron and B.D. Davis, J. Mol. Biol. 36 (1968) 71.
[2] R. Kaempfer and M. Meselson, Cold Spring Harbor Symp. Quant. Biol. 34 (1969) 209.
[3] R. Kaempfer, Nature 228 (1970) 534.
[4] A.R. Subramanian and B.D. Davis, Proc. Nat. Acad. Sci. U.S.A. 68 (1971) 2453.
[5] A.R. Subramanian and B.D. Davis, J. Mol. Biol. 74 (1973) 45.
[6] A.S. Spirin, FEBS Letters 14 (1971) 14.
[7] A.S. Spirin, M.I. Lerman, L.P. Gavrilova and N.V. Belitsina, Biokhimiya (USSR) 31 (1966) 424.
[8] A.S. Spirin, N.V. Belitsina, O. Gaal and T.M. Posdnyakova, Molecul. Biol. (USSR) 2 (1968) 2.
[9] C.G. Kurland, J. Mol. Biol. 90 (1966) 18.
[10] C. Guermant, V.V. Shcherbukhin and A.S. Spirin, Mol. Biol. Rept. 1 (1974) 289.
[11] S.M. Friedman, R. Axel and F.B. Weinstein, J. Bacteriol. 93 (1967) 1521.
[12] O.P. van Diggelen, H.L. Heinsius, F. Kalousek and L. Bosch, J. Mol. Biol. 55 (1971) 277.
[13] Y. Igarashi, T. Imamura, M. Suzuki and Y. Miyazawa, J. Biochem. 73 (1973) 683.
[14] T. Morimoto, Biochim. Biophys. Acta 182 (1969) 182.
[15] M. Nomura, P. Traub and H. Bechmann, Nature 219 (1968) 793.
[16] R.S. Zitomer and J.G. Flaks, J. Mol. Biol. 71 (1972) 263.
[17] L.A. Ball, P.M. Johnson and I.O. Walker, Eur. J. Biochem. 37 (1973) 12.

BIOPHYSICAL CHEMISTRY 2 (1974) 354–358. © NORTH-HOLLAND PUBLISHING COMPANY

THE DETECTION AND CONSEQUENCES OF ASSOCIATION OF TWO ENZYMES INVOLVED IN CATALYSING CONSECUTIVE REACTIONS

L.W. NICHOL, P.W. KUCHEL and P.D. JEFFREY

Department of Physical Biochemistry, John Curtin School of Medical Research, Australian National University, Australian Capital Territory, 2601, Australia

Received 2 July 1974

A set of differential rate equations is formulated for a system wherein two enzymes catalyse consecutive reactions of a pathway and also interact to form a 1:1 complex. The effect of this interaction on the time-dependence of final product formation is explored in terms of explicit expressions obtained with the use of Maclaurin polynomials applied to the rate equations. It is shown with the aid of numerical examples that provided complex formation between the enzymes leads to a species possessing different activity toward either substrate the interaction may potentially be detected by steady-state kinetic measurements on the enzymes studied alone and in a coupled assay. The introduction of a sigmoidal regulatory response arising as a sole consequence of the enzyme–enzyme interaction is also discussed.

1. Introduction

It has been pointed out that a sigmoidal kinetic response, frequently associated with allosteric effects [1], may also be observed with a system comprising an equilibrium mixture of different states of an enzyme possessing different activities toward substrate: these states may be isomeric [2, 3], polymeric [4] or comprise enzyme bound to a cell-membrane structure and unbound enzyme [5]. One purpose of the present communication is to show that a sigmoidal regulatory effect may also arise when interaction occurs between two different enzymes involved in catalysis of consecutive steps of a pathway, even though neither enzyme is itself of the control type. The mathematical development is based on an integration of the set of basic differential rate equations using Maclaurin polynomials [6] and suggests an experimental means by which enzyme–enzyme interactions may be detected from steady-state velocity measurements on the enzymes studied separately and in a coupled assay.

2. The differential rate equations

Consider a solution containing two enzymes A and B which associate to form a complex, C ($\equiv$ AB), the equilibrium being rapidly established and governed by the equilibrium constant,

$$X = [C]/[A][B] , \tag{1}$$

where [ ] denotes molar concentrations. A compound S_1 is added to the solution and binds instantaneously to p equivalent and independent sites on A and to q such sites on C with intrinsic association constants K_A and K_C, respectively. At equilibrium, the molar concentration of the A constituent, comprising unbound A and the complexes $A(S_1)_i$ ($i = 1, 2, ..., p$) is given by [7]

$$[\bar{A}] = [A](1+K_A[S_1])^p . \tag{2a}$$

Similarly, the molar concentration of the C constituent, comprising unbound C and the complexes $C(S_1)_j$ ($j = 1, 2, ..., q$) may be written

$$[\bar{C}] = [C](1+K_C[S_1])^q . \tag{2b}$$

Since each mole of C contains one mole of A, it follows that the total weight concentration of the A enzyme in all forms divided by the molecular weight of A is simply expressed as

$$[A]_T = [\bar{A}] + [\bar{C}] . \tag{2c}$$

The moles of ligand bound by the A constituent is given by

$$pK_A[A][S_1](1+K_A[S_1])^{p-1}$$

and to the C constituent by

$$qK_C[C][S_1](1+K_C[S_1])^{q-1}.$$

Thus constituent molar binding functions may be formulated as

$$\bar{r}_A = pK_A[A][S_1](1+K_A[S_1])^{p-1}/[A]_T, \quad (3a)$$

$$\bar{r}_C = qK_C[C][S_1](1+K_C[S_1])^{q-1}/[A]_T. \quad (3b)$$

If subsequent to the binding of S_1 to A, each complex breaks down to form product S_2 with the same intrinsic rate constant k_2, i.e.,

$$A(S_1)_i \xrightarrow{k_2} A(S_1)_{i-1} + S_2,$$

then the rate of depletion of S_1 from this source, v_1, may be deduced from eqs. (2) and (3a) to be

$$v_1 = -\frac{V_1 K_A[A][S_1](1+K_A[S_1])^{p-1}}{[A](1+K_A[S_1])^p + [C](1+K_C[S_1])^q}. \quad (4)$$

This formulation is based on the relationship suggested by Frieden [8] that $v_1/V_1 = -\bar{r}_A/p$, where the maximal velocity $V_1 = pk_2[A]_T$. There is an additional assumption implicit in eq. (4), inherent on its derivation from equilibrium binding equations. This may be seen most easily for the case $X = 0$, $[C] = 0$ (no interaction between A and B) when eq. (4) simplifies to the Michaelis–Menten equation with K_A identified as k_1^A/k_{-1}^A, where k_1^A and k_{-1}^A are microscopic (intrinsic) rate constants as defined by Dalziel [3]. The assumption implicit in eq. (4) is then that k_2 is relatively small. In this connection it is noted however that an equation of identical form to eq. (4) arises if it is assumed that all enzyme-substrate complexes are in a steady-state, with K_A now being identified as $k_1^A/(k_{-1}^A+k_2)$. When $X \neq 0$, S_1 is also depleted by the breakdown of complexes

$$C(S_1)_j \xrightarrow{k_3} C(S_1)_{j-1} + S_2$$

and the rate of its depletion from this source may be deduced from eqs. (2) and (3b) to be,

$$v_2 = -\frac{V_2 K_C[C][S_1](1+K_C[S_1])^{q-1}}{[A](1+K_A[S_1])^p + [C](1+K_C[S_1])^q}, \quad (5)$$

where $V_2 = qk_3[A]_T$ and $K_C = k_1^C/k_{-1}^C$ (if k_3 is small) or $K_C = k_1^C/(k_{-1}^C+k_3)$, if a steady-state of all $C(S_1)_j$ is assumed. In either case, the denominators of eqs. (4) and (5) equal $[A]_T$, which is invariant with time. Since the overall depletion of S_1 is given by the sum $v_1 + v_2$, it follows that

$$d[S_1]/dt = -\{V_1 K_A[A][S_1](1+K_A[S_1])^{p-1} + V_2 K_C[C][S_1](1+K_C[S_1])^{q-1}\}/[A]_T. \quad (6)$$

If instead of S_1, the substrate S_2 were added to the equilibrium mixture A + B ⇌ C and it bound to v equivalent and independent sites on B and to w such sites on C, each complex breaking down to form product S_3, then by entirely analogous reasoning, the overall rate of production of S_3 may be written

$$d[S_3]/dt = \{V_3 N_B[B][S_2](1+N_B[S_2])^{v-1} + V_4 N_C[C][S_2](1+N_C[S_2])^{w-1}\}/[B]_T, \quad (7)$$

where

$$[B]_T = [B](1+N_B[S_2])^v + [C](1+N_C[S_2])^w, \quad (8)$$

and N_B and N_C are the respective intrinsic binding constants (or reciprocal microscopic Michaelis constants) pertaining to the interactions of S_2 with B and C. In a coupled sequence of reactions ($S_1 \rightarrow S_2 \rightarrow S_3$), therefore, the basic set of differential rate equations is given by eqs. (6), (7) and the negative value of their sum,

$$d[S_2]/dt = +\{V_1 K_A[A][S_1](1+K_A[S_1])^{p-1} + V_2 K_C[C][S_1](1+K_C[S_1])^{q-1}\}/[A]_T - \{V_3 N_B[B][S_2](1+N_B[S_2])^{v-1} + V_4 N_C[C][S_2](1+N_C[S_2])^{w-1}\}/[B]_T. \quad (9)$$

Eq. (9) follows from the condition of mass conservation assuming that the amounts of substrates bound is small. It could also be noted that the set of rate equations assumes equilibrium (or steady) states of all enzyme–substrate complexes but not necessarily of the intermediate compound S_2 [6].

3. Application of Maclaurin polynomials

As has been discussed in detail previously [6], it is possible to express the concentrations $[S_n]_t$ ($n = 1$ or 2) as a function of time according to the Maclaurin polynomial

$$[S_n]_t = [S_n]_{t=0} + [S_n]'_{t=0}\, t + \{[S_n]''_{t=0}\, t^2/2!\}\,, \quad (10)$$

where $[S_n]'_{t=0}$ is the first derivative with respect to time evaluated at $t = 0$ and $[S_n]''_{t=0}$ is the corresponding second derivative: terms involving higher order derivatives have been truncated in writing eq. (10). Since $[S_3]_t = [S_1]_{t=0} - [S_1]_t - [S_2]_t$ and $[S_2]_{t=0} = 0$, it follows that

$$[S_3]_t = -\{([S_1]'_{t=0} + [S_2]'_{t=0})\, t + ([S_1]''_{t=0} + [S_2]''_{t=0})\, t^2/2\}\,. \quad (11)$$

It is now observed from eqs. (6) and (9) that $[S_1]'_{t=0} = -[S_2]'_{t=0}$ and therefore that the first term in eq. (11) is zero. It also follows from these equations that $[S_1]''_{t=0} + [S_2]''_{t=0}$ equals the differential of the second term of eq. (9) (or the differential of the negative of eq. (7)) evaluated at $t = 0$. With these observations eq. (11) becomes

$$[S_3]_t = \{d^2[S_3]/dt^2\}_{t=0}\, t^2/2\,. \quad (12)$$

With $\alpha = 1 + K_A[S_1]_0$ and $\beta = 1 + K_C[S_1]_0$, differentiation of eq. (7) yields,

$$[S_3]_t = \{(V_3 N_B [B]_0 + V_4 N_C [C]_0)(V_1 K_A [A]_0 [S_1]_0 \alpha^{p-1} + V_2 K_C [C]_0 [S_1]_0 \beta^{q-1})\, t^2\}/2[A]_T[B]_T\,, \quad (13)$$

where $[A]_0$, $[B]_0$ and $[C]_0$ are molar concentrations of *unbound* A, B and C, respectively, *at* $t = 0$. To obtain explicit expressions for these quantities, eqs. (1) and (2) are rewritten as

$$[C]_0 = X[A]_0[B]_0\,, \quad (14a)$$

$$[A]_0 = [A]_T/(\alpha^p + X\beta^q [B]_0)\,, \quad (14b)$$

and with the use of eq. (8) written as $[B]_T = [B]_0 + [C]_0$, the simultaneous solution is completed by

$$[B]_0 = -\{\alpha^p + X[A]_T - X\beta^q [B]_T - \sqrt{\Delta}\}/2X\beta^q\,, \quad (14c)$$

$$\Delta = \{\alpha^p + X[A]_T - X\beta^q [B]_T\}^2 + 4X\beta^q \alpha^p [B]_T\,. \quad (14d)$$

The negative root of eq. (14c) is excluded since $[B]_0 > 0$.

4. Discussion

Although the right-hand side of eq. (13) is the first non-zero term of a power series in time, it follows rigorously that

$$\lim_{t \to 0} \{d[S_3]_t/d(t^2)\} = m\,, \quad (15)$$

where m is given by the coefficient of t^2 in eq. (13) and is readily available to an experimenter from the slope of a plot of $[S_3]_t$ versus t^2. It is, therefore, possible from a set of coupled-assay experiments to construct a plot of m versus $[S_1]_0$. Previously [6], it has been shown that a plot of m versus $[S_1]_0$ would assume the form of a rectangular hyperbola when no interaction occurred between A and B, when these enzymes were of the Michaelis–Menten type. There is one situation where identical behavior would be observed even though interaction does occur: it is when the complex C possesses the same activity as A toward S_1 ($q = p, K_A = K_C, V_1 = V_2$) and the same activity as B toward S_2 ($v = w, N_B = N_C, V_3 = V_4$). With these equalities, eqs. (14a) and (14b) yield $[A]_0 + [C]_0 = [A]_T/\alpha^p$, and it follows from eq. (13) that

$$m = V_3 N_B V_1 K_A [S_1]_0/2(1 + K_A[S_1]_0)\,, \quad (16)$$

which is identical with eq. (5b) of ref. [6]. Except for this particular case, interaction between A and B in a coupled assay must give rise to deviations from the rectangular hyperbola described by eq. (16) even though separate studies on A and B have revealed that each is of the Michaelis–Menten type. Such separate studies permit the use of eq. (16) in the construction of a theoretical reference curve with which to compare the results of the coupled assay.

The type of deviation from the reference curve, which arises as a consequence of interaction between A and B leading to a complex with different activity toward S_1 and/or S_2, may be examined with the aid of eqs. (13) and (14). While these equations are general in that they would permit examination of any changes in the numbers of binding sites, intrinsic binding constants or break-down rate constants inherent on the formation of C, it suffices to illustrate the

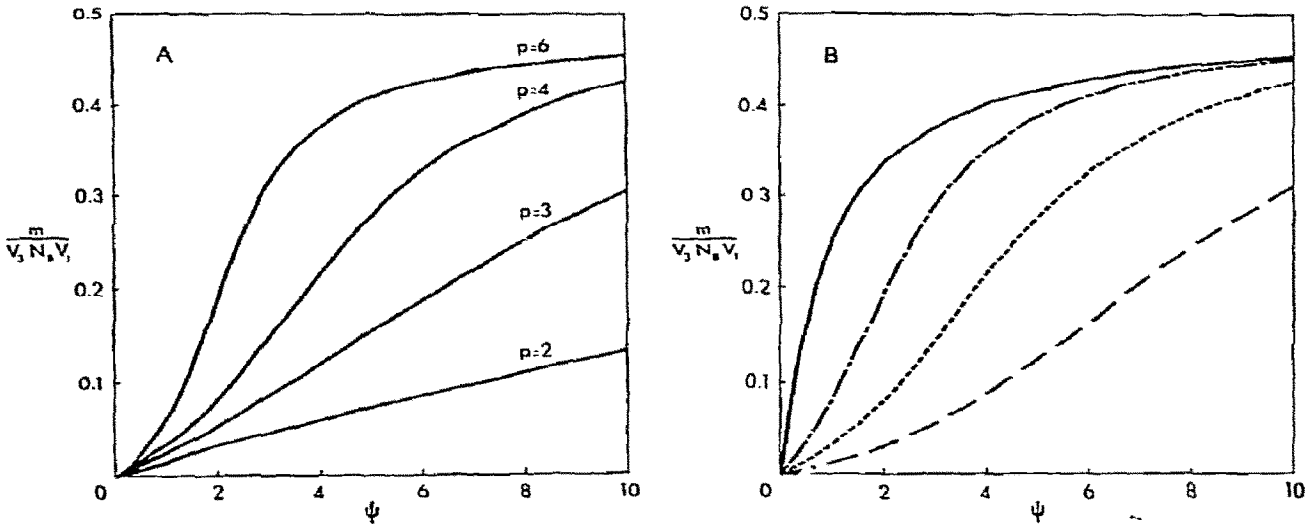


Fig. 1. Numerical examples illustrating the effect of interaction between two enzymes (A+B ⇌ C) catalysing consecutive reactions ($S_1 \rightarrow S_2 \rightarrow S_3$). A is enzymically active toward S_1 but C is not, while B and C are equally active toward S_2. The abscissa ψ equals the dimensionless product $K_A[S_1]_0$, where K_A is the intrinsic association constant for the interaction of S_1 with A and $[S_1]_0$ is the initial concentration of S_1. The ordinate is also dimensionless and equals $m/V_3 N_B V_1$ where m is the initial limiting slope of the plot of $[S_3]_t$ versus t^2, V_1 and V_3 are the respective maximal velocities of the first and second reaction and N_B is the intrinsic binding constant of S_2 to B or C. A. The effect of varying p, the number of binding sites on A for S_1, at fixed $X[B]_T = 10^3$. B. The effect of varying $X[B]_T$ with $p = 4$ where X is the equilibrium constant [C]/[A][B] and $[B]_T$ is the total molar concentration of B. (——), $X[B]_T = 0$; (—·—·—), $X[B]_T = 10^2$; (- - -), $X[B]_T = 10^3$; (– – –), $X[B]_T = 10^4$. For further details see text.

behavior of one system and we choose the following. A is enzymically active toward S_1 but C is not (q or $K_C = 0$), while B and C are equally active toward S_2 ($v = w, N_B = N_C, V_3 = V_4$). For this case,

$$m = \frac{V_3 N_B V_1 K_A [S_1]_0 (1+K_A[S_1]_0)^{p-1}}{(1+K_A[S_1]_0)^p + X([B]_T - [A]_T) + \sqrt{\Delta}}, \quad (17a)$$

$$\Delta = \{(1+K_A[S_1]_0)^p + X([A]_T - [B]_T)\}^2 + 4X[B]_T(1+K_A[S_1]_0)^p . \quad (17b)$$

Figs. 1A and 1B present plots of eq. (17) for the case $[A]_T = [B]_T$, when eq. (17) may be written with $\psi = K_A[S_1]_0$ as,

$$\frac{m}{V_3 N_B V_1} = \frac{\psi(1+\psi)^{p-1}}{(1+\psi)^p + \{(1+\psi)^{2p} + 4X[B]_T(1+\psi)^p\}^{0.5}} \quad (18)$$

which is seen to require examination of two variables p and the dimensionless product $X[B]_T$. Fig. 1A illustrates the effect of varying p at a fixed value of $X[B]_T = 10^3$, while in fig. 1B, $p = 4$ and the variation of $X[B]_T$ is examined. It follows from eq. (18) that

$$\lim_{X[B]_T \rightarrow 0} m = \frac{V_3 N_B V_1 \psi}{2(1+\psi)}, \quad (19)$$

which shows that the rectangular hyperbola in fig. 1B ($X[B]_T = 0$) is the reference curve described by eq. (16). It is clear from fig. 1B that deviations from the reference curve do indeed increase as $X[B]_T$ increases, the deviations being in the form of sigmoidality for all values of p examined (fig. 1A). In fact, in form, this behavior arising as a sole consequence of enzyme–enzyme interaction is indistinguishable from the behavior in a coupled assay of a control enzyme being monitored by but not interacting with an enzyme of the Michaelis–Menten type [6]. Since the plot basically reflects the time-dependence of final product formation as a function of $[S_1]_0$ [eq. (13)], the basic finding emerges that interaction between enzymes of the non-control type provides an alternate

means of obtaining a control response in a consecutive series of reactions. In addition it is now clear that the existence of such interactions (or their absence) may be tested experimentally at low enzymic concentration levels for any selected pair of enzymes simply by performing steady-state kinetic studies on the enzymes separately and in a coupled assay.

Thus, in the case of interaction, it is noted that the present treatment has provided explicit expressions describing the deviations to be expected from the reference curve [eq. (16)]. Moreover, the treatment may readily be extended to cases where one or both of the enzymes studied separately is of the control type. For these cases, the reference curve may itself be sigmoidal [6]; but interaction leading to a complex with different activity would act to change the extent of this sigmoidality.

References

[1] D.E. Koshland and K.E. Neet, Ann. Rev. Biochem. 37 (1968) 359.
[2] J. Monod, J. Wyman and J.P. Changeux, J. Mol. Biol. 12 (1965) 88.
[3] K. Dalziel, FEBS Letters 1 (1968) 346.
[4] L.W. Nichol, W.J.H. Jackson and D.J. Winzor, Biochemistry 6 (1967) 2449.
[5] C.J. Masters, R.J. Sheedy, D.J. Winzor and L.W. Nichol, Biochem. J. 112 (1969) 806.
[6] P.W. Kuchel, L.W. Nichol and P.D. Jeffrey, J. Theor. Biol., in press.
[7] I.M. Klotz, Arch. Biochem. 9 (1946) 109.
[8] C. Frieden, J. Biol. Chem. 242 (1967) 4045.

BIOPHYSICAL CHEMISTRY 2 (1974) 359–368. © NORTH-HOLLAND PUBLISHING COMPANY

THE MOLECULAR MECHANISM OF THE TEMPERATURE ENHANCEMENT OF PROTON MAGNETIC RELAXATION RATES IN METHAEMOPROTEIN SOLUTIONS

S. VUK-PAVLOVIĆ, B. BENKO and S. MARIČIĆ*
Institutes of Biology and Physics, University of Zagreb, Zagreb, Yugoslavia

Received 12 February 1974
Revised manuscript received 19 August 1974

The mechanism of water exchange between the haem-pocket and bulk solvent in aqueous methaemoprotein solutions was firmly substantiated by using the aliphatic protons of certain lower alcohols in an otherwise deuterated solution for measuring the incremental relaxation rates resulting from their magnetic interaction with the haem-iron. The fast-exchange condition was established for solutions of horse fluorometmyoglobin, human A fluoromethaemoglobin and Chironomus thummi aquomethaemoglobin. The distances between the exchangeable protons and the haem-iron obtained from these PMR measurements concur with the presence of the fluoride ion, while for Chironomus aquomethaemoglobin this distance is also much larger than that resulting from the location of the 6th site water molecule. The latter finding is the first clear-cut evidence that the exchanging protons belong to the next neighbour water molecule, a previously advanced hypothesis. The exchanging water molecule may thus serve as a natural probe for comparing the haem-pocket conformational state(s) under different conditions or in various haemoproteins.

1. Introduction

Met(ferri)haemoproteins contain an intrinsic paramagnetic probe, the ferric iron of the haem group. It is secluded within a part of the protein matrix, the haem-pocket, which is structurally well defined [1,2]. One would therefore hope that the finer details of the conformational state(s) of the haem-pocket under different conditions could be delineated by the proton magnetic relaxation (PMR) technique. In view of this the prime value of this method is in the structural parameters which in principle it may yield. The first is the distance of closest possible approach of solvent protons towards the haem-iron outside its immediate neighbourhood. Because of the shape of the haem-pocket, the relevant "outer-sphere" relaxation rate can only be used as an overall parameter of this accessibility, but no particular distance could be specified [3]. The second structural parameter is the distance, r, from the paramagnetic haem-iron to the protons which occupy a fixed site nearby but interchange with the bulk solvent at a rate, $1/\tau_B$, much larger than the longitudinal magnetic relaxation rate of the exchanging protons, $1/T_{1B}$. The values of r derived in our previous work [3,4] for the aquomethaemoproteins may thus be subject to criticism because the above condition was not satisfied.

Derzhansky et al. [5] interpreted their temperature study of PMR rates in a solution of dolphin metmyoglobin in a completely different way. Atanasov [6] used this alternative interpretation as, indeed, the only evidence of a structural kind in developing the hypothesis of "predenaturational conformation changes" as a functional mechanism for haemoproteins. In contrast to the "proton-exchange" idea which tacitly assumes no changes of protein conformation with temperature, the other hypothesis states that the water molecules with their protons are immobilized within the haem-pocket, but a shift of the haem towards the protein surface is assumed.

The purpose of this paper is twofold:

(i) to show the physical reality of the proton-exchange mechanism in the proton magnetic relaxation of methaemoprotein solutions, and,

(ii) to describe those cases in which the fast-exchange condition can be proven beyond doubt so that reliable iron–proton distances can be derived.

Our approach was to make use of inert marker molecules, larger than the molecule of water, bearing

* Mailing address: Dr. S. Maričić, Institute of Immunology, Rockefellerova 2, 41000 Zagreb, Yugoslavia.

chemically non-exchangeable aliphatic protons. In a fully deuterated solution of methaemoproteins the aliphatic protons of a sufficiently large marker molecule will sense the paramagnetic iron only via the "outer-sphere" relaxation, because they cannot enter the haem-pocket. If they do, the rate of their switching between the pocket and bulk solvent would be low enough not to affect the overall relaxation. Hence, the test of the "conformation" [6] hypothesis is the comparison of the relaxation rates in a solution fully deuterated, except for the aliphatic protons, with those rates measured in a similar solution with a sufficient amount of hydroxyl or hydronium ions. The two sets of measurements should be practically identical if the "conformation" hypothesis is valid. If they are not identical the proton-exchange mechanism plays an important role, depending on the temperature and other conditions.

2. Materials and method

2.1. Haemoproteins and solvents

Human haemoglobin was prepared from fresh blood (from the local blood bank) following the method of Cameron and George [7]. The met(ferri)-form was obtained by the addition of potassium ferricyanide with subsequent extensive dialysis against deionized water. After the initial liophylization the methaemoglobin solution was liophylized three times from D_2O allowing more than 24 h for the H → D exchange between each liophylization. The liophylized and deuterated methaemoglobin was then dissolved in the relevant solvent (vide infra).

Horse metmyoglobin solutions were prepared by dissolving liophylized metmyoglobin (Calbiochem, lot No. 100660) in the relevant solvent. To make deuterated solutions, metmyoglobin was subjected to the same deuteration procedure as were the methaemoglobin samples.

Methanol, 1,2-ethanediol, and 1,2,3-propanetriol (all Merck, reagent grade) were distilled five times with D_2O (Fluka, 99.7%, or Prochem B.O.C., 99.8%). High resolution proton magnetic resonance spectra indicated less than 0.1% HDO relative to the peak of the non-exchangeable protons.

The experiments shown in fig. 1 were performed

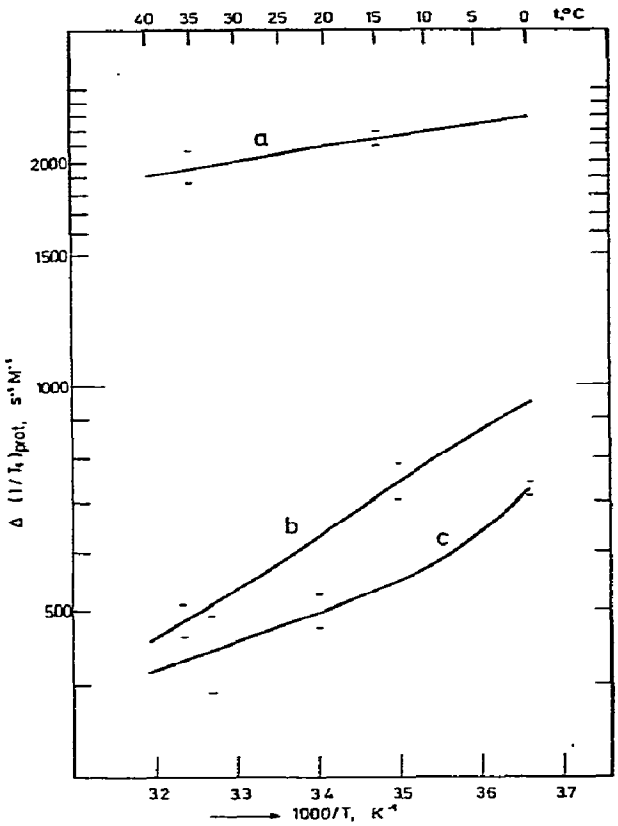


Fig. 1. The temperature dependence of the longitudinal magnetic relaxation rates of the solvent protons as increments induced per haem concentration of human A fluoromethaemoglobin dissolved in heavy water with addition of 2.95 M of: (a) CH_3^*OD, (b) $C_3H_5^*(OD)_3$, and (c) $C_2H_4^*(OD)_2$, where the asterisk denotes the solvent protons.

with equimolar (2.95 M) solutions of deuterated methanol, CH_3OD (curve a), 1,2-ethanediol, $C_2H_4(OD)_2$ (curve c), and 1,2,3-propanetriol, $C_3H_5(OD)_3$ (curve b). The protein concentrations were 5.05–5.27 mM (per haem). As in all the other experiments with fluoromethaemoproteins, the solutions contained 0.2 M sodium fluoride (Merck) in H_2O or D_2O. The measured pH was between 5.8 and 6.2 for reasons explained before [3].

Fluoromethaemoglobin and fluorometmyoglobin solutions (figs. 2 and 3, respectively) were prepared by dissolving the methaemoproteins in 0.2 M NaF + 5×10^{-4} M EDTA + 37.2 w% $C_2H_4(OH)_2$ in H_2O, pH 5.8, and in the case of the deuterated solution in 0.2 M NaF + 35.0 w% $C_2H_4(OD)_2$ in D_2O, measured

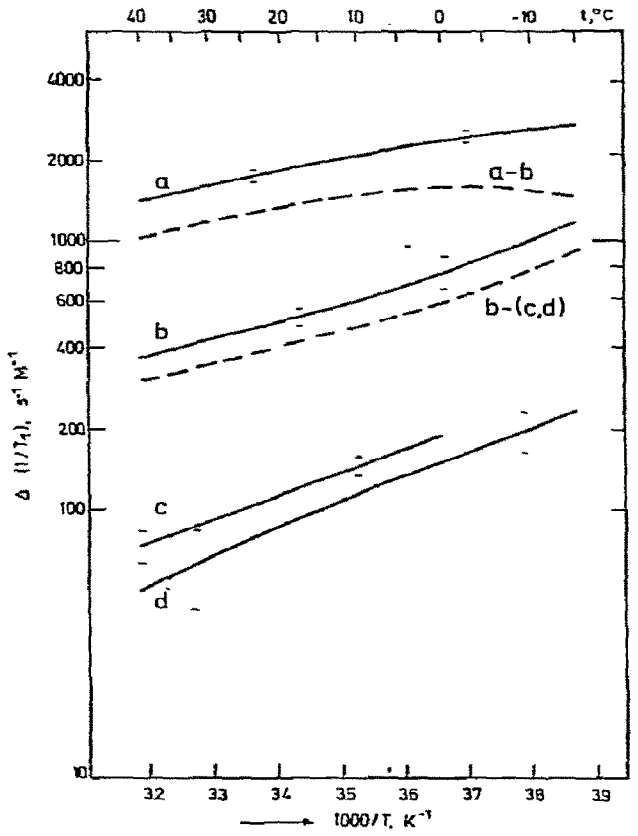


Fig. 2. The temperature dependence of the PMR rates as in fig. 1 induced by human A fluoromethaemoglobin and carbonmonoxyhaemoglobin in mixtures of water and ethanediol. (a) FluorometHb in 37.2 w% $C_2H_4^*(OH^*)_2$ + H_2^*O, and (b) $C_2H_4^*(OD)_2$ + D_2O. (c) COHb in 35.0 w% $C_2H_4^*(OD)_2$ + D_2O and (d) in 37.2 w% $C_2H_4^*(OH^*)_2$ + H_2^*O.

pH 6.4. The carbonmonoxyhaemoglobin samples (fig. 2) were prepared by reduction of methaemoglobin with sodium dithionite under a CO stream with subsequent dialysis against either 0.1 M NaCl with 35.0 w% $C_2H_4(OD)_2$ in D_2O (curve c) or 0.1 M NaCl with 37.2 w% $C_2H_4(OH)_2$ in H_2O (curve d), the latter being reproduced from ref. [8]. Curve (c) in fig. 3 was obtained with a solution of horse CO myoglobin in 0.1 M NaCl + 0.05 M Tris + 5×10^{-4} M EDTA + 37.2 w% $C_2H_4(OH)_2$, pH 5.8.

The methaemoglobin crystals from Chironomus thummi larvae originated from Dr. Huber's laboratory (Max Planck Institute, Munich). These crystals were dissolved and dialysed against 0.1 M NaCl + 5×10^{-4} M EDTA + 37.2 w% $C_2H_4(OH)_2$ in H_2O, pH 6.20, and 0.1 M NaCl + 35.0 w% $C_2H_4(OD)_2$ in D_2O, pH 6.25, respectively (fig. 4).

The human methaemoglobin samples in fig. 5 were obtained by dialysing the original, non-liophylized, methaemoglobin solutions against acid, pH 6.00 (curve Hb_{H_2O}), or alkaline, pH 9.65 (curve Hb_{OH^-}), 0.1 M NaCl + 0.05 M Tris + 5×10^{-4} EDTA solutions. The commercial, liophylized metmyoglobin was dissolved in the relevant solvent and dialyzed against it (curves Mb_{H_2O} and Mb_{OH^-}). Only the results represented by curve Hb_{OD^-} are due to a solution of the deuterated liophylized methaemoglobin in 0.1 M NaCl with 35.0 w% $C_2H_4(OD)_2$ in D_2O, pH_{meas} 9.40.

All the solutions were centrifuged at 15000 G for half an hour before PMR measurements.

The concentrations were determined using the cyanmet-method [9]. The examined haemoprotein solutions had spectra with the satisfactory ratios of maxima, which were also frequently checked after the relaxation measurements. The spectra in the visible range were taken for the described solutions with methanol, ethanediol, and propanetriol, and the maxima ratios of these spectra correspond to those published elsewhere [7]. The relaxation rates also show that the native state of haemoproteins was preserved under the described conditions (see section 4).

2.2. T_1-measurements

The proton magnetic longitudinal relaxation times, T_1, were measured by the π-t-$\pi/2$ pulse sequence. Variable t-delays were applied using a digital readout pulsed spectrometer (Jožef Stefan Institute, Ljubljana) with a high resolution magnet (Bruker-Physik, Karlsruhe), at 24 MHz, and also at 12 MHz for fluorometmyoglobin in H_2O. A computer programme yielded T_1 values, usually with a correlation coefficient not less than 0.99 for the least square straight lines with maximal errors in T_1 of 8%. The spectrometer was provided with a temperature controller and the temperature of the samples was kept constant within 1°C by a thermostated nitrogen stream. The actual temperatures of the solutions were checked by direct measurements with a calibrated thermistor probe (Yellow Springs, Ohio) before and after T_1 measurements.

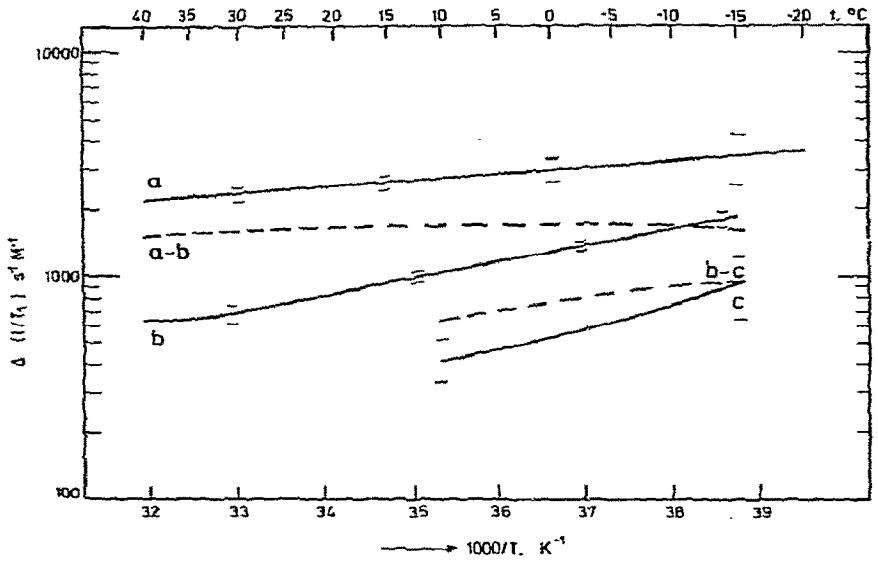


Fig. 3. The temperature dependence of the PMR rates for horse fluorometmyoglobin solutions as in *fig. 2a, b, and c.*

3. Results

3.1. Presentation of data

All the data presented in figs. 1 to 5 are plotted as the logarithms of the PMR rates versus reciprocal absolute temperature, with the linear temperature scale indicated as well. The relaxation rates, $\Delta(1/T_1)_{prot}$, are those induced by the magnetic interaction of solvent protons (those of H_2O *and* ethanediol, or only those from the aliphatic protons in "D_2O"-solutions) with the dissolved haemoprotein. They were obtained in the following way: the computer programme yielded the relaxation rates ($1/T_1$) for the haemoprotein solution and its corresponding solvent. The relatively small concentration of protein allows to deduct the relaxation rates for the solvent directly from those of the haemoprotein solutions. The differences obtained, normalized per haem concentration, are plotted in the figures described below. For more accurate calculations of stereochemical parameters (see section 4) the correction was made for the finite volume of the protein in solution. The curves shown in this paper are smoothed, with the indicated error (unless it equals the line-width) obtained from the points of largest deviation in drawing the mean curves for the haemoprotein solutions and the solvents relaxation rates. The original T_1-data may be obtained on request.

3.2. Description of the figures

Fig. 1 represents the relaxation rate measured for the aliphatic protons, i.e., CH_3-protons of methanol, CH_2-protons of 1,2-ethanediol, and CH_2- and CH-protons of 1,2,3-propanetriol. The chemically exchangeable protons (from hydroxyls or hydronium ions) were eliminated by the deuteration procedures as described in section 2.1. The results suggest that the relaxation rates observed for the methyl protons of methanol are comparable with those obtained with ordinary aqueous solutions, while the rates measured for the other two marker molecules are much lower, and the smaller of the latter two markers, 1,2-ethanediol, was used in the next experiments.

This evidence was taken to prove that the relaxation rates of the CH_2-protons of ethanediol, measured in completely deuterated solutions, represent the so called "outer-sphere" relaxation. Figs. 2, 3, and 4 were therefore obtained from measurements with human fluoromethaemoglobin, horse fluorometmyoglobin, and Chironomus thummi aquomethaemoglobin,

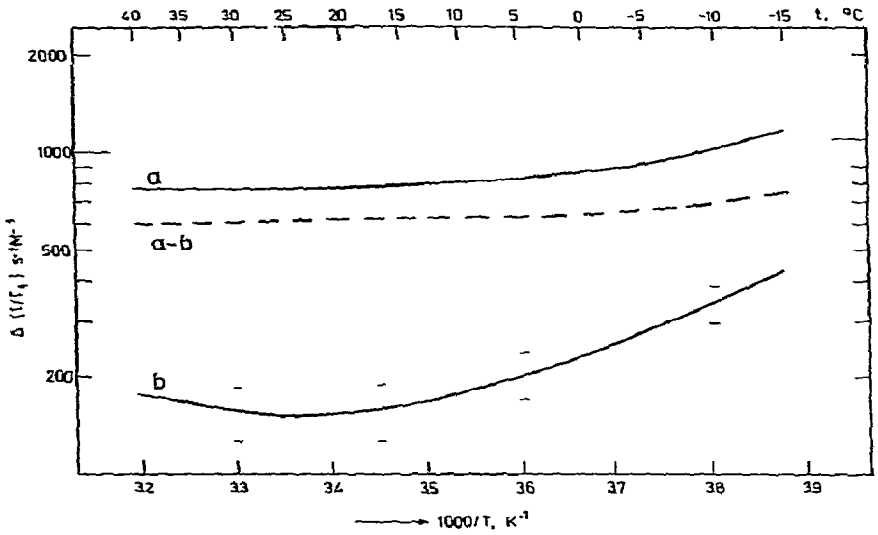


Fig. 4. The temperature dependence of the PMR rates for Chironomus thummi aquomethaemoglobin solutions as in fig. 2a and b.

respectively, in ordinary aqueous solutions with ordinary ethanediol added, and in deuterated solutions with only marker CH_2-protons present. The curves (a) in these figures refer to the first type of solutions, "H_2O", indicating the "fast-exchange" controlled relaxation rates, while those marked by (b) refer to the second type of solutions, "D_2O", induced by the "outer-sphere" relaxation. The difference in the relaxation rates between the two mechanisms is indicated in these figures by the broken lines marked (a – b), representing the pure, paramagnetic, "fast-exchange" relaxation rate. The "outer-sphere" relaxation, (b), is composed, again, of the pure paramagnetic part due to the dipole–dipole interaction of electron (haem-iron) and nuclear (proton) spins, and that due to the diamagnetic interaction between the solvent and protein protons. The latter contribution was measured for the carbonmonoxyhaemoglobin solutions using both "H_2O" and "D_2O" solvents. The results are represented by curves (c) and (d) in fig. 2 and curve (c) in fig. 3 for carbonmonoxymyoglobin in a "D_2O"-solution. The two sets of data almost coincide. Therefore, within the experimental error, the two solvents ("H_2O" versus "D_2O") do not significantly differ in their influence on the diamagnetic PMR rates. The difference between the curves (b) in figs. 2 and 3 and the mean diamagnetic relaxation rates equals the pure paramagnetic "outer-sphere" relaxation as represented in fig. 2 by the curve b – (c,d), or, for myoglobin, in fig. 3 (b – c).

Fig. 5 shows the comparison between the temperature dependence of methaemoglobin and metmyoglobin relaxation rates measured at different pH of the solvents (see section 2.1). In the first case both haemoproteins were in their aquomet-form, and in the second, in their hydroxomet-form. The latter form of methaemoglobin was also used in the "D_2O" measurements of hydroxomethaemoglobin (curve Hb_{OD}-) in order to compare them with those given by the curve Hb_{OH}-.

4. Discussion

4.1. Proton exchange

Methanol, ethanediol and propanetriol were used as the marker molecules in methaemoglobin aqueous solutions because they are practically inert towards this protein molecule as shown [10] by magnetochemical titration, and in other studies [8, 11–14]. Fluoromethaemoglobin was chosen for the comparison of

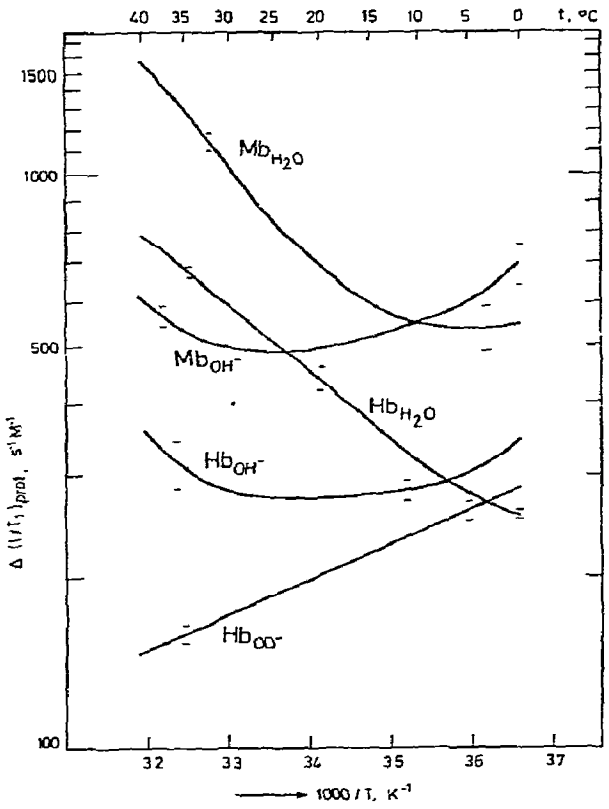


Fig. 5. The temperature dependence of the solvent protons longitudinal magnetic relaxation rates as increments induced per haem concentration in aqueous solutions of horse aquometmyoglobin, Mb_{H_2O}, and hydroxometmyoglobin, Mb_{OH^-}; human A aquomethaemoglobin, Hb_{H_2O}, and hydroxomethaemoglobin, Hb_{OH^-}. The Hb_{OD^-} curve was obtained with a solution of metHb in D_2O with 35 w% $C_2H_4(OD)_2$, pH_{meas} 9.40.

the three marker molecules because, like fluorometmyoglobin [15], its relaxation in aqueous solution seemed to be dominated by the mechanism of fast proton exchange between the haem-pocket and bulk solvent. On the other hand, if there is any slight interaction of aquomethaemoglobin with methanol [10], the haem-iron in fluoromethaemoglobin would be protected by the fluoride ion at the 6th site.

As no relaxation other than that of the aliphatic protons was measured in the experiments from fig. 1, one may conclude that there is a size limit between the molecules of methanol and ethanediol. While the methanol molecule can exchange between the haem-pocket and (deuterated) bulk solvent, ethanediol and propanetriol cannot. The small difference between the latter two may originate from differences in hydration sheaths around haemoglobin molecules in the two solutions, a point which requires further study. It is obvious that the "conformation" hypothesis is incompatible with these results, while they can be explained by the exchange mechanism. In the first case the (b) and (c) curves should in fact closely resemble that for methanol, (a). Because they do not, it must be concluded that they indeed represent only the "outer-sphere" relaxation, whereas the methanol curve also results from the much larger contribution due to the exchange mechanism.

We have also obtained results showing the transition from the purely "outer-sphere" relaxation [similar to (b) in fig. 1] through the partially to the fully-measured exchange contribution by varying the amount of exchanging protons in solutions of haemoglobin.

From such changes in the temperature dependence of the relaxation rates, the following conclusions can be drawn:

(i) There is indeed an exchange of protons between the haem-pocket and bulk solvent in solutions of aquomethaemoglobin. This does not imply that the fast-exchange condition (see Introduction) is fulfilled in this particular case, but the exchange is fast enough to dominate the overall relaxation rate at higher temperatures.

(ii) There is no shift in the conformational equilibrium for haemoglobin molecules on raising the temperature, of the kind postulated in references [5, 6]. Were there any such effect, curves like (b) in fig. 1 should have a negative instead of the observed positive slope with aquomethaemoglobin solution.

4.2. The iron–proton distance and the fast-exchange condition

Our experiments strongly support the physical reality of protons fluctuating between the haem-pocket and bulk solvent. It remains now to examine whether this proton exchange is fast enough for the existing theory to be applicable in calculating the distance, r, between the haem-iron and the nearest protons exchanging with bulk solvent. The only direct approach to this problem is to measure the residance

time, τ_B, of the protons in question inside the haem-pocket. This could be done by measuring the transverse relaxation time as a function of the pulse separation in a Carr–Purcell sequence, as applied for instance in the case of inorganic aquo-ions [16]. There are other, though less direct, criteria, by which one can define the fast-exchange conditions, and we shall apply them firstly to the fluoromethaemoproteins, and secondly to the aquomethaemoglobin from the Chironomus thummi larvae.

4.2.1. Fluoromethaemoproteins

We compare first our results for fluorometmyoglobin, fig. 3, with the similar measurements of Mildvan et al. [15]. As expected, the two sets of data are practically identical, and in agreement, again, with our experience that addition of ethanediol does not change the relaxation to any significant extent [8]. It should be pointed out that the curve (a) in fig. 3 represents the proton relaxation of a solution in which the protons can easily switch between the water and ethanediol hydroxyls and also between the haem-pocket and bulk solvent. Within the indicated error there was no difference between pairs of measurements at 24 and 12 MHz (the Larmor frequency used in ref. [15] was 24.3 MHz). It was hoped that by extending the measurements below zero centigrades, i.e., below the temperature limit in ref. [15], the curve (a) in fig. 3 would bend downwards owing to the diminished rate of proton exchange between the haem-pocket and bulk solvent. This would then seem to suggest, though not prove definitely, that the fast exchange condition, $T_{1B}/\tau_B > 10$, is maintained at the higher temperatures, as assumed by Mildvan et al. [15]. The expected curvature could not be detected even as low as –20°C. We therefore used our "marker method". In full confirmation of our data from fig. 1 for fluoromethaemoglobin, the "H_2O" (a) and the "D_2O" (b) curves in fig. 3 are quite different. This is strong experimental evidence for the "fast-exchange" at least above 0°C, because there is simply no other alternative (see the schematic fig. 6 in ref. [3]). Hence, the difference between the "H_2O" and "D_2O" curves, (a – b), represents the contribution to the relaxation from T_{1B}, the relaxation time of the exchanging protons while located near the iron inside the haem-pocket.

The values of $\Delta(1/T_1)_{a-b}$ from fig. 3 may be used to derive r, by the Solomon–Bloembergen equation [17], which, abbreviated, reads:

$$(1/T_1)_{a-b} = (n_h/N_p)(1/T_{1B}) = Kn_h F(\tau_C) r^{-6}. \quad (1)$$

$F(\tau_C)$ is a function of the correlation time, τ_C, for the dipole–dipole interaction of the haem-iron spin (= 5/2) and the proton spin (= 1/2). The most exact way of calculating r would be to first of all obtain τ_C for fluorometmyoglobin by measuring the frequency dispersion of $\Delta(1/T_1)_{a-b}$. Since we lack this data at present we take the value of $\tau_C = \tau_S$ (the electron spin relaxation time) = 1.5×10^{-10} s obtained in a study [18] of aquometmyoglobin at 5°C. While the fluoride complex is 100% high spin the aquomet may contain at 5°C a few percent of the low-spin form [19]. Because of this, and because of the different sixth ligands, (F versus H_2O) τ_S (= τ_C) in aquomet- and fluorometmyoglobin may not necessarily be identical. However, we assume that the two τ_C's are similar.

It is not definitely known how many protons [n_h in eq. (1)] from the haem-pocket of fluoromethaemoproteins exchange with bulk solvent. Mildvan et al. [15] seem to have assumed only one such proton. In agreement with these authors, who found r = 2.9 Å, we obtain $r_{1,MbF}$ = 2.99 Å. The difference of about 0.1 Å is due to our correction by the data of curve (b) in fig. 3. Using the same evaluation of the data for fluoromethaemoglobin (fig. 2), $r_{1,HbF}$ = 3.05 Å.

The question as to whether intact water molecules exchange between the two environments has been mentioned by Mildvan et al. [15] with regard to their measurements of ^{17}O-relaxation. However, no conclusion is attainable at all because ^{17}O-relaxation is not sensitive enough to the presence of paramagnetic ions. The pertinent factor is obtained from the magnetogyric ratios: $\gamma_{^{17}O}/\gamma_{^1H} = 0.018$, so that in order to obtain equal paramagnetic enhancement of ^{17}O-relaxation rates one would require concentrations of protein about 50 times the concentrations used in ^1H measurements. This is impossible to achieve.

If two protons of a water molecule were exchanging, r_2 will have a unique value only if the two of them were equidistant from the haem-iron. Thus, $r_{2,MbF}$ = 3.35 Å, and $r_{2,HbF}$ = 3.43 Å.

The asymmetric, Fe–F^- ··· HOH-bonded water molecule seems to be the most probable case (by extrapolation from pure ionic solutions, see ref. [20]). The observed relaxation rates for fluoromethaemo-

proteins then yield:

$r_{2,MbF,as}$: 3.03 Å and 4.55 Å;

$r_{2,HbF,as}$: 3.10 Å and 4.62 Å.

The latter values appear quite reasonable regarding the available space within the haem-pocket. This is also corroborated by deriving the iron-to-proton(s) distance(s) from the "methanol" results (see fig. 1, curve a – curve b), where $n_h = 3$. With the CH_3-free-rotation, an r_3 almost equal for all the three protons may be assumed, which results in

$r_{3,Hb} = 5.54$ Å.

It seems more likely that the methanol molecule faces the haem-iron with the CH_3-group, rather than with its OD-tail. For an asymmetric orientation the proximal proton of the CH_3-group will be at 5.05 Å, with the most distal proton at 6.29 Å from the haem-iron. Thus, with an approximate r of 5.5 ± 0.5 Å the CH_3-group of the methanol molecule is just about inside the haem-pocket but very close to its mouth-piece.

4.2.2. Aquomethaemoproteins

It may be concluded from fig. 4 along the same line of reasoning as for fluoromethaemoproteins that the proton magnetic relaxation of Chironomus aquomethaemoglobin solution is also governed by the fast exchange mechanism from +40°C down to at least −10°C. Further, using eq. (1) and the same numerical data as before, with $\Delta(1/T_1)_{a-b} = 620\ s^{-1}\ M^{-1}$ at 5°C,

$r_{1,Ch} = 3.53$ Å, $r_{2,Ch} = 3.96$ Å, or

$r_{2,Ch,as}$: 3.60 Å and 5.12 Å.

All these values are appreciably larger than the value 2.8 Å which follows from the fact that a molecule of water has been identified at the sixth ligand site of the haem-iron in the crystal structure analysis of Chironomus thummi aquomethaemoglobin [21]. The crystal structure data and our proton magnetic relaxation results obtained with the solution of this haemoglobin can be reconciled by the hypothesis [3,4] postulating the existence of protons exchanging with bulk solvent from a site inside the haem-pocket. This site is next to that occupied by the water molecule in the first coordination sphere of the haem-iron. The results from fig. 4 for Chironomus haemoglobin are in fact the first clear-cut evidence supporting this hypothesis. It is likely that the lamprey haemoglobin (Petromyzon marinus) fraction 2, as discussed in ref. [22], could be another such example.

We have not yet found a tetrameric aquomethaemoglobin with well defined "fast-exchange" relaxation mechanism under our experimental conditions. Fig. 5 illustrates the shape of the curves for solutions of mammalian methaemoproteins obtained under conditions comparable to other data in this paper. Pairs of measurements for horse myoglobin, a single unit protein like Chironomus, and for human haemoglobin A, a tetramer, both at pH close to either 6 or 10 are given. Neither the aquometmyoglobin nor the aquomethaemoglobin curves (pH 6) show any levelling off at the higher temperatures, which would be expected if the "fast-exchange" mechanism were to take over. In previous work carried out in this laboratory [3,4] it was assumed that the temperature and the corresponding relaxation rate of such a turning point is close to the highest available temperature in these measurements, i.e., 40°C. The result obtained with Chironomus haemoglobin is reassuring in that the basic conclusion about the exchangeable protons, which are not those from the water molecule in the first coordination sphere of the haem-iron, appears to be quite feasible in spite of the remaining doubts about the actual r-values for the aquomethaemoproteins of mammals.

The fluoromethaemoproteins are an example of the stereochemistry around the haem-iron with the sixth site occupied by a ligand without protons, the fluoride ion, and the exchangeable protons are from a next-neighbour site within the haem-pocket. Another such example was expected to be found in alcaline (pH ≈ 10) methaemoproteins in which the sixth ligand has long been assumed to be the hydroxyl ion hydrogen bonded to the imidazole nitrogen of the distal histidine. However, the results from fig. 5 (compare the Hb_{OH}- and Hb_{OD}- curves) clearly show that within the available temperature range the exchange of protons in hydroxomethaemoprotein is far from having the "fast-exchange" relaxation rate. For aquomethaemoglobin and aquometmyoglobin the contribution of the exchange mechanism becomes observable beyond the "outer-sphere" relaxation above

0°C and above 10°C, respectively. This temperature is raised to some 30°C for the hydroxometforms of both these proteins. The solutions of the latter exhibit therefore mostly the "outer-sphere" relaxation mechanism. Hence, comparisons between the relaxation behaviour of the two met-forms with the aim of drawing stereochemical conclusions as has been done in ref. [15] do not seem justified. The near coincidence at lower temperatures of the "H_2O" and "D_2O" curves for the hydroxomethaemoglobin solutions is yet additional evidence that under the conditions of our marker method the relaxation rates measured via the methyl protons of ethanediol do properly represent the "outer-sphere" relaxation. Whatever slight difference between these two curves there is, it may possibly be ascribed to differences in protein hydration.

4.3. The "outer-sphere" relaxation

The "D_2O"-curves, i.e., the "outer-sphere" relaxation rates, merit comment in spite of the fact that no quantitative structural parameter can be derived. It is necessary first to determine the pure paramagnetic contribution to these relaxation rates. It is usually done by subtracting the rates measured for the diamagnetic carbonmonoxyhaemoprotein, a contribution which is otherwise also inherently included in the measurements by "D_2O" experiments with paramagnetic haemoproteins.

The relaxation rates of the carbonmonoxyhaemoglobin and myoglobin solutions are reproduced in figs. 2 and 3, together with the curves obtained by subtracting these CO-curves from the "D_2O"-data, b − (c, d) and (b−c) respectively. The latter curves represent the "outer-sphere" relaxation due only to the rate induced by the paramagnetic haem-iron.

The diamagnetic rates are normalized per haem, and the rate ratio Mb/Hb is about four. This may be due to the fact that the monomeric myoglobin has a larger specific area of the protein surface exposed for interaction with solvent protons than the tetrameric haemoglobin. However, the remaining paramagnetic contribution to the "outer-sphere" relaxation of fluorometmyoglobin does not differ from that of fluoromethaemoglobin within the experimental error (20% to 10% from low to high temperature limits). Thus, in a qualitative way, which is the only possible one in discussing the "outer-sphere" relaxation for haemoproteins, one may conclude that the accessibility of the haem-pocket for the solvent molecules is very similar for fluorometmyoglobin and fluoromethaemoglobin from −15°C to +10°C.

5. Conclusions

A marker method has been developed by which one can distinguish between the mechanism of (i) "outer-sphere" relaxation, i.e., in the absence of any contribution to the rates from the relaxing species that may exchange between the site(s) of close association with the paramagnetic centre and bulk solvent, and (ii) "fast-exchange" by which the exchange contribution dominates over that of the "outer-sphere" relaxation.

The results obtained with this method eliminate the interpretation according to which the temperature enhancement of the relaxation rates in methaemoprotein solutions is due to the changes in the relative position of the haem-iron to the protein surface. They also strongly support the only other known interpretation, that of the thermally activated exchange rate. Hence, all those cases for haemoprotein solutions where such a temperature enhancement of PMR rates is observed may be discussed from the point of view of the energy of activation for the exchange mechanism as a parameter in defining the dynamics of the haem-pocket.

In the cases of established "fast-exchange" relaxation, i.e., for solutions of horse fluorometmyoglobin and human haemoglobin, and for aquomethaemoglobin of Chironomus, the site from which the protons exchange with bulk solvent from the haem-pocket, is at a distance greater than that defined by the sixth ligand site in the first coordination sphere of the haem-iron. This means that the PMR relaxation rate induced by these exchanging proton(s) may be useful as a parameter to describe the conformational state(s) of the haem-pocket in different haemoproteins and under different conditions.

The described marker method may also be applied in studies of the active sites of those enzymes activated by paramagnetic metal ions, or spin-labelled, for which an involved shape, like the haem-pocket, might be expected to exist.

Acknowledgement

This work was carried out under the PI-480 contract No. 02–004–1 between the N.I.H. (USA) and The Institute of Biology, University of Zagreb, with the partial support of the Research Fund of the S.R. Croatia. B.B. and S.V.-P thank the latter Fund and the Institute of Biology for postgraduate scholarships. The authors are indebted to Drs. R. Huber and H. Formanek for the invaluable donation of fine single crystals of Chironomus thummi haemoglobin.

We are grateful to Dr. G. Lahajnar for his critical remarks at a stage in this study, which prompted our experiments with different marker molecules.

We thank Mrs. V. Bračika for her continuous, excellent technical cooperation, and Mrs. L. Tomić, M.Sc., for recording the high resolution control spectra, at the Institute "Rudjer Bošković", Zagreb, and Dr. D. Šerman, Medical Faculty, University of Zagreb, for allowing us to use his laboratory for liophylization.

References

[1] H.C. Watson, in: Progress in stereochemistry, Vol. IV (Butterworths, London, 1968).
[2] M.F. Perutz, H. Muirhead, J.M. Cox and L.G.G. Goaman, Nature 219 (1968) 131.
[3] G. Pifat, S. Maričić and Š. Grandja, Biopolymers 12 (1973) 905.
[4] G. Pifat and S. Maričić, Biophys. Chem. 1 (1973) 112.
[5] A. Derzhanski, A. Georgieva, K. Kotev and B.P. Atanasov, Biochim. Biophys. Acta 214 (1970) 83.
[6] B.P. Atanasov, Nature 233 (1971) 560.
[7] B.F. Cameron and P. George, Biochim. Biophys. Acta 194 (1969) 16.
[8] J. Brnjas-Kraljević, S. Maričić and S. Vuk-Pavlović, Croat. Chem. Acta 45 (1973) 619.
[9] W.G. Zijlstra and E.J. Van Kampen, Clin. Chim. Acta 5 (1960) 719.
[10] Ch.D. Coryell and F. Stitt, J. Amer. Chem. Soc. 62 (1940) 2942;
F. Jung, H. Ankermann and W. Scheler, Biochem. Z. 328 (1956) 328.
[11] K. Kawahara, A.G. Kirshner and C. Tanford, Biochemistry 4 (1965) 1203.
[12] Th.T. Herskovits and J. Greenblatt, Arch. Biochem. Biophys. 130 (1969) 30.
[13] P. Douzou, Biochimie 53 (1971) 1135.
[14] K.D. Bartle, B.J. Dale, D.W. Jones and S. Maričić, J. Magn. Res. 12 (1973) 286.
[15] A.S. Mildvan, N.M. Rumen and B. Chance, in: Probes of structure and function of macromolecules and membranes, Vol. II – Probes of enzymes and haemoproteins (Academic Press, New York, 1971) p. 205.
[16] I.D. Campbell, P.E. Nixon and R.E. Richards, Mol. Phys. 20 (1971) 923.
[17] I. Solomon, Phys. Rev. 99 (1955) 559;
N. Bloembergen, J. Chem. Phys. 27 (1957) 595.
[18] G. Lahajnar, I. Zupančic, R. Blinc, G. Pifat and S. Maričić, Biopolymers 13 (1974) 1187.
[19] J. Beetlestone and P. George, Biochemistry 3 (1964) 707.
[20] H.G. Hertz, J. Solution Chem. 2 (1973) 239.
[21] R. Huber, O. Epp and H. Formanek, J. Mol. Biol. 42 (1969) 591.
[22] S. Maričić and N. Rumen, Biochim. Biophys. Acta 154 (1968) 496.

BIOPHYSICAL CHEMISTRY 2 (1974) 369–376. © NORTH-HOLLAND PUBLISHING COMPANY

MOLECULAR WEIGHT DETERMINATION OF BOVINE CARBONIC ANHYDRASE

S. LAPANJE and V. DOLEČEK
Department of Chemistry, University of Ljubljana, Yugoslavia

and

K. KAWAHARA and K. HIGASHI
Department of Pharmaceutical Chemistry, Nagasaki University, Bunkyo-machi, Nagasaki, Japan

Received 16 April 1974
Revised manuscript received 15 August 1974

The molecular weight of bovine carbonic anhydrase was determined by osmometric and sedimentation equilibrium methods. The solvents used were 0.15 M KCl and 6.0 M guanidinium chloride. The value found was 28300 ± 300 which is lower than the values found by other investigators.

As a part of the studies the intrinsic viscosities of the enzyme in 4.5 M guanidinium thiocyanate and 6.0 M guanidinium chloride were also ascertained. The values found, 25.4 ml/g and 24.7 ml/g, respectively, are smaller than expected on the basis of the molecular weight. This finding, however, is in agreement with the low value, 0.72×10^{-3} cm^3 mol/g^2, of the second virial coefficient in 6.0 M guanidinium chloride.

1. Introduction

In the course of our studies on the denaturation of globular proteins by guanidinium thiocyanate (Gdm SCN) [1] we noticed that the intrinsic viscosity of bovine carbonic anhydrase in concentrated solutions of this denaturant was much lower than expected considering the molecular weight given in the literature [2]. A detailed survey of the literature also revealed that most of the molecular weights determined were around 30000 and that very few, if any, extensive molecular weight studies of this enzyme were performed [3–6]. Therefore we performed osmometric and sedimentation equilibrium studies of the enzyme in dilute buffer and 6 M guanidinium chloride (Gdm Cl) solutions in order to arrive at a more accurate value of its molecular weight. The studies were complemented with viscosity measurements in solutions of the denaturants, Gdm SCN and Gdm Cl.

2. Experimental

2.1. Materials

Four samples of bovine carbonic anhydrase were used in the studies. One of them was a commercial product (Lot No. 35-C 8000) from Worthington Biochemical Corp. The other three were kindly supplied at different times by Dr. S. Lindskog. They were the form B which contained still small amounts of other forms as shown by acrylamide gel electrophoresis. They are practically identical with B (except in electrophoresis) and so they should not affect our experimental results. The Worthington sample also showed the presence of several components in acrylamide gel electrophoresis, but one was by far predominant. In viscometric experiments all four samples were used and identical results, within the limit of experimental error, were obtained. In osmometric experiments one of Lindskog's samples and the commercial sample were used, whereas sedimentation equilibrium experiments were performed with one

of Lindskog's preparations only. The zinc-free apoenzyme was prepared by dialysis for a week against 1,10-phenanthroline in 0.1 M acetate buffer, pH 5.2 [7].

Ultra-pure Gdm Cl was either prepared according to the method of Nozaki and Tanford [8] or purchased from Schwarz/Mann. Gdm SCN was purified from a crude sample (Dr. T. Schuchardt, G.m.b.H., Munich) as described previously [9].

From all of the samples, relatively concentrated stock solutions were prepared, which were then dialyzed against the solvent. The final dialysate was used as diluent for preparing other solutions. Where precipitation occurred, the pH was adjusted by adding a few drops of concn. NaOH. Since bovine carbonic anhydrase does not contain cystine usually no β-mercaptoethanol was added.

Protein concentrations were in most cases determined from dry weight content. However, with the last sample obtained from Lindskog as well as with the commercial sample the extinction coefficient $A^{1\%}_{280}$ was also determined and found to be 17.5 ± 0.2.

2.2. Intrinsic viscosity

Viscosity measurements were made in Cannon–Fenske capillary viscometers. 6 viscometers were used in the studies. They were filled with 5 ml of solvent or solution. Flow times for water were about 300 s and for Gdm Cl and Gdm SCN solutions around 400 s. No kinetic energy corrections were necessary. All measurements were made at 25.00 ± 0.01 °C. With each solution usually 6–8 flow time measurements were performed. The densities ρ of all solutions were calculated using the existing density equations for Gdm SNC and Gdm Cl, respectively [1, 10], and assuming contributions from components other than the denaturant to be additive.

2.3. Osmotic pressure

Osmotic pressure measurements were made with a Melabs recording osmometer, Model CSM-2 at 25°C. The solvents used were 0.15 M KCl, pH 6.5; 6.0 M Gdm Cl, pH 6.0 and for the apoenzyme the 0.1 M acetate buffer, pH 5.2. Membranes for measurements in 0.15 M KCl were cut from dialysis tubing, Union Carbide, which was treated similarly to that used in dialysis. In 6.0 M Gdm Cl membranes SM 117 36 (Sartorius-Membranfilter G.m.b.H., Göttingen) were used. Before use, the membranes were equilibrated with the solvent for at least 24 h. An important criterion for the accuracy of each series of measurements – in addition to pressure reaching a plateau after an initial rise – is the reproducibility of the solvent and solution readings. As in previous studies [11, 12], only those series of measurements in which the fluctuations were less than 0.15 cm were deemed satisfactory. In each solvent with each sample thus at least two independent series of measurements were performed.

2.4. Ultracentrifugation

Sedimentation equilibrium experiments were carried out in 12 and 30 mm double-sector cells in a Spinco Model E ultracentrifuge equipped with electric speed control and interference optics. The 0.1 M sodium phosphate buffer, pH 6.0, or 6.0 M Gdm Cl–0.1 M β-mercaptoethanol–0.1 M phosphate buffer were used as solvents for the enzyme. Both low-speed and high-speed equilibrium techniques were used.

The value of the partial specific volume, $\bar{v}_2$, for the enzyme is required for calculating the molecular weight. For buffer, the value 0.732 ml/g was obtained from densities of the commercial sample measured with an A. Paar precision densimeter, Model DMA 02D, at 25.00°C. For 6 M Gdm Cl, $\bar{v}_2$ was obtained from dilatometric measurements. A detailed account of these studies will be published separately [13]. The experimentally determined value of $\bar{v}_2$ for the native enzyme agrees well with the value 0.733 ml/g calculated by Wong and Tanford [6] from the amino acid composition.

3. Results and discussion

3.1. Intrinsic viscosity

Viscosity measurements usually started 1 h after preparing the solutions. They were extended over a period of several hours; final measurements were made next day. In 4.5 M Gdm SCN as well as in 6.0 M Gdm Cl constant flow times were observed. A separate study was made of the reduced viscosity of commercial

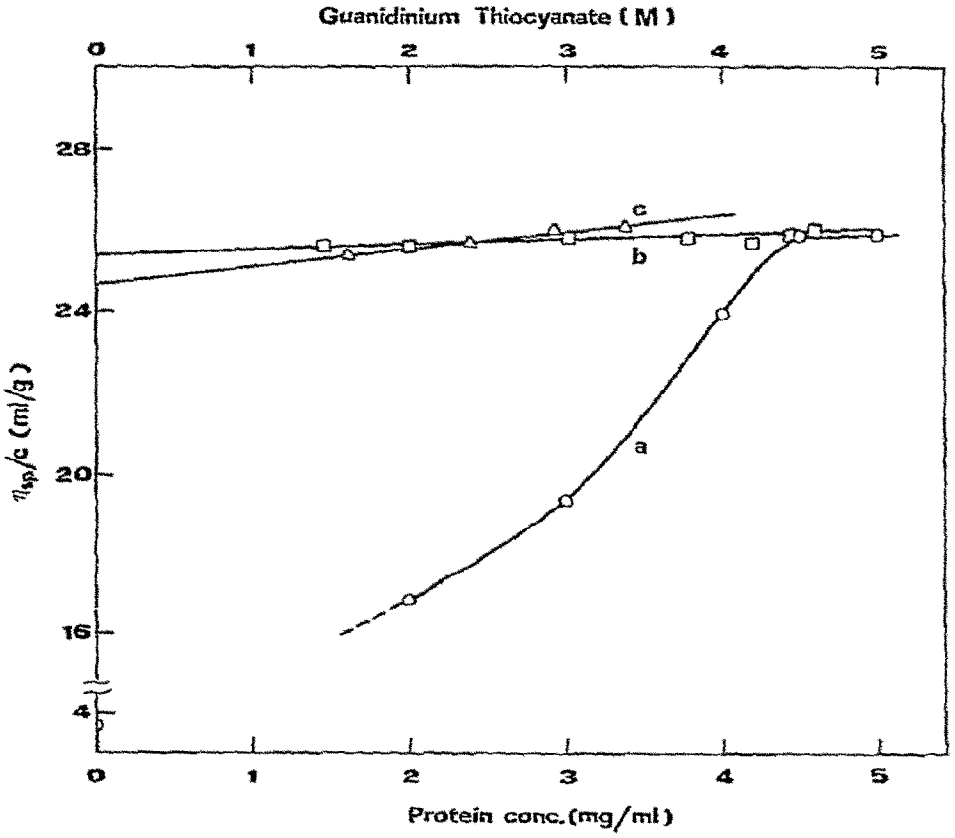


Fig. 1. (a) Reduced viscosity of bovine carbonic anhydrase (commercial sample) as a function of guanidinium thiocyanate concentration at 25°C. Protein concentration 4.4×10^{-3} g/ml.
(b) Reduced viscosity of bovine carbonic anhydrase in 4.5 M guanidinium thiocyanate as a function of protein concentration.
(c) The same in 6.0 M guanidinium chloride.

carbonic anhydrase as a function of Gdm SCN concentration. The results are presented in fig. 1. It can be seen that the transition from the native to the unfolded form is well expressed and at concentrations higher than 4.0 M the curve levels off.

The experimental data used in the determination of intrinsic viscosities are also given in fig. 1. The data were fitted by a least squares analysis to the equation

$$\eta_{sp}/c = [\eta] + k[\eta]^2 c, \qquad (1)$$

where η_{sp} is the specific viscosity, c the protein concentration in g/ml, $[\eta]$ the intrinsic viscosity, and k a dimensionless constant. The values of $[\eta]$ are 25.4 ml/g in 4.5 M Gdm SCN and 24.7 ml/g in 6.0 M Gdm Cl. The relative error is estimated at ± 2%.

Now it is possible to make use of the equations relating $[\eta]$ in the two solvents to the number of amino acid residues [1, 10]. Assuming the molecular weight to be around 29000 [6] there are 262 residues per enzyme molecule and we calculate $[\eta]$ = 27.7 ml/g in 4.5 M Gdm SCN and 28.4 ml/g in 6.0 M Gdm Cl. We see that these figures are about 10% higher than the experimental values. However, on the basis of our osmometric and sedimentation equilibrium measurements, see below, the molecular weight of bovine carbonic anhydrase appears to be closer to 28000 which would decrease the number of amino acid residues to about 253, yielding $[\eta]$ = 27.0 and 27.7, respectively. These values are still higher than those observed; the intrinsic viscosity measurements would therefore give too low a value for the molecular weight. Bovine carbonic anhydrase is not the only example

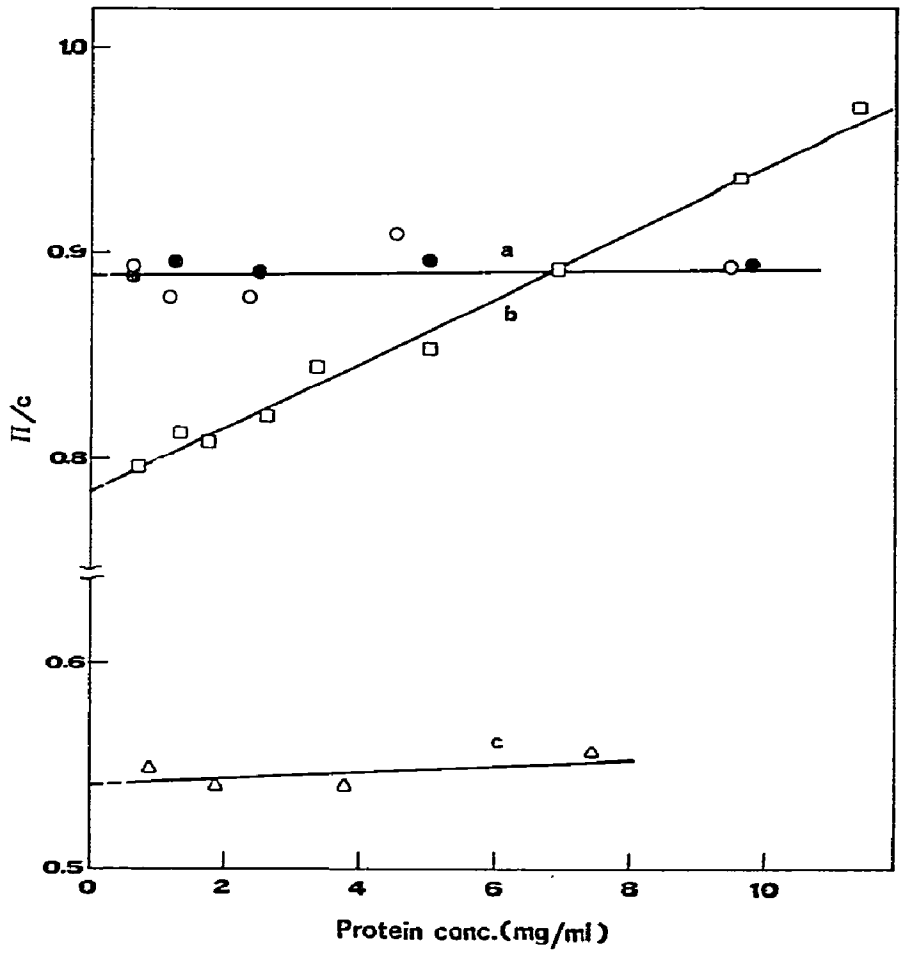


Fig. 2. (a) Osmotic pressure data for bovine carbonic anhydrase B (•) and for commercial sample (○) in 0.15 M KCl, pH 6.5.
(b) Osmotic pressure data for commercial enzyme sample in 6.0 M guanidinium chloride, pH 6.0.
(c) Osmotic pressure data for apoenzyme, prepared from commercial enzyme sample, in 0.1 M acetate buffer, pH 5.2.

of such a deviation. For pepsinogen, e.g., in 6.0 M Gdm Cl $[\eta]$ is 31.5 ml/g [10] which is quite low for a protein containing 376 residues per molecule. As has been mentioned above, the low value of $[\eta]$ for carbonic anhydrase in 4.5 M Gdm SCN prompted detailed investigations.

$[\eta]$ for the apoenzyme in 6.0 M Gdm Cl is 24.4 ml/g which is insignificantly lower than the value for the whole enzyme.

3.2. Osmotic pressure

The results obtained with one of the B samples and the commercial sample in osmotic experiments in 0.15 M KCl are given in fig. 2. The straight line observed has a slope of nearly zero, and the molecular weight calculated from the ordinate intercept is 28300 ± 200. Experiments in 6.0 M Gdm Cl were performed only with the commercial sample. The data again yield a straight line and the calculated molecular weight is 28200 ± 400. Moreover, from the slope which in this case has a measurable value, fig. 2, the second virial coefficient B is calculated to be $(0.72 \pm 0.07) \times 10^{-3}$ cm^3 mol/g^2. We see that the two values of the molecular weight are quite close and therefore can be considered as reliable. The

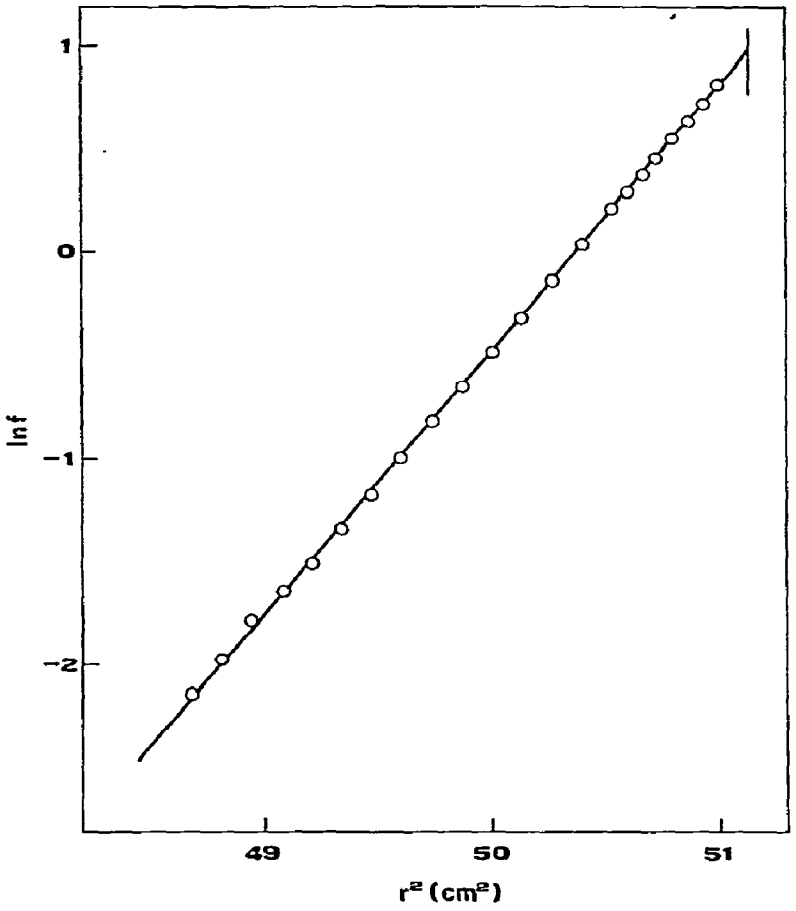


Fig. 3. Sedimentation equilibrium results by high-speed method for native bovine carbonic anhydrase B in 0.1 M phosphate buffer, pH 6.0, $c = 0.63$ mg/ml, cell length 12 mm. The rotor speed was 28000 rpm, and the solution column was 4.97 mm high, $T = 25°C$.

relatively small value of B should be commented upon, as by comparison with the values for other proteins in 6.0 M Gdm Cl [11] one would expect for B a value around 1.0×10^{-3}. However, the low value of B is in agreement with the unusually low intrinsic viscosity, cf. above. It is to be noted that for pepsinogen which also displays a low intrinsic viscosity in 6.0 M Gdm Cl, B in the same solvent is 1.17×10^{-3} [11] which is much above the expected value. We were not able to arrive at an explanation although even the possibility of an artifact was considered [11].

The results obtained with the apoenzyme in 0.1 M acetate buffer, pH 5.2, fig. 2, are quite interesting in that a molecular weight of 46400 ± 700 is calculated from the ordinate intercept. The high value apparently reflects considerable association which could partially be due to the absence of Zn-ions. This aspect was not further pursued.

3.3. Sedimentation equilibrium

The first run of the native enzyme in 0.1 M phosphate buffer at high-speed showed that during the experiment precipitation occurred. Later, the same behavior was observed in an experiment at low-speed. Therefore from all of the experiments with the native enzyme only two were considered as satisfactory, i.e., those where the amount precipitated was below 10%, figs. 3 and 4. Moreover, for the evaluation of molecular weight from the low-speed experiment the method

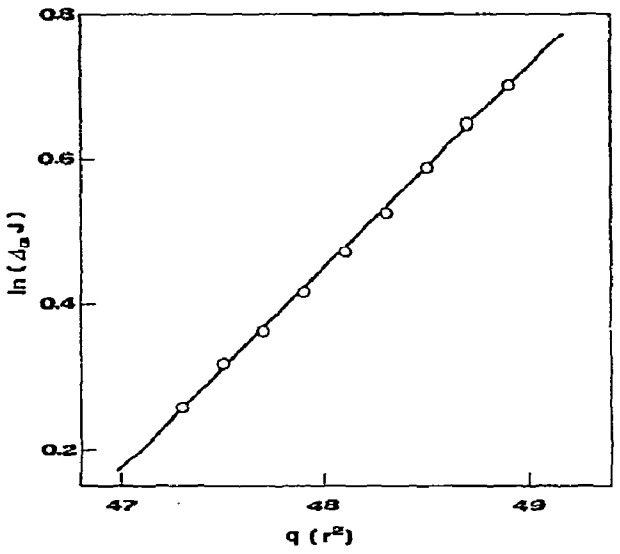


Fig. 4. Sedimentation equilibrium results by low-speed method for native carbonic anhydrase B in 0.1 M phosphate buffer, pH 6.0, $c = 3.14$ mg/ml, cell length 12 mm. The rotor speed was 13000 rpm and the solution column was 2.75 mm high, $T = 25°C$. $\Delta_Q J$ is the displacement of a fringe (in fringe numbers) between the positions $q^{1/2}$ and $(q+2)^{1/2}$.

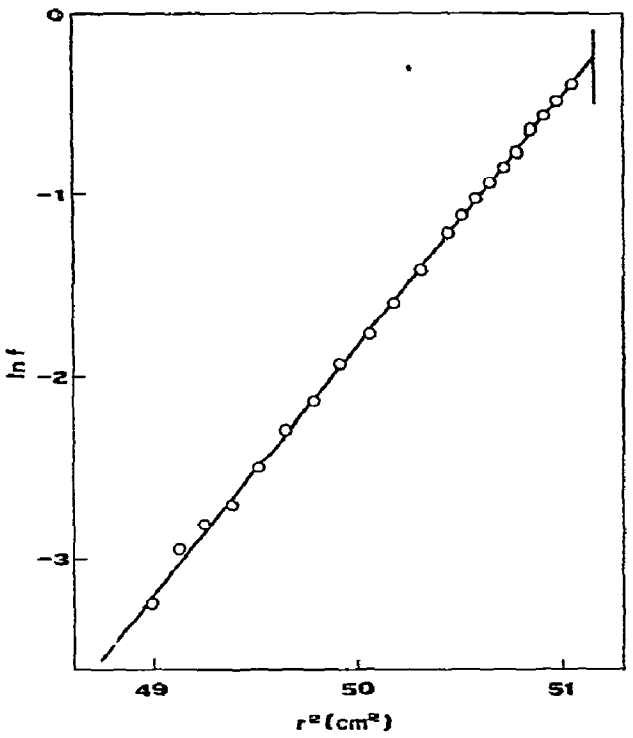


Fig. 5. Sedimentation equilibrium results by high-speed method for denatured bovine carbonic anhydrase B in 6.0 M guanidinium chloride–0.1 M β-mercaptoethanol–0.1 M phosphate buffer, pH 6.0, $c = 0.43$ mg/ml, cell length 12 mm. The rotor speed was 34000 rpm, and the solution column was 5.23 mm high, $T = 25°C$.

of Nazarian [14] had to be used.

In 6.0 M Gdm Cl–0.1 M β-mercaptoethanol–0.1 M phosphate buffer, pH 6.0, experiments were also carried out at low and high speeds. In these solutions precipitation was much higher, amounting to over 80%. Nevertheless the plots of $\ln f$ versus r^2 yielded straight lines, cf. fig. 5, indicating the homogeneity of the sample and regular distribution in the cell at sedimentation equilibrium.

The values of $M_2(1-\bar{v}_2\rho)$ found in the experiments with the native enzyme were 7.43×10^3 and 7.42×10^3, respectively. The relatively low buffer concentration allows us to treat the system as a 2-component one. Using the value 0.732 ml/g for $\bar{v}_2$, 28300 is calculated for M_2, the enzyme molecular weight.

In 6.0 M Gdm Cl the situation is more complicated. Neglecting the relatively small concentrations of β-mercaptoethanol and phosphate buffer the following relation applies [15]:

$$M_2(1-\Phi'\rho) = M_2(1-\bar{v}_2\rho) + \xi_3(1-\bar{v}_3\rho), \qquad (2)$$

where Φ' is an apparent quantity not simply related, as we can see, to $\bar{v}_2$; ξ_3 is the preferential solvation parameter and $\bar{v}_3$ the partial specific volume of component 3, i.e., Gdm Cl. The average value of the l.h.s. of eq. (2) determined in the experiments was $(5.0_2 \pm 0.20) \times 10^3$. Thus in order to calculate M_2 we have to know not only $\bar{v}_2$ but ξ_3 and $\bar{v}_3$ as well. $\bar{v}_2$ was obtained from dilatometric experiments which yielded for the difference between the partial specific volumes in 6.0 M Gdm Cl and water a value of 182 ml/mol [13], $\bar{v}_2$ in 6.0 M Gdm Cl is then 0.738 ml/g. The interaction parameter ξ_3 was not experimentally determined. Therefore we have to consider data for some other proteins in the same solvent. The value for β-lactoglobulin is 0.16 [16] and for bovine serum albumin 0.15 [17]. Using the latter value and for $\bar{v}_3$ 0.763 [15] we calculate 28200 for M_2. For lysozyme, on the other hand, ξ_3 was only 0.09 [16] and using this value M_2 is found to be 29500.

Table 1
Experimental data for bovine carbonic anhydrase B at 25°C. The molecular weight value in 6.0 M guanidinium chloride, pH 6.0, determined in osmometric experiments refers to the commercial enzyme sample. However, in 0.15 M KCl, pH 6.5, no difference was observed between the sample and pure form B. The molecular weight values by sedimentation equilibrium were calculated using the values 0.732 and 0.738 ml/g, respectively, for the partial specific volume of the enzyme in 0.1 M phosphate buffer, pH 6.0, and 6.0 M guanidinium chloride

Solvent	$[\eta]$ (ml/g)	Molecular weight	
		Osmotic pressure	Sed. equil.
0.15 M KCl, pH = 6.5	3.7 a)	28300 ± 200	
0.1 M phosphate buffer, pH 6.0			28300 ± 300
6.0 M Gdm Cl, pH 6.0	24.7	28300 ± 400	
4.5 M Gdm SCN, pH 6.0	25.2		
6.0 M Gdm Cl 0.1 M β-mercaptoethanol–0.1 M phosphate buffer, pH 6.0			28200 ± 1100 (29500) b)

a) The value found by Wong and Tanford [6] in 0.1 M NaCl, pH 7.0.
b) The value in parentheses calculated using the value 0.09 for the preferential interaction parameter ξ_3, see eq. (2) of the text.

Owing to the high extent of precipitation both values have to be considered as semi-quantitative only. However, the importance of knowing the correct value of the interaction parameter is clearly displayed. Thus this parameter as well as $\bar{v}_2$ have to be known for accurate molecular weight determinations. Incidentally, using the value of $\Phi' = 0.726$ ml/g assumed by Wong and Tanford [6] $M_2 = 29200$ is obtained.

We have deliberately avoided any discussion of the value 17.5 found for the extinction coefficient $A^{1\%}_{280}$. The determination was not considered as an important part of the studies. However, in those few instances where concentrations were determined by dry weight and photometric measurements complete agreement was observed. We are thus left with the fact that three different values for $A^{1\%}_{280}$ exist: Nyman–Lindskog's 19.0 [3]; Wong and Tanford's 18.3 [6], and ours, 17.5. The true value for the extinction coefficient is apparently not settled yet.

A comprehensive survey of all experimental data is given in table 1.

On the basis of osmometric and sedimentation equilibrium results we suggest that the molecular weight of bovine carbonic anhydrase is 28300 ± 300 which is significantly lower than the value of 31000 determined by Lindskog [2] by the approach to equilibrium technique, and also the value of 30000 estimated by Nyman and Lindskog [3] from amino acid composition.

Reynaud et al. [4,5], on the other hand, give values for the A and B forms of the enzyme ranging from 29200 to 33100 using especially the method of sedimentation and diffusion. Finally, Wong and Tanford [6] obtained by sedimentation equilibrium in 0.15 M NaCl, pH 7.0, and in 6.0 M Gdm Cl solutions a value of 29000. However, the agreement between our osmometric and sedimentation equilibrium results is probably not entirely fortuitous which supports our suggestion concerning the molecular weight of bovine carbonic anhydrase.

Acknowledgement

The authors express their gratitude to Dr. Sven Lindskog, Department of Biochemistry, University of Göteborg for his generous gift of samples without which these studies could not have been performed. They also thank S. Lenarčič and S. Regent for skilful technical assistance.

References

[1] S. Lapanje, Biochim. Biophys. Acta 243 (1971) 357.
[2] S. Lindskog, Biochim. Biophys. Acta 39 (1960) 218.
[3] P.-O. Nyman and S. Lindskog, Biochim. Biophys. Acta 85 (1964) 141.
[4] J. Reynaud, F. Luccioni, M. Bouthier, J. Savary and Y. Derrien, Biochim. Biophys. Acta 221 (1970) 367.
[5] J. Reynaud, F. Luccioni, M. Bouthier, J. Savary and

Y. Derrien, Biochimie 53 (1971) 1095.
[6] K.P. Wong and C. Tanford, J. Biol. Chem. 248 (1973) 8518.
[7] S. Lindskog and B.G. Malmström, J. Biol. Chem. 237 (1962) 1129.
[8] Y. Nozaki and C. Tanford, Methods Enzymol. 11 (1967) 732.
[9] S. Lapanje, Biochim. Biophys. Acta 243 (1971) 349.
[10] C. Tanford, K. Kawahara and S. Lapanje, J. Am. Chem. Soc. 89 (1967) 729.
[11] S. Lapanje and C. Tanford, J. Am. Chem. Soc. 89 (1967) 5030.
[12] S. Lapanje, Croat. Chem. Acta 41 (1969) 115.
[13] S. Lapanje and V. Doleček, paper in preparation.
[14] G.M. Nazarian, Anal. Chem. 40 (1968) 1766.
[15] E. Reisler and H. Eisenberg, Biochemistry 8 (1969) 4572.
[16] J. Špan, S. Lenarčič and S. Lapanje, Biochim. Biophys. Acta, in press.
[17] M.E. Noelken, Biochemistry 9 (1970) 4122.

BIOPHYSICAL CHEMISTRY 2 (1974) 377–384. © NORTH-HOLLAND PUBLISHING COMPANY

POSSIBLE IMPLICATIONS FOR ALLOSTERIC MODELS OF HEMOGLOBIN OF THE LAWS OF COMBINATION WITH CARBON MONOXIDE UNDER PHOTODISSOCIATING CONDITIONS

Edward WHITEHEAD

Istituto di Chimica Biologica dell'Università di Roma, and Centro di Biologia Molecolare del C.N.R., Citta Universitaria, 00185 Rome, Italy

Received 3 May 1974

It is shown that the data obtained by Brunori et al. on binding of carbon monoxide to hemoglobin in photodissociating conditions is explained by a simple allosteric model, the two-configuration exclusive-binding induced-fit model together with the simplest kinetic assumptions. Alternative models are considered. It is possible to calculate from the data of Brunori et al. a dissociation rate constant for carbon monoxide which agrees well with an independently determined rate constant.

1. Introduction

Brunori et al. [1] studied carbon monoxide binding to human hemoglobin under conditions of constant illumination where the apparent affinity of this ligand for the protein can be decreased by a factor of as much as 10^3 due to a process of photodissociation. The main experimental conclusions from this study are that

(i) the shape of the saturation curves as a function of log ligand concentration is not changed by light, i.e., the curves are all parallel, co-operativity is not changed;

(ii) the affinity is a linear function of light intensity;

(iii) the Bohr effect (the effect of pH on affinity) is invariant with light intensity; and

(iv) in photodissociating conditions change of temperature does not lead to change in the shapes of the saturation curves, as has long been known to be also the case in the dark. The effect of temperature on affinity in the presence of light is different from that in the dark; while in the dark increase in temperature leads to decrease in ligand affinity, in photodissociating conditions it *increases* affinity.

For the purposes of mathematical treatment the statements (i)–(iv) will be assumed to be exact laws. Insofar as they are exact, these laws as well as the classical laws of invariance of co-operativity with pH and temperature in the dark are completely accounted for by a simple model of allosteric equilibria – the two-configuration exclusive binding induced-fit model, plus the simplest possible kinetic assumptions.

2. The model

Consider an oligomer whose protomers can exist in only two configurations, termed T and R, and assume that a ligand ω can be found only to R. If there is only one site per protomer for ω and if the protein does not undergo an association-dissociation reaction then at equilibrium the relation between fractional saturation $\bar{\Omega}$ of the protein by the ligand and the concentration ω of the ligand ω in solution has the form

$$\bar{\Omega} = \frac{B\omega}{1+B\omega} \cdot \frac{\Sigma_{i=0}^{q} i L_i (1+B\omega)^i}{q \Sigma_{i=0}^{q} L_i (1+B\omega)^i}, \qquad (1)$$

where B is the association constant for binding of the ligand to the configuration R, q the number of protomers and the L_i a series of constants relating to the

interactions between protomers (see, e.g., eq. (26) of ref. [2]; eq. (7) of ref. [3]). This may be written

$$\bar{\Omega} = [B\omega/(1+B\omega)]\mathcal{R}(1+B\omega)\,, \qquad (2)$$

where $\mathcal{R}$ is a functional operator. It can be shown that the latter form is valid for the two-configuration exclusive binding hypothesis even in the presence of dissociation of the oligomer [4]. Now the long-established invariance of co-operativity of ligand binding to hemoglobin with pH and temperature may be explained [5] by the induced-fit hypothesis in which it is assumed, in addition to all the above, that for all measurable $\bar{\Omega}$, $B\omega \gg 1$. (This implies that there is never a significant proportion of free R in the system.) Applying this condition to eq. (2), we obtain

$$\bar{\Omega} = \mathcal{R}(B\omega)\,. \qquad (3)$$

3. Laws (i) and (ii)

As well as the above assumptions about allosteric equilibria, it is assumed that in the absence of light the reactions leading to the binding of CO to a subunit in the R form, and the dissociation of the RCO complex may be represented

$$\mathrm{R} + \mathrm{CO} \underset{b}{\overset{b'}{\rightleftarrows}} \mathrm{RCO}\,. \qquad (4)$$

Now B will be determined by two velocity constants, b' and b, respectively the forward and backward velocity constants for the reaction:

$$B = b'/b\,.$$

Then the facts can be explained by the reasonable assumption that light causes an extra "off" process

$$\mathrm{RCO} + h\nu \rightarrow \mathrm{R} + \mathrm{CO}\,, \qquad (5)$$

and that the first-order rate constant of this process is proportional to light intensity, I, and to the absorption coefficient, ϵ, and quantum yield, ϕ, of the chemophore. Thus the first-order rate constant for the photoinduced process (5) would be $\phi\epsilon I$. The total first-order rate constant for the decomposition of RCO directly into R + CO is the sum of those for (4) and (5), i.e.

$$b_I = b_0 + \phi\epsilon I\,,$$

(we shall adopt the convention of writing the effective value of any quantity in the presence of light intensity I with a subscript I, thus quantities with subscript 0 represent those quantities in the dark). Therefore

$$B_I = b'/(b_0 + \phi\epsilon I)\,.$$

From (3) constant $\bar{\Omega}$ corresponds to constant $B\omega$, therefore for any given constant saturation

$$b'\omega/(b_0 + \phi\epsilon I) = B_0\omega_0\,. \qquad (6)$$

Thus we have explained both the parallelism of the curves [law (i)] since we see in the above equation that at any fixed light intensity ω/ω_0 is independent of saturation, and also the linearity of the dependence of affinity on intensity [law (ii)], as can be seen rewriting (6) in the form

$$\omega = (B_0\omega_0/b')(b_0 + \phi\epsilon I)\,,$$

or

$$\omega = \omega_0(1 + \phi\epsilon I/b_0)\,. \qquad (7)$$

The experiments permit an estimation of the value of b_0. From (7) this is equal to the horizontal intercept multiplied by $-\phi\epsilon$ in a plot of ω against intensity at any constant $\bar{\Omega}$ (for instance $\bar{\Omega} = \frac{1}{2}$). Thus if the absolute intensities in the experiments of Brunori et al. were known an absolute value of b_0 could have been obtained. Unfortunately the intensities could not be measured absolutely, but only by their effect on the affinity of myoglobin. This means that in the first place a value of b_0 relative to a velocity constant of dissociation from myoglobin is what is obtained directly from the experiments. Thus we can write

$$\frac{b_{0(\mathrm{Hb})}}{b_{0(\mathrm{Mb})}} = \frac{\phi_{\mathrm{Hb}}\epsilon_{\mathrm{Hb}} I_{\omega=0(\mathrm{Hb})}}{\phi_{\mathrm{Mb}}\epsilon_{\mathrm{Mb}} I_{\omega=0(\mathrm{Mb})}} \approx \frac{\phi_{\mathrm{Hb}} I_{\omega=0(\mathrm{Hb})}}{\phi_{\mathrm{Mb}} I_{\omega=0(\mathrm{Mb})}}\,,$$

since the integrated extinction coefficients of hemoglobin and myoglobin are nearly equal. Using 0.37 as the value [6] of $\phi_{\mathrm{Hb}}/\phi_{\mathrm{Mb}}$, $b_{0(\mathrm{Hb})}/b_{0(\mathrm{Mb})}$ was estimated, using the results [1] of Brunori et al. as being close to 1. Now the kinetics of myoglobin's reactions with carbon monoxide can be adequately represented [7] by the scheme:

$$\mathrm{Mb} + \mathrm{CO} \underset{b_{0(\mathrm{Mb})}}{\overset{b'_{\mathrm{Mb}}}{\rightleftarrows}} \mathrm{MbCO}\,.$$

The velocity constant of CO dissociation from myo-

globin in the above scheme has been estimated [8] as $0.02\ s^{-1}$, so using the above ratio of the dissociation constants for hemoglobin and myoglobin, $b_{0(Hb)}$ is predicted to have roughly this value of $0.02\ s^{-1}$ too. The dissociation velocity constant of carbon monoxide from fully saturated human hemoglobin – "l_4" in hemoglobinologists' terminology – has also been (and is the only l_i to have been) directly measured [9] as $0.01 - 0.015\ s^{-1}$. But this velocity constant is expected from our model to be equal to $b_{0(Hb)}$ (the relation of kinetic dissociation constants is discussed below in more detail). It can be seen that the model gives good agreement between the predicted and observed values of l_4, when it is considered that the predicting computation uses data from five different publications.

4. Effect of pH – law (iii)

Brunori et al. [1] found that the effect of pH on affinity was the same at any light intensity as in the dark. The quantum yield of carbonmonoxyhemoglobin is known [6] to be independent of pH, and so therefore will be that of process (5) in our model. If then the pH variation of apparent affinity is independent of the relative contributions of the two processes – process (5) and the "off" process of scheme (4) – whose sum determines this affinity and one of which is pH independent, we must conclude that the rate constant b_0 is also independent of pH. This is what we should expect if binding is truly to a single configuration, and if we think of the Bohr protons as affecting the equilibrium between configurations rather than interacting in a direct manner with bound ligand. In agreement with this, and with the identity postulated above between b_0 and l_4, the latter is relatively independent [9] of pH.

5. The effect of temperature – law (iv)

Another constant of the model obtainable from the data of Brunori et al. [1] is the enthalpy of activation of the dissociation reaction in (4). Assuming that the process (5) and the quantum yield and extinction coefficient of the carbonmonoxyhemoglobin are not temperature-dependent, and simplifying eq. (7) slightly by taking the case where $\omega \gg \omega_0$ (a condition satisfied in many of the experiments) we see that this quantity is given by

$$\Delta H^{\ddagger} = -\mathrm{d}\ln b_0/\mathrm{d}(1/RT) = \mathrm{d}\ln(\omega_I/I\omega_0)/\mathrm{d}(1/RT)\,,$$

which is available experimentally. It is stating exactly the same thing in other terms to say that this enthalpy of activation is equal to the difference in the enthalpies of liganding of the hemoglobin at zero and at high light intensities.

$$\Delta H^{\ddagger} = \Delta H_I - \Delta H_0\,. \qquad (8)$$

From Brunori et al.'s values of +7 and −11.5 kcal/mole respectively for the quantities on the right-hand side, $\Delta H^{\ddagger}$ is approximately +18.5 kcal/mole. This may be compared with the value of 24 kcal/mole estimated [9] for directly measured l_4. The discrepancy between the two is equivalent to a better accord between the estimates of b_0 and l_4 at some temperatures than others.

6. Discussion

In this paper certain laws true to within a certain error of human hemoglobin, have been derived from a model, so supporting the model as an account of the real situation in this hemoglobin. However, the field of allosteric models is strewn with unwarranted inferences from experimental results springing from failure to recognise clearly which predictions are due to which features of the models. For this reason, and in view of the future usefulness of the photodissociation method for other systems, it will be important and illuminating to examine this relation closely in the present case, and to consider alternative models.

Concerning the laws (i) and (ii), the essential features of the model responsible for these are: the *exclusive binding hypothesis*, i.e., the assumption that CO is bound to one configuration only of the subunits, and the assumption that the processes of dissociation and photodissociation from this configuration can be adequately represented by scheme (4) and (5). The assumptions of only two configurations and of induced-fitwise binding are *not* necessary to *these* predictions, but were made above for convenience of exposition in the context of a discussion of human hemoglobin. Laws that *are* explained by the last two

assumptions are the invariance of co-operativity with pH and temperature in the dark and the linear relation between ligand saturation and configuration-dependent parameters. These last laws are not valid for hemoglobins in general, but only for some better-known mammalian (notably human and sheep) hemoglobins. The co-operativity of ligand binding by many fish hemoglobins, and among mammalian forms, cat and some abnormal human hemoglobins is on the other hand pH-dependent [10–12].

To see that the first-mentioned assumptions above are adequate to predict laws (i) and (ii) consider eq. (2). An equation of this form represents the case where binding of the ligand is to only one configuration however many non-binding configurations there may be. This equation can be written in the form:

$$\bar{\Omega} = f(B\omega) \,. \qquad (9)$$

Light affects B in the way already specified and the rest of the argument is exactly the same whether we use eq. (3) or (9).

The *kinetic* assumptions implicit in schemes (4) and (5) are essential to the explanations we have given.

A significant point about the assumption concerning photodissociation required by the explanation is that processes such as $E\Omega_i + h\nu \rightarrow E\Omega_0 + i\omega$, are excluded, or in other terms the quantum yield is independent of the degree of liganding (which has recently been confirmed experimentally by Brunori – personal communication) – or again that the photodissociation terms enters into the binding equation with the same statistical weights as does b_0. This need not exclude transfer of the photoexcitation between subunits, but does mean that such transfer cannot be specifically towards the liganded subunits.

With regard to the dark dissociation process, the pathway $RCO \rightarrow TCO \rightarrow T + CO$ must be assumed to contribute negligibly to it. A significant role for this pathway would allow the dissociation rate constants for CO to vary with the degree of liganding, but would not be compatible with the photodissociation experiments, whilst on the other hand in the model being proposed these constrants are independent of the degree of liganding. There is a general belief, based on kinetic and equilibrium studies and conflicting with the proposed model (or any model having its essential characteristics, as already emphasized by Brunori *et al.*) that these constants *do* vary with degree of liganding. Neither the author, not his colleagues at Rome have been able to devise a model satisfying both this belief and the photodissociation laws that is satisfactory on other grounds. It can only be noted that the belief in question is not based on any direct measurements of different CO dissociation rate constants (l_i has not been measured for $i = 1, 2, 3$). The values of the equilibrium constants for CO binding to sheep hemoglobin [13] on which the belief is mainly based are also in conflict with the theory [14] of the relation of CO and O_2 binding that gives a good account of the overall equilibrium behaviour of these ligands with hemoglobin. On the other hand the photodissociation experiments are the ones which most directly reflect effects of all the dissociation rate constants. It is quite reasonable to suspect current beliefs concerning CO dissociation kinetics may be mistaken; perhaps the experimental equilibrium constants for CO at extreme low and high saturations are affected by some extra factor that is not very important to the overall pattern of binding of CO. On the other hand the oxygen dissociation rate constants certainly do vary with degree of liganding. It is therefore expected that the photodissociation behaviour of oxyhemoglobin, which Professor Brunori is now preparing to study, will be quite different from that of carbonmonoxyhemoglobin*. Co-operatively should not be invariant with light, nor, under photodissociating conditions, with pH or temperature. Binding curves should become asymmetric. The equations have not suggested any particular simple positive features.

The appropriate model for oxygen reaction, then, will probably be different from that for carbon monoxide. Behaviour under photodissociating conditions thus reflects both allosteric equilibria and kinetics. The preceding discussion because of the simplicity of the model used has not yet brought out the essential character of binding under photodissociating conditions. A system under such conditions is not of course an equilibrium, but a steady-state, fully analogous to a steady-state of an enzyme during catalysis, and can be treated by the same mathemati-

* A condition under which the same laws as for CO would obtain is that the reaction of oxygen with the R form be even faster than that with dithionite, and that the $R \rightarrow T$ transformation be much slower than the $RO_2 \rightarrow TO_2$ transformation.

cal methods, notably the topological method of King and Altman [16]. Such steady-states in the general case (even in single-site proteins) allow kinetic contributions to co-operativity (see ref. [2] for review and references). These contributions are always dependent on the circulation of material around closed pathways, e.g., carbon monoxide can be in the sum result taken on by one configuration and discharged by another, a thing that does not happen at equilibrium. This circulation will not be significant when certain pathways are overwhelmingly favoured over others. Only in these and other special circumstances will the equation of binding in photodissociating conditions take a simple form similar to a possible equilibrium with only some of the constants changed by the photodissociation process, as happens in our proposed model. In such circumstances some, but not all species are present in their equilibrium ratios. As an example, if in a protein with an arbitrary number of configurations, liganded subunits may not undergo configurational transitions, light only changes the values of the B's without otherwise changing the binding equation from that at equilibrium.

A circumstance under which a *partial* simplification of the general steady-state binding equations results is when the configurational transitions are rapid in comparison with the binding and dissociation reactions. The binding of a single ligand can then be represented by an equation of Adair form, of which eq. (10) is an example.

Considering now alternative models, nonexclusive binding models, i.e., ones with binding of ligand to more than one conformation have been proposed for hemoglobin [17–21]. These models do not in general predict the laws (i)–(iv), and in this respect the observations of Brunori et al. give them no support. To see this, note that in such models equilibrium binding is determined by more than one association constant (B). While we have seen that the change of behaviour under photodissociation is not in general like that due to a change of B's in an equilibrium scheme, nevertheless, used with care, and when something can be assumed about the constants, such a way of thinking is often useful for the rapid prediction of qualitative effects. Thus light might change one of the B's much more than another in such a way that the system might come to resemble an exclusive binding equilibrium scheme, with consequent change in co-operativity. This is an extreme case, but light will in general change co-operativity in a nonexclusive scheme.

Still, it could be that there exists a departure from laws (i) and (ii) which is within the errors of the experiments, while the nonexclusive binding models may predict such *small* systematic effects which are not as yet observed experimentally in normal human hemoglobin. The same, it has been argued [5], is true of their predictions for the effects of pH and temperature in the dark. This corresponds to the fact that what is often being proposed in these models is something but slightly different from exclusive binding (and there would seem little enough justification for insisting on these minor modifications). The extent to which such models are falsified by the experiments is a matter for detailed calculation; but the photodissociation experiments certainly impose further constraint on nonexclusive models as accounts of this system.

Nonexclusive binding models with a kinetic basis and therefore susceptible to confrontation with photodissociation data have been proposed by Hopfield et al. [21] and Szabo and Karplus [22].

The attempt at a computation for the former model revealed some defects in it which will be detailed.

The value of the "nonexclusivity constant", c, proposed by Hopfield et al. [21] is 800 for CO. They do not appear to have noticed that in order to account for the correct value of the co-operativity ($n \approx 2.8$) this value of c demands a revision of their initially assumed value of the "allosteric constant", L. The revised value then alters the assignment of states of the protein which was the basis for their calculation of c and its four component velocity constants, such as to require an even more extreme value of c. Moreover, the equilibrium binding curves predicted by the revised values of the constants become noticeably asymmetric, in contradiction to the facts. However for illustrative purposes we shall investigate the effect of photodissociation using Hopfield et al.,'s kinetic constants and the eq. (10) corresponding to the symmetric transition model when all configurational changes are assumed rapid.

$$\bar{\Omega} = \frac{\sum_{i=1}^{4} \omega^i i \binom{4}{i} [(1+Lc^i)/(1+L)]\mathcal{P}_i}{4\left\{1 + \sum_{i=1}^{4} \omega^i \binom{4}{i} [(1+Lc^i)/(1+L)]\mathcal{P}_i\right\}}, \qquad (10)$$

where

$$\mathcal{P}_i = \prod_{j=1}^{i} \left\{ \frac{b'_R + b'_T L c^{j-1}}{b_{0(R)} + \phi\epsilon I + [b_{0(T)} + \phi\epsilon I]\, L c^j} \right\},$$

and where $c = B_{0(R)}/B_{0(T)}$.

The values of L consistent with $c = 800$ and $n_{1/2} = 2.8$ at equilibrium are 2.6×10^{-3} and 9×10^{-10}. With the second value light reduces $n_{1/2}$ to 1.9. This value would presumably not have been chosen because with oxygen ($c = 280$) it gives $n_{1/2} = 1.5$. With the other value of L saturating light would reduce $n_{1/2}$ to 2.3. A change of this order would have been detected in the experiments. There is also an obvious deviation from law (ii). Thus if this model were considered broadly applicable to the material of the photodissociation experiments, human hemoglobin at high dilutions, it would be eliminated. If alternatively the hypothesis is made that liganded subunit cannot undergo configurational transitions, in which case the binding equation is of equilibrium form, the deviations with $L = 2.6 \times 10^{-3}$ are less and might escape detection. This hardly rescues nonexclusivity since with these values of the constants, at 90% saturation the low-affinity conformation is only saturated to the extent of 1.5% at most in the dark. This is equivalent to saying that the exclusive-binding model is a good approximation. The difference between the two computations illustrates the influence of kinetics on the steady state photodissociation behaviour.

The constants proposed by Hopfield et al. are derived from measured equilibrium constants about which reservations were expressed above.

Szabo and Karplus [22] in their account assume implicitly that the dissociation rate constants for the two conformations are equal*. This is consistent with the view of the overall CO dissociation kinetics taken here, though not with the usual view. It is then true that this model describes the photodissociation laws exactly as does the exclusive binding model. But so does a model with thirty-six different configurations, all having the same "off" constants (at all temperatures!). If it be objected that a model with thirty-six binding conformations is more complicated than one with two, then so is the latter more complicated than a model with one. In other words, rather than supporting any particular nonexclusive model, the tendancy of these authors' arguments is towards the position that the photodissociation observations, ideally described by laws (i)–(iv), contain no information about allosteric equilibria (though they do contain the same value of b_0 calculated above). Since this is obviously relevant to the degree of confidence to be felt with any model, it will be further commented on in the conclusion.

Returning to the analysis of the relation of our own hypotheses and predictions, the exclusive binding hypothesis and the already mentioned kinetic assumptions are again by themselves adequate to predict invariance of the Bohr effect with respect to light [law (iii)]. By the concept of configuration itself one expects this to hold in an exclusive binding model. It is an indication of the participation of only one dissociation rate constant and one intrinsic equilibrium binding constant over a range of conditions where if there were more than one binding configuration, more than one constant would in general be expected to influence the observations. In other words it makes the conditions nonexclusive models have to satisfy yet more stringent than do observations at a single pH, while the exclusive binding hypothesis has no difficulty in meeting it.

Where the induced fit hypothesis comes in is in explaining an important feature of the Bohr effect namely invariance of co-operativity in the dark (and thereby automatically through the laws already considered in the light). The longknown pH and temperature invariance of the co-operativity of ligand binding to hemoglobin are highly relevant to the choice between induced-fit and nonexclusive models. The argument eventually becomes numerical: the former model predicts pH-invariance while the latter models not, but these may perhaps do so to within some approximation. The spirit of the rival models in this respect was commented above. The point could be phrased saying that it is the typical predictions of the induced-fit hypothesis that show up strongly with normal human hemoglobin, while nothing corresponding to the *typical* predictions of the nonexclusive models is seen.

* Strictly that the $\phi\epsilon$ of each of the two or more different species is proportional to their dark dissociation velocity constants. If the latter are different the author knows of no physical justification or precedent for such a proportionality.

But cat hemoglobin does show a marked effect typical of nonexclusive binding. While affinity for oxygen increases with pH, so does co-operativity [11]. On an exclusive-binding non-induced-fit model with positive co-operativity the opposite effect is expected. Possible simple explanations for the Bohr effect in cat hemoglobin are therefore: a nonexclusive binding model; an exclusive binding model with more than two configurations; and an exclusive binding model where B varies with pH (however as explained below the third of these is practically a special case of the second). Here is an example where the photodissociation method should be useful for distinguishing between models since there is a better chance than in human hemoglobin that the effects of nonexclusivity show up as deviations from the laws that apply to the latter.

Let us consider the possibility of explaining the Bohr effect in human hemoglobin without invoking induced-fit by postulating that variation of pH changes only one constant, B. The argument on photodissociation was based on change (by light) of B. With or without induced-fit this leaves co-operativity unchanged. Clearly in the same way, change of B by any agent is a possible formal explanation of its changing affinity without change of co-operativity. Applied to the effect of pH in the dark it seems at first somewhat contrary to notions of configuration. This formal explanation could however coincide with a configurational one if we assume, in addition to a pH-independent co-operative configurational change, other pH dependent non-co-operative ones. Wyman [12] has proposed just this in a "nonexclusive" model (one with two such effective pH dependent B's). According to his special assumption which cause both B's vary in the same way with pH, exact invariance of co-operativity with pH in the dark results. Like other nonexclusive models it needs further special assumptions to survive the photodissociation experiments. The idea can be put in an "exclusive" form (binding only to R which is a set of configurations related to each other through non-co-operative transitions) and then in general it satisfies laws (i) and (ii) but not (iii). The case where (iii) is satisfied without any special kinetic or other assumptions is when the binding is to one of these sub-configurations only – just a special case of exclusive binding. It must be added that in the type of model we are now considering, if it is not to reduce to exclusive binding, and induced fit, the observables – the $\overline{\Delta H^{\ddagger}}$, $\overline{\Delta H}$ and the other configuration-dependent parameters which vary linearly with saturation [7] are all correlated with non-co-operative transitions, and none as yet with the co-operative transition which must still be invoked. Law (iv) does not automatically follow either from exclusive binding or induced-fit. It requires the configurational equilibria to be temperature independent, i.e., the free energy differences between R and T to be entirely entropic. The induced-fit hypothesis is much more permissive – only the interactive parts of these free energy differences and not the much larger non-interactive parts need be purely entropic. In general (and with our usual kinetic assumptions) in the hypothesis of exclusive binding without induced-fit the effect of temperature on *co-operativity* would be the same in the light as in the dark (this is just saying that law (i) holds at different temperatures) but the effect on *affinity* would be quantitatively different, and eq. (8) would always apply, where the ΔH on the right-hand side are obtainable from

$$\Delta H = \mathrm{d} \ln \omega_{\mathrm{m}} / \mathrm{d}(1/RT) ,$$

where ω_{m} is the median ligand concentration as defined by Wyman [14].

The proposals of Szabo and Karplus [22] show that if one is prepared to accept very special kinetic assumptions infinite latitude is allowed the description of allosteric equilibria so far as the restrictions posed by the photodissociation experiments are concerned. The nearer the various "off" constants are to one another, the less constraint these experiments pose on schemes of equilibria. On the other hand the model proposed here allows considerable though not infinite latitude with respect to the kinetic constants (it suffices that b'_{T}/L_i, all i, is not comparable with or greater than b'_{R}) by making more special assumptions with respect to equilibria. These are however naturally suggested by the experimental equilibrium behaviour. It is not pretended that the induced fit model accurately accounts for all the facts taken into account here. Discrepancies of note, though perhaps not extremely grave, are the slight pH dependence of the directly measured l_4; and the difference in the estimated $\Delta H^{\ddagger}$ of l_4 and b_0. These might be weaknesses through which the way could be forced towards a better description of the system. But at this moment it seems fair to believe that an improved model for hemoglobin

equilibria and kinetics together would be situated somewhere within a small volume of the relevant parameter space which also contains the present model

Acknowledgement

I am greatly indebted to Professors E. Antonini, M. Brunori and J. Wyman for introducing me to the subject of photodissociation and for many helpful discussions and stimulating criticism. Computer calculations used in this work were done at the Medical Biological Laboratory of the TNO, Rijswijk, Holland and the University of Rome. I thank Drs. Wijnans and Salerno for assistance with computations. This work has been financed by the Consiglio Nazionale delle Ricerche and by Euratom. This is publication No. 1000 of the Euratom Biology Department of which the author is a staff member.

References

[1] M. Brunori, J. Bonaventura, C. Bonaventura, E. Antonini and J. Wyman, Proc. Natl. Acad. Sci. USA 69 (1972) 868.
[2] E.P. Whitehead, Prog. Biophys. Molec. Biol. 21 (1970) 321.
[3] E.P. Whitehead, Biochemistry 9 (1970) 1440.
[4] E.P. Whitehead, (1973), in preparation.
[5] E.P. Whitehead, Acta Biologica et Medica Germanica 31 (1973) 227.
[6] R.W. Noble, M. Brunori, J. Wyman and E. Antonini, Biochemistry 6 (1967) 1216.
[7] E. Antonini and M. Brunori, Hemoglobin and myoglobin in their reactions with ligands (North-Holland, Amsterdam, 1971).
[8] C. Bonaventura, J. Bonaventura, E. Antonini, M. Brunori and J. Wyman, Biochemistry 12 (1973) 3424.
[9] M.J. Mc Donald and R.W. Noble, J. Biol. Chem. 247 (1972) 4282.
[10] A. Riggs, in: Fish physiology, eds. W.S. Hoarr and D.J. Randall (Academic Press, New York, 1970) Vol. 4, p. 209.
[11] M.N. Hamilton and S.J. Edelstein, Science 178 (1972) 1104.
[12] J. Wyman, Current Topics in Cellular Regulation 6 (1972) 209.
[13] F.J.W. Roughton, A.B. Otis and R.L.J. Lyster, Proc. Roy. Soc. B144 (1955) 29.
[14] J. Wyman, Adv. Prot. Chem. 19 (1964) 223.
[15] Q.H. Gibson, Prog. Biophys. Biophys. Chem. 9 (1959) 1.
[16] E.L. King and C. Altman, J. Phys. Chem. 60 (1956) 1375.
[17] J. Monod, J. Wyman and J-P. Changeux, J. Mol. Biol. 12 (1965) 88.
[18] M.M. Rubin and J-P. Changeux, J. Mol. Biol. 21 (1966) 265.
[19] S.J. Edelstein, Nature 230 (1971) 224.
[20] J. Wyman, J. Am. Chem. Soc. 89 (1967) 2202.
[21] J.H. Hopfield, R.G. Shulman and S. Ogawa, J. Mol. Biol. 12 (1971) 625.
[22] A. Szabo and M. Karplus, Proc. Natl. Acad. Sci, USA 70 (1973) 673.

BIOPHYSICAL CHEMISTRY 2 (1974) 385–389. © NORTH-HOLLAND PUBLISHING COMPANY

KINETICS OF THE STACKING OF ETHIDIUM BROMIDE BY THE RAMAN LASER TEMPERATURE-JUMP METHOD

Douglas H. TURNER*‡, Raymond YUAN‡, George W. FLYNN**, and Norman SUTIN
Departments of Chemistry, Brookhaven National Laboratory, Upton, New York 11973, USA, and Columbia University, New York, New York 10027, USA

Received 2 July 1974
Revised manuscript received 4 September 1974

Raman laser temperature-jump measurements have been made on concentrated solutions of ethidium bromide. Two relaxations were observed. The faster has a lifetime of less than 30 ns and is attributed to rotation of the phenyl ring. The slower relaxation is concentration dependent and is due to the parallel stacking of two dye molecules. The forward and reverse rates for this process are $(4.6 \pm 1.4) \times 10^8$ M^{-1} s^{-1} and $(6.7 \pm 1.4) \times 10^6$ s^{-1}, respectively, at 25°C, 0.25 M ionic strength, and pH 6.9. This reverse rate and those of three similar reactions are found to fit a linear free energy plot. The implications of these results for studies of nucleic acid base stacking are discussed.

1. Introduction

Ethidium bromide, 2,7-diamino-9-phenyl-10-ethyl-phenanthridinium bromide, is extensively used in binding studies with nucleic acids [1–5]. This binding is assumed to occur via an intercalation mechanism in which the stacking interaction between the phenanthridinium ring and the nucleic acid bases stabilizes the complex. Similar stacking interactions are thought to be important in a wide variety of biological molecules [6]. NMR and X-ray results demonstrate that ethidium bromide is also capable of self-stacking into dimers [7–9]. We have investigated the kinetics of this dimerization as a model system for studying stacking interactions.

2. Materials and methods

The dimerization of ethidium bromide occurs too rapidly for study with conventional temperature-jump techniques. Therefore the recently developed Raman laser temperature-jump technique was used for these measurements [10, 11]. With this technique, a very thin sample solution is heated by absorption of a 15 ns wide (full width at half maximum) 1.41 μ laser pulse. The path lengths of the cells used in this study ranged from 0.013 to 0.080 cm, with corresponding average temperature jumps from 4.8 to 2.5 °C. A probe beam from a 450 watt xenon arc lamp was crossed with the laser beam at the cell and the time dependence of any absorption change was measured. Before it reached the cell, the probe beam was filtered with Corning #4602 and 5562 glass filters. Because ethidium bromide is photosensitive, it was exposed to the probe beam for very short times. A camera shutter was used to limit the total exposure time for each shot to 20 ms. A 4 ms wide square pulse from a bank of capacitors was applied to the xenon arc and served to enhance the light intensity by a factor of 4. The laser was synchronized to fire in the middle of this pulse. In order to avoid saturation of the detection system by the pulsed probe beam and yet amplify the small relaxation signal, the initial voltage change due to the lamp pulse was offset by a feedback loop. This loop was broken 400 ns before the laser pulse and therefore did not interfere with the relax-

* National Institutes of Health Predoctoral Fellow, Columbia University.
‡ Technical Collaborator, Brookhaven National Laboratory.
** Fellow of the Alfred P. Sloan Foundation and Research Collaborator, Brookhaven National Laboratory.

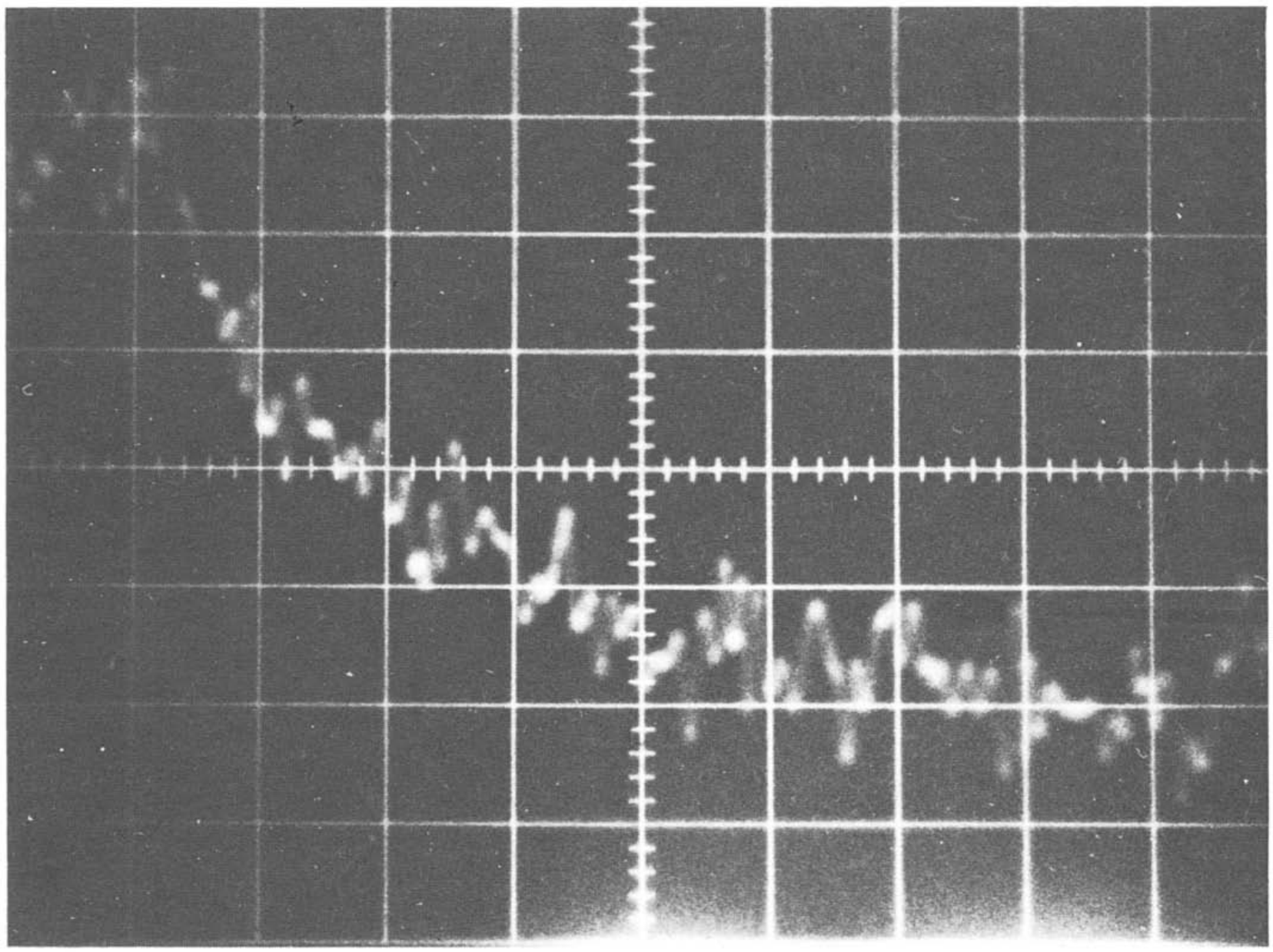


Fig. 1. Relaxation in 2.48×10^{-3} M ethidium bromide, 0.2 M KCl, 0.05 M phosphate, pH 6.9, wavelength is 480 nm, horizontal scale is 50 ns per division.

ation signal. The total rise time of the amplifier circuit was about 5 ns.

Ethidium bromide was obtained from Sigma Chemical Co and was used without further purification. A bromide analysis indicated the presence of 0.5 ethanol molecules (or one water molecule) per ethidium in the crystals. Solutions were made up in a 0.2 M KCl, 0.05 M phosphate buffer at pH 6.9 and were allowed to equilibrate thermally for at least 15 min. Fig. 1 shows a typical relaxation measured at 480 nm, which is an absorbance maximum of the monomer. Each reported lifetime represents the average of at least 12 measurements. Spectra taken before and after the temperature-jumps indicated no detectable decomposition of the sample.

3. Results

Two relaxations were observed with solutions of ethidium bromide in H_2O. However no signal was detected when D_2O was the solvent. The absorbance of D_2O at the laser wavelength, 1.41 μ, is 150 times smaller than the absorbance of H_2O and as a consequence the temperature jumps produced in D_2O are less than 0.04 °C. From these observations we conclude that the two relaxations observed in H_2O are due to heating caused by absorption of the laser pulse and not due to any photochemical effects. The faster relaxation corresponds to the heating time of the apparatus (30 ns). It is present in solutions containing 0.5 M HCl and in solutions without added KCl, as well as in the buffer solutions described above. In 0.5 M HCl this signal corresponds to a decrease in light intensity between 420

and 520 nm and to an increase in intensity in the wavelength region immediately below 380 nm. The latter wavelength corresponds to the beginning of a new absorption band. The slower relaxation is not observed in 0.5 M HCl, where presumably any dimers are broken up by protonation of both amino groups on the ethidium. It has a concentration-dependent lifetime and at pH 6.9 it can be observed without interference from the fast signal as an absorbance increase at wavelengths from 460 to 500 nm. We attribute the slower relaxation to the monomer–dimer equilibrium:

$$2E \underset{k_{-1}}{\overset{k_1}{\rightleftharpoons}} E_2. \qquad (1)$$

The concentration dependence of the lifetimes for such a reaction has the following form:

$$\tau^{-2} = k_{-1}^2 + 8k_1k_{-1}[E]_T, \qquad (2)$$

where $[E]_T$ is the total ethidium bromide dissolved. Fig. 2 shows the plot of the experimental data suggested by eq. (2). The forward and reverse rate constants derived from this plot are $(4.6 \pm 1.4) \times 10^8$ M^{-1} s^{-1} and $(6.7 \pm 1.4) \times 10^6$ s^{-1}, respectively, at 25 °C. The ratio of these rates gives a value of 69 M^{-1} for the equilibrium constant under these conditions. This equilibrium constant has previously been measured spectrophotometrically under somewhat different conditions. The kinetic result obtained in this work is consistent with the reported values of 30 M^{-1} and 230 M^{-1} measured in pure water and in 1 M NaCl, respectively [5, 9].

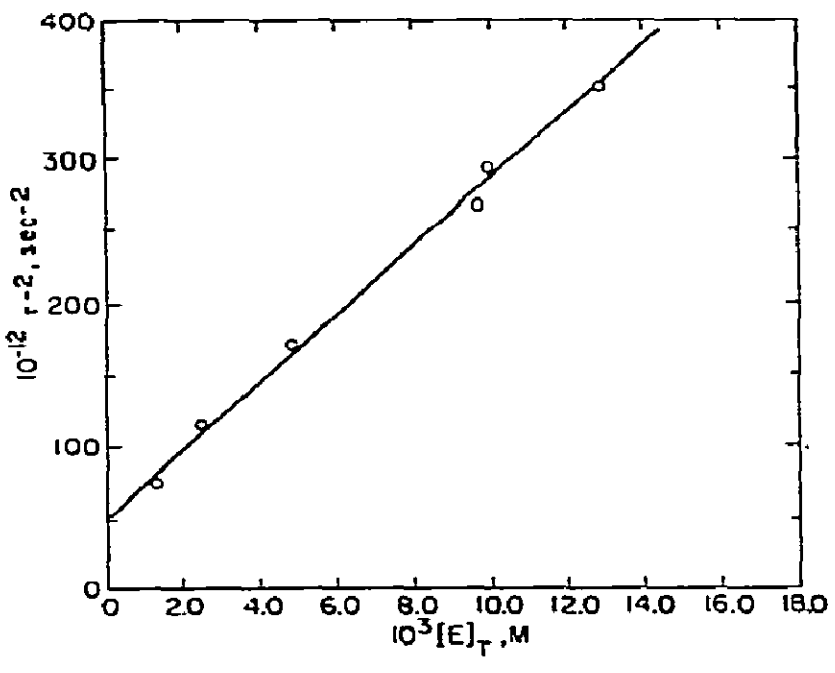


Fig. 2. Plot of square of reciprocal relaxation time versus total ethidium bromide concentration at 25 °C.

4. Discussion

An unusual feature of the ethidium system is the presence of two relaxation times. No similar effect is observed with proflavin (3,6-diamino-acridine) or acridine orange (3,6-*bis*dimethylacridine). The fact that the very rapid relaxation in the ethidium system is also present in 0.5 M HCl indicates that it is not coupled to the dimerization process. That it is unchanged in solutions without added KCl implies that it is not due to ion association. The increase in absorption above 420 nm and the decrease immediately below 380 nm observed in 0.5 M HCl could result from the electronic interaction between the two ring systems of ethidium. Due to the steric hindrance of the ethyl group, the preferred orientation of the phenyl ring in ethidium is perpendicular to the phenanthridinium system [7–9]. At higher temperatures increased rotation of the phenyl ring could bring it, on the average, more parallel to the phenanthridinium system. The direction of the transition moment for a given band would then determine whether the temperature increase produced hyper or hypochromism [12]. On the basis of these considerations we tentatively attribute the very rapid relaxation to increased rotation of the phenyl ring at the higher temperature. One obvious implication of this finding is that spectrophotometric measurements involving ethidium bromide are best performed at wavelengths, such as 480 nm, where this effect is negligible.

The rate constants for the slower ethidium dimerization reaction can be compared with those obtained for stacking reactions in proflavin, acridine orange, and N^6,N^9-dimethyladenine. These are listed in table 1. While these rates have been measured at ionic strengths ranging from 0.05 to 0.25 M, the reactions have been shown to be rather insensitive to this parameter [13, 14]. Thus a comparison of the rates is appropriate. The forward reaction rates are very high and are probably within an order of magnitude of the diffusion-controlled limit. The differences in the stability constants of the dimers are reflected primarily in their dissociation rates. This is shown in fig. 3 in which $\log k_{-1}$ is plotted versus $\log (k_1/k_{-1})$. A good linear relationship is obtained; the slope of the straight line is -1.15 ± 0.07. Evidently

Table 1

Summary of forward and reverse rate constants for dimerization reactions at 25 °C

System	$10^{-8}\,k_1$ ($M^{-1}\,s^{-1}$)	$10^{-6}\,k_{-1}$ (s^{-1})	Ref.
Ethidium bromide	4.6	6.7	a
Proflavine (3,6 diaminoacridine)	7.9	2.0	b
Acridine orange (3,6-*bis*dimethylaminoacridine)	2.7	0.018	c
N^6,N^9-dimethyladenine	9.3	50	d

a) This work. b) D.H. Turner, G.W. Flynn, S.K. Lundberg, L.D. Faller and N. Sutin, Nature 239 (1972) 215. c) G.G. Hammes and C.D. Hubbard, J. Phys. Chem. 70 (1966) 1615. d) D. Porschke and F. Eggers, Eur. J. Biochem. 26 (1972) 490.

the rates of dissociation of the dimers increase more rapidly than do the equilibrium constants for the dissociation reactions. Put somewhat differently, the dimerization rates tend to decrease with increasing driving force for the reactions. This effect is, however, small.

Additional information about the reaction mechanism can be obtained from a consideration of the following scheme:

$$M + M \underset{k_{21}}{\overset{k_{12}}{\rightleftharpoons}} M, M \underset{k_{32}}{\overset{k_{23}}{\rightleftharpoons}} M_2. \qquad (3)$$

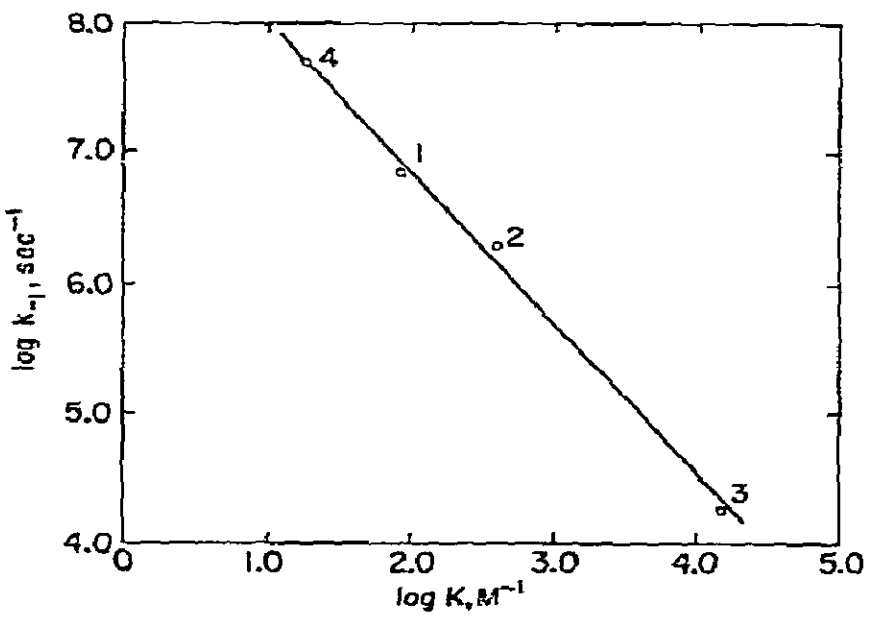


Fig. 3. Plot of log k_{-1} versus log k_1/k_{-1} for various dimers where k_{-1} is the dissociation rate constant and k_1/k_{-1} the stability constant at 25 °C: 1, ethidium bromide; 2, proflavine; 3, acridine orange; 4, N^6,N^9-dimethyladenine.

The first step represents the diffusion-controlled formation of an encounter complex, and the second step the activation controlled conversion of the encounter complex to the stable dimer. Two limiting forms of the rate law for this scheme are of interest.

Case (a): $k_{23} \gg k_{21}$. In this case $k_1 = k_{12}$ and $k_{-1} = k_{32}k_{21}/k_{23}$. Under these conditions the formation of M_2 is diffusion controlled. Since $K = k_1/k_{-1}$ it follows that

$$k_{-1} = k_{12}/K, \quad \log k_{-1} = \log k_{12} - \log K. \qquad (4)$$

In other words, if log k_{12} is constant for a series of reactions then a linear relationship between log k_{-1} and log K is predicted; the slope of this predicted plot is −1 and its intercept is log k_{12}. The slope of fig. 3 (−1.15 ± 0.07) is not too different from the predicted value. On the other hand the antilog of the intercept of fig. 3 (1.8×10^9 M^{-1} s^{-1}) is significantly higher than the measured k_1 values. Moreover inspection of table 1 shows that the forward rates shown are not equal, but differ by more than a factor of 3. This does not necessarily imply, however, that the reactions are not diffusion controlled since the variations in the dimensions and charges of the molecules could lead to differences in their diffusion controlled dimerizations. An estimate of the diffusion controlled rate can be obtained from eq. (5)

$$k_{diff} = 4\pi NRD/1000, \qquad (5)$$

where R is the encounter distance and D is the diffusion coefficient of the monomer. The diffusion coefficient of ethidium bromide has been measured [15], its value is $(3 \pm 1) \times 10^{-6}$ cm^2 s^{-1} in 0.1 M NaCl at 22 °C. A reasonable estimate of the encounter distance for ethidium bromide dimerization is 8×10^{-8} cm. Substitution of these values in eq. (5) gives $k_{diff} = 1.8 \times 10^9$ M^{-1} s^{-1}. The measured value of k_1 for ethidium bromide is about a factor 4 lower than this calculated value. While this lower rate may be due to the similar charges on the two dye molecules it may also suggest that the reactions of interest are primarily activation rather than diffusion controlled.

Case (b): $k_{23} \ll k_{21}$. In this case $k_1 = k_{12}k_{23}/k_{21}$ and $k_{-1} = k_{32}$. In terms of this interpretation the formation of M_2 is activation controlled and the slope of −1.15 for the free energy plot implies that only small

structural changes are required for the separated monomers to enter the transition state [16]. This conclusion is consistent with the high values of the forward rates for all four reactions, and it is further supported by the low activation enthalpies measured for proflavin and N^6,N^9-dimethyl adenine [11, 14]. A further implication of this interpretation is that all four reactions proceed by a similar mechanism. This conclusion assumes, of course, that the reactions under consideration are primarily activation controlled so that case (b) obtains [17]. Further studies are required to definitively differentiate between this case and simple diffusion control.

In view of their importance in stabilizing the structures of nucleic acids, the nature of the interactions involved in stacking has been the subject of much speculation [18–20]. Unfortunately, it is difficult to perform kinetic studies of the nucleic acid bases themselves because of their low association constants. Although the above analysis is almost certainly oversimplified, the results obtained in this work nevertheless indicate that suitable model systems can significantly augment the data obtained with the natural bases. Thus if the dimerization of N^6,N^9-dimethyladenine is representative of the stacking of other nucleic acid bases, then these studies suggest that dye molecules may serve as useful compounds for investigating stacking reactions [21]. The application of linear free energy (and enthalpy) relations to such data, coupled with measurements of the solvent dependence of the dimerization kinetics, could provide valuable information about the nature of the forces involved in stacking.

Acknowledgement

This research was performed under the auspices of the U.S. Atomic Energy Commission and was supported in part by the National Science Foundation and the National Institutes of Health. The authors wish to acknowledge helpful discussions with Dr. H.A. Schwarz, Dr. I Tinoco, Jr., and Dr. J. Yandell.

References

[1] T.R. Tritton and S.C. Mohr, Biochemistry 12 (1973) 905.
[2] I. Paoletti and J.B. Le Pecq, J. Mol. Biol. 59 (1971) 43.
[3] J.B. Le Pecq and C. Paoletti, J. Mol. Biol. 27 (1967) 87.
[4] M.J. Waring, J. Mol. Biol. 13 (1965) 269.
[5] J. Bresloff, Ph.D. Thesis, Yale University, New Haven (1974).
[6] B. Pullman, ed., Molecular associations in biology (Academic Press, New York, 1968).
[7] G.P. Kreishman, S.I. Chan and W. Bauer, J. Mol. Biol. 61 (1971) 45.
[8] E. Subramanian, J. Trotter and C.E. Bugg, J. Cryst. Mol. Struct. 1 (1971) 3.
[9] G. Thomas and B. Roques, FEBS Letters 26 (1972) 169.
[10] D.H. Turner, G.W. Flynn, N. Sutin and J.V. Beitz, J. Amer. Chem. Soc. 94 (1972) 1554.
[11] D.H. Turner, G.W. Flynn, S.K. Lundberg, L.D. Faller and N. Sutin, Nature 239 (1972) 215.
[12] I. Tinoco, Jr., A. Halpern and W.T. Simpson, in: Polyamino acids, polypeptides, and proteins, ed. M.A. Stahmann (University of Wisconsin Press, Madison, 1962) p. 147.
[13] G. Schwarz, S. Klose and W. Balthasar, Eur. J. Biochem. 12 (1970) 454.
[14] D. Pörschke and F. Eggers, Eur. J. Biochem. 26 (1972) 490.
[15] D. Magde, E.L. Elson and W.W. Webb, Biopolymers 13 (1974) 29.
[16] G.S. Hammond, J. Am. Chem. Soc. 77 (1955) 334.
[17] Note that it is not possible for k_{23} to be very much less than k_{21}; since k_1 is within a factor 4 of diffusion controlled limit, k_{21} cannot be greater than $4k_{23}$.
[18] D.M. Crothers and B.H. Zimm, J. Mol. Biol. 9 (1964) 1.
[19] O. Sinanoglu, ref. [6] p. 427.
[20] C.E. Bugg, J.M. Thomas, M .Sundaralingam and S.T. Rao, Biopolymers 10 (1971) 175.
[21] A recent kinetic study of 6-methylpurine, when combined with previous equilibrium data, indicates the aggregation of this base also conforms to the linear relationship shown in fig. 3. The values reported for this reaction are: $k_{-1} = 1.6 \times 10^8\ s^{-1}$, and $K = 6.7\ M^{-1}$ [22, 23].
[22] F. Garland and R.C. Patel, J. Phys. Chem. 78 (1974) 848.
[23] P.O.P. Ts'o and S.I. Chan, J. Amer. Chem. Soc. 86 (1964) 4176.

AUTHOR INDEX TO VOLUME 2

Avanesov, A.Ts., see C. Guermant 2 (1974) 345

Bańkowski, E. and W.M. Mitchell, Human procollagen I. An anionic tropocollagen precursor from skin fibroblasts in culture, Erratum 1 (1973) 73–86 2 (1974) 196
Baumgartner, E., see D. Turyn 2 (1974) 269
Benko, B., see S. Vuk-Pavlović 2 (1974) 359
Bertoli, D.A., see J.J. Breen 2 (1974) 49
Bontemps, J. and E. Fredericq, Comparative binding study of the interaction of quinacrine and ethidium bromide with DNA and nucleohistone 2 (1974) 1
Bontemps, J., C. Houssier and E. Fredericq, Optical and electro-optical properties of the complexes of dibutylproflavine with DNA and nucleohistone 2 (1974) 301
Breen, J.J., D.A. Bertoli, J. Dadok and C. Ho, Proton magnetic resonance studies of human adult hemoglobin in water 2 (1974) 49
Březina, M., A. Hofmanová-Matějková and J. Koryta, The dissociation-rate dependent electrochemical reduction of valinomycin complexes of monovalent ions 2 (1974) 264
Brunori, M., see A. Colosimo 2 (1974) 338

Chun, P.W., Determination of the equilibrium constants of self-associating protein systems. X. Evaluation of the weight fraction of monomer from the diffusion coefficient as a function of concentration 2 (1974) 170
Colosimo, A., M. Brunori and J. Wyman, Concerted changes in an allosteric macromolecule 2 (1974) 338
Crescenzi, V., see F. Quadrifoglio 2 (1974) 64

Dadok, J., see J.J. Breen 2 (1974) 49
De Goeij, A.F.P.M., see W.H.J. Stork 2 (1974) 127
De Haseth, P.L., see W.H.J. Stork 2 (1974) 127
Devore, D.I. and G.S. Manning, Application of polyelectrolyte limiting laws to virial and asymptotic expansions for the Donnan equilibrium 2 (1974) 42
Doleček, V., see S. Lapanje 2 (1974) 369

Eigen, M., see P.H. Richter 2 (1974) 255
Epand, R.M., see M.A. Moscarello 2 (1974) 290

Fernández-Prini, R., see D. Turyn 2 (1974) 269
Ferry, J.D., see C. Gerth 2 (1974) 208
Finazzi Agrò, A., L. Morpurgo and B. Mondovi, Effect of metal binding on the intrinsic fluorescence of bovine carbonic anhydrase 2 (1974) 151
Flynn, G.W., see D.H. Turner 2 (1974) 385
Fredericq, E., see J. Bontemps 2 (1974) 1
Fredericq, E., see J. Bontemps 2 (1974) 301
Fresco, J.R., see M.D. Topal 2 (1974) 193

Gerth, C., W.W. Roberts and J.D. Ferry, Rheology of fibrin clots. II. Linear viscoelastic behavior in shear creep 2 (1974) 208
González, J.J., Theoretical analysis of the oxidation of amylose by periodate ion as an example of cooperative effects in polymer kinetics 2 (1974) 23
Grafius, M.A., see D.B. Millar 2 (1974) 189
Grassi, H., see M.-A. Rix-Montel 2 (1974) 278
Guermant, C., V.V. Shcherbukhin and A.Ts. Avanesov, Thermodynamic equilibrium in reversibly interacting ribosomal systems of E. coli and Bac. coagulans 2 (1974) 345

Hesselink, F.Th., Monte Carlo generation of polypeptide random coil conformations; the persistence vector and the chain vector distribution 2 (1974) 76
Hiernaux, J., On some stochastic models for protein biosynthesis 2 (1974) 70
Higashi, K., see S. Lapanje 2 (1974) 369
Ho. C., see J.J. Breen 2 (1974) 49
Hofmanová-Matějková, A., see M. Březina 2 (1974) 264
Houssier, C., see J. Bontemps 2 (1974) 301

Inoue, I., I. Tasaki and Y. Kobatake, A study of the effects of externally applied sodium-ions and detection of spatial non-uniformity of the squid axon membrane under internal perfusion 2 (1974) 116

Jeffrey, P.D., see L.W. Nichol 2 (1974) 354
Johnson, M.L. and T.M. Schuster, Analysis of relaxation kinetics data by a nonlinear least squares method 2 (1974) 32
Joyce, D.E. and T. Kurucsev, Study of exciton interactions in some pyrimidine dinucleotides in aqueous solution by means of absorption spectroscopy 2 (1974) 273

Katona, E., see M.A. Moscarello 2 (1974) 290
Kawahara, K., see S. Lapanje 2 (1974) 369
Kobatake, Y., see I. Inoue 2 (1974) 116
Koryta, J., see M. Březina 2 (1974) 264
Koudelka, J., see G. Löber 2 (1974) 158
Kuchel, P.W., see L.W. Nichol 2 (1974) 354
Kurucsev, T., see D.E. Joyce 2 (1974) 273

Laiken, N., see R.H. Shafer 2 (1974) 180
Lapanje, S., V. Doleček, K. Kawahara and K. Higashi, Molecular weight determination of bovine carbonic anhydrase 2 (1974) 369
Löber, G., J. Koudelka and E. Smékal, Stacking interactions of ethidium bromide bound to a polyphosphate and phage DNA in situ 2 (1974) 158
Lorand, L., see L.F. Mockros 2 (1974) 164

Malkin, S., Energy transfer in the photosynthetic unit. I. The concept of independent units for photosystem II analyzed by flash yields for dichlorophenolindophenol reduction 2 (1974) 327
Mandel, M., see W.H.J. Stork 2 (1974) 127
Mandel, M. and W.H.J. Stork, A dye-binding induced conformational transition of poly-(methacrylic acid) by auramine O in aqueous solutions. II. Theoretical interpretation and discussion of the experimental results 2 (1974) 137
Mandel, M., see F. van der Touw 2 (1974) 218

Mandel, M., see F. van der Touw 2 (1974) 231
Mandel, M., see G. Müller 2 (1974) 242
Manning, G.S., see D.I. Devore 2 (1974) 42
Maričić, S., see S. Vuk-Pavlović 2 (1974) 359
Millar, D.B., M.A. Grafius, J.R. Wild and D.A. Palmer, High pressure stabilization of acetylcholinesterase sizeozymes against thermal denaturation 2 (1974) 189
Minton, A.P. and H.A. Saroff, A general formulation of the free energy of interaction in cooperative ligand binding: Application to hemoglobin 2 (1974) 296
Mitchell, W.M., see E. Bańkowski 2 (1974) 196
Mockros, L.F., W.W. Roberts and L. Lorand, Viscoelastic properties of ligation-inhibited fibrin clots 2 (1974) 164
Morpurgo, L., see A. Finazzi Agrò 2 (1974) 151
Moscarello, M.A., E. Katona, A.W. Neumann and R.M. Epand, The ordered structure of the encephalitogenic protein from normal human myelin 2 (1974) 290
Müller, G., F. van der Touw, S. Zwolle and M. Mandel, Dielectric properties of poly-L-glutamic acid in salt-free aqueous solutions 2 (1974) 242

Neet, K.E., Analysis of conformationally-linked dissociation of proteins 2 (1974) 102
Neher, E., see H.P. Zingsheim 2 (1974) 197
Neumann, A.W., see M.A. Moscarello 2 (1974) 290
Neumann, E., see A. Revzin 2 (1974) 144
Nichol, L.W., P.W. Kuchel and P.D. Jeffrey, The detection and consequences of association of two enzymes involved in catalysing consecutive reactions 2 (1974) 354

Oudshoorn, C., see R.J.M. Tausk 2 (1974) 53
Overbeek, J.Th.G., see R.J.M. Tausk 2 (1974) 53
Overbeek, J.Th.G., see R.J.M. Tausk 2 (1974) 175

Palmer, D.A., see D.B. Millar 2 (1974) 189
Pörschke, D., Model calculations on the kinetics of oligonucleotide double helix coil transitions. Evidence for a fast chain sliding reaction 2 (1974) 83
Pörschke, D., A direct measurement of the unzippering rate of a nucleic acid double helix 2 (1974) 97

Quadrifoglio, F. and V. Crescenzi, On the binding of actinomycin and of daunomycin to DNA: A calorimetric and spectroscopic investigation 2 (1974) 64

Revzin, A. and E. Neumann, Conformation changes in rRNA induced by electric impulses 2 (1974) 144
Richter, P.H. and M. Eigen, Diffusion controlled reaction rates in spheroidal geometry. Application to repressor–operator association and membrane bound enzymes 2 (1974) 255
Rix-Montel, M.-A., H. Grassi and D. Vasilescu, Experimental studies of thermal denaturation of the Na–DNA system with respect to Manning's model 2 (1974) 278
Roberts, W.W., see L. Mockros 2 (1974) 164
Roberts, W.W., see C. Gerth 2 (1974) 208

Saroff, H.A., see A.P. Minton 2 (1974) 296
Schuster, T.M., see M.L. Johnson 2 (1974) 32
Shafer, R.H., N. Laiken and B.H. Zimm, Radial migration of DNA molecules in cylindrical flow. I. Theory of the free-draining model 2 (1974) 180

Shafer, R.H., Radial migration of DNA molecules in cylindrical flow. II. The non-draining model and possible application to fractionation 2 (1974) 135
Shcherbukhin, V.V., see C. Guermant 2 (1974) 345
Sisco, K., see I. Tasaki 2 (1974) 316
Smékal, E., see G. Löber 2 (1974) 158
Stork, W.H.J., J.A.M. van Boxsel, A.F.P.M. de Goeij, P.L. de Haseth and M. Mandel, A dye-binding induced conformational transition of poly-(methacrylic acid) by auramine O in aqueous solutions. I. Experimental results 2 (1974) 127
Stork, W.H.J., see M. Mandel 2 (1974) 137
Sutin, N., see D.H. Turner 2 (1974) 385

Tasaki, I., see I. Inoue 2 (1974) 116
Tasaki, I., K. Sisco and A. Warashina, Alignment of anilinonaphthalene-sulfonate and related fluorescent probe molecules in squid axon membrane and in synthetic polymers 2 (1974) 316
Tausk, R.J.M., C. Oudshoorn and J.Th.G. Overbeek, Physical chemical studies of short-chain lecithin homologues. III. Phase separation and light scattering studies on aqueous dioctanoyllecithin solutions 2 (1974) 53
Tausk, R.J.M. and J.Th.G. Overbeek, Physical chemical studies of short-chain lecithin homologues. IV. A simple model for the influence of salt and the alkyl chain length on the micellar size 2 (1974) 175
Topal, M.D. and J.R. Fresco, Polynucleotides XV. A common error in the plotting of continuous variation (mixing curve) experiments 2 (1974) 193
Turner, D.H., R. Yuan, G.W. Flynn and N. Sutin, Kinetics of the stacking of ethidium bromide by the Raman laser temperature-jump method 2 (1974) 385
Turyn, D., E. Baumgartner and R. Fernández-Prini, Effect of polyelectrolytes on the kinetics of ionic reactions. III. Hydrolysis of pyrophosphate in poly-(ethyleneimine) solutions 2 (1974) 269

Van Boxsel, J.A.M., see W.H.J. Stork 2 (1974) 127
Van der Touw, F. and M. Mandel, Dielectric increment and dielectric dispersion of solutions containing simple charged linear macromolecules. I. Theory 2 (1974) 218
Van der Touw, F. and M. Mandel, Dielectric increment and dielectric dispersion of solutions containing simple charged linear macromolecules. II. Experimental results with synthetic polyelectrolytes 2 (1974) 231
Van der Touw, F., see G. Müller 2 (1974) 242
Vasilescu, D., see M.-A. Rix-Montel 2 (1974) 278
Vuk-Pavlović, S., B. Benko and S. Maričić, The molecular mechanism of the temperature enhancement of proton magnetic relaxation rates in methaemoprotein solutions 2 (1974) 359

Warashina, A., see I. Tasaki 2 (1974) 316
Whitehead, E., Possible implications for allosteric models of hemoglobin of the laws of combination with carbon monoxide under photodissociating conditions 2 (1974) 377
Wild, J.R., see D.B. Millar 2 (1974) 189
Wyman, J., see A. Colosimo 2 (1974) 338

Yuan, R., see D.H. Turner 2 (1974) 385

Zimm, B.H., see R.H. Shafer 2 (1974) 180
Zingsheim, H.P. and E. Neher, The equivalence of fluctuation analysis and chemical relaxation measurements: A kinetic study of ion pore formation in thin lipid membranes 2 (1974) 197
Zwolle, S., see G. Müller 2 (1974) 242

SUBJECT INDEX TO VOLUME 2

Each page number refers to the first page of a given reference

Actinomycin, binding to DNA, 64
Allosteric models, 338, 377
Amylose, oxidation of, 23
Anilinonaphthalene-sulfonate, 316
Auramine O, binding to poly-(methacrylic acid), 127, 137

Carbonic anhydrase, bovine, 151, 369
Catalysis, of consecutive reactions, 354
Conformation changes, in DNA, 97
Conformation changes, in oligonucleotides, 83
Conformation changes, in poly-(methacrylic acid), 127, 137
Conformation changes, in rRNA, 144
Cooperative effects, 23, 338
Cylindrical flow, of DNA, 180

Daunomycin, binding to DNA, 64
Dibutylproflavine, complexes with DNA, 301
Dichlorophenolindophenol, reduction of, 327
Dielectric properties, of poly-L-glutamic acid, 242
Dielectric properties, synthetic polyelectrolytes, 231
Dielectric properties, theory for charged macromolecules, 218
Diffusion coefficient, in protein systems, 170
Dissociation, rates of, 264
DNA, binding of antibiotics to, 64
DNA, binding of dyes to, 1, 158
DNA, complexes with dibutylproflavine, 301
DNA, kinetics of double helix unzippering, 97
DNA, thermal denaturation, 278
Donnan equilibrium, 42

Electrochemical reduction, 264
Electro-optical properties, of DNA complexes and nucleohistones, 301
Encephalitogenic protein, 290
Energy transfer, in photosynthesis, 327
Enzymes, association of, 354
Enzymes, membrane bound, 255
Equilibrium, in ribosomal systems, 345

Ethidium bromide, binding to DNA, 1
Ethidium bromide, kinetics of stacking, 385
Ethidium bromide, stacking interactions, 158
Exciton interactions, 273

Fibrin clots, viscoelastic properties, 164, 208
Fluctuation analysis, 197
Fluorescence, of carbonic anhydrase, 151
Fluorescence, probes, 316

Helix–coil transition, kinetics of, 83
Hemoglobin, allosteric models of, 377
Hemoglobin, ligand binding to, 296
Hemoglobin, NMR studies on, 49
Hemoglobin, photodissociation of, 377

Kinetics, 23, 83, 255, 269

Lecithin, homologues of, 53, 175
Ligand binding, cooperative, 296
Light scattering, lecithin homologues, 53

Manning's model, for polyelectrolytes, 42, 278
Membranes, squid axon, 116, 316
Membranes, thin lipid, 197
Methaemoprotein, 385
Micelles, size of, 175
Molecular weight, determination of, 369
Monte Carlo calculations, polypeptides, 76
Myelin, human, 280

Nucleohistones, 1, 301
Nucleotides, oligo-, 83
Nucleotides, pyrimidine, 273

Oligonucleotides, model calculations for, 83
Optical properties, of DNA complexes and nucleohistones, 301

Phase separation, in lecithin homologues solutions, 53
Photodissociation, of hemoglobin, 377

Photosystems, 327
Polyelectrolytes, dielectric properties, 218, 231
Polyelectrolytes, Donnan equilibrium, 42
Polyelectrolytes, effects on reaction rates, 273
Polyelectrolytes, Manning's model, 42, 278
Poly-(ethyleneimine), effects on reaction rates, 269
Poly-L-glutamic acid, 242
Poly-(methacrylic acid), binding of dyes to, 127, 137
Polypeptides, Monte Carlo calculations, 76
Polyphosphates, 158
Pore formation, ion, 197
Proteins, biosynthesis, 70
Proteins, dissociation of, 97
Proteins, self-associating systems, 170
Proton magnetic resonance, 49, 385
Pyrophosphates, hydrolysis of, 269

Quinacrine, binding to DNA, 1

Relaxation, chemical, 197
Relaxation, dielectric, 218, 231, 242
Relaxation, kinetics of, 32
Relaxation, NMR, 385
Repressor–operator, association, 255
Ribosomal systems, 345

Structures, ordered (myelin), 290

Temperature-jump method, Raman laser, 385

Valinomycin, 264
Viscoelastic behaviour, of fibrin clots, 164, 208